OAK RIDGE NATIONAL LABORATORY LIBRARIES
3 4456 0570482 3

CENTRAL RESEARCH LIBRARY

ORNL-4998

cy 1

MECHANICAL PROPERTIES TEST DATA FOR STRUCTURAL MATERIALS QUARTERLY PROGRESS REPORT FOR PERIOD ENDING JULY 31, 1974

[redacted]

OAK RIDGE NATIONAL LABORATORY
CENTRAL RESEARCH LIBRARY
DOCUMENT COLLECTION
LIBRARY LOAN COPY
DO NOT TRANSFER TO ANOTHER PERSON
If you wish someone else to see this document, send in name with document and the library will arrange a loan.
UCN-7969
(3 3-67)

OAK RIDGE NATIONAL LABORATORY
OPERATED BY UNION CARBIDE CORPORATION • FOR THE U.S. ATOMIC ENERGY COMMISSION

Printed in the United States of America. Available from
the U.S. Atomic Energy Commission, Technical Information Center
P.O. Box 62, Oak Ridge, Tennessee 37830
Price: Printed Copy $10.60 ; Microfiche $1.45

This report was prepared as an account of work sponsored by the United States Government. Neither the United States nor the United States Atomic Energy Commission, nor any of their employees, nor any of their contractors, subcontractors, or their employees, makes any warranty, express or implied, or assumes any legal liability or responsibility for the accuracy, completeness or usefulness of any information, apparatus, product or process disclosed, or represents that its use would not infringe privately owned rights.

ORNL-4998
UC-79b, -h, -k
(Liquid Metal Fast
Breeder Reactors)

Contract No. W-7405-eng-26

METALS AND CERAMICS DIVISION

MECHANICAL PROPERTIES TEST DATA FOR STRUCTURAL MATERIALS QUARTERLY PROGRESS REPORT FOR PERIOD ENDING JULY 31, 1974

Aerojet Nuclear Company
Argonne National Laboratory
Hanford Engineering Development Laboratory
Naval Research Laboratory
Oak Ridge National Laboratory
Westinghouse Advanced Reactors Division
University of Cincinnati
University of California at Los Angeles

Compiled by M. R. Hill

SEPTEMBER 1974

OAK RIDGE NATIONAL LABORATORY
Oak Ridge, Tennessee 37830
operated by
UNION CARBIDE CORPORATION
for the
U.S. ATOMIC ENERGY COMMISSION

FOREWORD

This is the fourth in a series of progress reports, the purpose of which is to record and distribute quarterly the collected results of all structural materials mechanical properties test programs sponsored by the Reactor Research and Development Division of the USAEC.

To be useful as resource documents, the reports in this series must be published and distributed in a timely manner to those in the reactor design and materials technology community who have a need of mechanical property test data for nuclear reactor and power plant applications. A materials index, lists of measurement units and conversion factors, and stress unit conversion tables are included to increase the effectiveness of the report.

Reports previously issued in this series are as follows: ORNL-4936, period ending October 31, 1973; ORNL-4948, period ending January 31, 1974; and ORNL-4963, period ending April 30, 1974. The next quarterly report will be for the period ending October 31, 1974, and contributions are due at ORNL by November 15, 1974.

W. R. Martin
Metals and Ceramics Division
Oak Ridge National Laboratory

CONTENTS

SUMMARY xi

1. AEROJET NUCLEAR COMPANY 1

1.1 INTRODUCTION 1

1.2 FATIGUE TESTS ON CLADDING AND STRUCTURAL MATERIALS . . . 1

1.2.1 Fatigue and Creep-Fatigue of Type 316 Stainless Steel with 20% Cold Work 1

1.3 INCONEL 718 MECHANICAL PROPERTY PROGRAM 12

1.3.1 Development and Optimization of a Modified Heat Treatment for Inconel 718 12

2. ARGONNE NATIONAL LABORATORY 15

2.1 INTRODUCTION 15

2.2 FRACTURE AND FATIGUE STUDIES ON STAINLESS STEELS 15

2.2.1 Some Considerations Involved in the Application of Strain-range Partitioning to the Prediction of Low-cycle Fatigue Life for Type 304 Stainless Steel 15

2.2.2 Low-cycle Creep Fatigue and Crack Propagation of SMA Type 304/308 Stainless Steel Weldments . . 22

2.3 SODIUM EFFECTS ON LMFBR MATERIALS 35

2.3.1 Influence of Sodium Environment on Tensile and Creep Behavior of Austenitic Stainless Steels . . 35

2.4 REFERENCES 51

3. HANFORD ENGINEERING DEVELOPMENT LABORATORY (For Period Ending April 30, 1974) 55

3.1 INTRODUCTION 55

3.2 MATERIALS PERFORMANCE AND SURVEILLANCE 55

3.2.1 Subcritical Crack Growth 55

3.2.1.1 Accomplishments and Status 55

3.3 HIGH STRAIN RATE EFFECTS 63

3.3.1 Accomplishments and Status 63

3.3.2 Expected Achievements 65

3.4 REFERENCES 65

3. HANFORD ENGINEERING DEVELOPMENT LABORATORY (For Period Ending July 31, 1974) 75

3.1 INTRODUCTION 75

3.2 IRRADIATION DAMAGE TO REACTOR METALS 75

3.2.1 Low Temperature Creep of 20% Cold Worked Type 316 Stainless Steel 75

3.2.1.1 Objective 75

3.2.1.2 Accomplishments and Status 75

3.2.1.3 Expected Achievements 83

3.3 MATERIALS PERFORMANCE AND SURVEILLANCE 83

3.3.1 FFTF Component Materials Evaluation 83

3.3.1.1 Objective. 83

3.3.1.2 Accomplishments and Status 84

3.3.2 Subcritical Crack Growth 90

3.3.2.1 Objective 90

3.3.2.2 Accomplishments and Status 90

3.4 CLADDING DEVELOPMENT AND PROCESS 91

3.4.1 Fuel and Cladding Characterization 91

3.4.1.1 Objective 91

3.4.1.2 Accomplishments and Status 97

3.5 REFERENCES 100

4. NAVAL RESEARCH LABORATORY 103

4.1 INTRODUCTION 103

4.2 FATIGUE CRACK GROWTH IN THERMALLY-AGED TYPES 304 and 316 STAINLESS STEEL PLATE 103

4.2.1 Background 103

4.2.2 Materials and Test Procedures 103

4.2.3 Results and Discussion 104

4.3 TOUGHNESS OF TYPE 316 STAINLESS STEEL FORGING AND WELD METAL USING THE J INTEGRAL 110

4.3.1 Background 110

4.3.2 Experimental Investigation 110

4.3.2.1 Material and Specimen Types 110

4.3.2.2 Results 111

4.3.3 Discussion 112

4.4 REFERENCES 116

5. OAK RIDGE NATIONAL LABORATORY 119

5.1 INTRODUCTION 119

5.2 MECHANICAL PROPERTIES AND BEHAVIOR FOR STRUCTURAL MATERIALS 119

5.2.1 Mechanical Property Characterization of Type 304 Stainless Steel Reference Heat 120

5.2.1.1 Creep and Rupture Properties of the 2-in. (51-mm) Plate of Reference Heat. . 120

5.2.1.2 Uniaxial Tensile Tests Following Periods of Creep 120

5.2.2 Materials Behavior in Support of Development and Evaluation of Failure Criteria for Materials. 122

5.2.3 Heat-to-Heat Variation of Mechanical Properties of Types 304 and 316 Stainless Steel. 132

5.2.3.1 Long-Term Creep Tests in Heat-to-Heat Variation Study of Type 304 Stainless Steel 132

5.2.3.2 Effect of Aging on the Tensile Properties of Type 304 Stainless Steel 132

5.2.3.3 Influence of Aging on Creep Properties of Type 304 Stainless Steel 141

5.2.3.4 Heat-to-Heat Variation of Type 316 Stainless Steel 143

5.2.3.5 Influence of Aging on Tensile and Creep Properties of Type 316 Stainless Steel . 143

5.2.3.6 Correlation of Tensile Properties with Chemical Composition and Microstructure. 155

5.2.4 Mechanical Property Characterization of Type 316 Stainless Steel Reference Heat 163

5.2.4.1 Procurement of Type 316 Stainless Steel Reference Heat 163

5.2.5 Structural Materials Information Center 168

5.2.6 Elastic Properties of Engineering Structural Materials 172

5.2.6.1 Program Plan 172

5.2.6.2 Elastic Properties Determined by Dynamic Tests 174

5.2.6.3 Elastic Properties Determined by Static Tests 175

5.2.7 Analytical Studies of Mechanical Properties Testing 175

5.2.7.1 Efficacy of Diametral Extensometry for Monotonic Loading of the Hourglass Specimen 176

5.2.7.2 Stresses in the Hourglass Specimen . . . 177

5.2.7.3 Buckling Analysis of a Hollow Tubular Specimen 178

5.3 MECHANICAL AND METALLURGICAL BEHAVIOR OF WELDMENTS FOR LMFBR 178

5.3.1 Tensile Properties of "Heat-Affected Zone" of FFTF Vessel Test Welds 178

5.3.2 Creep and Creep-Rupture Properties of Type 308 CRE Stainless Steel Weld Metal From the FFTF Vessel Test Weld 187

5.4 MECHANICAL PROPERTIES OF STEAM GENERATOR AND HEAT EXCHANGER MATERIALS 197

5.4.1 Tensile Properties of 2 1/4 Cr-1 Mo Steel 197

5.4.2 Creep Properties of 2 1/4 Cr-1 Mo Steel 202

5.4.3 Effect of Sodium on the Mechanical Properties of 2 1/4 Cr-1 Mo Steel 207

5.4.4 Heat-to-Heat Variations of 2 1/4 Cr-1 Mo Steel . . 213

5.4.5 Fatigue Behavior of 2 1/4 Cr-1 Mo Steel 213

5.4.6 Biaxial Fatigue Testing of 2 1/4 Cr-1 Mo Steel . . 219

5.4.7 Mechanical Properties Correlations of 2 1/4 Cr-1 Mo Steel for LMFBR Steam Generator 221

5.4.7.1 Time to Rupture 223

5.4.7.2 Yield and Ultimate Tensile Strength . . . 224

5.4.7.3 Minimum Creep Rate 224

5.4.8 Mechanical Properties of Weld-Overlaid Stainless Steel 225

5.5 HIGH TEMPERATURE DESIGN 232

5.5.1 Exploratory Studies on Type 304 Stainless Steel in Support of Structural Design Methods 232

5.5.1.1 Tensile Testing 232

5.5.1.2 Creep Testing 236

5.5.1.3 Relaxation Testing 238

5.5.1.4 Strain-Cycling 239

5.5.2 Investigations of Creep Failure under Uniaxial and Multiaxial Conditions 241

5.6 MECHANICAL PROPERTIES OF HTGR STEAM GENERATOR AND PRIMARY CIRCUIT MATERIALS 256

5.6.1 Materials 256

5.6.2 Mechanical Property Testing 256

5.6.3 Environmental Facilities 257

5.7 REFERENCES 259

6. WESTINGHOUSE ADVANCED REACTORS DIVISION 263

6.1 INTRODUCTION 263

6.2 BASIC SPECIMEN TESTING 263

6.2.1 Uniaxially Loaded Specimen Models with Uniform Gage Section (304 SS, Heat 9T2796) 263

6.2.1.1 Test Piece Description 263

6.2.1.2 Current Results 263

6.2.2 Uniaxially Loaded Specimen Models with Non-Uniform Gage Section 271

6.2.2.1 Test Piece Description 271

6.2.2.2 Current Results 271

6.2.3 Specimens with Welds (304 SS Heat 9T2796) 272

6.2.3.1 Test Piece Description 272

6.2.3.2 Current Results 272

6.2.4 Topical Report 272

6.3 TUBULAR SPECIMEN TESTING 272

6.3.1 Test Piece Description 272

6.3.2 Test Results and Planning (304SS, Heat 9T2796 ORNL Reference Heat) 274

6.3.3 Data Reduction and Analysis 283

6.3.4 316SS Tubular Testing 300

6.4 REFERENCES 301

7. UNIVERSITY OF CINCINNATI 305

7.1 INTRODUCTION 305

7.2 EXPERIMENTAL PROGRAM 305

7.2.1 Characterization of the Creep and Tensile Substructure of 304 Stainless Steel, Reference Heat 9T2796 306

7.2.2 Analysis of Relationships of Creep Rate, Stress and Temperature for 304 Stainless Steel 310

7.2.3 The Role of Twin Boundary - Grain Boundary Intersections on Microcracking Behavior of AISI 304 Stainless Steel Deformed in Slow Tension and Creep at 650°C 314

7.2.4 Comparison of the Fatigue Induced Microstructure in Incoloy 800 When Tested in the Bend and Push-Pull Modes 322

7.3 REFERENCES 327

8. UNIVERSITY OF CALIFORNIA AT LOS ANGELES 329

8.1 MICROSTRUCTURE AND HIGH TEMPERATURE DEFORMATION OF Cr-Mo STEELS FOR LMFBR HEAT EXCHANGER 329

8.1.1 Introduction 329

8.1.2 Microstructures of Intermediate Carbon (0.03%) 2 1/4 Cr-1 Mo Alloy 330

8.1.2.1 Long-Term-Tempered at 850°F. 330

8.1.2.2 Long-Term-Tempered at 950°F 333

8.1.2.3 Long-Term-Tempered at 1050°F 335

8.1.3 Microstructure of High Carbon (0.12%) 2 1/4 Cr-1 Mo Alloy 336

8.1.3.1 Long-Term-Tempered at 850 and 950°F . . 336

8.1.3.2 Long-Term-Tempered at 1050°F 340

8.2 Creep Studies in Lightly Cold-Worked Stainless Steels . 340

8.2.1 Introduction. 340

8.2.2 Experimental Details 341

8.2.2.1 Testing Equipment 341

8.2.2.2 Test Material and Specimen Preparation . 342

8.2.3 Results and Discussion 342

8.2.3.1 Steady-State Creep and Rupture Behavior. 342

8.2.3.2 Transient Creep Behavior 343

8.3 The Effects of Carbon on the Elevated Temperature Tensile Properties of Type 316 Stainless Steel 347

8.3.1 Introduction. 347

8.3.2 Experimental Procedures 348

8.3.2.1 Specimen Preparation 348

8.3.2.2 Mechanical Test Procedures 349

8.3.2.3 Carbon Analysis 351

8.3.2.4 Measurement of Volume Fraction of Carbon Case 351

8.3.3 Results 353

8.3.3.1 Mechanical Properties vs. Bulk Carbon Content 353

8.3.3.2 Mechanical Properties vs. Volume Fraction of Case 356

8.3.4 Fracture Model 356

8.3.4.1 Fibered Composite Model 359

8.3.4.2 Fracture Controlling Process 360

8.4 REFERENCES 363

SI CONVERSION TABLES AND FACTORS 365

INDEX 409

SUMMARY

1. AEROJET NUCLEAR COMPANY

Fatigue and creep-fatigue tests at room temperature and 593°C (1100°F) of Type 316 stainless steel with 20% cold work are reported. Aging at 593°C (1100°F) for 1000 hours prior to testing markedly improves the creep-fatigue properties of this material which is believed to be due to fine carbides precipitating out on the cold work bands. Aging or solution annealing also has a slight effect on the zero hold time fatigue properties at the higher strain ranges (>∿0.8%).

Additional tests are reported from efforts to improve the mechanical properties of Inconel Alloy 718 through modifications of conventional thermal treatments. Strain fatigue data are summarized for one heat of material solution-annealed at 1093°C (2000°F), slow cooled at 55.5°C (100°F) per hour to below the aging temperature, then aged four hours at 718°C (1325°F) and variously 16 hours or 25 hours at 621°C (1150°F). For comparison, heat treatment of a portion of the samples was performed in vacuum rather than in air.

2. ARGONNE NATIONAL LABORATORY

Strain-range partitioning is being considered as a possible creep-fatigue life predictive method for Type 304 stainless steel. However, before the inelastic strain range for existing cyclic relaxation data could be partitioned in a completely unambiguous fashion, a basic difficulty in the load-relaxation curves had to be resolved. The difficulty is related to the load change that is observed to accompany an abrupt change in plastic strain rate. This relationship between applied load and plastic strain rate is discussed, and the proper partitioning of the inelastic strain accompanying the load change is considered. In addition, a testing mode is suggested whereby unambiguous strain range versus fatigue life data may be generated.

An evaluation was made of the low-cycle creep fatigue and crack propagation of SMA Type 304/308 stainless steel welded plates (with controlled residual elements made by Combustion Engineering to simulate the seam and girth welds of the FFTF vessel). The creep-fatigue tests were conducted in air at 1100°F in the axially controlled strain mode, fully reversed at a fixed strain rate of 4×10^{-3} sec^{-1}, and at a total strain range ($\Delta\varepsilon_t$) of 0.5-2%. Preliminary data indicate that the fatigue life of the core section of the aged weld metal in the longitudinal direction behaves in a manner similar to that of the corresponding base metal. A slight increase in fatigue life of the weld metal is observed as one moves from the core toward the surface. In the transverse welding direction, no obvious difference is observed in the fatigue life at the core, the surface weld, or the base metal. The crack-propagation tests were conducted with single-edge-notch (SEN) specimens under uniaxial tension loading in sawtooth stress waveform at a temperature of 1100°F, a stress ratio of 0.05, and a frequency of 30 cpm. The crack-growth rate is about the same for

the base metal in the as-received condition ($m = 2.19 \pm 0.08$) as for the aged condition ($m = 2.01 \pm 0.04$). The growth rate for the weld metal in the aged condition ($m = 2.20 \pm 0.13$) is also about the same as for the base metal; only weld metal in the as-welded condition exhibited a lower growth rate ($m = 1.75 \pm 0.04$). This lower growth rate may be a consequence of the locked-in residual stress during welding fabrication.

Tensile tests and preliminary creep-rupture tests were conducted on Types 304, 316, and Ti-modified 316 stainless steel upon exposure to flowing sodium of controlled nonmetallic element concentrations. True stress-true strain behavior of these materials in the annealed and carburized conditions are reported at temperatures of 650 and 700°C. In general, a degradation in the tensile properties of these materials was observed upon carburization in the sodium environment.

3. HANFORD ENGINEERING DEVELOPMENT LABORATORY
(For Period Ending April 30, 1974)

The fatigue-crack propagation behavior of Incoloy 800 (ASME SB-409) in an air environment was studied at temperatures of 75, 600, 800, 1000, and 1200°F. Material in both Grades 1 and 2 was studied, and in general, the crack extension behavior of the two grades was similar over this temperature range. Fatigue-crack growth rates increased with increasing test temperatures, although the increases were not as great as observed in types 304 and 316 stainless steels tested under identical conditions. The improved behavior of Incoloy 800 is thought to be related to its superior oxidation resistance.

The effect of thermal aging on the tensile properties and strain rate sensitivity of type 304 stainless steel has been determined. Specimens were thermally aged at temperatures of 800, 1000 and 1200°F for exposure times of 1000, 3500 and 10,000 hr. Testing was performed at the aging temperatures and at strain rates from 3×10^{-5} to sec^{-1}. Results of these tests indicate thermal aging to 1200°F does not greatly alter the tensile properties or strain rate sensitivity of type 304 stainless steel.

3. HANFORD ENGINEERING DEVELOPMENT LABORATORY
(For Period Ending July 31, 1974)

Creep strains in 20% cold worked type 316 stainless steel at 850°F under a stress of 20,000 psi are small (i.e., a strain of 120×10^{-6} in 1000 hr), but readily measurable using the microwave extensometer. Creep strains measured during an in-reactor test were about seven times larger than those measured in the present laboratory experiment.

Creep rupture testing on three heats of FFTF 28-in.-diam type 316H stainless steel primary piping has been completed. Tests were performed at temperatures of 1050, 1200 and 1400°F and rupture times to 2500 hr. Results of these tests and tensile properties previously reported show the piping material has excellent high temperature strength and ductility.

The fatigue-crack propagation behavior of SA-351, Grade CF8 cast stainless steel was investigated over the temperature range 75–1200°F. Crack growth rates were slightly lower than in plate material tested under similar conditions. No effect of crack orientation was noted for the two orientations studied.

The recovery and recrystallization characteristics of eleven prototypic and production fuel cladding lots of 1400, 1500 and 1600°F have been determined to establish lot-to-lot variations and to provide a basis for possible improvement in cladding recrystallization characteristics. Recrystallization at these temperatures was found to be very sensitive to the heat treatment used just prior to the final 20% reduction in area.

4. NAVAL RESEARCH LABORATORY

The effect of thermal aging at 1100°F (593°C) for 5000 hours on fatigue crack growth in Types 304 and 316 stainless steel was investigated at 1100°F. For the solution-annealed material, thermal aging produced a slight increase in fatigue crack growth resistance compared to that of unaged material tested at the same temperature. The cold-worked materials, however, exhibited a decrease in fatigue crack growth resistance after thermal aging. No substantial effect of thermal aging was observed for fatigue crack growth in Type 308 weld metal.

The toughness of Type 316 stainless steel forging and weld metal is being evaluated with the J-Integral technique. Notched, three-point bend specimens of 0.2 in. (5.1 mm) and 0.4 in. (10.2 mm) thickness were loaded statically at 500°F (260°C) and the J integral was calculated using an approximate equation. The results are expressed in terms of an R curve which was extrapolated to yield the critical J_{Ic} at crack initiation. The J_{Ic} value for the weld metal is significantly below that of the forging. Even with its reduced toughness, the weld metal is expected to exhibit elastic plastic behavior in structural applications. Results from forging specimens of 0.2 in. and 0.4 in. thickness suggest a thickness dependence of J_{Ic} when the thickness is insufficient to meet a proposed minimum requirement of $25J/\sigma_{flow}$ based on results of ferritic steels.

5. OAK RIDGE NATIONAL LABORATORY

Elevated-temperature creep and tensile testing of the ORNL reference heat of type 304 stainless steel is continuing. Minimum creep rate and rupture data are reported from tests that reached over 14,000 hr in duration. Values of the so-called "stable" creep elongation, one of the possible strain limits criteria, were calculated for the tests run to date, and it was generally shown to be a function of both temperature and rupture time. Plans for interrupted creep tests followed by tensile tests are given and initial test data are reported.

Ten long-term (50,000-hr) creep tests are in progress on several different heats of type 304 stainless steel. Two of the creep tests have reached test times of 23,000 hr.

Aging studies to date on type 304 stainless steel generally indicate a small decrease in the short-term tensile ductility. Changes in short-term properties resulting from aging depend upon material composition and time at temperature. The influence of aging time on creep properties (i.e., minimum creep rate and rupture time) is mixed in that for the several heats studied to date increases, decreases, and little change or stability of these properties have been found.

Aging similarly influenced the tensile and creep behavior of type 316 stainless steel. Both increases and decreases in the yield and ultimate tensile strength occurred, while the ductility generally decreased. However, for material deformed by creep both the uniform and total elongation increased, indicating the importance of strain rate.

The effects of carbon, nitrogen, and grain size on the short-term mechanical properties of types 304 and 316 stainless steel obtained from this program are compared with predictions from relations given in the literature. Differences between calculated and measured values are explained.

Progress in the procurement of various product forms of the type 316 stainless steel reference heat is reported. Methods of maintaining traceability of various product forms to specific ingots and their pouring sequence are explained. Delivery of all plate, sheet, and bar items should be complete by mid-September.

The ORNL computerized data management system for data acquisition, storage, and calculation is described, and both examples of current capabilities and plans for future development are given.

Plans are discussed for determining the elastic constants, both static and dynamic, of a number of structural materials. Test variables include temperature, heat-to-heat variations, heat treatment, prior cyclic straining, and anisotropy.

Analytical studies are under way to define optimum specimen design for mechanical properties tests and to compare experimental behavior with analytical behavior where appropriate. Highlights of current results from analytical studies using the hourglass-shaped fatigue specimen are presented. This work showed that differences would be expected between the uniaxial stress-strain curves of cylindrical and hourglass specimens.

Design creep data for type 308 stainless steel welds with controlled residual elements (CRE) are presented graphically. Times to important levels of strain (0.5, 1, and 2%) and to various characteristic events during creep, including tertiary creep, are presented, and some comparisons are made with the properties of type 304 stainless steel base metal. Creep rate correlations and data that are useful for strain limit evaluation are presented. As support for the evaluation of whole weldment cross-

section behavior, the tensile property variation is the "heat-affected zone" of these welds has been explored. Significant increases in the yield strength occur in this region.

Correlation efforts are actively under way to determine the best physical and mechanical properties from available data, and their time and temperature dependences, for 2 1/4 Cr-1 Mo steel. A number of correlations and their respective tolerance limits have been completed and are currently undergoing review by the technical community before being placed in the *Nuclear Systems Materials Handbook*. These include time to rupture, ultimate tensile strength, and yield strength.

Uniaxial strain-controlled fatigue data are reported for 2 1/4 Cr-1 Mo steel. Results from cyclic tests with and without tensile or compressive hold times are reported. Low-cycle strain-controlled fatigue data obtained in this program are compared with high-cycle load-controlled fatigue data reported in the literature. The material underwent both cyclic hardening and softening, depending upon the temperature and strain range. Compressive hold times were more damaging to cyclic lives than tensile hold times in the tests conducted to date. Plans and design details for elevated-temperature biaxial fatigue tests are briefly reported.

Results of mechanical property (i.e., tensile and creep) determinations from tests conducted on 2 1/4 Cr-1 Mo steel are reported. Tensile curves are given over the range 25 to 593°C for strain rates of 0.004 to 0.4/min. Creep curves are given for 454, 510, and 565°C. Plans for heat-to-heat variation studies are also given.

The effect of sodium exposure on the mechanical properties of 2 1/4 Cr-1 Mo steel is also of interest since both decarburization and aging reactions are possible. Specifically, the cyclic creep behavior of decarburized tubes is under investigation. Photomicrographs of material as annealed, aged in helium, and decarburized in sodium are compared.

Creep-rupture properties of type 304 stainless steel forging material weld-overlaid with type 308 are reported for the region adjacent to the fusion line.

Current results from exploratory deformation studies being conducted on the ORNL reference heat of type 304 stainless steel are reported. Results from tests performed over large deformation ranges at various temperatures and strain rates are compared with predictions based on several flow models. Variable strain rate tests were also conducted, and preliminary results indicate that damage at one strain rate could not be summed linearly and used to estimate retained ductility at another rate. The influence of temperature and cyclic and monotonic prestraining on the monotonic creep behavior of the reference heat is being investigated. Results from cyclic creep tests and short-term single- and multiple-temperature relaxation tests are also reported. Monotonic creep behavior interrupted by periods of short-term cycling is also being investigated, and results from these tests are reported.

Progress on uniaxial and multiaxial creep rupture tests of type 304 stainless steel is reported. In uniaxial tests, strain was not significantly localized before tertiary creep. Variations in rupture life in constant-load and step-load tests are attributed to grain size variations.

Several alloys (i.e., 2 1/4 Cr-1 Mo and 9 Cr-1 Mo steels, Hastelloy X, and Hastelloy S) have been obtained for use in our HTGR mechanical property tests. Procurement of other materials (e.g., Incoloy 800) is in progress. Mechanical testing to date has been confined to elevated-temperature tensile tests of the Cr-Mo steels. Matrices for FY 1975 creep-rupture and subcritical crack growth tests are being prepared. Our environmental testing facilities are essentially complete, including the chromatographic equipment. A bottled environmental supply exhibited good stability during a 600-hr bleed-down test.

6. WESTINGHOUSE ADVANCED REACTORS DIVISION

Basic specimen creep testing of plate type specimens of the reference ORNL type 304 stainless steel heat (9T2796) was continued and the planned tests for uniaxial, uniform gage specimens were completed at 1100°F. Tubular creep testing of the same heat of material was continued and one uniaxial and one multiaxial tubular creep test were completed at 1100°F. Three multiaxial tubular creep tests were initiated during the present report period. The test matrix and the load specification for the multiaxial tubular creep tests of type 304 stainless steel were finalized. A tentative test matrix for type 316 stainless steel was prepared. Test equipment and instrumentation were modified so that all four tubular creep test machines have the same high quality furnace and instrumentation. Progress was continued in establishing the procedure to be used to reduce the test data to obtain a mathematical model for creep behavior.

7. UNIVERSITY OF CINCINNATI

Characterization of creep and tensile substructure of type 304 stainless steel reference heat 9T2796 was initiated. Work has been completed on three specimens tensile tested at 650°C at various strain rates. The fast strain rates have been shown to produce dislocation cell structure whereas slow strain rate produce a subgrain structure.

Minimum creep rate for the reference heat was plotted as a function of modulated compensated true stress. The stress exponent and activation energy have been shown to be 7 ± 1 and 85 ± 5 kcal/mole.

The role of twin boundary-grain boundary intersection on microcracking behavior of type 304 stainless steel deformed in slow tension and creep at 650°C have been investigated. The number of cracks associated with twin boundary-grain boundary intersection have been shown to increase with decreasing strain rate.

Microstructure has been compared for Incoloy 800 specimens tested in push-pull and bend fatigue. It has been suggested that the stress levels in the region of the surface of bend fatigue specimens were approximately 14% higher than that along the diameter of the push-pull specimens.

8. UNIVERSITY OF CALIFORNIA AT LOS ANGELES

This report describes the progress made on three separate projects. The first is a study of microstructure-mechanical property relationships in ferritic Cr-Mo steels containing various carbon contents. The contribution in this project consists of a description of the microstructure of two alloys, containing 0.03 and 0.12%C, after long-term tempering of the microstructure resulting from a standard initial treatment of 1300°F for 1 hr. Tempering was done at 850 and 950°F for times ranging up to 19 months.

The second project is concerned with the effects of small amounts of prior cold work (up to 10%) on the creep behavior of types 316 and 304 stainless steel at temperatures from 1100 to 1400°F. Initial results suggest that at high stresses (19 and 25 ksi) and temperatures (1400°F), the rupture life, steady-state creep rate and ductility are not strongly affected by prior cold work. However, the transient creep behavior is influenced. Preliminary attempts to characterize the transient creep behavior are described.

The third project is a study of elevated temperature fracture of carburized type 316 stainless steel. The yield strength, ultimate tensile strength, true fracture strength and tensile ductility of gas-carburized sheet samples were determined at 1400°F and correlated with the volume fraction of the carbon case, since the carbon is not distributed uniformly throughout the sample but instead promotes a carbide layer, the thickness of which varies with the carburizing time. A continuous fibered composite model was found to describe the data quite accurately, as described in this report.

1. AEROJET NUCLEAR COMPANY

W. C. Francis

1.1 INTRODUCTION

Aerojet Nuclear Company is conducting mechanical properties investigations under two programs sponsored by the AEC Division of Reactor Research and Development. Program 06031, Fatigue Tests on Cladding and Structural Materials, involves experimental fatigue tests on stainless steel Types 304 and 316 as well as Type 304/308 weldments. These tests are intended to determine the influence of irradiation, cold work, heat treatment, heat-to-heat property variations, and temperature on fatigue behavior. Irradiated, thermal control, as-received, and annealed specimens are being tested at 427 to 700°C (800 to 1292°F). Current work on irradiated material is reported in the Semi-Annual Progress Report for the Irradiation Effects on Reactor Structural Materials Program compiled at HEDL. Unirradiated work currently involves low cycle fatigue and creep-fatigue tests of Type 316 stainless steel with 20% cold work and is reported in this document.

Program 06084, Inconel 718 Mechanical Property Program, has as its primary objective the acquisition of the necessary mechanical property data to permit safe, efficient use of this material in LMFBR service. The specific immediate application is for selected structural components of the Clinch River Breeder Reactor Project. Other reactor service applications which require high levels of mechanical properties at temperatures up to 649°C (1200°F) are also expected to make use of this material.

What has been considered standard heat treatments for Inconel 718 has not consistently yielded acceptable ductility values for the welded material. Current work involves scoping tests on material subjected to modified thermal treatments in an effort to optimize the heat treatment that will yield the best mechanical properties of both base and weld metal.

1.2 FATIGUE TESTS ON CLADDING AND STRUCTURAL MATERIALS - G. E. Korth, and M. D. Harper

1.2.1 Fatigue and Creep-Fatigue of Type 316 Stainless Steel with 20% Cold Work

Hourglass fatigue specimens with a minimum diameter of 5.08 mm

(0.200 inch) were machined from a 12.7 mm (0.50 inch) diameter rod of Type 316 stainless steel with 20% nominal cold work. Some of the specimens were then aged in an argon environment for 1000 hours at 593°C (1100°F) and another batch was vacuum annealed at 1075°C (1967°F) for 0.5 hour and then helium quenched. All three conditions were tested in low cycle fatigue at room temperature and 593°C (1100°F) with tensile hold times incorporated into some of the elevated temperature tests. Tests were conducted in air using induction heating. Testing was performed using strain control with a fully reversed ramp waveform and a strain rate of $4 \times 10^{-3} s^{-1}$.

Results of the tests are tabulated in Table 1.1 where:

$\Delta \varepsilon_t$ = total strain range

$\Delta \varepsilon_p$ = plastic strain range at ∿1/2 cycle life

$\Delta \sigma_{max}$ = maximum stress range

$\Delta \sigma$ = stress range

$\sigma_{t,max}$ = maximum tensile stress amplitude

$\sigma_{t,min}$ = tensile stress amplitude at the end of a hold time

N_o = number of cycles to the point where a marked decrease in stress amplitude is noted indicating crack initiation

N_5 = number of cycles to the point where a 5 per cent decrease in stress amplitude occurs

N_f = number of cycles to failure

t_f = total time to fail

All the zero hold time data at room temperature and 593°C (1100°F) is plotted in Figure 1.1 and the hold time data in Figure 1.2. At 593°C (1100°F) and zero hold time the cold worked material had a slightly lower fatigue life at the higher strain ranges (>∿.8%) when compared to the annealed stainless. The cold worked plus aged material had the longest cyclic life. At lower strain ranges (<∿0.6%) the data of all three conditions merges together and no one type appears to be superior. At room temperature no significant difference is noted between the various conditions. At both test temperatures cyclic softening was observed with the cold worked material. The maximum stress

Table 1.1 Strain Fatigue Behavior of 316 Stainless Steel 20% Cold Worked, HT. 81583, Tested at 22 & 593°C

Specimen No.	Material Condition[a]	Hold Time, h	$\Delta\varepsilon_t$, %	$\Delta\varepsilon_p$, %	$\Delta\sigma$ max MPA	$\Delta\sigma$ max ksi	Cycle of $\Delta\sigma$ max	$\Delta\sigma$ @ $N_f/2$ MPA	$\Delta\sigma$ @ $N_f/2$ ksi	σ_t max @ $N_f/2$ MPA	σ_t max @ $N_f/2$ ksi	σ_t min @ $N_f/2$ MPA	σ_t min @ $N_f/2$ ksi	N_5	N_o	N_f	t_f, h	Test °C Temp
E2-53	As Rec	0	2.04	1.42	1312.1	190.3	1	1070.1	155.2	535.0	77.6	-----	-----	1,826	1,818	1,832	4.92	22
E2-5	Aged	0	1.98	1.32	1196.9	173.6	6	1071.4	155.4	529.5	76.8	-----	-----	2,157	2,116	2,257	6.07	22
E2-37	Ann	0	1.98	1.48	966.0	140.1	2432	865.3	125.5	428.2	62.1	-----	-----	2,458	2,448	2,494	6.71	22
E2-36	Ann	0	1.10	0.74	717.7	104.1	~9000	654.3	94.9	324.7	47.1	-----	-----	9,427	9,414	9,438	14.20	22
E2-54	As Rec	0	1.00	0.39	1170.0	169.7	3	961.8	139.5	452.3	65.6	-----	-----	13,083	13,034	13,261	18.53	22
E2-26	Aged	0	0.88	0.39	1017.0	147.5	1	847.4	122.9	413.0	59.9	-----	-----	23,547	23,537	23,621	30.47	22
E2-25	Aged	0	0.60	0.16	911.2	132.2	1	795.0	115.3	388.6	56.4	-----	-----	------	------	55,060	44.42	22
E2-39	Ann	0	0.55	0.30	495.2	71.8	127	482.0	69.9	237.1	34.4	-----	-----	61,909	61,627	62,458	46.38	22
E2-55	As Rec	0	0.51	0.05	852.9	123.7	1	804.6	116.7	415.1	60.2	-----	-----	------	------	120,179	80.13	22
E2-49	As Rec	0	2.00	1.52	986.6	143.1	3	892.2	129.4	430.2	62.4	-----	-----	407	372	518	1.38	593
E2-23	Aged	0	2.00	1.53	852.9	123.7	3	773.6	112.2	370.2	53.7	-----	-----	674	656	726	1.95	593
E2-43	Ann	0	2.05	1.50	875.6	127.0	110	839.1	121.7	406.1	58.9	-----	-----	574	472	639	1.72	593
E2-31	Aged	0	1.88	1.47	837.7	121.5	1	760.5	110.3	370.2	53.7	-----	-----	740	620	873	2.15	593
E2-48	As Rec	0	1.01	0.56	867.4	125.8	1	812.9	117.9	371.6	53.9	-----	-----	1,320	1,217	1,517	2.09	593
E2-64	As Rec	0	1.01	0.56	861.8	125.0	5	743.9	107.9	356.5	51.7	-----	-----	2,069	2,069	2,240	3.06	593
E2-30	Aged	0	1.00	0.53	755.7	109.6	5	667.4	96.8	329.6	47.8	-----	-----	2,713	2,692	2,807	3.93	593
E2-50	Ann	0	1.00	0.62	604.7	87.7	138	604.7	87.7	300.6	43.6	-----	-----	2,211	2,195	2,308	3.17	593
E2-42	Ann	0	0.90	0.51	556.4	80.7	200	580.5	84.2	285.4	41.4	-----	-----	3,176	3,092	3,512	4.15	593
E2-32	Aged	0	0.81	0.44	695.7	100.9	1	585.4	84.9	276.5	40.1	-----	-----	5,124	5,110	5,432	6.01	593
E2-38	Ann	0	0.62	0.23	595.0	86.3	300	559.8	81.2	276.5	40.1	-----	-----	7,924	7,739	9,092	7.42	593
E2-52	As Rec	0	0.52	0.15	708.1	102.7	1	645.3	93.6	293.7	42.6	-----	-----	12,613	12,226	14,065	9.59	593
E2-24	Aged	0	0.50	0.16	639.1	92.7	1	551.6	80.0	266.8	38.7	-----	-----	28,494	28,326	29,376	20.04	593
E2-44	Ann	0	0.51	0.23	450.9	65.4	436	437.1	63.4	201.3	29.2	-----	-----	10,266	10,156	10,780	7.35	593
E2-33	Aged	0	0.46	0.13	624.0	90.5	1	555.7	80.6	235.1	34.1	-----	-----	15,555	15,116	16,077	9.73	593
E2-47	Ann	0	0.42	0.19	355.8	51.6	429	355.8	51.6	177.9	25.8	-----	-----	31,971	31,724	32,969	17.96	593
E2-56	As Rec	0	0.41	0.07	677.1	98.2	1	617.1	89.5	274.4	39.8	-----	-----	------	------	45,441	24.76	593
E2-29	Aged	0	0.38	0.06	576.4	83.6	1	499.9	72.5	246.8	35.8	-----	-----	------	------	184,500[b]	94.91[b]	593
E2-66	As Rec	0.01	2.00	1.58	949.4	137.7	2	814.3	118.1	394.4	57.2	340.6	49.4	491	475	514	6.64	593
E2-35	Aged	0.01	2.00	1.60	822.5	119.3	2	738.4	107.1	353.7	51.3	315.1	45.7	705	691	761	9.98	593
E2-46	Ann	0.01	2.00	1.57	784.6	113.8	78	773.6	112.2	375.8	54.5	353.7	51.3	580	546	596	7.72	593
E2-59	As Rec	0.01	1.00	0.55	857.7	124.4	1	732.2	106.2	351.6	51.0	327.5	47.5	1,908	1,881	2,016	22.02	593
E2-58	As Rec	0.01	1.00	0.56	770.1	111.7	1	676.4	98.1	327.5	47.5	308.9	44.8	------	------	2,021	22.07	593
E2-22	Aged	0.01	1.00	0.62	733.6	109.3	1	628.8	91.2	295.8	42.9	289.6	42.0	2,670	2,650	2,912	31.94	593
E2-45	Ann	0.01	1.01	0.65	621.2	90.1	147	611.6	88.7	297.2	43.1	270.3	39.2	1,714	1,699	1,821	20.00	593
E2-63	As Rec	0.01	0.50	0.12	698.4	101.3	1	624.0	90.5	288.9	41.9	281.3	40.8	------	------	9,000[b]	99.98[b]	593
E2-28	Aged	0.01	0.51	0.14	610.2	88.5	1	526.1	76.3	233.7	33.9	220.6	32.0	------	------	20,863[b]	220.93[b]	593
E2-67	As Rec	0.1	2.00	1.52	954.2	138.4	3	799.8	116.0	386.1	56.0	307.5	44.6	371	354	384	39.52	593
E2-21	Aged	0.1	1.98	1.64	828.1	120.1	2	707.4	102.6	331.6	48.1	287.5	41.7	748	738	758	77.22	593
E2-41	Ann	0.1	2.00	1.60	746.0	108.2	44	733.6	106.4	349.6	50.7	304.1	44.1	318	307	327	33.52	593
E2-57	As Rec	0.1	1.00	0.62	803.9	116.6	1	662.6	96.1	304.1	44.1	252.3	36.6	917	915	1,017	103.29	593
E2-34	Aged	0.1	1.00	0.65	723.3	104.9	1	616.4	89.4	291.6	42.3	256.5	37.2	2,674	2,515	2,882	291.76	593
E2-51	Ann	0.1	1.00	0.65	625.4	90.7	347	823.3	90.4	296.6	43.0	296.6	39.1	974	926	1,136	114.82	593
E2-65	As Rec	0.5	2.00	1.63	926.0	134.3	2	762.6	110.6	370.2	53.7	276.5	40.1	246	233	275	136.31	593
E2-27	Aged	0.5	2.01	1.52	839.8	121.8	2	728.8	105.7	354.4	51.4	259.9	37.7	537	504	566	280.65	593
E2-40	Ann	0.5	2.00	1.64	751.5	109.0	17	727.4	105.5	359.2	52.1	271.6	39.4	173	148	197	97.49	593
E2-60	As Rec	0.5	1.03	0.62	823.2	119.4	1	622.6	90.3	292.3	42.4	224.8	32.6	537	499	587	291.21	593

[a]As Rec = as machined condition, 20% CW
Aged = 20% CW plus 1000 h at 593°C
Ann = solution annealed at 1075°C for 1/2 h and helium quench
[b]Did not fail

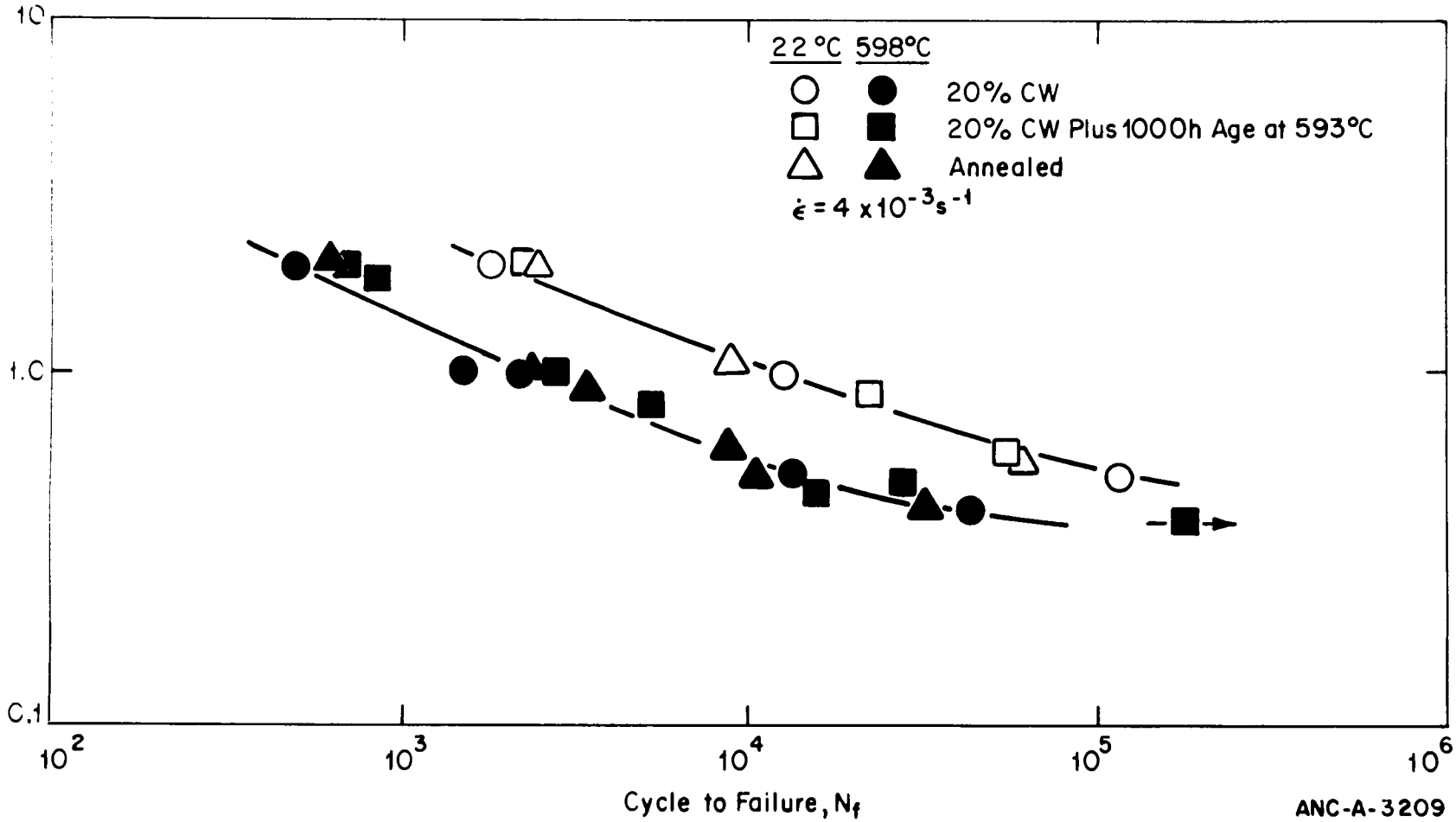

Figure 1.1 Strain Fatigue Behavior Of Type 316 Stainless Steel at 22°C and 593°C In The 20% CW, Plus Aged, And Annealed Conditions

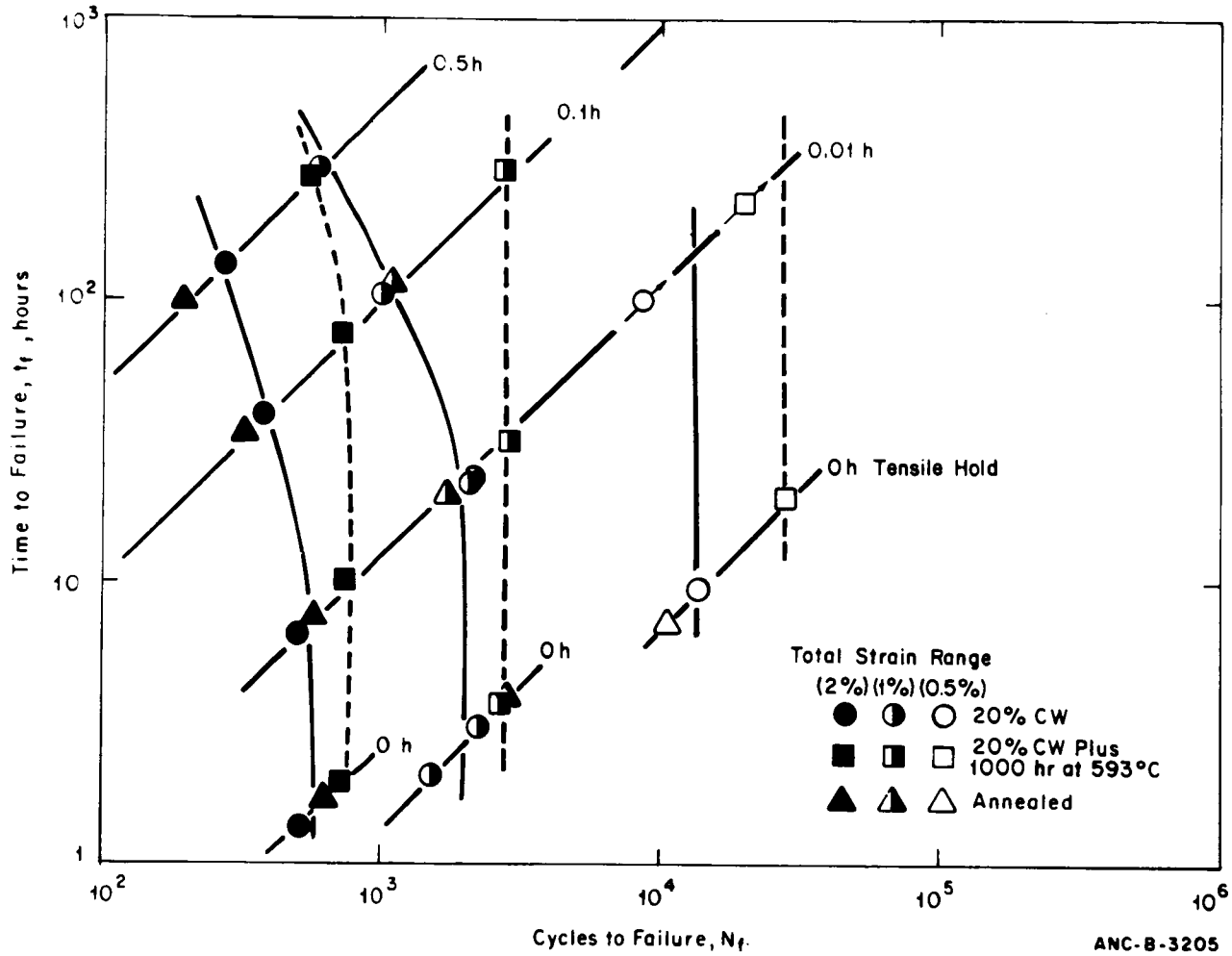

Figure 1.2 Cycles-to-Fail Vs Time-to-Fail Plot Of Type 316 Stainless Steel Tested at 593°C (1100°F) With Tensile Hold Periods

and corresponding cycle are listed in the tabulated data as well as half-cycle life values to demonstrate the softening observed. The annealed material showed the classical cyclic hardening.

When hold times were included at the peak tensile strain of each fatigue cycle a rather marked increase in creep-fatigue resistance was seen for the aged material when compared to the annealed and the as-cold worked stainless steel. All conditions showed no hold time effect for 0.01 hour dwell periods; but as hold times were increased a steady decrease in cycle life was observed for the annealed and cold worked material. The cold worked plus aged stainless, however, showed no effect of hold times except one test at 2% strain range and 0.5 hour hold. With tests run to date the annealed material shows a tendency towards more creep-fatigue damage than the as-cold worked, especially at the highest strain range and longer hold times.

Optical and electron metallography was performed on all three conditions and is shown in Figures 1.3 through 1.7. The aging treatment precipitated carbides on the cold work lines as can be seen in Figures 1.3 and 1.4. Closer examination with TEM showed the carbides to be quite small in size (5 to 50 nm) and electron diffraction showed them to be of the $M_{23}C_6$ type. It was undoubtedly the fine carbides that gave the aged material the better creep-fatigue resistance. A similar phenomenon of fine carbides and superior creep-fatigue properties has also been seen in Type 304 stainless steel[1]. All the specimens examined by TEM were from 1% strain range with 0.1 hour hold time tests so that the test section of the specimens was at 593°C (1100°F) from 100 to 300 hours. Foils taken from the gage section did show the fine carbides were starting to precipitate out in the as-cold worked and annealed material due to the long time at test temperature. However carbides formed during test were smaller and less dense than those from the previously aged material.

---

[1]C. R. Brinkman and G. E. Korth, J. Nucl. Mats 48 (1973) 293-306.

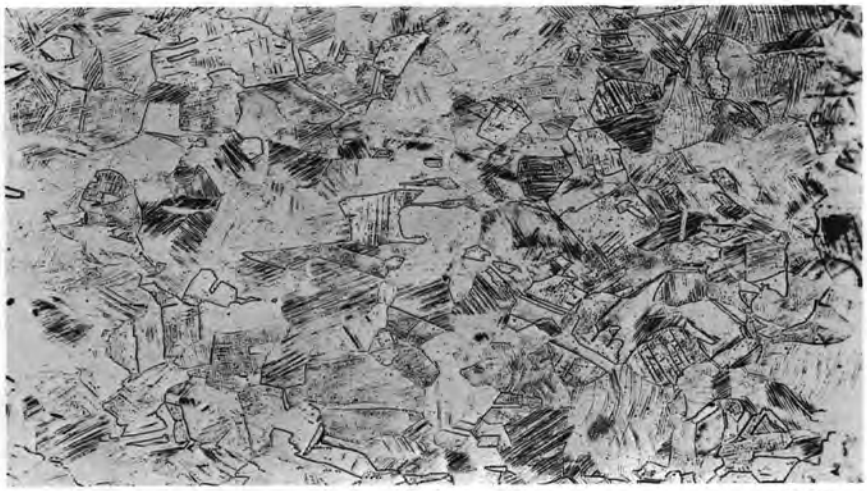

(a) 100X

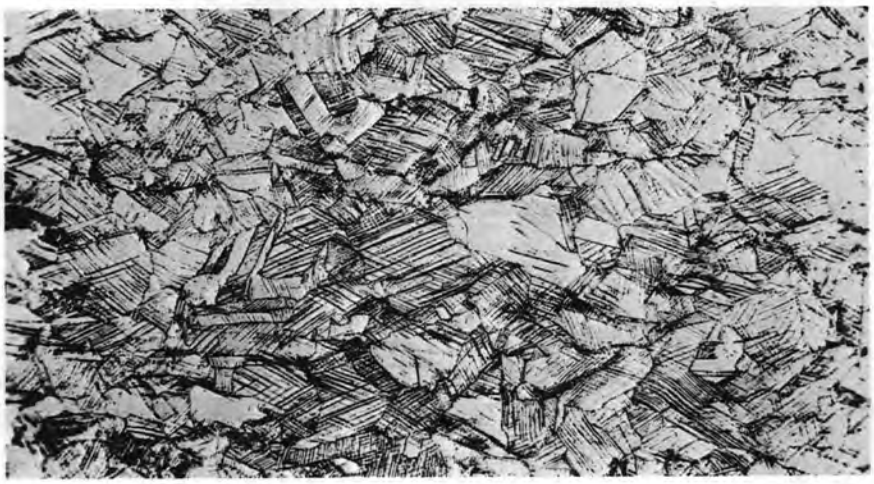

(b) 100X

(c) 100X

Fig. 1.3. Microstructure of Type 316 stainless steel in the (a) 20% CW condition, (b) 20% CW + 1000 h age at 593°C (1100°F), and (c) solution annealed (oxalic acid etch).

(a) 1500X

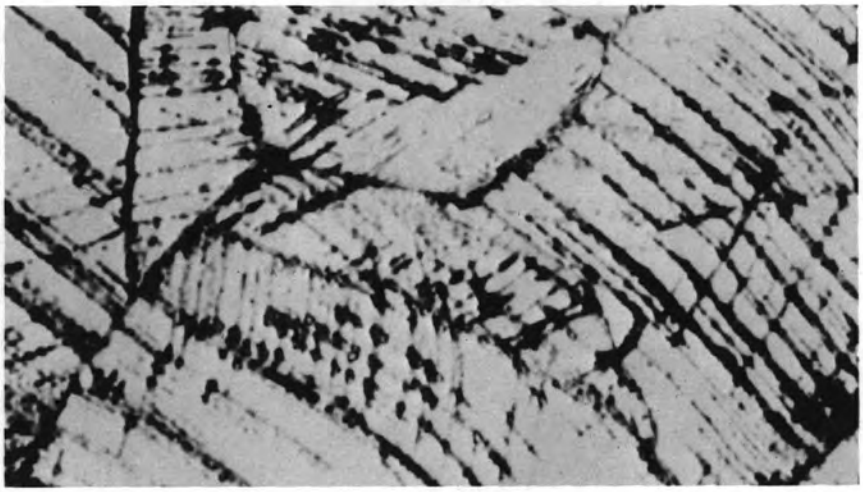

(b) 1500X

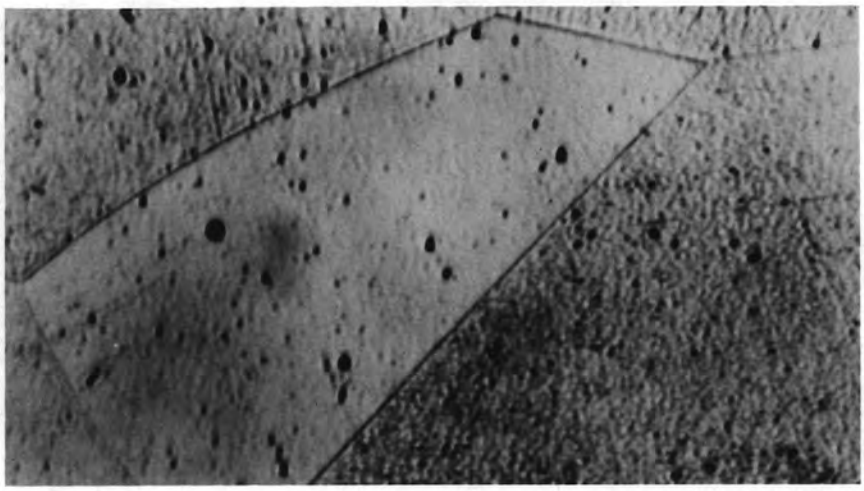

(c) 1500X

Fig. 1.4. Microstructure of Type 316 stainless steel in the (a) 20% CW condition, (b) 20% CW + 1000 h age at 593°C (1100°F), and (c) solution annealed (oxalic acid etch).

7-74-487 (a) 10,000X

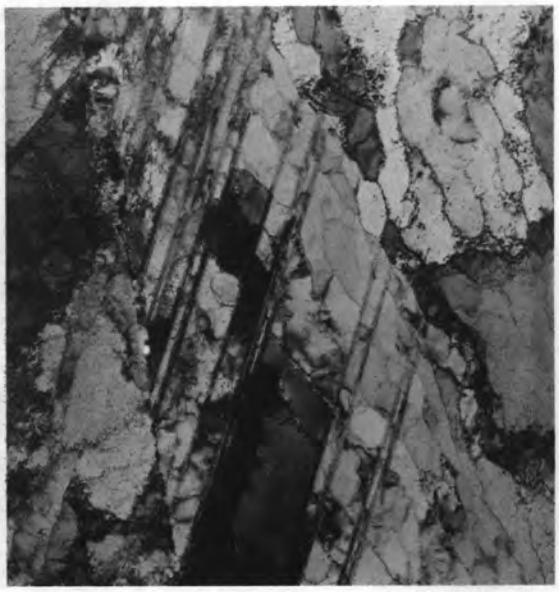

7-74-485 (b) 10,000X

8-74-514 (c) 30,000X

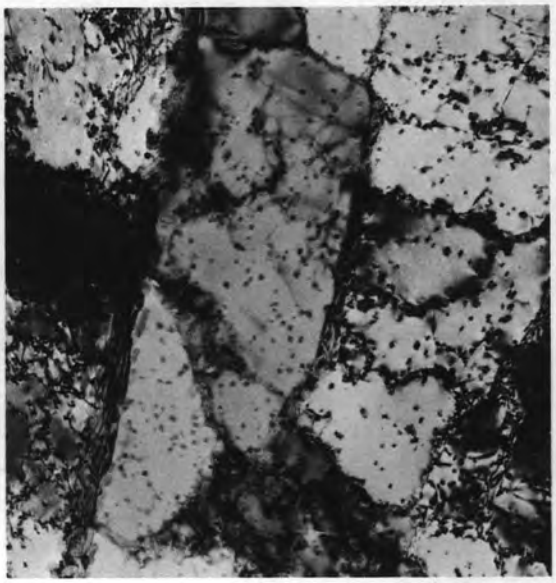

8-74-518 (d) 30,000X

Fig. 1.5. Transmission electron micrographs of Type 316 stainless steel fatigue specimen with 20% CW (E2-57) showing cold work, dislocation, and precipitate interaction. (a) shoulder section, (b) (c), and (d) gage section.

7-74-496 (a) 10,000X

7-74-503 (b) 60,000X

7-74-492 (c) 10,000X

8-74-509 (d) 30,000X

Fig. 1.6. Transmission electron micrographs of Type 316 stainless steel fatigue specimen with 20% CW + 1000 h age at 593°C (1100°F) prior to test (E2-34). (a), (b) shoulder section, (c), (d) gage section.

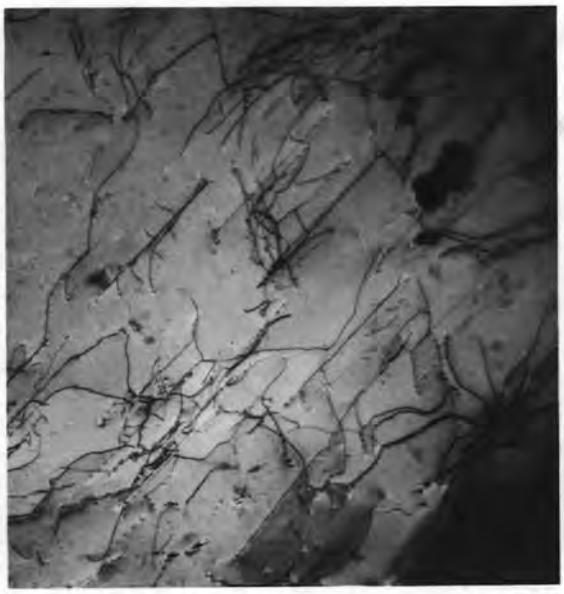

7-74-469 (a) 12,000X

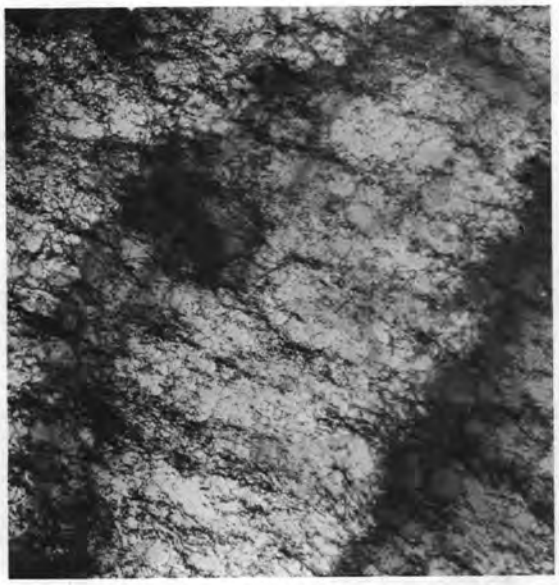

7-74-482 (b) 10,000X

8-74-511 (c) 15,000X

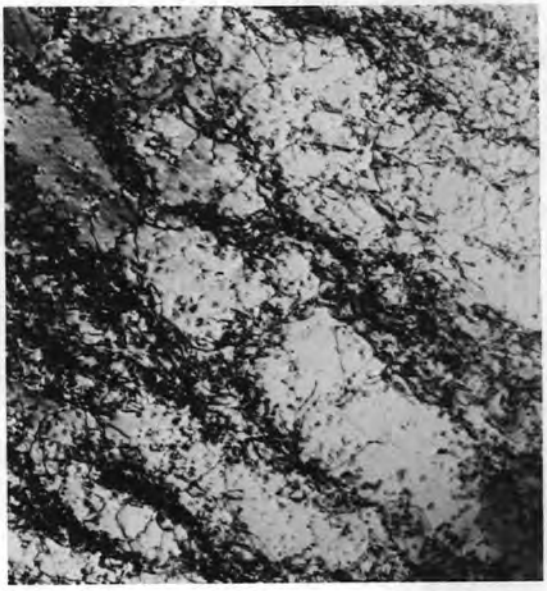

8-74-513 (d) 30,000X

Fig. 1.7. Transmission electron micrographs of Type 316 stainless steel fatigue specimen in the annealed condition (E2-51). (a) shoulder section, (b) (c) and (d) gage section.

1.3 INCONEL 718 MECHANICAL PROPERTY PROGRAM - D. D. Keiser, W. G. Reuter, G. R. Smolik, H. L. Brown

1.3.1 Development and Optimization of a Modified Heat Treatment for Inconel 718

In the program to improve the mechanical properties of Inconel 718 via modified heat treatment, activity continues on elevated temperature tensile testing for strain-age-cracking susceptibility and on elevated temperature stress-rupture testing. The data reported here represent only the completed and evaluated test efforts. It must be emphasized, however, that they are preliminary and may not adequately describe the general behavior of Inconel 718.

Table 1.2 presents data from strain-controlled, fully-reversed fatigue tests at 538°C (1000°F) for heat 2180-2-9251. In Figure 1.8, the data points are compared with best-fit curves[2] for fatigue data from similar material receiving either of the commonly-used heat treatments based on 940°C (1725°F) solution anneal plus age or 1038°C (1900°F) solution-anneal plus age. For total strains below 4.2% the data agree well with the curve for 1038°C (1900°F) anneal plus age. Above 4.2% strain, both scatter and departure from the best-fit curve are evident. No difference is seen in the fatigue behavior of these samples for either the longer aging cycle or vacuum versus air heat-treatment environment.

---

[2]C. R. Brinkman and G. E. Korth, "Strain Fatigue and Tensile Behavior of Inconel 718 from Room Temperature to 650°C," ANCR-1125 (1973).

Table 1.2. Strain Fatigue Behavior of Inconel 718 with Modified Heat Treatments

Specimen No.	Modified Heat Treat	Total Strain Range, $\Delta\varepsilon_t$,%	Plastic Strain Range at $N_f/2$, $\Delta\varepsilon_p$,%	Elastic Strain Range at $N_f/2$, $\Delta\varepsilon_e$, %	Stress Range, $\Delta\sigma$ at $N_f/2$ MPA	Stress Range, $\Delta\sigma$ at $N_f/2$ ksi	Stress Amplitude σ_t at $N_f/2$ MPA	Stress Amplitude σ_t at $N_f/2$ ksi	Cycles to Crack Initation N_o	Cycles for 5% Tensile Load Dec. N_5	Cycles to Failure, N_f	Strain Rate, $\dot{\varepsilon}$,s^{-1}	Test Temp °C	Heat No.
1-1-5-14	b	5.61	3.89	1.72	2533.9	367.5	1203.1	174.5	47	47	48	$4x10^{-3}$	538	1[e]
1-1-3-38	b	5.25	3.75	1.50	2591.1	375.8	1238.3	179.6	46	48	48	$4x10^{-3}$	538	1
1-1-4-40	a	5.19	3.50	1.69	2552.5	370.2	1201.1	174.2	37	37	38	$4x10^{-3}$	538	1
1-1-4-49	b	4.05	2.40	1.65	2340.8	339.5	1132.8	164.3	108	132	138	$4x10^{-3}$	538	1
1-1-5-11	c	3.53	1.97	1.56	2231.2	323.6	1071.4	155.4	195	197	197	$4x10^{-3}$	538	1
1-1-5-9	a	2.98	1.54	1.44	2132.6	309.3	1042.5	151.2	304	319	324	$4x10^{-3}$	538	1
1-1-5-12	c	2.02	0.72	1.30	2040.2	295.9	990.1	143.6	616	631	635	$4x10^{-3}$	538	1
1-1-4-39	a	2.00	0.69	1.31	1967.0	286.6	952.2	138.1	743	751	758	$4x10^{-3}$	538	1
1-1-4-38	a	1.00	0.08	0.92	1683.7	244.2	809.4	117.4	6,427	6,460	6,558	$4x10^{-3}$	538	1
1-1-4-37	a	0.91	0.03	0.88	1477.5	214.3	702.6	101.9	11,772	11,817	12,045	$4x10^{-3}$	538	1
1-1-5-10	c	0.75	0.01	0.74	1251.4	181.5	616.4	89.4	28,156	28,290	28,392	$4x10^{-3}$	538	1
1-1-3-20	b	0.70	0	0.70	1134.9	164.6	559.9	81.2	36,264	36,684	37,089	$4x10^{-3}$	538	1
1-1-4-47	b	0.65	0	0.65	1036.4	150.3	476.4	69.1	d	d	139,895	d	538	1

[a]1093°C(2000°F) Solution anneal, cool at 55.5°C(100°F) per hour to below aging temperature, duplex age 718°C(1325°F) four hours and 621°C(1150°F) sixteen hours
[b]Same as (a) except all heat treating performed in vacuum
[c]Same as (a) except 621°C(1150°F) age was for 25 hours
[d]Run in strain control to 83,300 cycles at $\dot{\varepsilon} = 4x10^{-3}s^{-1}$ then run in load control at 1 Hz to failure
[e]ANC Heat No. 1 is Cabot 2180-2-9251

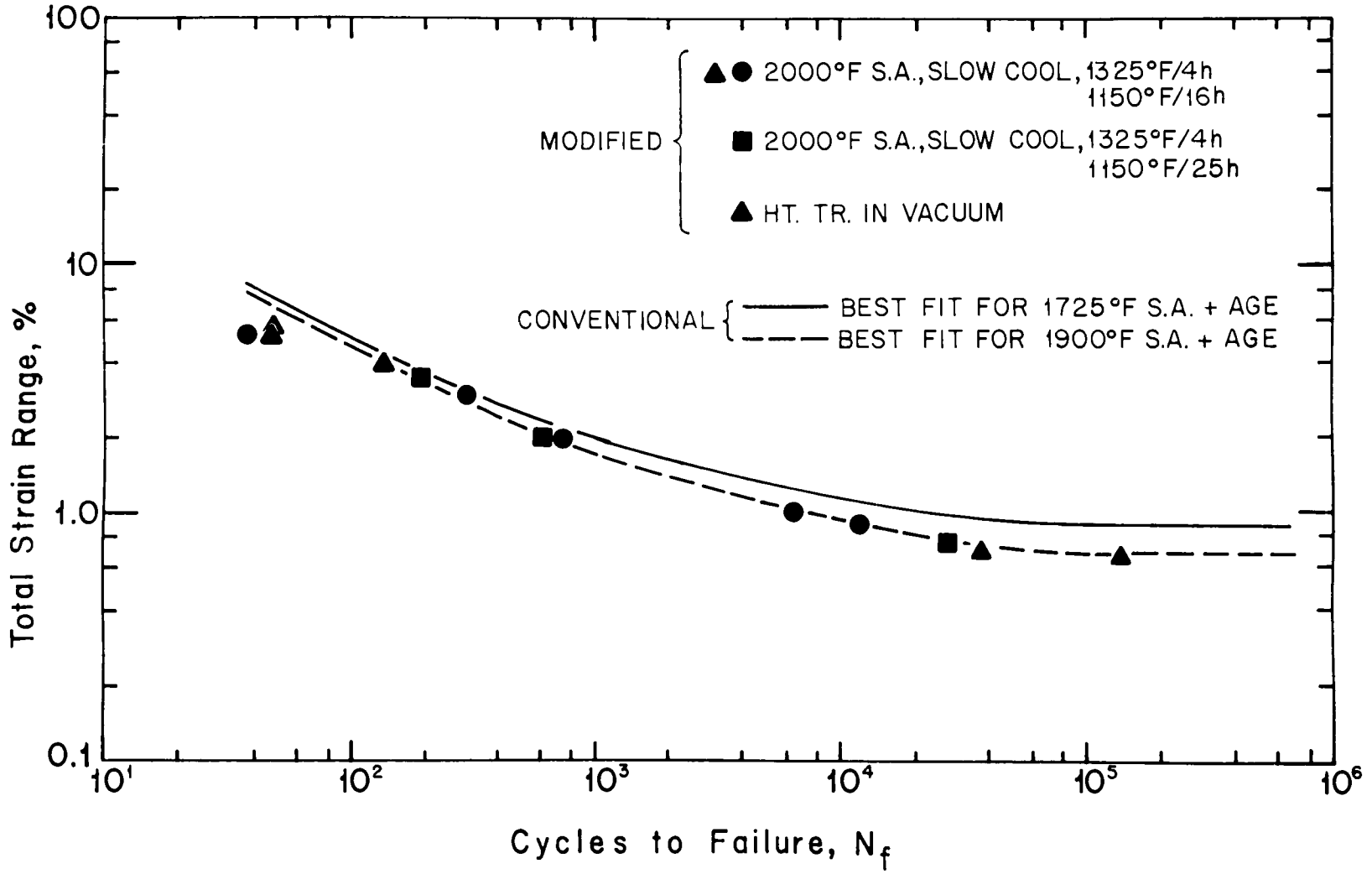

Figure 1.8 Fatigue Behavior Of Inconel 718 at 1000°F With Various Heat Treatments Compared to Best Fit Curves From Conventional Heat Treat (Ref. ANCR-1125)

2. ARGONNE NATIONAL LABORATORY

R. W. Weeks

2.1 INTRODUCTION

Argonne National Laboratory (ANL) is conducting an extensive program to provide low-cycle, high-temperature fatigue data on Types 304 and 316 stainless steel in support of LMFBR component design, as outlined in a previous report.[1] The present report describes some considerations involved in the application of strain-range partitioning to elevated-temperature fatigue life prediction, crack-propagation work on Type 304/308 stainless steel weldments, and the effect of sodium on the tensile and creep behavior of austenitic stainless steels.

2.2 FRACTURE AND FATIGUE STUDIES ON STAINLESS STEELS -- D. R. Diercks, C. F. Cheng, and P. S. Maiya

2.2.1 Some Considerations Involved in the Application of Strain-range Partitioning to the Prediction of Low-cycle Fatigue Life for Type 304 Stainless Steel -- D. R. Diercks

Manson and co-workers[2,3] have proposed a life-predictive method, known as strain-range partitioning, that is applicable to combined creep-fatigue testing conditions. This method is based upon the premise that the inelastic strain which a component or specimen experiences may be classified as either plastic (time-independent) strain or creep (time-dependent, nonrecoverable) strain. Anelastic strains are ignored. For reversed loading, four possible types of strain ranges exist: $\Delta\varepsilon_{pp}$, plastic strain in tension reversed by plastic strain in compression; $\Delta\varepsilon_{pc}$, plastic strain reversed by creep strain; $\Delta\varepsilon_{cp}$, creep strain reversed by plastic strain; and $\Delta\varepsilon_{cc}$, creep strain reversed by creep strain. In general, each of the

strain components is considered to make a different contribution to the damage process, and the damage from each component is summed linearly when the method is applied to the life prediction.

We are, at present, checking the predictions of the strain-range partitioning method against our experimental results for selected 593°C (1100°F) hold-time tests. However, before the strain ranges for these selected tests could be partitioned in a completely unambiguous fashion, a basic difficulty in the load versus time curves had to be resolved. Figure 2.1(a) shows the total strain versus time waveform for a strain-controlled test with tension hold time, and Fig. 2.1(b) shows the somewhat idealized load waveform required to obtain this response. At time t_1, where the total strain rate is abruptly changed from $\dot{\varepsilon}_t = \dot{\varepsilon}_1$ to $\dot{\varepsilon}_t = 0$, an abrupt drop in the load is observed, followed by the usual load relaxation during the hold time at constant strain. Similarly at time t_2, an abrupt strain-rate change is accompanied by an abrupt change in load. (In the actual load records, of course, inertial effects in both the hydraulic system of the test machine and the recorders cause these load drops to occur over a short, but finite time rather than instantaneously.) It has now become evident that these abrupt load changes are manifestations of a general relationship between applied stress and plastic strain rate. Thus, when all other conditions are constant, the applied stress necessary to impose a given plastic strain rate increases with an increase in plastic strain rate. At times t_1 and t_2 in Fig. 2.1, abrupt changes in load are necessary to achieve the programmed abrupt changes in total and plastic strain rates. This variation in applied stress, or flow stress, with imposed strain rate is a familiar effect in the monotonic tensile deformation

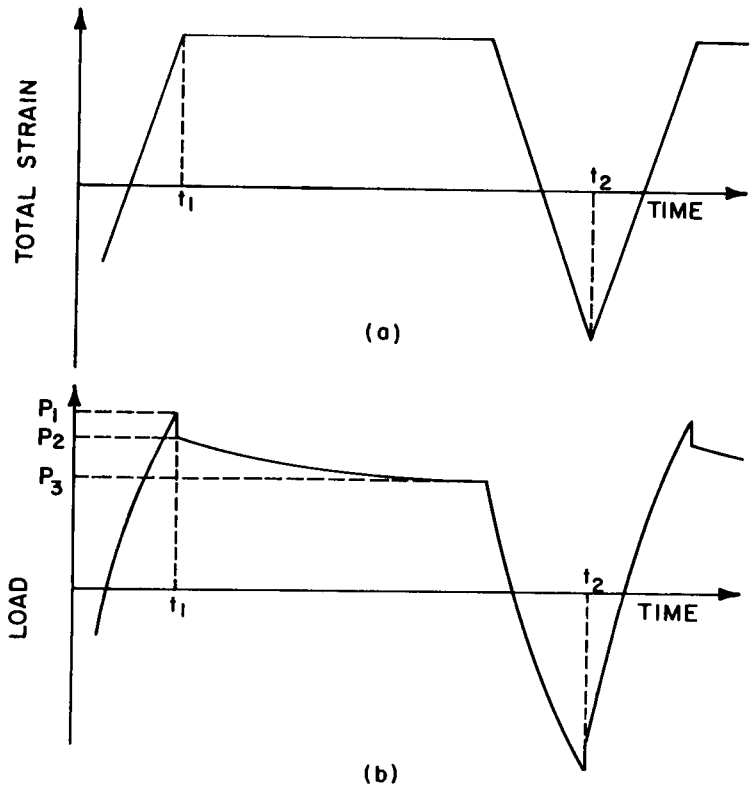

Fig. 2.1. Strain and Load vs Time Waveforms for Strain-controlled, Tension Hold-time Test.

of Type 304 stainless steel[4,5] and is now becoming apparent in the cyclic deformation. As further evidence, we observe experimentally that the load drop associated with a change in total strain rate from 4×10^{-5} sec^{-1} to zero is much less than that associated with a change from 4×10^{-3} sec^{-1} to zero. It should be noted that Hart and co-workers[6,7] have mathematically formalized this variation of flow stress with plastic strain rate into the concept of a mechanical equation of state with the state variables being flow stress, plastic strain rate, "hardness state" (or resistance to plastic flow), and temperature. Furthermore, Yamada and Li[8] have obtained experimental results indicating that Types 304 and 316 stainless steel behave according to this sort of mechanical equation of state, at least at room temperature.

We now turn to a consideration of partitioning the strain range for a cyclic-relaxation test. The relaxation portion of the load record of Fig. 2.1(b) ($P_2 - P_3$) can be related to a creep strain (in this case $\Delta\varepsilon_{cp}$). However, an inelastic strain is also associated with the abrupt load drop $P_1 - P_2$, since it occurs at constant total strain, and typically this strain is found to be of the order of 2×10^{-4} or 0.02% for the 593°C (1100°F) hold-time tests partitioned to date. This is about equal to the $\Delta\varepsilon_{cp}$ strain associated with a tension hold time of 15 min at a 2% total strain range or 60 min at a 1% total strain range. Thus, the inelastic load-drop strain is significant and must be properly taken into account in strain-range partitioning. Since a finite time is required for the load drop to occur in a real test, the drop may be expected to include some creep strain associated with the load relaxation that would occur in this finite time increment. However, the preponderence of the load

drop appears to be a strain-rate-change effect, and this portion is more properly classified as a plastic (here $\Delta\varepsilon_{pp}$) strain. Since the time required for the drop to occur is found to be negligible compared with the constant strain hold times, we have decided to treat the strain associated with the load drop entirely as a plastic component.

One must now be concerned with generating the partitioned strain range versus life curves. Let us consider the $\Delta\varepsilon_{cp}$ data specifically. An apparent method of generating these data is that of cycling in load control, as shown in Fig. 2.2(b), where the loading rates between hold times are sufficiently great so that negligible creep damage occurs. The loading rate is switched to zero at time t_1 when the strain reaches ε_1 [Fig. 2.2(a)], and the load is held constant until the strain reaches ε_3. This would appear to give a $\Delta\varepsilon_{cp}$ strain range of $\varepsilon_3 - \varepsilon_1$ per cycle. However, closer examination reveals that the strain $\varepsilon_3 - \varepsilon_1$ is actually mixed $\Delta\varepsilon_{cp}$ and $\Delta\varepsilon_{pp}$. At time t_1 when strain ε_1 is reached, the applied load is P_1 and the corresponding plastic strain rate is $\dot{\varepsilon}_1$. At some small time increment Δt later, the applied load is still P_1 and, since the specimen has undergone very little further deformation and hardening, the plastic strain rate will still be $\sim \dot{\varepsilon}_1$. The deformation mode of the specimen will only gradually change from plasticity to creep as it deforms at constant load P_1. The $\Delta\varepsilon_{cp}$ strain will thus be $\varepsilon_3 - \varepsilon_2$ rather than $\varepsilon_3 - \varepsilon_1$, where ε_2 is, in general, rather poorly defined [Fig. 2.2(a)].

To circumvent this difficulty, we have developed an alternative loading waveform for generating the partitioned strain range versus life data. The computer-controlled testing machine is employed to conduct the test. The situation will again be illustrated for the $\Delta\varepsilon_{cp}$ data (Fig. 2.3). The

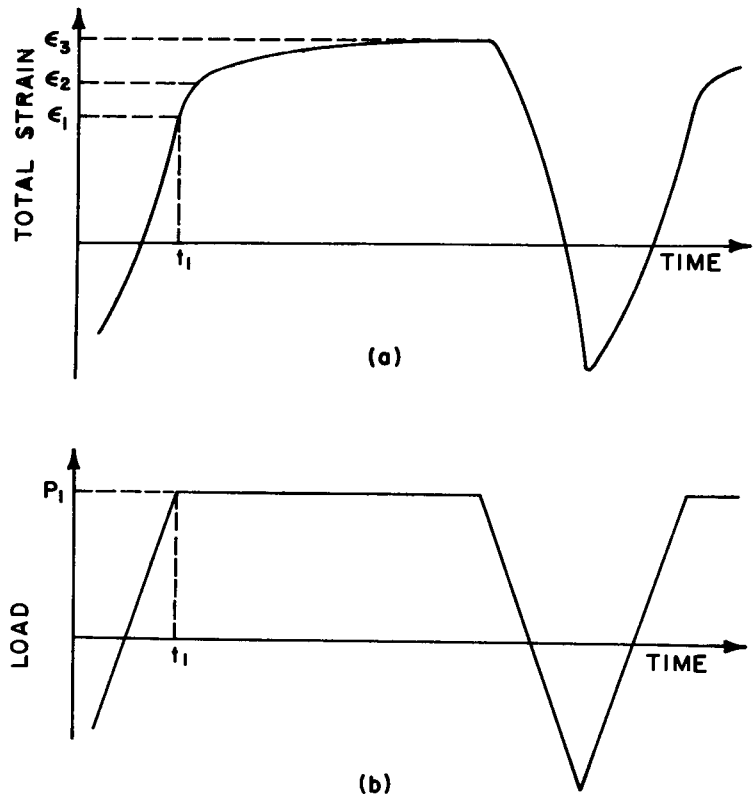

Fig. 2.2. Strain and Load vs Time Waveforms for Load-controlled Test with Hold Time at Peak Tensile Load.

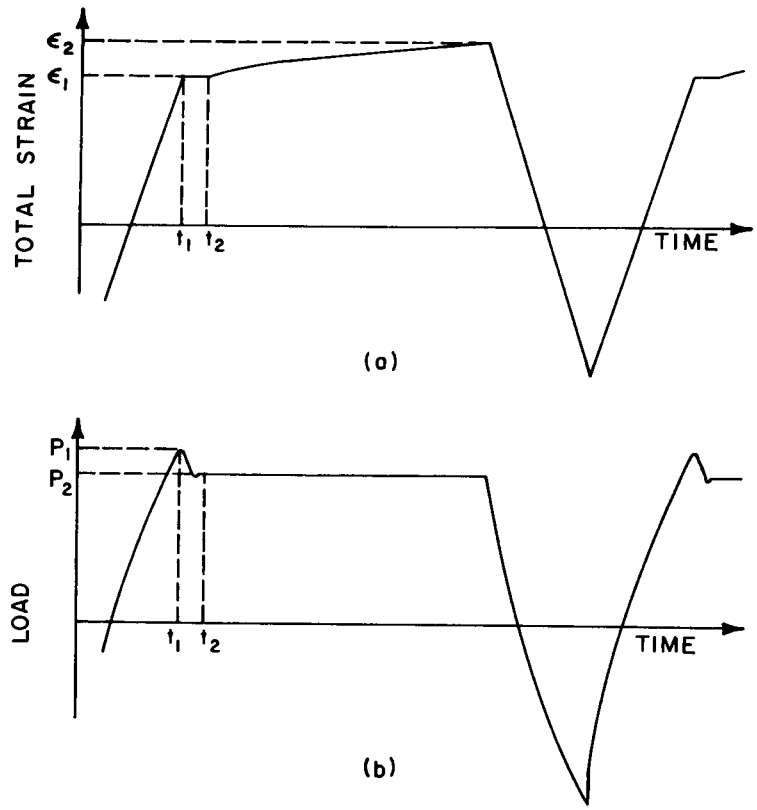

Fig. 2.3. Suggested Strain and Load vs Time Waveforms to Determine $\Delta\varepsilon_{cp}$ Strain-Life Relationship.

cyclic portion of the loading is accomplished in strain control, with a relatively high strain rate to minimize creep effects. When the strain reaches the value ε_1 at time t_1 [Fig. 2.3(a)], the strain rate is changed abruptly to zero, but the test remains in strain control. This causes a readjustment in load from P_1, corresponding to the plastic strain rate just before t_1, to P_2, corresponding to the plastic strain rate just after t_1. After a short delay (typically, $\sim$ 3 sec), the test is switched to load control at constant load P_2, and the specimen is permitted to creep to the upper strain limit ε_2. At ε_2 the test returns to strain control, and the specimen is cycled into compression. In this manner, the strain $\varepsilon_2 - \varepsilon_1$ is entirely $\Delta\varepsilon_{cp}$ in character. The strain corresponding to the load change $P_1 - P_2$ is interpreted as entirely $\Delta\varepsilon_{pp}$, as described above for the cyclic-relaxation tests. The hysteresis loop that corresponds to the test described here is shown in Fig. 2.4.

To date, the above procedures have been used to partition the strain range for $\sim$ 30 cyclic-relaxation tests. In addition, $\Delta\varepsilon_{pp}$ versus N_{pp} and limited $\Delta\varepsilon_{cp}$ versus N_{cp} data have been generated. These data will be included in a future report, when more complete results are available.

2.2.2 Low-cycle Creep Fatigue and Crack Propagation of SMA Type 304/308 Stainless Steel Weldments -- C. F. Cheng

ANL is studying the low-cycle creep fatigue and crack growth of SMA Type 304/308 stainless steel welded plates with controlled residual elements made by Combustion Engineering to simulate the seam and girth welds of the FFTF vessel. The details of the fabrication and mechanical properties of the welded plates have been reported by ORNL.[9,10] Weld-metal and base-metal specimens were sectioned from welded plates as shown in Fig. 2.5.

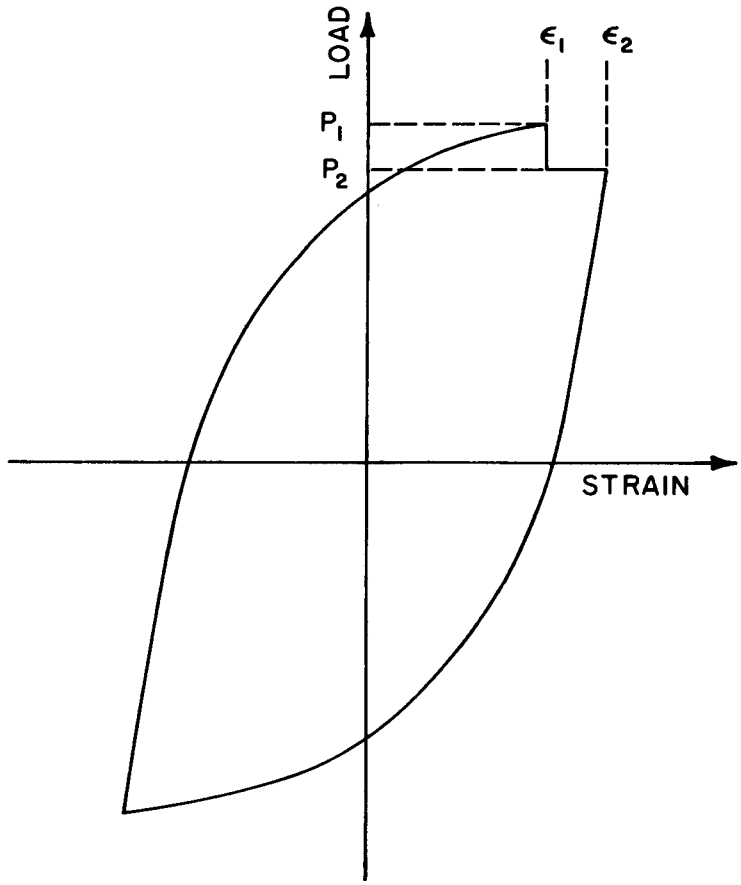

Fig. 2.4. Hysteresis Loop that Corresponds to Strain and Load Waveforms of Fig. 2.3.

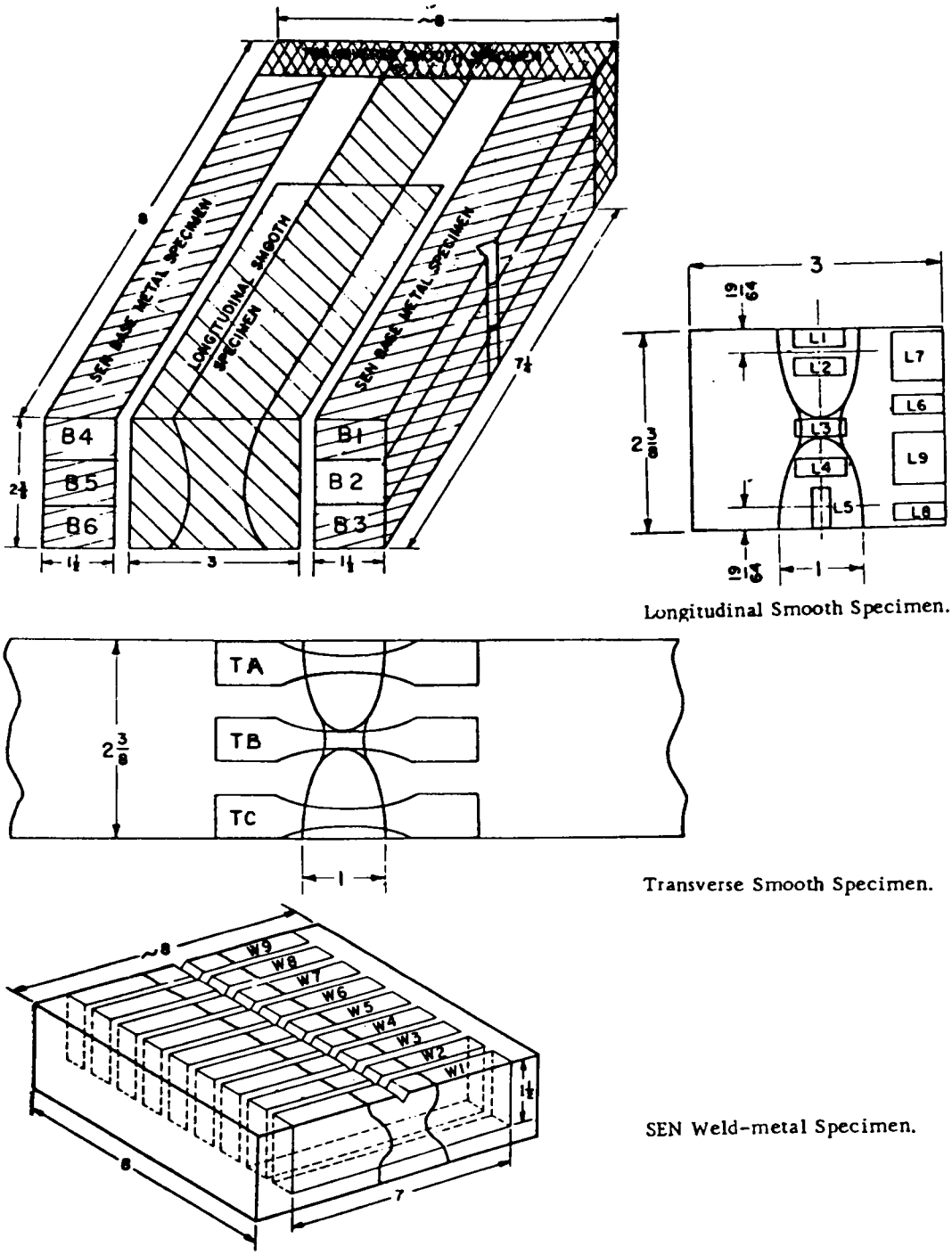

Longitudinal Smooth Specimen.

Transverse Smooth Specimen.

SEN Weld-metal Specimen.

All dimensions are in inches.

Fig. 2.5. Weld-metal and Base-metal Specimens.

The machined and ground specimens were then tested in either the as-fabricated condition or a subsequently aged condition. The specifications of smooth specimens for the creep-fatigue tests and the SEN specimens for the crack-propagation tests are shown in Fig. 2.6.

All low-cycle, creep-fatigue tests were conducted in a closed-loop hydraulic machine.[11] The machine uses a set of two horizontally oriented diametral extensometers 90° apart, a load cell, and an analog strain computer to monitor continuously the average diameter change, axial load, and axial strain at the gauge section of the specimen, respectively.[12] Dual diametral extensometers were used to compensate for the anisotropic deformation of the weldment. The elastic Poisson's ratio for different orientations and locations of the weldment (Fig. 2.5) was determined from tensile tests using a uniform gauge-section specimen with simultaneous recordings of axial and diametral extensometers. The plastic Poisson's ratio was taken as 0.5, and Young's modulus, E, was obtained from the hysteresis loop of stress versus strain in the low-cycle, creep-fatigue test.

All tests were conducted in air in the fully reversed, axially controlled strain mode at a fixed strain rate of 4×10^{-3} sec^{-1}. The tests were performed in the total strain range from 0.5 to 2.0% at a temperature of 1100°F. Data showing the logarithmic relationship between total strain range ($\Delta\varepsilon_t$) and plastic strain range ($\Delta\varepsilon_p$) versus fatigue life (N_f) are plotted in Fig. 2.7. The ANC data are for base metal in the as-fabricated condition using either hourglass specimens with a diametral extensometer (solid lines) or uniform gauge specimens with an axial extensometer (dashed lines). All other ANL and ANC data points are included for

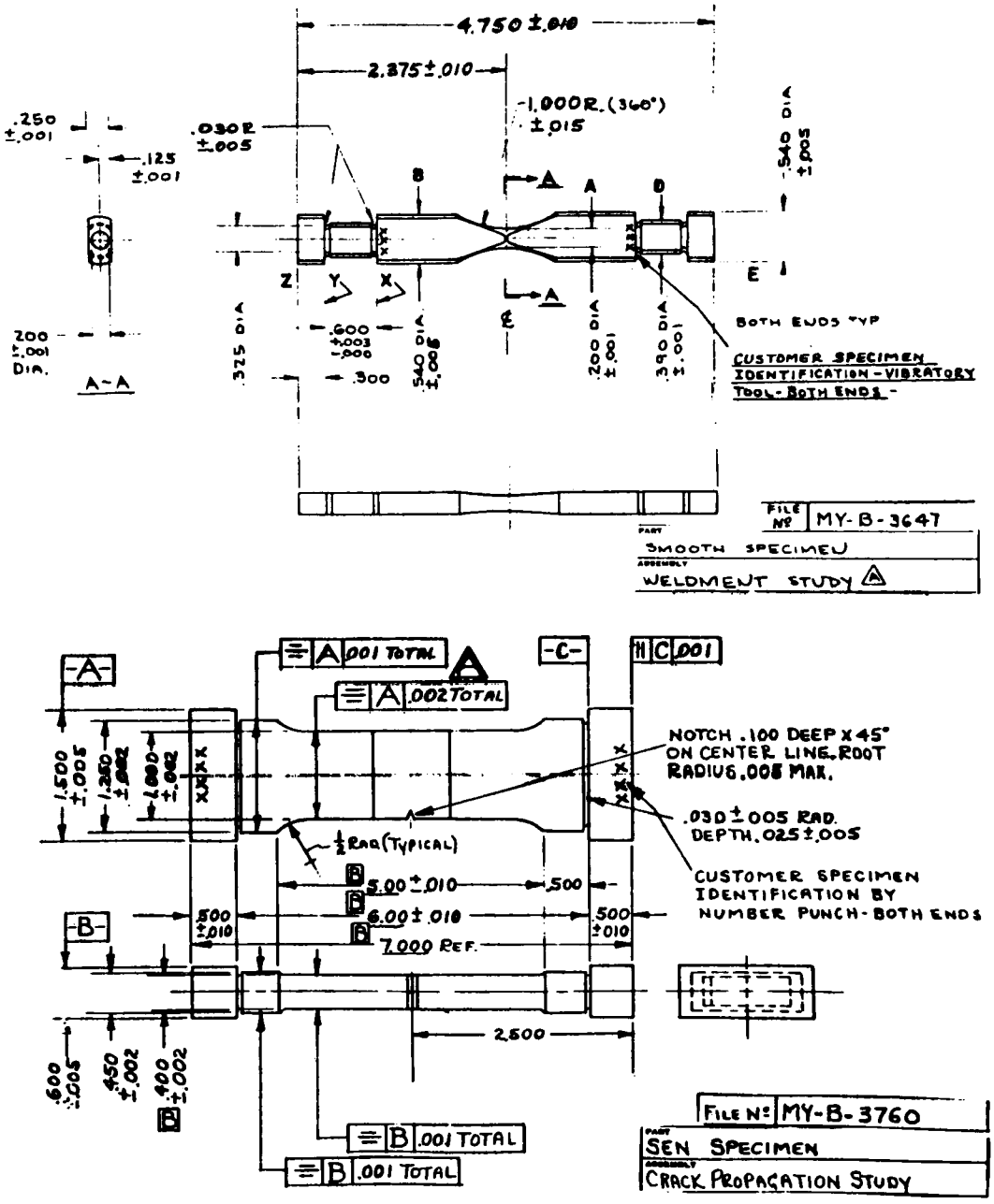

Fig. 2.6. Specifications for Smooth and SEN Specimens.

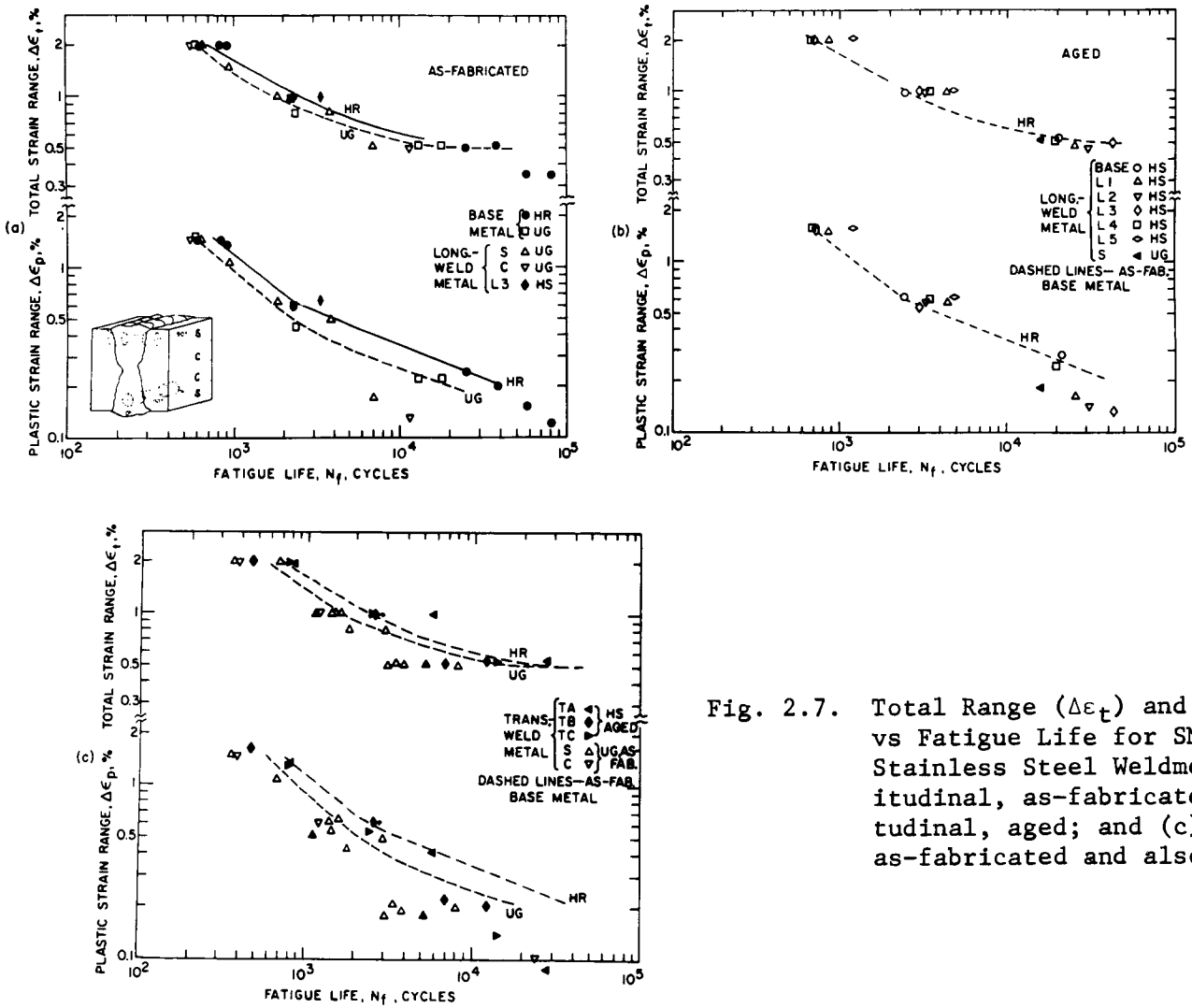

Fig. 2.7. Total Range ($\Delta\varepsilon_t$) and Plastic Range vs Fatigue Life for SMA Type 304/308 Stainless Steel Weldment. (a) Longitudinal, as-fabricated; (b) longitudinal, aged; and (c) transverse, as-fabricated and also aged.

comparison. At $\sim$ 1/2% $\Delta\varepsilon_t$, the two lines merge. Note in Fig. 2.7(a) that the data points for the ANC uniform gauge specimens at both the surface (S) and center (C) sections of the weld metal lie on the dashed line for the corresponding base-metal specimens, whereas the single data point at the weld-metal core (L3) of the ANL smooth specimen lies on the solid line for the base-metal hourglass specimens. The preliminary data in Fig. 2.7(b) indicate that the data points for the aged base-metal smooth specimens lie on the dashed line for as-fabricated base-metal hourglass specimens. The same is true for the longitudinal weld metal at the core (L3). In general, for weld-metal specimens (L1, L2, L4, L5), the fatigue life decreases slightly as the distance from the core increases. Additional tests are needed to confirm the observation. It is suspected that the differences in ferrite content may influence the fatigue life; metallographic examinations of the failed specimens are in progress. Figure 2.7(c) is a plot of data points for the transverse weld-metal specimens. All data points for the aged smooth specimens at different locations in the weld metal fall on the dashed line for base-metal hourglass specimens in the as-fabricated condition. The scattered points that do not follow the general pattern may be the result of localized difference in microstructure, and the failed specimens will be examined metallographically to determine the microstructure.

Crack Propagation

Weld-metal and base-metal specimens in the single-edge-notch (SEN) configuration were machined from welded plates, as shown in Fig. 2.8. Each specimen (Fig. 2.6) was cycled under uniaxial tension loading using a saw-tooth waveform at a constant stress ratio ($R = \sigma_{min}/\sigma_{max}$). The

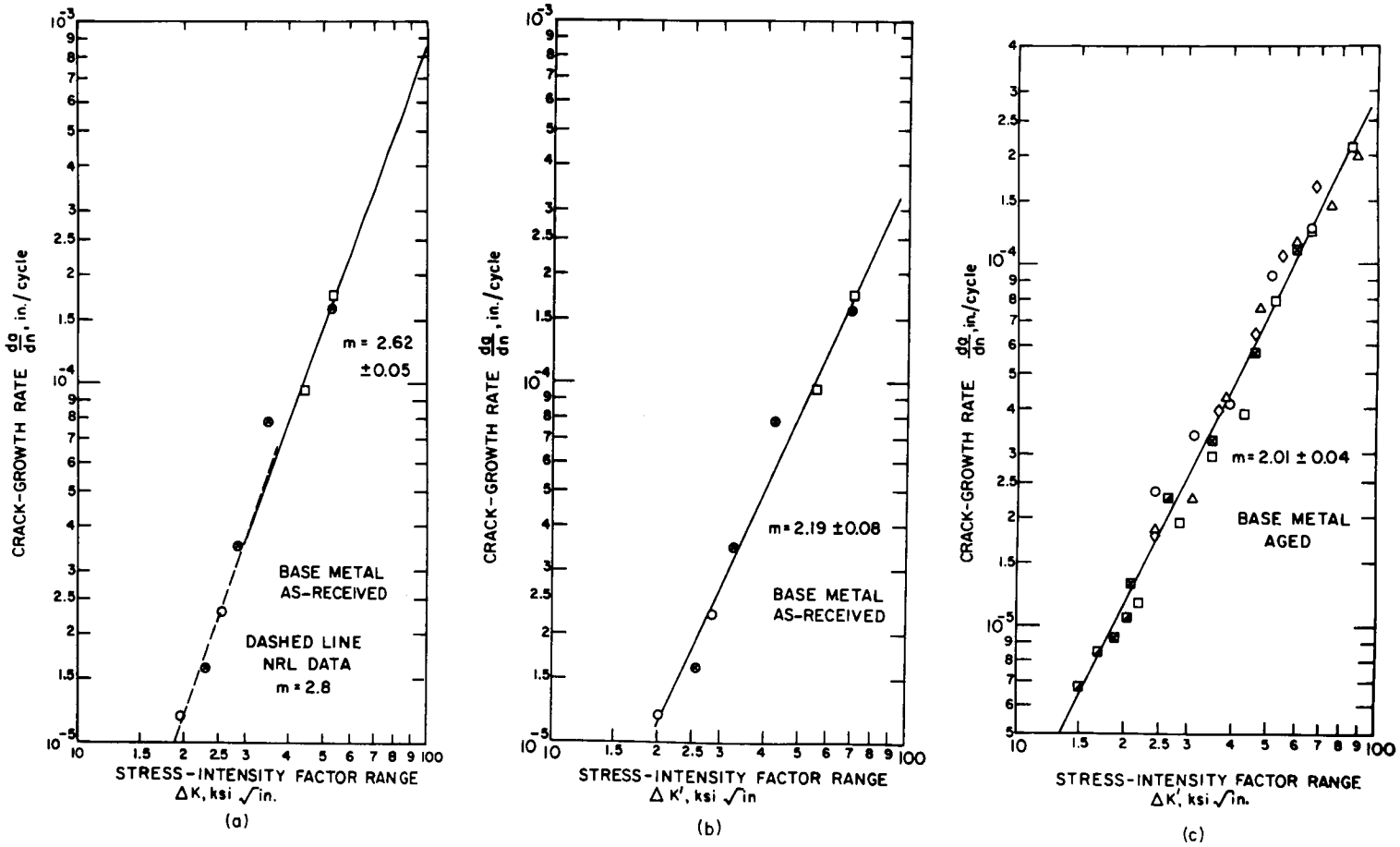

Fig. 2.8. Crack-growth Rate vs Stress-intensity Factor Range at 1100°F in Base Metal for SMA Type 304/308 Stainless Steel Weldment. (a) As-received (ΔK), (b) as-received, and (c) aged. Symbols: Continuous cycling (circles), 1-min tension hold at scribe marks (squares), reduce frequency to 0.3 cpm at each scribe mark (diamonds), stop test and restart at each scribe mark (triangles). Separate tests are denoted by open, cross, or half-solid symbols.

crack growth was viewed through a microscope, and the number of cycles was recorded as the crack traversed a series of parallel scribe marks at 50-mil increments from the side notch. The average crack length is determined by the cross-sectional area of the cracked surface up to the crack front of the fracture surface divided by the thickness of the specimen. The test conditions and results are summarized in Table 2.1. The crack-growth rate da/dN was determined for each increment of crack extension, and the stress-instensity factor range was calculated, as previously described,[14] based on the average crack length for that increment.

Analysis of the fatigue crack-growth data was made on the basis of the power law relating da/dN to $\Delta K'$, which is expressed as

$$da/dN = C\ (\Delta K')^m,$$

where C and m are constants, and $\Delta K'$ is selected over ΔK because $\Delta K'$ corrects for the plastic zone.

Figures 2.8 and 2.9 are logarithmic plots of da/dN versus $\Delta K'$ (or ΔK) for base metal in the as-received or aged condition and weld metal in the as-welded or aged condition, respectively. Figure 2.8(a) shows our data points are in good agreement with NRL data,[15] represented by the dashed line in the da/dN versus ΔK plot. Furthermore, no significant difference in the crack-growth rate is observed (Figs. 2.8 and 2.9) as the crack traverses the scribe marks under the following test conditions: (a) continuous cycling, (b) 1-min tension hold, (c) reduce frequency to 0.3 cpm, and (d) stop and restart. Test condition (b) gives a clear demarcation of the crack contour.

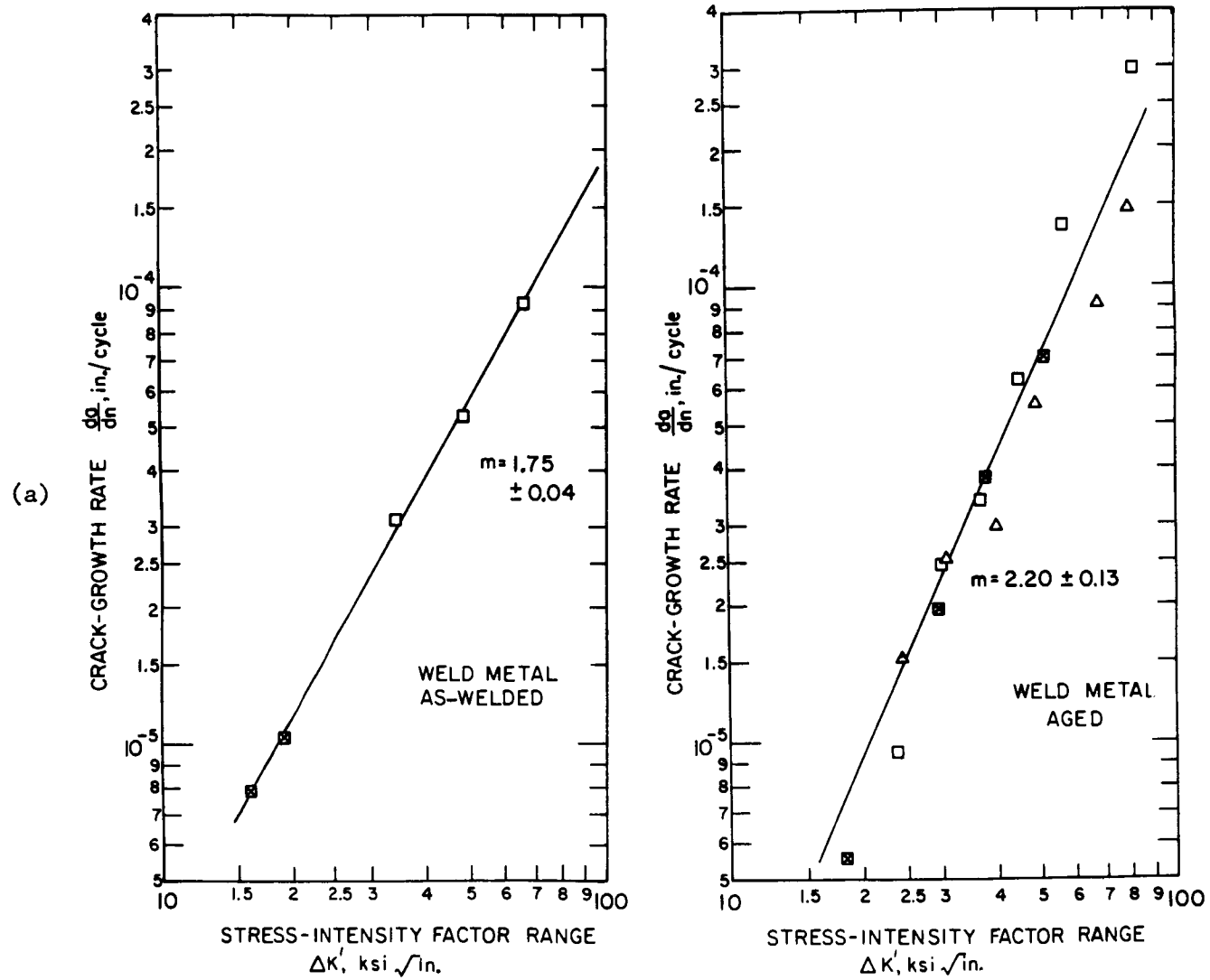

Fig. 2.9. Crack-growth Rate vs Stress-intensity Factor Range at 1100°F in Weld Metal for SMA Type 304/308 Stainless Steel Weldment. (a) As-welded and (b) aged.

Table 2.1. Crack Propagation of SMA Type 304/308 Stainless Steel Weldments

Frequency: 30 cpm; Stress Ratio R: 0.05; Temperature: 1100°F

Test Number	Specimen Number	a_{avg}, 10^{-3} in.	P_{avg}, 10^3 lb	da/dN, 10^{-6}/in.	ΔK, ksi$\sqrt{in.}$	r_p,[a] 10^{-3} in.	$\Delta K'$, ksi$\sqrt{in.}$	Cycling Conditions[b]
				Base Metal: As-received				
1C	CE32B3	294.7	4.830	11.79	19.08	41.7	20.39	
		377.2	4.820	22.80	25.79	76.1	28.61	
2C	CE32B1	220.4	7.743	16.17	22.92	60.1	25.86	(1)
		276.4	7.738	35.05	28.62	93.7	33.12	
		360.6	7.723	78.11	34.90	182.1	42.82	
		441.7	7.678	160.29	53.44	326.7	70.48	
4C	CE32B5	403.9	7.531	95.75	44.80	229.6	56.11	
		447.0	7.606	176.16	54.00	333.6	71.36	
				Base Metal: Aged (1000 hr at 1100°F)				
6C	CE33B5	191.3	7.629	11.49	19.91	45.3	22.14	
		247.9	7.629	19.23	25.25	72.9	28.72	
		294.9	7.614	29.27	30.08	103.5	34.96	
		340.1	7.594	38.36	35.69	145.7	42.66	
		386.3	7.599	78.59	42.10	202.8	51.99	
		433.6	7.593	120.11	51.17	299.5	66.54	
		479.6	7.588	209.4	61.77	436.5	85.37	
11C	CE33B6	224.6	5.774	9.30	17.43	34.7	18.73	
		252.6	5.754	13.12	19.28	42.5	20.84	(2)
		374.9	5.758	32.30	30.58	107.0	34.97	
		433.2	5.753	56.86	38.66	171.0	45.66	
		486.7	5.753	107.88	48.32	267.1	60.13	
14C	CE33B2	226.2	4.740	6.81	14.36	23.6	15.09	
		256.3	4.740	8.55	16.07	29.5	16.99	
		298.6	4.750	10.60	19.02	41.4	20.30	
		363.6	4.745	21.77	24.27	67.4	26.42	
7C	CE33B1	213.7	7.599	17.69	21.81	54.4	24.33	
		304.9	7.600	39.40	31.31	112.1	36.41	
		356.9	7.590	63.48	37.87	164.1	45.76	(3)
		395.5	7.590	105.00	43.72	218.7	54.48	
		440.1	7.590	163.60	52.37	313.7	68.54	

Table 2.1. Crack Propagation of SMA Type 304/308 Stainless Steel Weldments (Contd.)

Frequency: 30 cpm; Stress Ratio R: 0.05; Temperature: 1100°F

Test Number	Specimen Number	a_{avg}, 10^{-3} in.	P_{avg}, 10^3 lb	da/dN, 10^{-6}/in.	ΔK, ksi$\sqrt{in.}$	r_p,[a] 10^{-3} in.	$\Delta K'$, ksi$\sqrt{in.}$	Cycling Conditions[b]
				Base Metal: Aged (1000 hr at 1100°F) (Contd.)				
18C	CE33B4	210.8	7.599	18.57	21.73	54.0	24.35	
		265.7	7.598	22.43	26.82	82.3	30.69	
		314.4	7.599	43.09	32.37	119.9	38.05	
		363.1	7.599	74.91	38.68	171.1	46.91	(4)
		412.0	7.599	116.30	46.96	252.3	59.63	
		457.7	7.599	143.70	56.23	361.7	75.24	
		487.8	7.599	199.50	63.83	466.1	89.26	
19C	CE34B2	209.6	7.620	23.45	21.57	53.2	24.15	
		268.4	7.620	31.76	27.05	83.7	30.98	
		316.3	7.640	40.71	32.85	123.4	38.74	(1)
		379.5	7.640	92.87	41.33	195.4	50.87	
		432.9	7.620	123.20	50.98	297.3	66.21	
				Weld Metal: As-welded				
10C	CE39W8	189.6	5.695	7.96	14.81	27.9	15.86	
		231.3	5.690	10.24	17.53	39.0	18.95	
16C	CE41W6	284.8	7.606	31.24	28.90	106.1	33.86	
		366.3	7.599	52.67	39.14	194.6	48.43	
		426.6	7.604	94.51	49.73	314.1	65.52	
				Weld Metal: Aged (1000 hr at 1100°F)				
12C	CE39W1	204.1	7.596	9.61	21.04	56.2	23.76	
		256.9	7.596	24.33	25.83	84.7	29.79	(2)
		306.5	7.593	37.76	31.66	127.3	37.67	
		348.0	7.596	61.18	36.76	171.6	44.92	
		398.8	7.596	136.20	44.21	248.2	56.31	
		467.9	7.592	294.10	58.46	434.1	81.17	
13C	CE39W2	219.6	5.700	5.61	16.87	36.2	18.21	
		335.6	5.693	19.40	26.41	88.6	29.69	
		390.7	5.685	33.51	32.06	130.6	37.03	
		454.9	5.690	69.57	41.77	221.6	50.94	

Table 2.1. Crack Propagation of SMA Type 304/308 Stainless Steel Weldments (Contd.)

Frequency: 30 cpm; Stress Ratio R: 0.05; Temperature: 1100°F

Test Number	Specimen Number	a_{avg}, 10^{-3} in.	P_{avg}, 10^3 lb	da/dN, 10^{-6}/in.	ΔK, ksi$\sqrt{in.}$	r_p,[a] 10^{-3} in.	$\Delta K'$, ksi$\sqrt{in.}$	Cycling Conditions[b]
				Weld Metal: Aged (1000 hr at 1100°F) (Contd.)				
17C	CE39W5	210.7	7.600	15.23	21.58	57.6	24.35	(4)
		267.0	7.624	25.07	26.99	90.2	31.22	
		320.1	7.647	29.36	33.42	138.3	39.99	
		369.0	7.612	55.00	39.65	194.6	49.00	
		420.5	7.612	91.19	48.72	293.8	63.49	
		460.7	7.647	147.34	57.35	407.1	78.71	

[a]Calculated value based on cyclic yield strength at 1100°F at 37.3 ksi for base metal and 35.8 for weld metal.[13]

[b](1) Continuous cycling (circles in figures); (2) 1-min tension hold at each scribe mark (squares in figures); (3) reduce frequency cpm to 0.3 at each scribe mark (diamonds in figures); (4) stop test and restart at each scribe mark (triangles in figures).

The crack-growth rate is about the same for the base metal in the as-received ($m = 2.19 \pm 0.08$) and aged (2.01 ± 0.04) conditions. The growth rate for the weld metal in the aged condition ($m = 2.20 \pm 0.13$) is also about the same as that for the base metal; only the weld metal in the as-welded condition exhibited a lower growth rate ($m = 1.75 \pm 0.04$). This lower growth rate may be a consequence of the locked-in residual stress during welding fabrication.

2.3 SODIUM EFFECTS ON LMFBR MATERIALS -- T. F. Kassner

2.3.1 Influence of Sodium Environment on Tensile and Creep Behavior of Austenitic Stainless Steels -- K. Natesan, D. L. Smith, and J. Y. N. Wang

The effect of carburization on the tensile and creep-rupture properties of Types 304, 316, and Ti-modified 316 stainless steel is being determined after exposure of the materials to well-characterized sodium at temperatures between 550 and 700°C. Although prior work[16-21] has shown that carburization of austenitic stainless steels increases the ultimate tensile strength and proof stress with a corresponding decrease in ductility, the tensile properties have been correlated with the average carbon concentration in the materials rather than with the surface carbon concentration and the depth of carbon penetration in relation to the specimen thickness. In most instances, both the surface and average carbon concentrations in the materials were considerably higher than can reasonably be expected[22] for stainless steels after long-term service in reactor heat-transport systems.

In this program, the initial criterion chosen for comparison of the property data at various temperatures is the constancy of the depth of penetration of carbon in the specimens, since the surface carbon

concentration in the steels decreases as the exposure temperature increases at a fixed carbon concentration in sodium. The surface carbon concentration for the three materials will also be different at any temperature. The relationship between the carbon concentration profiles and the mechanical behavior will be further explored at several temperatures between 500 and 650°C by varying the surface carbon concentrations in the materials over a range that could occur in the intermediate heat exchanger and the primary and secondary system piping. This will be accomplished by controlling the carbon concentration in the sodium at different levels during the exposure period.

The composition of the three austenitic stainless steels is given in Table 2.2 along with the final heat treatment of the 15-mil-thick sheet. Tensile and creep specimens of these materials, which were fabricated according to ASTM standard E8-69, have been exposed to flowing sodium at temperatures of 550, 600, 650, and 700°C for ∿5000, 1500, 300, and 100 hr, respectively, to yield ∿4 mils of carbon penetration. Additional specimens are being exposed to sodium of the same carbon concentration to produce ∿8 mils of carbon penetration in the materials at 600, 650, and 700°C (exposure times of ∿5000, 1500, and 500 hr, respectively).

A number of the annealed specimens and those with 4- and 8-mil carbon penetration depths have been tensile tested in an Instron machine at a crosshead speed of 0.02 in./min. This corresponds to an initial strain rate of 4×10^{-4} sec^{-1} for the 0.875-in. gauge-length specimens. Representative true stress-true strain curves for Types 304, 316, and Ti-modified 316 stainless steel are shown in Figs. 2.10 to 2.12, respectively, at test temperatures of 25, 550, 600, 650, 700, and 750°C. The results

Table 2.2. Composition of Austenitic Stainless Steels

Material	Heat	Concentration, wt%											
		C	N	P	S	Cr	Ni	Mn	Si	Mo	Ti	Cu	Co
304 SS[a]	9T2796	0.046	0.038	0.026	0.012	17.7	9.3	1.17	0.47	0.33	0.03	0.20	0.10
316 SS[a]	V87210	0.058	0.007	0.026	0.011	16.7	13.9	1.43	0.46	2.84	0.04	0.06	0.03
Ti-modified 316 SS[b]	82190	0.080	0.010	0.010	0.008	17.0	13.9	1.46	0.05	2.90	0.24	0.01	0.03

[a]The 15-mil-thick material was solution annealed for 30 min in argon at 1025°C and water quenched.

[b]Same as a, except the annealing temperature was 1100°C.

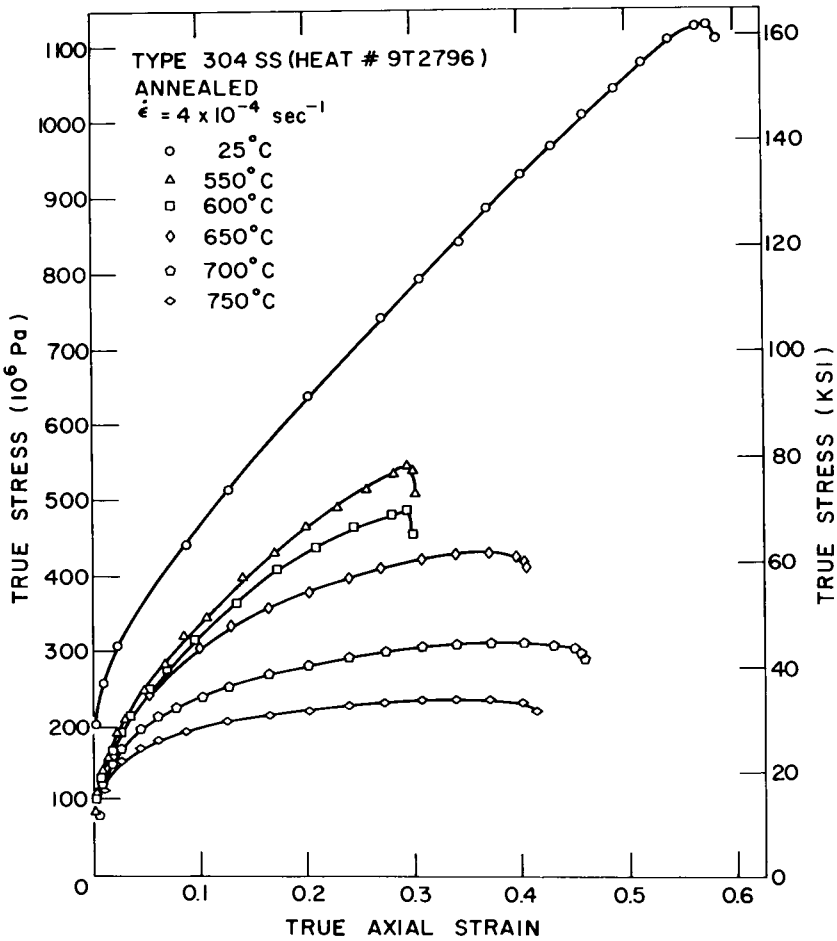

Fig. 2.10. True Stress-True Strain Behavior of Annealed Type 304 Stainless Steel at Various Temperatures.

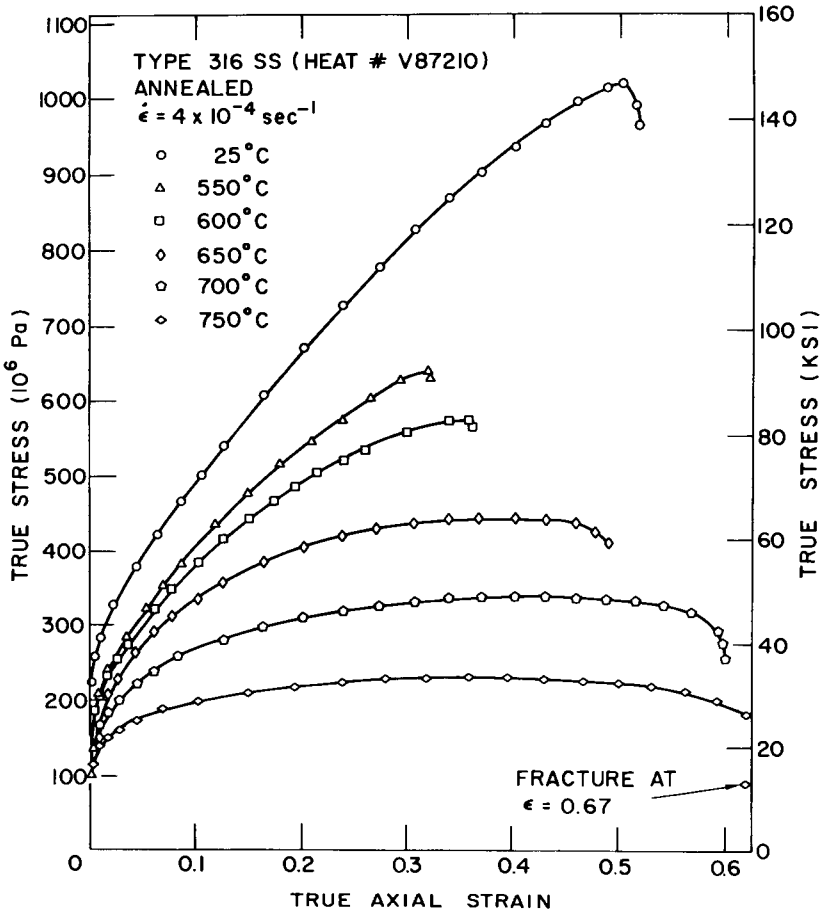

Fig. 2.11. True Stress-True Strain Behavior of Annealed Type 316 Stainless Steel at Various Temperatures.

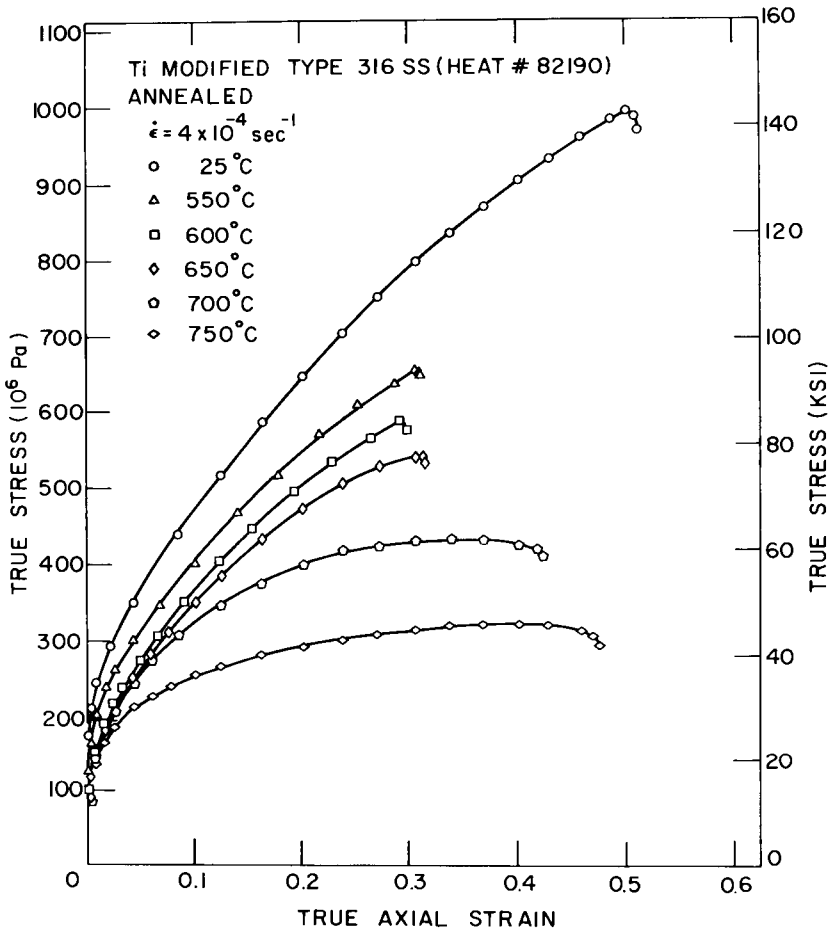

Fig. 2.12. True Stress-True Strain Behavior of Ti-modified Type 316 Stainless Steel in the Annealed Condition at Various Temperatures.

are in good agreement with prior data[23-25] obtained on these heats of materials and will be used as base-line information for comparison with the tensile properties after exposure to the high-temperature sodium environment.

The true stress-true strain behavior of Types 304, 316, and Ti-modified 316 stainless steel after exposure to flowing sodium for 312 and 1512 hr at 650°C is shown in Figs. 2.13 to 2.15. The surface carbon concentrations in the specimens were determined from combustion analyses of 2-mil-thick foils of the three materials, which were equilibrated in the sodium during the specimen-exposure period. These surface carbon concentration values were used with the kinetic analysis for carbon diffusion[22] to obtain the concentration profiles shown in Figs. 2.13 to 2.15. The mechanical test specimens are being analyzed to determine the average carbon concentrations for comparison with the amount of carburization associated with the curves in these figures. This approach is necessary, since an evaluation of the profiles by hardness measurements or metallography will not be quantitative at the indicated carbon concentration levels.

Similar true stress-true strain behavior for the three materials is shown in Figs. 2.16 to 2.18 after exposure to 700°C sodium for 120 and 504 hr. The degree of carburization in these specimens is somewhat less than that for the corresponding material at 650°C because of the lower surface carbon concentrations. Shorter exposure times were required to achieve the ∿4- and 8-mil carbon penetration depths at 700°C. Figure 2.19 shows the engineering tensile strength as a function of temperature for Types 304, 316, and Ti-modified 316 stainless steel in the annealed

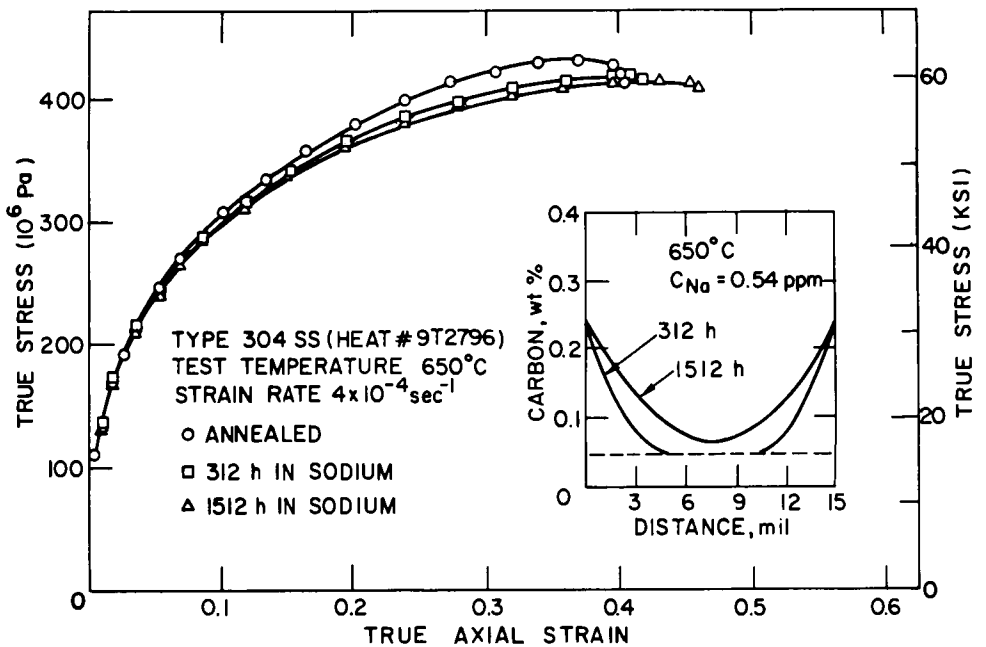

Fig. 2.13. True Stress-True Strain Curves for Type 304 Stainless Steel at 650°C in the Annealed and Carburized Conditions.

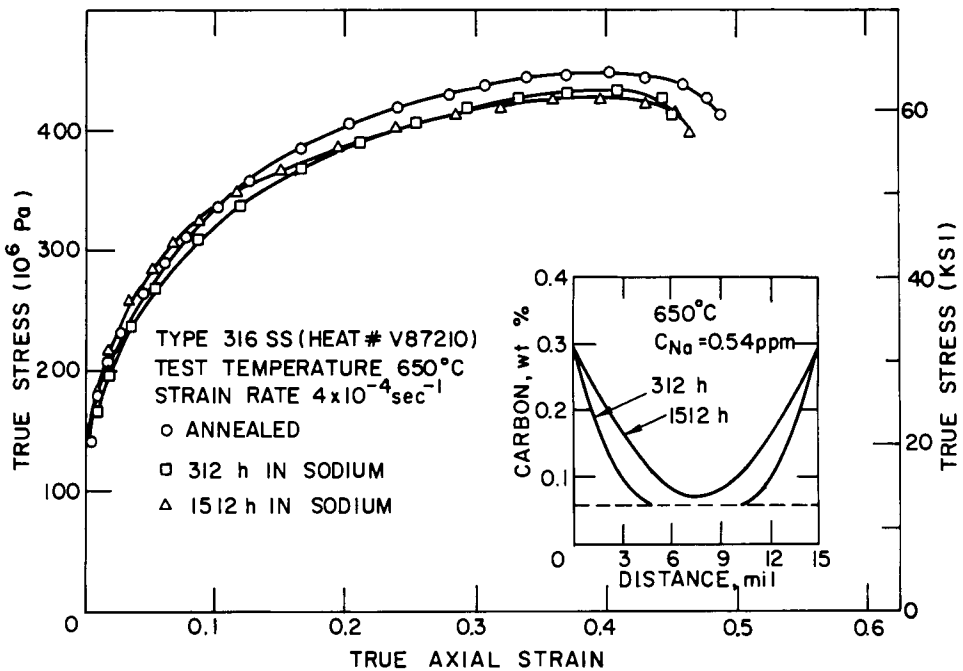

Fig. 2.14. True Stress-True Strain Curves for Type 316 Stainless Steel at 650°C in the Annealed and Carburized Conditions.

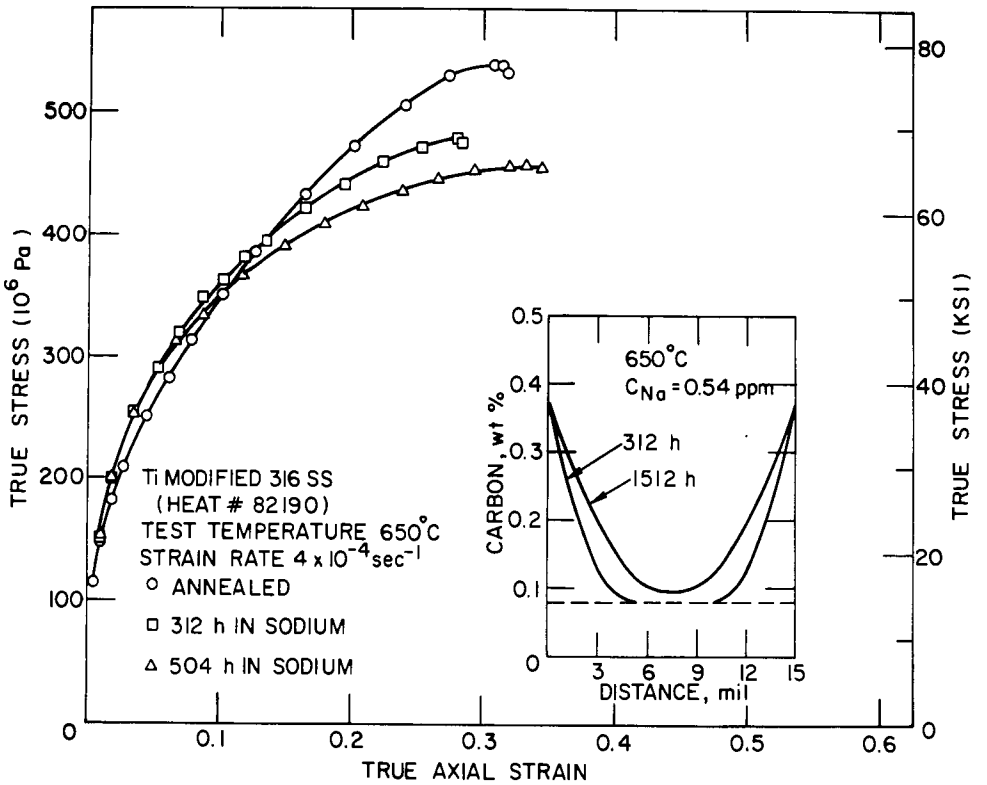

Fig. 2.15. True Stress-True Strain Curves for Ti-modified Type 316 Stainless Steel at 650°C in the Annealed and Carburized Conditions.

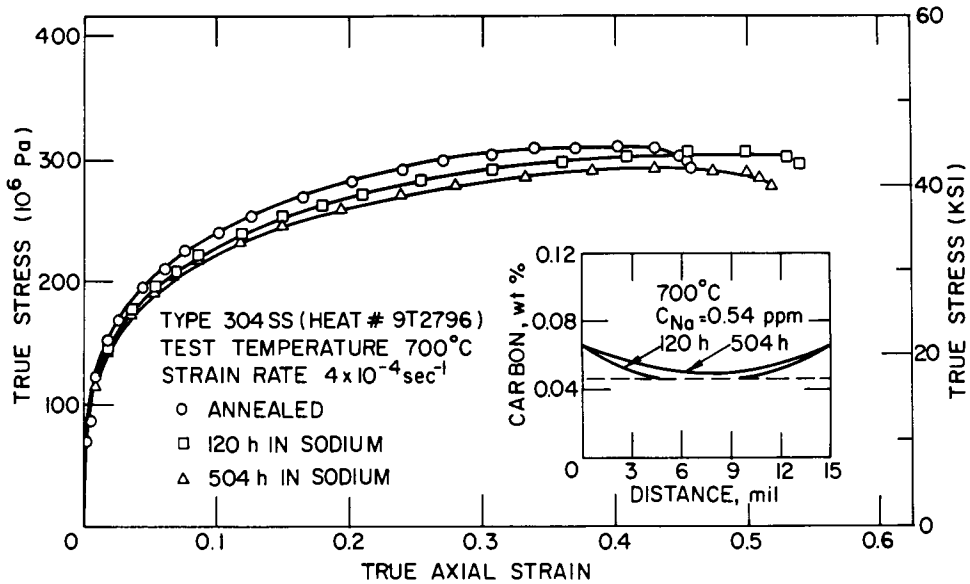

Fig. 2.16. True Stress-True Strain Behavior of Annealed Type 304 Stainless Steel at 700°C in the Annealed and Carburized Conditions.

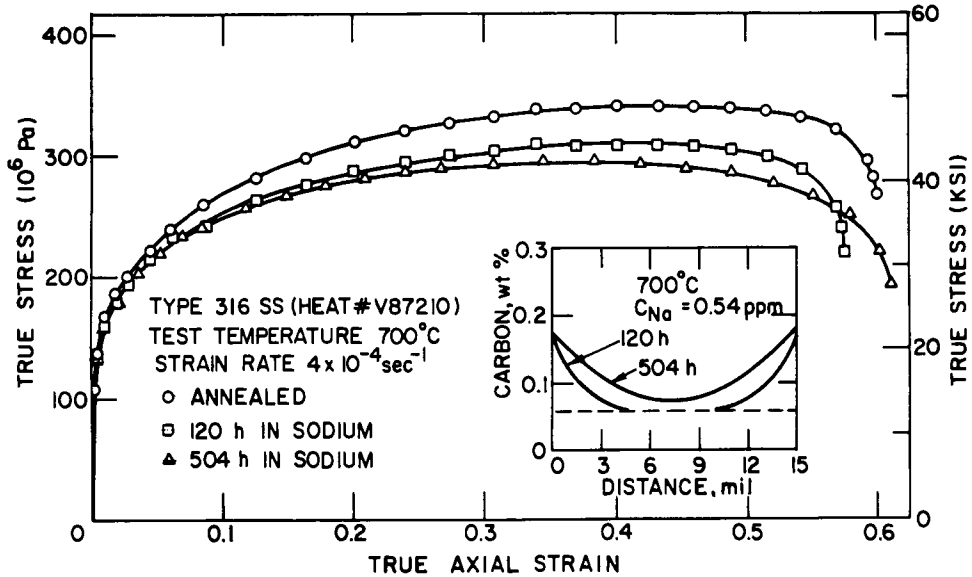

Fig. 2.17. True Stress-True Strain Behavior of Annealed Type 316 Stainless Steel at 700°C in the Annealed and Carburized Conditions.

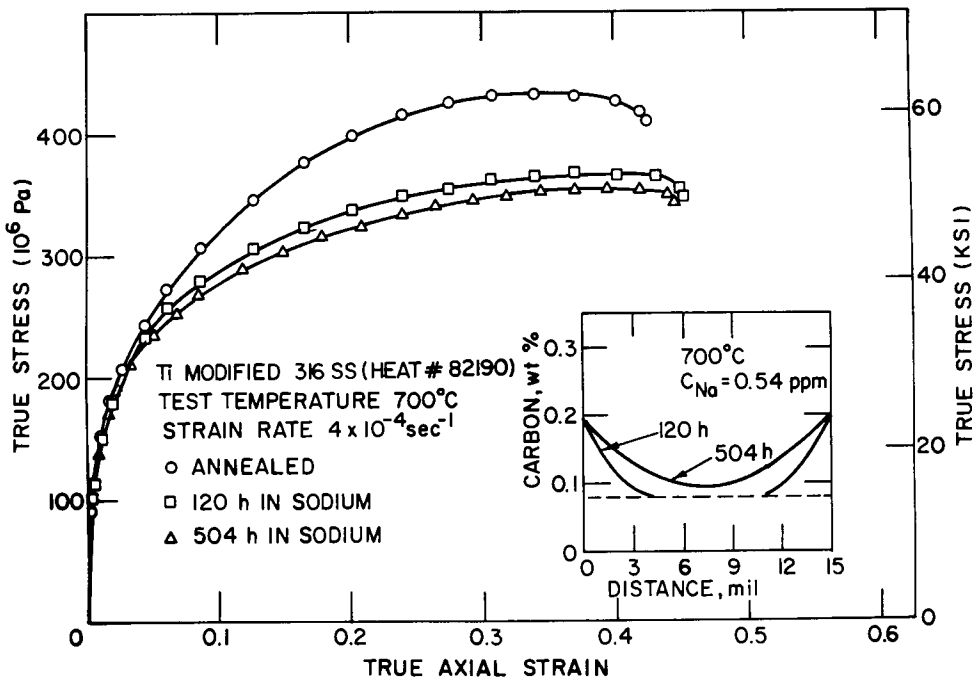

Fig. 2.18. True Stress-True Strain Behavior of Annealed Ti-modified Type 316 Stainless Steel at 700°C in the Annealed and Carburized Conditions.

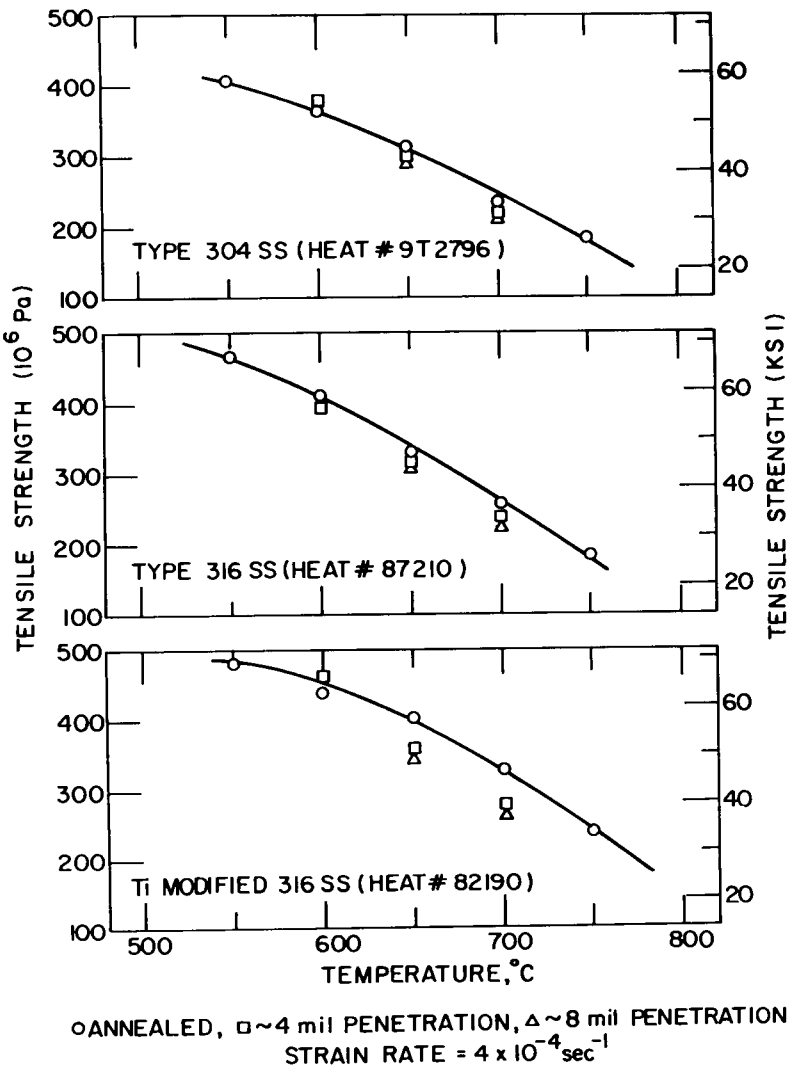

Fig. 2.19. Variation of the Engineering Tensile Strength with Temperature for Types 304, 316, and Ti-modified 316 Stainless Steel in the Annealed and Carburized Conditions.

condition and for the sodium-exposed specimens with a small degree of carburization. At these carbon levels, a small reduction in the tensile properties of the materials occurs. Additional data for these materials are being obtained at different carbon levels. The data will be used to develop quantitative relationships between the tensile properties and the carbon concentration profiles, which are dependent on the exposure time, temperature, and the carbon concentration in sodium.

Specimens with 4-mil carbon penetration depths are also being creep tested at 650 and 700°C in an argon environment using dead-load testing machines. The creep strain in the specimens is measured by a linear variable differential transducer in which displacements of 0.02 mil can be accurately determined. Figure 2.20 shows the strain versus time for Type 304 stainless steel at 700°C for applied stresses of 90 and 128 MPa. Data of this type are being obtained for the three materials after exposure to sodium at different carbon levels to evaluate the start of secondary and tertiary creep stages, the minimum creep rate for different values of applied stress, and the time to rupture. The results obtained will be compared with the creep-rupture properties of annealed materials to establish quantitatively the influence of the sodium environment.

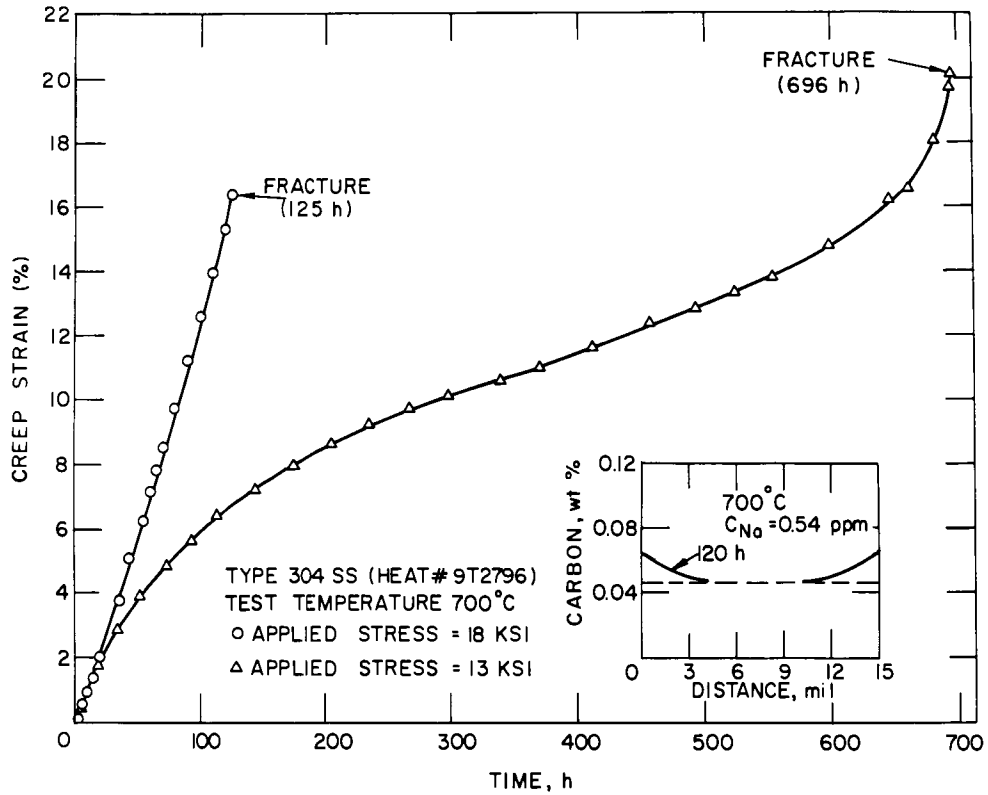

Fig. 2.20. Creep Strain vs Time for Carburized Type 304 Stainless Steel at 700°C under Applied Stresses of 90 and 128 MPa.

2.4 REFERENCES

1. Mechanical Properties Test Data for Structural Materials Quarterly Progress Report for Period Ending October 31, 1973, Oak Ridge National Laboratory, ORNL-4936, pp. 15-33.

2. S. S. Manson, G. R. Halford, and M. H. Hirschberg, "Creep-Fatigue Analysis by Strain-Range Partitioning," pp. 12-28 in Design for Elevated Temperature Environment, Am. Soc. Mechan. Eng., ASME (1971).

3. S. S. Manson, "The Challenge to Unify Treatment of High Temperature Fatigue - A Partisan Proposal Based on Strain-Range Partitioning," pp. 744-782 in Fatigue at Elevated Temperatures, Am. Soc. Testing, ASTM (1973).

4. D. R. Diercks and W. F. Burke, "Elevated-temperature True Stress-True Strain Tensile Behavior of AISI Type 304 Stainless Steel," in Elevated Temperature Properties of Austenitic Stainless Steels, Am. Soc. Mechan. Eng., ASME (1974).

5. Mechanical Properties Test Data for Structural Materials Quarterly Progress Report for Period Ending January 31, 1974, Oak Ridge National Laboratory, ORNL-4948, pp. 15-21.

6. E. W. Hart, "A Phenomenological Theory for Plastic Deformation of Polycrystalline Metals," Acta Met. 18(6), 599-610 (June 1970).

7. E. W. Hart, Che-Yu Li, H. Yamada, and G. L. Wire, "Phenomenological Theory: A Guide to Constitutive Relations and Fundamental Deformation Properties," in Constitutive Equations in Plasticity, A. Argon, Ed., to be published.

8. H. Yamada and Che-Yu Li, "Stress Relaxation and Mechanical Equation of State in Austenitic Stainless Steels," Met. Trans. 4(9), 2133-2136 (Sept 1973).

9. R. T. King, J. O. Stiegler, and G. M. Goodwin, "Properties of Thick Type 308 Stainless Steel Welds with Controlled Residual Elements," Oak Ridge National Laboratory, ORNL-TM-4206 (June 1974).

10. R. T. King, J. O. Stiegler, and G. M. Goodwin, "Creep Properties of a Type 308 Stainless Steel Pressured Vessel Weld with Controlled Residual Elements," Oak Ridge National Laboratory, ORNL-TM-4131 (May 1973).

11. C. F. Cheng, C. Y. Cheng, D. R. Diercks, and R. W. Weeks, "Low-Cycle Fatigue Behavior of Types 304 and 316 Stainless Steel at LMFBR Operating Temperature," in Fatigue at Elevated Temperatures, Am. Soc. Testing, ASTM STP 520, August 1973, pp. 355-364.

12. T. Slot, R. H. Stentz and J. T. Berling, in Manual of Low-Cycle Fatigue Testing, Am. Soc. Testing, ASTM STP 465, 1969, p. 100.

13. C. R. Brinkman and G. E. Korth, "Heat to Heat Variations in the Fatigue and Creep-Fatigue Behavior of AISI Type 304 Stainless Steel and Fatigue Behavior of Type 308 Stainless Steel Weld Material," ANCR-1097, May, 1973.

14. Mechanical Properties Test Data for Structural Materials Quarterly Progress Report for Period Ending April 30, 1974, Oak Ridge National Laboratory, ORNL-4963, pp. 18 and 20.

15. P. Shahinian, H. H. Smith, and J. R. Hawthorne, "Fatigue Crack Propagation in Stainless Steel Weldments at High Temperature," Welding J., Research Supplement, 51, 527S-532S (Nov 1972).

16. L. H. Kirschler and R. C. Andrews, Proceedings of the International Conference on Sodium Technology and Large Fast Reactor Design, Argonne National Laboratory, ANL-7520 (Part I), p. 41 (1968).

17. L. H. Kirschler, R. H. Hiltz, and S. J. Rodgers, MSA Research Corp., MSAR-70-76 (1970).

18. A Thorley and C. Tyzack, "The Carburization of Stainless Steels in Sodium Containing Carbon Impurities and Its Effect on Mechanical Properties," Effects of Environment on Material Properties in Nuclear Systems, Conf. Proc., July 1971, Brit. Nucl. Energy Soc., London (1971).

19. A. Thorley, B. Longson, and J. Prescott, "Effect of Exposure to Sodium on the Mechanical Properties and Structure of Some Ferritic, Austenitic, and High Nickel Alloys," Culcheth, TRG-Report-1909(c) (1969).

20. W. Charnock, J. E. Cordwell, J. R. Gwyther, M. R. Hobdell, P. Marshall, and I. R. McLauchlin, "The Effect of High Carbon Activity Sodium upon the Mechanical Properties of AISI 316 Stainless Steel," Intl. Conf. on Physical Metallurgy of Reactor Fuel Elements, Central Electricity Generating Board, Berkeley Nuclear Laboratories, 1973.

21. K. Natesan, T. F. Kassner, and Che-Yu Li, "Effect of Sodium on Mechanical Properties and Friction-Wear Behavior of LMFBR Materials," Reactor Technol. 15(4), 244-247 (Winter 1972-1973).

22. R. B. Snyder, K. Natesan, and T. F. Kassner, "Kinetics of the Carburization-Decarburization Process of Austenitic Stainless Steels in Sodium," J. Nucl. Mater. 50, 259-274 (1974).

23. Mechanical Properties Test Data for Structural Materials Quarterly Progress Report for Period Ending October 21, 1973, Oak Ridge National Laboratory, ORNL-4936, pp. 81-94.

24. Materials Considerations in Support of the FFTF Preliminary Safety Analysis, Report-RM9, Vol. 1, Hanford Engineering Development Laboratory, HEDL-TME 71-53 (1971).

25. D. Fahr, "Tensile Properties of Ti-modified 316 Stainless Steel," Quarterly Progress Report Irradiation Effects on Reactor Structural Materials, Feb.-April 1973, Hanford Engineering Development Laboratory, HEDL-TME 73-47 (May 1973).

3. HANFORD ENGINEERING DEVELOPMENT LABORATORY
(For Period Ending April 30, 1974)

T. T. Claudson

3.1 INTRODUCTION

The objectives of the structural materials investigation conducted at the Hanford Engineering Development Laboratory are to provide control data for the in-reactor and postirradiation tests and to provide direct and timely assistance to FFTF and Demonstration plant structural design and analysis programs. The HEDL efforts involve evaluation of mechanical properties at high strain rates, creep testing and analysis, fatigue crack growth, and tensile tests of such materials as FFTF weldments, vessel and piping, core support structures, reflectors as well as duct and cladding. Those test results and analyses appropriate to the "Structural Materials Quarterly Report" will be reported herein; however those investigations associated with irradiation effects per se will continue to be reported in the "Irradiation Damage to Reactor Structural Materials" Quarterly Report published at HEDL.

3.2 MATERIALS PERFORMANCE AND SURVEILLANCE - T. T. Claudson and J. J. Holmes

3.2.1 Subcritical Crack Growth

3.2.1.1 Accomplishments and Status

Linear-elastic fracture mechanics techniques were used to characterize the fatigue-crack propagation behavior of Incoloy 800. Two material heats were utilized representing material Grades 1 and 2 (mill-annealed and solution-annealed, respectively). The mechanical properties and chemical analyses are given in Tables 3.1 and 3.2, respectively. Since the objective of this study was to characterize the effect of temperature upon crack extension behavior, all elevated temperature tests were conducted at a constant cyclic frequency and stress ratio.

The results for the tests conducted over the range 75-1200°F are shown in Figures 3.1-3.5. Also shown are the results of Carden[1] who tested Grade 1 material at 75°F and 1200°F. It will be noted that good agreement is obtained between the results of the present study and Carden's results. Comparison

Table 3.1. Chemical Composition (Percent by Weight)

	C	Mn	Fe	S	Si	Cu	Ni	Cr	Al	Ti	B
Heat A*	.07	.86	48.01	.007	.35	.18	30.29	19.26	.28	.31	-----
Heat B**	.03	1.05	46.48	.007	.26	.16	32.44	19.25	.10	.20	.0002
Carden***	.05	.95	45.28	.007	.36	.32	31.39	20.78	.38	.46	-----

*Huntington Heat No. HH2531A; ASME SB-409, Grade 2

**Huntington Heat No. HH7531A; ASME SB-409, Grade 1

***Huntington Heat No. HH2521A; ASME SB-409, Grade 1

Table 3.2. Room Temperature Mechanical Properties

	0.2% Yield Strength	Ultimate Strength	Percent Elong.	Percent Red. Area	Hardness (R_b)	ASTM Grain Size	Condition
Heat A*	27,000 psi 18.98 kg/mm^2	76,500 psi 53.76 kg/mm^2	53.0	----	69	1.5	Hot rolled, descaled, solution annealed
Heat B**	35,500 psi 24.96 kg/mm^2	75,500 psi 53.08 kg/mm^2	48.0	72.0	71	4.5	Hot rolled, descaled, mill annealed
Carden***	42,500 psi 29.88 kg/mm^2	85,500 psi 60.12 kg/mm^2	39.0	----	76	8.0	Cold rolled, pickled, mill annealed

*Huntington Heat No. HH2531A; ASME SB-409, Grade 2; 0.5 in. plate.

**Huntington Heat No. HH7531A; ASME SB-409, Grade 1; 1.0 in. plate.

***Huntington Heat No. HH2521A; ASME SB-409, Grade 1; 0.062 in. sheet.

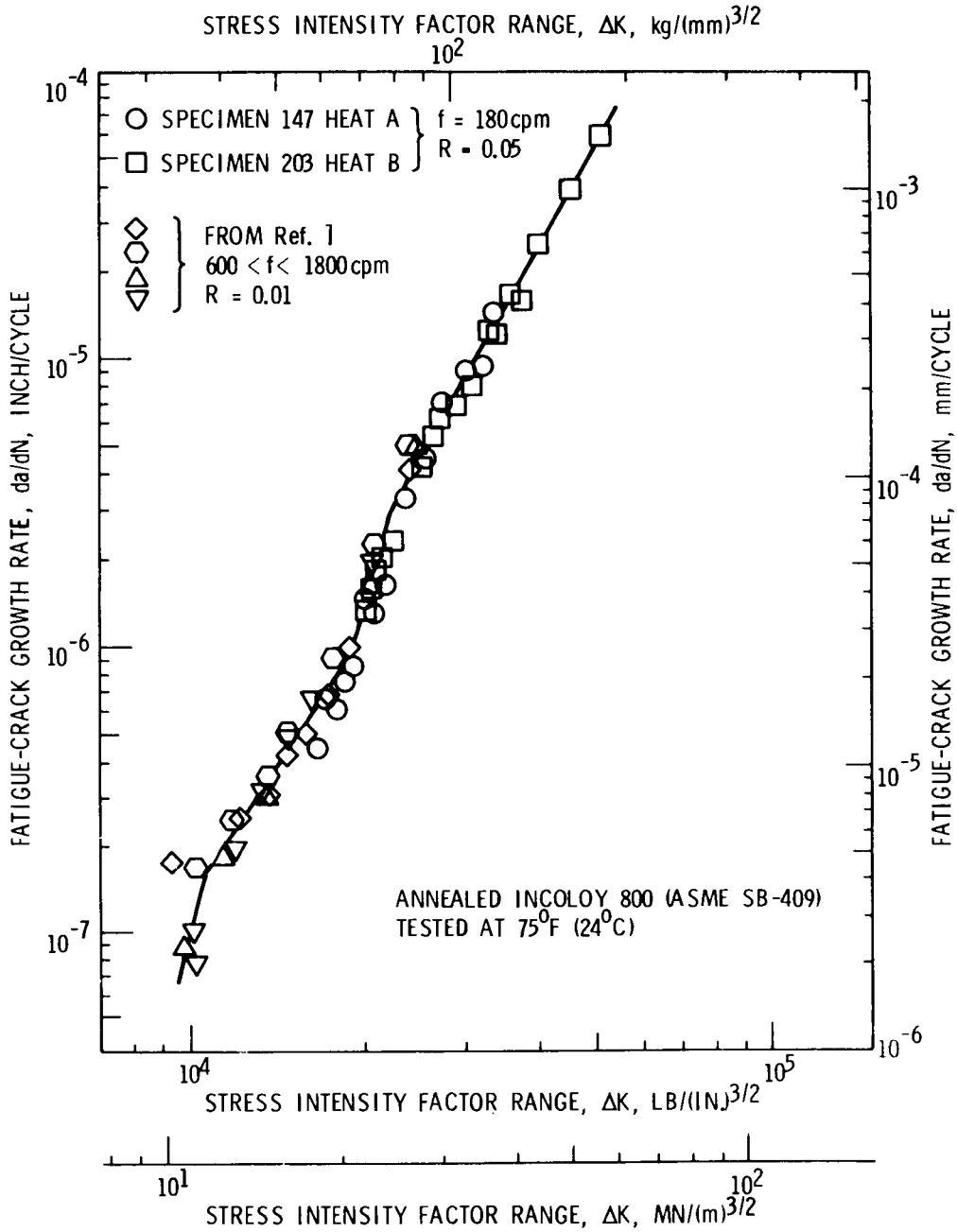

Figure 3.1. Fatigue-Crack Propagation Behavior of Incoloy 800 at 75°F (24°C).

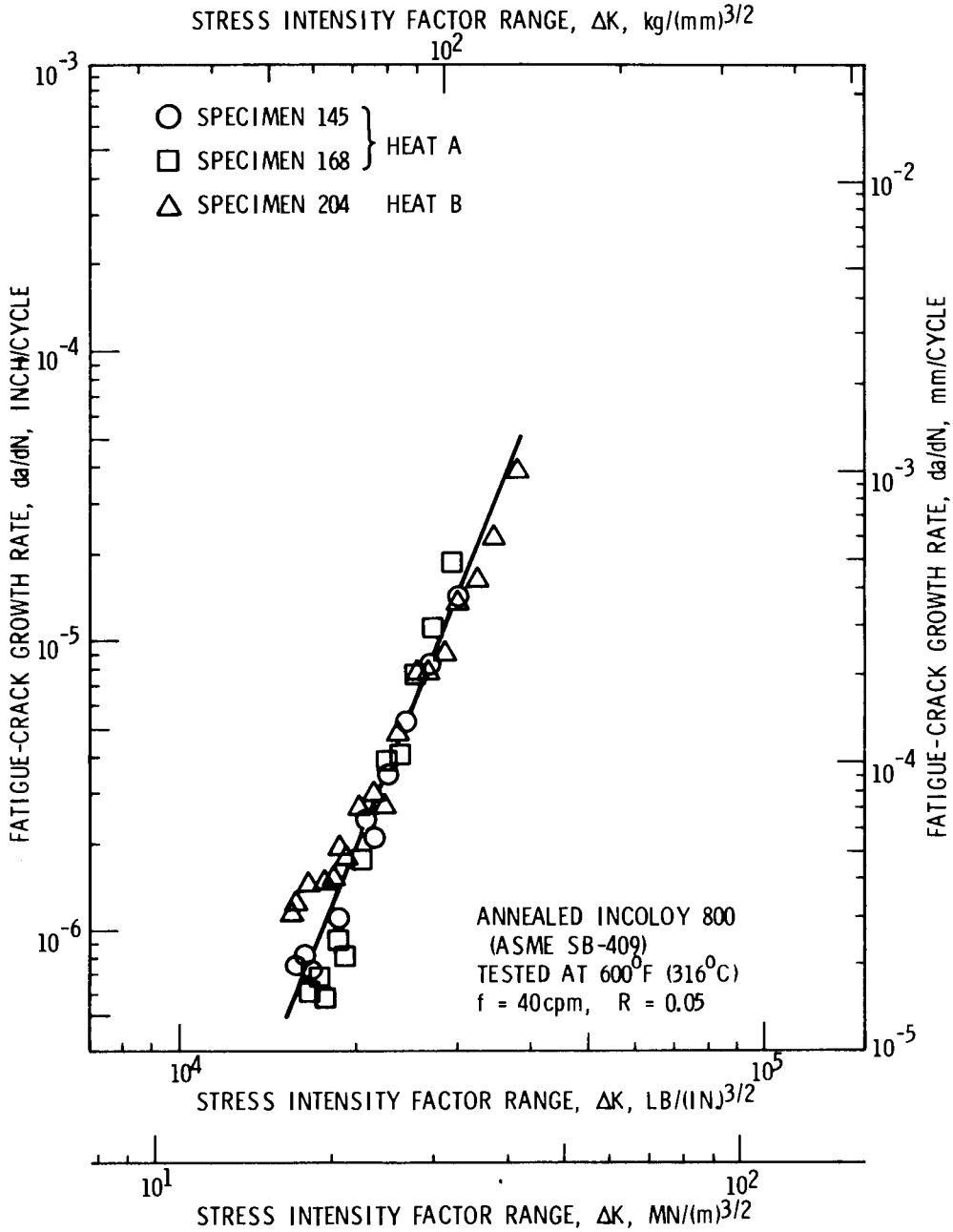

Figure 3.2. Fatigue-Crack Propagation Behavior of Incoloy 800 at 600°F (316°C).

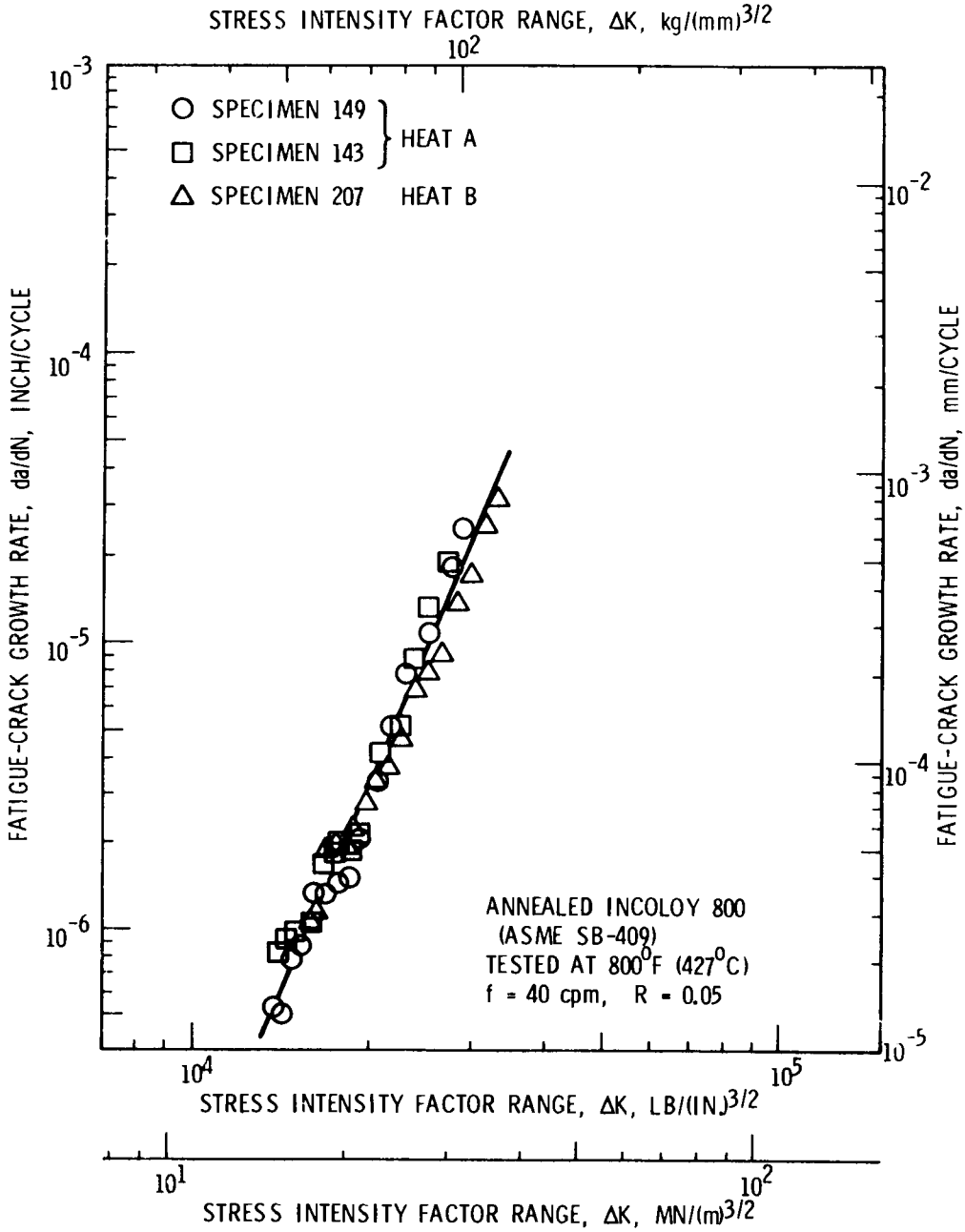

Figure 3.3. Fatigue-Crack Propagation Behavior of Incoloy 800 at 800°F (427°C).

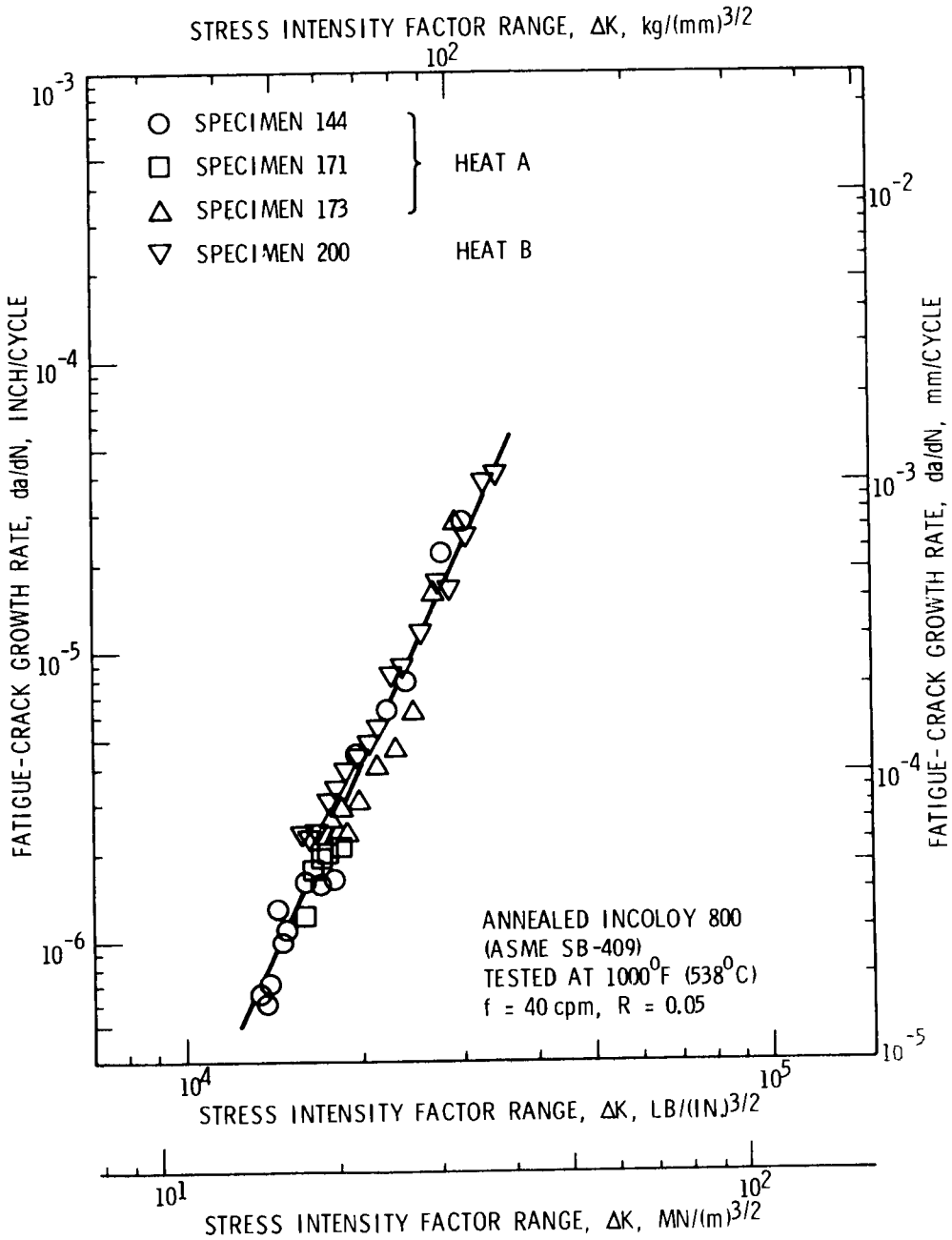

Figure 3.4. Fatigue-Crack Propagation Behavior of Incoloy 800 at 1000°F (538°C).

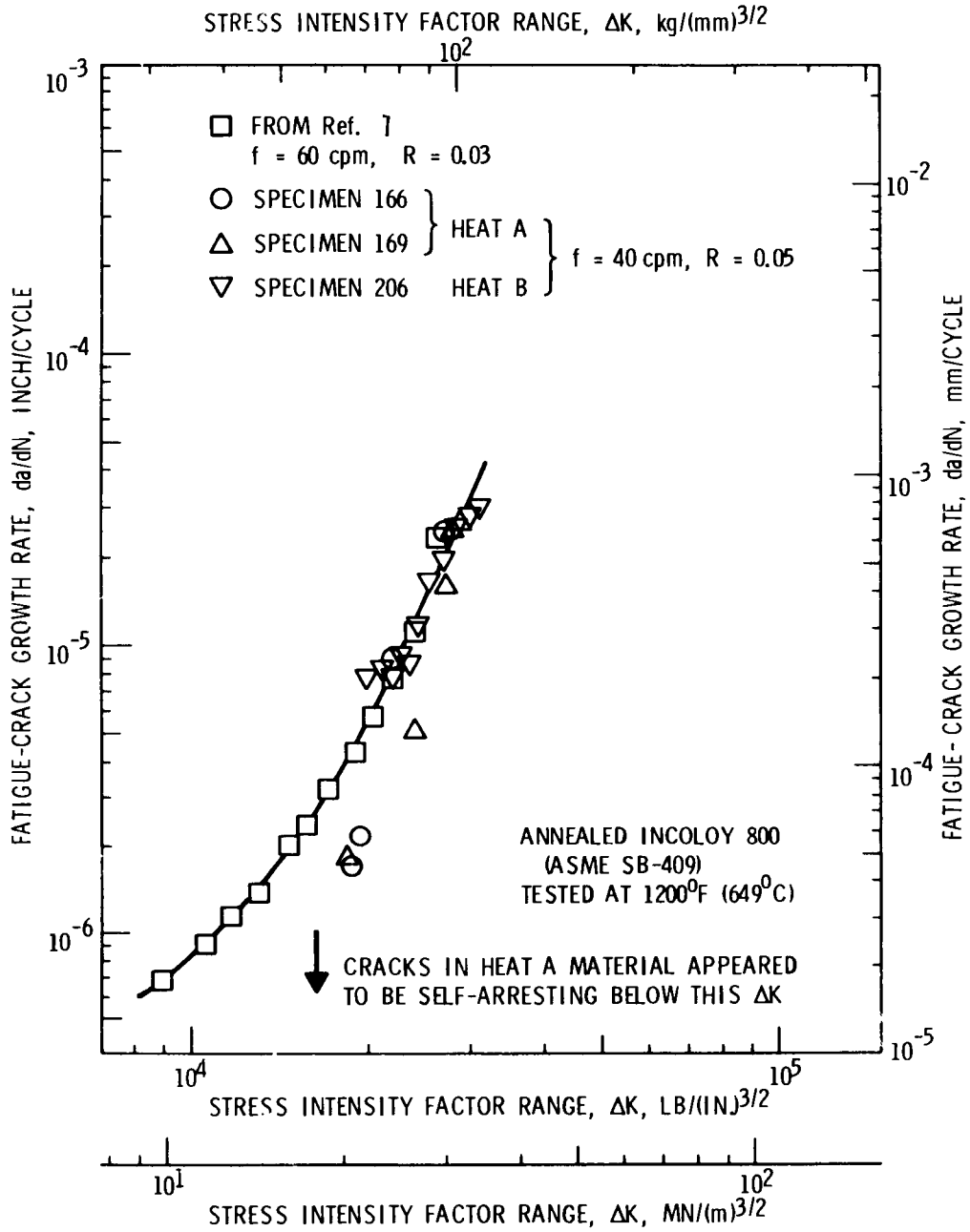

Figure 3.5. Fatigue-Crack Propagation Behavior of Incoloy 800 at 1200°F (649°C).

of Figures 3.1-3.5 reveals that the fatigue-crack growth rate increases with increasing test temperature. The increase, however, is considerably less than that observed for austenitic stainless steels tested under identical conditions.[2] For example, at $\Delta K = 20{,}000$ lb/(in)$^{3/2}$, the crack growth rate of Incoloy 800 increased by a factor of 4.1 between 75°F and 1200°F, while the crack growth of annealed Type 316 tested under identical conditions increased by a factor of 11.8 over the same temperature range.[2] The reason for this difference in behavior is not known, but is thought to be related to the superior oxidation resistance of Incoloy 800.[3]

Tests conducted on the Heat A (Grade 2) material at 1200°F suggested the possible existence of a crack growth threshold at $\Delta K \simeq 16{,}000$ lb/(in)$^{3/2}$. At this temperature, cracks loaded below this level of ΔK did not propagate, even after the application of a great many cycles and crack extension would not proceed until the loads were increased such that ΔK exceeded 16,000 lb/(in)$^{3/2}$. Sufficient testing was not done to determine if this behavior was unique to Grade 2 material, or due to some other factor, but the phenomenon deserves further study.

Two specimens were aged in an air environment at 1000°F to determine if thermal aging (i.e., the precipitation of carbides and intermetallics) had any effect on the crack growth behavior. The results of these tests, shown in Figure 3.6, show that there is a very slight tendency for crack growth rates to decrease in the aged material. This is consistent with the results for several austenitic stainless steels.[4] The decrease in crack growth rates of the aged stainless steels was attributed to a partial crack blunting and subsequent reinitiation as the crack encountered second-phase particles. Such a mechanism could also apply to the observed behavior in Incoloy 800.

3.3 HIGH STRAIN RATE EFFECTS - J. M. Steichen/R. L. Knecht, J. J. Holmes

3.3.1 Accomplishments and Status

High strain rate testing of thermally aged Type 304 stainless steel has been completed. Specimens were aged in static sodium at temperatures of 800, 1000 and 1200°F for exposure times of 1000, 3500 and 10,000 hours. Testing was performed at the aging temperatures and strain rates from 3×10^{-5} to

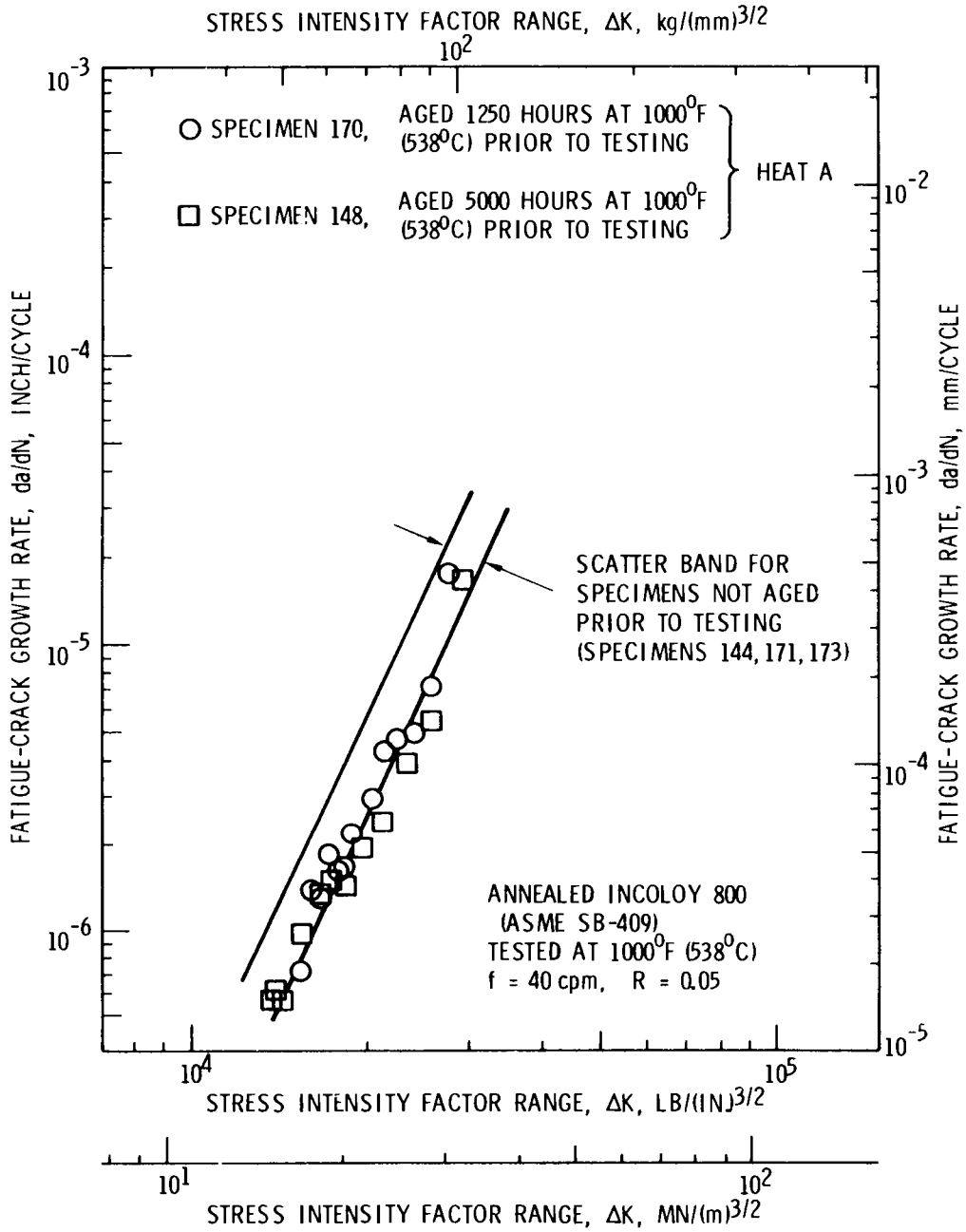

Figure 3.6. Comparison of the Fatigue-Crack Propagation Behavior of Aged and Unaged Incoloy 800 at 1000°F (538°C).

10 sec^{-1}. Data from these tests included ultimate and 0.2% yield strengths, total and uniform elongations, and reduction of area. These data are listed in Table 3.3 and illustrated in Figures 3.7-3.12.

The effect of strain rate on the ultimate and 0.2% yield stress of thermally aged Type 304 stainless steel for aging and test temperatures of 800, 1000 and 1200°F is presented in Figures 3.7 through 3.9, respectively. Included in the figures are data representing unaged behavior. No effect of thermal aging on strength properties is observed.

At aging and test temperatures of 800 and 1000°F, the ductility (total and uniform elongation) of the aged and unaged materials is essentially identical for all strain rates (Figures 3.10 and 3.11). Ductility at 1200°F is slightly influenced by thermal aging as shown in Figure 3.12. At the lowest strain rate, the total elongation of the aged material is significantly higher than the unaged material. As strain rate increases the aged material total elongation is reduced and at a rate of 10 in./in./sec it is slightly lower than the unaged material. The uniform elongation of the aged material at 1200°F is essentially identical to that of the unaged material to a rate of ∿9.91 in./in./sec and is slightly lower for higher strain rates.

3.3.2 Expected Achievements

A topical report describing the influence of thermal aging on the high strain rate tensile properties of Type 304 stainless steel will be prepared and the effect of strain rate on the tensile properties of A-286, the IVHM bolting material, will be completed.

3.4 REFERENCES

1. A. E. Carden, *A Phenomenological Analysis of the Interaction of Creep and Fatigue*, PhD Dissertation, Department of Metallurgy, University of Connecticut, 1972.
2. L. A. James, *The Effect of Elevated Temperature Upon the Fatigue-Crack Propagation Behavior of Two Austenitic Stainless Steels*, Mechanical Behavior of Materials, Vol. III, pp. 341-352, The Society of Materials Science, Japan, 1972.

Table 3.3. Tensile Properties of Thermally Aged Type 304 Stainless Steel

Aging Conditions		Test Conditions		Strength, ksi		Elongation, %		Reduction of Area, %
Temp., °F	Exposure, Hr.	Temp., °F	Strain Rate, sec^{-1}	0.2% Yield	Ultimate	Total	Uniform	
800	1000	800	3×10^{-5}	15.6	65.6	41.5	33.7	65.6
			3.5×10^{-3}	16.4	61.4	36.7	30.9	64.8
			0.1	16.7	58.9	36.4	31.2	69.6
			1.0	16.0	56.2	36.0	31.4	72.0
			10.0	21.3	59.3	36.0	30.4	74.0
800	3500	800	3×10^{-5}	14.2	64.7	41.4	37.6	65.0
			3×10^{-5}	14.3	65.3	36.3	31.8	63.4
			3.5×10^{-3}	16.3	60.7	37.0	32.2	65.0
			0.1	21.7	56.6	37.0	32.8	56.1
			10.0	20.0	57.4	34.9	29.2	68.8
800	10,000	72	3×10^{-5}	33.1	84.6	74.8	66.7	79.7
		800	3×10^{-5}	15.9	63.0	39.8	36.1	67.2
			3.5×10^{-3}	16.7	62.3	37.2	32.8	72.4
			1.0	16.5	56.3	35.8	30.6	77.8
1000	1000	1000	3×10^{-5}	15.4	56.6	37.0	31.6	64.6
			3.5×10^{-3}	18.7	50.5	36.5	30.7	71.5
			0.1	15.0	54.1	34.2	30.6	71.5
			1.0	15.6	55.4	35.2	30.1	72.4
			10.0	16.5	56.2	34.2	29.4	77.2
1000	3500	1000	3×10^{-5}	12.4	55.3	37.5	31.5	59.3
			3.5×10^{-3}	13.0	51.1	34.9	29.6	70.7
			0.1	14.4	52.6	29.9	24.5	69.6
			1.0	17.9	53.8	34.3	30.0	69.6
			10.0	18.5	52.0	30.7	25.6	69.6
1000	10,000	72	3×10^{-5}	26.2	83.4	69.8	64.2	76.2
		1000	3×10^{-5}	14.9	53.7	32.7	28.7	55.3
			3.5×10^{-3}	15.2	55.3	33.5	29.1	69.1
			1.0	16.0	53.8	33.5	28.3	69.6

Table 3.3. (Continued)

Aging Conditions		Test Conditions		Strength, ksi		Elongation, %		Reduction of
Temp., °F	Exposure, Hr.	Temp., °F	Strain Rate, sec^{-1}	0.2% Yield	Ultimate	Total	Uniform	Area, %
1200	1000	1200	3×10^{-5}	13.3	34.6	47.1	20.8	50.4
			3.5×10^{-3}	11.9	45.2	31.8	26.1	65.9
			0.1	13.0	48.9	31.9	26.8	61.8
			1.0	14.9	47.4	32.4	26.4	68.3
			10.0	16.8	48.8	33.4	26.4	67.5
1200	3500	1200	3×10^{-5}	11.1	34.0	46.4	21.0	54.9
			3.5×10^{-3}	10.6	42.7	31.9	26.3	61.8
			0.1	12.3	44.7	30.8	25.8	61.5
			1.0	14.0	46.3	30.7	25.6	64.2
			10.0	16.7	47.1	31.4	25.9	63.9
1200	10,000	72	3×10^{-5}	26.2	86.3	63.6	59.4	64.2
		1200	3×10^{-5}	12.8	34.3	46.8	22.3	65.0
			3.5×10^{-3}	12.2	44.0	28.4	23.6	55.3
			1.0	13.8	44.4	26.5	21.8	66.8

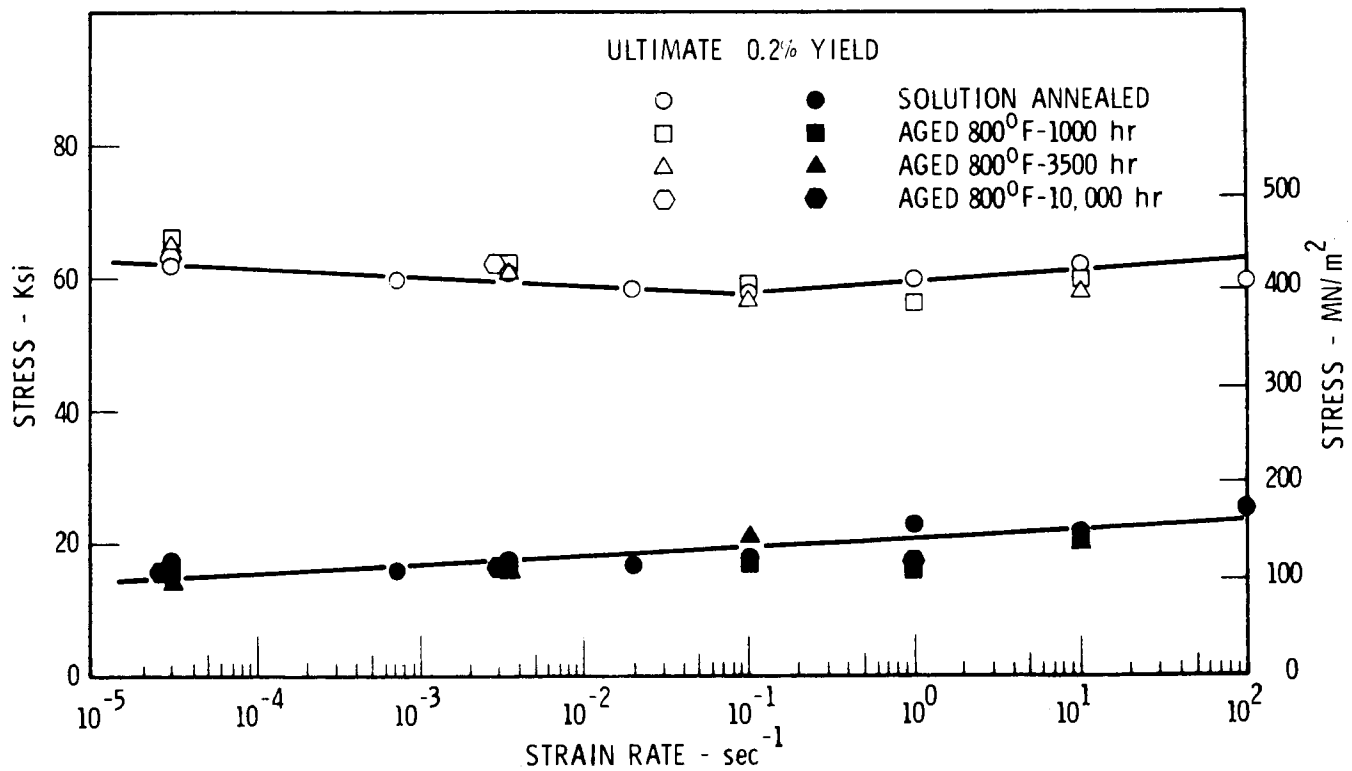

Figure 3.7. Effect of Strain Rate on Strength Properties of Thermally Aged Type 304 Stainless Steel at 800°F.

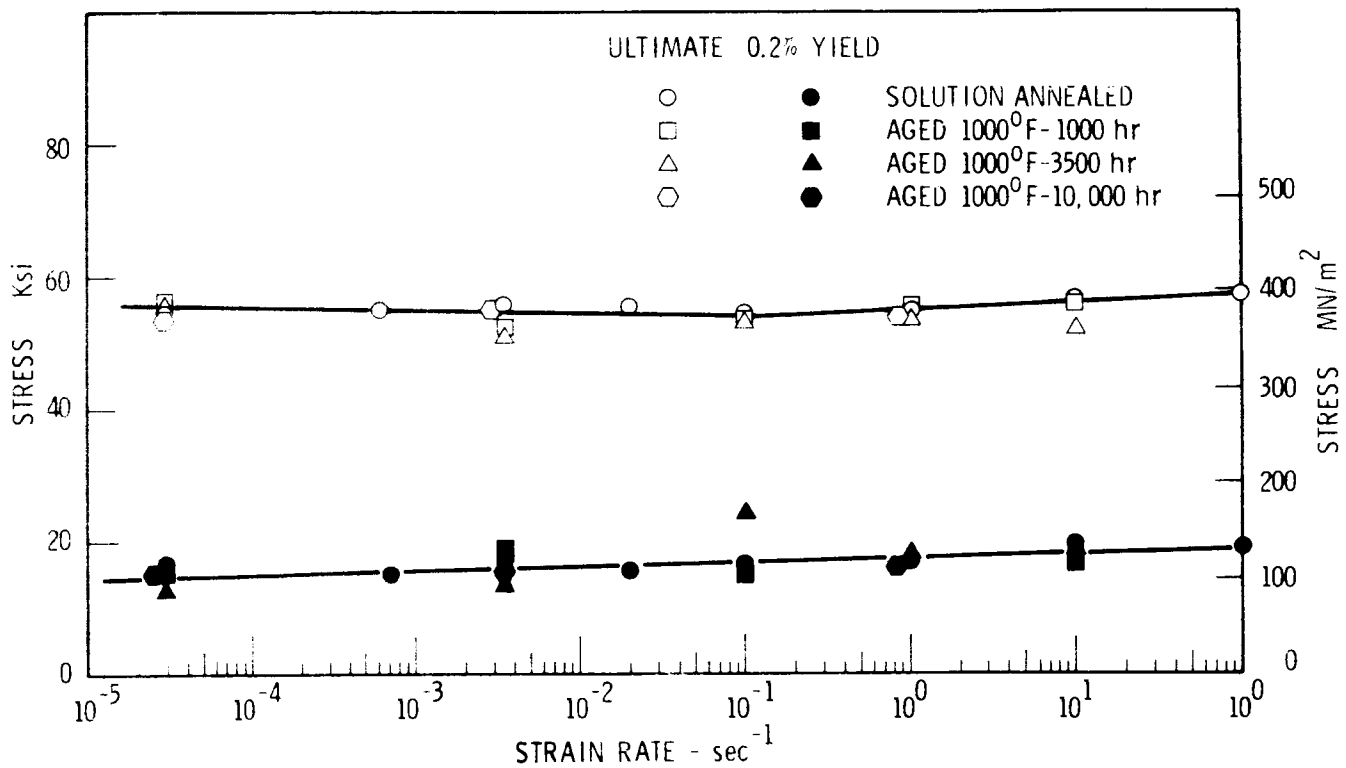

Figure 3.8. Effect of Strain Rate on Strength Properties of Thermally Aged Type 304 Stainless Steel at 1000°F.

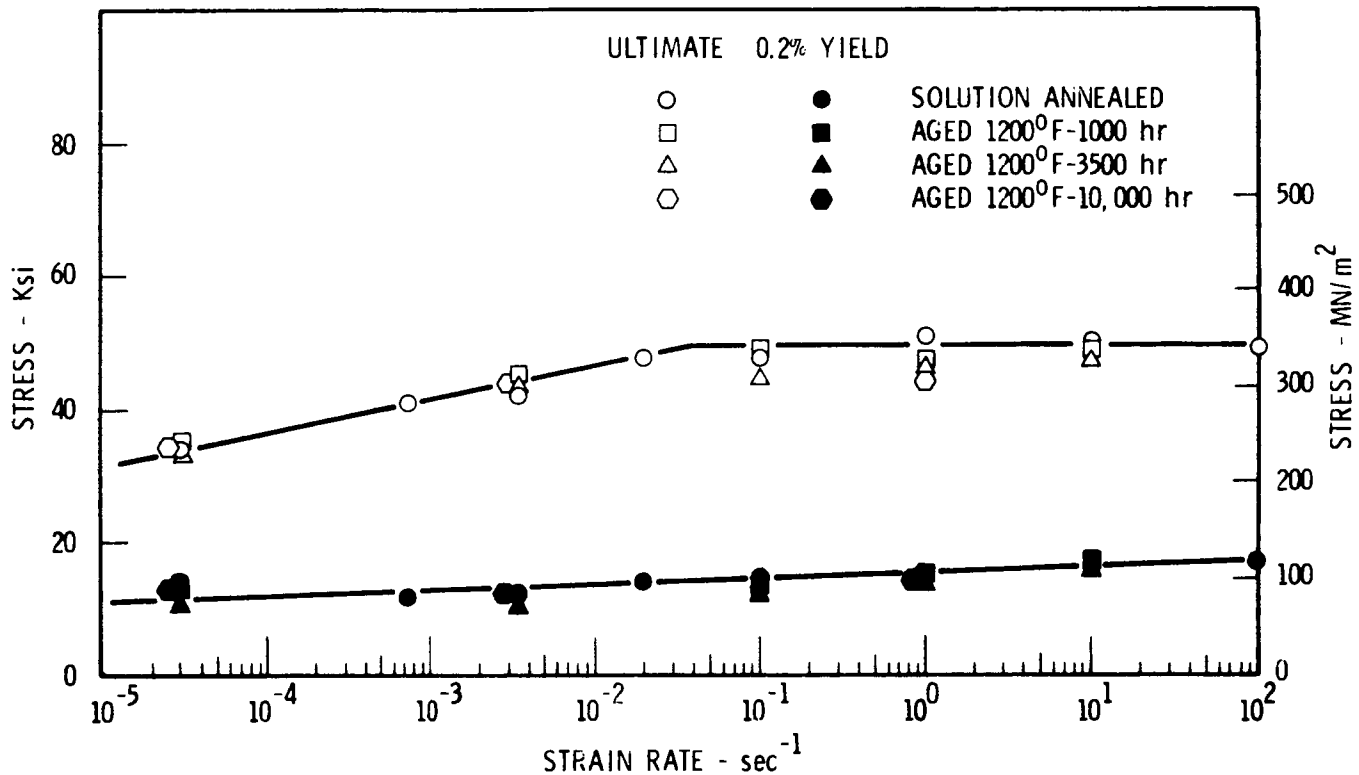

Figure 3.9. Effect of Strain Rate on Strength Properties of Thermally Aged Type 304 Stainless Steel at 1200°F.

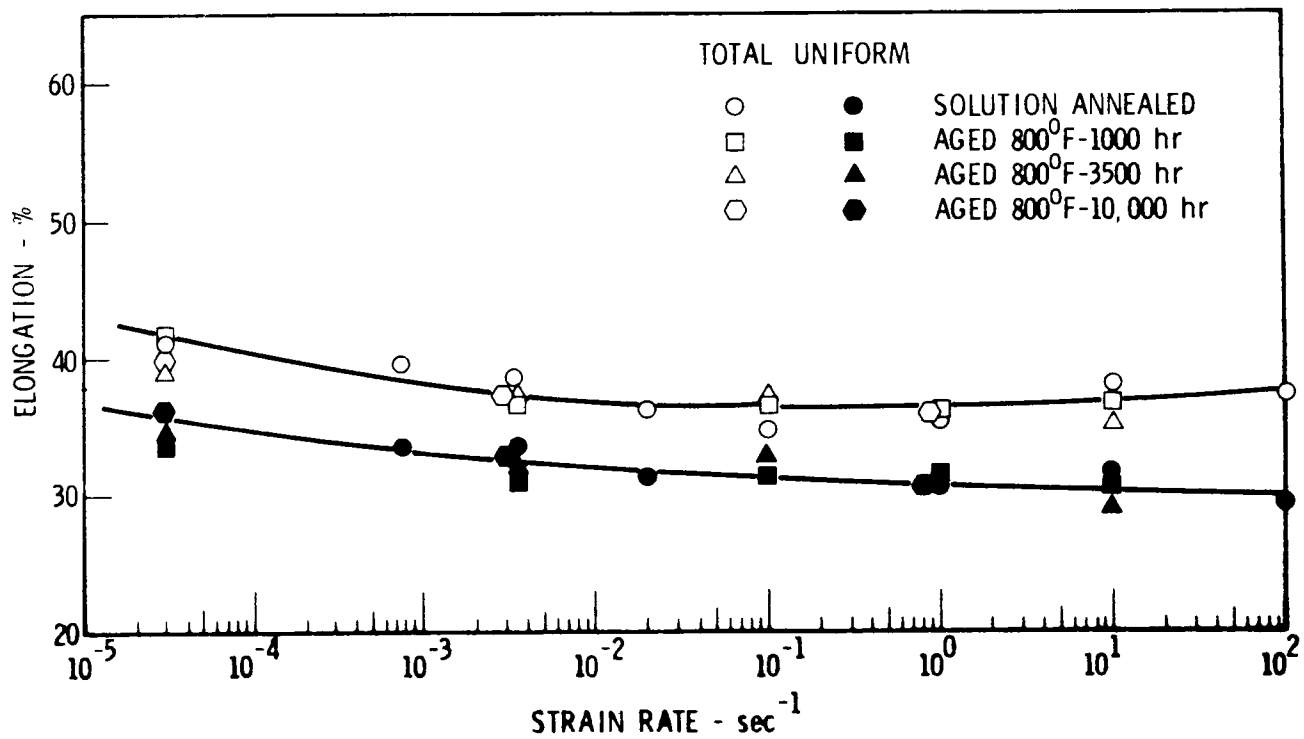

Figure 3.10. Effect of Strain Rate on Ductility of Thermally Aged Type 304 Stainless Steel at 800°F.

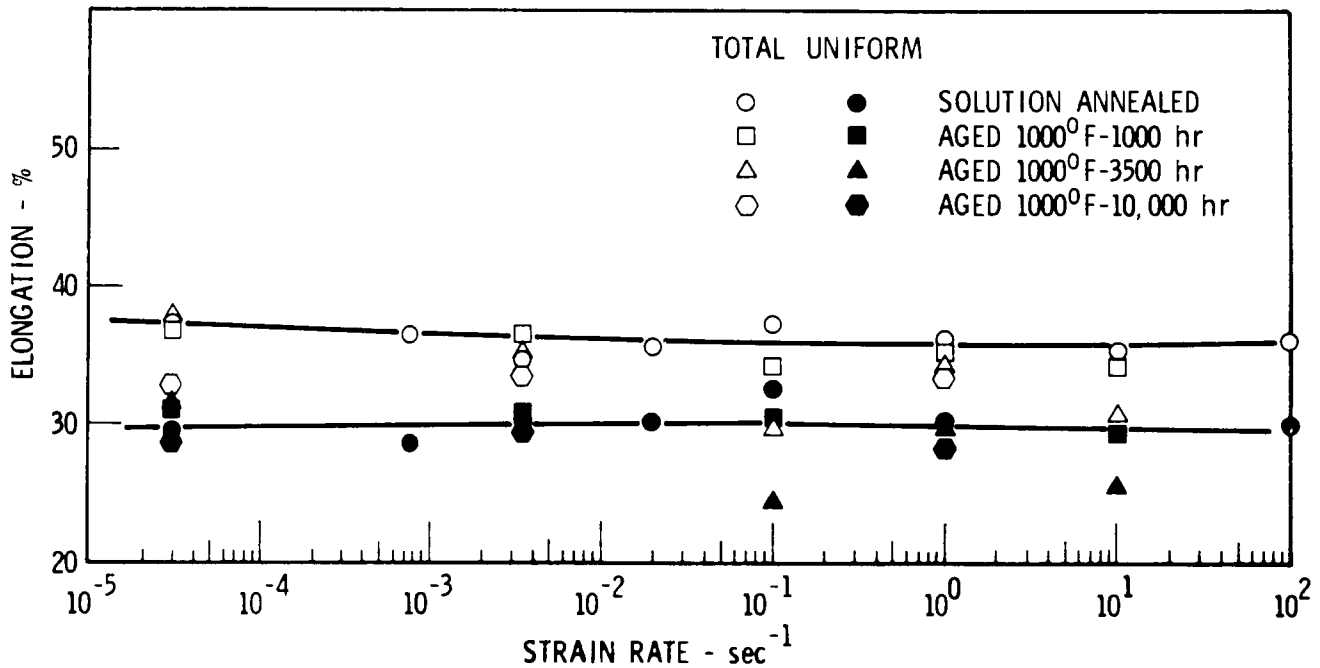

Figure 3.11. Effect of Strain Rate on Ductility of Thermally Aged Type 304 Stainless Steel at 1000°F.

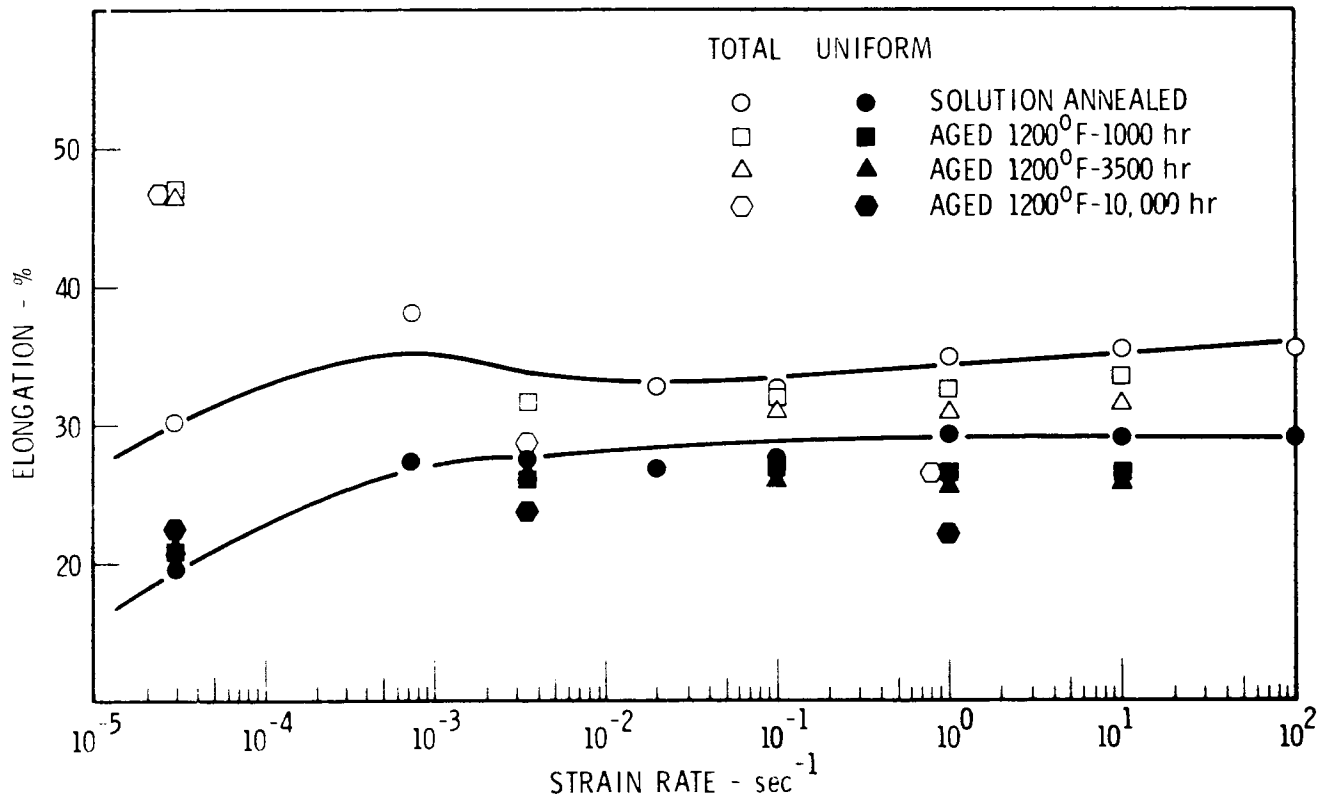

Figure 3.12. Effect of Strain Rate on Ductility of Thermally Aged Type 304 Stainless Steel at 1200°F.

3. H. L. Eiselstein and E. N. Skinner, *The Effect of Composition on the Scaling of Iron-Chromium-Nickel Alloys Subjected to Cyclic Temperature Conditions*, ASTM STP-165, pp. 162-172, 1954.

4. L. A. James, *Effect of Thermal Aging Upon the Fatigue-Crack Propagation Behavior of Austenitic Stainless Steels*, Metallurgical Transactions, Vol. 5, No. 4, 1974.

3. HANDFORD ENGINEERING DEVELOPMENT LABORATORY
(For Period Ending July 31, 1974)

T. T. Claudson

3.1 INTRODUCTION

The objectives of the structural materials investigation conducted at the Hanford Engineering Development Laboratory are to provide control data for the in-reactor and postirradiation tests and to provide direct and timely assistance to FFTF and Demonstration plant structural design and analysis programs. The HEDL efforts involve evaluation of mechanical properties at high strain rates, creep testing and analysis, fatigue crack growth, and tensile tests of such materials as FFTF weldments, vessel and piping, core support structures, reflectors as well as duct and cladding. Those test results and analyses appropriate to the "Structural Materials Quarterly Report" will be reported herein; however those investigations associated with irradiation effects per se will continue to be reported in the "Irradiation Damage to Reactor Structural Materials" Quarterly Report published at HEDL.

3.2 IRRADIATION DAMAGE TO REACTOR METALS - T. T. Claudson and J. J. Holmes

3.2.1 Low Temperature Creep of 20% Cold Worked Type 316 Stainless Steel

3.2.1.1 Objective

The objectives of this work are: (1) to accurately measure thermal creep in 20% cold worked Type 316 stainless steel for comparison with in-reactor creep results, and (2) to further demonstrate the application of microwave extensometers for high precision creep strain measurements.

3.2.1.2 Accomplishments and Status

3.2.1.2.1 Scope of Work. A constant-load creep test was performed on 20% cold worked Type 316 stainless steel at 850°F under a stress of 20,000 psi using a high precision microwave extensometer to measure strain. Details of specimen and extensometer design were described previously.[1]

The specimen was manufactured from the same heat of steel employed in an earlier in-reactor experiment,[2] but the grain size in the present specimen is ASTM 6 or an average grain intercept of 40 microns, compared to a grain size of ASTM 7 (average grain intercept 25 microns) for the in-reactor test material.

The specimen was heated to 800°F in about 75 hours, was held at approximately 800°F for 175 hours, and then heated to 850°F and held for 15 hours prior to applying the test load. Temperature control during the test was within ± 0.5°F. The test environment was a gas mixture of 94% helium - 6% hydrogen, employed to prevent oxidation of the pure copper linings in the microwave sensors.

Each microwave sensor of the averaging extensometer was calibrated separately at room temperature using a precision micrometer. Calibration displacement was correlated with sensor frequency using a third degree polynomial in frequency. For one sensor, the standard error for the calibration displacement was 12.9 microinches and the maximum deviation was 25.4 microinches. For the other sensor, the standard error and maximum deviation were 19 and 37 microinches, respectively. The accuracy of the calibration micrometer was not better than 20 microinches. The measured specimen gage length at room temperature was 2.9997 inches, so the extensometer qualifies as ASTM Class A. All strains were computed based on the room temperature specimen gage length and sensor calibrations.

3.2.1.2.2 Results. The specimen was loaded in increments of about 2000 psi, and the deformation was totally elastic, as shown in Figure 1. The experimental value of Young's modulus was 24.5×10^6 psi, in good agreement with reported values for Type 316 stainless steel.[3]

Time-dependent creep deformation measurements are presented in Figure 2. These data were fit to a fourth degree polynomial in $t^{0.15}$, and the standard error of the estimate of creep strain was 1×10^{-6}. Essentially identical results were obtained with polynomials of degree five and six. The polynomial relation was differentiated to obtain creep rate and the results are shown in Figure 3. Creep rate decreases by almost three orders of magnitude over the 1000-hour test, and there is no indication of approach to a minimum or steady-state creep rate. Creep strains

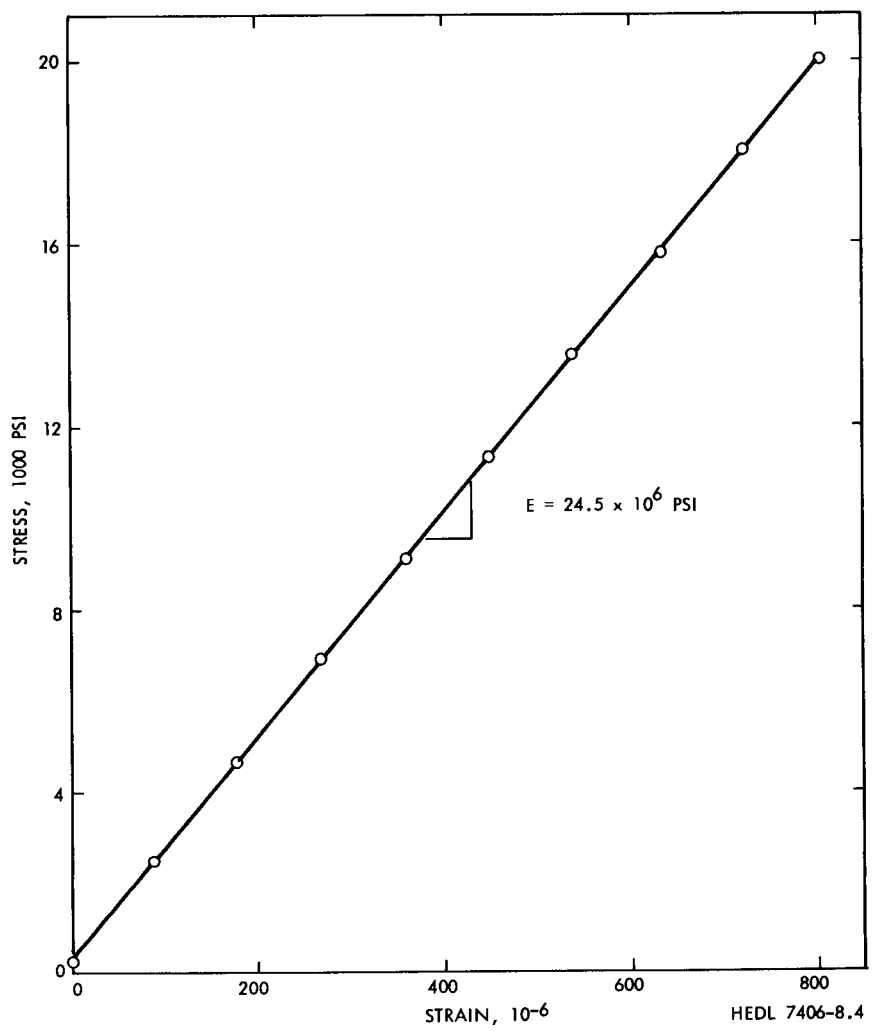

Fig. 3.1. Elastic loading of 20% C.W. 316 stainless steel at 850°F.

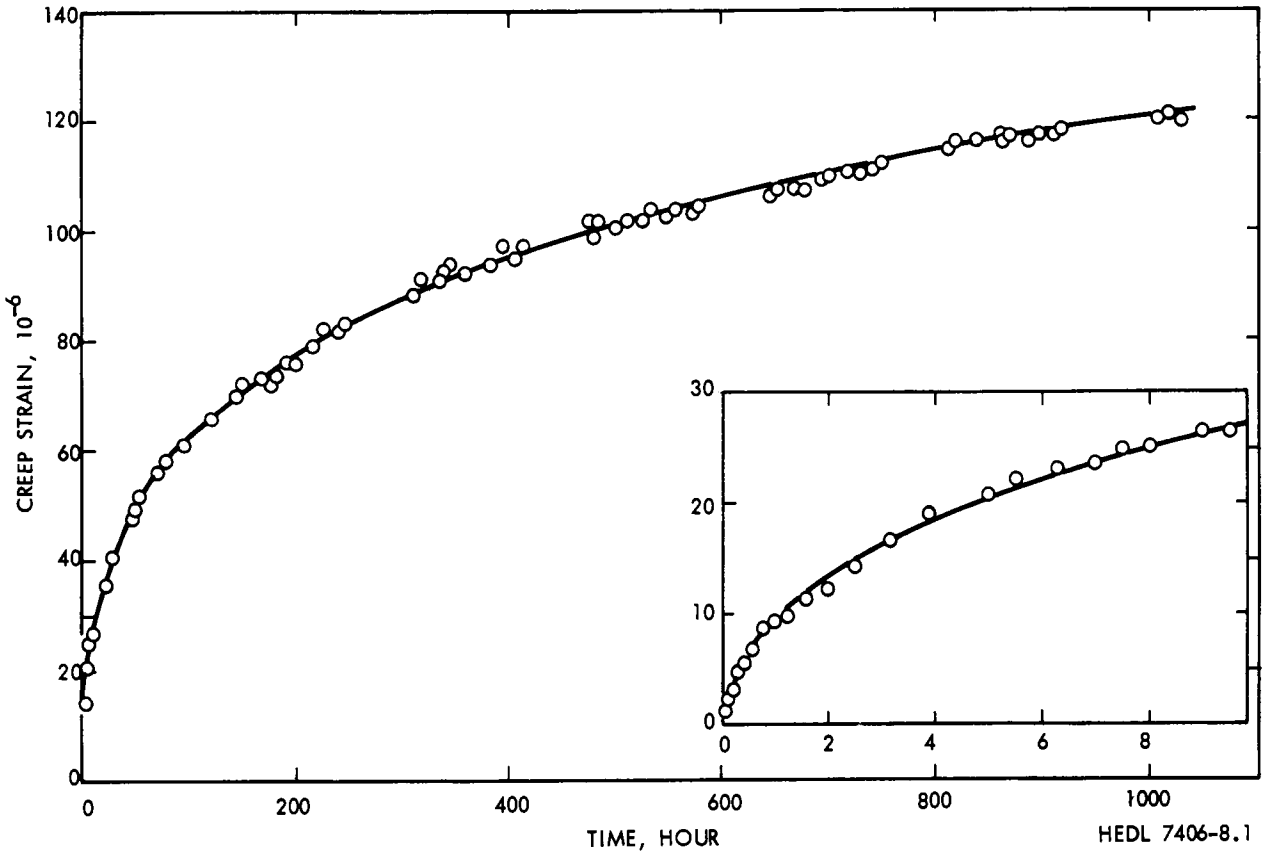

Fig. 3.2. Creep curve for 20% C.W. 316 stainless steel at 850°F/20,000 psi.

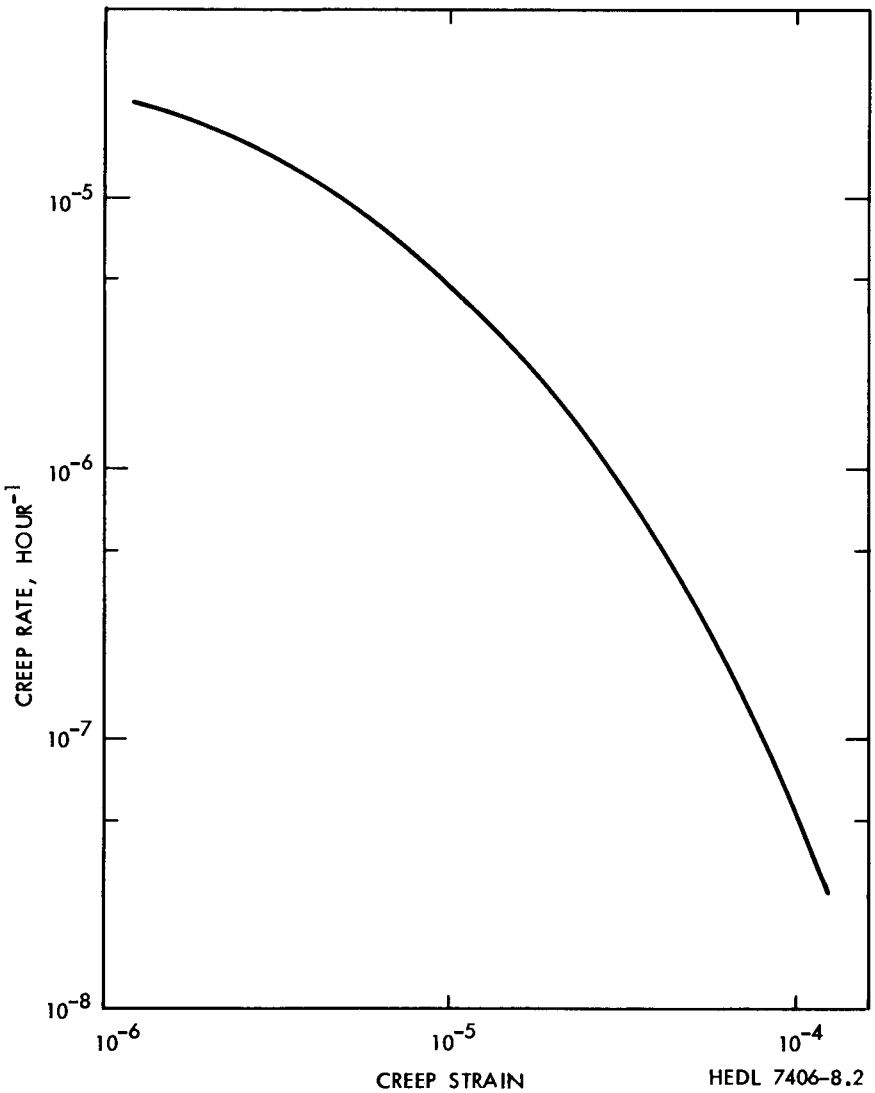

Fig. 3.3. Creep rate as a function of creep strain in 20% C.W. 316 stainless steel at 850°F/20,000 psi.

measured in an in-reactor (EBR-II) test[2] under the same conditions were about seven times larger than strains reported here, as shown in Figure 4.

At 1031 hours, the specimen was unloaded to a stress of 220 psi. The measured elastic contraction agreed with the elastic loading strain to within 6×10^{-6}. Initial measurements indicate significant time-dependent strain recovery in the unloaded condition, and these results will be presented in future reports.

3.2.1.2.3 Evaluation of Results. Several factors affect the accuracy of the strain measurements reported here. First, of course, is the calibration procedure, which was described earlier. The microwave sensors were calibrated at room temperature, but were then used at 850°F in the creep test. The potential error associated with this difference between calibration temperature and operation temperature was estimated from the theory relating microwave frequency, sensor dimensions and mode of excitation; it was found that the ratio of strain values based on room temperature calibration to strain values based on 850°F calibration should be about 1.006. Small changes in sensor radius were detected during the creep test by monitoring a mode frequency which depends only on sensor radius. However, these sensor radius changes in themselves affect the frequency of the mode which is sensitive to length changes, and therefore introduce an additional error in reported strains. The measured radius changes and the associated correction to axial strain as computed from the theoretical relation between resonant frequency and sensor dimensions are shown in Figure 5. These changes in sensor dimensions may result from reaction between hydrogen from the test atmosphere and dissolved oxygen in the OFHC copper liner of the sensor, but they are much smaller than the effects observed for impure copper liners.[1]

Several analytical representations were examined in formulating a quantitative description of the strain-time data. For the low temperature and stress and the short time of this test, steady-state creep was not expected to contribute significantly to the observed strains, and this was confirmed by the polynomial representation (see Figure 3). Therefore, the following analytical forms were considered in describing the creep strain (ε_c) data:

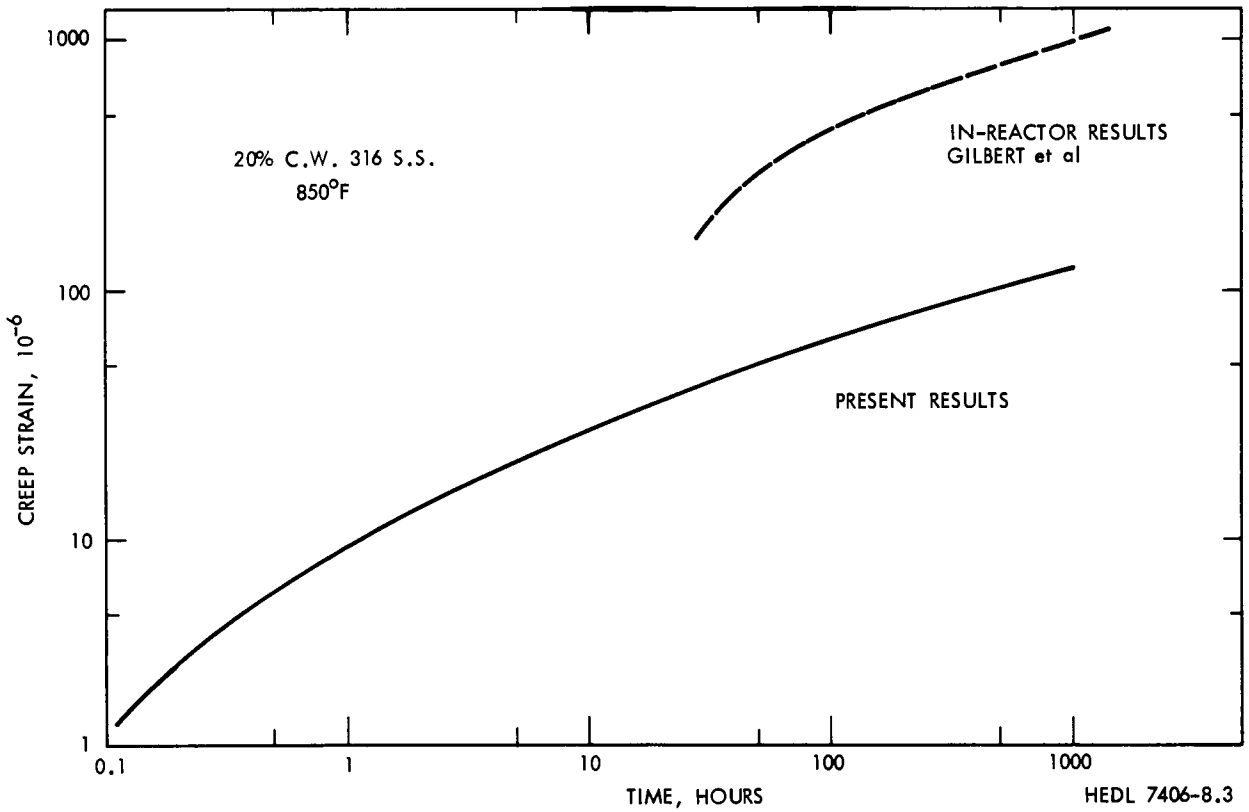

Fig. 3.4. Comparison of laboratory creep test with in-reactor creep test.

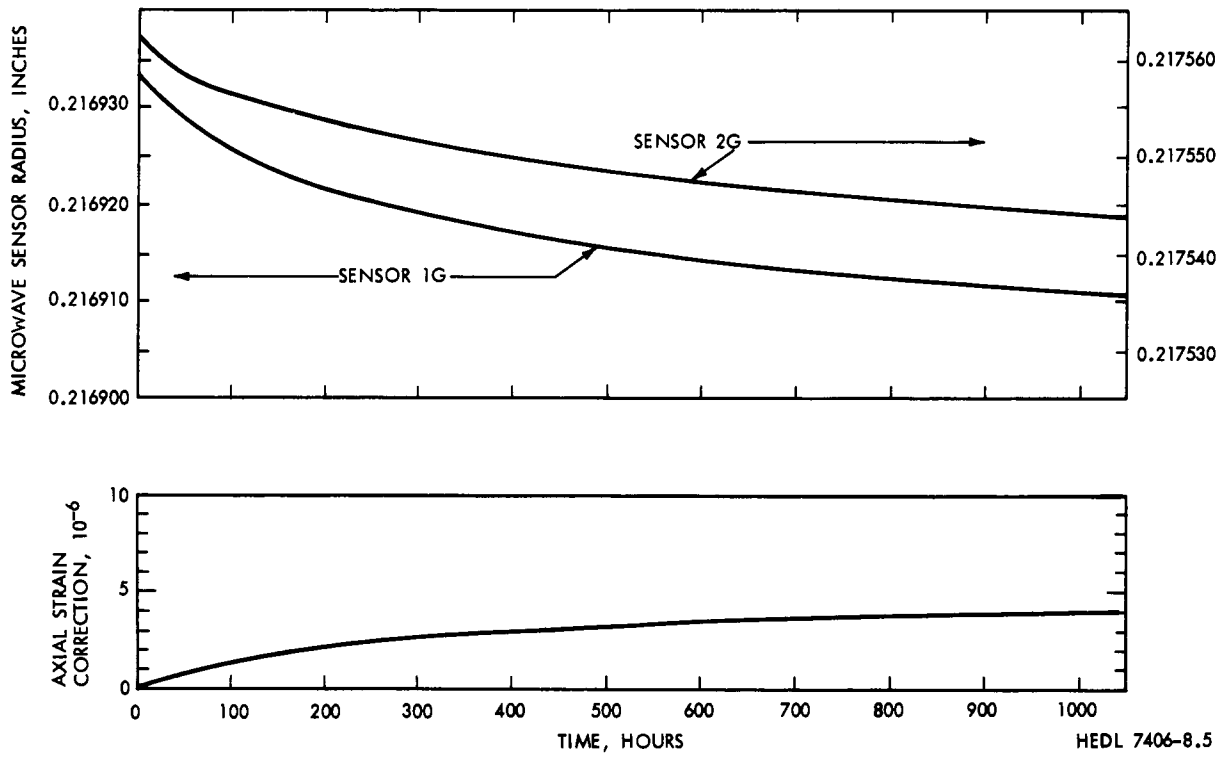

Fig. 3.5. Variation of microwave sensor radius during creep test and associated axial strain correction.

$$\varepsilon_c = At^m \quad (3.1)$$

$$\varepsilon_c = \varepsilon_o + At^m \quad (3.2)$$

$$\varepsilon_c = A + B \ln t \quad (3.3)$$

$$\varepsilon_c = B \ln (1 + t) \quad (3.4)$$

$$\varepsilon_c = B \ln (1 + ct) \quad (3.5)$$

$$\varepsilon_c = A (1 - e^{-Bt}) \quad (3.6)$$

$$\varepsilon_c = t/(A + Bt) \quad (3.7)$$

$$\varepsilon_c = t/(A + Bt^m) \quad (3.8)$$

None of these representations were completely satisfactory in describing the experimental data, and the polynomial representation described earlier was selected as the best description.

3.2.1.2.4 Conclusions And/Or Recommendations. Thermal creep strain in 20% cold worked Type 316 stainless steel at 850°F and 20,000 psi is small, reaching a value of 1.2×10^{-4} in 1000 hours. Even at these low strain levels, the course of creep deformation can be followed in detail using microwave extensometry. Creep strain measured in the present experiment is substantially smaller than in-reactor creep strain determined under the same test conditions.

3.2.1.3 Expected Achievements

Results of stress changed (unloading and reloading) on creep behavior will be obtained during the next reporting period.

3.3 MATERIALS PERFORMANCE AND SURVEILLANCE - T. T. Claudson and J. J. Holmes

3.3.1 FFTF Component Materials Evaluation

3.3.1.1 Objective

The objective of this program is to determine the mechanical properties of FTR component materials for anticipated service conditions. Included as an integral part of the program is the influence of both thermal history

and fast neutron irradiation on observed behavior. Results of this work are used for design confirmation, operations support of FFTF and for optimizing materials selection and application for future LMFBRs.

3.3.1.2 Accomplishments and Status

The creep rupture properties of actual FTR primary piping (316H stainless steel, ∿ 28-inch diameter) have been determined. Tests were performed on three heats of material at temperatures of 1050, 1200 and 1400°F and at stress levels to produce rupture in times to 2500 hours. Preliminary results from these tests are presented herein.

The Type 316H stainless steel FTR 28-inch diameter primary pipe was formed by the Rollmet process[4] followed by a final anneal at 1850°F for 45 minutes and then force air cooled. Three heats of piping material were tested. The chemical composition and tensile properties of these heats have been reported previously.[5]

All testing was performed in argon within recommended ASTM practice.

3.3.1.2.1 Results. Preliminary results of creep rupture tests at the three test temperatures for three heats of piping material are listed in Table 3.1 and illustrated in Figures 6-9. In Figure 6, stress versus rupture life for specimens fabricated from the longitudinal forming direction of the pipe for the three heats and the transverse direction for one heat (Heat 55320) are presented. A linear relationship between log stress and log rupture time is observed. All three heats of material (including the transverse orientation on Heat 55320) exhibit essentially the same stress dependence on rupture life indicating very consistent properties between the three heats. Similar behavior is observed in Figure 7 where log stress versus log minimum creep rate is presented.

The ductility (total elongation) of the subject materials for the various temperatures and rupture lives is illustrated in Figure 8. At 1050°F total elongation slightly decreases with increasing rupture life. At the higher test temperatures (1200 and 1400°F) an opposite trend is observed since ductility increases with rupture life. All three heats of material exhibit similar ductility over the temperature-rupture time range

Table 3.1. Creep Rupture Properties of FTR Type 316H Stainless Steel Primary Piping

Heat No.	Temp., °F	Stress, ksi	Min. Creep Rate in/in/hr	Rupture Life, hr.	Elongation at Fracture, %
55320	1050	65	3.2×10^{-3}	23.4	42.9
		60	9.5×10^{-4}	91.5	34.9
		50	2.7×10^{-4}	360.5	27.3
		45	4.3×10^{-5}	2,483.2	28.3
55320-Trans.	1050	62	1.2×10^{-3}	33.8	41.3
		48	1.7×10^{-4}	502.6	22.0
55318	1050	60	1.1×10^{-3}	67.3	32.5
55319	1050	60	1.9×10^{-3}	60.5	38.9
		48	1.0×10^{-4}	> 512	> 24.0
55320	1200	40	7.7×10^{-3}	30.3	47.2
		34	1.8×10^{-3}	120.6	51.2
		30	3.9×10^{-4}	448.8	55.8
		26	2.1×10^{-4}	970.0	61.5
		24	9.4×10^{-5}	2,132.6	59.5
55320-Trans.	1200	35	2.9×10^{-3}	73.2	48.9
		29	3.9×10^{-4}	529.5	46.6
55318	1200	35	3.1×10^{-3}	76.9	47.7
		30	5.7×10^{-4}	290.5	51.1
55319	1400	35	2.6×10^{-3}	88.8	40.0
		30	4.5×10^{-4}	367.6	51.8
55320	1400	20	8.5×10^{-3}	19.5	68.2
		15	2.0×10^{-3}	121.5	67.7
		12	4.8×10^{-4}	548.1	> 69.5
55320-Trans.	1400	14	1.0×10^{-3}	222.7	74.0
55318	1400	14	1.6×10^{-3}	196.2	74.7
55319	1400	14	1.4×10^{-3}	222.3	80.0

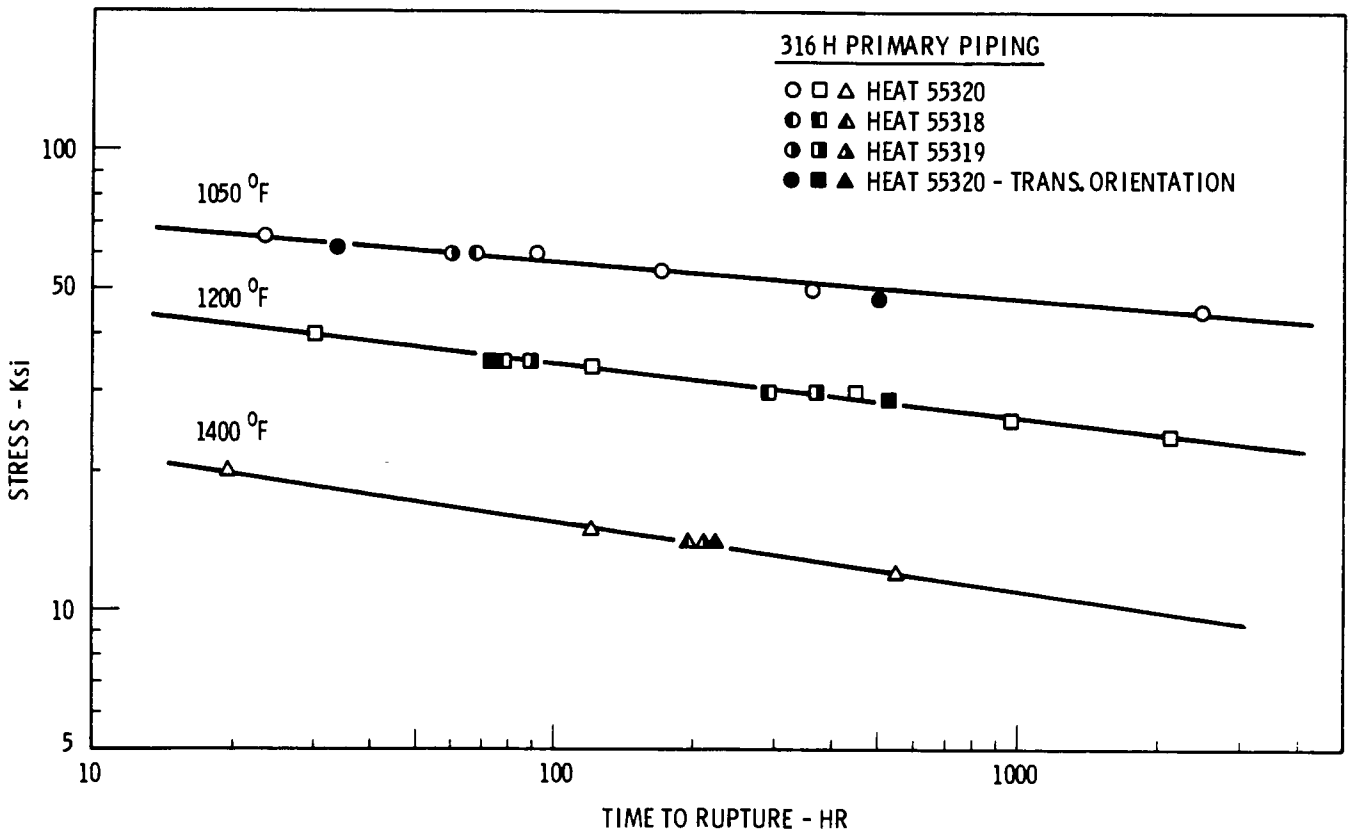

Fig. 3.6. Stress rupture behavior of 316H FTR primary piping.

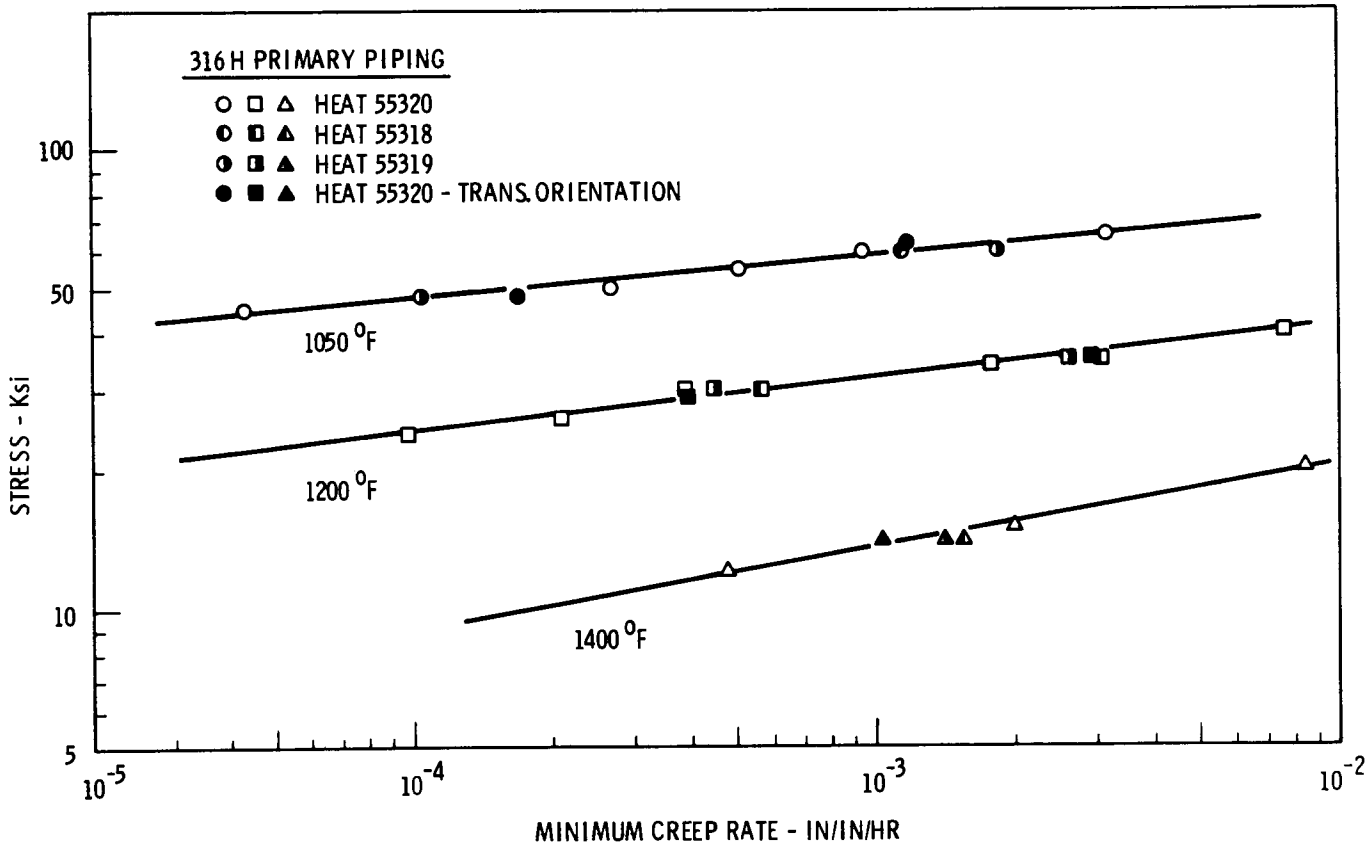

Fig. 3.7. Stress versus minimum creep rate for 316H FTR primary piping.

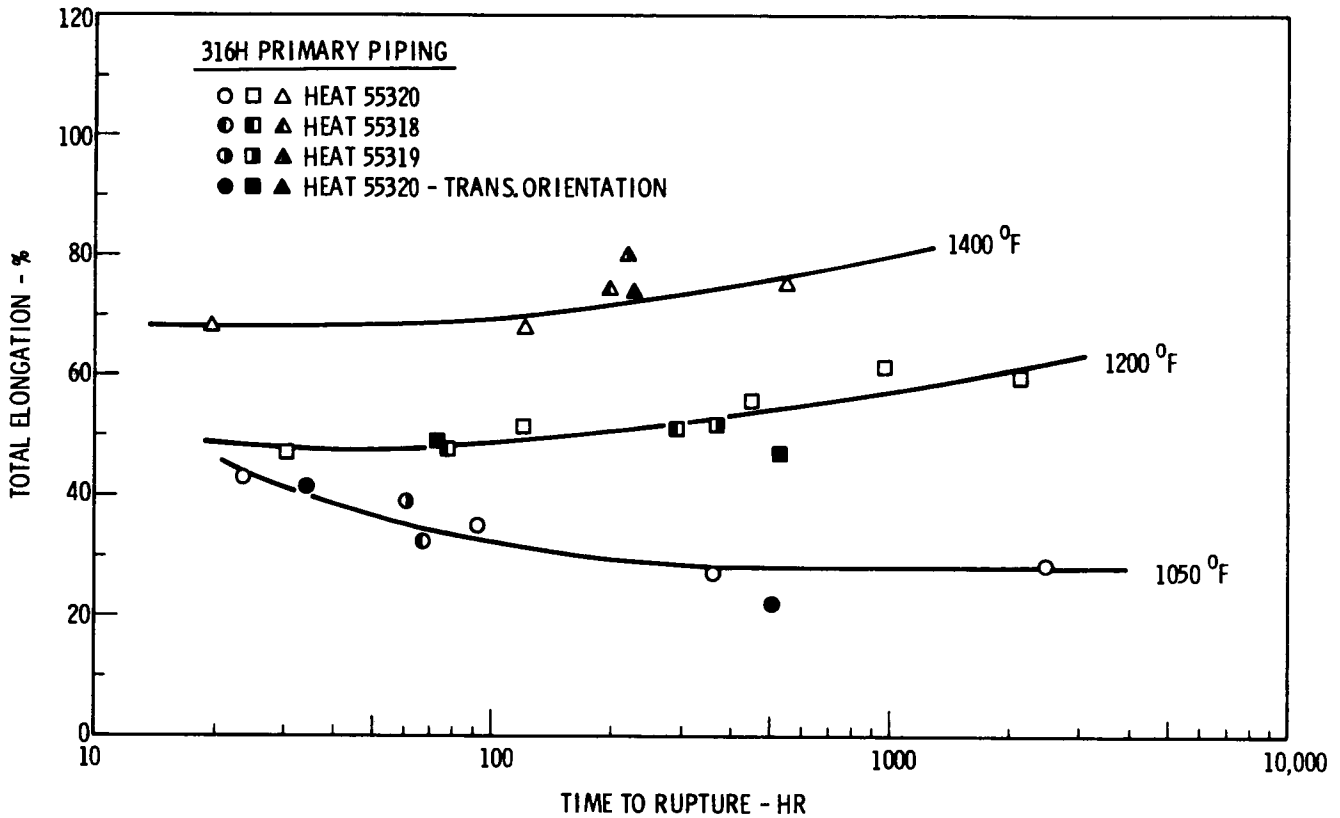

Fig. 3.8. Rupture ductility of 316H FTR primary piping.

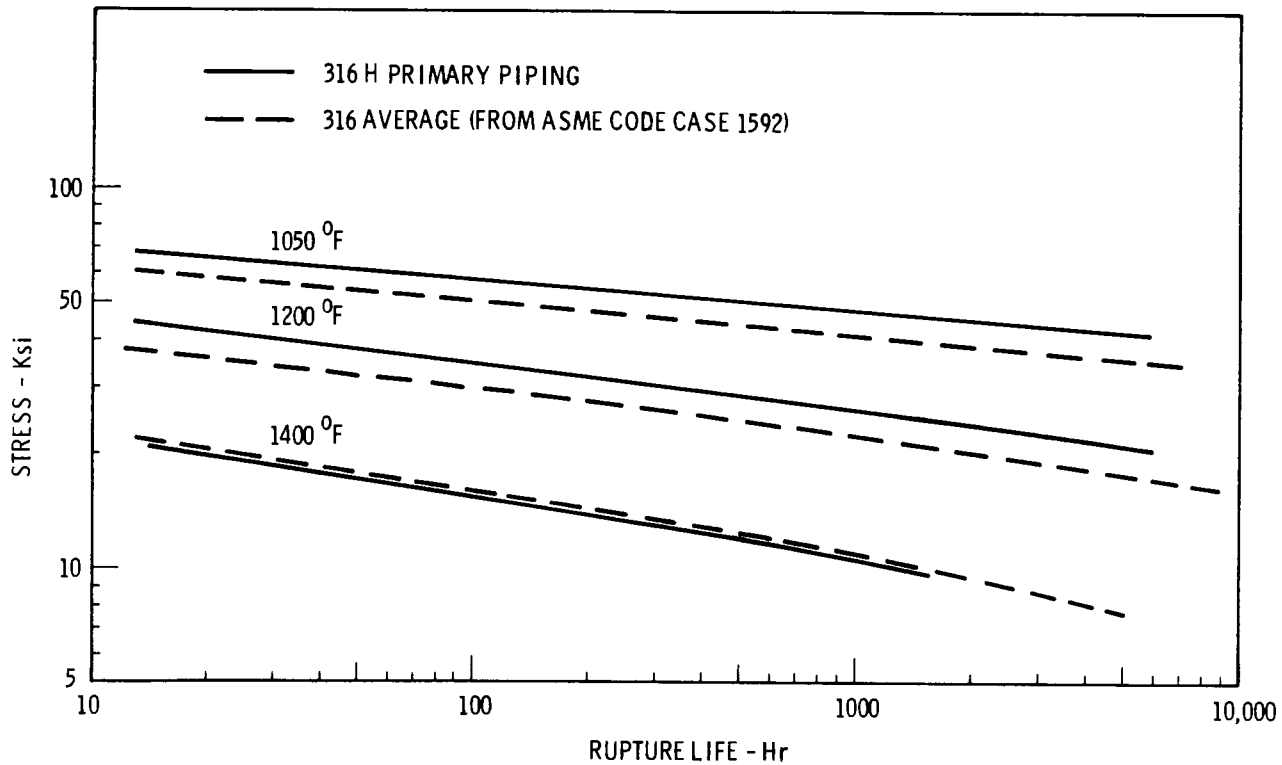

Fig. 3.9. Comparison of stress rupture behavior of FTR 316H primary piping to ASME Code Case 1592.

of this study. Also, little effect of specimen orientation is observed.

To provide an indication of the quality of the piping material, stress rupture properties were compared to those obtained on other heats of material (ASME Code Case 1592). As shown in Figure 9, the piping material exhibits higher stress rupture behavior for temperatures of 1050 and 1200°F and slightly lower behavior at a temperature of 1400°F. The stress dependence on rupture life for the piping material parallels that of ASME Code Case 1592 for all three test temperatures. A direct comparison between the stress rupture ductility of the piping material and that of other Type 316 stainless steel cannot be made since large variations in ductility were observed between previous studies. However, inspection of ductility data indicates the piping material has greater ductility than the average of the other materials.

3.3.2 Subcritical Crack Growth

3.3.2.1 Objective

The objectives of this study are to determine the subcritical crack growth properties of FFTF/LMFBR structural materials for various operating environments, and to perform fatigue failure analyses for the vessel, primary coolant boundary components and other FFTF structures.

3.3.2.2 Accomplishments and Status

Cast austenitic stainless steels are employed in a number of structural applications (e.g., core support structures, valve bodies, pump housings and impellers, etc.) in FFTF/CRBRP designs. Some of these components will be subjected to loadings in service that are cyclic in nature, and knowledge of the fatigue-crack growth behavior of cast stainless steels is necessary for design and safety analyses. Therefore, the present study characterized the effect of temperature upon the fatigue-crack growth behavior of one cast austenitic stainless steel: ASTM SA-351, Grade CF8 (procured to RDT M4-2T).

The specimens employed were of the ASTM "Compact Specimen" design, and had the planar dimensions corresponding to a one-inch thick specimen. The thickness was, however, approximately 0.51 inch. Two orientations of

the crack, relative to the casting, were tested, and these were designated "A" and "B". The crack propagation direction in orientation "A" was perpendicular to that of orientation "B". Tests were conducted on an MTS testing machine using load as the control parameter. A sinusoidal waveform was employed, and the stress ratio R was 0.05 for all tests. A cyclic frequency of 40 cpm was used for all tests except at room temperature where frequency would not be expected to be an important parameter. Tests were conducted in an air-circulating furnace at 75, 600, 800, 1000 and 1200°F.

The experimental results are shown in Figures 10-14. Also given, for comparison, are scatter bands for annealed Types 304 and/or 316 stainless steel tested under similar conditions. Several observations may be made concerning these results: 1) The fatigue-crack growth rate at a given value of ΔK increases with increasing test temperature. This is consistent with the behavior of other austenitic steels tested in an air environment. 2) In general, the crack growth rates in the cast stainless steel were slightly lower than those in annealed plate material tested under similar conditions. This is consistent with observations on Types 304/308[9] and 316/316[10] weldments which also represented crack growth in a cast structure. 3) There does not appear to be any observable difference between the crack growth behavior for orientations "A" and "B". Another observation, not apparent in Figures 10-14, is that there was more crack branching observed (microscopically and macroscopically) in the cast material than normally observed in plate material. This is consistent with observations on crack growth in weldments,[9,10] and may account for the slightly lower crack growth rates in the castings, relative to plate material.

3.4 CLADDING DEVELOPMENT AND PROCESS - L. H. Rice and J. J. Holmes

3.4.1 Fuel and Cladding Characterization

3.4.1.1 Objective

The program objective is to define the mechanical properties, metallurgical structure, chemistry and metallurgical stability of prototypic and production FTR fuel cladding purchased under the cladding development

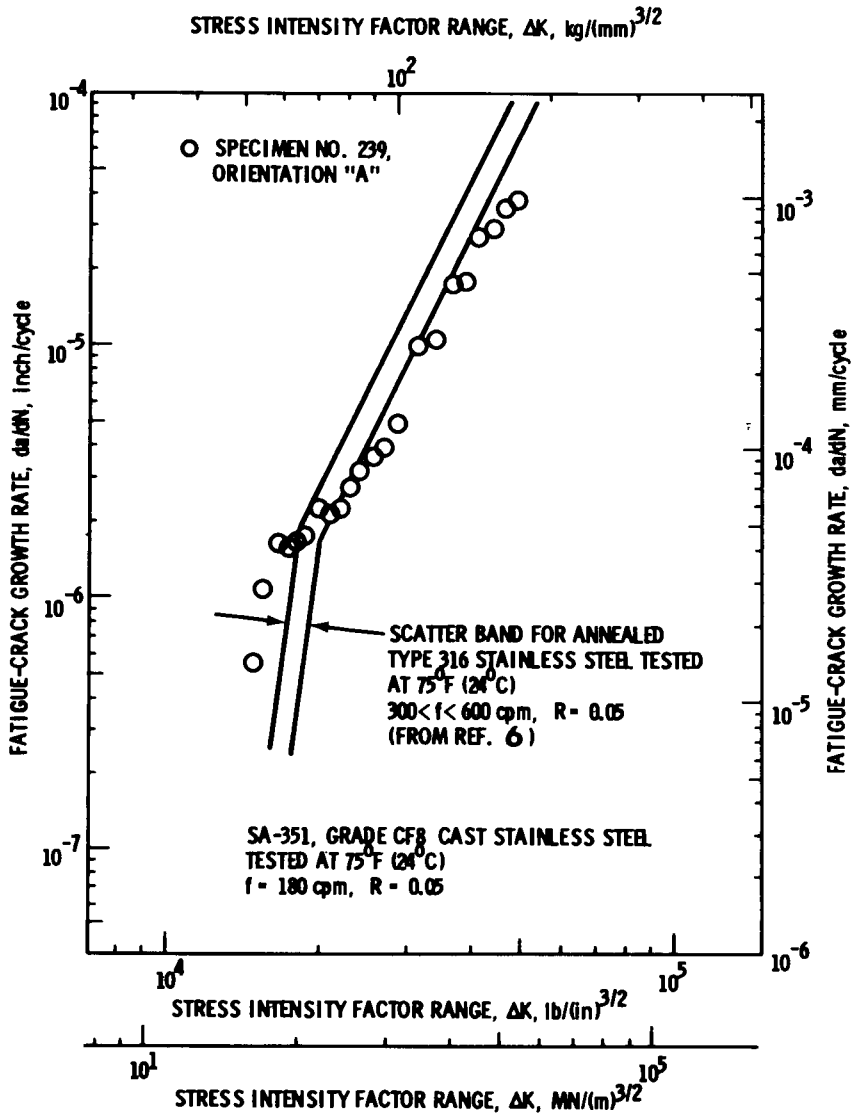

Fig. 3.10. Fatigue crack propagation behavior of ASME SA-351 Grade CF8 cast stainless steel at 75°F (24°C).

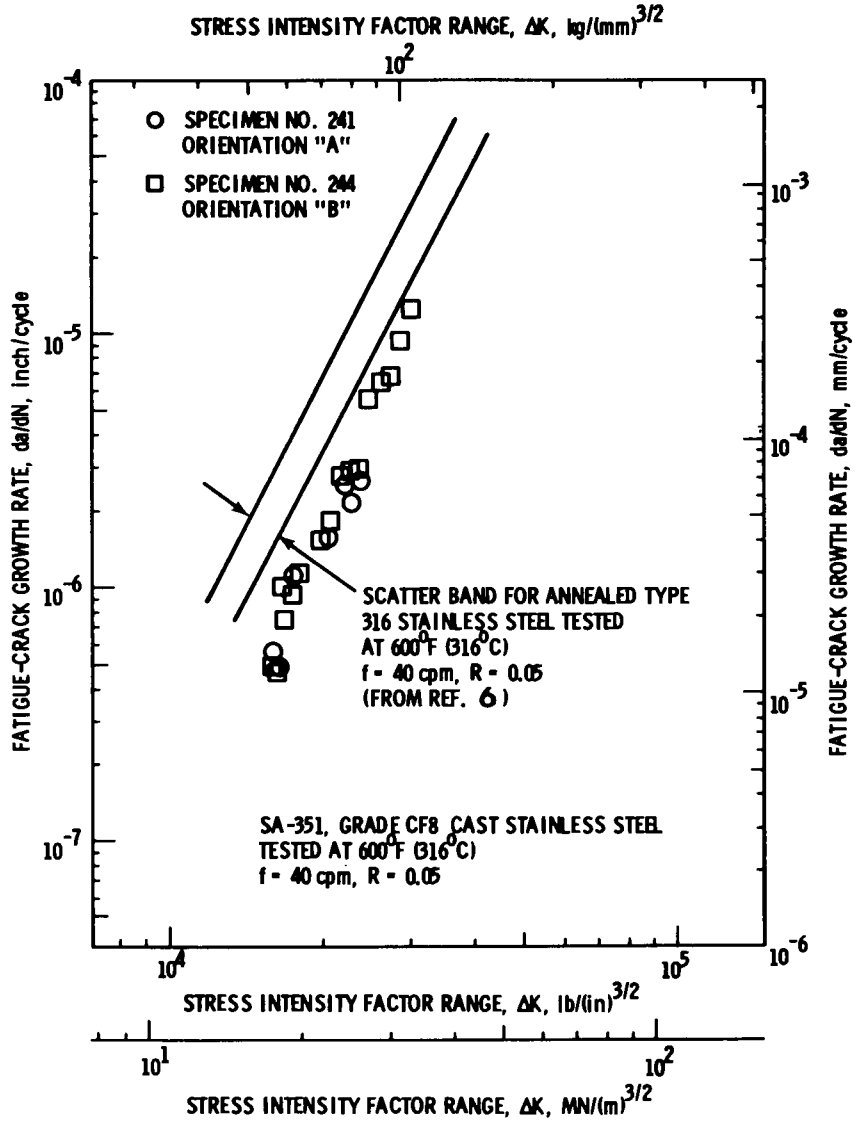

Fig. 3.11. Fatigue crack propagation behavior of ASME SA-351 Grade CF8 cast stainless steel at 600°F (316°C).

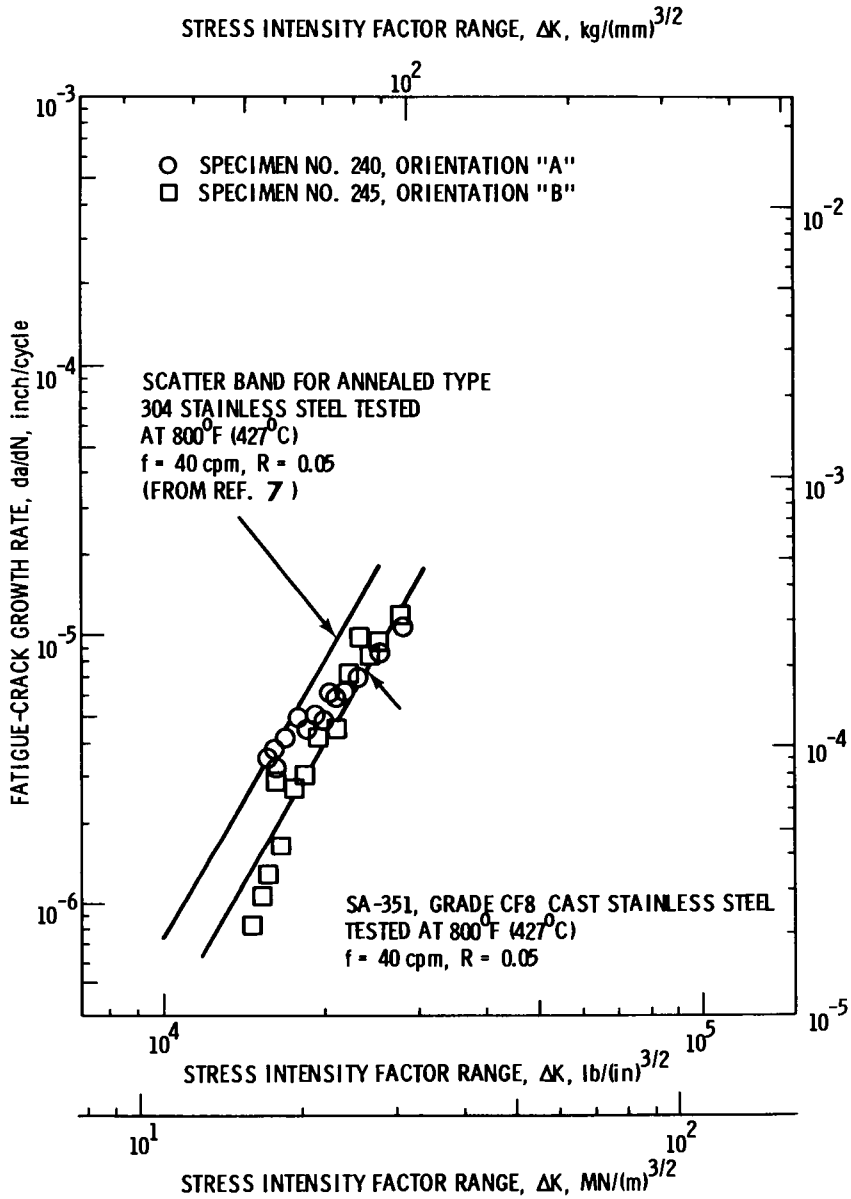

Fig. 3.12. Fatigue crack propagation behavior of ASME SA-351 Grade CF8 cast stainless steel at 800°F (427°C).

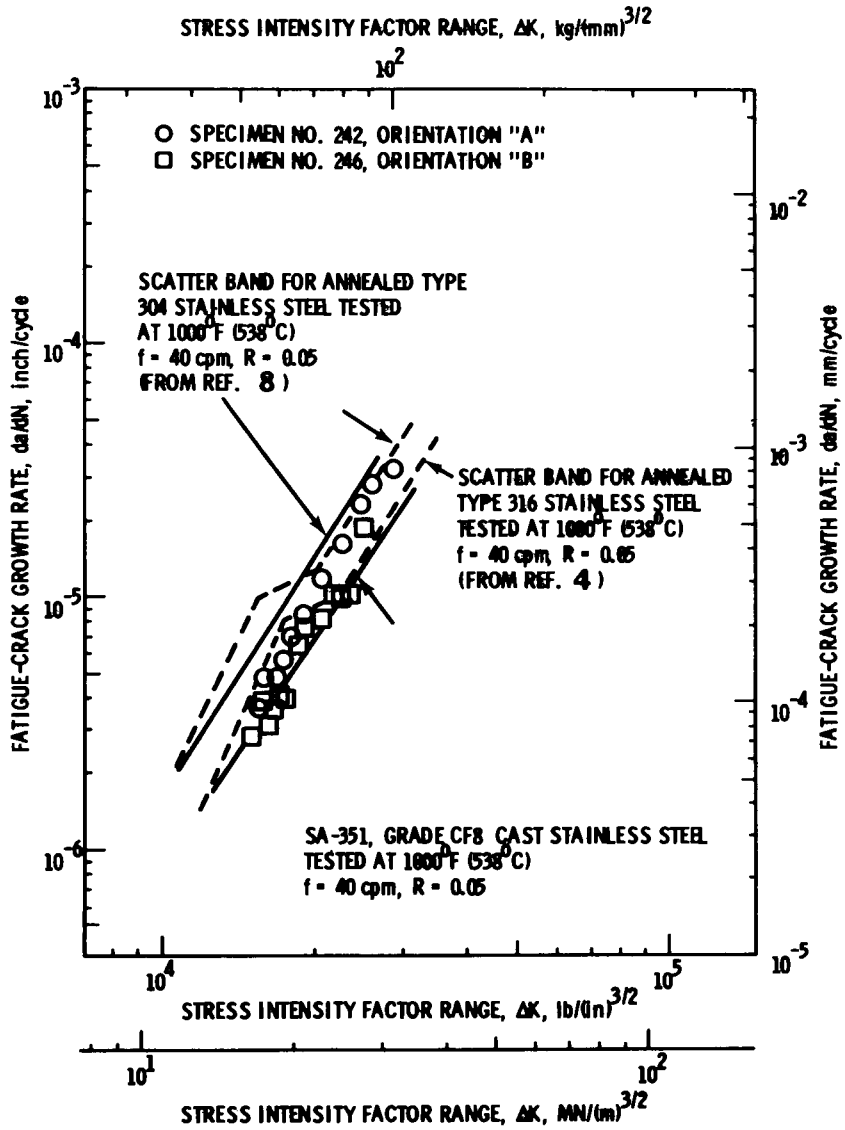

Fig. 3.13. Fatigue crack propagation behavior of ASME SA-351 Grade CF8 cast stainless steel at 1000°F (538°C).

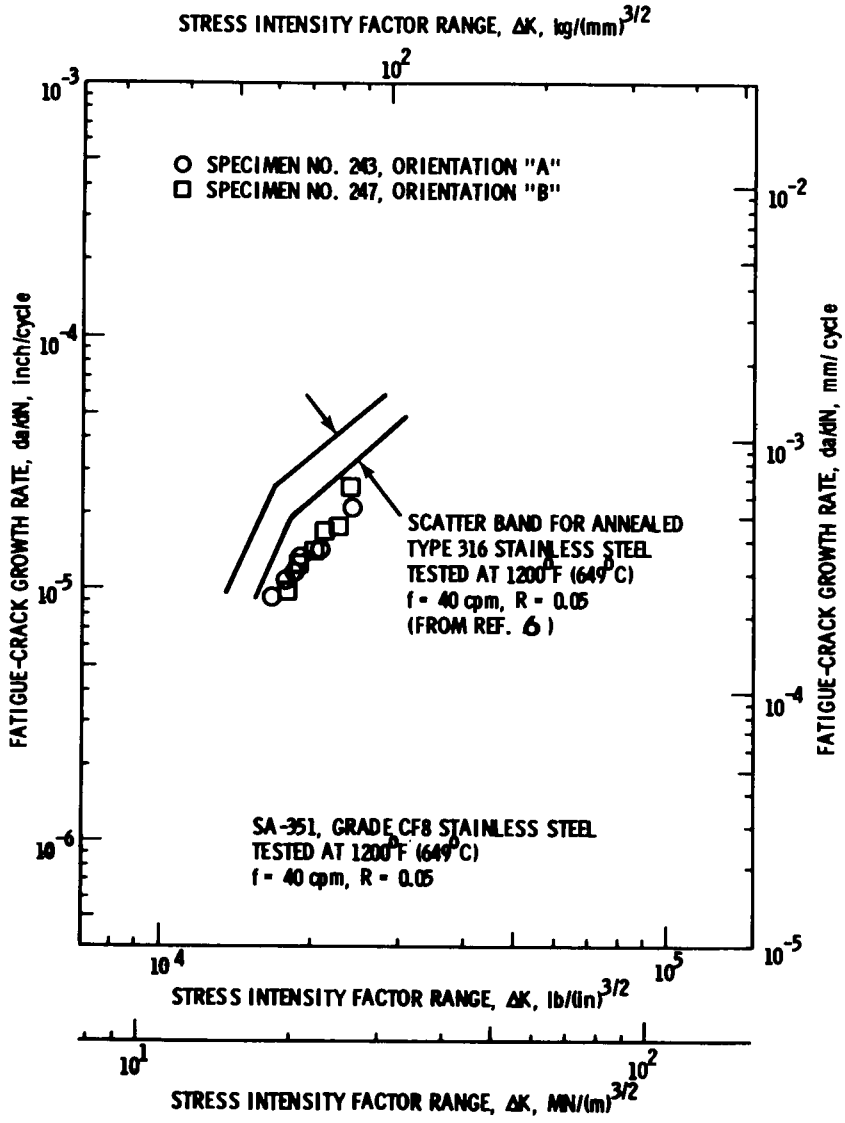

Fig. 3.14. Fatigue crack propagation behavior of ASME SA-351 Grade CF8 cast stainless steel at 1200°F (649°C).

program. Cladding from this program is utilized for vendor qualification, FFTF development programs and FTR core loadings.

3.4.1.2 Accomplishments and Status

3.4.1.2.1 Scope of Work. The recovery and recrystallization characteristics of one 20% cold worked Type 316 stainless steel tubing series (N Lot) have been established. The recovery and recrystallization characteristics of 11 prototypic and production fuel cladding tubing lots of 1400, 1500 and 1600°F have been determined to establish lot-to-lot variations and to provide a basis for possible improvements in cladding recrystallization characteristics.

3.4.1.2.2 Results. Eleven lots of 20% cold worked Type 316 stainless steel tubing (N, O, R, T, U, X, BB, CN-13, CN-17, P and S) were utilized in this study. Isothermal annealing curves were established for each tube lot by aging four-inch tubular specimens in helium at 1400 to 1600°F for times from 0.1 to 2000 hours. The aged specimens were subsequently tensile tested in vacuum (5-10 microns) at 1000°F at a strain rate of 0.01 min^{-1} utilizing an Instron tensile machine. Specimens were gripped by using a compression fitting technique.

The 0.2% yield stress at 1000°F was used as the measure of the annealing effects of time at temperature. The resulting isothermal annealing curves at 1500 and 1600°F, Figures 15 and 16, clearly show that the recrystallization time at these two temperatures can vary significantly from lot to lot. At 1600°F the recrystallization time ranges from a low of $\leq$ 0.2 hour to a high of 7 hours. At 1500°F, the range is 10 hours to 200 hours.

Because the variations in recrystallization times were greater than would be expected from data scatter, an attempt was made to correlate the variations to some variable that exists between the tube lots. Correlations with respect to chemistry variations, drawing sequence, drawing technique, and melting practice were all unsuccessful. However, the recrystallization time for a temperature correlated quite well with the heat treatment temperature used prior to the final 20% reduction in area.

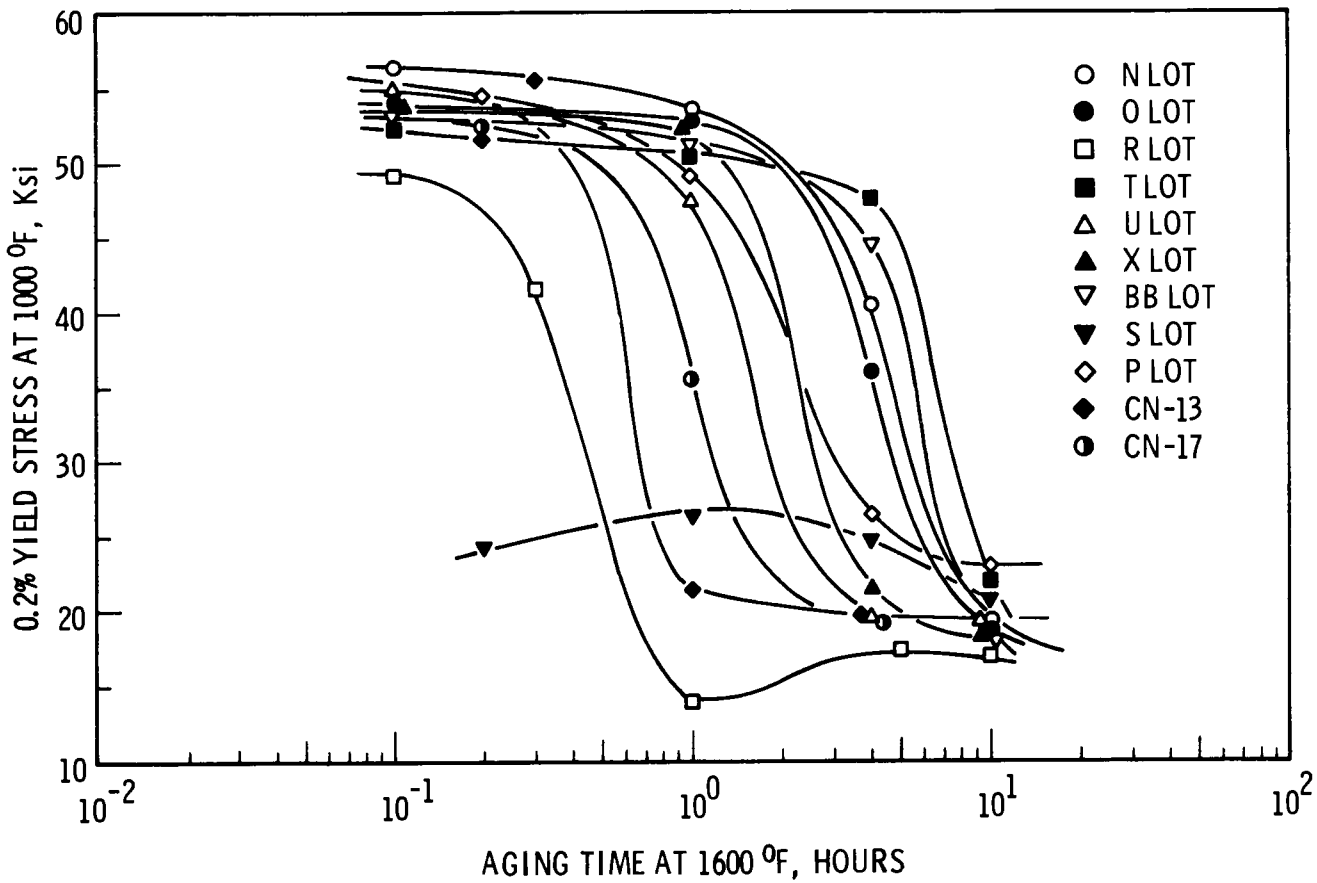

Fig. 3.15. Isothermal annealing curves at 1600°F for eleven prototypic FTR fuel cladding tube lots.

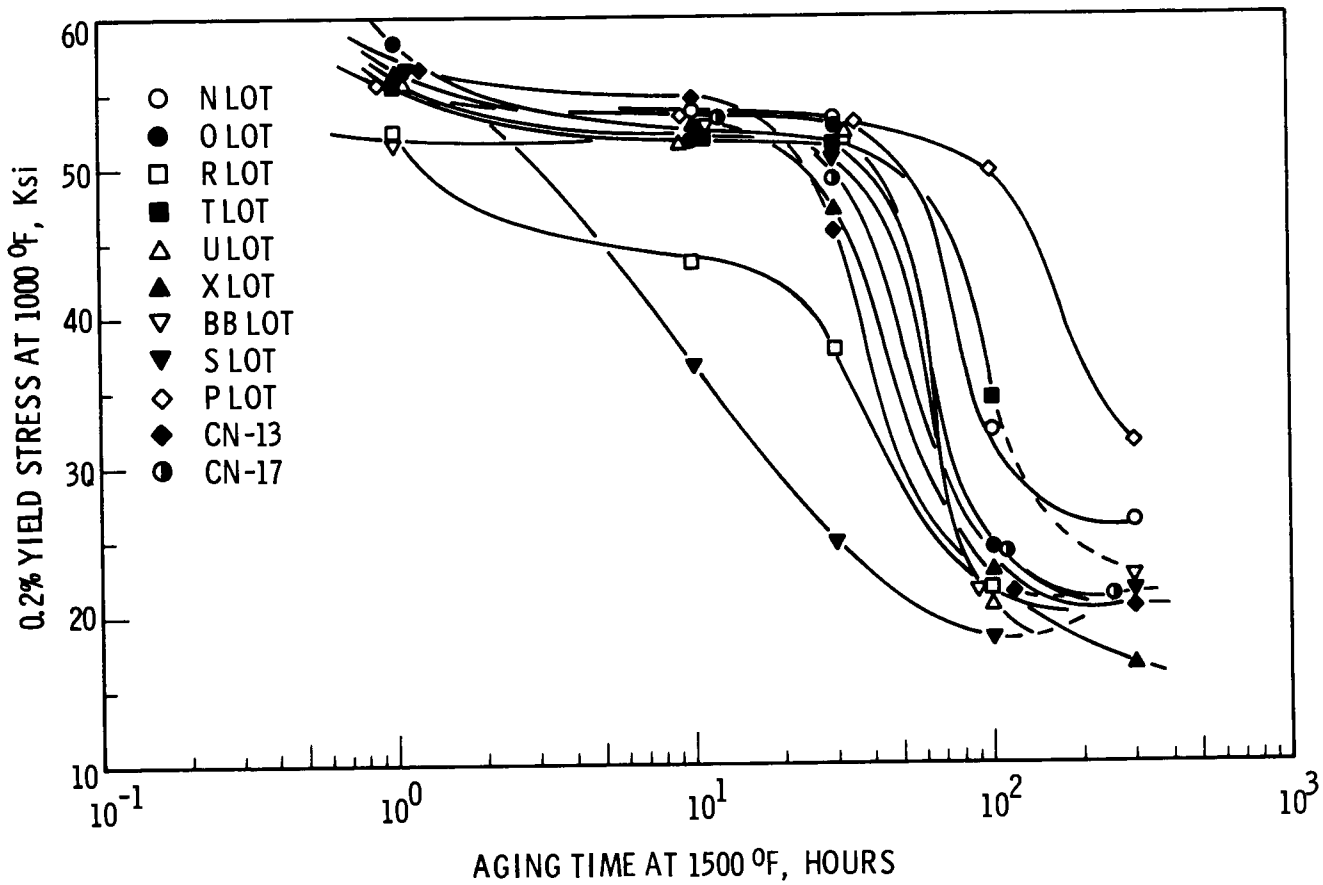

Fig. 3.16. Isothermal annealing curves at 1500°F for eleven prototypic FTR fuel cladding tube lots.

This correlation is shown in Figure 17 for the seven tube lots for which there are sufficient processing data.

These data show some thermally activated process which occurs during the heat treatment before the final draw has a pronounced effect on the subsequent recrystallization kinetics. No detailed in-depth study was attempted using these due to lot-to-lot variations in chemistry, time at temperature during heat treatment, and exact cold work level. However, a series of tubes processed in a commercial tube mill were selected from a single processing lot (consisting of ∿ 200 tubes) just prior to the final anneal, and three tubes were given each of the following heat treatments:

Temperature °F	Furnace Feed Rate	Time at Temperature (Peak ± 5°F)
1850	36"/min.	7-10 sec.
1900	36"/min.	7-10 sec.
1950	36"/min.	7-10 sec.
2000	36"/min.	7-10 sec.
2050	36"/min.	7-10 sec.
1950	48"/min.	2-4 sec.
2050	48"/min.	2-4 sec.

These tubes were subsequently given a 20% reduction in area sequentially using the same dies to minimize or eliminate any change in cold work level due to die wear. Recrystallization studies on the above listed material will be reported in the near future.

3.5 REFERENCES

1. L. D. Blackburn, R. W. Barker and T. R. Billeter, *HEDL Quarterly Technical Progress Report -- July, August, September 1973*, HEDL-TME 73-5, Vol. 1, October 1973, p. B-1.
2. E. R. Gilbert, D. C. Kaulitz, J. J. Holmes and T. T. Claudson, *Fast Reactor Induced Creep in 20% Cold Worked Type 316 Stainless Steel*, BNES Conference on Irradiation Embrittlement and Creep in Fuel Cladding and Core Components, November 1972.
3. F. Garofalo, P. R. Malenoch and G. V. Smith, *The Influence of Temperature on the Elastic Constants of Some Commercial Steels*, Symposium on Determination of Elastic Constants, ASTM STP 129, American Society for Testing and Materials, Philadelphia,

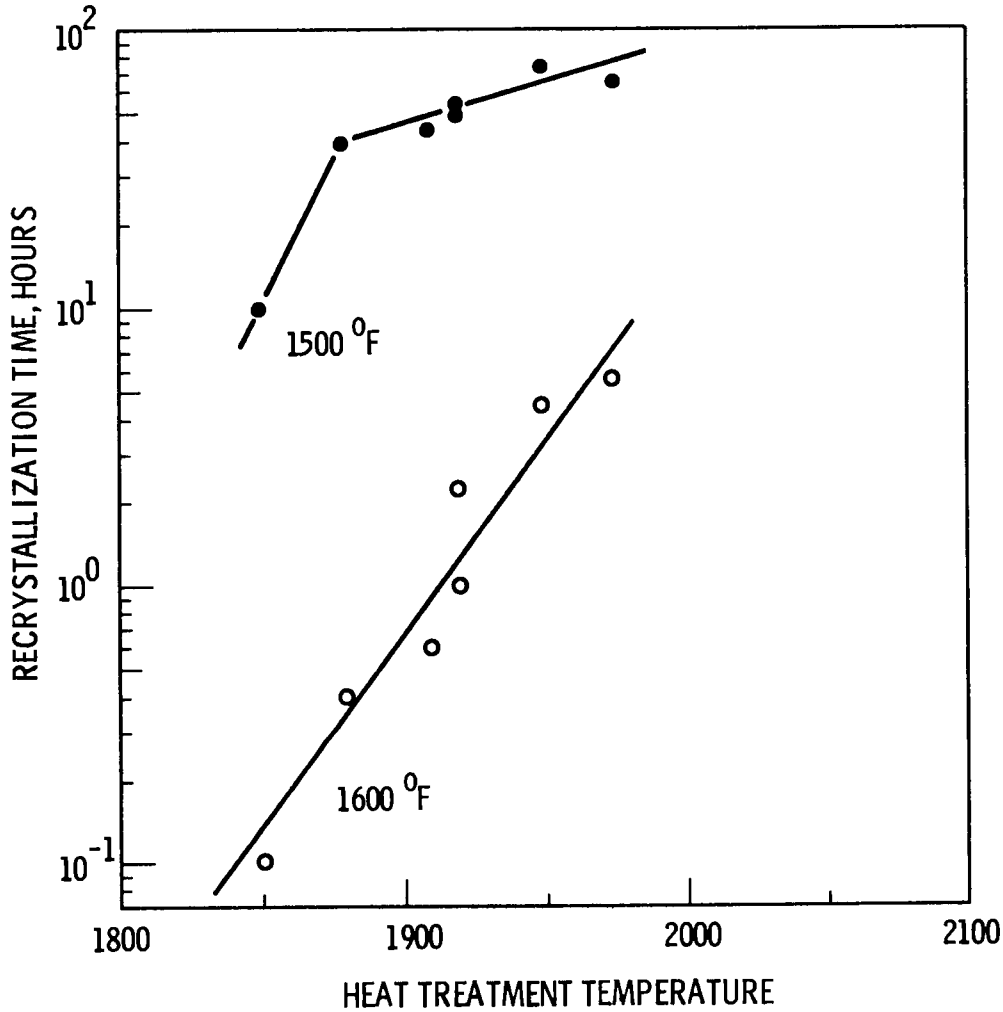

Fig. 3.17. A correlation of heat treatment temperature prior to the final 20% reduction in area and recrystallization time at 1500 and 1600°F.

Pennsylvania, 1952, p. 10.

4. J. M. Steichen, *FFTF Primary Piping Fabrication Comparison*, Hanford Engineering Development Laboratory, HEDL-TME 72-133, October 1972.
5. J. M. Steichen, *HEDL Quarterly Report*, HEDL-TME 73-6, Vol. I, January 1974.
6. L. A. James, "The Effect of Elevated Temperature Upon the Fatigue Crack Propagation Behavior of Two Austenitic Stainless Steels," *Mechanical Behavior of Materials*, Vol. III, pp. 341-352, The Society of Materials Science, Japan, 1972.
7. L. A. James and R. L. Knecht, "Fatigue-Crack Propagation in Fast-Neutron-Irradiated Types-304 and -316 Stainless Steels," *Nucl. Technol.* 19(3): 158-155 (September 1973).
8. L. A. James, "Fatigue-Crack Growth in Type 304 Stainless Steel Weldments at Elevated Temperature," *Jnl. of Testing and Evaluation*, 1(1): 52-57 (January 1974).
9. L. A. James, "Crack Propagation Behavior in Type 304 Stainless Steel Weldments at Elevated Temperature," *Welding Jnl. Res. Suppl.*, 52(4): 173s-179s (April 1973).
10. P. Shahinian, H. H. Smith and J. R. Hawthorne, "Fatigue Crack Propagation in Stainless Steel Weldments at High Temperature," *Welding Jnl. Res. Suppl.*, 51(11): 527s-532s (November 1972).

4. NAVAL RESEARCH LABORATORY

L. E. Steele

4.1 INTRODUCTION - L. E. Steele

The research program of the NRL, Metallurgy Division, Reactor Materials Branch, includes the study of the behavior of structural materials useful in reactor construction. This report is developed using such data to support the USAEC objective of compiling structural materials properties data for the use in national reactor development programs. The NRL program is sponsored by the Office of Naval Research, the U. S. Atomic Energy Commission, and the U. S. Army Engineer Power Group. The unirradiated materials properties data contributed here include those developed in the course of research in the areas of high temperature materials, radiation damage, and fracture mechanics.

4.2 FATIGUE CRACK GROWTH IN THERMALLY-AGED TYPES 304 AND 316 STAINLESS STEEL PLATE - D. J. Michel, H. H. Smith, and H. E. Watson

4.2.1 Background

The long term exposure of austenitic stainless steels to elevated temperatures is known to be responsible for precipitate formation [1,2] which may influence the mechanical properties of these steels.[3-6] Few studies, however, have considered the effect of thermal aging on fatigue crack propagation in these steels.[7] The present experiments represent the initial phase of an NRL program to investigate the effect of thermal aging on the fatigue crack growth resistance of Types 304 and 316 stainless steel. The emphasis of this study is to correlate crack growth behavior with microstructural changes produced by extended elevated temperature exposure.

4.2.2 Materials and Test Procedures

The chemical composition and tensile properties of the Types 304 and 316 stainless steels used in this work were given in previous reports.[8,9] Single-edge-notched specimens containing side grooves and oriented in the RW direction were cycled at 10 cpm in cantilever bending under zero-to-tension loading to a constant maximum load. The experimental data

were analyzed to determine crack growth rate, da/dN, as a function of the stress intensity factor range, ΔK. Induction heating was used for the elevated temperature tests. The thermally-aged condition specimens were machined from blanks aged in air for 5000 hours at 1100°F (593°C).

4.2.3 Results and Discussion

Figures 4.1 and 4.2 show the effect of thermal aging on the fatigue crack growth resistance at 1100°F (593°C) of solution-annealed and 25 percent cold-worked Type 304 stainless steel respectively. The results for thermally aged Type 308 stainless steel weld material at 1100°F (593°C) are shown in Fig. 4.3. Figures 4.4 and 4.5 present the results for solution-annealed and 20 percent cold-worked Type 316 stainless steel.

Comparison of Figs. 4.1 and 4.4 indicates that thermal aging produced only a slight increase in the fatigue crack growth resistance of both solution-annealed Types 304 and 316 stainless steel when compared to unaged material.[8] For the cold-worked specimens, however, Figs. 4.2 and 4.5 indicate that thermal aging decreased the fatigue crack growth resistance for both the annealed and cold worked conditions the effect of aging is seen to be larger for the Type 316 steel than for the Type 304 steel. Examination of Fig. 4.3 suggests that thermal aging decreased the fatigue crack growth resistance of Type 308 stainless steel weld material at the lower ΔK values but produced a slightly beneficial effect at the higher ΔK values. With the exception of the cold-worked Type 316 data, the present results are in general agreement with a recent fatigue study[7] where similar aging treatments and test temperatures were employed. In that study no effect of aging on fatigue crack growth rate was seen for cold-worked Type 316 stainless steel. It should be noted, however, that the referenced investigations were carried out at lower ΔK values than used in the current study.

Examination of the present results indicates that thermal aging produced a decrease in fatigue crack growth resistance of the cold-worked condition while slightly increasing the fatigue crack growth resistance of the solution-annealed condition. Since it is known that cold-work enhances precipitation of carbide and intermetallic phases during thermal aging[1,2], it is believed that this enhanced precipitation provided a

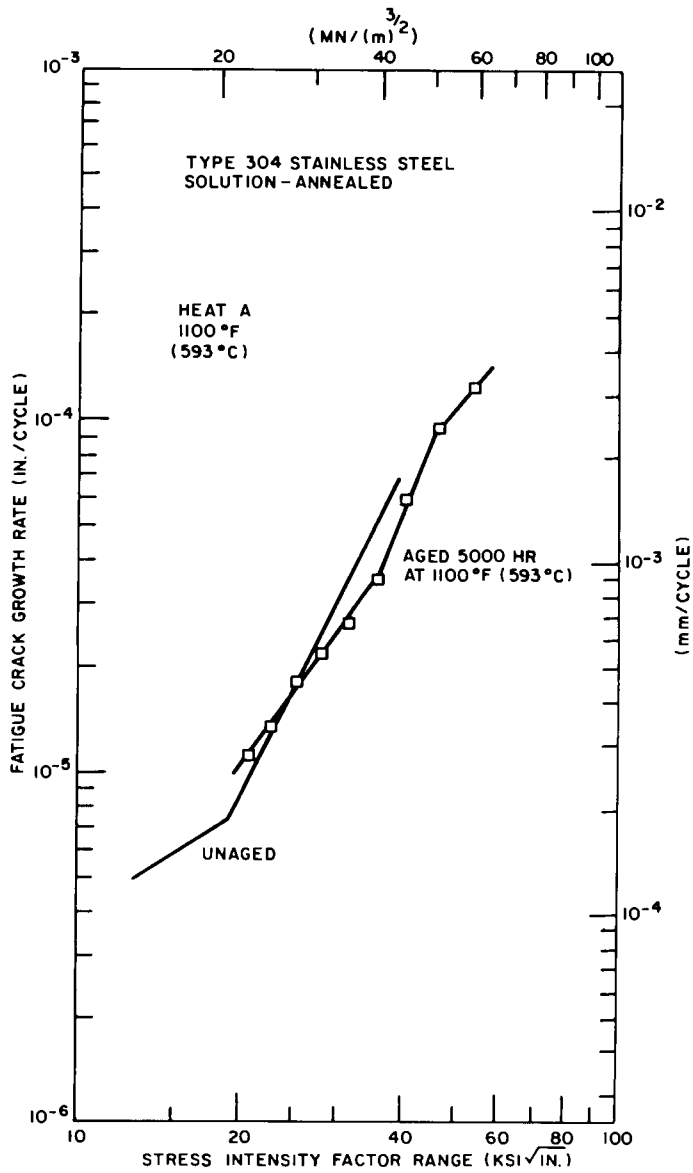

Fig. 4.1. Effect of thermal aging on fatigue crack growth rate in solution-annealed Type 304 stainless steel as a function of the stress intensity factor range.

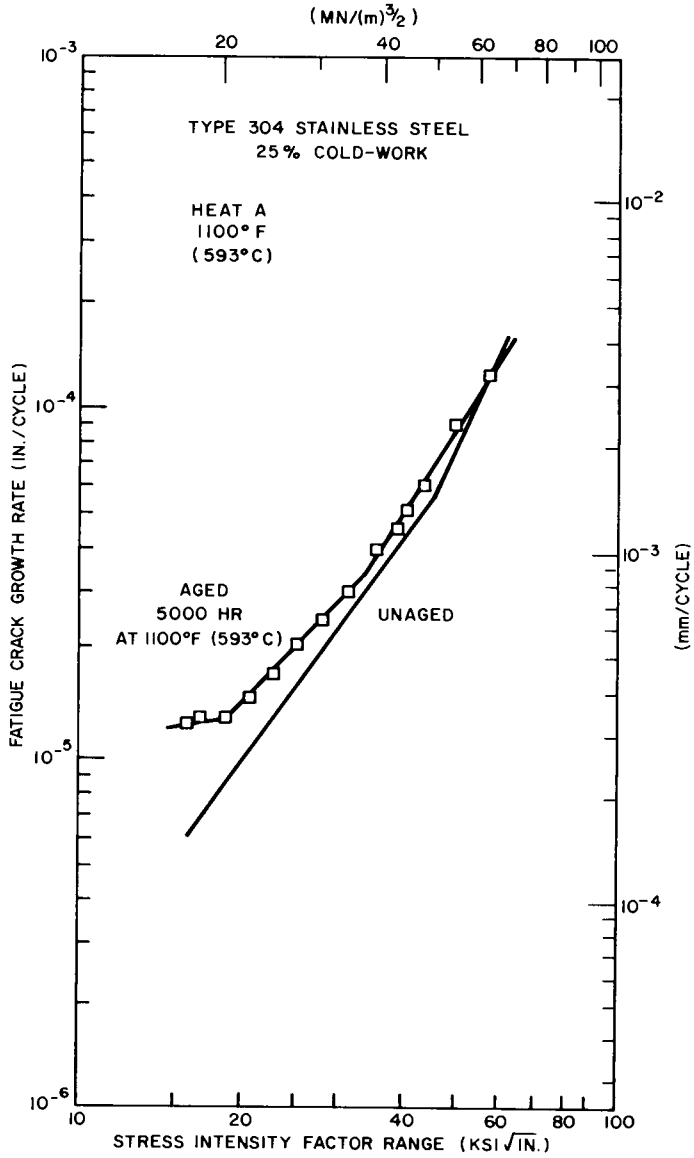

Fig. 4.2. Effect of thermal aging on fatigue crack growth rate in 25% cold-worked Type 304 stainless steel as a function of the stress intensity factor range.

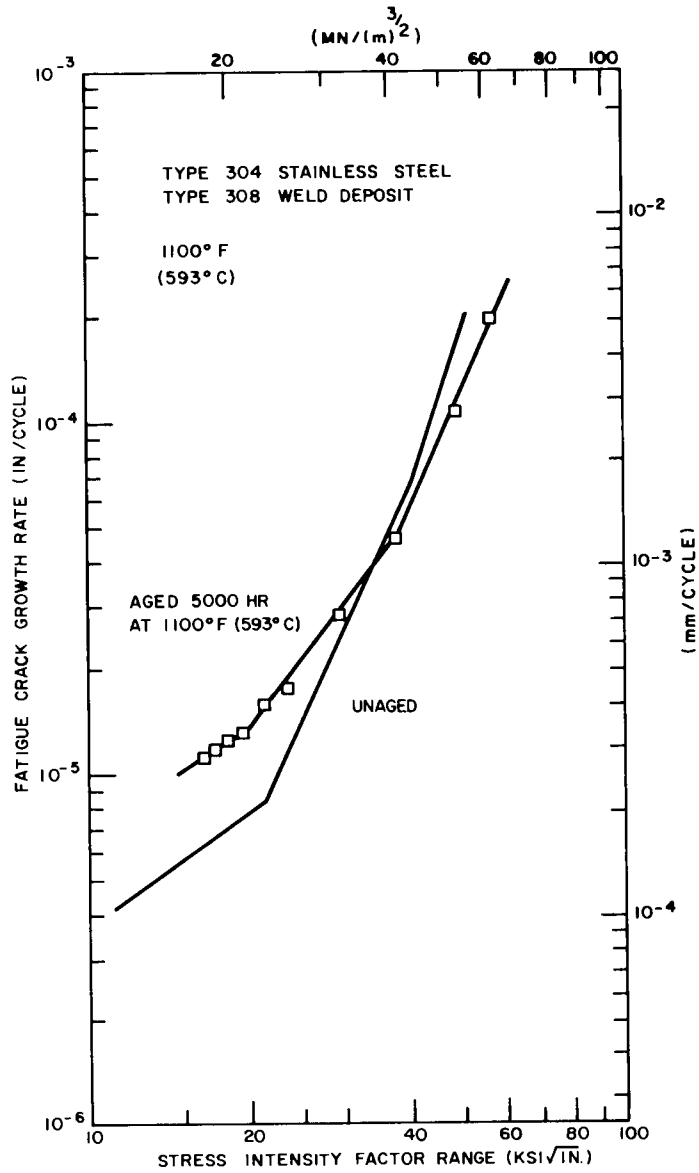

Fig. 4.3. Effect of thermal aging on fatigue crack growth rate in Type 308 stainless steel weld metal as a function of the stress intensity factor range.

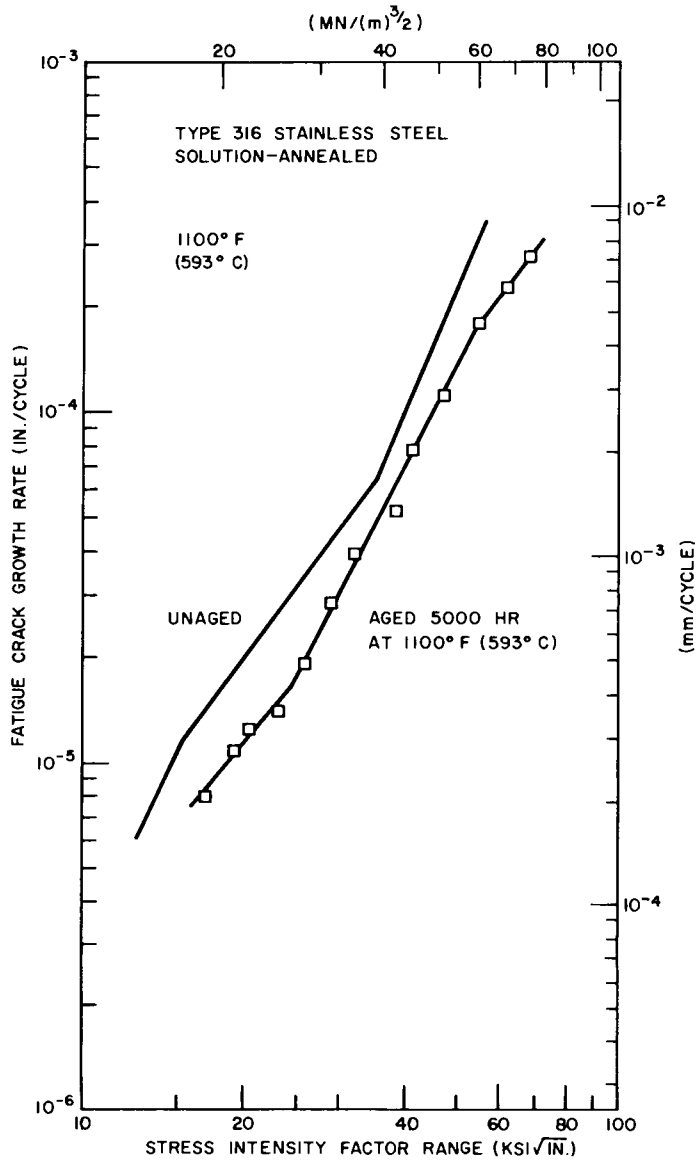

Fig. 4.4. Effect of thermal aging on fatigue crack growth rate in solution-annealed Type 316 stainless steel as a function of the stress intensity factor range.

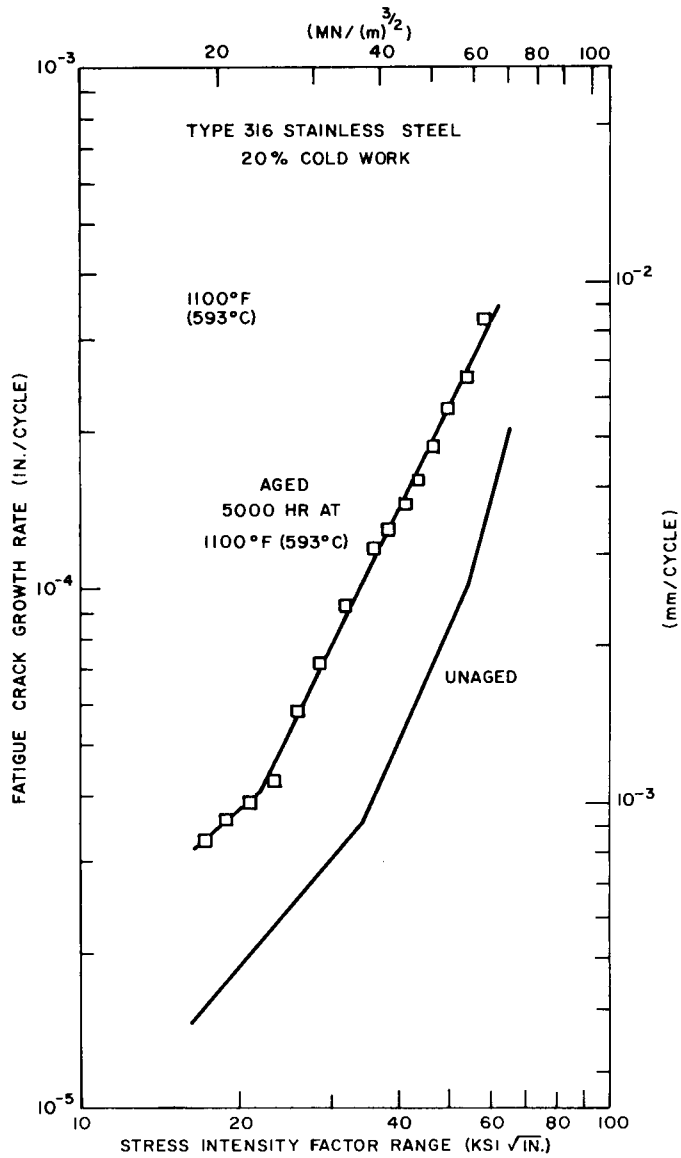

Fig. 4.5. Effect of thermal aging on fatigue crack growth rate in 20% cold-worked Type 316 stainless steel as a function of the stress intensity factor range.

major microstructural contribution to the different fatigue crack growth behavior observed for the solution-treated and cold-worked steels. Further, the effect of the increased availability of intragranular precipitation sites (i.e., dislocations and stacking faults) in the cold-worked material may substantially influence the crack growth process when compared to solution-treated material. A detailed metallographic examination of the specimens tested in this study is now in progress to determine the relationship between the observed crack growth behavior and precipitate formation. These results will be presented in future reports.

4.3 TOUGHNESS OF TYPE 316 STAINLESS STEEL FORGING AND WELD METAL USING THE J INTEGRAL - F. J. Loss and R. A. Gray

4.3.1 Background

The fracture toughness of austenitic stainless steel and nickel-base alloys for fast breeder reactors is being characterized in terms of the J Integral. These alloys, when employed at elevated temperatures, generally exhibit elastic plastic or fully plastic behavior. The J-Integral concept provides a means with which to define the initiation of crack extension in the elastic plastic regime and to relate this phenomenon to structural parameters used in design (e.g., critical flaw size and stress level). Current emphasis is directed toward (a) characterization of different high temperature alloys by means of the J Integral, and (b) assessment of specimen geometry dependence of the J Integral at crack initiation (i.e., J_{Ic}). The data reported here relate to Type 316 forging and weld metal at elevated temperature.

4.3.2 Experimental Investigation

4.3.2.1 Material and Specimen Types

Weld metal test specimens were machined from a 1-in. thick weldment formed by joining Type 316 stainless steel plates by submerged arc welding, using a Type 316 stainless steel filler. The weldment was specially prepared to simulate that used in the Army's MH-1A reactor pressure vessel. Specimens of 316 stainless steel were prepared from a 3-1/8 in. thick ring forging (nozzle cutout) from the MH-1A vessel. Chemical and tensile properties as well as specimen orientation are given in Ref. 10.

Notched, three point bend specimens were machined from both the forging and weld metal. Three different specimen types, having the following geometries, were investigated.

Type 1: width (W) = 0.394 in., thickness (B) = 0.197 in., and span (S) between supports = 1.758 in.

Type 2: geometrically similar to type 1 but twice as large.

Type 3: same as type 1 except W = 0.282 in.

The specimens were fatigue precracked at a ΔK of 25 ksi$\sqrt{\text{in.}}$ (27.5 MPa$\cdot m^{\frac{1}{2}}$) using a zero-tension cycle. The majority of the specimens had a nominal a/W ratio of 0.35 (0.28 to 0.46 range in a/W).

The testing was conducted statically with specimen load and midspan deflection monitored on an x-y recorder. All tests were conducted at 500°F (260°C) as achieved with an induction heating coil.

4.3.2.2 Results

Specimens of a given a/W ratio were loaded to various fractions of the maximum load as determined from one of the specimens. This procedure resulted in the specimens undergoing different amounts of slow stable crack extension (Δa) with rising load while attaining the desired load or deflection. In preliminary interpretation of the data, no attempt was made to distinguish a stretch zone at the tip of the fatigue crack from the total crack extension values that are reported. The specimens were unloaded and heat tinted at 900°F (482°C) and then broken open at room temperature. In this way it was possible to measure the amount of stable growth that had taken place up to the point where the test was terminated. With the weld metal specimens, the slow crack extension could be distinguished from the fatigue precrack due to a difference in texture between these two regions. However, this difference in texture was extremely difficult to detect in the forged specimens. Consequently, it was necessary to ink stain the latter specimens before testing in order to mark the fatigue precrack region. The unstained heat tinted region was then attributed to slow crack extension that occurred with rising load during the course of the test.

The J-Integral value was computed from the total area (A) under the load versus midspan deflection record (i.e., energy) using the approximate

equation for a deeply notched beam in pure bending derived simultaneously be Rice[11] and Srawley[12]:

$$J = \frac{2A}{B(W-a)} \qquad \text{Eq. (1)}$$

In all cases the deflections of the bend jig were negligible so that the area under the load versus deflection trace represents energy imparted to the specimen. The original crack length (a) to the tip of the fatigue crack was used in Eq. (1) (as opposed to using the final crack length, $a + \Delta a$).

The values of J for forging and weldment, calculated from Eq. (1), are presented in Fig. 4.6 as a function of the average slow crack extension at the specimen quarter points. This method of representation is termed an R-curve. In a strict sense, crack extension is not permitted by the J concept since the J_{Ic} value is defined as the toughness at crack initiation. The J_{Ic} is defined here by extrapolating the R-curve to some small crack extension such as may be acceptable in a valid K_{Ic} test.* A 1 percent crack extension was arbitrarily chosen for this investigation. It is evident that any criterion of a fixed percentage crack extension will result in different values of absolute crack extension for different size specimens (See Fig. 4.6). For the present investigation, however, this difference is not considered detrimental to the data interpretation.

4.3.3 Discussion

The data in Fig. 4.6 show that the J_{Ic} of the weld metal is significantly below that of the forging (600 vs 3500 in.lb/in.^{2}). With a J_{Ic} of 600 in.lb/in.^{2}, it is expected that elastic plastic conditions will prevail and that plane strain behavior (as defined by ASTM Standard E-399) will not be attained for this material, even in very thick sections. Nevertheless, an assessment is required of the structural significance of the reduced toughness of the weld metal in comparison with that of the forging. It is felt that considerable research is required before this goal can be achieved.

---

*2% crack extension is permitted in a K_{Ic} test by ASTM Standard E-399.

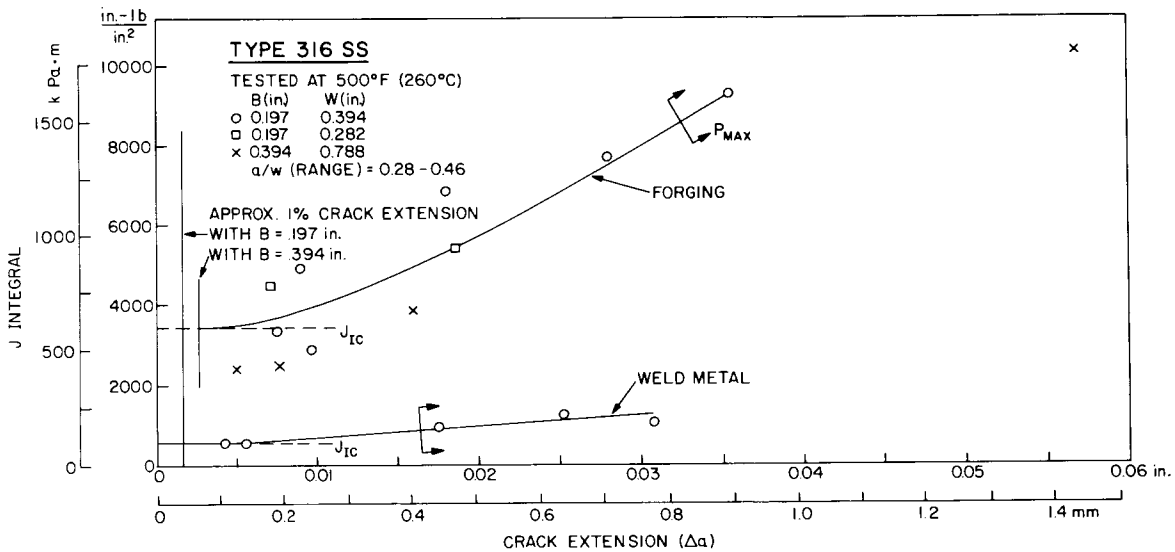

Figure 4.6 - The critical J, or J_{Ic}, at crack initiation is defined by the intersection of the curve through the data with an arbitrarily chosen value of 1% crack extension. The J values for the forging obtained with the thick specimens (0.394 in.) suggest a thickness dependence of J_{Ic} when proposed minimum requirements are not met. The arrows labeled P_{MAX} denote those points based on J computed using the specimen energy to maximum load.

As a way of pointing out differences in the behavior of the weld metal and forging, Fig. 4.7 illustrates the load vs midspan deflection records of two identical specimens cut from these two materials. The specimens are compared on the basis of both having exhibited the same degree of slow crack extension. The illustrated weld metal record is near the maximum load for this size specimen. In comparison to the forging specimen, the weld metal exhibits only a small fraction of the deformation capability of the forging (0.044 in. as compared to 0.323 in. for a forging specimen if taken to maximum load).

For J_{Ic} data to be considered valid it is reasonable to require that certain minimum dimensions be maintained as in the case of plane strain testing. Landes and Begley[13], on the basis of data from ferritic steels have suggested that a, B, and W/a, be greater than 25 J/σ_{flow} where $\sigma_{flow} = 1/2\ (\sigma_{ys} + \sigma_{ts})$. This requirement would necessitate specimen thicknesses of 0.27 in. and 1.8 in. for the weld metal and forging, respectively, as opposed to the maximum thickness specimens of 0.2 in. (weld metal) and 0.4 in. (forging) that were investigated. Unfortunately, material in larger sections does not exist with which to verify the proposed thickness requirements.

The forging data of Fig. 4.6 suggest a dependence of J_{Ic} upon specimen thickness. The data for the thicker specimens (B = 0.394 in.) form the lower boundary of the scatterband for the forging. An R-curve connecting only the data of the thicker specimens would result in a value of J_{Ic} close to 2400 in.lb/in.^{2} in comparison with the value of 3500 in.lb/in.^{2} illustrated in the figure. It is apparent from these data that additional research is necessary to qualify the effects of specimen geometry on the J_{Ic} value.

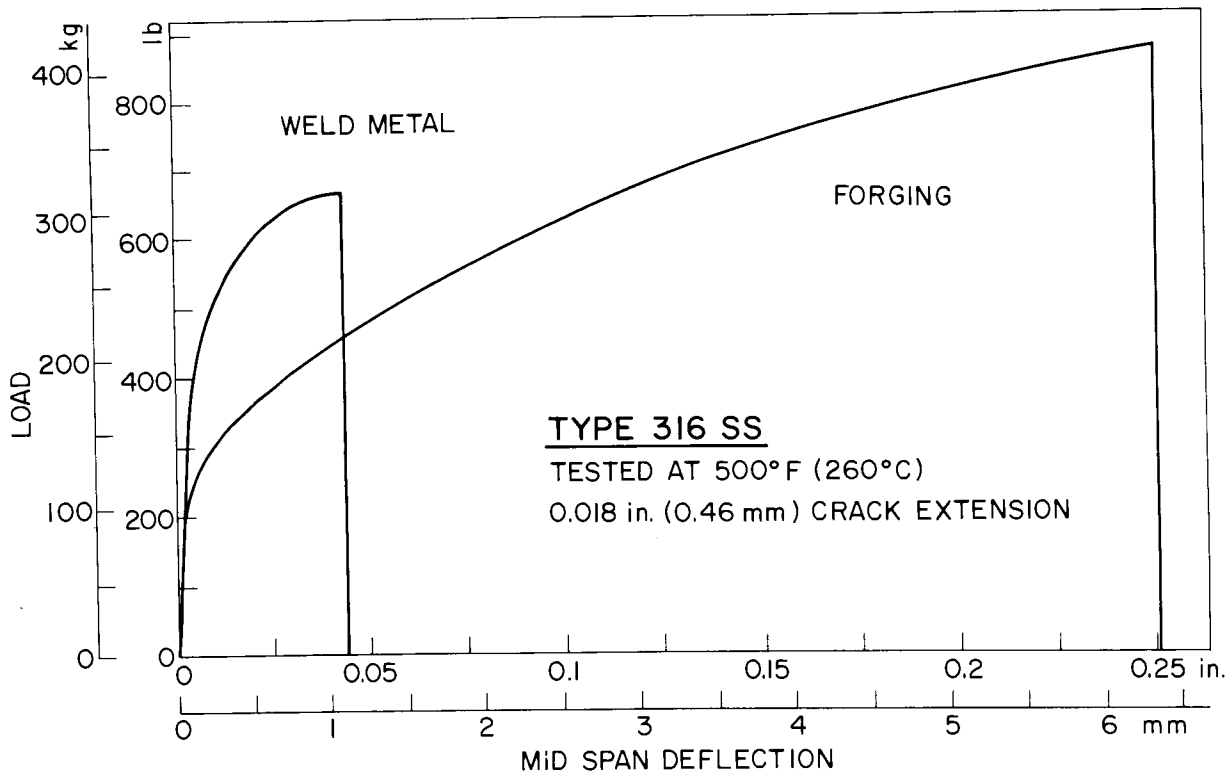

Figure 4.7 - Load vs midspan deflection records for identical specimens (including crack length) cut from weld metal and forging. Both specimens exhibited the same slow crack extension up to point where the test was terminated. The forging specimen is at maximum load whereas a similar weld metal specimen attained a maximum load of 900 lb (4×10^3 N).

4.4 REFERENCES

1. B. Weiss and R. Stickler, Phase Instabilities During High Temperature Exposure of 316 Austenitic Stainless Steel, Met. Trans. 3, 851, 1972.
2. J. E. Spruiell, J. A. Scott, C. S. Ary, and R. L. Hardin, Microstructural Stability of Thermal Mechanically Pretreated Type 316 Austenitic Stainless Steel, Met. Trans. 4, 1533, 1973.
3. F. Garogalo, F. von Gemmingen, and W. F. Domis, The Creep Behavior of an Austenitic Stainless Steel as Effected by Carbides Precipitated on Dislocations, Trans. ASM 54, 430, 1961.
4. J. T. Barnby and F. M. Peace, The Effect of Carbides on the High Strain Fatigue Resistance of an Austenitic Steel, Acta Met. 19, 1351, 1971.
5. J. T. Barnby and F. M. Peace, "Influence of Carbides on the Low-Cycle Fatigue Strength of an Austenitic Steel," in Effect of Second-Phase Particles on the Mechanical Properties of Steel, The Iron and Steel Institute, London, 1971, p. 124
6. J. H. Driver, The Effect of Boundary Precipitates on the High-Temperature Fatigue Strength of Austenitic Stainless Steels, Met. Sci. Journal 5, 47, 1971.
7. L. A. James, Effect of Thermal Aging Upon the Fatigue-Crack Propagation of Austenitic Stainless Steels, Met. Trans. 5, 831, 1974.
8. D. J. Michel and H. H. Smith, Fatigue Crack Growth in Type 304 Stainless Steel, in Mechanical Properties Test Data for Structural Materials, Quarterly Progress Report for period ending Oct. 31,1973, ORNL-4936, Oak Ridge National Laboratory, Oak Ridge, Tennessee, January 1974, pp. 37-45.
9. D. J. Michel and H. H. Smith, Fatigue Crack Growth in Type 316 Stainless Steel, in Mechanical Properties Test Data for Structural Materials Quarterly Progress Report for period ending Jan. 31, 1974, ORNL-4948, Oak Ridge National Laboratory, Oak Ridge, Tennessee, March 1974, pp. 157-165.
10. F. J. Loss and R. A. Gray, Irradiation Effects on Reactor Structural Materials, 1 February-31 July 1974, NRL Memorandum Report 2875, Naval Research Laboratory, August 1974, pp. 23-30.

11. J. R. Rice, P. C. Paris, and J. G. Merkle, "Some Further Results of J-Integral Analysis and Estimates," ASTM STP 536, Progress in Flaw Growth and Fracture Toughness Testing, 1973, pp. 231-245.

12. J. E. Srawley, On the Rice J Integral Concept in Fracture Mechanics, lecture notes, NASA-Lewis Research Center, Cleveland, Ohio, July 1972.

13. J. D. Landes and J. A. Begley, Test Results From J Integral Studies--An Attempt to Establish a J_{Ic} Testing Procedure, Scientific Paper 73-1E7-FMPWR-P3, Westinghouse Research Laboratories, Pittsburgh, Pa., Oct. 18, 1973.

5. OAK RIDGE NATIONAL LABORATORY

W. R. Martin

5.1 INTRODUCTION

The ORNL mechanical properties effort comprises several programs. The program Mechanical Properties and Behavior for Structural Materials deals with materials of general applicability to the LMFBR program. Other programs are concerned with the mechanical properties of weldments in LMFBR components, the specific materials of interest for LMFBR steam generators, collection and correlation of mechanical data needed for design of high-temperature LMFBR systems, and materials for the primary circuit and steam generators of HTGR systems.

5.2 MECHANICAL PROPERTIES AND BEHAVIOR FOR STRUCTURAL MATERIALS — C. R. Brinkman

The objective of this program is to collect mechanical property data and material behavior for LMFBR structural and component materials. Included in the scope of this effort are the following: (1) basic tensile, creep, creep-rupture, and relaxation base-line data that are directly applicable to design criteria and methods for types 304 and 316 stainless steel reference heats and cyclic stress-strain tests performed with emphasis on loading and history effects, (2) find the variations in properties for several heats of types 304 and 316 stainless steel to allow establishment of minimum and average values of specific properties and the equation parameters required for design purposes. This work will include determination of property variation of samples from different mill products within a given heat of stainless steel.

5.2.1 Mechanical Property Characterization of Type 304 Stainless Steel Reference Heat — V. K. Sikka

5.2.1.1 Creep and Rupture Properties of the 2-in. (51-mm) Plate of Reference Heat

Several creep tests on 2-in. (51-mm) plate of reference heat of type 304 stainless steel (9T2796) continued. The test times and creep strains for all tests have been updated and are summarized in Table 5.1. One test at 538°C (1000°F) and 14 ksi (97 MPa) was discontinued after 4498 hr. The machine made available was loaded with a specimen at 593°C (1100°F) and a stress of 10 ksi (69 MPa). All creep curves have been updated. Three creep tests have reached test times over 14,000 hr, whereas two other tests have exceeded 12,000 hr. All creep tests are progressing smoothly and will be continued during the next quarter.

5.2.1.2 Uniaxial Tensile Tests Following Periods of Creep

These tests involve performing creep tests to different periods, discontinuing the test, cooling under the load, and tensile testing at the creep test temperature. The test matrix for this type of tests is presented in Table 5.2. For each creep stress and temperature, four tests, discontinued at periods of 100, 500, 2000, and 10,000 hr, are required. Nine creep tests are to be stopped when total strains at the end of creep periods are equal to those for the 10-ksi (69-MPa) tests at the same temperature and with a 10,000 hr creep period. According to the test matrix in Table 5.2, a total of 105 tests would be required.

Two creep tests have been completed and are represented by closed symbols in Table 5.2. Tests that will rupture or have ruptured before the discontinuing period are marked by half closed symbols in Table 5.2. Tensile data are available on only one of the two completed tests. Meanwhile, preliminary results were obtained on specimens that had discontinued in our regular creep program and are compared in Table 5.3 with tensile results previously obtained on uncrept specimens of slightly different design.

Table 5.1. Creep Tests on Type 340 Stainless Steel Reference Heat 9T2796 2-in.-thick (51-mm) Plate[a]

Test	Temperature (°C)	Temperature (°F)	Stress ksi	Stress MPa	Time in Test (hr)	Strain, % Loading	Strain, % Creep	Ratio of Creep Stress to Yield Stress[b]	Comments[c]
11595	427	800	20.0	138	8,749	2.67	0.051	1.57	
12368	427	800	18.0	124	5,771	1.91	0.003	1.42	
12472	427	800	16.0	110	5,047	1.17	0.038	1.26	
12570	427	800	14.9	97	4,695	0.83	0.027	1.10	
11569	482	900	20.0	138	8,919	3.27	0.082	1.70	
12375	482	900	18.0	124	5,777	2.40	0.032	1.53	
11675	482	900	16.0	110	2,451	1.48	0.032	1.36	Discontinued
11693	482	900	14.0	97	2,202	0.92	0.14	1.19	Discontinued
11830	482	900	12.0	83	1,682	0.35	0.04	1.02	Discontinued
13152	482	900	10.0	69	2,873	0.089	0.008	0.85	
13020	482	900	10.0	69	3,344	0.085	0.035	0.85	
10489	538	1000	20.0	138	13,953	3.80	0.562	1.80	
12250	538	1000	18.0	124	6,250	2.62	0.225	1.62	
11625	538	1000	16.0	110	8,674	1.79	0.196	1.44	
10491	538	1000	14.0	97	16,974	1.16	0.0231	1.26	
12444	538	1000	14.0	97	5,292	1.18	0.163	1.26	
12445	538	1000	14.0	97	4,498	1.17	0.090	1.26	Discontinued
11568	538	1000	12.0	83	8,819	0.53	0.077	1.08	
11626	538	1000	10.0	69	8,604	0.071	0.066	0.90	
11641	538	1000	8.0	55	3,170	0.040	0.027	0.72	Discontinued
10853	593	1100	18.0	124	4,545	2.84	5.94	1.65	Ruptured
10852	593	1100	16.0	110	12,194	2.29	1.742	1.47	
10554	593	1100	14.0	97	8,710	1.40	0.65	1.28	Discontinued
11596	593	1100	12.0	83	8,772	0.52	0.375	1.10	
10490	593	1100	10.0	69	13,952	0.22	0.333	0.92	
13710	593	1100	10.0	69	663	0.096	0.024	0.92	
11227	593	1100	8.0	55	6,103	0.041	0.080	0.73	Discontinued
12459	593	1100	5.0	34	5,131	0.024	0.076	0.46	
10855	649	1200	16.0	110	304	2.41	12.0	1.57	Ruptured
10854	649	1200	14.0	97	761	1.60	13.0	1.37	Ruptured
11563	649	1200	12.0	83	2,674	0.59	13.4	1.18	Ruptured
11226	649	1200	10.0	69	7,278	0.18	7.0	0.98	Ruptured
10851	649	1200	8.0	55	12,057	0.044	1.245	0.78	
12255	649	1200	5.0	34	992	0.030	0.08	0.49	Discontinued
12443	649	1200	5.0	34	5,255	0.024	0.098	0.49	
12460	649	1200	3.0	21	5,104	0.020	0.167	0.29	
10856	704	1300	10.0	69	568	0.067	15.6	0.90	Ruptured
11562	704	1300	10.0	69	653	0.12	22.5	0.90	Ruptured
11222	704	1300	8.0	55	2,760	0.031	16.4	0.72	Ruptured
12254	704	1300	5.0	34	6,136	0.030	0.910	0.45	
12461	704	1300	3.0	21	5,038	0.018	0.284	0.27	
12462	704	1300	2.0	14	4,951	0.010	0.202	0.18	

[a]Annealed 0.5 hr at 1093°C before testing. All tests loaded at a strain rate of 0.004/min.

[b]Yield stresses used in this ratio we 12,700 psi (88 MPa) at 427°C (800°F), 11,800 psi (81 MPa) at 482°C (900°F), 11,100 psi (77 MPa) at 538°C (1000°F), 10,900 psi (75 MPa) at 593°C (1100°F), 10,200 psi (70 MPa) at 649°C (1200°F), 11,100 psi (77 MPa) at 704°C (1300°F).

[c]Unless otherwise noted, tests in progress.

Table 5.2. Uniaxial Tensile Tests Following Periods of Creep on Reference Heat of Type 304 Stainless Steel

ORNL-DWG 74-7614

STRESS ksi (MPa)	TEMPERATURE °C (°F)			
	482 (900)	538 (1000)	593 (1100)	649 (1200)
5 (34)			○ △ □ ◊	○ △ □ ◊
7 (48)		○ △ □ ◊	○ △ □ ◊	○ △ □ ◊
10 (69)	○ △ □ ◊	○ △ □ ◊	○ △ □ ◊	○ △ □ ◊
-10 (-69)	○ △ □ ◊	○ △ □ ◊	○ △ □ ◊	○ △ □ ◊
12 (83)	○ △ □ ◊	○ △ □ ◊	○ △ □ ◊	○ △ □ ◊
12 (83)	▽	▽	▽	
16 (110)	○ △ □ ◊	○ △ □ ◊	○ △ □ ◊	● ▲ ◨ ◊
16 (110)	▽	▽	▽	
20 (138)	○ △ □ ◊	○ △ □ ◊	● △ □ ◊	
20 (138)	▽	▽	▽	

SYMBOLS ARE FOR DIFFERENT CREEP TEST PERIODS

○= 100, △= 500, = 2000, ◊= 10,000 hr.

▽= TEST DURATIONS ESTABLISHED WHEN THE TOTAL STRAINS AT THE END OF CREEP PERIODS ARE EQUAL TO THOSE FOR THE 10 ksi TESTS AT THE SAME TEMPERATURE AND WITH A 10,000 hr CREEP PERIOD.

CLOSED SYMBOL REPRESENTS A COMPLETED CREEP TEST. HALF CLOSED SYMBOL REPRESENTS TEST, WHICH WILL RUPTURE OR HAVE RUPTURED BEFORE DISCONTINUING PERIOD.

5.2.2 Materials Behavior in Support of Development and Evaluation of Failure Criteria for Materials — V. K. Sikka

The workable "strain limits" for design applications, which should reflect material ductility, were described in earlier reports.[1,2] The ductility measures chosen were total elongation, product of minimum creep rate times time to rupture, and strain to the end of secondary creep. These measures were used[2] to analyze the data on type 316 stainless steel.

In this report ductility measures used include total elongation, product of minimum creep rate times time to rupture, and reduction of area. These have been applied to analyze the data reported in Sec. 5.2.1.1 (Table 5.1) for the reference heat of type 304 stainless steel.

Minimum creep rates have been calculated from the updated creep curves and are plotted against initial creep stress in Fig. 5.1. The stress rupture plot is shown in Fig. 5.2. The present ORNL creep data are compared with HEDL creep data[3] in Figs. 5.3 and 5.4 and with previously reported ORNL data[4] [ORNL, reference heat 9T2796 1-in. plate (25 mm)]

Table 5.3. Tensile Properties on Reference Heat of Type 304 Stainless Steel After Creep Tests

Creep Conditions[a]						Tensile Results at 0.040/min Strain Rate									
Test	Stress		Duration (hr)	Strain, %		Test	Temperature		Proportional Limit		Strength, ksi(MPa)		Elongation, %		Reduction of Area (%)
	(ksi)	(MPa)		Creep	Total		(°C)	(°F)	(ksi)	(MPa)	0.2% Yield	Ultimate Tensile	Uniform	Total	
						11798[b]	482	900	6.1	42	12.2(84)	55.8(385)	46.4	51.5	71.4
11693	14	97	2690	0.14	1.06	13701	482	900	7.2	50	15.8(109)	57.3(395)	38.0	40.7	63.2
11675	16	110	2451	0.03	1.51	13702	482	900	12.4	85	21.9(151)	55.8(385)	33.8	39.5	67.9
						11794[b]	649	1200	6.7	46	10.4(72)	40.2(277)	36.0	48.3	49.2
13824	16	110	102	2.87	5.18	13869	649	1200	19.5	134	21.1(145)	39.8(274)	20.2	25.8	35.0

[a]Creep at eventual tensile temperature; second stage had been reached.

[b]Specimen gage length-to-diameter ratio = 5 for specimens without prior creep; specimen gage length-to-diameter ratio = 9 for crept specimens.

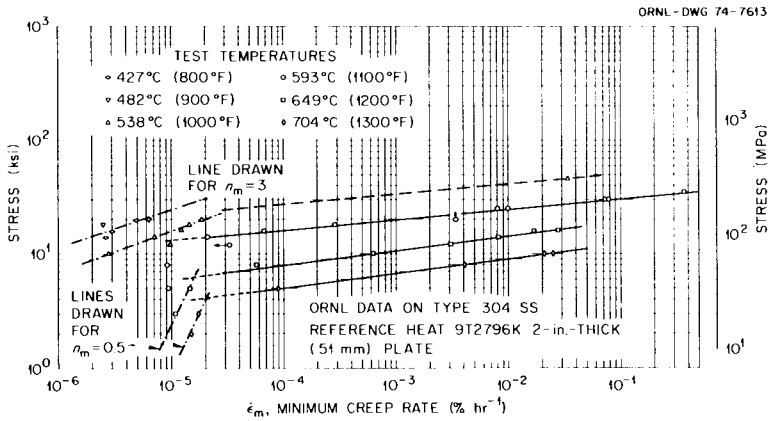

Fig. 5.1 Stress Versus Minimum Creep Rate for Reference Heat 9T2796K of Type 304 Stainless Steel.

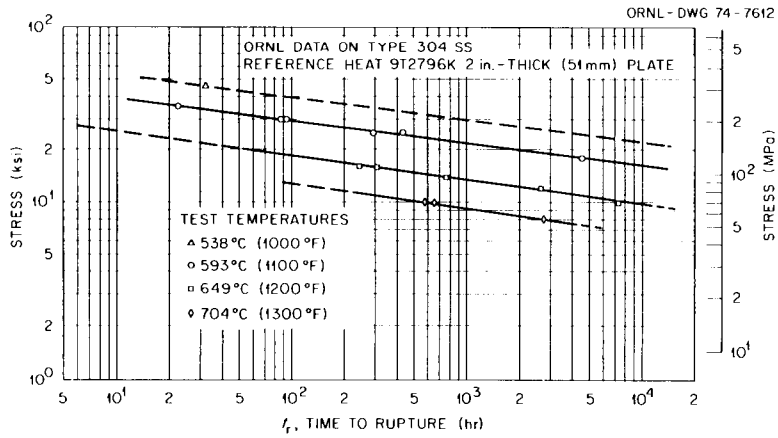

Fig. 5.2. Stress Versus Time to Rupture for Reference Heat 9T2796K of Type 304 Stainless Steel.

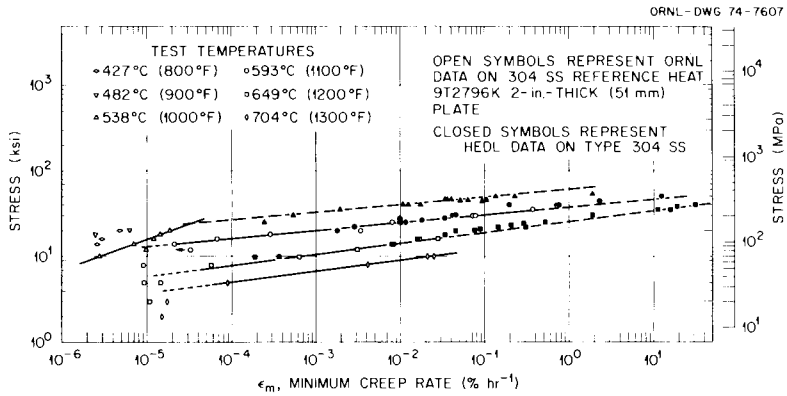

Fig. 5.3. Stress Versus Minimum Creep Rate for Reference Heat 9T2796K of Type 304 Stainless Steel Compared with Hanford Data.

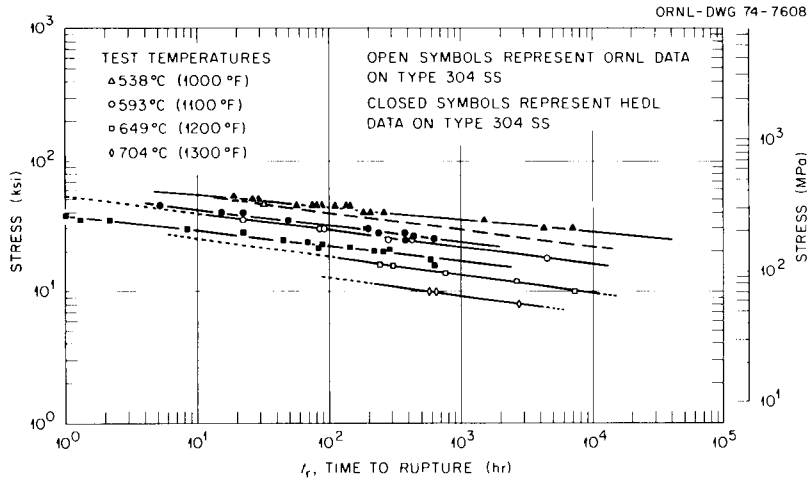

Fig. 5.4. Stress Versus Time to Rupture for Reference Heat 9T2796K of Type 304 Stainless Steel Compared with Hanford Data.

in Fig. 5.5. The ORNL minimum creep data on reference heat 2-in. plate (51-mm) and 1-in. (25-mm) plate,[2] Fig. 5.5, show very good agreement for all test conditions.

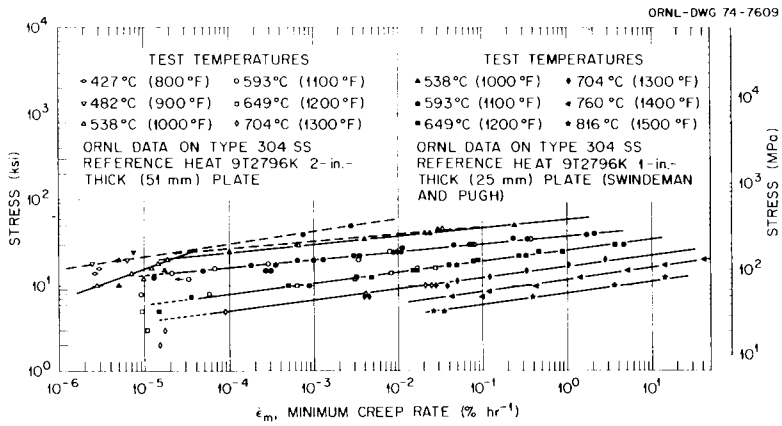

Fig. 5.5. Stress Versus Minimum Creep Rate for Reference Heat 9T2796 of Type 304 Stainless Steel Compared with Reference Heat Data of Swindeman and Pugh.

The HEDL[3] creep data are limited to only three test temperatures and test times less than 7000 hr, whereas Swindeman and Pugh[4] data extend to seven different test temperatures and to test times yielding minimum creep rates values down to approximately 5×10^{-6} %/hr. The present creep data on reference heat 2-in. (51-mm) plate are at six different temperatures and test times reaching 14,000 hr, and testing is still continuing.

In general, minimum creep rate versus stress data fit a power law of the type

$$\dot{\varepsilon}_m = A_m \, \sigma^{n_m} \, . \tag{1}$$

For minimum creep rate values greater than a critical minimum, which increases with increasing test temperature in the range 593 to 704°C (1100–1300°F), Eq. (1) is obeyed and yields values of stress exponent, n_m, in the range 7.9 to 10.9. In the same temperature range for minimum creep rate values less than critical the stress exponent, n_m, approaches

values in the range 0.5 to 1. For the test temperature range of 427 to 538°C (800–1000°F), the minimum creep rate values are in the range of 2×10^{-6}%/hr to 2×10^{-5}%/hr and seem to show a stress exponent of about 2.8 to 3.0.

The stress versus time to rupture data can also be approximated by a power law, similar to Eq. (1), as:

$$1/t_r = A_r \, \sigma^{n_r} \, . \tag{2}$$

Constants from Eqs. (1) and (2) and their ranges are summarized in Table 5.4. It is interesting to note that the stress exponent n_r for stress versus time to rupture data is essentially the same in the temperature range 593 to 704°C (1100–1300°F), whereas n_m is significantly different for 593°C (1100°F) then for 649 and 704°C (1200 and 1300°F). A similar conclusion holds true for A_r and A_m.

Equations (1) and (2) have significance from a design point of view, because the combination of these two equations gives a measure of the so-called[5] stable creep elongation, e_s. The combination of Eqs. (1) and (2) gives

$$\dot{\varepsilon}_m t_r = e_s = \left(A_m/A_r\right) \sigma^{n_m - n_r} \, . \tag{3}$$

Elimination of σ from Eqs. (2) and (3) gives a relationship of the form

$$\dot{\varepsilon}_m t_r = e_s = C t_r^{-k} \, , \tag{4}$$

and if the value of the exponent k is zero, then

$$\dot{\varepsilon}_m t_r = e_s = C \, . \tag{5}$$

Values of C and k have been calculated for the data obtained to date and are listed in Table 5.4. For test temperatures of 649°C (1200°F) and 704°C (1300°F), the exponent k has values approaching zero, whereas for 593°C (1100°F) k is 0.35. If k is zero, one would expect the coefficient

Table 5.4. Parameters[a] in Creep Power Laws from the Present Data on Reference Heat 9T2796K 2-in. Plate (51 mm) of Type 304 Stainless Steel

Test Temperature		Stress Range		$\dot{\varepsilon}_m$ Range (%/hr)	$\dot{\varepsilon}_m = A_m \sigma^{n_m}$		$1/t_r = A_r \sigma^{n_r}$		$\dot{\varepsilon}_m t_r = e_s = C t_r^{-k}$	
(°C)	(°F)	(ksi)	(MPa)		n_m	A_m	n_r	A_r	(C)	(k)
427	800	14–20	96–138	$2 \times 10^{-6} - 6.4 \times 10^{-6}$	~3	6.9×10^{-8}				
482	900									
538	1000	10–20	60–138	$2.8 \times 10^{-6} - 3.5 \times 10^{-5}$	2.8	4.5×10^{-9}				
593	1100	14–35	96–241	$2.0 \times 10^{-5} - 3.7 \times 10^{-1}$	10.9	6.8×10^{-18}	8.1	1.4×10^{-14}	35.4	0.35
649	1200	6–16	41–110	$1.3 \times 10^{-5} - 2.8 \times 10^{-2}$	7.9	8.0×10^{-12}	7.3	6.0×10^{-12}	12.8	0.08
649	1200	3–5	21–34	$1 \times 10^{-5} - 4 \times 10^{-5}$	0.5					
704	1300	4–10	28–69	$1.5 \times 10^{-5} - 2.5 \times 10^{-2}$	7.9	3.1×10^{-10}	7.2	9.9×10^{-11}	24.8	0.09
704	1300	2–4	14–28	$1.5 \times 10^{-5} - 1.8 \times 10^{-5}$	0.5					

[a]Values are based on stresses in ksi.

C to increase with increasing test temperature; however, in the present case k deviated from zero, and thus increasing values of C were not observed over the whole test temperature range.

The significance of quantity e_s in relation to the creep curve is shown in Fig. 5.6. The values of e_s calculated from the present data are plotted in Fig. 5.7. The solid lines have been calculated from Eq. (4). The "stable" creep strain values were also calculated for the HEDL creep data[3] and are compared with the present data in Fig. 5.8. Some tenative conclusions from Figs. 5.7 and 5.8 are as follows:

1. Stable creep strain e_s decreases with decreasing test temperature.
2. Generally e_s decreases with increasing time to rupture.
3. In particular at temperatures up to 593°C (1100°F) e_s decreases sharply with increasing time to rupture.
4. The lowest value of e_s observed at test times approaching 7500 hr is approximately 2% at 528 and 593°C (1000 and 1100°F).

No tests at 427 and 482°C (800 and 900°F) have ruptured at present; however, data from these tests are expected to be available in the future.

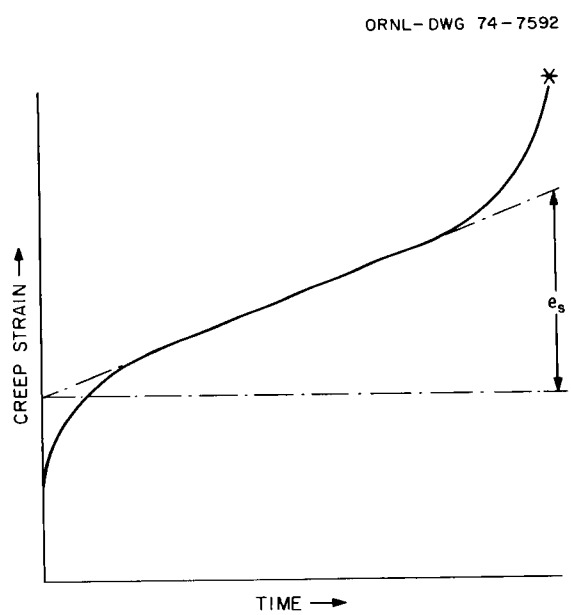

Fig. 5.6. Definition of the Quantity e_s.

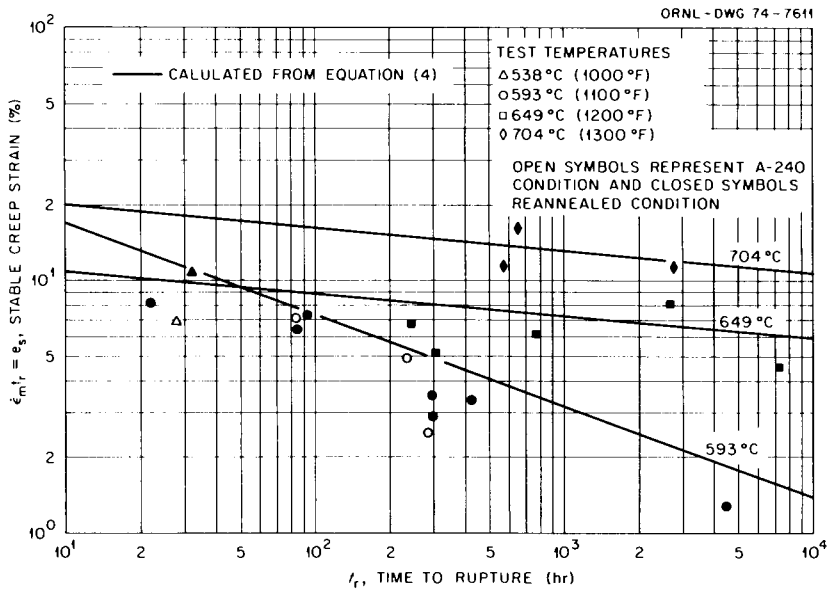

Fig. 5.7. Stable Creep Strain Versus Time to Rupture for Reference Heat 9T2796K 2-in. (51-mm) Plate of Type 304 Stainless Steel.

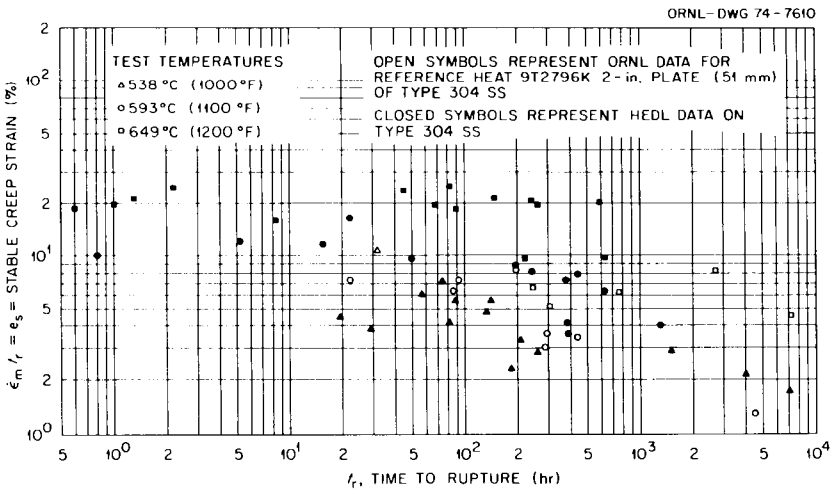

Fig. 5.8. Stable Creep Strain Versus Time to Rupture; Comparison Between ORNL and Hanford Data.

Although e_s is a rather useful measure of ductility, total elongation at rupture and reduction of area can also be used as a guide in defining a long-term ductility or strain limit. Krisch[6] reported elongation at rupture and reduction of area data for creep tests on stainless steel to test times reaching 30,000 hr. Krisch's data are compared in Fig. 5.9 with ORNL reference heat data. One of our creep tests on heat 845 of type 304 stainless steel ruptured at 14,077 hr (longest ruptured test available) and thus has also been included in Fig. 5.9. Chemical analysis of ORNL heats and that of the material used by Kirsch have been included on Fig. 5.9. The present data for reference heat and test temperatures of 593 and 649°C (1100 and 1200°F) compare reasonably well with data by Kirsch.[6] The important point to note is that at 593 and 649°C (1100 and 1200°F) the rupture elongations reach values of 2 and 3%, respectively, and reduction of area values of 5% at time periods of 25,000 to 30,000 hr.

Work will continue in this area, and more results will be plotted as they become available.

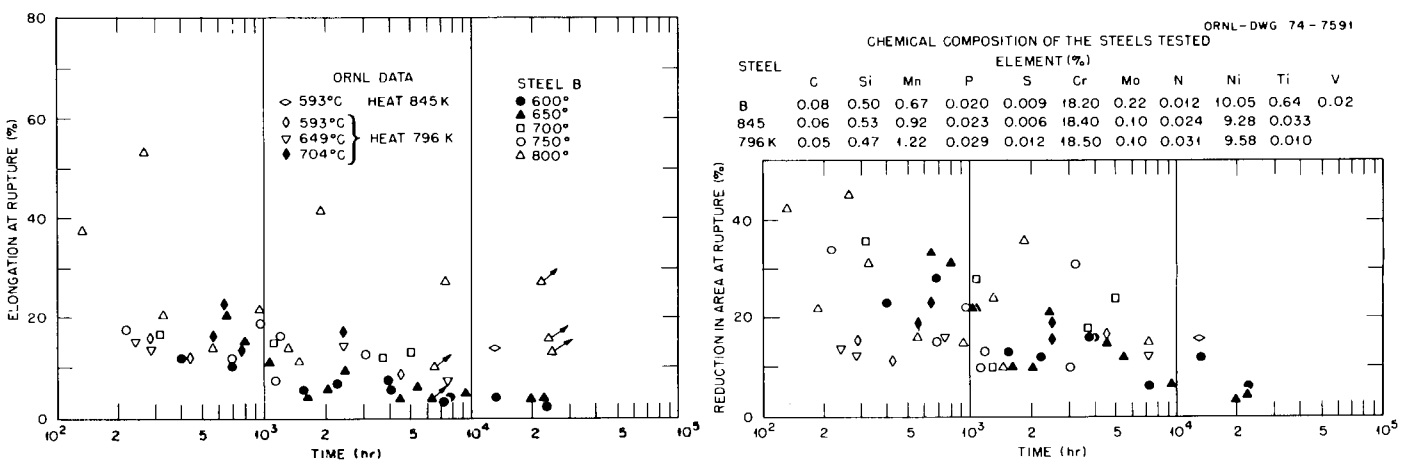

CHEMICAL COMPOSITION OF THE STEELS TESTED

STEEL	ELEMENT (%)										
	C	Si	Mn	P	S	Cr	Mo	N	Ni	Ti	V
B	0.08	0.50	0.67	0.020	0.009	18.20	0.22	0.012	10.05	0.64	0.02
845	0.06	0.53	0.92	0.023	0.006	18.40	0.10	0.024	9.28	0.033	
796 K	0.05	0.47	1.22	0.029	0.012	18.50	0.10	0.031	9.58	0.010	

Fig. 5.9. Ductility of Reference Heat of Type 304 Stainless Steel Compared with Data Reported by Kirsch, *Joint Intern. Conf. Creep*, The Institute of Mechanical Engineers, London, 1963, pp. 1-81—1-89.

5.2.3. Heat-to-Heat Variation of Mechanical Properties of Types 304 and 316 Stainless Steel — V. K. Sikka

5.2.3.1 Long-Term Creep Tests in Heat-to-Heat Variation Study of Type 304 Stainless Steel

Ten long-term creep tests are in progress on several heats of type 304 stainless steel at 593°C (1100°F). One test on heat 845 went to rupture after 14,077 hr. The creep curve for this long-term test is shown in Fig. 5.10. The time to third stage (0.2% offset) in this test was 11,000 hr, and the creep strain at that time was 3.6%. The rupture elongation was 12.8%, whereas creep strain to rupture was 11.4%. The reduction of area at rupture was 15%. The stable creep strain (defined in Fig. 5.6) was 1.97%.

The other nine long-term creep tests are still in progress, and their present status is shown in Table 5.5. Two of the creep tests have reached test times of 23,000 hr and seem to be moving much faster and might rupture in the next three months. These tests will add very useful information concerning the strain limit problem, the effect of variation in composition on long-term tests, and a more reliable creep equation. The ruptured creep specimen will be used to study the microstructural stability, type of precipitation, nature of cracking, and substructure.

5.2.3.2 Effect of Aging on the Tensile Properties of Type 304 Stainless Steel

The investigation of influence of aging on the mechanical properties of various heats of type 304 stainless steel continued. The program involves nine heats of type 304 stainless steel and various combinations of aging time and temperature. The scope of the aging program is shown in Fig. 5.11(a). Six more blocks of heat 544 aged 4000 hr were removed from the furnace. The present status of the aging program is shown in Fig. 5.11(b). Some of the blocks of heats 845 and 926 had come out after aging periods of 10,000 hr. Blocks of other heats are about to reach 10,000 hr and will become available for machining into specimens during the next three months.

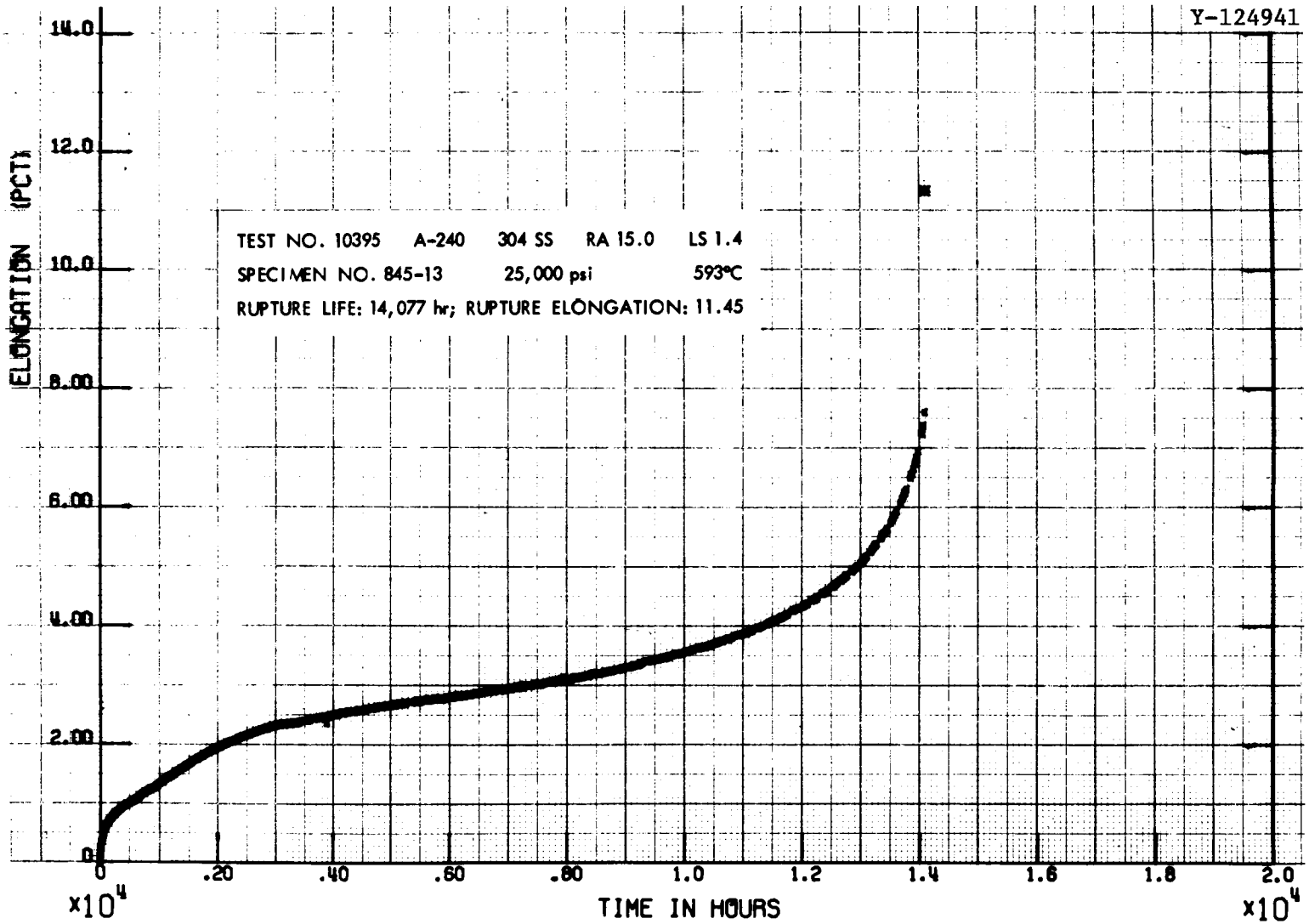

Fig. 5.10. Creep Curve for Heat 845, Tested at 593°C (1100°F) and a Stress of 25 ksi (207 MPa).

Table 5.5 Status of Several Long-Term Creep Tests of Type 304 Stainless Steel at 593°C (1100°F)

Test	Heat	Condition[a]	Stress, (ksi)	Stress, (MPa)	Test Time (hr)	Strain, % Loading	Strain, % Creep	Minimum Creep Rate (%/hr)	Time to Onset of Tertiary Creep (hr)
10396	60551	A 479	25.0	172	15,035	1.81	3.962	1.4×10^{-4}	>12,732
10395	346845	A 240	25.0	172	Ruptured	1.37	11.35	1.4×10^{-4}	11,000
9499	300380	Reannealed	17.0	117	21,230	0.72	0.91	~0	>18,878
9483	600414	Reannealed	17.0	117	21,300	1.49	0.926	1.1×10^{-5}	>18,999
9464	337330	A 240	17.0	117	21,564	−0.20	0.98	5.5×10^{-6}	>19,212
9446	9T2796	A 479	17.0	117	21,565	0.13	1.14	2.1×10^{-5}	>19,262
9443	337187	A 240	17.0	117	21,528	0.47	4.455	9.7×10^{-5}	17,000
9371	55697	A 479	17.0	117	21,765	0.62	3.63	1.4×10^{-4}	15,500
9221	600414	A 240	17.0	117	23,702	0.18	0.712	1.0×10^{-5}	>21.398
9508	346544	A 240	17.0	117	21,128	0.22	3.00	3.5×10^{-5}	17,300

[a]As received per indicated specification or reannealed 0.5 hr at 1065°C (1950°F).

[b]Unless otherwise noted tests are in progress.

(a)

X-22807
600414
300380
9T2796K
R22926
346845
8043813
346544
3121

Aging Program

Time (hr)	Temperature (°F)
1,000	900
2,000	1100
4,000	1200
10,000	

(1) Microstructure
(2) Tensile Properties, RT, 1100°F
(3) Creep Behavior at

1100°F – 30 ksi (100 to 2000 hr)
1100°F – 17 ksi (Disc. 2000 hr)
1200°F – 14 ksi (Disc. 2000 hr)
900°F – 20 ksi (Disc. 2000 hr)

(b)

ORNL-DWG 73-11407R3

AGING TIME (hr)	482	593	649
10,000	121 □ 414 ○,□ 380 ○,□ 796 ○,□ 845 ○,■ 807 ○,□ 813 ○,□ 926 ■ 544 ○,□	414 ○,□ 380 ○,□ 796 ○,□ 845 ○,■ 807 ○,□ 813 ○,□ 926 ■ 544 ○,□	121 □ 414 ○,□ 380 ○,□ 796 ○,□ 845 ○,■ 807 ○,□ 813 ○,□ 926 ■ 544 ○,□
4000	414 ●,■ 380 ●,■ 796 ●,■ 845 ●,■ 807 ●,■ 813 ■ 926 ■ 544 ○,□	414 ●,■ 380 ●,■ 796 ●,■ 845 ●,■ 807 ■ 813 ■ 926 ■ 544 ○,□	414 ●,■ 380 ●,■ 796 ●,■ 845 ●,■ 807 ●,■ 813 ■ 926 ■ 544 ●,■
2000	121 ■	845 ■ 807 ■ 813 ■ 544 ●,■	121 ■ 414 ● 380 ● 796 ●,■ 845 ●,■ 807 ●,■ 813 ■ 544 ●,■
1000			414 ● 380 ● 796 ●,■ 845 ●,■ 807 ●,■ 813 ■ 544 ●,■

AGING TEMPERATURE (°C)

○ ANNEALED 0.5 hr AT 1065°C PRIOR TO AGING
□ AGED IN AS-RECEIVED CONDITION
OPEN SYMBOLS – AGING IN PROGRESS
CLOSED SYMBOLS – COMPLETED

Fig. 5.11. Aging Program for Type 304 Stainless Steel. (a) Scope. (b) Status.

Several of the aged samples have been tensile tested at both room temperature and 593°C (1100°F). The tensile data on heats 845 and 926 have become available on specimens aged for 10,000 hr. The properties for these heats have been plotted as bar charts in Figs. 5.12 through 5.17. The results suggest that the changes in tensile properties are functions of (a) pretreatment, (b) aging temperature, (c) aging time, and (d) test temperature.

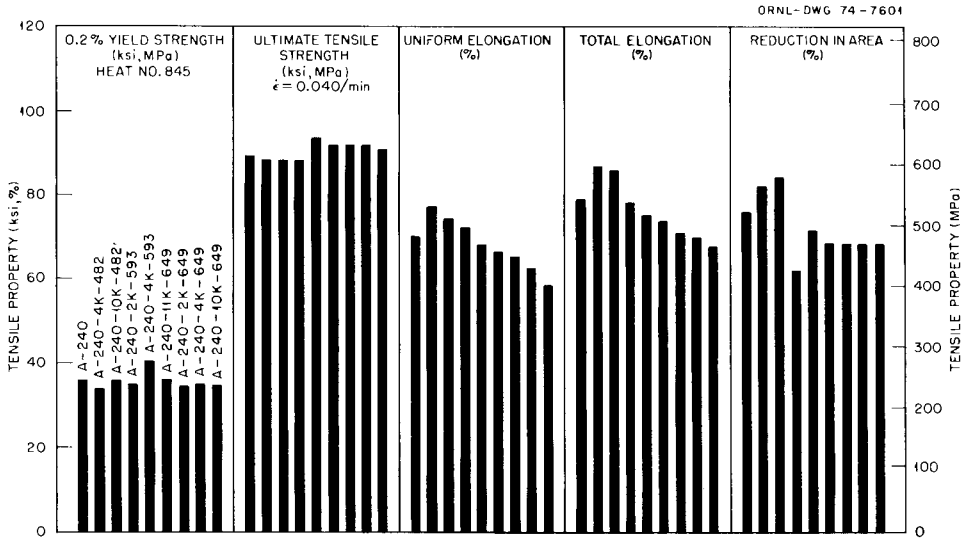

Fig. 5.12. Effect of Aging on Tensile Properties at Room Temperature for Heat 346845 Aged in the As-Received Condition.

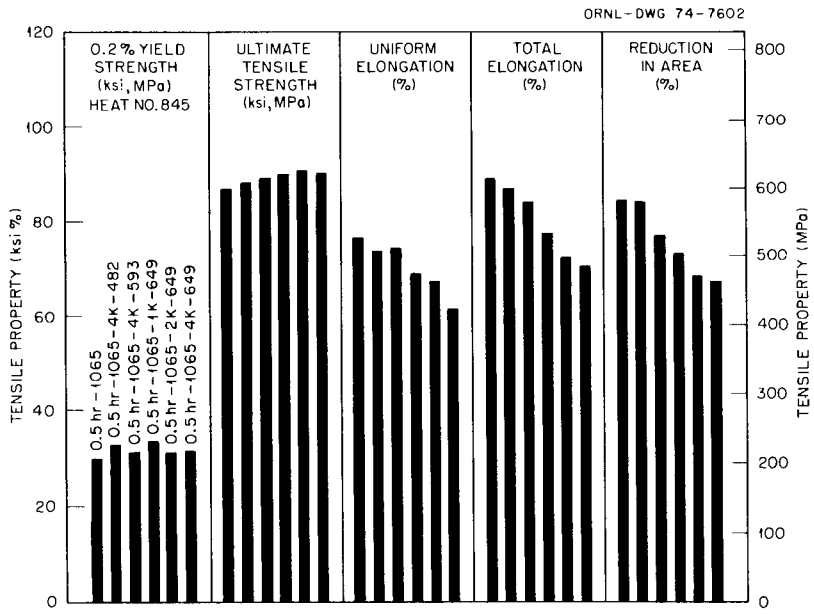

Fig. 5.13. Effect of Aging on Tensile Properties at Room Temperature for Heat 346845 Aged in the Reannealed Condition.

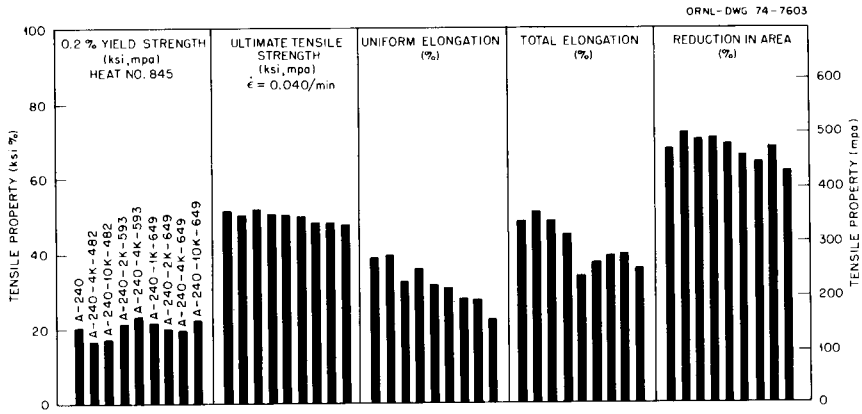

Fig. 5.14. Effect of Aging on Tensile Properties at 593°C (1100°F) for Heat 346845 Aged in the As-Received Condition.

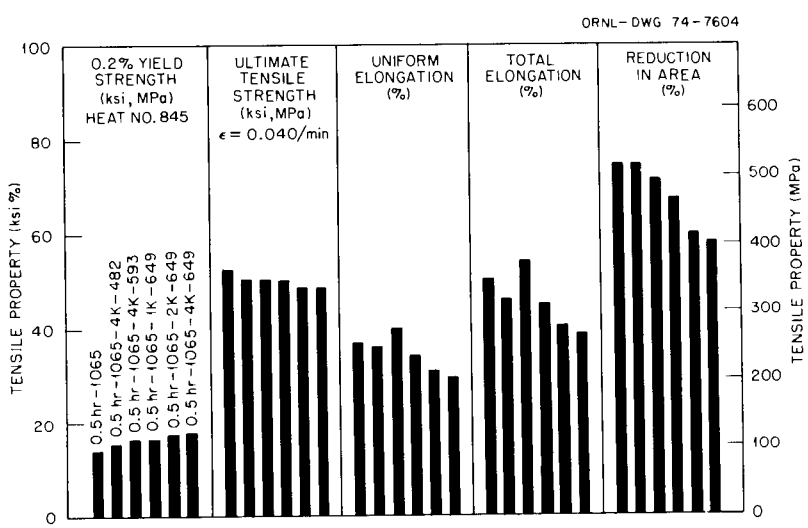

Fig. 5.15. Effect of Aging on Tensile Properties at 593°C (1100°F) for Heat 346845 Aged in the Reannealed Condition.

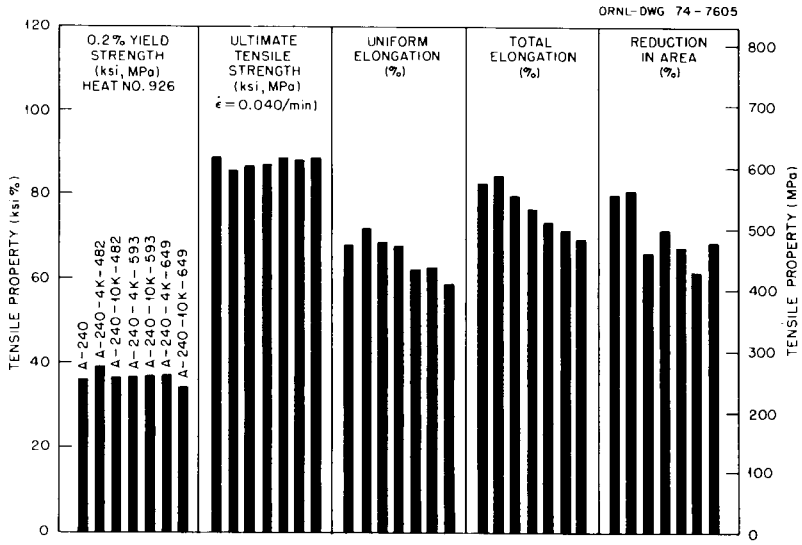

Fig. 5.16. Effect of Aging on Tensile Properties at Room Temperature for Heat R22926 Aged in the As-Received Condition.

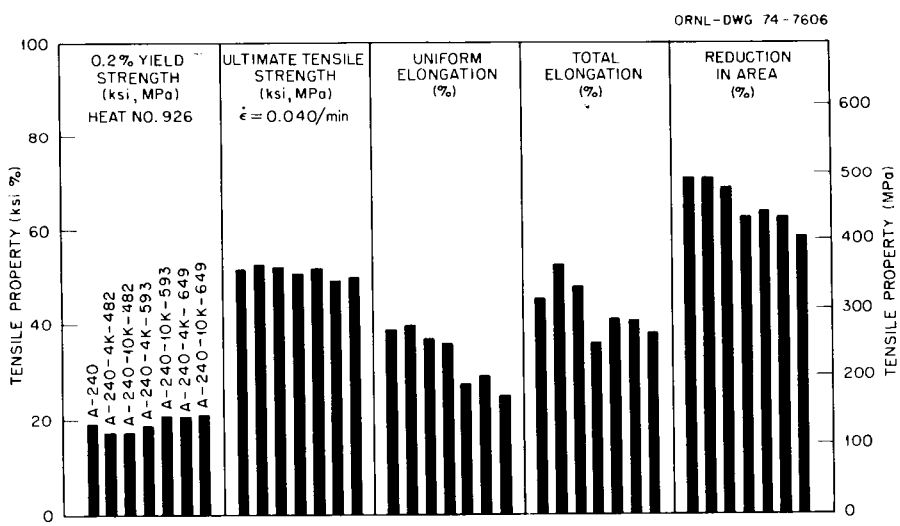

Fig. 5.17. Effect of Aging on Tensile Properties at 593°C (1100°F) for Heat R22926 Aged in the As-Received Condition.

5.2.3.2.1 Effect of Aging Time. The changes in tensile properties for specimens tested at room temperature and 593°C (1100°F) for heat 845 in the A 240 condition, then aged at 649°C (1200°F), are plotted as a function of aging time in Fig. 5.18.

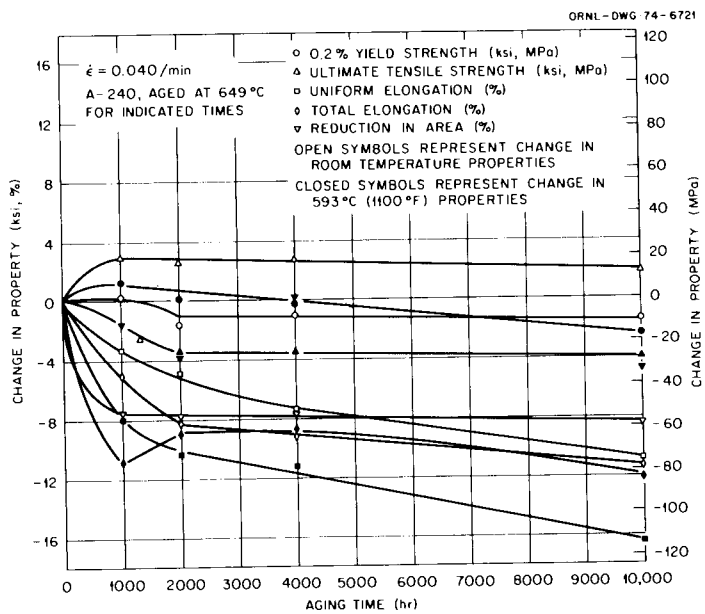

Fig. 5.18. Change in Tensile Properties at Room Temperature and 593°C (1100°F) as Functions of Aging Time for Heat 346845 of Type 304 Stainless Steel in A 240 Condition.

Several comments on Fig. 5.18 are:

1. The 0.2% yield strength showed relatively large changes for a test temperature of 593°C (1100°F) as compared with room temperature.

2. Ultimate tensile strength at room temperature increased and that at 593°C (1100°F) decreased, but the changes were not affected significantly by aging times up to 10,000 hr.

3. Uniform elongation decreased continuously as a function of aging time. The decrease was much greater for specimens tested at 593°C (1100°F) as compared with room temperature. The maximum reduction in uniform elongation observed for 10,000 hr aging and test temperature of 593°C (1100°F) was 16.6%.

4. Total elongation also decreased continuously with increasing aging time. The amount of change for room temperature and 593°C (1100°F) was essentially the same.

5. Consistent with uniform elongation, reduction of area showed small changes for test temperature of 593°C (1100°F) as compared with room temperature. The changes in reduction of area were maximum for 1000 hr and then remained constant with further increase in aging time.

Effect of aging time and temperature on tensile properties at room temperature and 593°C (1100°F) for heat 926 is shown in Fig. 5.19.

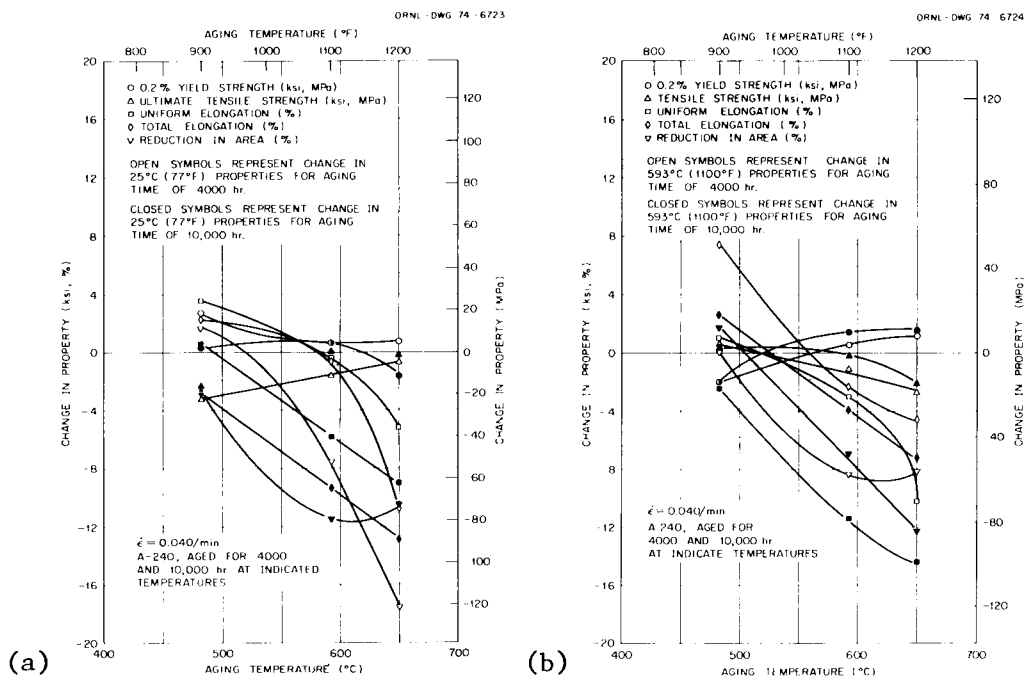

Fig. 5.19. Change in Tensile Properties As Functions of Aging Temperature for Heat R22926 of Type 304 Stainless Steel in A 240 Condition Aged 4000 and 10,000 hr. (a) Tested at room temperature. (b) Tested at 593°C (1100°F).

Some comments from Fig. 5.19 are as follows:

1. The 0.2% yield strength for room-temperature tests did not show any significant effect of aging time or temperature, while those at 593°C (1100°F) showed a decrease for an aging temperature of 482°C (900°F), followed by an increase with increasing temperature and time.

2. Room-temperature ultimate tensile strength showed a maximum decrease at an aging temperature of 482°C (900°F), but recovered with increasing aging temperature. The changes in ultimate tensile strength were smaller for longer aging time. At a test temperature of 593°C (1100°F)

and an aging temperature of 482°C (900°F), there were no changes in ultimate tensile strength. For higher aging temperatures tensile strength decreased, and the amount of decrease was smaller for a 10,000 hr aging time as compared with 4000 hr.

3. Uniform elongation for tensile tests at room temperature increased slightly at an aging temperature of 482°C (900°F), but decreased continuously with increasing temperature and time. At a test temperature of 593°C (1100°F) uniform elongation decreased even at an aging temperature of 482°C (900°F), and showed further decrease with decreasing aging temperature. The decrease was again more for 10,000 hr aging than for 4000 hr.

4. Total elongation and reduction of area followed the same trends as uniform elongation for both test temperatures.

5.2.3.2.2 Effect of Aging and Test Temperatures. Effect of aging temperature on the room-temperature and 593°C (1100°F) properties of heats 845 and 807 aged in A 240 conditions for 4000 hr is shown in Fig. 5.20. Similar plots for heat 926 have already been shown in Fig. 5.19. Some general comments on all heats are:

1. A maximum influence on tensile properties is observed for an aging temperature of 649°C (1200°F).

2. For relatively small changes in strength properties, ductility shows a considerable decrease.

3. Uniform elongation at 593°C (1100°F) can decrease by 15 to 20% at an aging temperature of 649°C (1200°F).

4. Heat 807, which is more close in chemical composition to type 304L stainless steel, shows large changes in properties, even after aging at 482°C (900°F). Further increase in aging temperature only produces a small increment.

5.2.3.3 Influence of Aging on Creep Properties of Type 304 Stainless Steel

Several heats of type 304 stainless steel are being aged in both the as-received and reannealed condition at 482, 593, and 649°C (900, 1100 and 1200°F) for aging periods of 1000, 2000, 4000, and 10,000 hr.

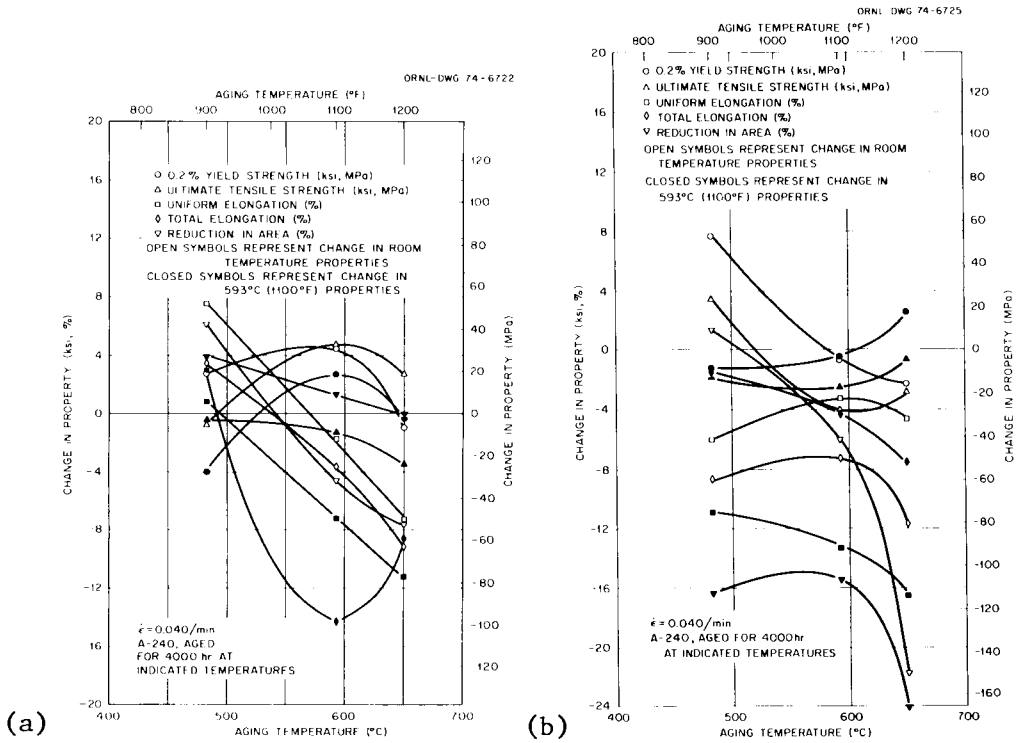

Fig. 5.20. Change in Tensile Properties at Room Temperature and 593°C (1100°F) as Functions of Aging Temperature of Type 304 Stainless Steel in A 240 Condition. (a) Heat 346845. (b) Heat X22807.

The scope and the status of this program have already been presented in Fig. 5.11. In addition to the tensile tests (described in the previous section), creep tests are also being conducted on the aged specimens. A total of 37 creep tests has been completed, 13 on heat 845, nine on the reference heat (796K), ten on heat 807, two on heats 544 and 121, and one on heat 380.

All creep tests on the aged specimens have been performed at a test temperature of 593°C (1100°F), initial creep stress of 30 ksi (207 MPa), and test times up to 1450 hr. Although more tests of longer duration and on other aged heats of type 304 stainless steels are continuing, the present results show the following:

1. The minimum creep rate and time to rupture may both increase.
2. The minimum creep rate may decrease and time to rupture increase.
3. Both minimum creep rate and time to rupture may remain unchanged.

Out of the six differene heats studied, two heats showed increase in both minimum creep rate and time to rupture, two of them showed

decrease in minimum creep rate and increase in time to rupture, whereas one heat showed the mixed behavior.

5.2.3.4 Heat-to-Heat Variation of Type 316 Stainless Steel

Seven wrought and one as-cast heats of type 316 stainless steel are currently included in this program. The reference heat will be added to this program as soon as it becomes available. The test program being followed in this program is outlined in Fig. 5.21.

Parts A, B, and C have been completed on all heats except the reference heat. Tensile properties for parts A and B were reported previously.[7] Effects of composition and grain size variation were investigated and are presented in Sec. 5.2.3.6. All creep tests in Part C have been completed. One of the heats, 686, was exceptionally strong, and thus additional creep tests were performed at a stress of 50 ksi (345 MPa).

The status of the aging program in part D is shown in Fig. 5.22. All blocks aged for periods of 4000 hr have been taken out of the furnace and machined into specimens. The tensile tests on all aged specimens have been completed, whereas creep tests are still in progress. Tensile and creep tests listed in parts F and G of Fig. 5.21 will be started on the reference heat when it becomes available.

5.2.3.5. Influence of Aging on Tensile and Creep Properties of Type 316 Stainless Steel

Tensile tests have been performed on aged specimens at room temperature and 593°C (1100°F) at a strain rate of 0.040/min. The results for heats 613, 686, and 212 are summarized in Tables 5.6 through 5.11. Change in tensile properties at room temperature and 593°C (1100°F) in the as-received and reannealed condition are plotted as a function of aging temperature in Fig. 5.23. Some general comments on this figure are as follows:

1. Yield strength at room temperature decreases, whereas at 593°C (1100°F) it increases with the increasing aging temperature.

2. Ultimate tensile strength at room temperature increases, whereas at 593°C (1100°F) it decreases with increasing aging temperature.

Select 8 Heats

(A)

As-Received
Tensile Tests
Strain rate 0.04/min
RT, 427, 593, and 649°C (800, 1100, and 1200°F)

Complete

Complete

(B)

Annealed 0.5 hr at 1065°C (1950°F)
Tensile Tests
Strain rate 0.04/min
RT, 427, 593, and 649°C (800, 1100, and 1200°F)

8 Heats

(C)

Creep and Rupture Study
593°C (1100°F)
(10 to 3000 hr tests)

As-Received	Annealed
35 ksi (241 MPa)	35 ksi (241 MPa)
40 ksi (276 MPa)	40 ksi (276 MPa)

Complete

(E)

Tests on Selected Heats to Determine Stress and Temperature Dependence
4 Heats

538°C (1000°F): 40 ksi (276 MPa)
593°C (1100°F): 40, 30, and 20 ksi (276, 207, and 138 MPa)
649°C (1200°F): 40 ksi (276 MPa)

In Progress

4 Selected Heats

(D)

Heats	Aging Program Time (hr)	Temperature (°C)	Temperature (°F)
915509	1,000	482	900
327686 com-	2,000	593	1100
500613 plete	4,000	649	1200
2P3212	10,000		

In Progress (1) Microstructure.
Complete (2) Tensile Properties, RT, 593°C (1100°F)
In Progress (3) Creep Behavior at:
593°C (1100°F) - 40 ksi (276 MPa)
593°C (1100°F) - 35,000 (241 MPa)

Select One Heat for Detailed Study in Reannealed* Condition

(F)

Tensile Tests in Addition to Above†

Temperature (°C)	(°F)	Strain Rate (min^{-1})
538	1000	0.004
593	1100	0.004
649	1200	0.004
593	1100	0.0004

To Start on Reference Heat

To Start on Reference Heat

(G)

Creep Tests in Addition to Above†

Temperature (°C)	(°F)	Stress (ksi)	(MPa)	Loading Strain Rate (min^{-1})	Duration (hr)
538	1000	14	97	0.005	50,000
593	1100	10	69	0.0005	1,000
593	1100	10	69	0.005	50,000
593	1100	10	69	0.25	1,000
593	1100	14	97	0.005	35,000
593	1100	16	110	0.0005	1,000
593	1100	16	110	0.005	10,000
593	1100	16	110	0.25	1,000
648	1200	14	97	0.005	10,000

*Reannealed for 0.5 hr at 1065°C (1950°F) in argon and air cooled.
†Tests will be started after the procurement of the reference heat.

Fig. 5.21. Heat-to-Heat Variation Program, Type 316 Stainless Steel.

ORNL-DWG 73-11408R2

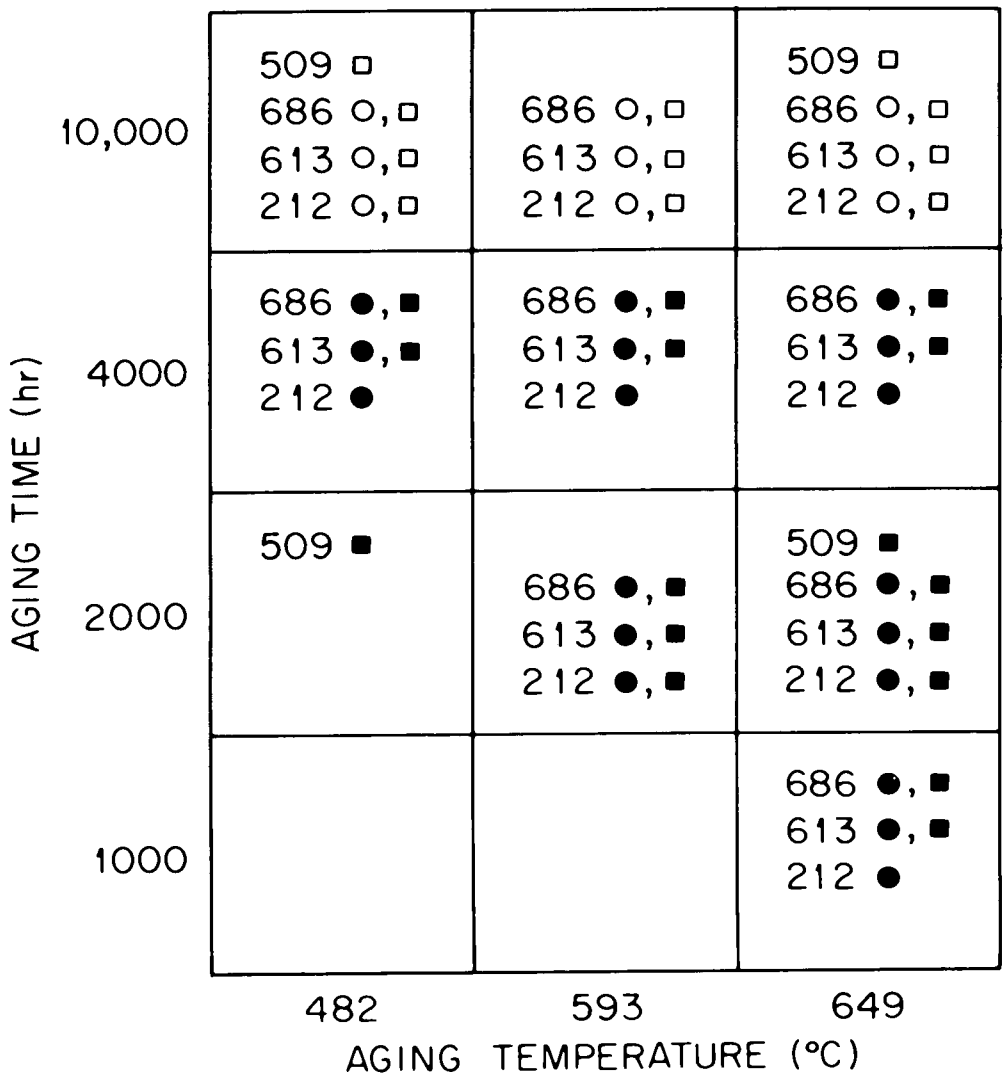

○ ANNEALED 0.5 hr AT 1065°C PRIOR TO AGING
□ AGED IN AS-RECEIVED CONDITION
OPEN SYMBOLS – AGING IN PROGRESS
CLOSED SYMBOLS – COMPLETED

Fig. 5.22. Aging Program for Type 316 Stainless Steel.

Table 5.6. Tensile Properties of Type 316 Stainless Steel Heat 613 at 25°C (77°F) and a Strain Rate of 0.040/min

Condition	Treatment			Stress, ksi(MPa)		Strain, %		Reduction of Area (%)
	Time (hr)	Temperature (°C)	Temperature (°F)	Yield	Ultimate Tensile	Uniform	Total	
A 240				37.8(261)	86.5(596)	54.4	69.0	67.0
A 240, aged	4000	482	900	41.9(289)	88.7(612)	48.3	65.4	64.3
A 240, aged	2000	593	1100	41.2(284)	90.9(627)	53.0	61.9	57.8
A 240, aged	4000	593	1100	40.1(276)	91.4(630)	47.0	61.6	58.6
A 240, aged	1000	649	1200	41.9(289)	92.9(641)	44.0	55.1	57.1
A 240, aged	2000	649	1200	39.0(267)	91.5(631)	46.5	55.2	57.8
A 240, aged	4000	649	1200	39.0(267)	92.5(638)	40.7	52.2	53.4
Reannealed	0.5	1065	1950	35.1(242)	85.7(591)	64.0	72.4	65.8
Reannealed, aged	4000	482	900	38.2(263)	88.2(608)	52.7	68.6	53.7
Reannealed, aged	2000	593	1100	52.6(363)	102.7(708)	40.9	52.6	61.5
Reannealed, aged	4000	593	1100	37.7(260)	89.6(618)	54.0	62.0	61.2
Reannealed, aged	1000	649	1200	35.5(245)	89.4(616)	48.8	60.3	58.5
Reannealed, aged	2000	649	1200	37.4(258)	89.6(618)	48.0	58.9	58.9
Reannealed, aged	4000	649	1200	37.0(255)	91.0(627)		55.6	53.2

Table 5.7. Tensile Properties of Type 316 Stainless Steel Heat 613 at 593°C (1100°F) and a Strain Rate of 0.040/min

Condition	Treatment			Stress, ksi(MPa)		Strain, %		Reduction of Area (%)
	Time (hr)	Temperature (°C)	Temperature (°F)	Yield	Ultimate Tensile	Uniform	Total	
A 240				18.1(125)	63.2(436)	45.6	45.5	53.9
A 240, aged	4000	482	900	20.0(138)	64.2(443)	37.9	46.3	54.9
A 240, aged	2000	593	1100	21.6(149)	62.5(431)	33.0	44.5	52.5
A 240, aged	4000	593	1100	21.8(150)	59.4(410)	29.3	42.2	49.3
A 240, aged	1000	649	1200	22.0(152)	62.7(432)	33.6	41.9	49.9
A 240, aged	2000	649	1200	23.3(161)	59.8(412)	26.7	35.6	52.8
A 240, aged	4000	649	1200	21.4(148)	59.3(409)	23.9	37.3	44.5
Reannealed	0.5	1065	1950	16.3(112)	63.5(438)	45.6	53.9	53.9
Reannealed, aged	4000	482	900	18.6(128)	63.1(435)	39.0	50.4	51.3
Reannealed, aged	2000	593	1100	31.1(214)	69.8(481)	31.5	40.7	55.6
Reannealed, aged	4000	593	1100	19.5(134)	59.8(412)	35.9	46.1	49.8
Reannealed, aged	1000	649	1200	20.2(139)	60.0(414)	33.6	42.4	51.9
Reannealed, aged	2000	649	1200	21.1(145)	60.8(419)		41.2	50.0
Reannealed, aged	4000	649	1200	20.9(144)	58.7(405)	24.8	36.4	45.9

Table 5.8. Tensile Properties of Type 316 Stainless Steel Heat 686 at 25°C (77°F) and a Strain Rate of 0.040/min

Condition	Treatment			Stress, ksi(MPa)		Strain, %		Reduction of Area (%)
	Time (hr)	Temperature (°C)	Temperature (°F)	Yield	Ultimate Tensile	Uniform	Total	
A 240				53.4(368)	100.3(698)	38.8	57.0	69.0
A 240, aged	4000	482	900	54.5(376)	103.9(716)	36.1	53.7	68.5
A 240, aged	2000	593	1100	57.5(396)	105.3(726)	39.0	51.0	60.9
A 240, aged	4000	593	1100	54.1(373)	104.1(718)	34.9	47.7	58.0
A 240, aged	1000	649	1200	55.6(383)	105.2(725)	36.0	45.9	59.3
A 240, aged	2000	649	1200	60.0(414)	106.7(736)	36.2	47.4	54.3
A 240, aged	4000	649	1200	54.6(376)	108.6(749)	29.4	41.3	51.6
Reannealed	0.5	1065	1950	52.2(360)	98.5(679)	39.8	57.0	70.7
Reannealed, aged	4000	482	900	53.9(372)	103.5(714)	37.0	53.9	66.5
Reannealed, aged	2000	593	1100	36.9(254)	87.5(610)	54.5	64.9	62.8
Reannealed, aged	4000	593	1100	52.2(360)	102.8(709)	35.4	48.4	58.8
Reannealed, aged	1000	649	1200	50.3(347)	103.1(711)	39.2	48.4	58.5
Reannealed, aged	2000	649	1200	49.8(343)	103.4(713)	37.8	46.4	50.2
Reannealed, aged	4000	649	1200	47.4(327)	103.7(715)	32.5	47.5	54.0

Table 5.9. Tensile Properties of Type 316 Stainless Steel Heat 686 at 593°C (1100°F) and a Strain Rate of 0.040/min

Condition	Treatment			Stress, ksi(MPa)		Strain, %		Reduction of Area (%)
	Time (hr)	Temperature (°C)	Temperature (°F)	Yield	Ultimate Tensile	Uniform	Total	
A 240				30.2(208)	75.0(517)	35.2	46.5	59.5
A 240, aged	4000	482	900	32.0(220)	83.9(578)	27.8	44.1	53.5
A 240, aged	2000	593	1100	37.3(257)	72.0(496)	27.4	40.4	50.2
A 240, aged	4000	593	1100	33.7(232)	68.6(473)	28.1	40.2	54.9
A 240, aged	1000	649	1200	35.5(245)	68.2(470)	27.2	35.7	49.5
A 240, aged	2000	649	1200	33.4(230)	69.5(479)	24.8	36.6	51.3
A 240, aged	4000	649	1200	35.9(248)	69.8(481)	18.5	28.5	45.4
Reannealed	0.5	1065	1950	28.8(199)	72.6(501)	38.4	48.8	60.5
Reannealed, aged	4000	482	900	29.1(201)	73.8(509)	30.7	42.2	54.4
Reannealed, aged	2000	593	1100	19.5(134)	62.5(431)	36.5	44.3	55.6
Reannealed, aged	4000	593	1100	29.3(202)	68.9(475)	26.1	42.9	52.1
Reannealed, aged	1000	649	1200	30.0(207)	67.8(467)	28.8	36.0	47.5
Reannealed, aged	2000	649	1200	30.6(211)	68.5(472)	26.0	34.4	48.4
Reannealed, aged	4000	649	1200	29.7(205)	68.0(469)	21.3	32.2	48.8

Table 5.10. Tensile Properties of Type 316 Stainless Steel Heat 212 at 25°C (77°F) and a Strain Rate of 0.040/min

Condition	Treatment			Stress, ksi(MPa)		Strain, %		Reduction of Area (%)
	Time (hr)	Temperature (°C)	Temperature (°F)	Yield	Ultimate Tensile	Uniform	Total	
A 240				36.8(254)	86.6(597)	60.7	72.0	73.0
A 240, aged	2000	593	1100	37.3(257)	88.6(611)	53.4	62.4	64.5
A 240, aged	1000	649	1200	35.9(218)	87.1(601)	53.6	65.7	61.6
A 240, aged	2000	649	1200	37.3(257)	91.7(632)	46.6	56.0	60.1
Reannealed	0.5	1065	1950	34.8(240)	85.0(586)	56.8	72.0	72.9
Reannealed, aged	4000	482	900	36.4(251)	86.7(612)	53.0	68.5	71.4
Reannealed, aged	2000	593	1100	36.1(249)	86.7(598)	55.7	64.4	66.4
Reannealed, aged	4000	593	1100	35.8(247)	87.6(604)	54.3	68.3	65.3
Reannealed, aged	1000	649	1200	35.9(248)	87.1(601)	53.6	65.7	61.6
Reannealed, aged	2000	649	1200	37.2(256)	90.1(621)	47.8	53.3	59.7
Reannealed, aged	4000	649	1200	38.7(267)	92.7(639)	41.1	53.7	55.2

Table 5.11. Tensile Properties of Type 316 Stainless Steel Heat 212 at 593°C (1100°F) and a Strain Rate of 0.040/min

Condition	Treatment			Stress, ksi(MPa)		Strain, %		Reduction of Area (%)
	Time (hr)	Temperature (°C)	Temperature (°F)	Yield	Ultimate Tensile	Uniform	Total	
A 240				19.2(132)	66.3(457)	44.0	49.0	60.4
A 240, aged	2000	593	1100	20.9(144)	60.6(418)	35.0	47.0	60.7
A 240, aged	1000	649	1200	18.4(127)	61.5(424)	37.6	51.4	57.2
A 240, aged	2000	649	1200	22.0(152)	60.0(414)	27.7	38.4	58.9
Reannealed	0.5	1065	1950	14.5(100)	60.6(418)	49.6	51.0	60.7
Reannealed, aged	4000	482	900	17.1(118)	60.8(419)	45.6	52.5	58.9
Reannealed, aged	2000	593	1100	18.3(126)			49.2	56.8
Reannealed, aged	4000	593	1100	19.5(134)	59.8(412)	35.9	46.1	49.8
Reannealed, aged	1000	649	1200	18.4(127)	61.5(424)	37.6	51.4	57.2
Reannealed, aged	2000	649	1200	21.7(150)	59.4(410)	37.2	35.9	53.8
Reannealed, aged	4000	649	1200	21.3(147)	59.5(410)	25.5	36.5	50.6

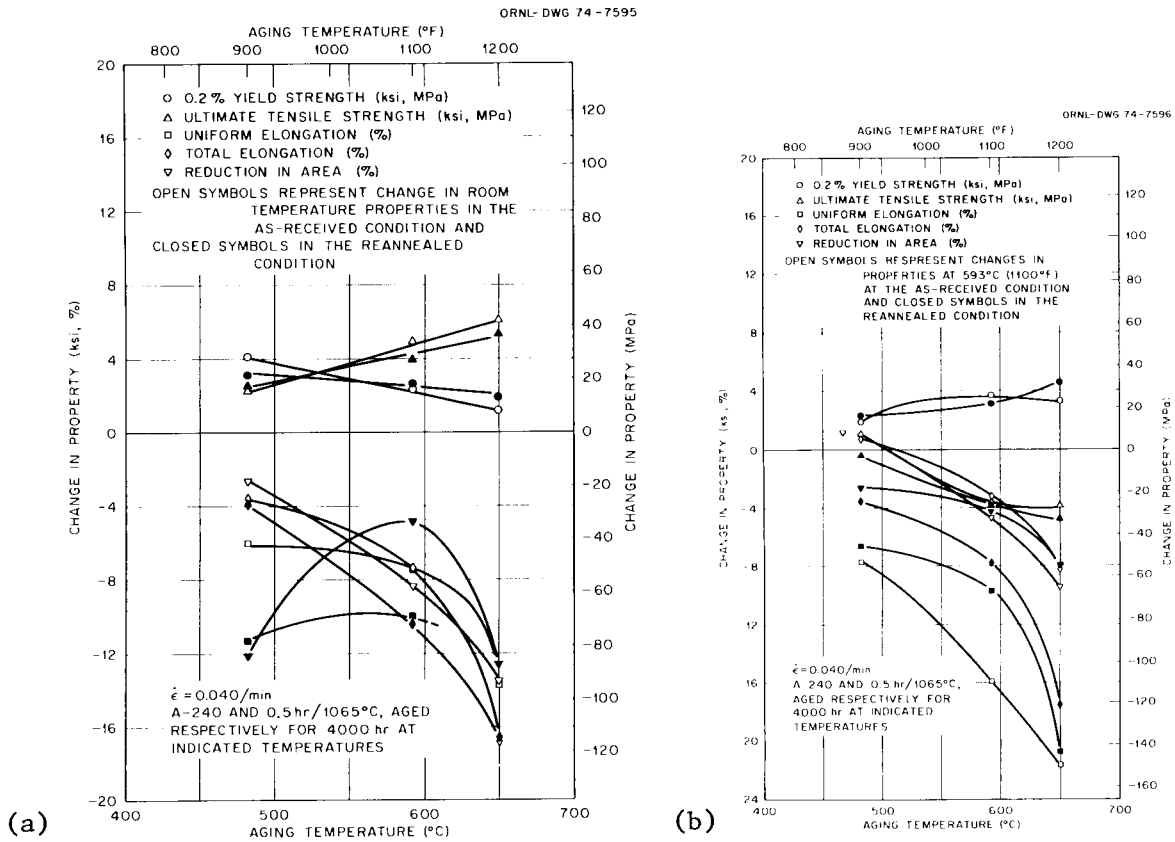

Fig. 5.23. Change in Tensile Properties as Functions of Aging Temperature for Heat 500613 of Type 316 Stainless Steel in A 240 and Reannealed Conditions. (a) Tested at room temperature, (b) Tested at 593°C (1100°F).

3. Changes in yield and ultimate tensile strengths are quite similar for both as-received and reannealed conditions.

4. Uniform elongation at room temperature and 593°C (1100°F) decreases for all aging temperatures. Furthermore, the amount of decrease increases with increasing aging temperature.

5. Uniform elongation at room temperature shows a small decrease for the as-received condition as compared with the reannealed condition, whereas at 593°C (1100°F) it shows a great decrease for the as-received condition as opposed to the reannealed.

6. The decrease in uniform elongation at 593°C (1100°F) is about 22%, compared with only 17% at room temperature.

7. Both total elongation and reduction of area at room temperature decrease for all aging temperatures, and the amount of decrease increases

with increasing aging temperature. Similar results are also observed for 593°C (1100°F).

8. The changes in total elongation and reduction of area are smaller for the as-received than reannealed condition for both room temperature and 593°C (1100°F).

The influence of aging on tensile properties at room temperature and 593°C (1100°F) for heats 613, 686, and 212 is shown in Figs. 5.24 and 5.25.

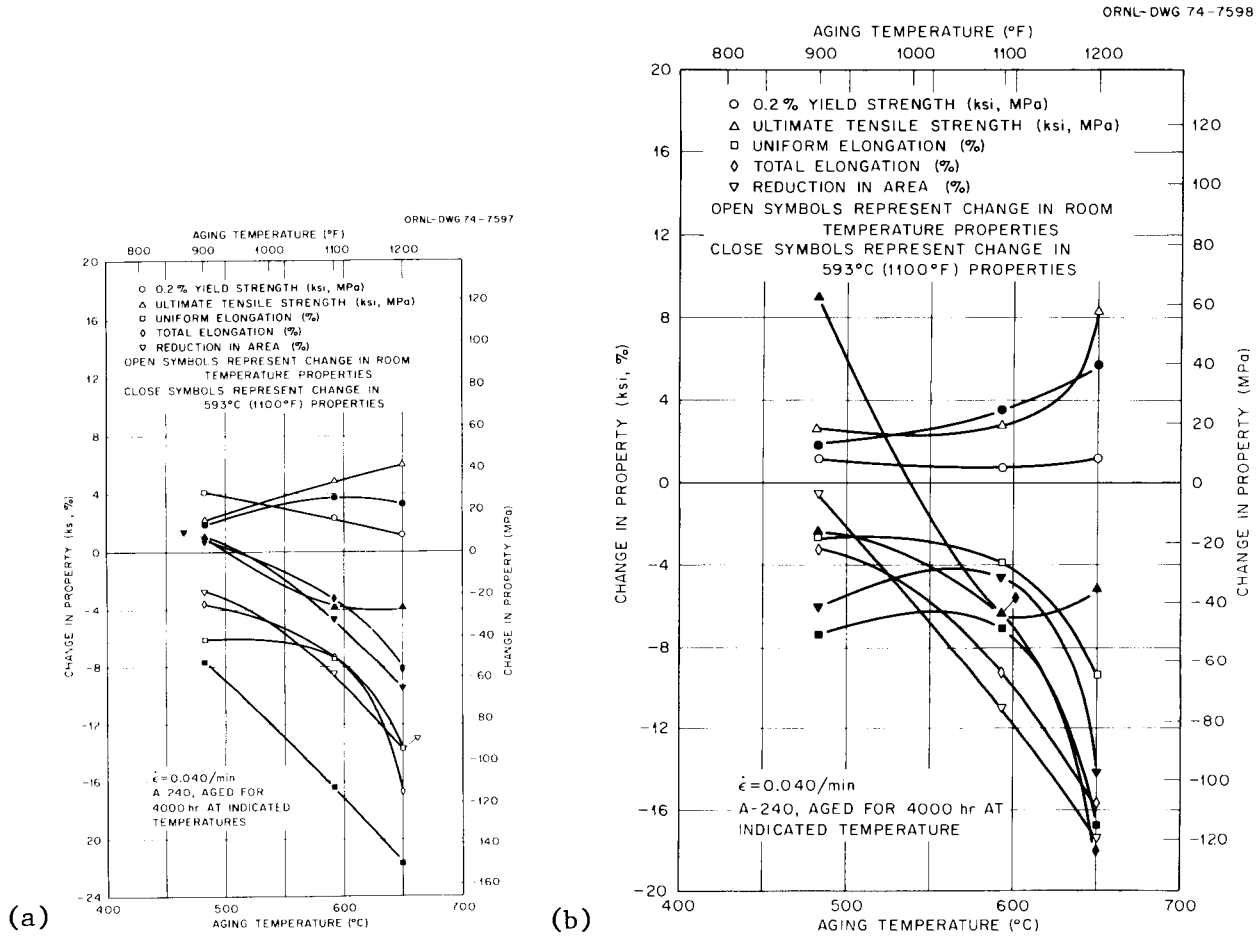

Fig. 5.24. Changes in Tensile Properties at Room Temperature and 593°C (1100°F) as Functions of Aging Temperature for Type 316 Stainless Steel in A 240 Condition. (a) Heat 500613. (b) Heat 327686.

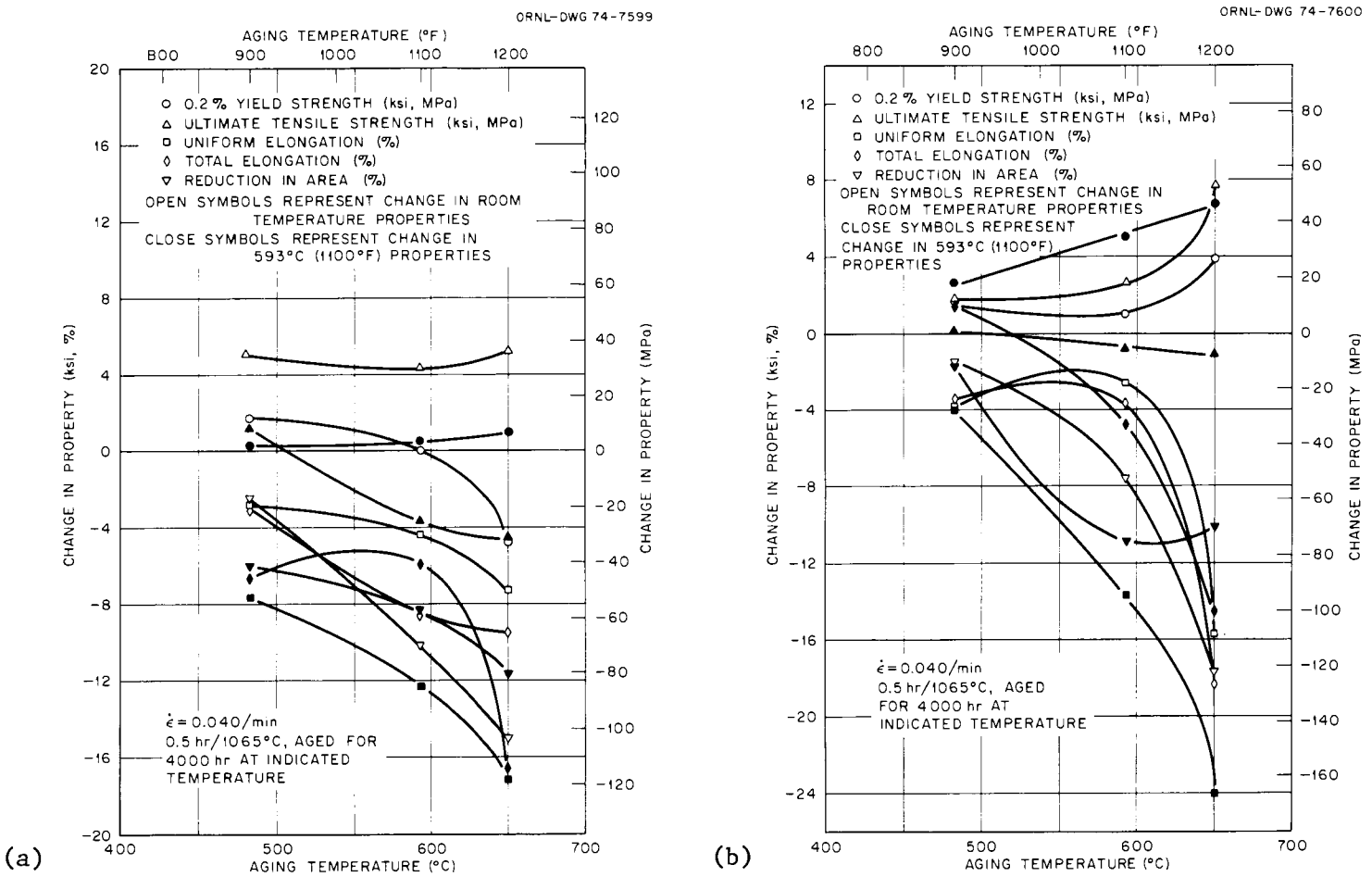

Fig. 5.25. Changes in Tensile Properties at Room Temperature and 593°C (1100°F) as Functions of Aging Temperature for Type 316 Stainless Steel in the Reannealed Condition. (a) Heat 327686. (b) Heat 2P3212.

Some very general comments on these figures are as follows:

1. Uniform elongation at 593°C (1100°F) for all heats decreases for all aging temperatures. The amount of decrease in uniform elongation is maximum for an aging temperature of 649°C (1200°F) and a period of 4000 hr.

2. The maximum decreases in uniform elongation at 593°C (1100°F) for heats 613, 686, and 212 are 22, 17, and 24%, respectively.

3. The maximum decreases in uniform elongation at room temperature for heats 613, 686, 212, are 14, 9, and 16%, respectively.

It is interesting to note that although aging decreases the uniform and total elongations during a tensile test, it increases them during a creep test. Work in progress will help explain these differences.

5.2.3.6 Correlation of Tensile Properties with Chemical Composition and Microstructure

High-temperature tensile and creep properties are being studied at ORNL for 20 different heats of wrought type 304 stainless steel and seven heats of wrought and one cast type 316 stainless steel. A wide variation exists in tensile and creep properties of various heats of both types 304 and 316 stainless steel. These variations in high-temperature mechanical properties could even increase due to the pickup of interstitial impurities from exposure to the sodium environment. The most important interstitials that affect the mechanical properties are carbon, nitrogen, and boron. A review on the effect of other impurities is available.[8] Various approaches have been tried to explain the effect of composition and microstructure on the room-temperature and high-temperature tensile properties of austenitic stainless steels. The purpose of this section is to review various approaches in context to the heats being used in the heat-to-heat program.

Irvine et al.[9] gave a regression equation describing the relation between 0.2% yield stress (95% confidence) and the microstructure and composition. The regression equation was of the type:

$$\sigma_y = 4.1 + 32(N,\%) + 23(C,\%) + 1.3(Si,\%) + 0.24(Cr,\%) + 0.94(Mo,\%) + 1.2(V,\%) + 0.29(W,\%) + 2.6(Nb,\%) + 1.7(Ti,\%) + 0.82(Al,\%) + 0.16(\delta,\%) + 0.46(d^{-1/2}) \ . \quad (6)$$

The 0.2% yield strength (σ_y) was expressed in tsi (1 tsi = 13.8 MPa) and the grain size (d) in mm. All chemical elements were expressed as weight percent; δ represented the δ-ferrite phase in stainless steel. Similar equations were also given for ultimate tensile strength and reduction of area. In less stable austenitic steels, a martensite content less than 30% had little effect on 0.2% yield strength. The tensile strength was shown to increase because of the presence of martensite, and its contribution could be calculated from the relation:

$$UTS_{martensite} = 12 + 0.82(\text{martensite } \%) \ . \quad (7)$$

The constant term of 12 arises from the formation of strain-induced martensite during the tensile test at strains up to maximum load.

Dyson and Holmes[10] investigated the effect of alloying additions on the lattice parameter of austenite to determine the strengthening contributions due to different elements. A multiple regression analysis for the lattice parameter change due to various elements gave:

$$a = 3.5780 + 0.0330C + 0.0220N + 0.00095Mn - 0.0002Ni + 0.0006Cr + 0.0056Al - 0.0004Co + 0.0015Cu + 0.0031Mo + 0.0051Nb + 0.0039Ti + 0.0018V + 0.0018W \ , \quad (8)$$

where the symbols for the elements represent their contents in weight percent. A linear multiple regression analysis was also carried out to relate the 0.2% yield stress to the austenite composition and microstructure and was similar to that of Irvine et al.[9]

Dyson and Holmes[10] converted the regression coefficients for proof stress to an atomic percent basis; these are shown together with the corresponding changes in lattice parameter in Fig. 5.26. In general, an increase in the distortion of the austenite lattice produced by the

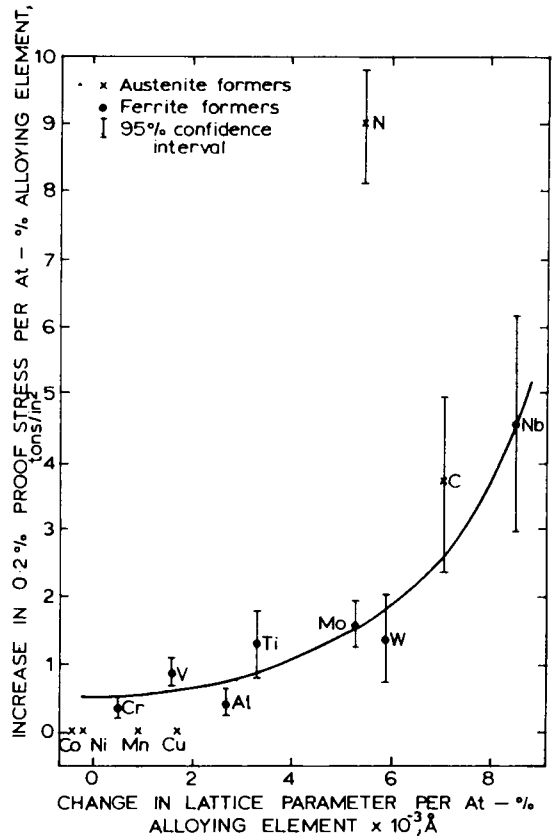

Fig. 5.26. The Increase in 0.2% Proof Stress as a Function of the Change in Lattice Parameter.

addition of substitutional ferrite-forming elements causes an increase in the strengthening effect of the solute. The austenite-forming substitutional elements, however, produce no significant strengthening. Nitrogen and, to a lesser extent, carbon produce large increases in 0.2% yield stress for a given lattice strain than is observed for the ferrite-forming elements. Dyson and Holmes[10] suggested that the large effect of nitrogen could be due to the interstitial positions adopted by these elements, although the large effect of nitrogen may be due to clustering in these positions.

Soo and Horton[11] recently reviewed the effect of carbon and nitrogen on the short-term tensile behavior of solution-treated types 304 and 316 stainless steel. The yield and tensile strengths and total elongations of solution-treated type 304 stainless steel were give, respectively, by equations:

$$\sigma_y = 89.952 + 181.167(C + N) - 0.148T(C + N) - 5.727T^{1/2} + 0.105T ,$$
standard deviation = 2.236, (valid for $297 \leq T \leq 922$ K, 75–1200°F); (9)

$$\sigma_u = -1.806 - 227.391(C + N) + 1218.392T^{-1/2} + 1.127T(C + N) - 8.446 \times 10^{-4}T^2(C + N),$$
standard deviation = 2.645, (valid for $366 \leq T \leq 866$ K, 200–1100°F); (10)

$$\varepsilon = 29.595 - 89.898(C + N) + 468.414T^{-1/2},$$
standard deviation = 2.955, (valid for $477 \leq T \leq 922$ K, 400–1200°F). (11)

Equations 9 through 11 were shown[11] to be valid for $(C + N) \leq 0.13$ wt % and to apply to plate, bar, pipe, and forged material. The stresses σ_y and σ_u are in ksi (1 ksi = 6.895 MPa), and ε is expressed in percent.

For type 316 stainless steel, the equations were:

$$\sigma_y = 88.474 + 211.640(C + N) - 0.206T(C + N) - 5.762T^{1/2} + 0.111T,$$
standard deviation = 2.806, (valid for $297 \leq T \leq 977$ K, 75–1300°F); (12)

$$\sigma_u = 8.563 - 461.665(C + N) + 1064.154T^{-1/2} + 2.722T(C + N) - 2.330 \times 10^{-3}T^2(C + N),$$
standard deviation = 6.458, (valid for $297 \leq T \leq 977$ K, 75–1300°F); (13)

$$\varepsilon = 28.000 - 99.139(C + N) + 653.926T^{-1/2},$$
standard deviation = 6.703, (valid for $297 \leq T \leq 977$ K, 75–1300°F). (14)

The above equations, (12–14), were said to be valid[11] for $(C + N) \lesssim 0.10$ wt %. These equations may be used for plate, bar, pipe, rod, sheet, strip, and forged material.

Several papers presented in a symposium[12] on elevated-temperature properties discuss the influence of nitrogen additions on the behavior of types 304 and 316 austenitic stainless steel. Natesan et al.[13] have also reviewed the effect of carbon and nitrogen on the mechanical properties of stainless steels.

The chemical analysis and grain size of 20 heats of type 304 stainless steel and seven heats of type 316 stainless steel being investigated in the present program were used in Eq. (6) to calculate the 0.2% yield strength. The calculated and experimental results at room temperature are compared for these heats in Fig. 5.27. For most of the cases, calculated yield strength values are lower than observed. Only one possible error in calculation can arise from the fact that for 20 heats of type 304 stainless steel, aluminum and tungsten contents are not available, and for both these elements, the coefficients of these elements in Eq. (6) are relatively large. Furthermore, a few of the heats of type 304 stainless steel might have some δ-ferrite, which has also not been considered. The agreement between the calculated and observed values for type 316 stainless steel is very good for six heats. One heat, 686, is the strongest and has 0.01% B and the smallest grain size. Equation (6)

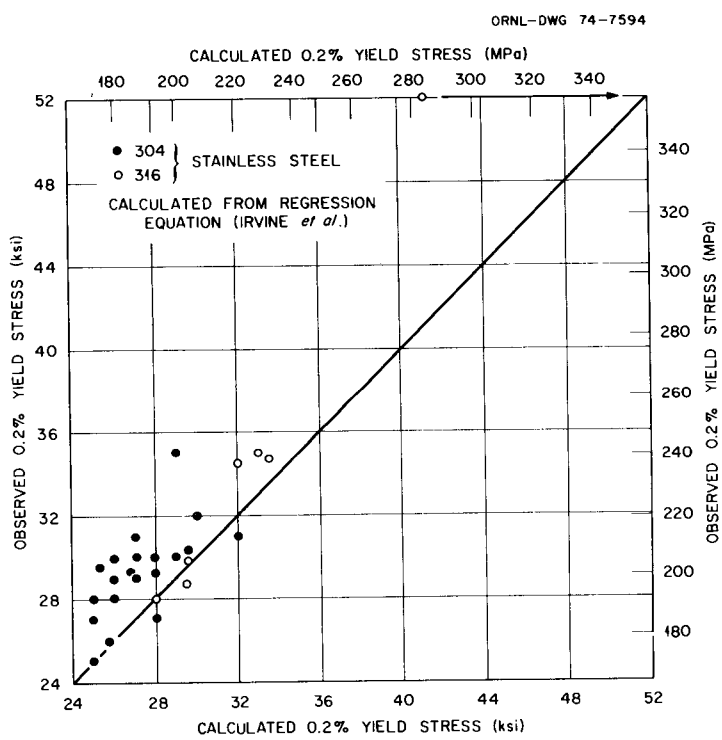

Fig. 5.27. Comparison Between the Calculated and Observed Yield Stress for 20 Heats of Type 304 and Seven Heats of Type 316 Stainless Steel in the Reannealed Condition.

does not take boron into account, and, furthermore, for such a small grain size (8 μm) the linear addition may not be valid. Although regression analysis in Eq. (6) gives an order-of-magnitude value of yield strength at room temperature, no mention has been made as to its use at high temperature.

Yield strength (0.2%) data for both types 304 and 316 stainless steel at room temperature, 427, 593, and 649°C (800, 1100, and 1200°F) have been compared with Eqs. (9) through (14) in Figs. 5.28 through 5.33. Interestingly enough, these equations do not fit the present data. Some of the possible reasons for such differences could be the assumptions made in the HEDL analysis:

1. Alloy grain size was assumed to be a negligible variable.
2. The test strain rate was assumed to be negligible.

Thus it appears that one needs a better correlation between tensile properties and material variables, such as composition and microstructure. One such analysis is under way at ORNL.

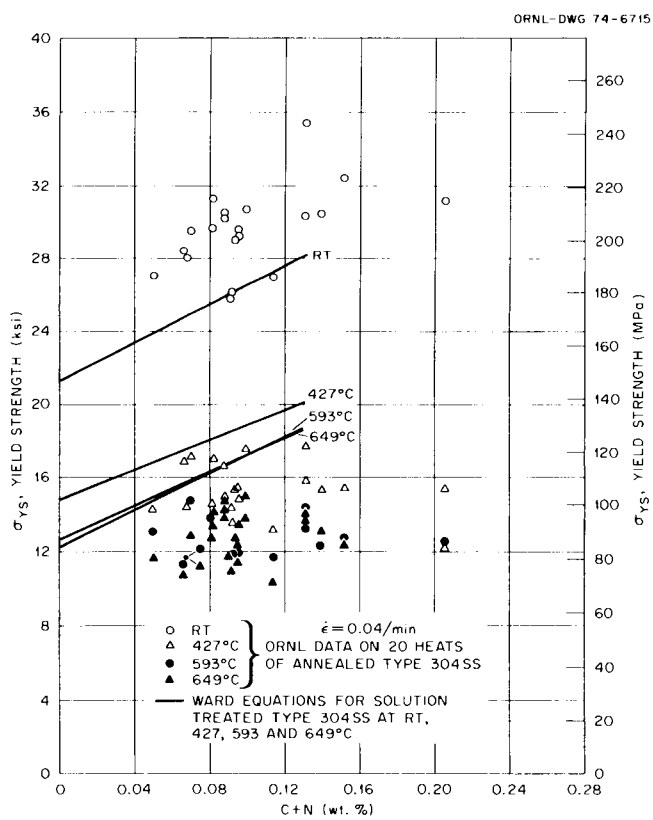

Fig. 5.28. Comparison of 0.2% Yield Strength of 20 Heats of Annealed Type 304 Stainless Steel with WARD Equations.

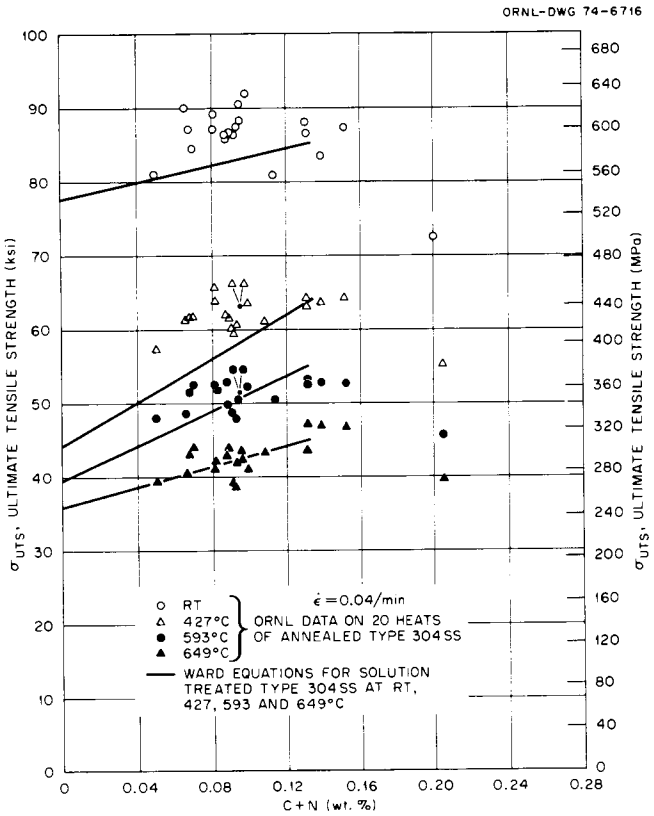

Fig. 5.29. Comparison of Ultimate Tensile Strength of 20 Heats of Annealed Type 304 Stainless Steel with WARD Equation.

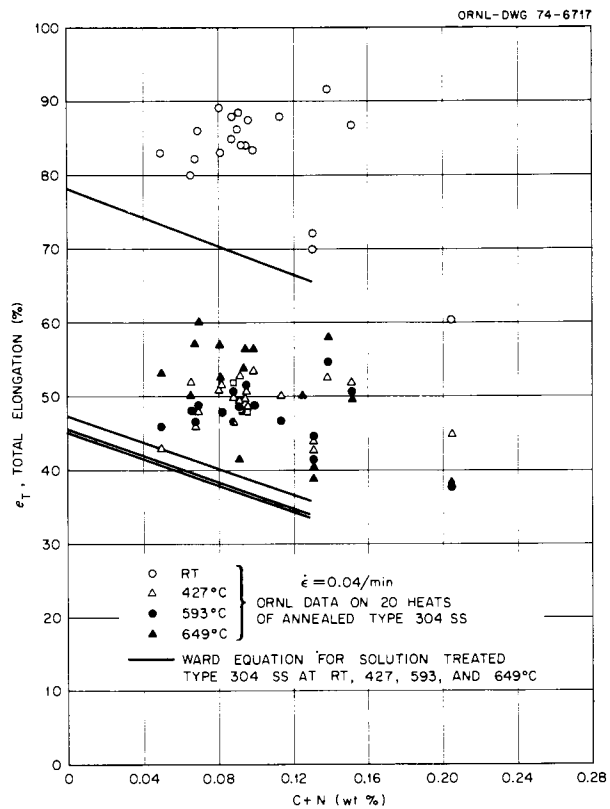

Fig. 5.30. Comparison of Total Elongation of 20 Heats of Annealed Type 304 Stainless Steel with WARD Equation.

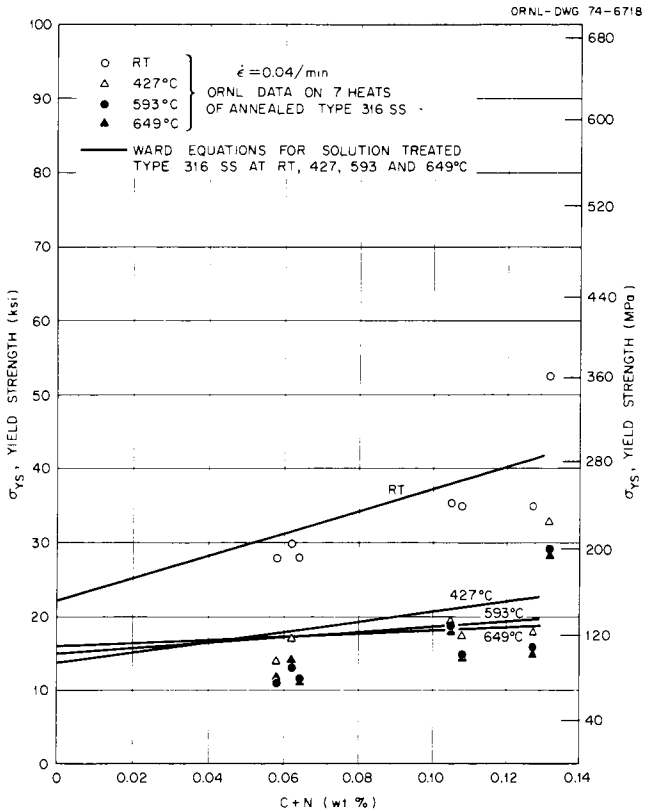

Fig. 5.31. Comparison of 0.2% Yield Strength of Seven Heats of Annealed Type 316 Stainless Steel with WARD Equation.

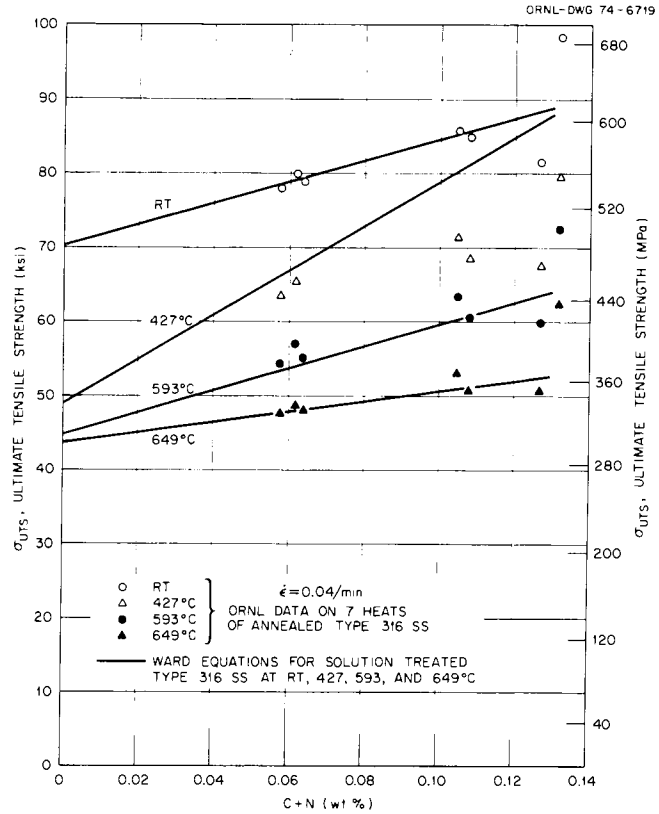

Fig. 5.32. Comparison of Ultimate Tensile Strength of Seven Heats of Annealed Type 316 Stainless Steel with WARD Equation.

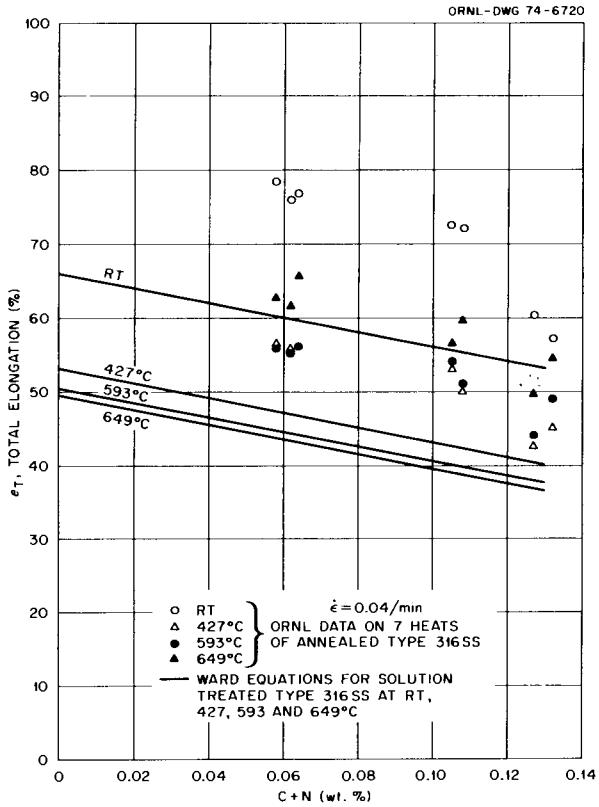

Fig. 5.33. Comparison of Total Elongation of Seven Heats of Annealed Type 316 Stainless Steel with WARD Equation.

5.2.4 Mechanical Property Characterization of Type 316 Stainless Steel Reference Heat

5.2.4.1 Procurement of Type 316 Stainless Steel Reference Heat — R. J. Beaver

Production of all items required by this order has been completed except for the finishing operations on the bar items and rounds to be used for pipe manufacturing, the breakdown of ingot 7 to provide the two remaining 24- by 24-in. (610- × 610-mm) forgings, the production of pipe at the Ellwood Plant of the U.S. Steel Corporation (the Republic Steel Corporation subcontractor), and the production of 16- and 28-in.-diam (406 and 711 mm) pipe at Rollmet, Inc. (the UCC-ND subcontractor). Inspections at CONAM (Republic Steel Corporation subcontractor) were initiated early in July, and all inspections of the plate items except

the 2-in. plate were completed. Inspections will be continuous throughout August and September, and delivery of all plate, sheet, and bar items should be complete by mid-September.

Periodic surveillances were made of the Republic Steel Corporation activities, with emphasis on traceability by the aircraft identification system. Disposition of items produced relative to the pouring sequence of the ingots is summarized in Table 5.12, and the specific identities of the items in relationship to concise traceability to position in the ingot are listed in Table 5.13. The results of check chemical analyses and mechanical properties tests are summarized in Table 5.14.

Pipe production remained in the planning stages. Manufacture of all pipe items at the Ellwood Plant is anticipated shortly after delivery of the rounds by Republic Steel early in August, with complete delivery expected in late fall 1974. A contract with Rollmet, Inc., was arranged for production of 16- and 28-in.-diam (406 and 711 mm) pipe, and shipment of pieces of the 24- by 24-in. (610- × 610-mm) forgings, produced by Republic Steel Corporation, to the Carlton Forge Co. (the Rollmet subcontractor for manufacturing forged rings) is planned for late August. Delivery of these items is estimated as January 1975.

Table 5.12. Summary Showing Disposition of Items Relative to Pouring Sequence of the Ingots 316 Stainless Reference Heat

Ingot Pour Sequence	Ingot Size (in.)	Ingot Size (m)	Nominal Ingot Weight (lb)	Nominal Ingot Weight (Mg)	Product Form
1	25 × 27	0.64 × 0.19	12,000	5.44	8-in. (203-mm) rounds (pipe)
2	25 × 27	0.64 × 0.19	12,000	5.44	1/2- and 5/8-in. (13- and 16-mm) plate
3	25 × 27	0.64 × 0.19	12,000	5.44	5/8-in. plate
4	43-in. octagon	1.09	25,390	11.52	24 × 24-in. (610 × 610 mm) forging
5	43-in. octagon	1.09	25,390	11.52	24 × 24-in. (610 × 610 mm) forging
6	43-in. octagon	1.09	25,390	11.52	Scrapped
7	43-in. octagon	1.09	25,390	11.52	Reserved (probably for forging)
8	20 × 41	0.51 × 1.04	14,670	6.66	0.125- and 0.060-in. (3.18- and 1.52-mm) sheet
9	20 × 41	0.51 × 1.04	14,670	6.66	1- and 2-in. (25- and 51-mm) plate
10	20 × 41	0.51 × 1.04	14,670	6.66	1- and 2-in. (25- and 51-mm) plate
11	20 × 41	0.51 × 1.04	14,670	6.66	1- and 2-in. (25- and 51-mm) plate
12	20 × 41	0.51 × 1.04	14,670	6.66	2-in. (51-mm) plate
13	20 × 41	0.51 × 1.04	14,670	6.66	1-in. (25-mm) plate
14	20 × 41	0.51 × 1.04	14,670	6.66	1- and 2-in. (25- and 51-mm) plate
15	20 × 41	0.51 × 1.04	14,670	6.66	2-in. (51-mm) plate
16	20 × 41	0.51 × 1.04	14,670	6.66	2-in. (51-mm) plate
17	25 × 27	0.64 × 0.69	12,000	5.44	8-in. (203-mm) rounds (pipe)
18	25 × 27	0.64 × 0.69	12,000	5.44	8-in. (203-mm) rounds (pipe)
19	25 × 27	0.64 × 0.69	12,000	5.44	8-in. (203-mm) rounds (pipe)
20	25 × 27	0.64 × 0.69	12,000	5.44	3 3/4-in. (95-mm) rounds (pipe)
21	25 × 27	0.64 × 0.69	12,000	5.44	4 1/2-in.-diam (114-mm) bar
22	25 × 27	0.64 × 0.69	12,000	5.44	4 1/2-in.-diam (114-mm) bar
23	25 × 27	0.64 × 0.69	12,000	5.44	1-in.-diam (25-mm) bar
24	25 × 27	0.64 × 0.69	12,000	5.44	2- and 2 1/2-in.-diam (51- and 64-mm) bar
25	25 × 27	0.64 × 0.69	12,000	5.44	2-in.-diam (51-mm) bar
26	25 × 27	0.64 × 0.69	12,000	5.44	1- and 2-in.-diam (25- and 51-mm) bar
27	25 × 27	0.64 × 0.69	12,000	5.44	3 1/4-in.-diam (83-mm) rounds (pipe)
28	25 × 27	0.64 × 0.69	12,000	5.44	24 × 15-in. (610 × 380-mm) blooms - spare
29	25 × 27	0.64 × 0.69	12,000	5.44	24 × 15-in. (610 × 380-mm) blooms - spare

Table 5.13. Listing of Items in Relation to Identification and Traceability for Type 316 Stainless Steel Reference Heat

Forms Identified by Aircraft Identity System		
Form	Dimension, in.[a]	Aircraft Identity of Forms
Plate	1/2	2AB, 2AC, 2CA, 2CB
	5/8	2BA, 2BB, 2BC, 2CC, 3AA, 3AB, 3AC, 3BA, 3BB, 3BC, 3CA, 3CB, 3CC
	1	9A, 9B, 9C, 10A, 10B, 10C, 11A, 11B, 11C, 13A, 13B, 13C, 13D, 13E, 13F, 14B, 14C, 14D, 14E, 14F
	2	9D, 9E, 10D, 10E, 11D, 11E, 12A, 12B, 12C, 12D, 14A, 15A, 15B, 15C, 15D, 16B, 16C, 16D
Rounds (for pipe)[b]	8 8	1A, 1B, 1C, 1D, 17A, 17B, 17C, 17D, 18A, 18B, 18C, 18D, 19A, 19B, 19C, 19D
	4 1/2 4	21AA, 21AB, 21BA, 21BB, 21CA, 21CB, 21DA, 21DB
	3 3/4 2 1/2	20AA, 20AB, 20AC, 20BA, 20BB, 20BC
	3 1/4 2	27AA, 27AB, 27BA, 27BB
Forging[c]	24 × 24	4A, 4B, 5A, 5B

Bar Identification			Sheet Identification	
Diameter (in.)	Billet Aircraft Identity	Bar Identities	Thickness (in.)	Sequential Identification Relative to Top of Ingot 8
1	26AAA	1	0.125	2, 9, 10, 11, 12, 14, 15 16, 17, 18, 19, 20
	26ABA	2		
	26BAA	3		
2	24CAA	1–9	0.060	38–67, 69–88
	24CBA	10–14		
	25AAA	20–24		
	25ABA	30–34		
	25BAA	40–44		
	25BBA	50–54		
	25CAA	60–64		
	25CBA	70–74		
	26CBA	80–84		
2 1/2	24AAA	1–9		
	24ABA	10–14		
	24BAA	20–24		
	24BBA	30–34		

[a]1 in. = 25.4 mm. Dimensions are thickness for plate, diameter followed by subsequent pipe diameter for rounds.

[b]Each pipe per size will be numbered sequentially relative to the round from which it is produced. Pipe diameter follows round diameter.

[c]Two additional pieces are to be produced from ingot 7.

Table 5.14. Summary of Republic Steel Corporation Chemical Check Analyses and Mechanical Properties Results for the Product Forms Produced from Type 316 Stainless Steel Reference Heat

Property	Value for Each Product Form				
	Plate (6 lots)	Sheet (2 lots)	Bar (4 lots)	Rounds (3 lots)	Forgings (4 lots)
Content, wt %					
C	0.059–0.065	0.058–0.060	0.060–0.063	0.060–0.068	0.063–0.065
Mn	1.82–1.88	1.82–1.86	1.84–1.86	1.84–1.86	1.82–1.84
P	0.022–0.024	0.023	0.023–0.024	0.020–0.023	0.022–0.034
S	0.018–0.020	0.018–0.019	0.018–0.019	0.018–0.019	0.017–0.019
Si	0.57–0.62	0.58–0.60	0.57–0.59	0.56–0.60	0.57–0.58
Cu	0.08–0.10	0.08–0.10	0.09–0.10	0.08–0.09	0.08–0.10
Ni	13.30–13.40	13.35–13.50	13.35–13.70	13.40–13.45	13.40–13.60
Cr	16.40–17.30	17.05–17.35	17.10–17.15	17.05–17.19	17.00–17.30
Mo	2.29–2.34	2.33–2.34	2.34–2.35	2.33–2.36	2.34–2.35
Ti	0.00	0.00–0.01	0.00–0.01	0.00–0.02	0.00
Co	0.01–0.02	0.02	0.01–0.02	0.01–0.02	0.02
N	0.031–0.034	0.032–0.035	0.029–0.032	0.030–0.032	0.030–0.032
B	0.0005–0.0006	0.0004–0.0006	0.0005–0.0006	0.0005–0.0006	0.0005
Strength, ksi					
Yield	35.0–46.0	48.7–49.1	31.2–33.6	32.0–32.9	34.0–37.5
Ultimate tensile	77.5–82.0	85.0–86.5	78.0–79.2	77.5–80.2	70.0–73.5
Strength, MPa					
Yield	241–317	336–339	215–232	221–227	234–259
Ultimate tensile	534–565	586–596	538–546	534–553	483–507
Elongation (%)	50.0–56.0	46.0–50.0	56.0–60.0	54.0–70.0	51.5–58.0
Reduction of Area (%)	66.5–72.5		75.0–77.8	75.5–82.0	62.0–72.5
Hardness, Brinell	131–143	156–160	131–137	143–156	131–137

[a]Nb + Ta not detected: 0.00%.

5.2.5 Structural Materials Information Center — M. K. Booker

The computerized system for management of mechanical properties data has been described earlier.[14] Figure 5.34 is a simplified diagram of the projected flow of information within the system. This system continues to expand and develop in an effort to make it increasingly flexible and useful in the study of mechanical properties.

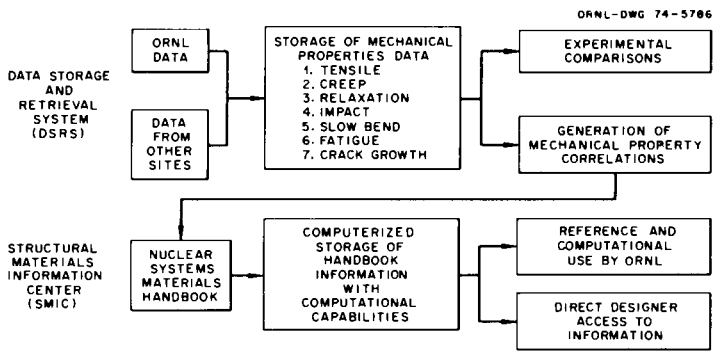

Fig. 5.34. Simplified Diagram of the Flow of Mechanical Properties Data in the ORNL Computerized Data Management System.

The Data Storage and Retrieval System (DSRS) now contains the results of 1690 tests, including tensile, creep, impact, slow-bend, and relaxation tests, all conducted at ORNL. Plans are under way to begin input of fatigue and crack-growth test results in the near future. The input of data from sources outside ORNL is also presently being studied. However, extensive efforts must be made to assure uniformity and standardization of information in DSRS. Thus, when a user retrieves information from the system, he can be sure that he knows what he is getting. To this end, the thesaurus of terms used to identify data in DSRS has been re-written to ensure clarity and completeness in the definitions of the identifiers. Also, a manual on standard methods of measurement of DSRS identifiers is being prepared, along with a new, comprehensive user's guide.

DSRS provides for fast, efficient retrieval of data; it does not perform calculations. However, the data stored in the system may be accessed by other programs, which can in turn perform calculations and other manipulations.

For example, a plotting program has been developed to output graphical representations of data stored in DSRS. Using this program one may plot any numerical field contained in DSRS against any other numerical field contained in the system, for any subset of the stored tests. Linear, semilog, and log-log plots are possible. Examples of plots produced by this program are shown in Figs. 5.35 and 5.36. Currently, plots are produced through the CALCOMP plotter in the ORNL Computing Center, but capacity to produce plots quickly and easily by in-shop facilities is expected soon.

Another feature that will greatly increase the power and flexibility of DSRS is the automatic data acquisition system. A PDP-8/E computer has been acquired for taking creep data by computer, thus allowing more points to be read with greater accuracy. The computer is being fitted with peripheral devices, and the data acquisition system should be in operation soon.

Work is continuing on development of the Structural Materials Information Center (SMIC). The demonstration version of the computer program for SMIC, HANDBK,[14] has been tested and modified where necessary. The computer program that will operate SMIC in its final form is currently being developed. As a first step, a new main program has been written to allow the system to operate in overlay, bringing portions of the program into core from peripheral devices only as needed, providing much more efficient use of core space than the current program.

When complete, SMIC will contain a complete on-line version of the *Nuclear Systems Materials Handbook*. The user will be able to access any of the handbook information quickly and easily, receiving output in various forms. Forms under consideration include tabular, graphical, curve fits, etc. In addition, a wide range of computational subroutines will be available to allow the user to use handbook information in calculations. Increased access flexibility will make it possible to ask questions of the system in a variety of ways, allowing the user to get the information he needs rapidly. The program will guide the user throughout, requiring a minimum of skill and labor on his part.

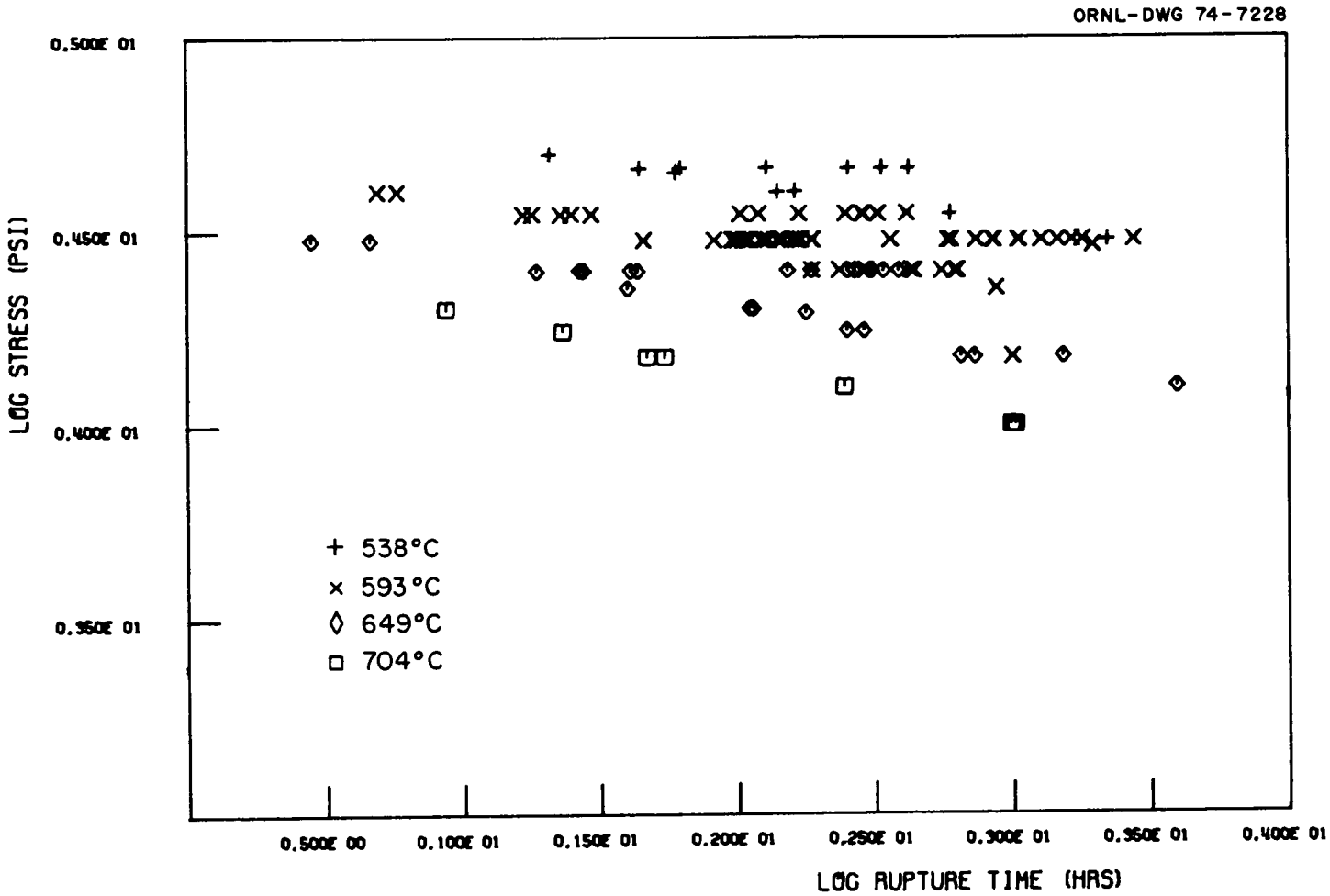

Fig. 5.35. Computer-Drawn Plot of Ultimate Tensile Strength Against Temperature For Type 304 Stainless Steel (Several Heats) From Room Temperature to 816°C (1500°F).

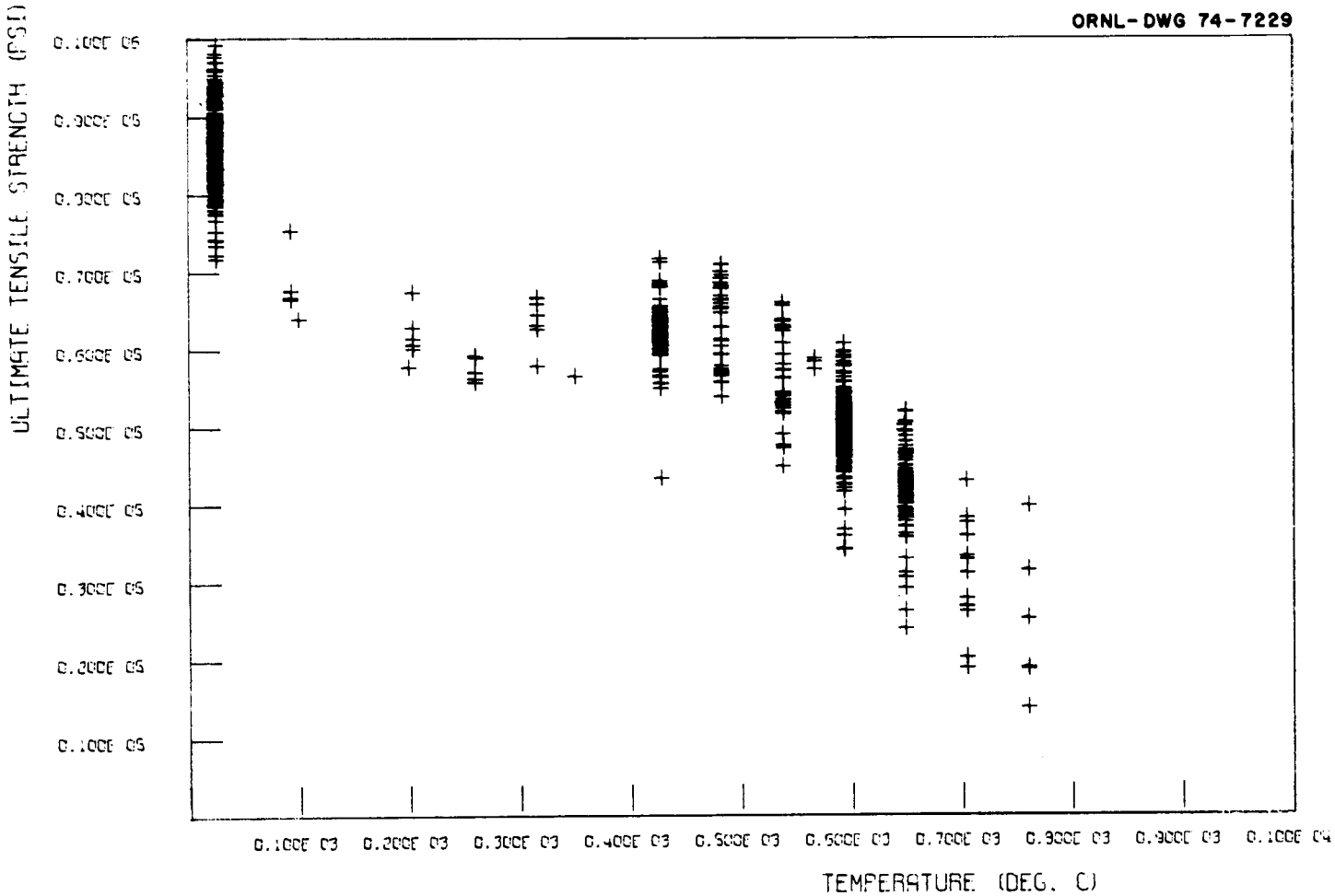

Fig. 5.36. Computer-Drawn Stress-Rupture Diagram for Type 304 Stainless Steel (Seven Heats) From 538 to 704°C (1000–1300°F).

Moreover, accurate, timely computer updating will ensure that SMIC information is current, eliminating much of the confusion and possible error involved in updating the looseleaf version of the handbook.

5.2.6 Elastic Properties of Engineering Structural Materials — J. P. Hammond

Elastic constants are the proportionality constants in equations relating stress to strain under specified conditions. Precise measurements show that for metals the elastic stress-strain relationships are not perfectly linear, even at very low strain levels, and become progressively more nonlinear as strain increases. With increasing maximum strain, measurements reveal evidence of incipient plastic behavior, with strain a function of instantaneous stress, time, temperature, and prior strain history. As a consequence, discrepancies often occur between elastic constants determined at different strain levels and rates of strain and between constants established by dynamic and static means.

The purpose of this program is to correlate the two separate categories of elastic constants (dynamic and static) for reactor materials of interest, giving specific attention to the significant test variables. In addition to elastic constants (Young's modulus, E; shear modulus, G; and Poisson's ratio, ν), elastic and proportional limits (E.L. and P.L.) will be determined. This information is needed to enable more exact and enlightened use of this class of information in engineering design and structural verification work.

5.2.6.1 Program Plan

A diagram scheduling the dynamic and static property phases of this program through the calendar year 1975 is shown in Fig. 5.37. The dynamic moduli and Poisson's ratio will be determined by ultrasonic methods using total maximum strain levels and frequencies of about 0.003 μin./in. (0.003 μm/m, με) and 5 MHz, respectively. Room-temperature determinations of these constants will be made on block samples by the highly accurate contact pulse-echo method, whereas elevated-temperature values will be determined by the thin-wire, magnetostrictive method, which enables

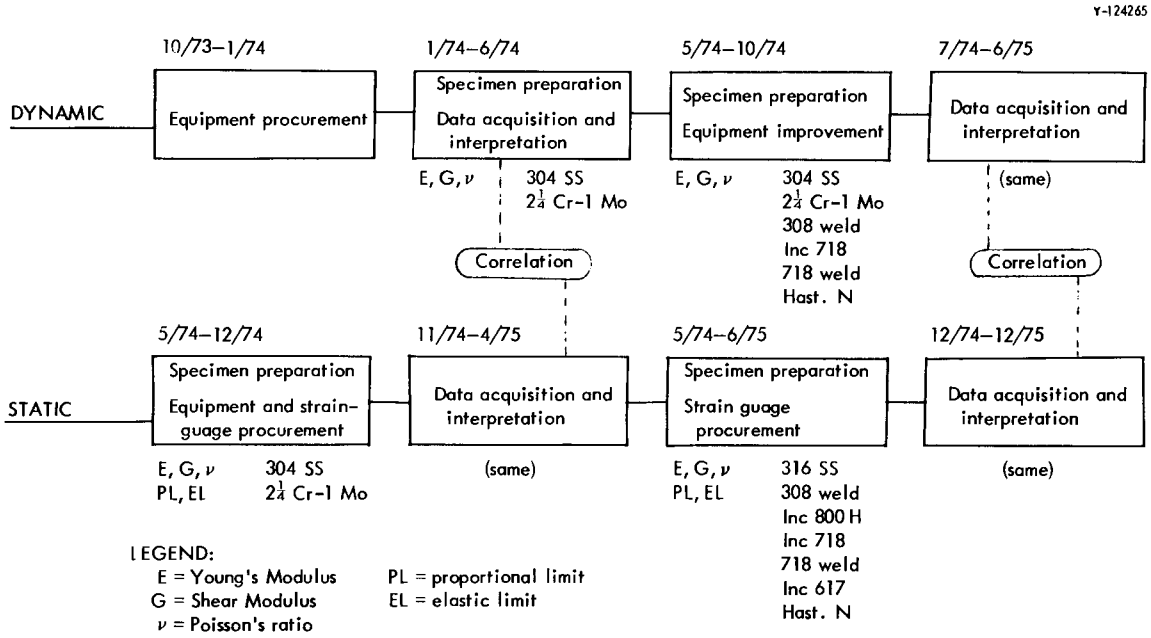

Fig. 5.37. Schedule of Elastic Properties Study Tasks.

remote operation of the transducer. The elevated-temperature data will be normalized to the more accurate room-temperature determinations. Four sets of data will be gathered and treated statictically for establishing property values at room temperature and at 28°C (50°F) increments from 38°C (100°F) to the range 650 to 760°C (1200–1400°F).

The static property determinations will be made with an Instron tensile testing machine using high-sensitivity resistance strain gages to sense strain and the standard load cells that accompany Instron machines to sense stress. Tensile bars of rectangular cross-section will be employed to eliminate any need to preform the resistance strain gages. The gages will be mounted both longitudinally and laterally for determining Poisson's ratio. To correct for nonaxial specimen alignment, gages will be installed in duplicate on opposite sides of the specimen to enable strain averaging. The tensile specimen with attached gages is shown in Fig. 5.38. A mechanical-electrical (LVDT) extensometer will be mounted over the resistance strain gages at 2-in.-gage-length positions to enable checking for spurious gage behavior. Signals from the respective extensometer systems will be treated electronically for plotting strain as a function of stress on x-y recorders and subsequent analysis.

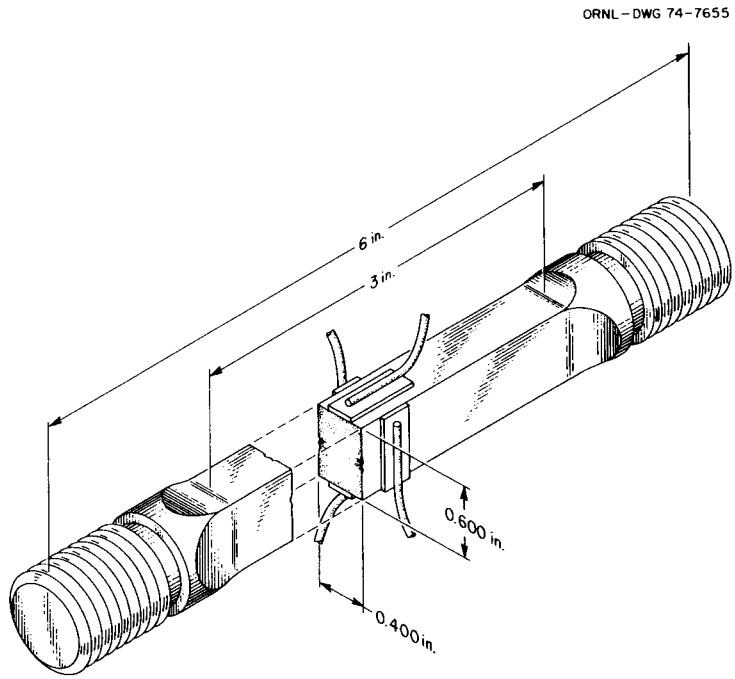

Fig. 5.38. Tensile Test Specimen of Rectangular Cross Section Showing Mounted MG-425 Strain Gages.

Elastic modulus values will be established by the static method at tentative maximum strain levels of 100, 250, 500, and 1000 $\mu\varepsilon$ and strain rates of 0.2, 0.02, 0.002, and 0.0002/min. The tests in this case will be performed at room temperature and at 56°C (100°F) increments from 38 to 649°C (100–1200°F), the approximate temperature limit for resistance strain gages. Tests more damaging to the specimen and gages — namely, runs above 480°C (900°F) and ones conducted to establish elastic limits — will be conducted last.

In addition to the test condition variables, a number of material variables will be examined. These include the effects of heat-to-heat variation, heat treatment, prior cyclic straining, orientation within standard stock forms, and preferred crystallographic texture.

5.2.6.2 Elastic Properties Determined By Dynamic Tests — J. P. Hammond and M. W. Moyer*

Information on the dynamic moduli and Poisson's ratio for 2 1/4 Cr-1 Mo steel in the annealed condition (for 1-in.-thick plate with specimen

*Laboratory Development, Y-12.

axis in the rolling direction) was determined and presented in the last quarterly report.[15] Details on the methods of gathering the sound data, calculating property values, and treating the results statistically were included.

During the last quarter the block and wire specimens for determining dynamic moduli and Poisson's ratio by the room-temperature double-pulse and the elevated-temperature thin-wire sonic methods were completed for the first round of data acquisition, planned to start July 1. The materials included various heats of type 304 stainless steel, type 308 (FFTF) weld deposit, 2 1/4 Cr-1 Mo steel, and Inconel 718 base metal and weld deposit. Suitable material samples of type 316 stainless steel, Incoloy 800, Inconel 617, and Hastelloy N are yet to be secured.

5.2.6.3 Elastic Properties Determined by Static Tests

The preparation of rectangular tensile test specimens (Fig. 5.38) in the materials on hand was begun, and resistance strain gages for the type 304 stainless steel and 2 1/4 Cr-1 Mo steel are on order. Weldable type MG425 wire gages that are fully compensated for temperature effects (Ailteck product) will be employed in elevated-temperature tests and type EA-06-250 foil gages (Micro-Measurements) for room temperature use. The electronic circuits for treating strain signals preparatory to introduction in x-y recorders will be developed by the Instruments and Controls Division. The initial circuit plan uses the attractive full-bridge concept for averaging strain signals and instituting temperature compensation. However, certain resistance balances associated with temperature compensation, which are ordinarily performed for the MG425 gages in half-bridge circuits, will have to be performed at operational amplifiers if the full-bridge circuit is used. We shall perform early testing of the favored circuit. A conservative but more costly design employing two half bridges is being held in abeyance in case it is needed.

5.2.7. Analytical Studies of Mechanical Properties Testing — B. R. Dewey*

The analysis of the hourglass fatigue specimen has progressed through

---

*Subcontractor from Department of Engineering Science and Mechanics, University of Tennessee, Knoxville.

the completion of the monotonic plasticity solutions for 0.5 and 2.0% strain. The results have given not only detailed stress and strain distributions for the specimen, but also a check of the possible accuracy of the diametral extensometer. Triaxiality induced by the specimen geometry can be used to explain the apparent increase in the stress level observed on this specimen.

The application to 2 1/4 Cr-1 Mo steel at 538°C (1000°F) of the CREEP-PLAST[16] finite element program has shown sensitivity to the fineness of the mesh work and to the selection of loading steps. Bilinear stress-strain representations for 0.5 and 2.0% strain were used in accordance with the recommended[17] procedures for FFTF.

5.2.7.1 Efficacy of Diametral Extensometry for Monotonic Loading of the Hourglass Specimen

A well-known relationship for the axial strain ε_a as a function of the instantaneous diameter D of the neck of the hourglass is

$$\varepsilon_a = \frac{4P}{\pi E D^2}\left(1 - \frac{\nu_e}{\nu_p}\right) - \frac{1}{\nu_p} \ln \frac{D}{D_0} , \tag{15}$$

where

P is the axial load,
E is the modulus of elasticity,
ν_e is the elastic Poisson's ratio,
ν_p is the plastic Poisson's ratio = 0.5, and
D_0 is the original diameter of the neck.

Note that Eq. (15) uses true stress and true strain in the calculation of ε_a. If Eq. (15) is recast in terms of axial engineering stress σ and diametral engineering strain ε_1, we have

$$\varepsilon_a = \frac{\sigma}{E}\left(1 - \frac{\nu_e}{\nu_p}\right) - \frac{\varepsilon_1}{\nu_p} . \tag{16}$$

The derivations of Eqs. (15) and (16) are based on the definition of Poisson's ratio and on a uniform state of strain. Some uncertainty

exists in the use of these equations because of the triaxial stress at the neck and the nonuniform strain distribution. To assess the results that might be experimentally obtained from Eqs. (15) and (16), the axial strain predicted from these equations has been compared with the average axial strain computed by CREEP-PLAST. The results in Table 5.15 use the diameter change, the average axial engineering stress, and the average diametral engineering strain as appropriate from CREEP-PLAST. We see good agreement for the three methods of calculations for three strain states.

Table 5.15. Diametral Extensometry Comparisons

Nominal Strain State	Axial Strain (Microstrain) As Computed From		
	Eq. (15)	Eq. (16)	CREEP-PLAST Average
Elastic at yield	999.8	1,001.4	998.1
0.5% nominal	4,987	5,016	4,998
2% nominal	19,540	19,438	19,445

5.2.7.2 Stresses in the Hourglass Specimen

The finite-element results show, aside from the outer surface and the singularity at the axis, that the axial, radial, and tangential components of stress are all positive. This produces an effective stress that is less than the axial stress. Typically the effective stress is 2 to 5% lower than the axial stress. Since these two stresses are virtually equal in a cylindrical specimen, the stress-strain curve produced by the hourglass specimen is not expected to agree with one produced by a cylindrical specimen.

For elastic material, stress on the outer surface at the waist of the hourglass is some 6% higher than the stress at the core. However, as plasticity commences, the computations show that the location of the peak stress moves to the center of the specimen, and that the axial stress varies less than 1.5% across the cross section.

Presently, the analysis is being continued into the regime of tensile hold time to determine if the results on extensometry and stress distribution are affected.

5.2.7.3 Buckling Analysis of a Hollow Tubular Specimen

We have completed an informal report to aid in the application of the hollow tubular specimen for biaxial tension-compression and torsion. Buckling is possible in a local sense (shell buckling) or in an overall sense (column buckling). With the dimensions of the specimen considered, local buckling is predicted[18] at an axial stress level σ_{cr} given by $\sigma_{cr} = 0.127E$, where E is the modulus of elasticity. If σ_{cr} is over the proportional limit the buckling stress is lowered, and the above formula may be corrected by replacing E with $\sqrt{EE_t}$ (where E_t is the tangent modulus evaluated at σ_{cr}). The problem is complicated somewhat when a combined compression and torsional load are applied, because the state of stress depends on the order in which the axial and torsional loads are applied. A general solution of this type of stability problem was not found in the buckling literature, although a tentative interaction formula is suggested by combining known results for column buckling (Euler's equation) and for torsional buckling. In any event, addition of the torsional load increases the likelihood of buckling.

5.3 MECHANICAL AND METALLURGICAL BEHAVIOR OF WELDMENTS FOR LMFBR — P. Patriarca, G. M. Slaughter, W. R. Martin, and C. R. Brinkman

5.3.1 Tensile Properties of "Heat-Affected Zone" of FFTF Vessel Test Welds — R. T. King, E. Bolling, and L. T. Ratcliff

Type 308 stainless steel welds were made in 6.0-cm-thick (2 3/8-in.) type 304 stainless steel plate for evaluation. These welds are prototypic of the FFTF vessel girth and seam welds, and they were made with the heats of base metal and lots of electrodes used in the vessel.[19] One aim of the program is to evaluate the behavior of the entire weldment cross section under load, by experimentally and analytically determining the stress and strain concentrations that develop. Some of the whole-weld cross section preliminary evaluations have been reported previously.[20,21]

The earlier work demonstrated that the microstructure[22] and creep properties[23] of the adjacent base metal (heat-affected zone or HAZ) were affected by the thermal and mechanical cycling that occurs during

welding. To perform elastic and elastic-plastic numerical evaluations of whole weld cross-section behavior for comparison with experimental results, we need to determine the tensile properties of the base metals in the HAZ. This report describes the tensile behavior of HAZ base metal.

A 6:2—2 weldment[19] was sectioned to produce tensile specimens whose gage lengths were parallel to the welding direction. The specimens had gage section center lines that were 0.6, 1.5, and 2.4 cm (0.24, 0.59, and 0.94 in.) from the fusion line. The specimen layout is shown in Fig. 5.39. Specimens are numbered FF03-BXX, and they were cut from near the surface (L1 layer[24]), near the root passes (L2 layer[24]), and an intermediate location (L3 layer[24]). These specimens had a 0.61-cm-diam by 3.12-cm-long (0.25 by 1.25 in.) reduced section, and were tested at 0.004/min

PHOTO 2065-74

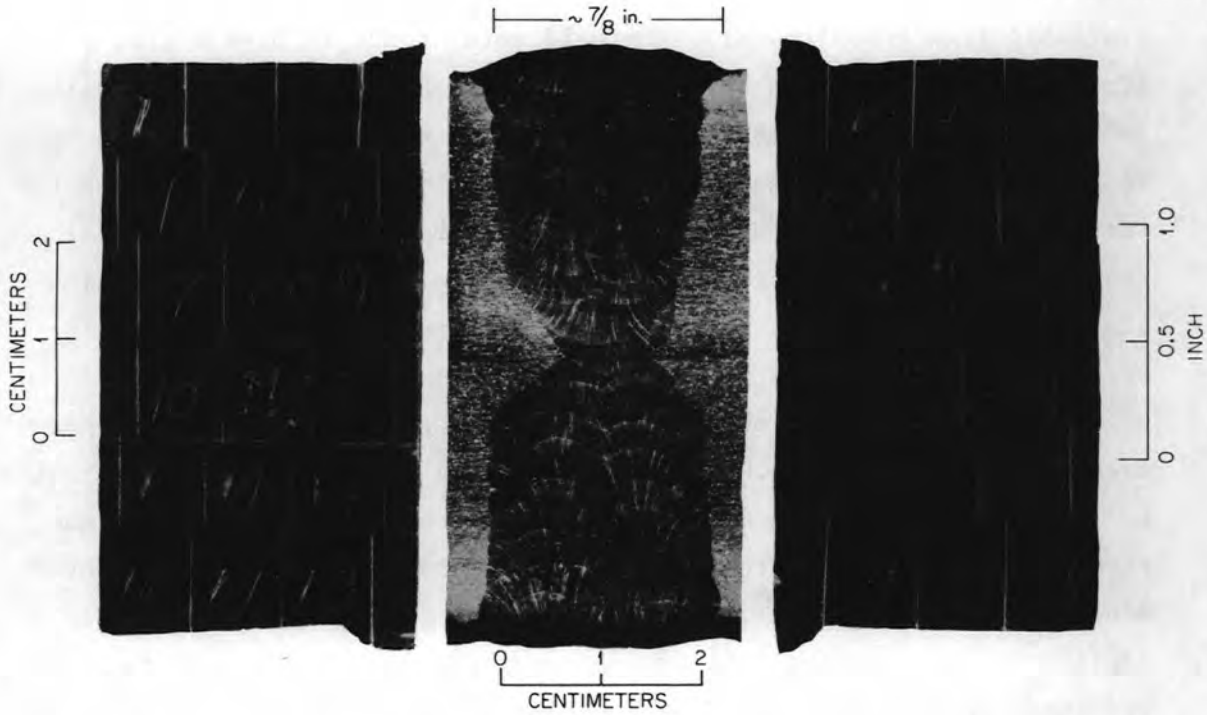

Fig. 5.39. Location of Base Metal Specimens from Near the Fusion Line in FFTF Vessel Test Welds. Areas shown are not all to same scale.

by use of the same techniques used to test comparable weld-metal specimens.[24,25] The data reduction techniques have been described previously;[25] the tensile data are summarized in Tables 5.16 through 5.19 for tests performed at room temperature, 482°C, and 593°C (900 and 1100°F). Probably the most important single factor for the base metal is the variation of yield strength that occurs. At all three test temperatures, the 0.2% offset yield strength increased significantly as the fusion line was neared; the observed increase was on the order of 15,000 to 20,000 psi (103–138 MPa). (See Figs. 5.40 and 5.41). The increment in strength tends to be smallest near the surface of the weld. Two other sets of data are plotted for comparison: (1) the yield strength data for longitudinal all-weld-metal specimens from a 6:2-2 weld are plotted with bars representing the range of values measured for other combinations of weld metal and base metal[26] and (2) yield strength data from specimens made and tested in the same manner, from "virgin" base metal located about 5 cm (2 in.) from the fusion line (only yield strength data are now available from these tests). The weld metal tends to have higher yield strength than the virgin base metal, but the HAZ material can sometimes be stronger or weaker than the weld metal at the same level for the specimen orientations that were tested. The virgin base metal near the surface appears to have higher yield strength than virgin base metal near the center of the plate, and less thermal and mechanical cycling occurs near the surface, apparently causing somewhat lower HAZ yield strength adjacent to the fusion line.

Transmission electron microscopy[23] for wafer specimens cut approximately 0.1 and 1.0 cm (0.04 and 0.4 in.) from the fusion line at about the L2 level showed that the dislocation line density in the HAZ increased near the fusion line as though the material had been worked. To determine whether the thermal and mechanical cycling does produce effects similar to cold working, the true-stress true-strain curves for all HAZ specimens were plotted on transparent graph paper and translated parallel to the strain ordinate until reasonable superposition occurred in the 0.1 to 0.3 strain regime. (See Fig. 5.42.) The translations required to superpose the curves are:

Table 5.16. Tensile Properties at Room Temperature of Base Metal Adjacent to FFTF Vessel Test Welds

Specimen Number and Location		Strength,[a] ksi(MPa)				Strain,[a] %		Extensometer Measurements, ksi(MPa)		Reduction of Area (%)
		Apparent Elastic Limit	0.2% Offset Yield	Ultimate	Fracture	Uniform	Total	Elastic Limit	0.2% Offset Engineering Yield Stress	
B16	L1	31.8(219)	41.6(287)	87.8(605)	64.3(443)	72.1	83.9	16.9(117)	41.4(285)	66.5
			41.7	151.0(1041)	192.0(1324)	54	109			
B17	L1	39.7(274)	49.3(340)	87.5(603)	63.6(439)	68.6	85.3	33.9(234)	50.1(345)	71.0
			49.4	147.5(1017)	219.0(1510)	52	124			
B18	L1	47.6(328)	56.3(388)	91.9(634)	71.4(492)	58.3	72.4	24.8(171)	56.7(391)	58.1
			56.4	145.5(1003)	170.4(1175)	46	87			
B13	L2	30.3(209)	36.6(252)	87.1(601)	64.1(442)	95.5	111.2	23.1(159)	37.0(255)	61.7
			36.6	170.2(1174)	167.4(1154)	67	96			
B14	L2	35.2(243)	43.7(301)	88.8(612)	63.0(434)	74.8	85.1	22.8(157)	43.5(300)	68.6
			43.8	155.3(1071)	200.6(1383)	56	116			
B15	L2	50.7(350)	59.0(407)	93.2(643)	68.2(470)	74.2	90.2	28.0(193)	60.0(414)	65.2
			59.1	162.3(1119)	196.1(1352)	55	106			
B10	L3	27.7(191)	38.0(262)	88.1(607)	70.4(485)	74.0	85.2	7.4(51)	37.0(255)	62.2
			38.1	153.3(1057)	186.5(1286)	55	97			
B11	L3	34.9(241)	45.2(312)	89.3(616)	69.8(481)	67.5	84.8	17.8(123)	32.4(223)	70.6
			45.3	162.7(1122)	237.5(1638)	51				
B12	L3	50.3(347)	64.7(446)	95.3(657)	79.1(545)	57.6	69.3	14.4(99)	58.7(405)	60.7
			64.8	150.2(1036)	201.3(1388)	45	93			

[a]First line gives engineering values; second gives true.

Table 5.17. Tensile Properties at 482°C (900°F) of Base Metal Adjacent to FFTF Vessel Test Welds

Specimen Number and Location		Strength,[a] ksi(MPa)				Strain,[a] %		Extensometer Measurements, ksi(MPa)		Reduction of Area (%)
		Apparent Elastic Limit	0.2% Offset Yield	Ultimate	Fracture	Uniform	Total	Elastic Limit	0.2% Offset Engineering Yield Stress	
B1	L1	21.7(150)	26.5(183)	67.2(463)	52.1(359)	40.3	49.3	14.1(97)	25.7(177)	60.3
			26.6	94.3(650)	129.1(890)	34	92			
B2	L1	25.0(172)	30.4(210)	66.3(457)	50.2(346)	37.5	46.5	11.3(78)	29.6(204)	55.9
			30.5	91.2(629)	113.9(785)	32	82			
B3	L1	31.3(216)	39.9(275)	68.2(470)	53.5(369)	31.3	40.0	27.0(186)	39.3(271)	59.4
			40.0	89.6(618)	131.8(909)	27	90			
B4	L2	16.8(116)	21.7(150)	65.8(454)	51.3(354)	44.8	51.8	10.3(71)	19.9(137)	53.7
			21.8	95.2(656)	110.8(764)	37	77			
B5	L2	21.0(145)	26.1(180)	65.0(448)	51.0(352)	39.2	47.1	14.7(101)	25.3(174)	57.1
			26.2	90.5(624)	119.1(821)	33	85			
B6	L2	36.8(254)	41.4(285)	68.1(470)	52.2(360)	32.2	40.1	20.5(141)	44.0(303)	58.7
			41.4	90.0(621)	126.4(872)	28	88			
B7	L3	14.7(101)	22.2(153)	64.7(446)	52.1(359)	42.0	48.9	6.95(48)	20.8(143)	53.9
			22.2	91.8(633)	113.0(779)	35	77			
B8	L3	21.2(146)	26.8(185)	65.5(452)	50.9(351)	39.7	48.2	15.5(107)	27.3(188)	60.3
			26.8	91.6(632)	126.3(871)	33	92			
B9	L3	35.1(242)	44.6(308)	68.4(472)	54.1(373)	26.9	35.5	32.3(223)	41.9(289)	61.2

[a]First line gives engineering values; second gives true.

Table 5.18. Tensile Properties at 593°C (1100°F) of Base Metal Adjacent to FFTF Vessel Test Welds

Specimen Number and Location		Strength,[a] ksi(MPa)				Strain,[a] %		Extensometer Measurements, ksi(MPa)		Reduction of Area (%)
		Apparent Elastic Limit	0.2% Offset Yield	Ultimate	Fracture	Uniform	Total	Elastic Limit	0.2% Offset Engineering Yield Stress	
B21	L1	15.2(105)	22.3(154)	51.3(354)	49.9(344)	33.2	36.5	11.3(78)	21.5(148)	37.1
			22.4	68.3(471)	79.4(547)	29	46			
B20	L1	20.5(141)	27.4(189)	52.3(361)	49.1(339)	31.8	36.6	15.3(105)	26.7(184)	32.8
			27.5	68.9(475)	73.0(503)	28	40			
B19	L1	29.5(203)	36.7(253)	54.0(372)	46.0(317)	22.7	34.7	19.0(131)	36.4(251)	37.6
			36.8	66.3(457)	73.8(509)	20	47			
B24	L2	14.4(99)	19.6(135)	51.7(356)	49.9(344)	32.4	35.6	7.8(54)	18.2(126)	34.6
			19.6	68.4(472)	76.4(527)	28	42			
B23	L2	16.7(115)	22.3(154)	51.8(357)	47.7(329)	35.7	41.7	8.6(59)	21.3(147)	34.3
			22.4	70.3(485)	72.6(501)	30	42			
B22	L2	19.7(136)	34.3(236)	54.1(373)	44.9(310)	25.6	36.5	11.7(81)	35.2(243)	41.7
			34.4	67.9(452)	77.1(532)	23	54			
B27	L3	15.0(103)	19.7(136)	50.8(350)	45.4(313)	34.4	43.0	7.7(53)	19.1(132)	38.5
			19.8	68.3(471)	73.9(510)	30	49			
B26	L3	15.9(110)	24.2(167)	51.8(357)	42.0(290)	31.1	42.8	11.3(78)	23.3(161)	47.6
			24.2	67.9(468)	80.1(552)	27	65			
B25	L3	28.6(197)	39.2(270)	54.1(373)	43.9(303)	21.1	32.8	12.2(84)	39.4(272)	41.5
			39.3	65.5(452)	75.0(517)	19	54			

[a]First line gives engineering values; second gives true.

Table 5.19. Diametral Strain and Hollomon Constants for Base Metal Adjacent to FFTF Vessel Test Welds

Specimen Number and Location		Diametral Strain: At Fracture, % Max	Min	Ratio	Diametral Strain: Away From Fracture, % Max	Min	Ratio	Constants of $\sigma = k\varepsilon^n$: ln k, k in ksi	MPa	n
				Tested at Room Temperature						
B16	L1	43.8	40.6	1.08	19.3	18.1	1.07	11.78	13.71	0.210
B17	L1	48.6	43.8	1.11	20.5	20.5	1.00	11.77	13.70	0.177
B18	L1	36.7	33.9	1.08	17.7	17.3	1.02	11.81	13.74	0.161
B13	L2	39.8	36.5	1.09	22.9	21.7	1.06	11.80	13.73	0.239
B14	L2	45.2	42.7	1.06	18.5	17.7	1.05	11.80	13.73	0.205
B15	L2	41.7	40.3	1.03	18.5	18.1	1.02	11.82	13.75	0.149
B10	L3	39.4	37.7	1.04	19.7	18.5	1.07	11.79	13.72	0.226
B11	L3	46.6	45.0	1.04	24.1	19.7	1.22			
B12	L3	39.0	35.7	1.09	20.5	18.9	1.09	11.82	13.75	0.138
				Tested at 482°C (900°F)						
B1	L1	37.4	36.6	1.02	14.4	13.9	1.03	11.46	13.39	0.230
B2	L1	33.8	33.4	1.01	13.7	13.9	1.01	11.45	13.38	0.206
B3	L1	36.5	36.1	1.01	12.3	11.5	1.07	11.46	13.39	0.151
B4	L2	32.2	31.7	1.01	14.1	13.7	1.03	11.49	13.42	0.269
B5	L2	34.7	34.3	1.01	13.5	13.1	1.03	11.45	13.38	0.230
B6	L2	35.8	35.6	1.01	12.2	12.0	1.02	11.47	13.40	0.151
B7	L3	32.3	31.9	1.01	14.7	14.3	1.03	11.44	13.37	0.254
B8	L3	37.2	36.8	1.01	13.6	13.0	1.05	11.46	13.39	0.145
B9	L3	38.3	37.1	1.03	10.3	9.7	1.06	11.45	13.38	0.133
				Tested at 593°C (1100°F)						
B21	L1	22.9	18.5	1.24	13.1	12.9	1.02	11.28	13.21	0.225
B20	L1	19.4	16.6	1.17	12.8	12.4	1.03	11.25	13.18	0.185
B19	L1	21.8	20.2	1.08	12.6	12.2	1.03	11.21	13.14	0.123
B24	L2	19.3	18.9	1.02	12.7	12.5	1.02	11.27	13.20	0.240
B23	L2	19.5	18.3	1.07	14.7	14.3	1.03	11.29	13.22	0.226
B22	L2	24.0	23.2	1.03	11.6	11.2	1.04	11.23	13.16	0.138
B27	L3	25.7	17.7	1.45	14.9	14.5	1.03	11.28	13.21	0.244
B26	L3	27.8	27.4	1.01	14.6	14.2	1.03	11.28	13.21	0.211
B25	L3	24.3	22.7	1.07	10.7	10.5	1.02	11.21	13.14	0.109

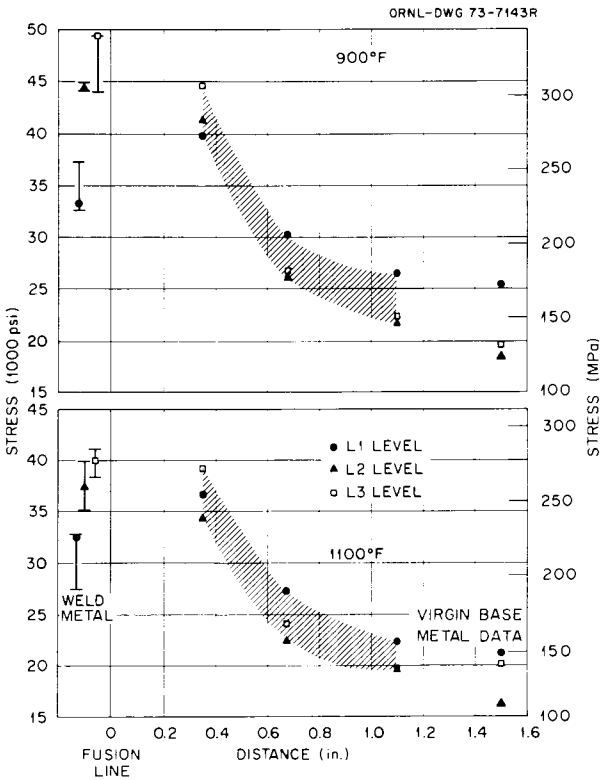

Fig. 5.40. Variation of Yield Strength at 482 and 593°C (900 and 1100°F) in Weld Metal and HAZ of Type 308 Stainless Steel Weldment.

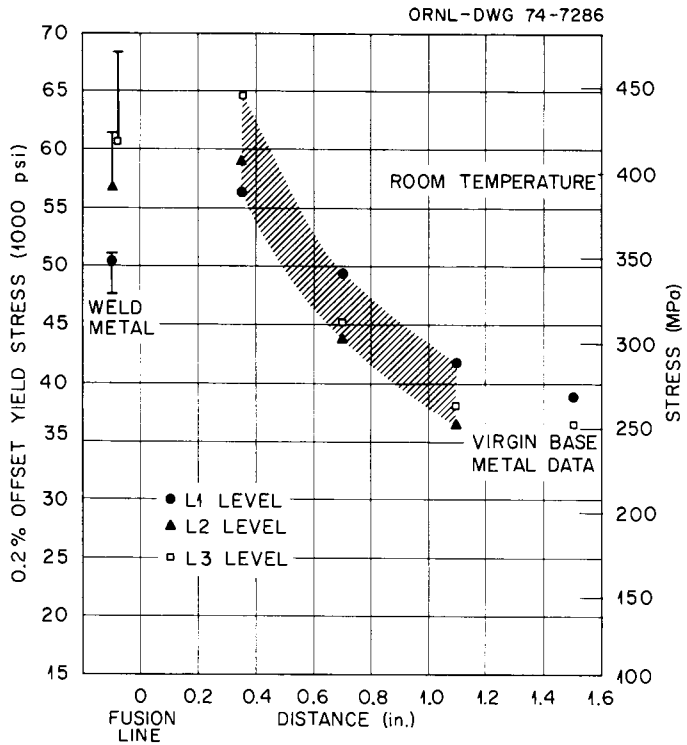

Fig. 5.41. Variation of Yield Strength at Room Temperature in Weld Metal and HAZ of Type 308 Stainless Steel Weldment. 1 in. = 25.4 mm.

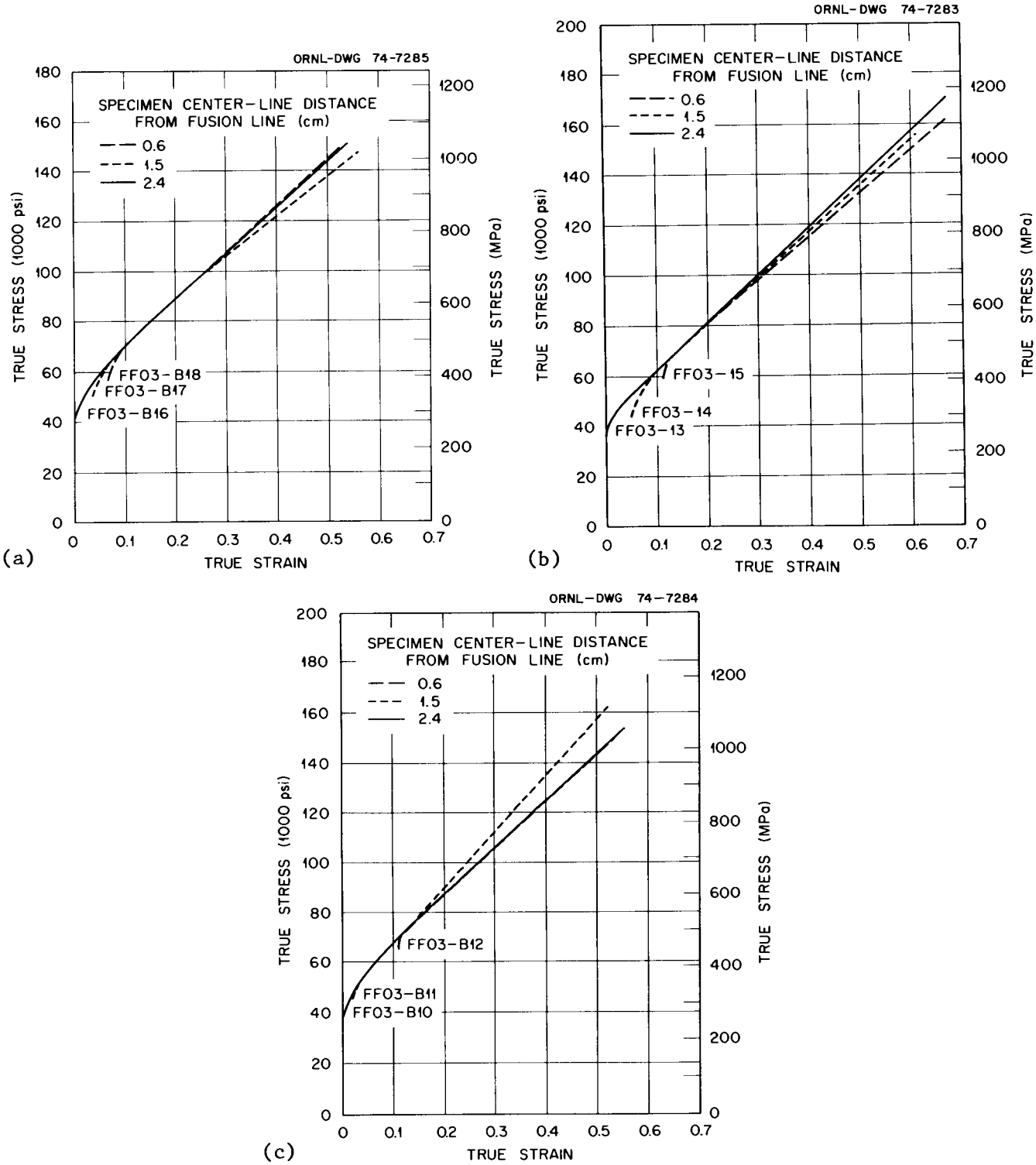

Fig. 5.42. Room Temperature Tensile True-Stress vs True-Strain Curves From 0.2% to Ultimate Strain for Type 304 Stainless Steel Near Fusion Line. (a) L1 Level. (b) L2 Level. (c) L3 Level.

Specimen Locations Distance from Fusion Line	True Strain to Cause Superposition at		
	25°C(77°F)	482°C(900°F)	593°C(1100°F)
1.5-cm specimen onto 2.4-cm specimen	0.035	0.05	0.02
0.6-cm specimen onto 2.4-cm specimen	0.07	0.115	0.11

The shapes of the curves are sufficiently similar that these results coupled with the transmission microscopy indicate that the HAZ is a region in which the dominant effect on tensile properties is the cold or warm working that occurs during welding. This apparant strain hardening increases as the fusion line is neared.

5.3.2 Creep and Creep-Rupture Properties of Type 308 CRE Stainless Steel Weld Metal From the FFTF Vessel Test Weld — R. T. King and E. Bolling

The creep and creep-rupture data for the as-deposited longitudinal all-weld metal specimens of type 308 CRE stainless steel that are prototypic of longitudinal seam and girth welds in the FFTF vessel were tabulated in the last report of this series.[27] This report gives the graphical representation of those data.

Creep tests were performed at several temperatures, and they are represented by use of a time-temperature parameter method. The Larson-Miller parameter is used here because of its relative simplicity and widespread acceptance, but it is only a convenient method whose use is not based on any fundamental considerations. The Larson-Miller representation has the form:

$$\log_{10} \sigma = f[T(c \pm \log_{10} t)] \ , \qquad (17)$$

where T is temperature (°R), σ is applied stress (psi), and the constant c is arbitrarily set equal to 20. The time, t, refers to several specific identifiable times in a creep test, for which data are plotted as follows. Figures 5.43, 5.44, and 5.45 show, respectively, the time to 0.5, 1.0, and 2.0% total strain, together with the corresponding isochronous

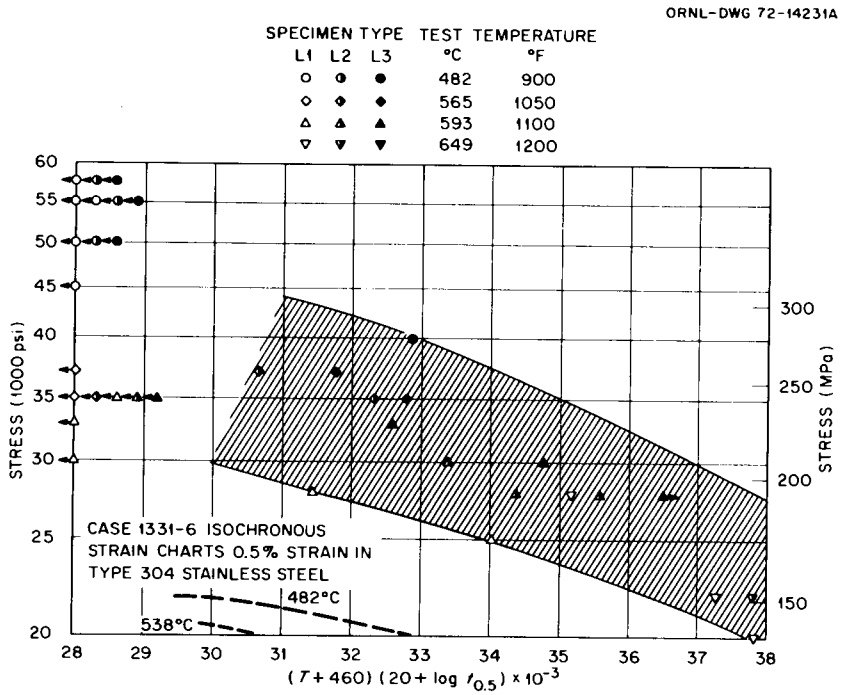

Fig. 5.43. Larson-Miller Parameter for Time to 0.5% Strain in Type 308 CRE Stainless Steel Weld Metal.

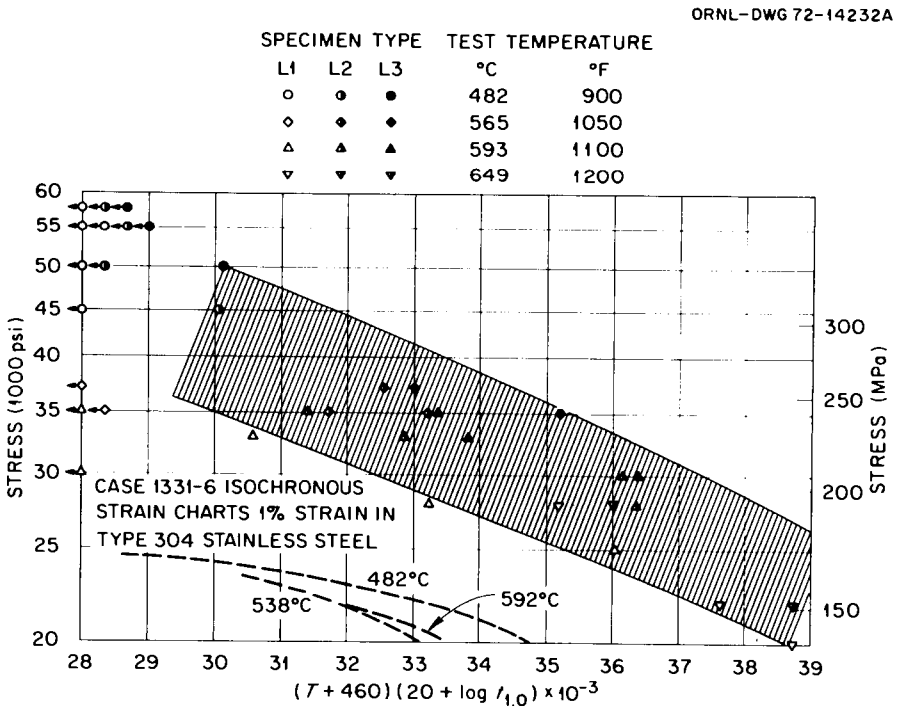

Fig. 5.44. Larson-Miller Parameter for Time to 1.0% Strain in Type 308 CRE Stainless Steel Weld Metal.

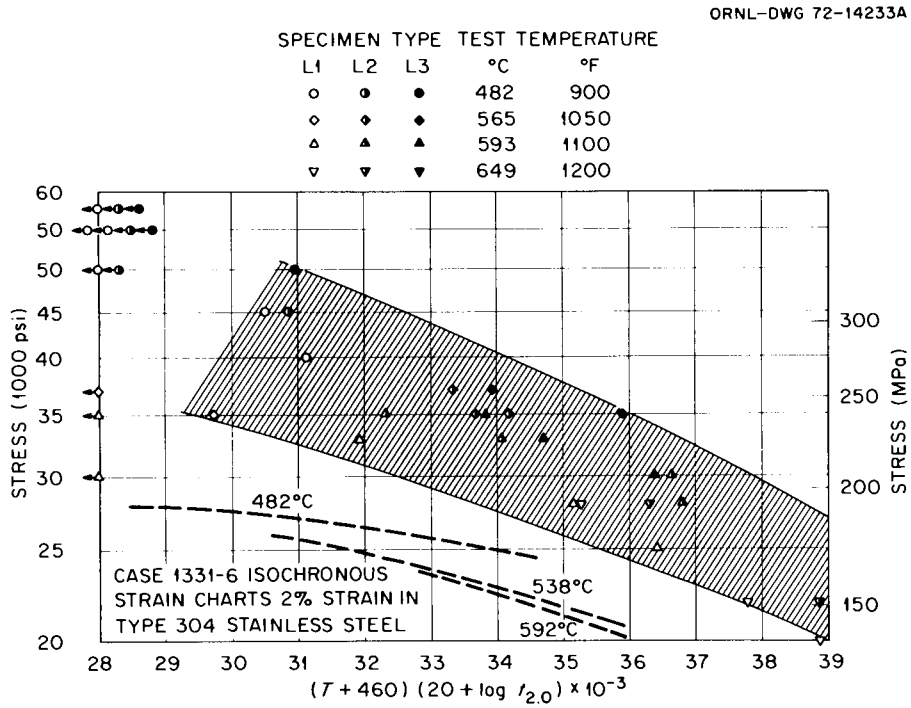

Fig. 5.45. Larson-Miller Parameter for Time to 2.0% Strain in Type 308 Stainless Steel Weld Metal.

stress-strain curve values[28] for type 304 stainless steel base metal. Figure 5.46 shows the time to the end of primary creep, and Fig. 5.47 the time to the end of second-stage creep, as determined by visual observation of the start of nonlinear strain-time data. Figure 5.58 shows the time to the onset of tertiary creep as determined by intersection of a line displaced by +0.2% strain from second-stage creep data with the strain-time curve. Figure 5.49 shows the time to rupture, combined with expected[29] values and lower (λ=0.95, P=0.90) tolerance limits* for type 304 stainless steel base metal at various temperatures.

Above 482°C (900°F), L3 specimens (from the root pass region) tend to be strongest, L2 specimens (from the intermediate region) to be intermediate in strength, and L1 specimens (from the surface pass region) to be the weakest material. This is in agreement with tensile test results, and it has been explained on the basis of the microstructure of the

*The curves above which there is 95% confidence that 95% of the data lie.

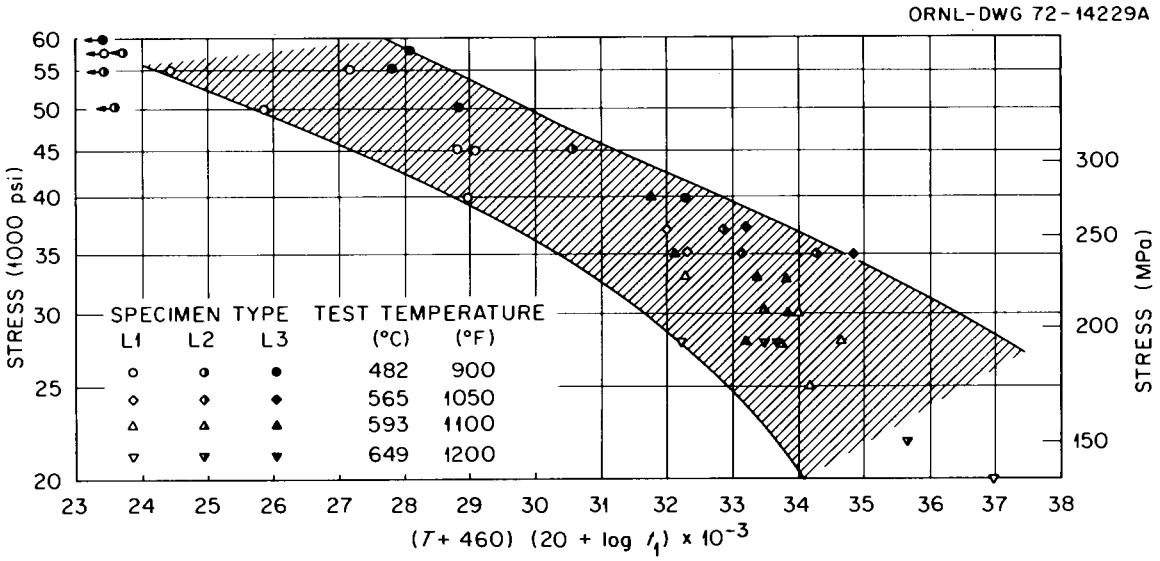

Fig. 5.46. Larson-Miller Parameter for Time to End of First-Stage Creep in Type 308 CRE Stainless Steel Weld Metal.

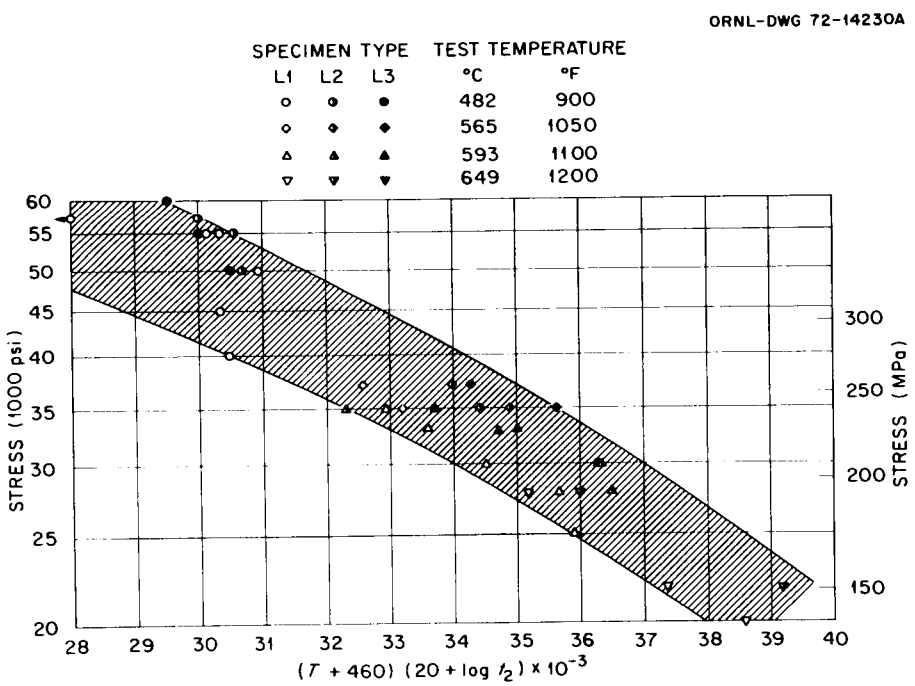

Fig. 5.47. Larson-Miller Parameter for Time to End of Second-Stage Creep in Type 308 CRE Stainless Steel Weld Metal.

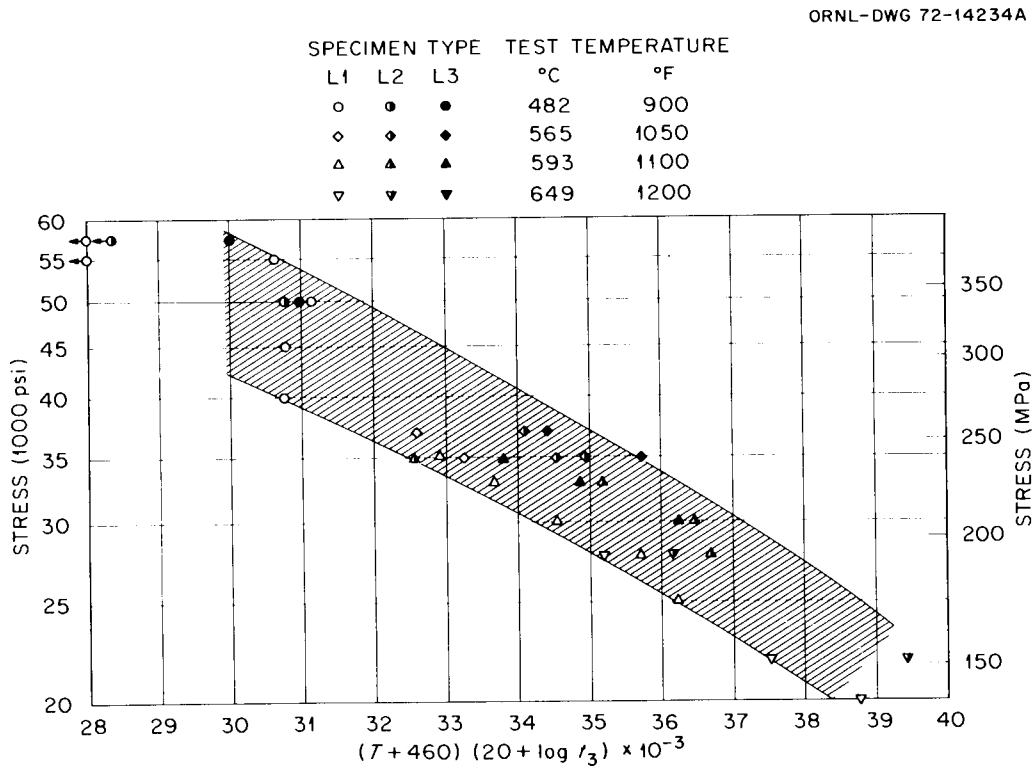

Fig. 5.48. Larson-Miller Parameter for Time to Third-Stage Creep by 0.2% Strain Offset Method in Type 308 CRE Stainless Steel Weld Metal.

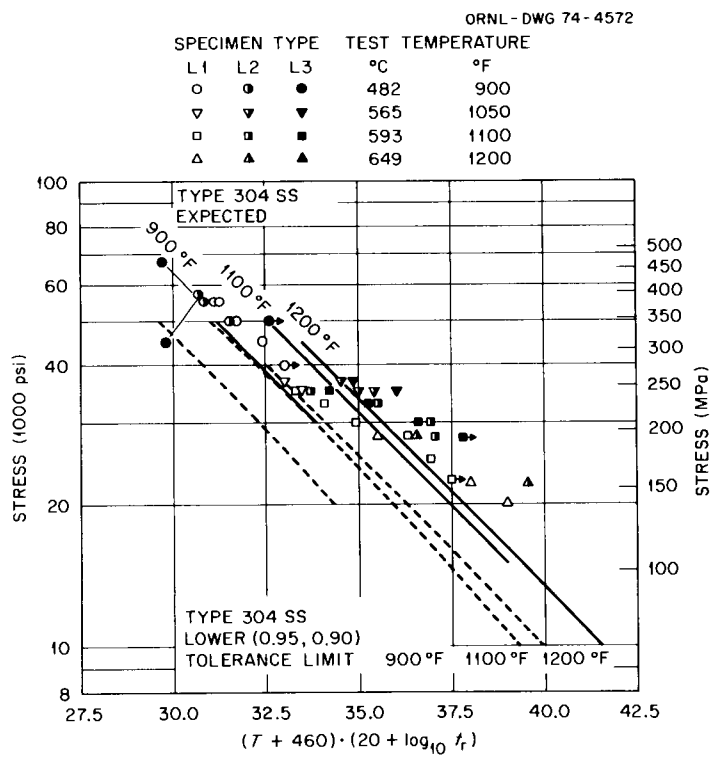

Fig. 5.49. Stress-Rupture Data for Type 308 CRE Stainless Steel Longitudinal All-Weld-Metal Specimens.

weld metal.[23] At 482°C (900°F), it was necessary to load specimens to relatively high strains. The usual order of strengths by distance from the weld surface is frequently reversed at 482°C, but it is not clear whether this effect is real, due to factors in testing, or due to exact specimen location. For example, the exact test temperature and the method of specimen loading (step-type or smooth) can both influence the data. These variations may result from improvements in test methods over the span of this project. However, the strength properties are quite sensitive to the precise location of the specimen in the weld, and that variable could be affecting these high-stress creep tests. A small number of identical carefully controlled creep tests are now being run to investigate these possibilities.

The test results show that the times to the various total strains of 0.5, 1.0, and 2.0% exceed those for type 304 stainless steel base metal given in Code Case 1331. Further, the rupture times of all weld metal specimens exceed the (λ=0.95, P=0.90) lower tolerance limits for type 304 stainless steel base metal, and they are often well above the expected values for base metal (Fig. 5.49). Except for short-time tests at 482°C (900°F), L3 specimens tend to have the longest rupture times and L1 specimens the shortest. The fraction of total test time before tertiary creep is usually between 0.2 and 0.8, although values below 0.1 have been observed at 482°C (Fig. 5.50).

The ranking of strength is also apparent in the minimum creep rate data (Fig. 5.51). We have plotted the minimum creep rate, obtained manually from the strain-time data, against the rupture time, to investigate whether these two parameters are related (Fig. 5.52). All the data fall in a single scatter band that is about 1.5 log cycles wide in rupture time, and no particular distinction can be made between L1, L2, and L3 specimens. Tests that are still in progress are indicated by arrows. The average creep rate (rupture strain/rupture time) correlates better with rupture time than does the true minimum creep rate (see Fig. 5.53). (This simply reflects the relatively small variation in rupture strain observed in these tests.)

The creep strain before the onset of tertiary creep (Fig. 5.54) is of some interest for current design practice. An envelope that decreases

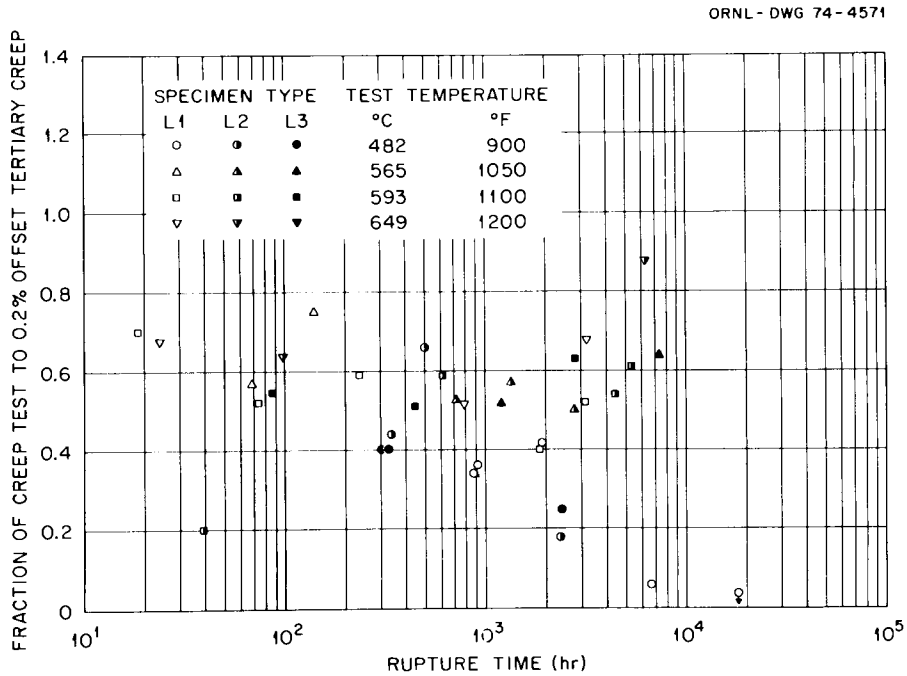

Fig. 5.50. Fraction of Total Creep Test Time Before 0.2% Offset Tertiary Creep for Type 308 CRE Stainless Steel Weld-Metal Specimens.

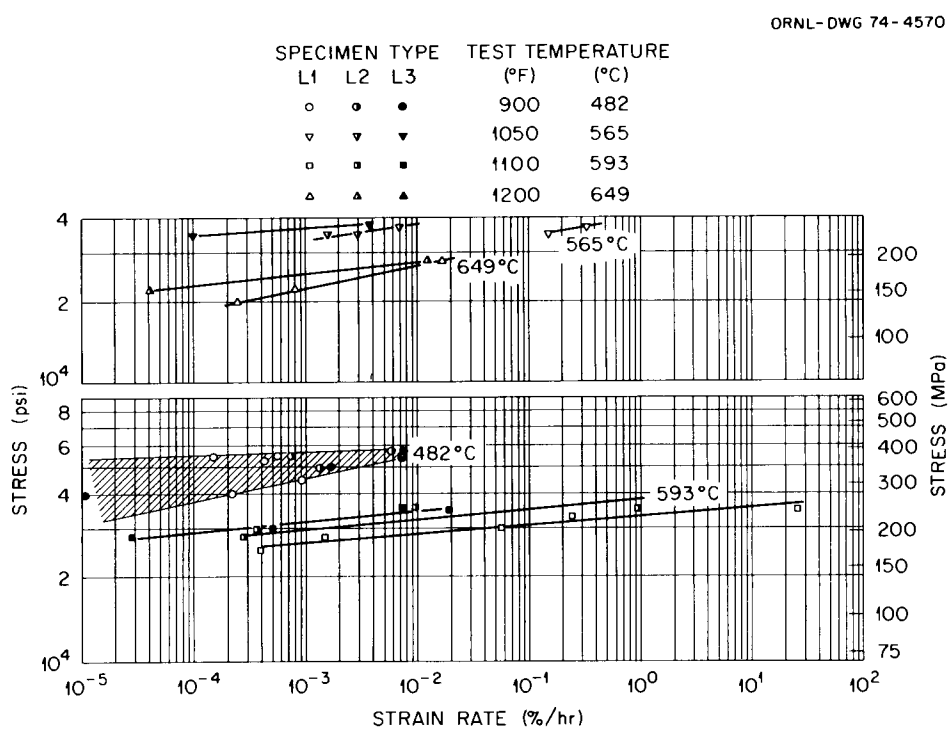

Fig. 5.51. Minimum Creep Rates for Type 308 CRE Stainless Steel Longitudinal All-Weld-Metal Specimens.

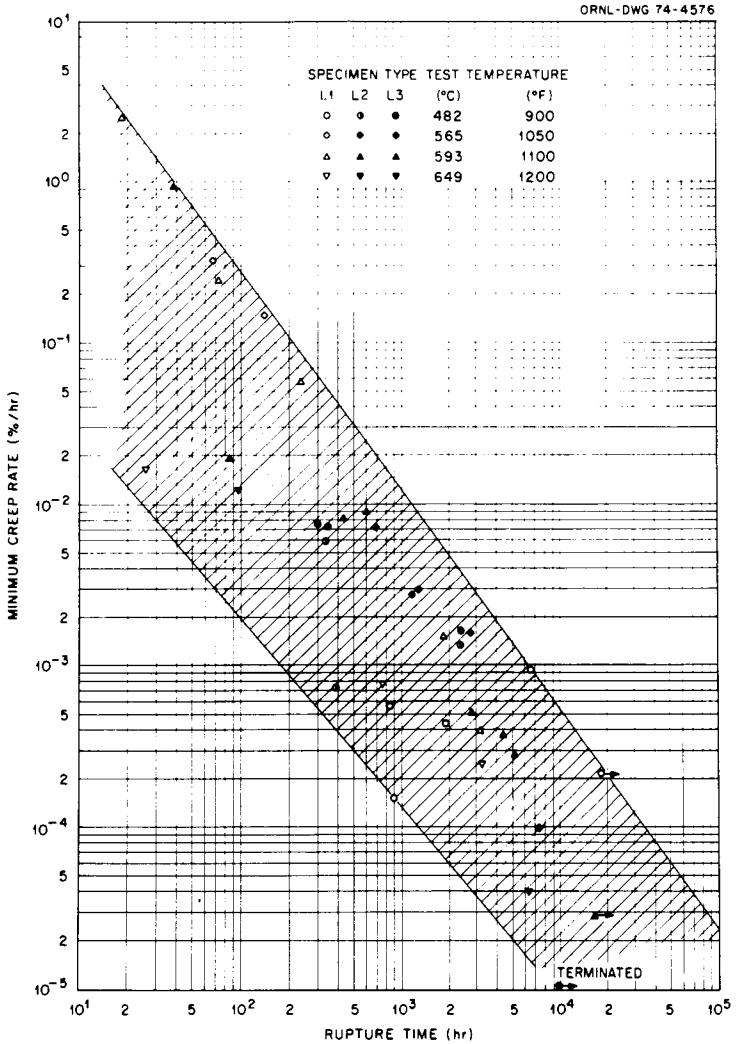

Fig. 5.52. Relation Between Minimum Creep Rate and Rupture Time for Type 308 CRE Stainless Steel Welds.

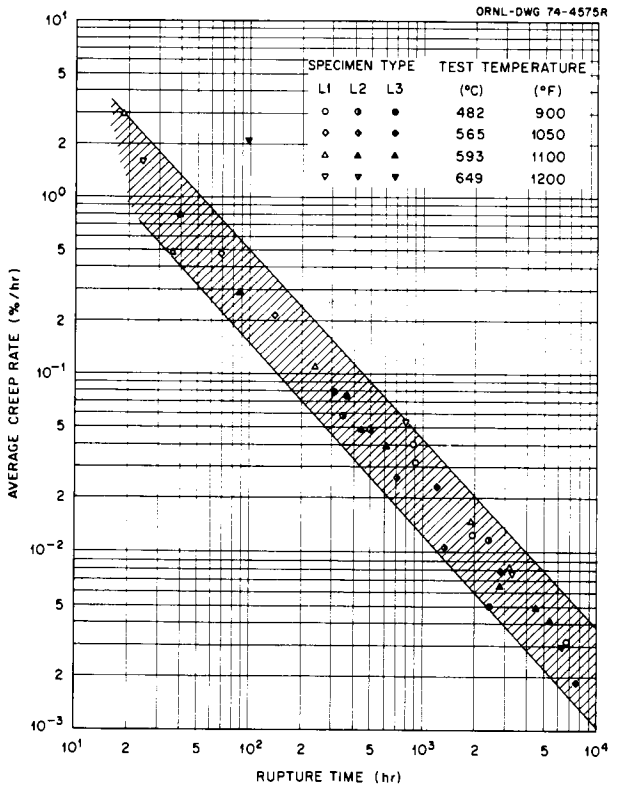

Fig. 5.53. Relation Between Average Creep Rate and Rupture Time for Type 308 CRE Stainless Steel Welds.

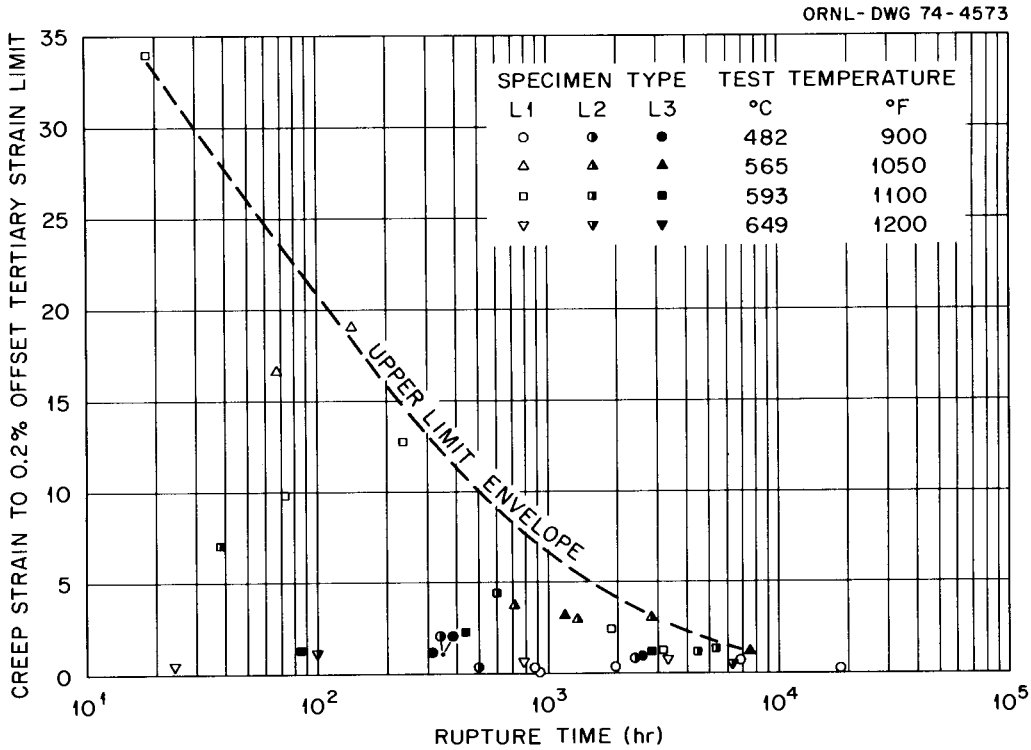

Fig. 5.54. Relationship Between Strain to Tertiary Creep and Rupture Life for Type 308 CRE Stainless Steel Welds.

with rupture time contains all these data. For rupture times approaching 10,000 hr, the strains tend to be small, about 1%. In tests lasting less than 1000 hr at 482 and 565°C (900 and 1050°F), creep strains before tertiary creep in some surface and intermediate specimens exceed 5%, but they are far outnumbered by the tests exhibiting less than 5% creep strain before tertiary creep.

The total elongations of ruptured Type 308 CRE stainless steel weld metal specimens all exceed 12% (Fig. 5.55). The trend band for type 308 CRE weld metal has ductilities much higher than those reported for conventional type 308 weld metal for times approaching 10,000 hr. The four tests in progress include two specimens that have already strained more than 5% (for times between 9000 and 19,000 hr). The surface (L1) specimens tend to be somewhat more ductile than the root pass (L3) specimens.

With one exception, the reduction of area measurements exceed 25% (Fig. 5.56), and some are as large as 65%. This measure of ductility does not decrease markedly with increasing rupture time, and the lowest value occurred in a short-time test.

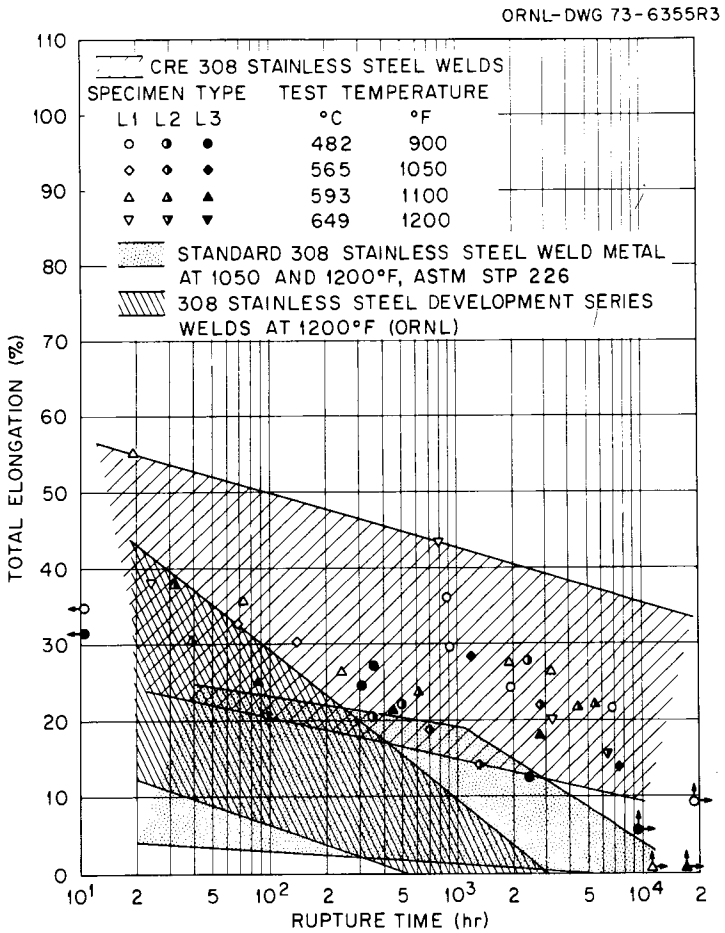

Fig. 5.55. Creep Ductility of Type 308 CRE Stainless Steel Weld Metal.

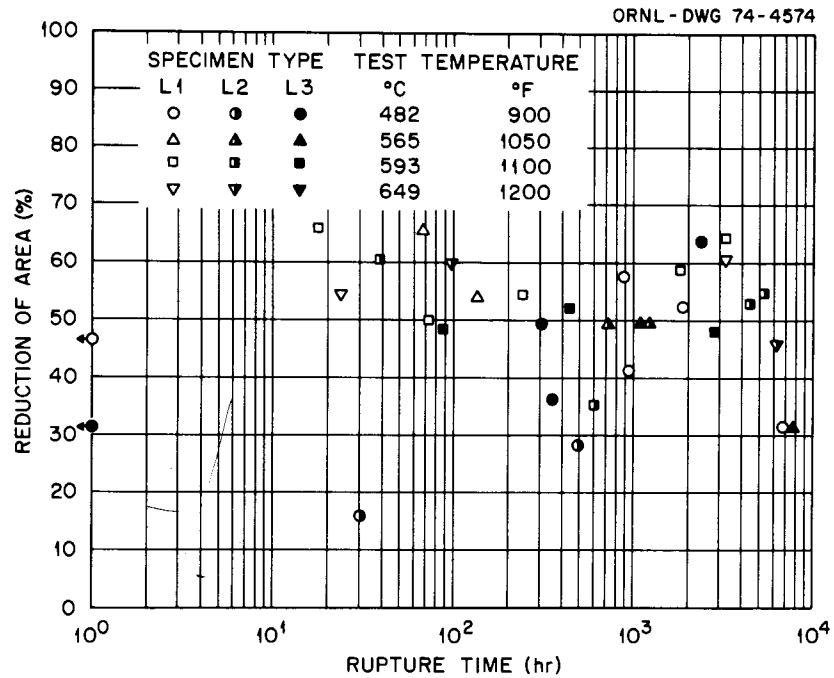

Fig. 5.56. Reduction of Area of Type 308 CRE Stainless Steel Longitudinal, All-Weld-Metal Specimens.

A statistical analysis of these tests based on characteristics obtained from more formal treatments of the strain-time curves is planned. The reader is warned that the values published here are subject to change as a result of this more rigorous analysis.

5.4 MECHANICAL PROPERTIES OF STEAM GENERATOR AND HEAT EXCHANGER MATERIALS — C. R. Brinkman

Extensive mechanical properties studies are under way on 2 1/4 Cr-1 Mo low-alloy steel. These include tensile, creep, fatigue, and heat-to-heat variations. A number of correlations, with their tolerance limits, have also been made for inclusion in the *Nuclear Systems Materials Handbook*. A small study is also under way to determine the properties of weld-overlaid stainless steel for intermediate heat exchanger applications.

5.4.1. Tensile Properties of 2 1/4 Cr-1 Mo Steel — R. L. Klueh

Last quarter[30] we reported tensile data on annealed 2 1/4 Cr-1 Mo steel that covered the range room temperature to 593°C (1100°F) and the strain range of 0.0004 to 0.4/min. In addition to determining the usual tensile data there reported (i.e., yield stress, ultimate tensile strength, etc.), we also determined accurate stress-strain curves by attaching an extensometer to the specimen gage length. In this way, we were able to obtain accurate curves to 5% strain, the strain region of interest to the designer.

Figures 5.57 through 5.60 show such data for the four strain rates tested (at 0.0004/min, only four tests have been completed). In general, these curves reflect the observations[30] made on the ultimate tensile strength variation with temperature and strain rate. That is, the effect of strain aging, which gives rise to the peak in ultimate tensile strength at 371°C (700°F), is seen to become a factor at low strains. Even at low strains the 371 and 454°C (850°F) curves often exceed those for tests at lower temperatures.

Last quarter[30] we discussed the analysis of the tensile data to determine a true-stress—true-strain relationship for the plastic behavior between the 0.2% offset yield stress and the ultimate tensile strength

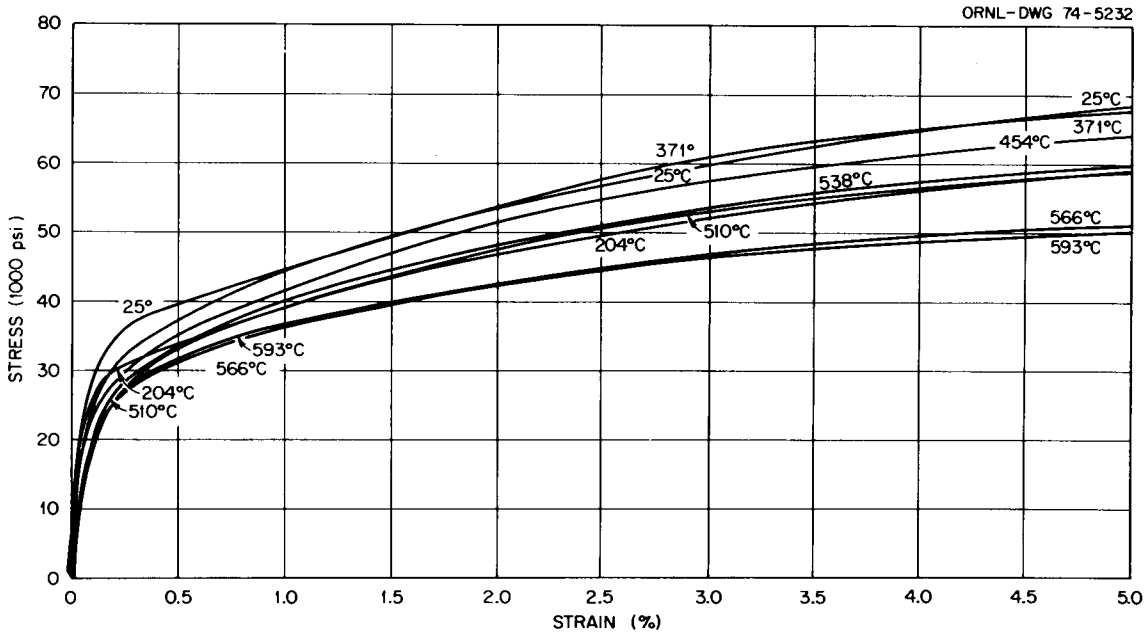

Fig. 5.57. Tensile Curves for Annealed 2 1/4 Cr-1 Mo Steel at 0.4/min.

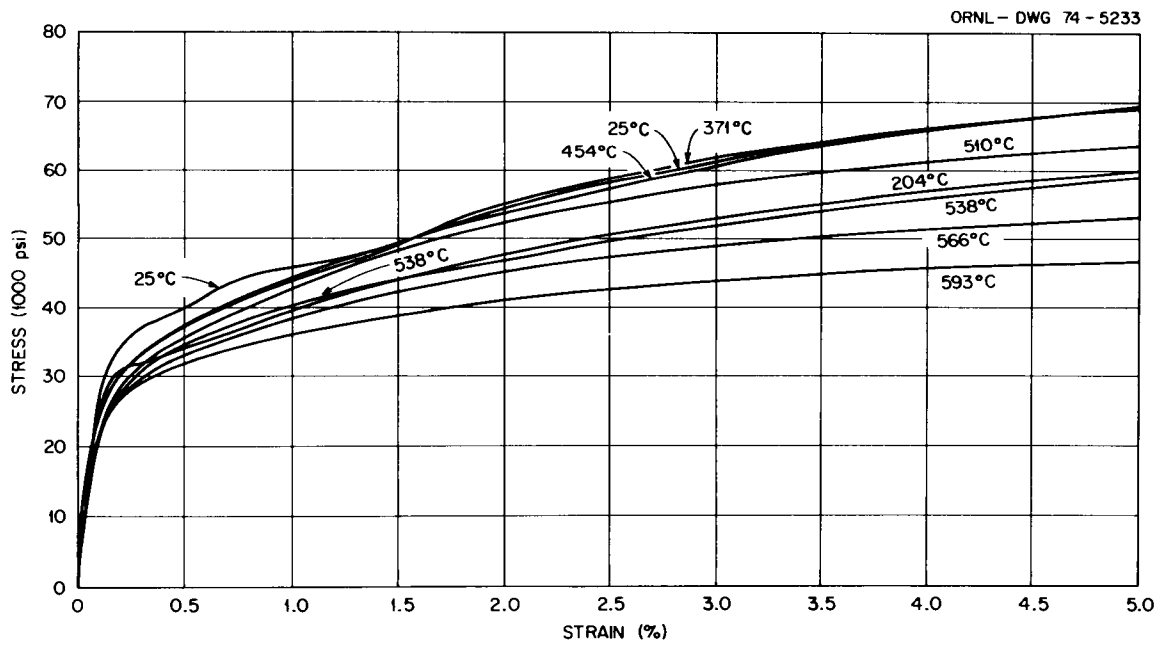

Fig. 5.58. Tensile Curves for Annealed 2 1/4 Cr-1 Mo Steel at 0.04/min.

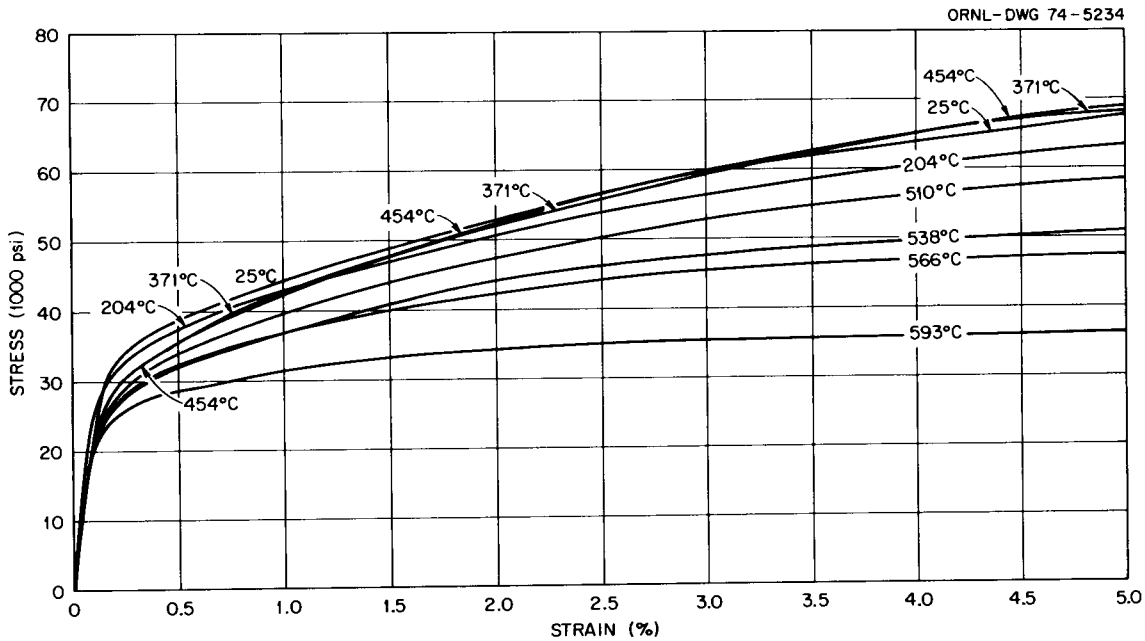

Fig. 5.59. Tensile Curves for Annealed 2 1/4 Cr-1 Mo Steel at 0.004/min.

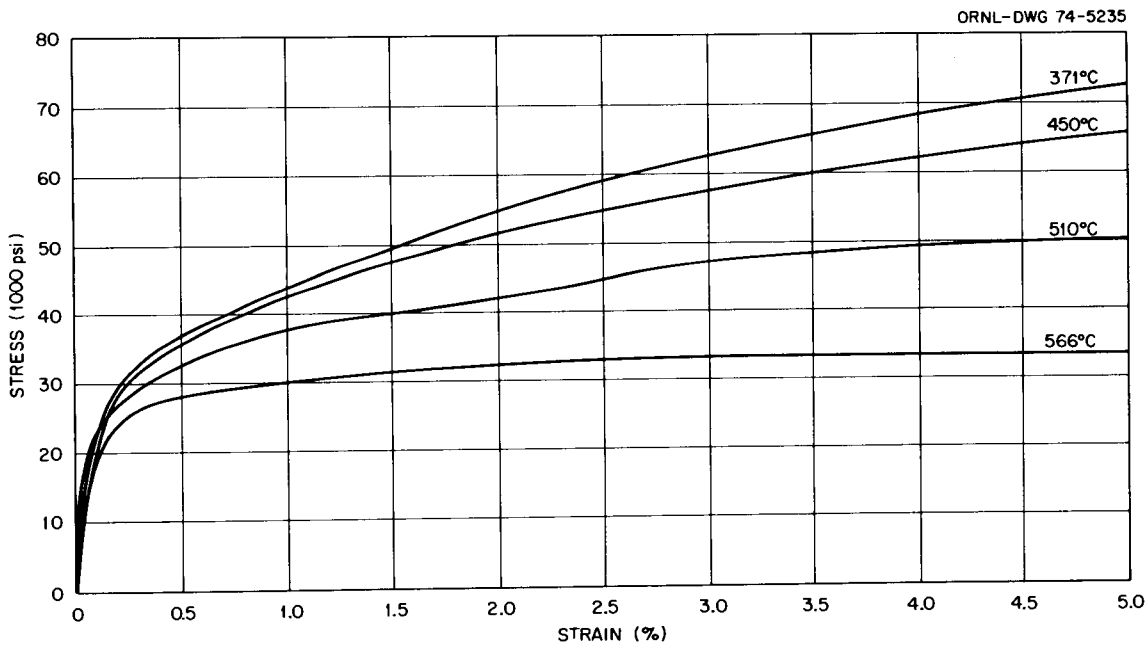

Fig. 5.60. Tensile Cruves for Annealed 2 1/4 Cr-1 Mo Steel at 0.0004/min.

and presented the data for the fit to the Holloman[31] and Ludwik[32] equations. We are now investigating the fit of those data to the Voce[33] and Ludwigson[34] equations.

We are also determining the toughness of the annealed 2 1/4 Cr-1 Mo steel during tensile deformation. The toughness of a material is its ability to absorb energy in the plastic range. A measurement of toughness is the area under the stress-strain curve. To get a measure for toughness for neck formation, we have determined the area under the engineering stress-strain curve out to the ultimate tensile strength. The results are shown in Fig. 5.61 and Table 5.20. The trend of the data with strain rate and temperature follow that of the ultimate tensile strength. It is interesting to note that the toughness of this heat of 2 1/4 Cr-1 Mo steel can be estimated to less than ±10% by the simple relation $144\sigma_u\varepsilon_u$,

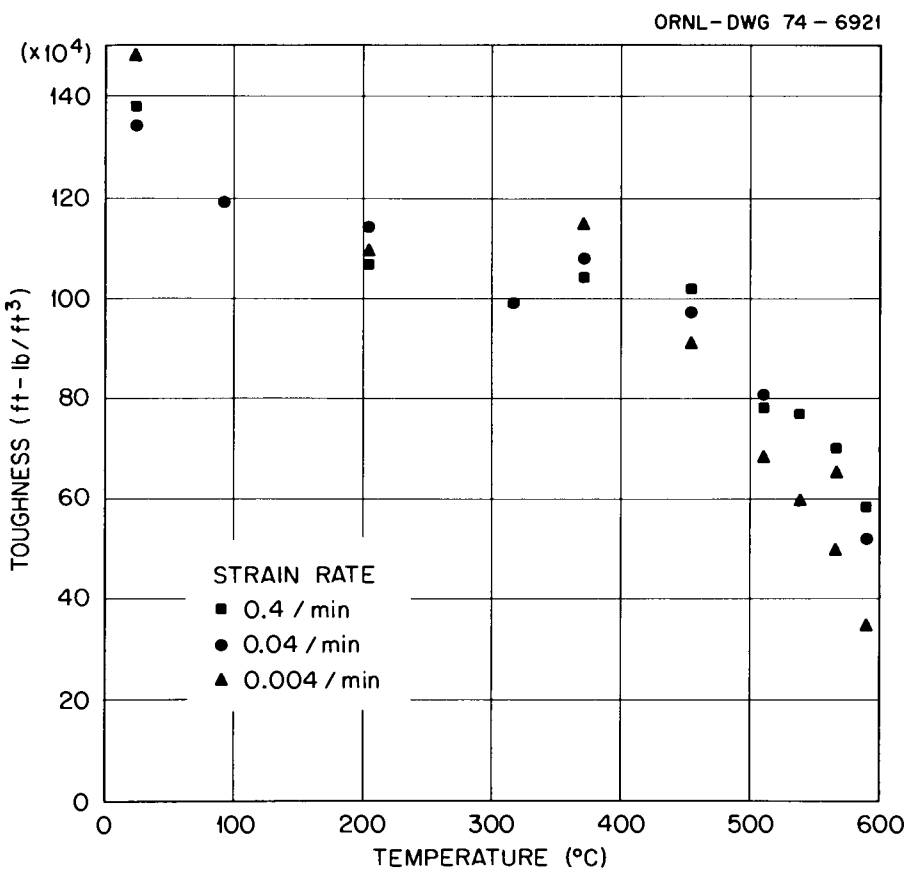

Fig. 5.61. Variation of Tensile Toughness for Neck Formation as a Function of Temperature.

Table 5.20. Toughness of Annealed 2 1/4 Cr-1 Mo Steel in Tensile Deformation (Energy Absorbed in Neck Formation)

Strain Rate (min^{-1})	Temperature (°C)	(°F)	Energy Absorbed $\left(\frac{ft\text{-}lb}{ft^3}\right)$	(MJ/m^3)
0.4	25	77	1.38×10^6	660
	204	400	1.07	512
	371	700	1.04	498
	454	850	1.02	488
	510	950	0.78	373
	538	1000	0.77	368
	566	1050	0.70	335
	593	1100	0.58	278
0.04	25	77	1.34	641
	93	200	1.19	570
	204	400	1.14	546
	316	600	0.99	474
	371	700	1.08	517
	454	850	0.97	464
	510	950	0.80	383
	538	1000	0.77	368
	566	1050	0.65	311
	593	1100	0.52	249
0.004	25	77	1.49	713
	204	400	1.09	522
	371	700	1.15	550
	454	850	0.92	440
	510	950	0.68	325
	538	1000	0.59	283
	566	1050	0.49	235
	593	1100	0.34	163

where σ_u is the ultimate tensile strength, ε_u the uniform elongation, and 144 is a conversion factor from in.-lb/in^3 to ft-lb/ft^3. During the next quarter, we will fit this data with a polynomial and submit the results for inclusion in the *Nuclear Systems Materials Handbook*.

5.4.2 Creep Properties of 2 1/4 Cr-1 Mo Steel — R. L. Klueh

We previously[35] gave test matrices for the uniaxial tensile creep tests planned for annealed and normalized-and-tempered 2 1/4 Cr-1 Mo steel over the range 371 to 593°C (700 to 1100°F). Since that time, a decision has been made to emphasize the tests on annealed material (the heat treatment to be used in the LMFBR demonstration plant), and at present, all our efforts are directed at determining the properties in that condition. From these creep tests, precise base-line data are to be obtained for one heat of material (B & W heat 20017) at stresses of interest to the steam generator. These data will be used to develop the constitutive equations that define the stress-strain-time-temperature behavior of the material.

Table 5.21 summarizes the data for tests completed or run past 1000 hr (tests are run for 2000 hr or 1% strain). Figures 5.62, 5.63, and 5.64 show creep and creep-rupture curves for the tests completed at 454, 510, and 566°C (850, 950, and 1050°F). As seen, the creep studies are at such stresses that the amount of creep during test is often quite small. This is especially true at 454°C, where the creep rates are about 7×10^{-6}%/hr or less. In this case, the data scatter has obscured the difference in the curves shown in Fig. 5.62 for stresses of 14, 18, and 22 ksi (97, 124, and 152 MPa). Since these tests were completed, some improvements have been made in our measurement techniques, and several of these tests will be repeated.

We are also conducting creep-rupture studies on the same material at 454, 510, and 566°C (850, 950, and 1050°F), and the results are given in Table 5.22. In Fig. 5.65, the rupture life and minimum creep rates are shown as a function of stress. When these results are compared with those given by Smith[36] in his compilation of elevated temperature properties for 2 1/4 Cr-1 Mo steel, good agreement is obtained at 510 and 566°C; at 454°C, Smith gives no data.

Table 5.21. Creep Properties of Annealed 2 1/4 Cr-1 Mo Steel

Temperature		Stress		Minimum Creep Rate	Creep Elongation in 1000 hr	Time to 1% Creep Strain[a]
(°C)	(°F)	(ksi)	(MPa)	(%/hr)	(%)	(hr)
454	850	14	97	0.0000036	0.032	271,000
		18[b]	124	0.0000053	0.029	187,000
		22	152	0.000007	0.026	140,000
		30	207	0.000023	0.107	41,000
		40[c]	276	0.00019	0.48	3,700
510	950	8[c]	55			
		10[b]	69	0.000018	0.035	55,000
		12[c]	83			
		14[b]	97	0.000025	0.043	40,000
		18	124	0.000032	0.064	6,000[d]
		22[c]	152	0.00013	0.031	1,550[e]
538	1000	8[c]	55	0.000012	0.041	81,000
		10[c]	69			
		12	83	0.000034	0.115	27,000
		14	97	0.000066	0.168	14,000
		18[c]	124	0.00013	1.30	6,700
566	1050	6[c]	41			
		8[c]	55	0.000019	0.064	50,000
		10	69	0.000033	0.21	26,000
		12	83	0.000062	0.22	14,000
		14	97	0.00021	0.44	3,700
593	1100	10[c]	69			
		12[c]	83	0.00035	0.47	2,500

[a]Extrapolated assuming steady-state creep continues to 1% strain.

[b]Test to be repeated.

[c]Test in progress.

[d]No longer in steady-state creep after 600 hr. Estimate takes this into account.

[e]No longer in steady-state creep after 500 hr. Estimate takes this into account.

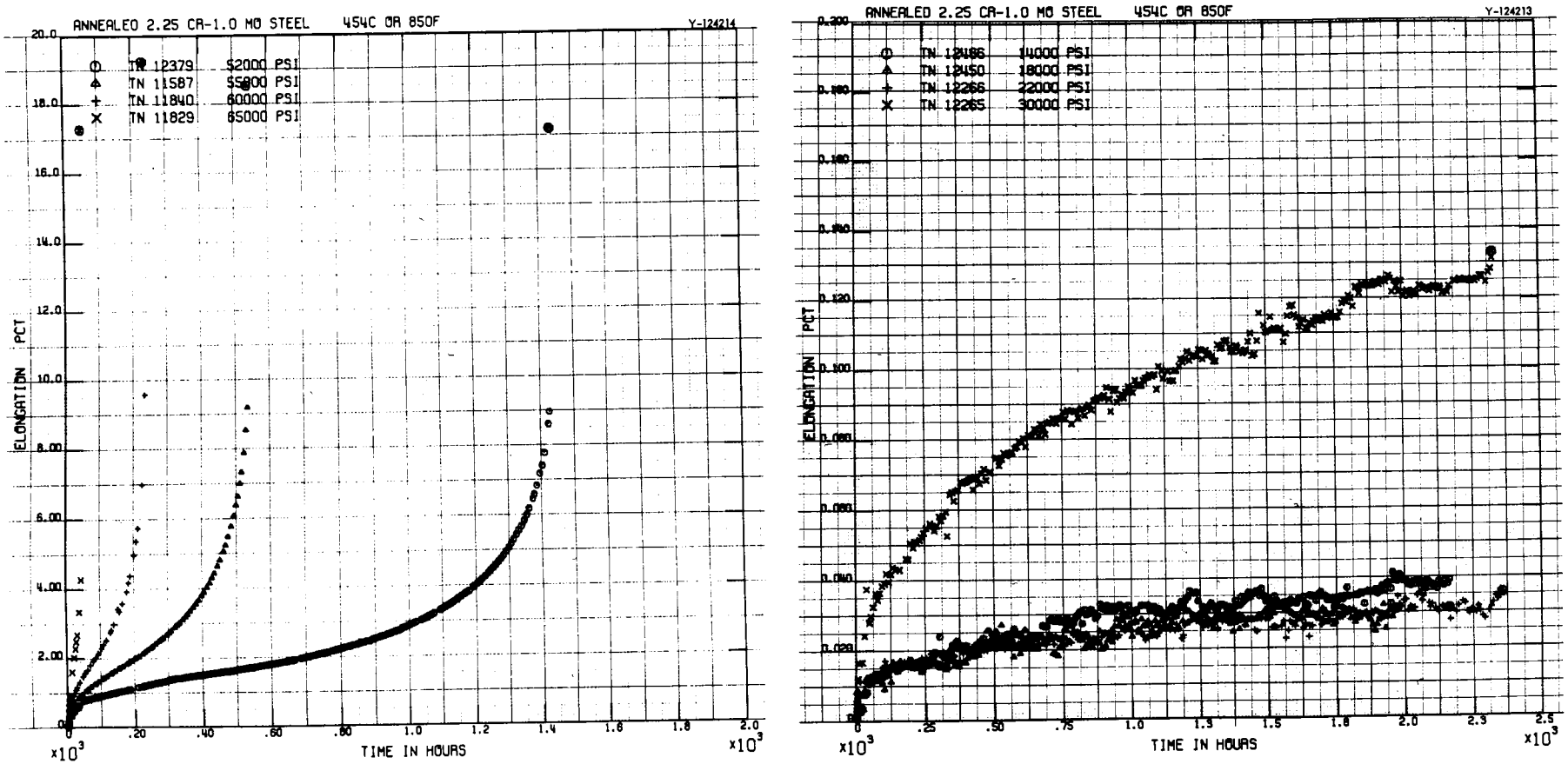

Fig. 5.62. Creep Curves for Annealed 2 1/4 Cr-1 Mo Steel at 454°C (850°F).

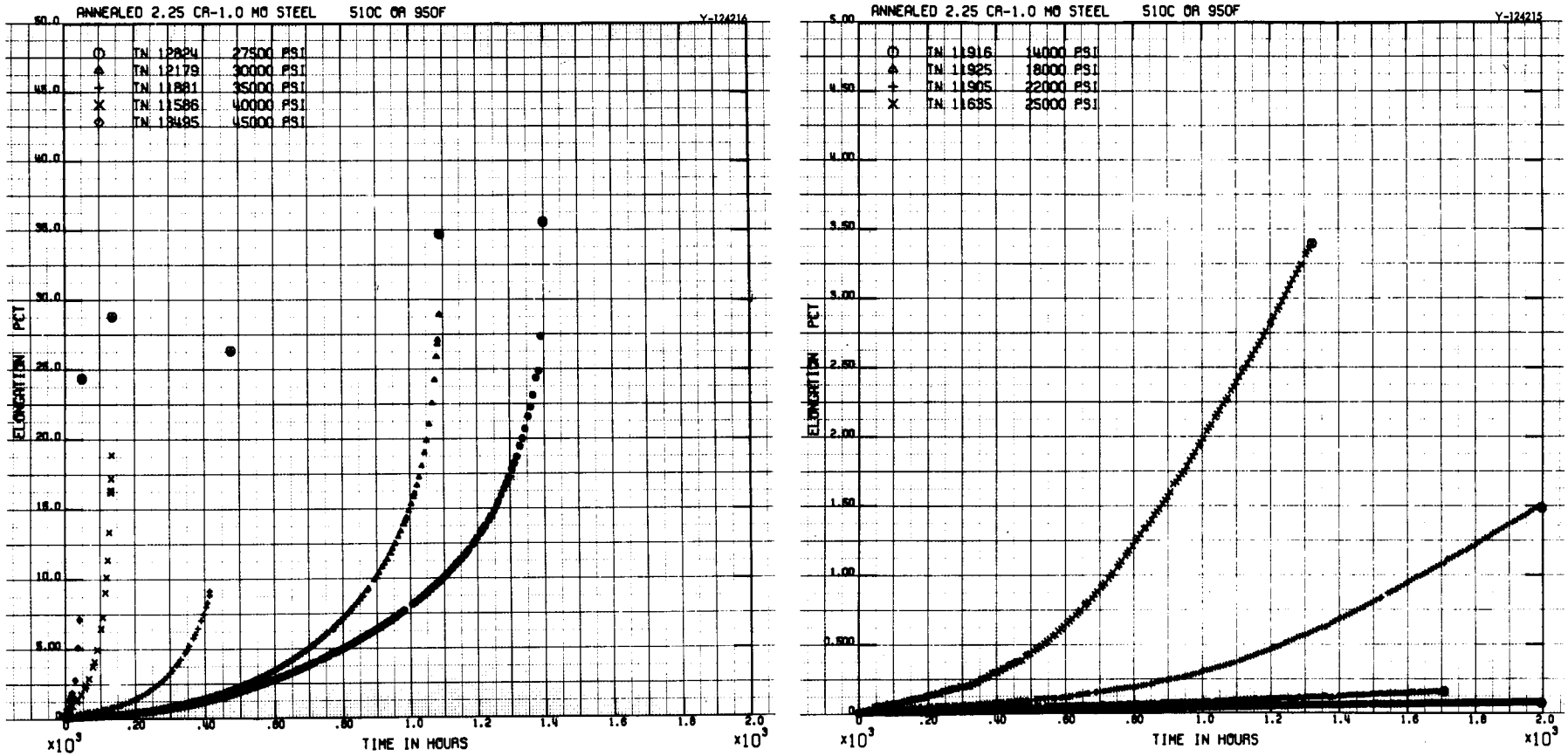

Fig. 5.63. Creep Curves for Annealed 2 1/4 Cr-1 Mo Steel at 510°C (950°F).

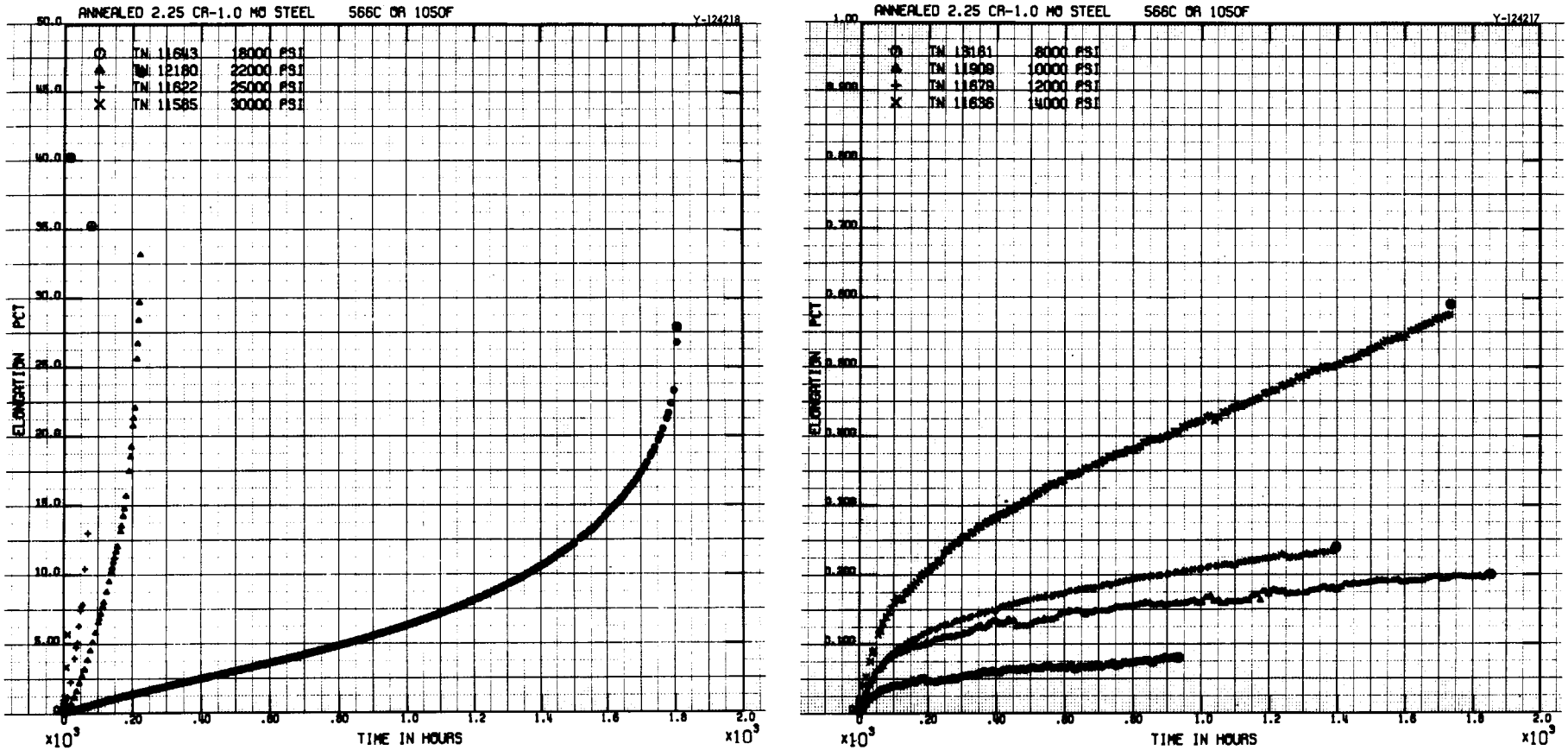

Fig. 5.64. Creep Curves for Annealed 2 1/4 Cr-1 Mo Steel at 565°C (1050°F).

Table 5.22. Creep-Rupture Properties of Annealed 2 1/4 Cr-1 Mo Steel

Stress (ksi)	Stress (MPa)	Rupture Life (hr)	Strain (%)	Reduction of Area (%)	Minimum Creep Rate (%/hr)
			454°C (850°F)		
65	448	48.9	17.3	66.4	0.062
60	414	233.4	19.2	64.4	0.0148
55	379	539.1	18.5	71.4	0.0061
52	359	1435.3	17.2	70.8	0.00142
47.5	328	a			
			510°C (950°F)		
45	310	47.5	24.4		0.069
40	276	135.5	28.8	76.3	0.030
35	241	476.0	26.4	77.0	0.00467
30	207	1089.3	34.7	82.3	0.0015
27.5	190	1396.4	35.6	81.4	0.00125
25	172	2788.0	36.4	76.1	0.00050
22	152	a			
			566°C (1050°F)		
30	207	40.2	16.3	85.1	0.51
25	172	78.2	35.2	83.9	0.115
22	152	222.9	46.4	82.3	0.030
18	124	1804.6	27.9	66.1	0.0055
15	103	a			0.0065

[a]Test in progress

5.4.3 Effect of Sodium on the Mechanical Properties of 2 1/4 Cr-1 Mo Steel — R. L. Klueh

In a sodium-heated steam generator 2 1/4 Cr-1 Mo steel can decarburize, affecting the mechanical properties. For this reason, we are studying the cyclic creep of decarburized tubes, as discussed last quarter.[37] We have also obtained some tensile specimens of annealed 2 1/4 Cr-1 Mo steel from MSA Research Corporation, Evans City, Pennsylvania, that have been decarburized in sodium in a type 316 stainless steel retort for 26,000 hr at 566°C (1050°F) in an effort to obtain information on the effect of decarburization and aging.

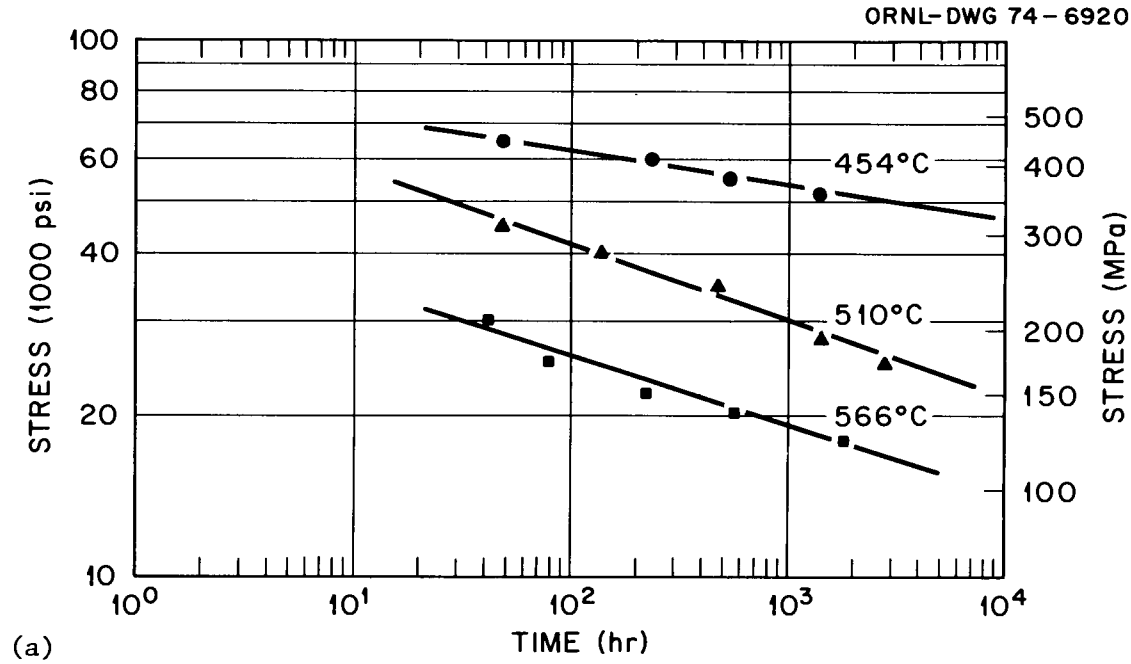

(a)

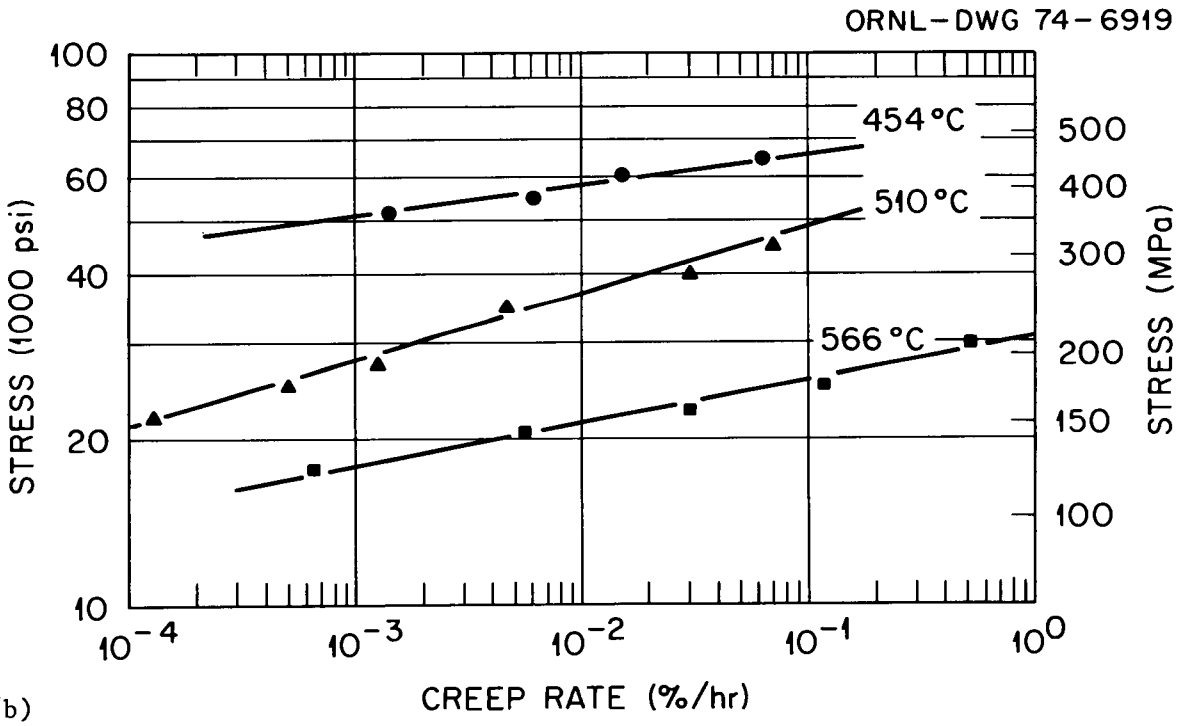

(b)

Fig. 5.65. Creep-Rupture Properties of Annealed 2 1/4 Cr-1 Mo Steel at 454, 510, and 565°C (850, 950, and 1050°F). (a) Rupture life. (b) Minimum creep rate.

Although these results are not directly applicable to the demonstration LMFBR steam generator, which operates at a maximum temperature of 520°C (968°F), these specimens were exposed to sodium for a longer period of time and a lower temperature than has been any previous 2 1/4 Cr-1 Mo steel. By extrapolation therefore, these results should offer the best estimate presently available as to the behavior of this material after prolonged periods (greater than 100,000 hr) at 520°C. This assumes that similar decarburization and aging mechanisms apply at 520 and 566°C (1050°F).

The MSA investigators studied the effect of sodium exposure and thermal aging at 566°C (1050°F) on tensile properties, metallography, and carbon content after 10,000, 20,000, and 26,500 hr. Because the program was discontinued, these investigations were reported in limited detail.[38,39,40]

After 10,000 hr, MSA found that carbide spheroidization of both the helium- and sodium-exposed specimens was well under way; all indications of the prior pearlite platelets had disappeared.[38] The only reported difference between the helium- and sodium-exposed specimens was a slightly lower density of carbide particles in the specimens exposed to sodium. No metallography was reported after 20,000 and 26,500 hr.

The carbon content of the sodium-exposed specimens decreased from 0.110 to 0.093 and 0.075 wt % C after 10,000 and 20,000 hr exposures,[39] respectively. During the final 6500-hr exposure, no further change in the carbon content could be detected.[40]

After 26,500 hr, the tensile properties of the decarburized and aged specimens at 25 and 566°C (77 and 1050°F) had decreased, the greatest effect occurring at 566°C. At this temperature, there was little difference between the specimens exposed to sodium and those exposed to helium.[40]

Since we were unable to obtain any of the MSA material that was put into test (i.e., material not aged or decarburized) and we wish to study the starting microstructure by electron microscopy, we heat treated end pieces (shoulders) from tensile specimens that had been aged in helium and not decarburized. With these specimens we felt we could get some understanding of the representative before-test microstructure. These

specimens were austenitized for 1 hr at 927°C (1700°F), furnace cooled to 704°C (1300°F), held at that temperature for 2 hr, and then air cooled. The microstructure of this "annealed" steel is shown in Fig. 5.66 and consists of large amounts of proeutectoid ferrite and a fine pearlite. This microstructure is similar to that published by MSA.[41]

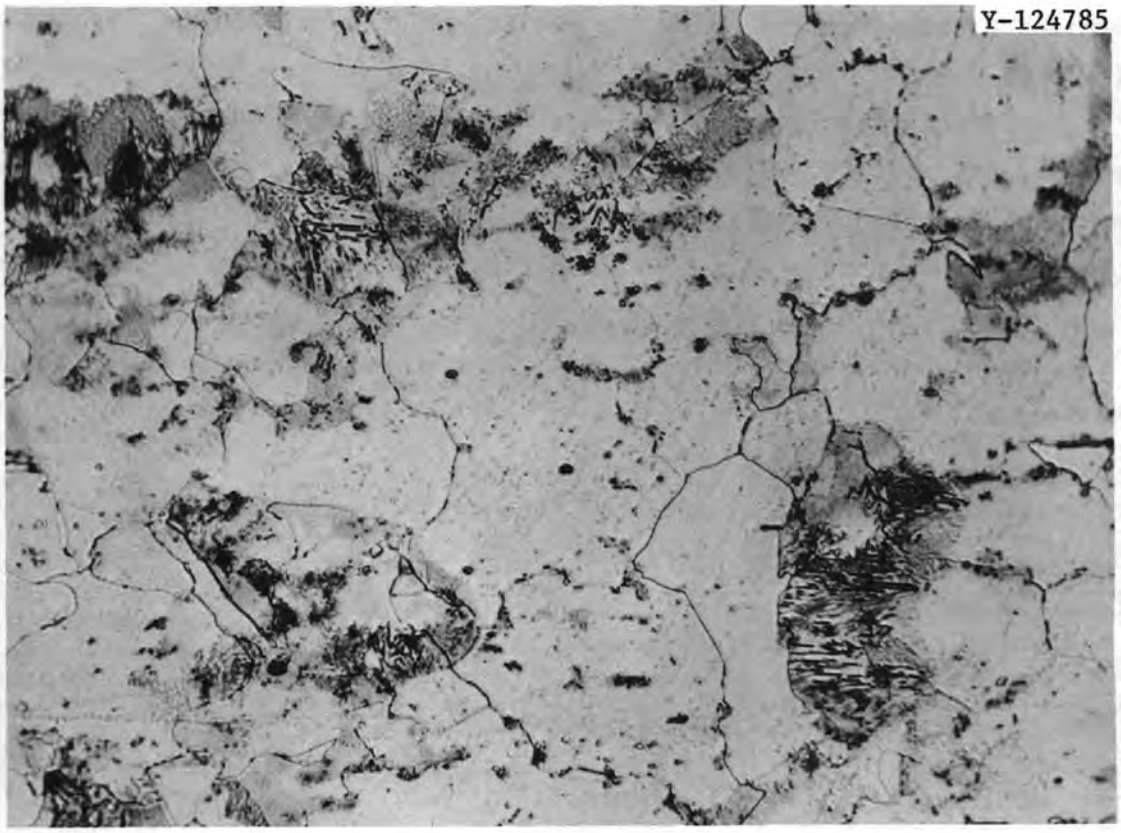

Fig. 5.66. Microstructure of Annealed 2 1/4 Cr-1 Mo Steel Heat-Treated to Simulate the MSA Starting Material. 1000×.

Figures 5.67 and 5.68(a) are photomicrographs of the centers of the helium- and sodium-exposed specimens after 26,500 hr. Both specimens contained large globular carbide particles with the helium-exposed specimen containing the higher density of precipitate particles. In the helium-exposed specimen, the density of particles remains quite constant through the specimen cross section, but, as expected, it was less than that previously purlished[38] after 10,000 hr. Figure 5.68(b) shows a photomicrograph from near the surface of the

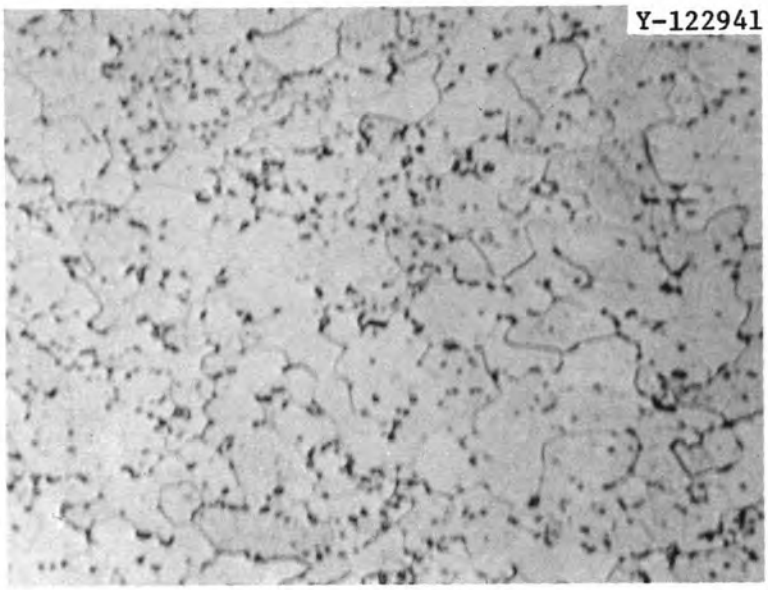

Fig. 5.67. Microstructure of 2 1/4 Cr-1 Mo Steel Aged in Helium for 26,500 hr. 500×.

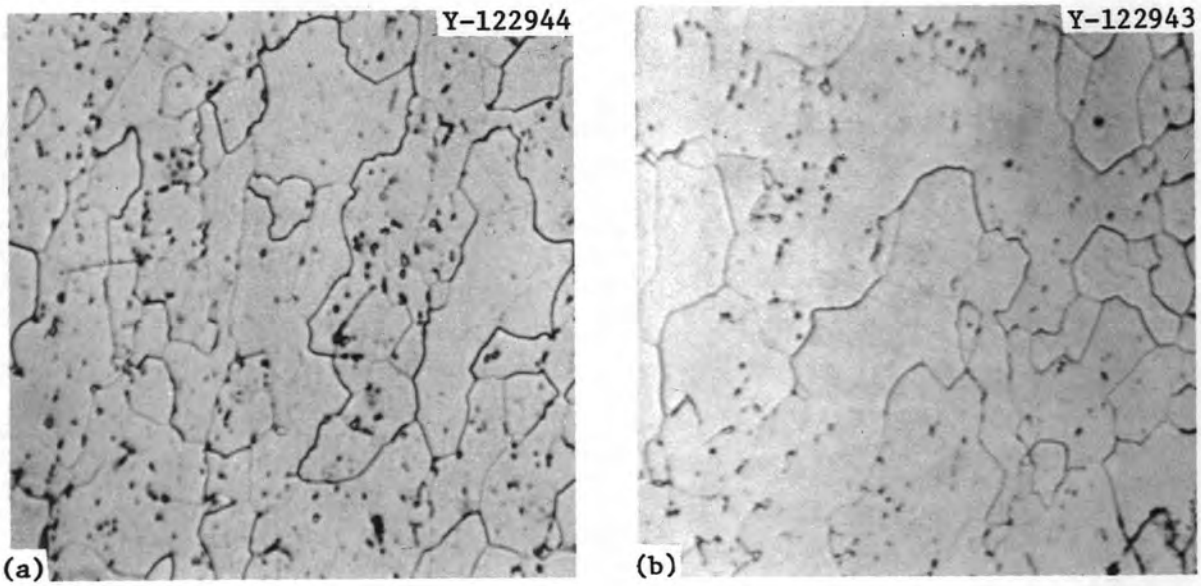

Fig. 5.68. Microstructure of 2 1/4 Cr-1 Mo Steel Decarburized by Sodium in a Type 316 Stainless Steel Retort for 26,500 hr. (a) Center. (b) Edge of 0.060-in.-thick (1.5-mm) specimen. 500×.

sodium-exposed specimen. Comparing with Fig. 5.68(a) shows the precipitate density near the surface is obviously lower than that at the center.

In addition to the observations on the general microstructure of the specimen, we found a surface "penetration" effect in the sodium-exposed specimens; penetration proceeds to a depth of about 0.0005 in. (13 μm). This is showh in Fig. 5.69. Since similar penetrations were not present in the helium-exposed specimens, we assumed that they result from sodium exposure.

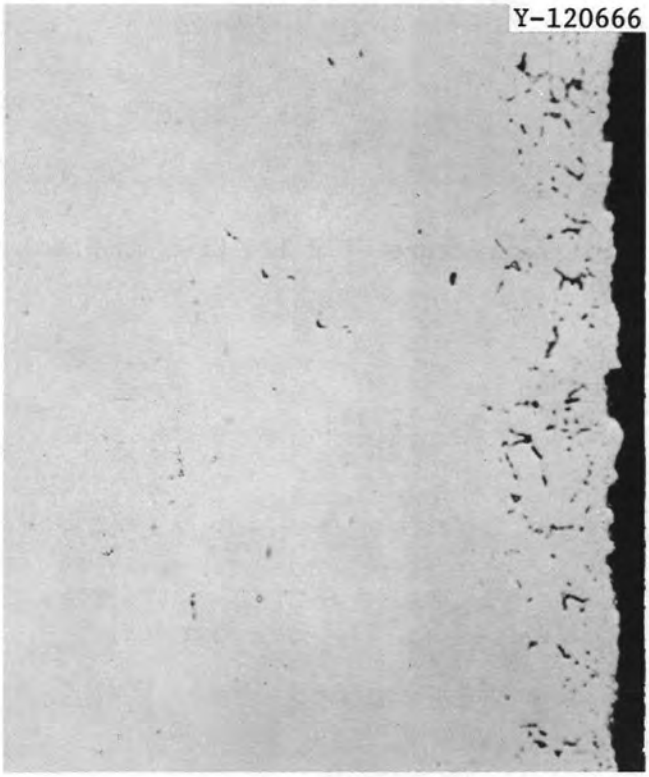

Fig. 5.69. Edge of 2 1/4 Cr-1 Mo Steel Decarburized for 26,500 hr. As Polished. 500×.

In an effort to determine whether decarburization for 26,500 hr led to a hardness gradient, a microhardness traverse was made through the cross section of helium- and sodium-exposed specimens. Within the scatter of the hardness measurements, we could not discern a gradient. Furthermore, there was essentially no difference in the microhardness of the two specimens.

5.4.4 Heat-to-Heat Variations of 2 1/4 Cr-1 Mo Steel — R. L. Klueh

Even though a heat of 2 1/4 Cr-1 Mo steel is purchased to applicable ASTM standards, a comparison with heats purchased to identical specifications often reveals a considerable variation in mechanical properties. Such differences in properties can arise because of differences in the cooling rates, composition, austenite grain size, etc. Therefore, for a truly representative statistical analysis of the mechanical property data, several heats must be tested. Although the extent of the tensile and creep testing per heat will not need to be as great as that indicated[35] for heat 20017, sufficient tests are required to establish the values for each heat at the temperatures of interest.

To meet the above objective, we propose to compare the tensile and creep-rupture behavior of several heats of annealed 2 1/4 Cr-1 Mo steel in the as-received condition (as heat treated by the vendor) and after identical heat treatments in our laboratory. Potential heats include: vacuum-arc remelt (VAR), forging, electroslag remelt (ESR) forging, air-melted forging, tubing, and plate.

At present we have acquired two pieces of VAR forging, a piece of ESR forging, and four tubing heats, and we are purchasing an air-melted forging. During the next quarter, we will obtain specimens from these various heats and begin testing.

5.4.5 Fatigue Behavior of 2 1/4 Cr-1 Mo Steel — C. R. Brinkman and J. P. Strizak

Strain-controlled fatigue tests are currently being conducted on 2 1/4 Cr-1 Mo steel according to a recently defined test matrix.[42] The material presently being used in these tests is commercial 1-in.-thick (2.54 cm) Croloy plate. Carbon content was 0.135%; other specifics concerning chemical composition and mechanical behavior can be found elsewhere.[43] Before specimen preparation sample plates were isothermally annealed as follows: austenitized at 926 ± 12°C (1700 ± 25°F) for 1 hr and cooled at a maximum rate of 85°C/hr (150°F/hr) to an isothermal transformation temperature of 705 ± 12°C (1300 ± 25°F). The plate was then held at this temperature for 2 hr and cooled to room temperature at a rate not to exceed 5°C/min (10°F/min).

Hourglass-shaped specimens (0.25 in. or 0.64 cm in diameter) were prepared and tested by Mar-Test Inc. Results of the fully reversed strain-controlled tests obtained to date are shown over the range 24 to 538°C (75–1000°F) in Fig. 5.70. High-cycle load-controlled fatigue data obtained by BNL investigators[44] on another heat of this material in the annealed condition is also shown for comparison. Blending the low-cycle strain-controlled data into the high-cycle load-controlled data, however, must be done with caution since ratcheting may have occurred in the high-cycle tests. No check for ratcheting was performed by those investigators. The emphasis of the first part of this program is to determine fatigue data over the range 315 to 427°C (600–800°F) for initial steam

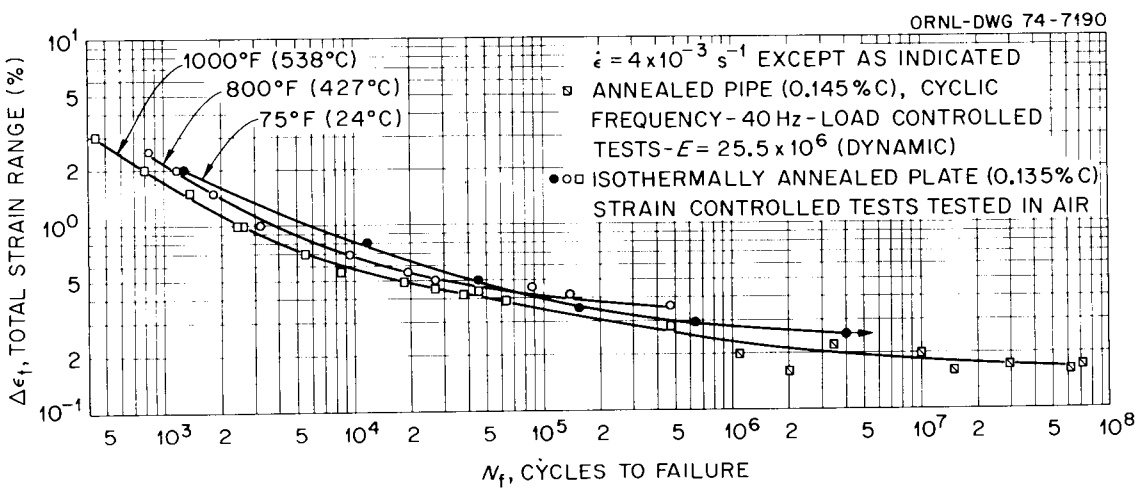

Fig. 5.70. Total Strain Range Versus Cycles to Failure For 2 1/4 Cr-1 Mo Steel.

generator design. The results presented in Fig. 5.70 show only small to moderate temperature dependence in the low-cycle fatigue behavior of this material, while the temperature dependence in the high-cycle region is still inconclusive.

Elastic, plastic, and total strain range are plotted against cycles to failure in Figs. 5.71 through 5.73 for the various temperatures considered to date. Linearity of the log-log plots of plastic strain range versus cycles to failure is in general agreement with the Coffin-Manson low cycle fatigue law. However, a break or deviation from linearity

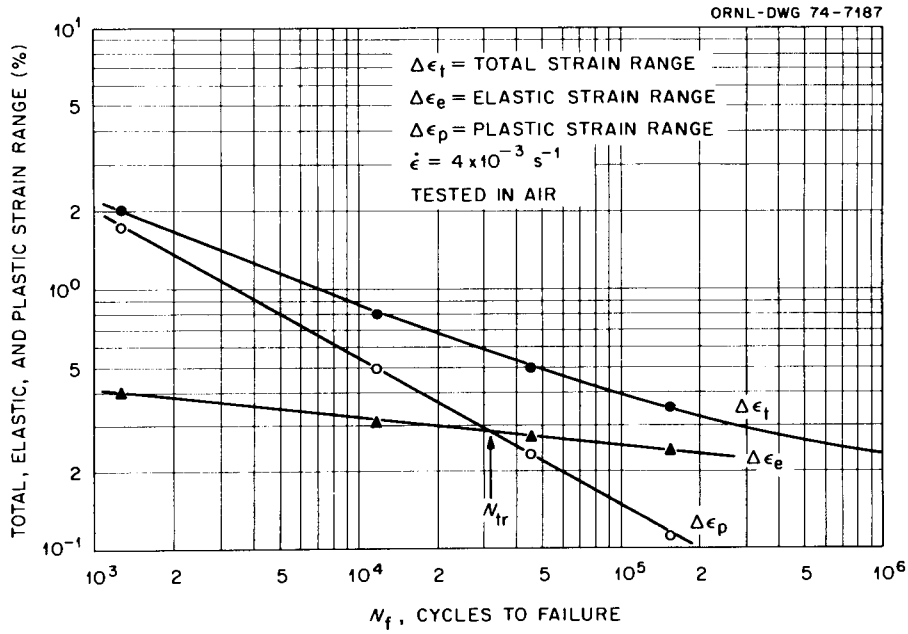

Fig. 5.71. Total, Elastic, and Plastic Strain Range Versus Cycles to Failure at Room Temperature for Isothermally Annealed 2 1/4 Cr-1 Mo Steel Showing Transition Fatigue Life, N_{tr}.

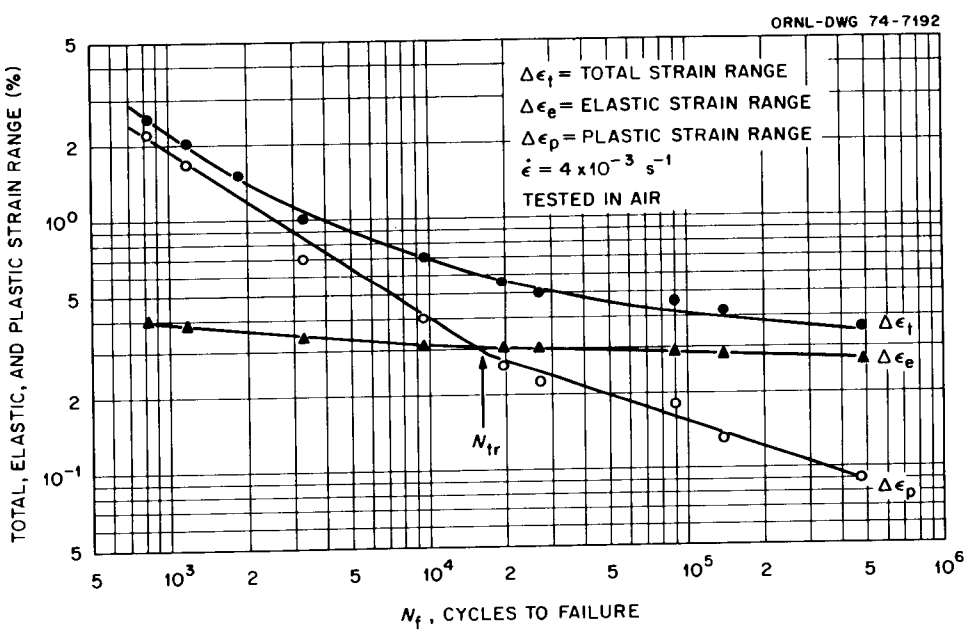

Fig. 5.72. Total, Elastic, and Plastic Strain Range Versus Cycles to Failure at 427°C (800°F) for Isothermally Annealed 2 1/4 Cr-1 Mo Steel Showing Transition Fatigue Life, N_{tr}.

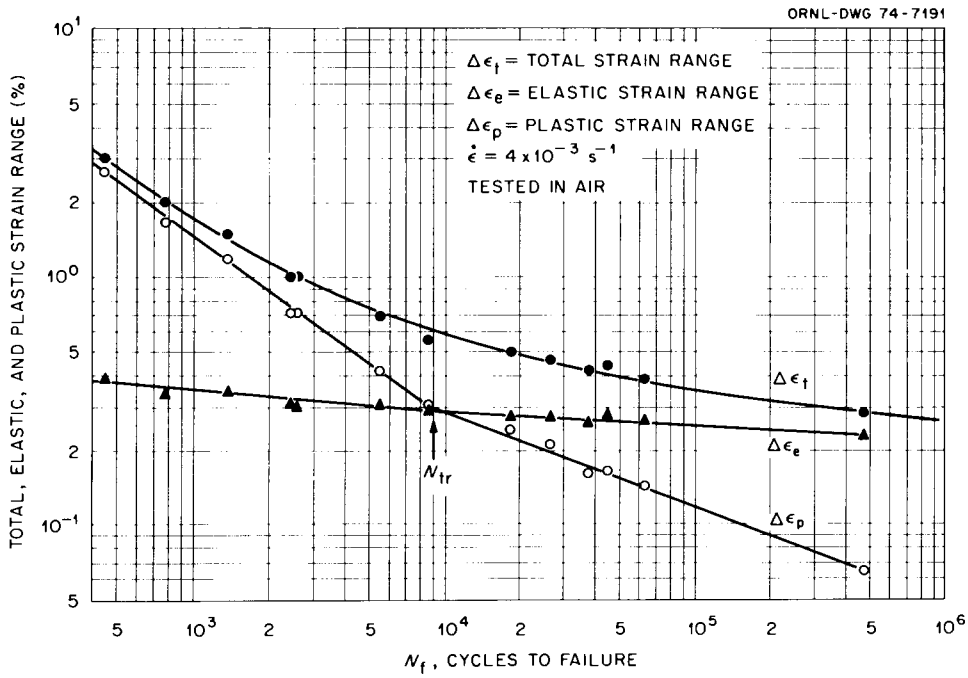

Fig. 5.73. Total, Elastic, and Plastic Strain Range Versus Cycles to Failure at 538°C (1000°F) for Isothermally Annealed 2 1/4 Cr-1 Mo Steel Showing Transition Fatigue Life, N_{tr}.

does occur at approximately the cyclic transition life, N_{tr}, defined as the point at which the elastic and plastic strain ranges are equivalent. Further, this transition point shifts to the left (lower cycle life) with increasing temperature. The transition fatigue life is of particular significance at 427 and 538°C (800 and 1000°F) for this material in that in the low-cycle region (i.e., cycles to failure less than the transition life) the material underwent a period of initial cyclic hardening followed by near stress stabilization until a significantly large crack developed, as shown in Fig. 5.74. However, in the high-cycle region the material underwent a similar period of initial hardening followed by a period of cyclic softening until stabilization occurred, as shown in Fig. 5.75. Hence, for this particular heat of 2 1/4 Cr-1 Mo steel, heat-treated as specified above, whether or not the material will strain soften following cyclic hardening depends on strain range and temperature. Figure 5.75 shows that coincident with the softening process the plastic strain ranges tend to increase. This in turn, accounts for the upward break in the plastic strain range curves shown in Figs. 5.72 and 5.73 beyond N_{tr}.

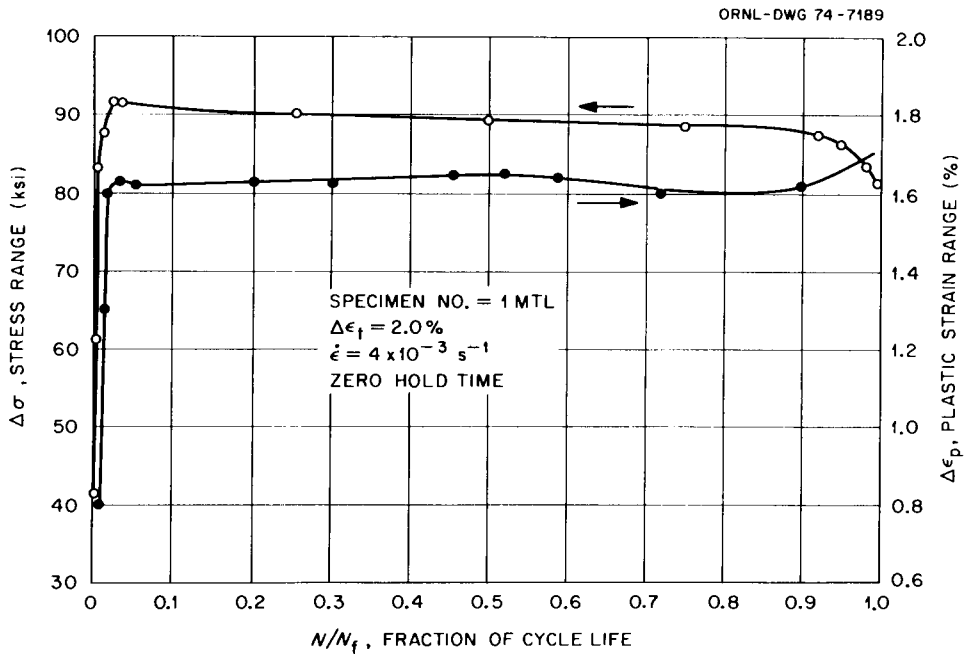

Fig. 5.74. Typical Stress and Plastic Strain Range as Functions of Fraction of Cyclic Life for Isothermally Annealed 2 1/4 Cr-1 Mo Steel at 538°C (1000°F). Low-cycle range.

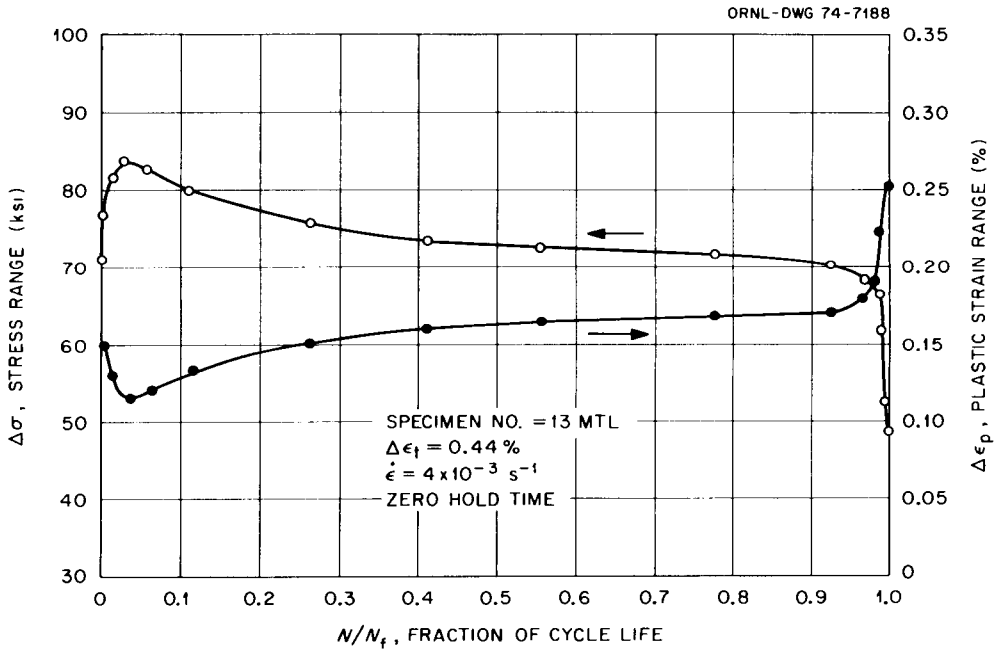

Fig. 5.75. Typical Stress and Plastic Strain Range as Functions of Fraction of Cyclic Life for Isothermally Annealed 2 1/4 Cr-1 Mo Steel at 538°C (1000°F). High-cycle range.

Cyclic stress-strain curves determined at the three test temperatures under consideration are given in Fig. 5.76. These were simply determined by connecting the stress amplitudes of the appropriate hysteresis loops at half the cyclic life for a given strain range.

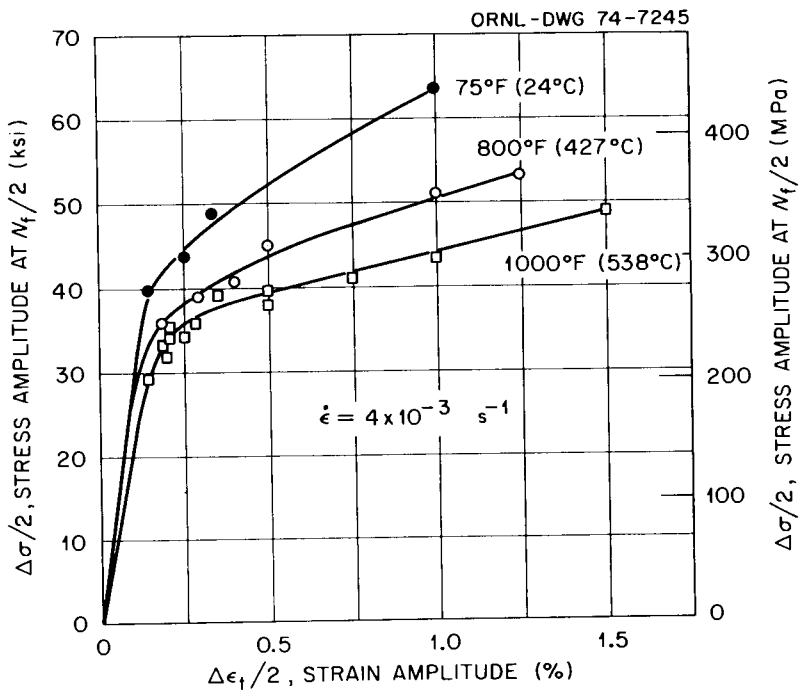

Fig. 5.76. Cyclic Stress-Strain Curves for Isothermally Annealed 2 1/4 Cr-1 Mo Steel.

Hold time tests, both tensile and compressive, are also under way at 538 and 427°C (1000 and 800°F). The results of the tests completed to date at 538°C are shown in Fig. 5.77. The limited data shown here indicate that the influence of the hold period is greater at lower strain ranges (i.e., larger reduction in fatigue life occurs) and that the compressive hold time is more deleterious than the tensile hold time at this temperature and for the strain ranges considered to date. The influence of cyclic softening on the hold time effect will receive more attention.

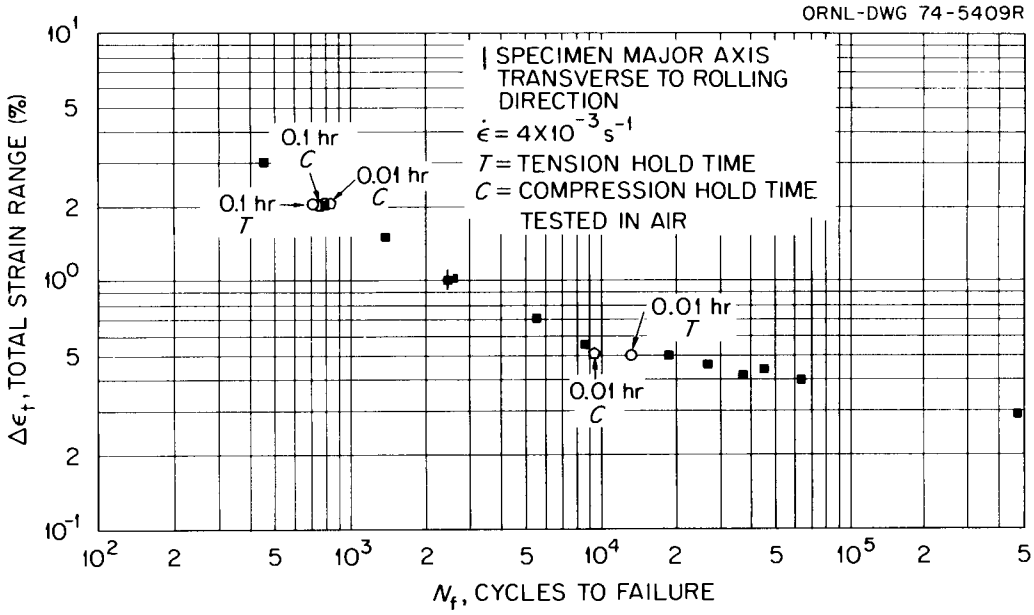

Fig. 5.77. Total Strain Range Versus Cycles to Failure for 2 1/4 Cr-1 Mo Steel Tested at 538°C (1000°F) in Strain Control. The influence of tension and compression hold times (t_h) is also shown.

5.4.6 Biaxial Fatigue Testing of 2 1/4 Cr-1 Mo Steel — C. R. Brinkman and J. P. Strizak

Elevated-temperature multiaxial data are urgently needed to substantiate current design concepts. In particular, the influence of state of stress or strain on fatigue and creep-fatigue interaction is needed to substantiate methods of correlating uniaxial data with actual design loading conditions.

ORNL has access to a servo-controlled axial push-pull and torsion fatigue machine with independent loop control, which could be adapted to perform either push-pull and torsion, or push-pull and internal or external specimen pressurization fatigue tests. The biaxial push-pull torsion capability, however, is the easier of the two concepts to develop and so is being pursued on a budget permitting basis. Conceptually, a uniform gage specimen would be subjected to biaxial loading as shown in Fig. 5.78. The specimen, a thin-walled hollow tube shown in Fig. 5.79, would be heated internally so as to leave the external surface free for dual extensometer

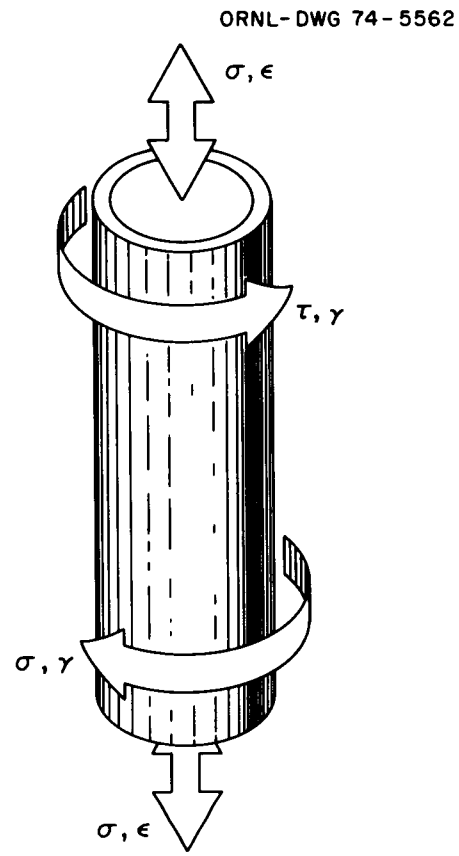

EXPERIMENTAL VARIABLES
TEMPERATURE: 75-1000°F
STRAIN RATIO: $\frac{\Delta\gamma}{\Delta\epsilon_a}$ = CONSTANT
HOLD TIME: 0.01 TO 0.1 hr
HOLD TIME MODE: TENSION OR COMPRESSION

Fig. 5.78. Push-Pull Torsion Elevated Temperature Fatigue Tests. Temperature range is 24 to 538°C.

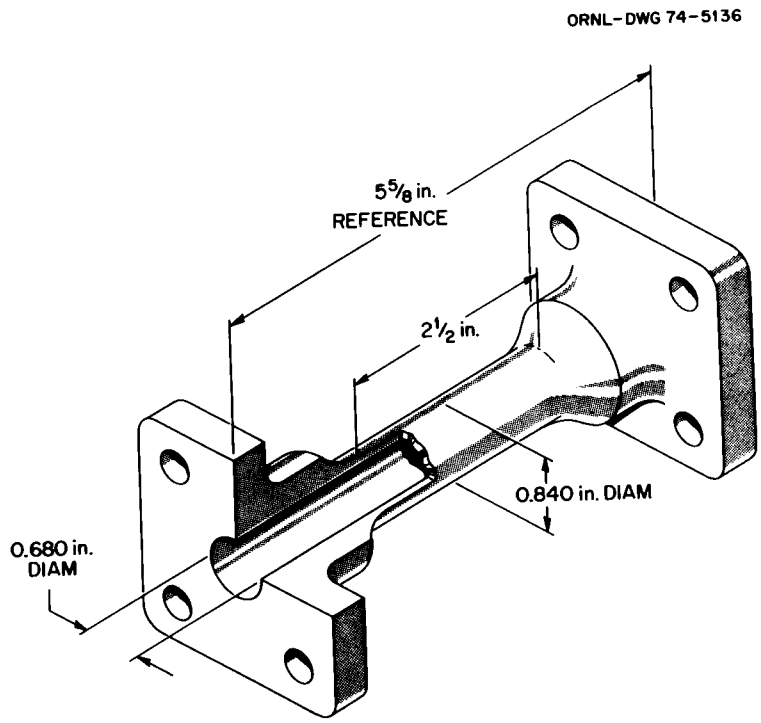

Fig. 5.79. Prototype Multiaxial Test Specimen. 1 in. = 25.4 mm.

attachment. The specimen would be rigidly held and aligned via a die set arrangement similar in concept to the type used for uniaxial fatigue testing. This loading fixture has been designed and is shown in Fig. 5.80. During an actual test, the heating element chambers would be sealed so as to allow a slight internal pressurization. Specimen failure could then be defined by a pressure decrease. Extensometer development is under way.

5.4.7 Mechanical Properties Correlations of 2 1/4 Cr-1 Mo Steel for LMFBR Steam Generator — D. O. Hobson and T. L. Hebble*

In a continuation of efforts to provide input to the *Nuclear Systems Materials Handbook* (NSMH), a number of correlations with their respective tolerance limits have been finished during the past quarter. These are: time to rupture, ultimate tensile strength, and yield strength, with their appropriate tolerance limits, as well as the tolerance limits for the minimum creep rate equation reported previously.[45]

---

*Mathematics Research Staff.

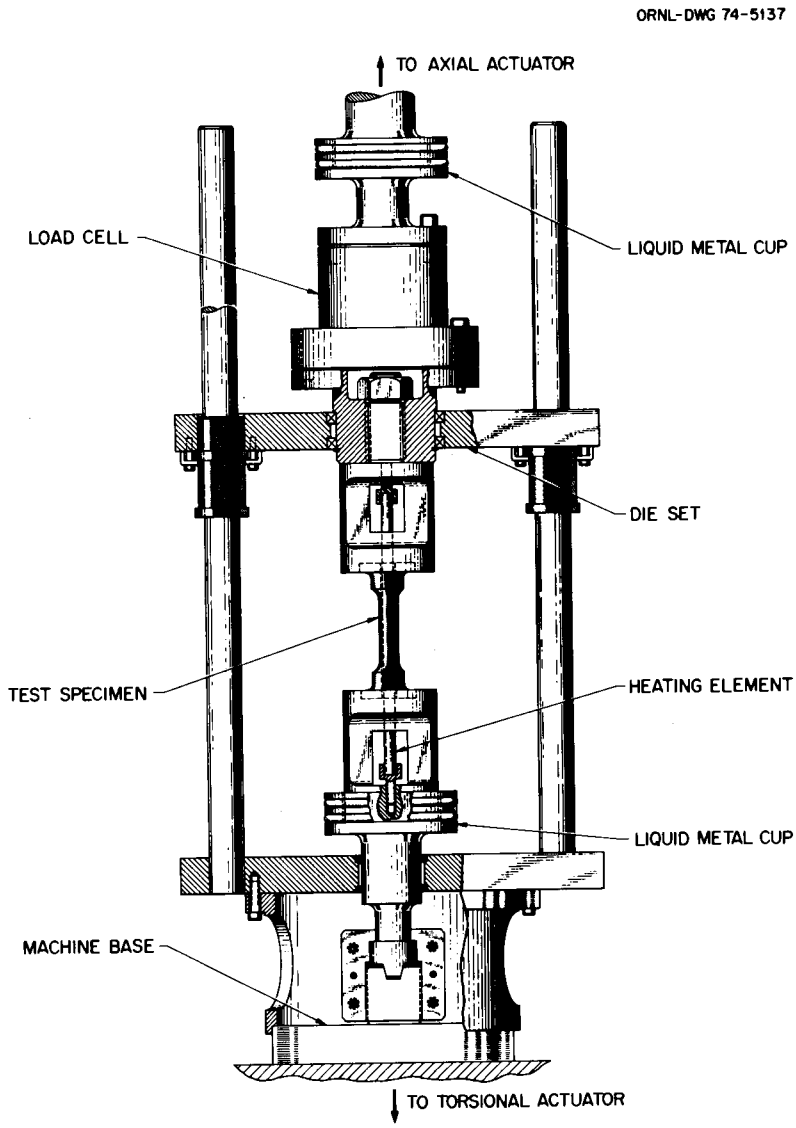

Fig. 5.80. Biaxial Fatigue Test Fixture.

The ferritic 2 1/4 Cr-1 Ni alloy depends in some of its mechanical properties upon room-temperature ultimate tensile strength as well as the temperature and stress parameters that suffice for correlating the austenitic alloys. This dependence is not general, but instead appears to hold for those properties that are directly time-dependent, such as creep rate.

The data bases for the various correlations differed widely in both number and quality. Much time was spent in screening the data to achieve a homogeneous and coherent set for each of the correlations. The most

important consideration in data selection was to ensure that both the material composition and heat treatment fell within the applicable specifications for the alloy. The data bases were also characterized by the type of heat treatment and product form and by test temperatures to determine the ranges of applicability of the correlations. Data sources were listed previously.[46]

The various correlations and their corresponding tolerance limits have been developed in both English and SI units and, to conserve space, will not be presented here. Rather, the engineering-unit models will be shown and discussed, and numerical examples of the tolerance limits will be given.

5.4.7.1 Time to Rupture

The mathematical model for this property is given by

$$\widehat{\log_{10} t_r} = 25.92 - 0.2067\sigma - 0.01306T + 1.061 \times 10^{-6}\ \sigma^2 T\ ,$$

where t_r = time to rupture (hr), σ = creep stress (ksi), and T = test temperature (°F + 460). The model is applicable within the range 371 to 593°C (700–1100°F) and to a maximum stress of (97,400/T) ksi. It is strictly empirical and should not be extrapolated beyond the data set upon which it is based. The applicable specifications are SA-335-P22, SA-213-T22, SA-387-D, and SA-336-F22a (annealed or normalized-and-tempered only). The lower tolerance limit is applicable in this model and, in general, gives values that are approximately 10% of the expected values predicted by the model.

The maximum and minimum values for the models are defined to be the upper and lower central tolerance limits (λ = 0.95, P = 0.90) about the expected values obtained from the models. Thus, with a confidence level of 0.95, 95% of all observed values are expected to be greater than the lower limit. Similarly, with a confidence level of 0.95, 95% of all observed values are expected to be less than the upper limit. The actual tolerance limit is based on the Bonferroni inequality and is explained in greater detail by Lieberman and Miller.[47] This limit is simultaneous in all levels of the independent variables. That is, the limits can be

calculated repeatedly for different levels of the independent variables without affecting the level of confidence.

5.4.7.2 Yield and Ultimate Tensile Strength

A third-order polynomial in temperature was found to adequately describe both properties.

$$\widehat{\mathrm{UTS}} = 181.7 - 0.3811T + 4.057 \times 10^{-4}\ T^2 - 1.393 \times 10^{-7}\ T^3$$

$$\widehat{\mathrm{YS}} = 74.44 - 0.1191T + 1.161 \times 10^{-4}\ T^2 - 3.829 \times 10^{-8}\ T^3$$

where

$\widehat{\mathrm{UTS}}$ = expected value of ultimate tensile strength, ksi,

$\widehat{\mathrm{YS}}$ = expected value of yield strength, ksi, and

T = test temperature (°F + 460).

These models are applicable from room temperature to 593°C (1100°F) and for the following specifications: SA-335-P22, SA-213-T22, SA-387-D, and SA-336-F22a (annealed only). Both upper and lower tolerance limits are applicable, and selected values are shown in Table 5.23.

5.4.7.3 Minimum Creep Rate

The model for minimum creep rate was given previously[45] as

$$\widehat{\log \mathrm{MCR}} = -3.24 + 3.17\sigma - 4.80 \times 10^{-3}\ \sigma T + 1.87 \times 10^{-6}\ \sigma T^2$$

$$-9.16 \times 10^{-4}\ \tau + 3.05 \times 10^{-7}\ T\tau^2$$

where

MCR = minimum creep rate, %/hr,

σ = creep stress, ksi,

T = test temperature, °F + 460, and

τ = room temperature ultimate tensile strength, ksi.

Table 5.23. Calculated Values of Ultimate Tensile Strength, Yield Strength, and Tolerance Limits

Temperature		Strength, ksi (MPa)		
(°C)	(°F)	Lower Limit	Expected Value	Upper Limit
		Ultimate Tensile Strength		
21	70	57.9 (399)	72.9 (503)	87.9 (606)
149	300	51.1 (352)	65.2 (449)	79.4 (547)
316	600	54.3 (374)	67.7 (467)	81.1 (559)
482	900	50.2 (346)	63.4 (437)	76.5 (527)
593	1100	32.2 (222)	45.7 (315)	59.1 (407)
		Yield Strength		
21	70	28.3 (195)	38.2 (243)	48.2 (332)
149	300	24.8 (171)	34.2 (236)	43.6 (301)
316	600	24.0 (165)	33.0 (228)	42.0 (290)
482	900	22.0 (152)	30.9 (213)	39.8 (274)
593	1100	16.7 (115)	25.8 (178)	35.0 (241)

The upper tolerance limit is applicable to this model and typical values are given in Table 5.24 for 538°C (1000°F) and τ values of 60, 70, and 75 ksi (414, 483, and 517 MPa).

Work continues on models for primary creep, elongation, and reduction of area. Properties for which models are required have been listed.[46]

5.4.8 Mechanical Properties of Weld-Overlaid Stainless Steel — R. L. Klueh

Last quarter[48] we reported on the creep-rupture properties at 593°C (1100°F) of the type 304 stainless steel forgings that were unaffected by the overlay process. We have now completed tests on specimens taken from the forging immediately adjacent to the fusion line and specimens taken from the type 308 stainless steel weld metal. Tests were made on radial and tangential specimens at 593°C.

Table 5.25 gives the creep-rupture properties for the forging immediately adjacent to the overlay fusion line; Fig. 5.81 shows the rupture life and minimum creep rates as functions of stress. As seen in Fig. 5.81, orientation has essentially no effect on the creep-rupture

Table 5.24. Approximate[a] Values of Minimum Creep Rates (MCR) and Upper Tolerance Limits (L) for 538°C (1000°F) Tests

Creep Stress σ,		Value, %/hr, for Different Room-Temperature Ultimate Strengths, τ					
		τ = 60 ksi (414 MPa)		70 ksi (483 MPa)		75 ksi (517 MPa)	
(ksi)	(MPa)	MCR	L	MCR	L	MCR	L
5	34	7×10^{-5}	1.6×10^{-3}	1.6×10^{-5}	4.3×10^{-4}	7.3×10^{-6}	2.1×10^{-4}
10	69	4×10^{-4}	9.5×10^{-3}	1×10^{-4}	2.1×10^{-4}	4.2×10^{-5}	1×10^{-3}
15	103	2.3×10^{-3}	5.3×10^{-2}	5.4×10^{-4}	1.1×10^{-2}	2.4×10^{-4}	5×10^{-3}
20	138	1.3×10^{-2}	3.4×10^{-1}	3.2×10^{-3}	7×10^{-2}	1.4×10^{-3}	2.5×10^{-2}
25	172	8.1×10^{-2}	2.2	1.9×10^{-2}	3.9×10^{-1}	8.3×10^{-3}	1.5×10^{-1}

[a]Read from graph.

Table 5.25. Creep-Rupture Properties of Type 304 Stainless Steel Forging Adjacent to the Fusion Line at 593°C (1100°F)

Stress (ksi)	Stress (MPa)	Rupture Life (hr)	Elongation (%)	Reduction of Area (%)	Minimum Creep Rate (%/hr)
			Tangential Specimens		
50	345	47.6	21.6	21.8	0.162
48	331	121.8	16.1	16.3	0.039
45	310	186.8	11.8	13.0	0.0190
42.5	299	654.5	14.4	17.6	0.0057
40	276	1298.4	17.0	23.3	0.0026
40	276	1126.4	16.9	20.5	0.0030
			Radial Specimens		
45	310	174.0	8.7	15.0	0.011
42.5	299	727.5	16.9	24.7	0.0053
40	276	1140.1	9.4	15.5	0.0020
35	241	a			0.00028

[a]Test discontinued.

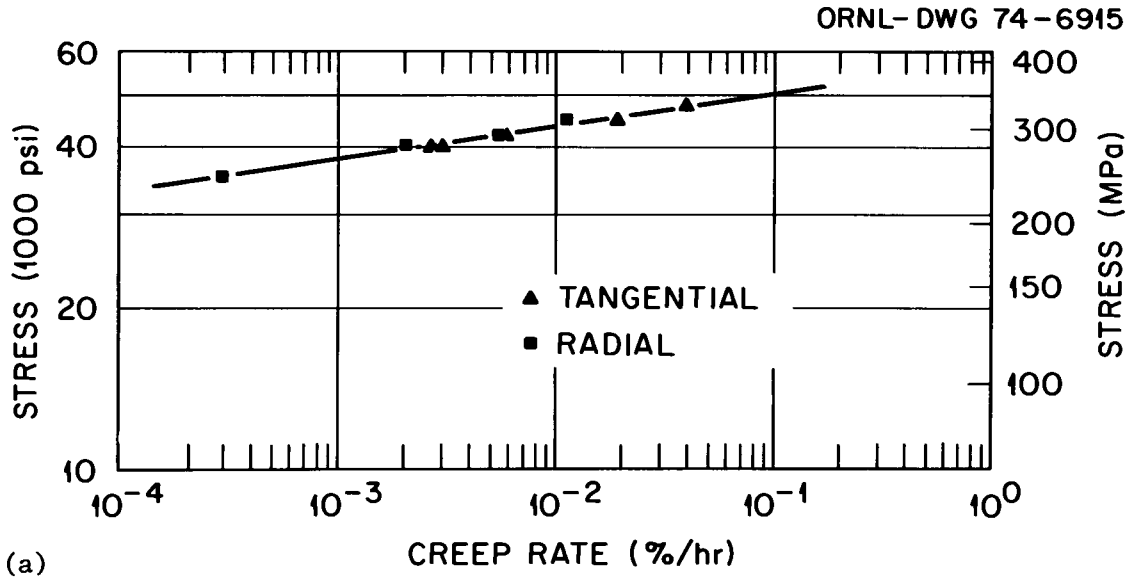

(a)

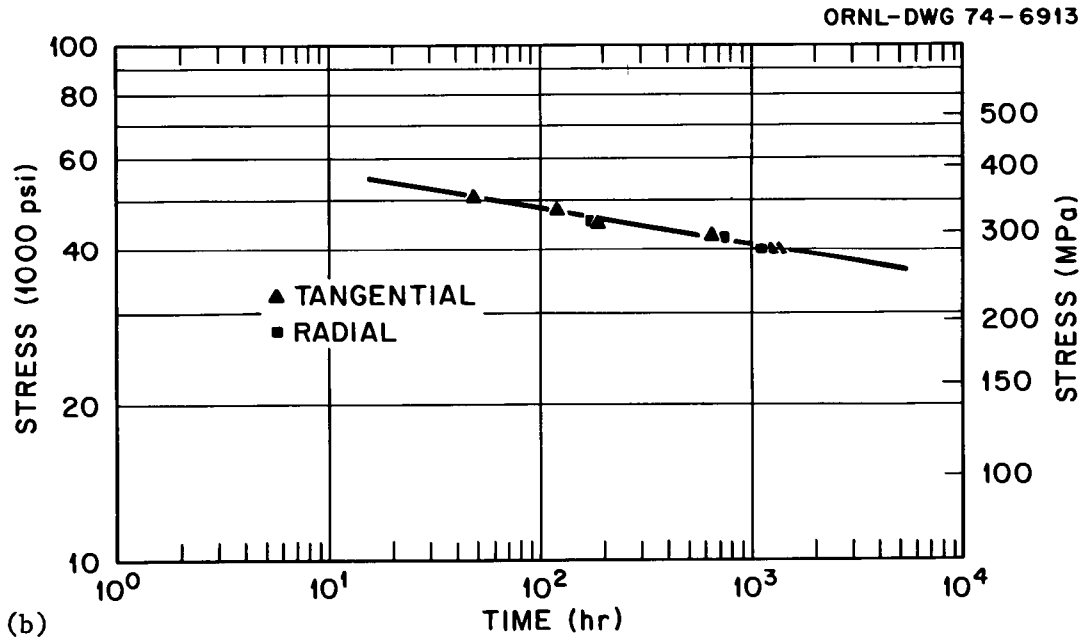

(b)

Fig. 5.81. Creep-Rupture Properties of Type 304 Stainless Steel Forging Adjacent to the Weld Overlay Fusion Line at 593°C (1100°F). (a) Rupture life. (b) Minimum creep rate.

behavior, which agrees with the previous observations on the unaffected forging.[48] This similarity in behavior is illustrated in Fig. 5.82, which shows the creep curves for a radial and two tangential specimens tested at 40 ksi (276 MPa).

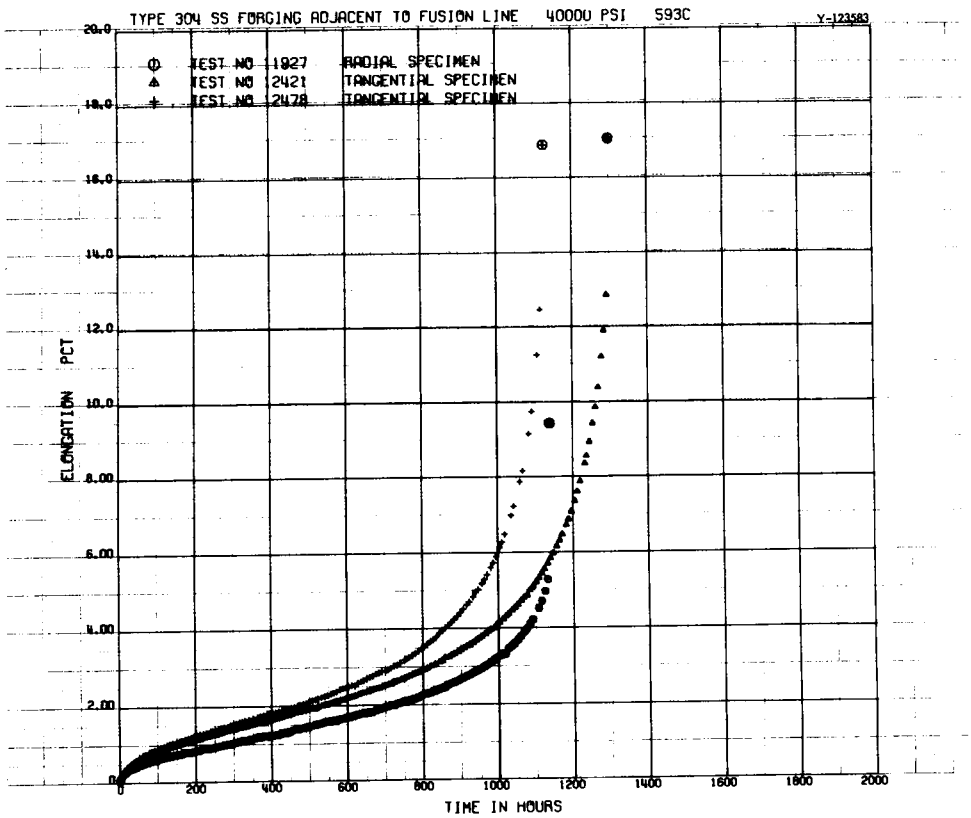

Fig. 5.82. A Comparison of Creep Curves for Radial and Tangential Specimens Taken from the Type 304 Stainless Steel Forging Immediately Adjacent to the Overlay-Forging Fusion Line.

The results for the type 308 stainless steel weld metal are given in Table 5.26, and Fig. 5.83 shows the rupture life and minimum creep rate as functions of stress. For weld metal, orientation appears to affect the rupture life. However, although the rupture lives of the tangential specimens are consistently greater than those for the radial specimens [Fig. 5.83(a)], only at the higher stresses (shorter rupture life) was there any significant difference in the creep rates for the two orientations [Fig. 5.83(b)]. For both orientations, a precipitous drop in ductility with decreasing stress is noted.

Table 5.26. Creep-Rupture Properties of Type 308 Stainless Steel Weld Metal at 593°C (1100°F)

Stress (ksi)	Stress (MPa)	Rupture Life (hr)	Elongation (%)	Reduction of Area (%)	Minimum Creep Rate (%/hr)
			Radial Specimens		
45	310	2.4	24.7	42.6	5.24
40	276	14.1	22.2	44.6	0.82
35	241	95.6	15.8	24.1	0.052
30	207	546.6	9.9	15.4	0.0040
27.5	190	1294.1	5.0	7.4	0.0014
25	172	a			
			Tangential Specimens		
40	276	58.9	24.6	26.0	0.19
35	241	151.4	21.4	23.4	0.053
32.5	224	379.6	16.2	23.2	0.016
30	207	1030.9	9.9	8.2	0.0030

[a]Test in progress.

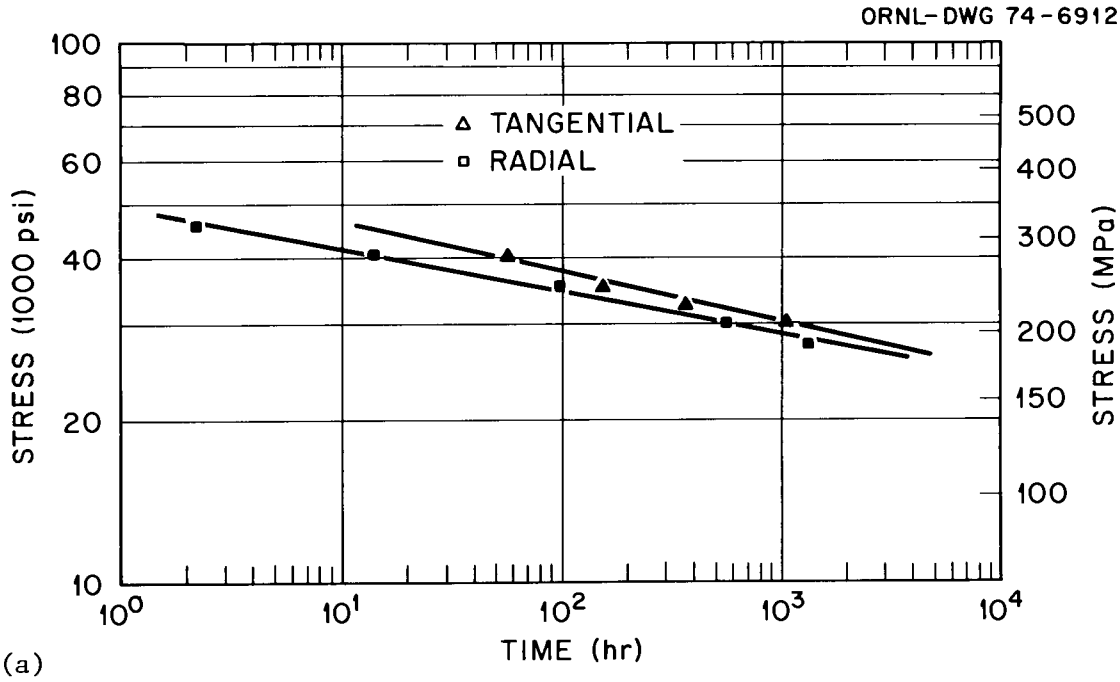

(a)

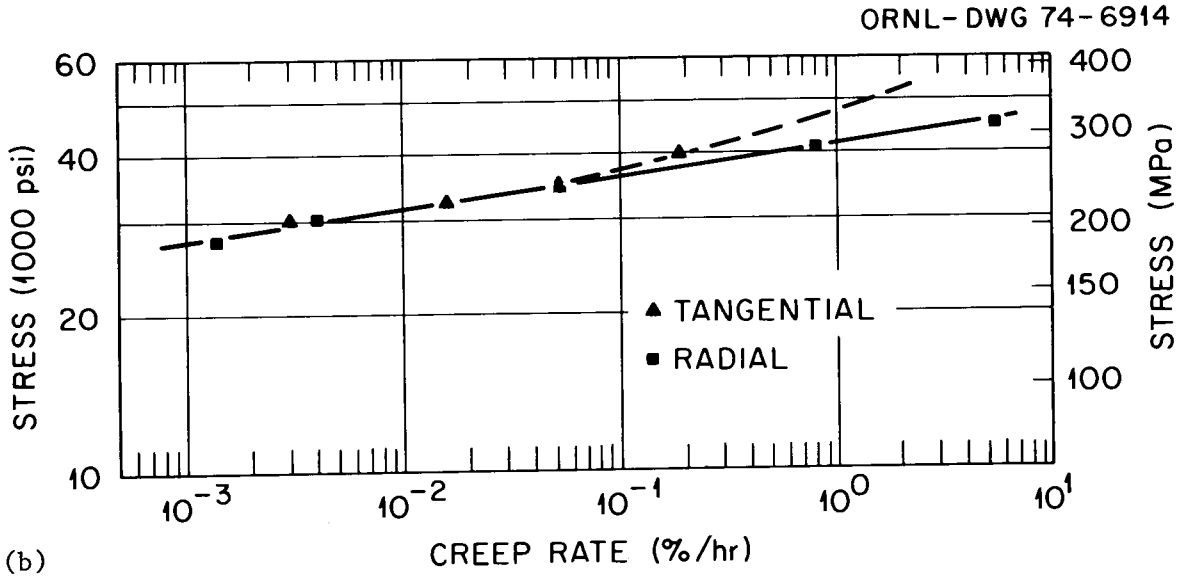

(b)

Fig. 5.83. Creep-Rupture Properties of Type 308 Stainless Steel Weld Overlay at 593°C (1100°F). (a) Rupture life. (b) Minimum creep rate.

5.5 HIGH TEMPERATURE DESIGN — W. L. Greenstreet,* J. M. Corum,* and C. E. Pugh*

5.5.1 Exploratory Studies on Type 304 Stainless Steel in Support of Structural Design Methods — R. W. Swindeman

5.5.1.1 Tensile Testing

Attempts to represent the monotonic tensile curve for reannealed type 304 stainless steel (heat 9T2796) were described previously.[49] The approach involved the development of several relationships, each restricted in its range of applicability. We intend to refine the model, but first we are investigating the tensile flow behavior under variable testing conditions. The results can be used to assess the capabilities of the existing model and also indicate desirable refinements. Tests are being performed over large deformation ranges, and we are examining the flow stress change that results from temperature and strain rate variation. Studies of deformation under variable conditions in the low strain range will be worked into the studies on strain cycling behavior.

The results of some tests at varying temperature follow. In the first test (Fig. 5.84) the specimen was strained approximately 1% at each of several temperatures increasing from 25 to 538°C (77–1000°F). The specimen was unloaded during temperature changes. After the straining at 538°C (1000°F), tests were performed at decreasing temperatures to 25°C (77°F). The heavy solid line in Fig. 5.84 represents the plastic component of strain at each temperature, while the light solid line represents the prediction based on the Voce flow model, assuming the validity of the hardening assumption. The dashed line represents the prediction based on the Ludwik flow model, again with the assumption of strain hardening. The Voce model did a poor job of representing the first period of straining at 25°C, but did a fairly good job for increasing temperatures after this. However, it was not as good as the Ludwik model for representing behavior for decreasing temperatures. Figure 5.85 shows the results of a test that was started the same way as that shown in Fig. 5.84. After straining at

---

*Reactor Division.

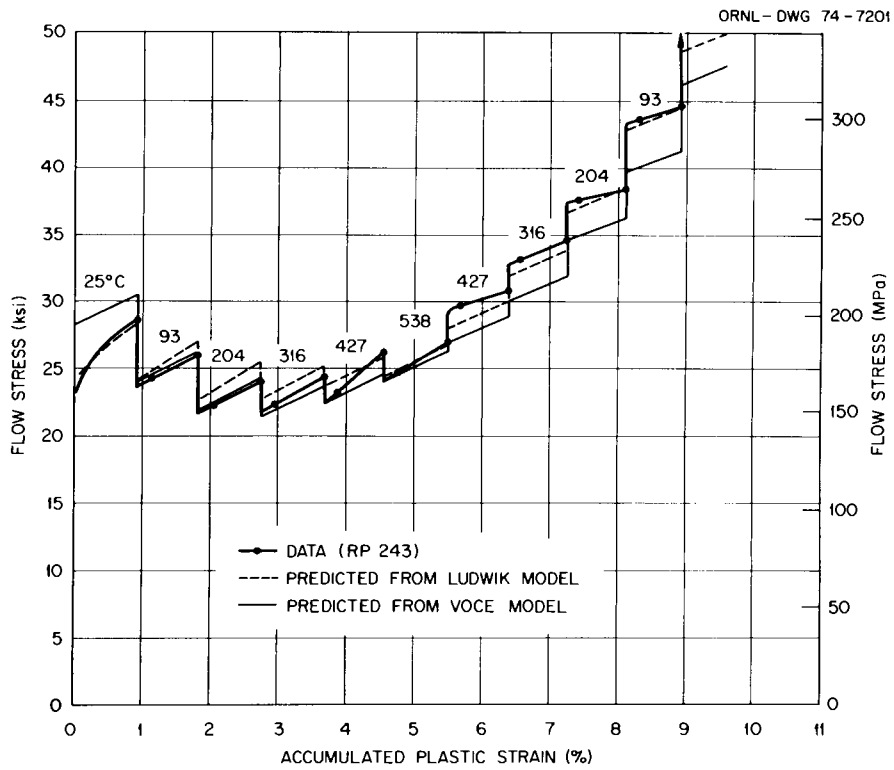

Fig. 5.84. Influence of Changing Temperature on the Flow Stress of Type 304 Stainless Steel (Heat 9T2796). Temperature was increased in steps from 25°C (77°F) to 538°C (1000°F) and then reduced in steps to 25°C.

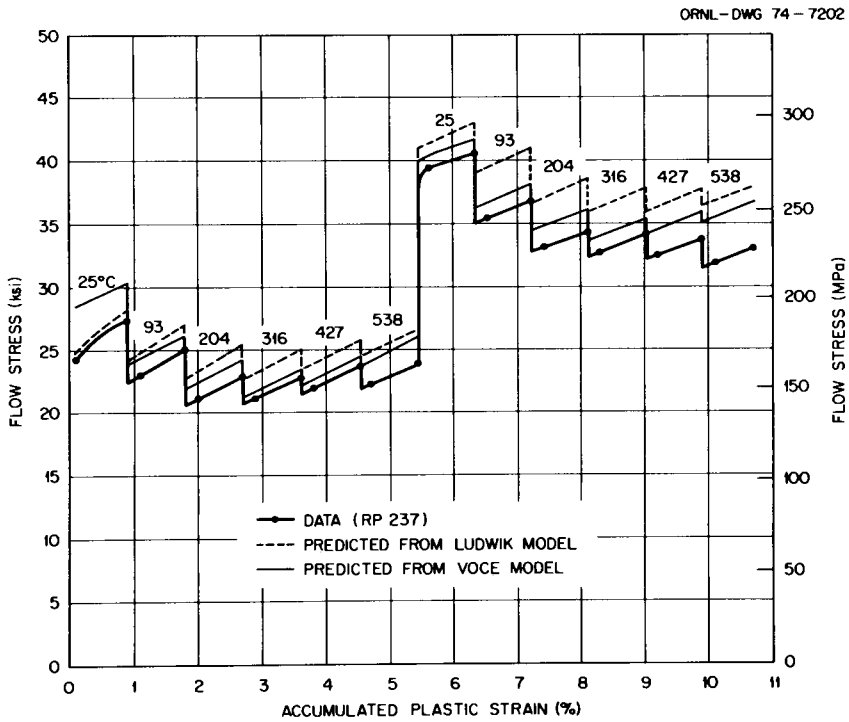

Fig. 5.85. Influence of Changing Temperature on the Flow Stress of Type 304 Stainless Steel (Heat 9T2796). Temperature was increased in steps from 25°C (77°F) to 538°C (1000°F), reduced to 25°C, and increased in steps to 538°C again.

538°C, however, the temperature was reduced to 25°C and another heating series was begun. The specimen tested in this series appeared to be weaker than would be predicted by either flow model. The Voce model came closer to representing behavior (except for the first straining period) than the Ludwik model. The results of a test that started at 538°C (1000°F) is shown in Fig. 5.86. More often than not the specimen behavior fell between the predictions of the two models. Except for the inability of the Voce model to predict the early part of the room-temperature yield, both models predict the flow stress within about 10%, and the differences in the strength from one specimen to another can vary by that much. Further work along the lines described here has been planned.

A few change-of-strain-rate tests were performed to evaluate history effects on the large strain behavior. Some results for 593°C (1100°F) are shown in Fig. 5.87, which is a plot of tensile strain against time in test. Shown at the left in the figure is the strain-time plot for a tensile test at

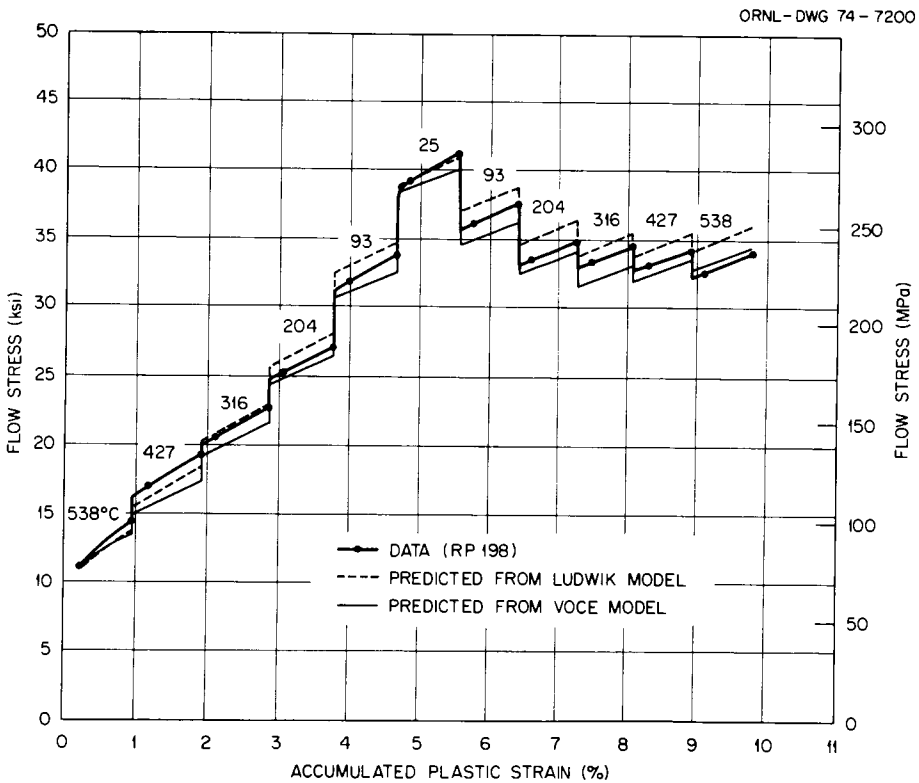

Fig. 5.86. Influence of Changing Temperature on the Flow Stress of Type 304 Stainless Steel (Heat 9T2796). Temperature was reduced in steps from 538°C (1000°F) to 25°C (77°F) and then increased in steps to 538°C.

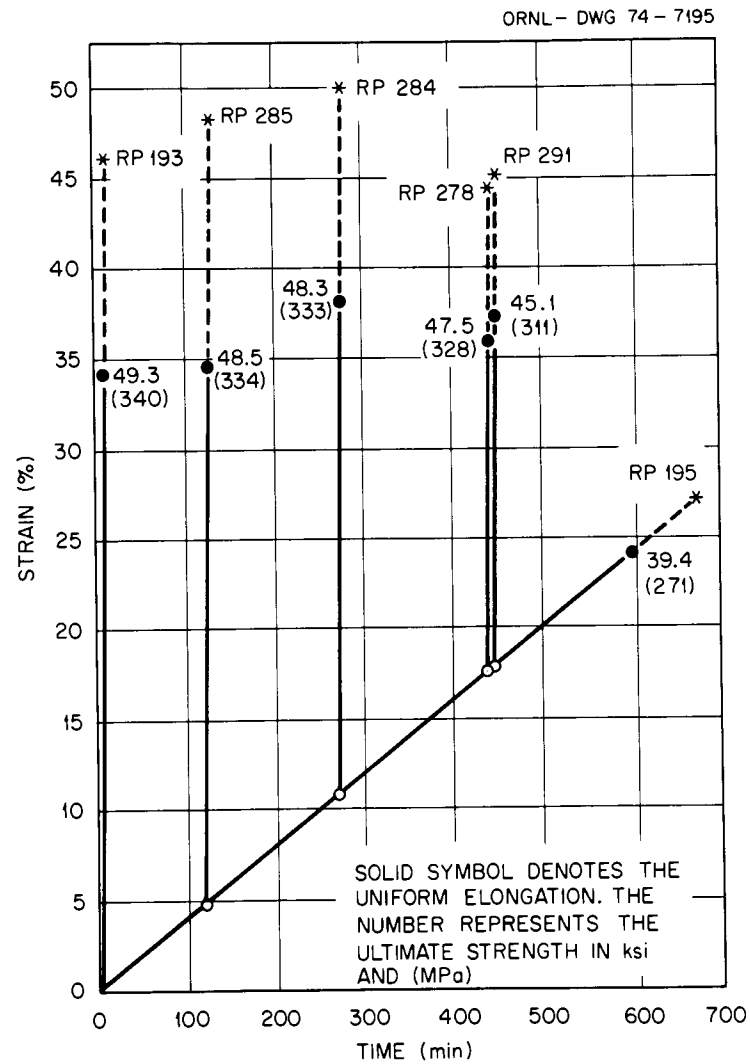

Fig. 5.87. Influence of Changing Strain Rate on the Elongation of Type 304 Stainless Steel (Heat 9T2796) at 593°C (1100F°).

0.04/min (specimen RP 193). This specimen had an ultimate strength near 49.3 ksi (340 MPa), uniform elongation near 34%, and a total elongation near 46%. The straight line at the left in the figure represents a test at 0.0004 strain rate (RP 195). The tensile strength is near 39.4 ksi (271 MPa), the uniform elongation near 24%, and the total elongation near 27%. Data for the four other tests are provided, and these were all started at the 0.0004/min rate. After different times (or strains) the rate was increased to 0.04/min. We found that neither the uniform nor the total elongation was affected by the strain accumulated at the lower rate. This suggests that it is not possible for the short times covered in these experiments to linearly sum damage at one strain rate and use the summation to estimate retained ductility at another strain rate. On the other hand, there did appear to be a slight loss in ultimate strength at the 0.04/min rate after strain accumulation at the 0.0004/min rate.

Strain rate effects have been accommodated by the high-temperature Voce model described previously.[49] It is also possible with this model to relate changes in the ultimate strength and uniform elongation to changes in the flow stress. As an example, the Voce constants σ_∞, ε_c, and σ_0 were determined for a room-temperature tensile test on one product form of the reference heat of type 304 stainless steel (heat 9T2796). We then assumed that σ_0 could be replaced by the yield strength. A relation that describes the variation in the ultimate strength with the Voce constants[49] was used to calculate the increase in the ultimate strength that should develop by increasing the yield via cold work. The calculated trend is shown by the line in Fig. 5.88. The data shown in the figure represent tensile data obtained from the different product forms of the reference heat. The trend of the data is similar to the curve.

5.5.1.2 Creep Testing

Exploratory tests on the reference heat of type 304 stainless steel (heat 9T2796) are continuing, with emphasis on gathering additional data at temperatures below 649°C (1200°F). Further testing is under way at 621, 538, and 482°C (1150, 1000, and 900°F). The purpose of the work is

ORNL-DWG 74-7197

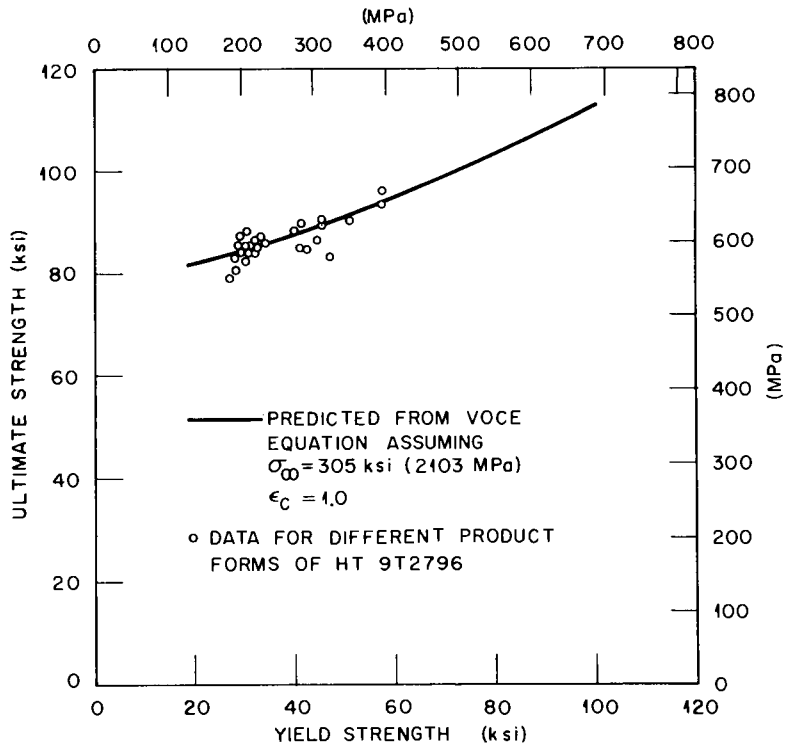

Fig. 5.88. Comparison of the Relation Between Yield Strength and Ultimate Strength Predicted by the Voce Equation with Actual Data Obtained for Different Product Forms for Type 304 Stainless Steel (Heat 9T2796) at Room Temperature.

to collect more creep and rupture data in the region where the stress and temperature dependence of creep is changing most rapidly.

Tests are also under way to examine the influence of both cyclic and monotonic prestraining on the creep behavior at 593°C (1100°F). Cyclic creep tests are continuing, and the results from a recent test at 593°C (1100°F) are shown in Fig. 5.89. The test (specimen CRP 20) was started by cycling between 15 and −12.5 ksi (103 and −86 MPa) using a two week cycle period. After five cycles the stresses were increased to +17.5 and −15 ksi (121 and −103 MPA). The results were qualitatively similar to earlier findings in that the cyclic strains were nearly stabilized after the second cycle. The tensile creep component in the first cycle was about 30% higher than the strain expected from monotonic tests, and the compressive component was 50% of the strain in a virgin specimen.

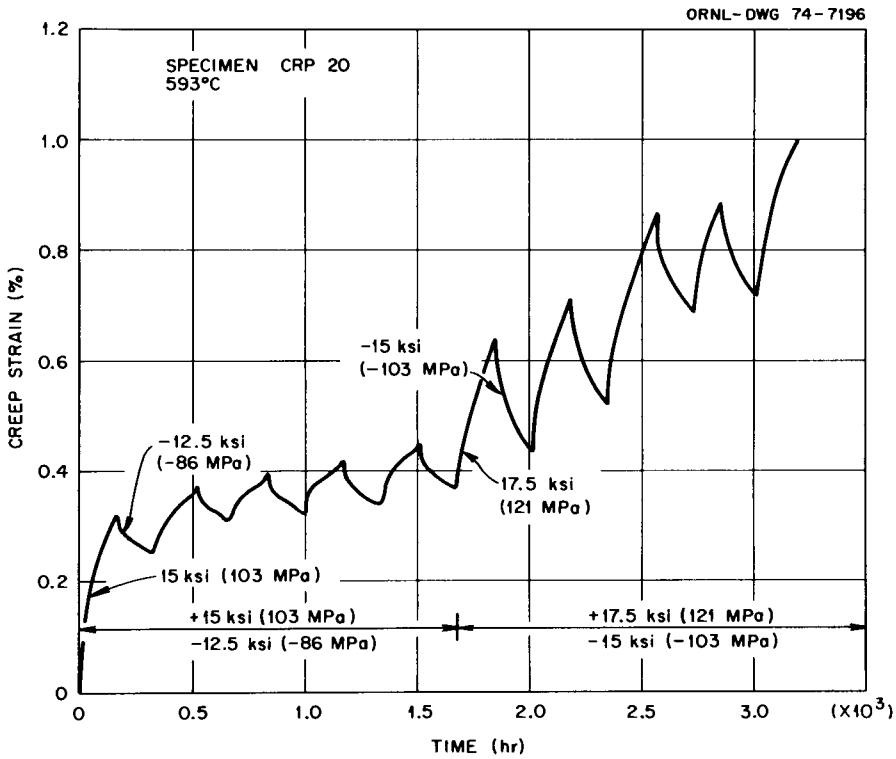

Fig. 5.89. Cyclic Creep Curve for Type 304 Stainless Steel (Heat 9T2796) at 593°C (1100°F).

After the stresses were increased we saw a similar behavior pattern. The trend of the data generally support the approach recommended for describing creep behavior under cyclic stresses.[17]

5.5.1.3 Relaxation Testing

Several relaxation tests were performed for times extending to 100 hr. Most tests were at 593°C (1100°F), but after the initial relaxation period, test temperatures were changed to examine the behavior for other conditions. The relaxation behavior at 760°C (1400°F) was relatively independent of history, providing the specimen was strained plastically before holding strain constant. Similar behavior was observed at 704°C (1300°F). At 649°C (1200°F) a very gradual rate of hardening was observed in the sense that each time the specimen was strained, and then held, the relaxed stress was greater for any given time; at temperatures below 649°C, relaxation rates depended strongly on history.

5.5.1.4 Strain-Cycling

The results of two tests involving creep-plasticity studies at 593°C (1100°F) are shown in Figs. 5.90 and 5.91. Figure 5.90 is a plot of accumulated creep strain against time in test. Dashed lines represent the results from three constant-load tests at 15 ksi (103 MPa) on the reference heat of type 304 stainless steel. The creep curve for a specimen (FRP81) that received one cycle of plastic strain every week appears to fall quite close to the trend for monotonic straining conditions. The creep curve for a specimen (FRP96) subjected to 10 cycles of straining every week exhibited a suppression of the early transient creep behavior. However, the curve appeared to follow a trend similar to the monotonic tests after the second cycling period. The suppression of early transient creep was also observed in a similar test performed at the Battelle Memorial Institute.[50] The specimen, machined from the same material, was subjected to 20 cycles before creep at 15 ksi (103 MPa). Plastic hardening data obtained on the specimens during the cycling periods are summarized in Fig. 5.91. In all cases the cyclic strains were near 0.6%. Specimen FRP81, which was subjected to only one cycle per week, hardened

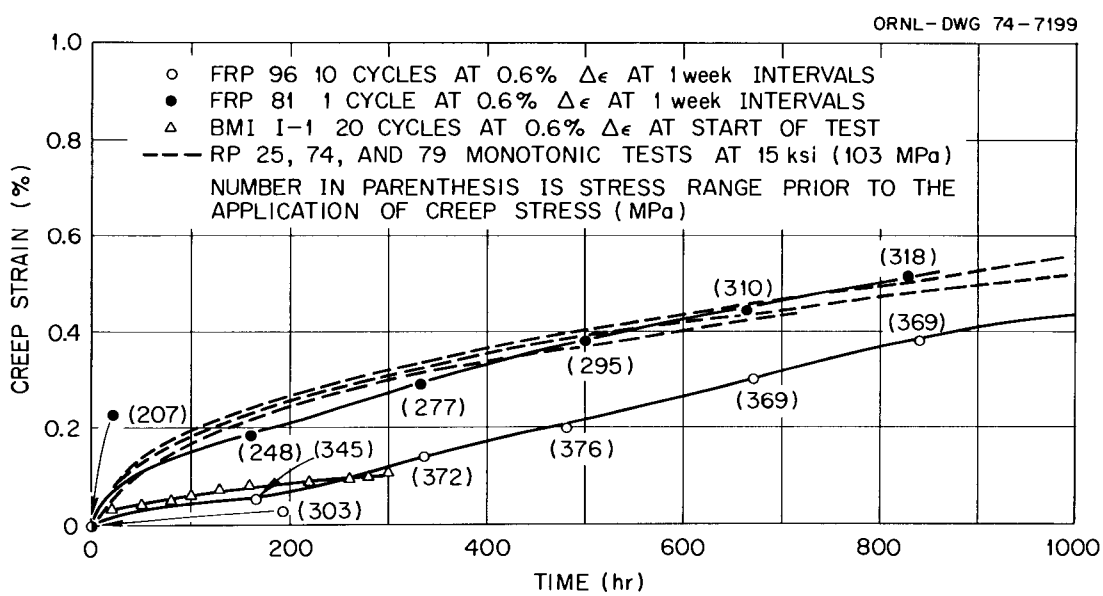

Fig. 5.90. Influence of Cyclic Strain on the Creep Curve for Type 304 Stainless Steel (Heat 9T2796) at 593°C (1100°F) and 15,000 psi (103 MPa).

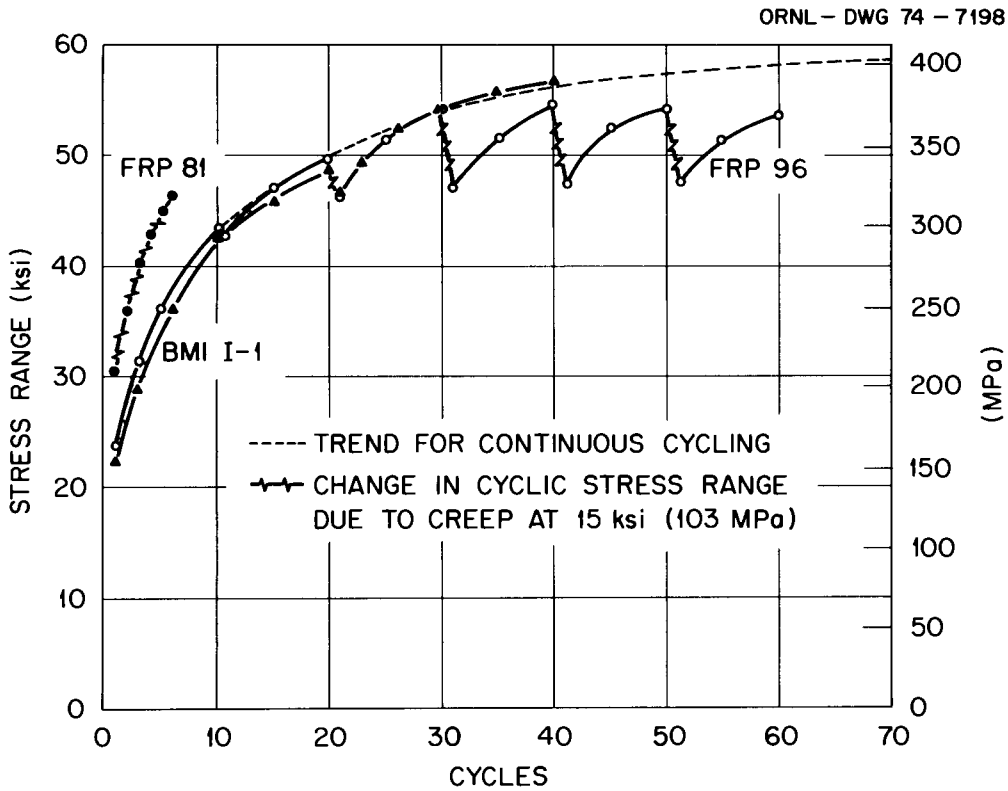

Fig. 5.91. Influence of Creep at 15,000 psi (103 MPa) on the Rate of Cyclic Strain Hardening of Type 304 Stainless Steel (Heat 9T2796) at 593°C (1100°F) and 0.6% Strain Range.

very rapidly and the creep strains appeared to be contributing to the rate of cyclic hardening. Specimens FRP96 and BMI I—1 hardened at a rate typical of a specimen subjected to continuous cycling. Specimen FRP96 showed very little change in strength after it was subjected to creep after ten cycles. After 20 cycles both specimens FRP96 and BMI I—1 were again placed in creep, and both showed a loss in strength when cycling was resumed. With continued periods of cycling and creeping, specimen FRP96 established a stable condition. After creep, the stress range was around 47 ksi (324 MPa), and after ten continuous cycles the stress range increased to near 54 ksi (372 MPa). The "relaxed stress range" of 47 ksi (324 MPa) was fairly close to the stress range observed by ANL for relaxation-type cycling conditions when the hold time was about 1 hr.

5.5.2 Investigations of Creep Failure under Uniaxial and Multiaxial Conditions — C. C. Schultz, Babcock and Wilcox

Progress on the constant-load and step-load uniaxial creep tests for this quarter is summarized in Tables 5.27 and 5.28, respectively. Minor corrections have been made to the rupture times for tests BWR-10 and BWR-12 in Table 5.28. Four uniaxial and two tubular specimens ruptured during this reporting period.

Rupture occurred in 6868 hr in constant-load test BWR-14 (at 20 ksi). This result is in poor agreement with the previously reported rupture time of 9584 hr for test BWC-5B (also at 20 ksi). The stress-strain response, on loading, for these two tests did not differ enough to indicate any significant differences in grain size. The microstructure of specimen 2-9 (test BWR-14) has not yet been examined for comparison with that of specimen 2-16 (test BWC-5B). The creep strain-time data for these two tests are shown in Fig. 5.92.

As previously reported,[51] the primary purpose of test BWR-14 (see Fig. 5.93) was to determine if significant deformation occurs outside the 2-in. gage length in the threaded-type specimen or if bending in this type of specimen is greater than that in the 3-in. button-head creep machine specimen. Test BWC-10 (Fig. 5.94), also directed to establishing the cause for the apparent differences in strain-time responses obtained from the two types of specimens and testing machines, is still in progress. As previously reported, the purpose of this test is to establish if the strain becomes significantly localized prior to tertiary creep. The data shown in Fig. 5.94 indicate that the strain is not being localized. The strain-time results of four tests, all at 20 ksi (BWR-5, BWR-14, BWC-5B, and BWC-10), are compared in Fig. 5.95. Irrespective of the actual strain magnitudes, it may be seen that the two 3-in. creep machine specimens respond similarly, as do the two 2-in. rupture machine specimens. Further review of our present data must precede complete definition of future action in this area.

Three step-load uniaxial specimens ruptured this reporting period. Two of these (tests BWC-6 and BWR-8) were transferred to this test series after elimination from the interrupted test series. All six specimens involved in this transfer have now ruptured, with calculated life fractions

Table 5.27. Status of Uniaxial Constant-Load Rupture Tests Type 304 Stainless Steel (Heat 9T2796); 593°C (1100°F)

Test No.	Specimen No.	Stress (ksi)	Total strain on loading[a] (%)	Time to secondary creep (hr)	Minimum creep rate (%/hr)	Time to tertiary creep[b] (hr)	Intercept creep strain[c] (%)	Test time[d] (hr)	Fracture elongation[e] (%)	Reduction in area (%)
BWC-1	7-15	30	4.7					187 R	19.0	30.5
BWR-1	7-1	30						138 R	21.5	32.9
BWC-2	2-22	28	5.8	40	0.016	195	0.50	227 R	13.0	20.4
BWR-2	2-1	28		40	0.022	230	0.65	368 R	16.5	29.0
BWR-13	7-13	28		60	0.023	215	0.88	276 R	16.5	18.9
BWC-9	7-25	28	3.8	85	0.021		1.16	415 R	18.3	25.2
BWC-3[f]	7-28	25	NA	80	0.0065	500	0.45	667 R	12.7	12.0
BWR-3	7-8	25		100	0.0079	585	0.71	948 R	17.0	23.2
BWC-4	2-28	22	3.7	175	0.0014	1400	0.60	2,130 R	10.7	13.7
BWR-4	7-7	22		160	0.0030	1170	0.72	2,026 R	12.5	16.6
BWC-5[g]	2-15	20						D		
BWC-5B	2-16	20	1.8	5000	0.000165	8700	1.84	9,584 R	10.5	12.0
BWR-5[h]	2-14	20						4,842 D		
BWR-6	7-14	19						14,570 I		
BWR-9	7-11	18						13,580 I		
BWR-11[i]	2-12	17						94 D		
BWR-11B	2-10	17						13,750 I		
BWR-7	2-4	16						14,250 I		
BWR-14	2-9	20	2.02	3200	0.00044	5800	1.88	6,868 R	8.5	13.1
BWC-10	7-18	20	1.52					2,690 I		

[a]All specimens were step loaded at 1.87-ksi increments, except test BWC-5B, which was step loaded at 1.49-ksi increments. Loading curves on BWR series include load train displacements, thus not reported. NA = not available.

[b]Based on the 0.2% offset from the minimum rate line.

[c]Does not include the elastic and initial plastic components.

[d]R = rupture; D = discontinued; I = in test.

[e]Elongation over 3 in. in BWC series; over 2 in. in BWR series.

[f]Failure occurred near end of gage length.

[g]Temperature excursion to 1300°F prior to loading; replaced by test BWC-5B.

[h]Temperature excursion to 1380°F at 4842 hr; terminated.

[i]Temperature excursion at 1300°F at 94 hr; replaced by test BWR-11B.

Table 5.28. Status of Uniaxial Step-Load Rupture Tests Type 304 Stainless Steel (Heat 9T2796); 593°C (1100°F)

Test No.	Specimen No.	Stress (ksi)	Total strain on loading (hr)	Time at Load[a] (hr)	Life fraction (%)	Fracture elongation[b] (%)	Reduction in area (%)
BWC-6	2-17	16	0.42	3,871	6		
		25		136	17		
		20		9,251	123		
				13,258 R		9.0	16.0
BWR-10	2-11	16		3,871	6		
		25		136	17		
		20		5,655	75		
				9,662 R	98	11.5	17.8
BWC-7	2-18	17	0.76	3,699	11		
		25		136	17		
		20		5,066	68		
				8,901 R	96	12.0	20.6
BWR-8	2-5	17		3,703	11		
		25		136	17		
		20		8,901	119		
				12,740 R	147	11.0	13.8
BWLF-5	2-25	20	2.06	503	7		
		25		198	25		
		20		5,246	70		
				5,947 R	102	12.5	17.0
BWC-8	7-16	18	1.78	5,071	25		
		25		136	17		
		20		5,420	72		
				10,627 R	114	8.0	15.5

Table 5.28. (Continued)

Test No.	Specimen No.	Stress (ksi)	Total strain on loading (%)	Time at load[a] (hr)	Life fraction (%)	Fracture elongation[b] (%)	Reduction in area (%)
BWR-12	7-12	18		4,897	24		
		25		136	17		
		20		3,996	53		
				9,029 R	94	11.5	17.2
BWLF-5B	2-21	21	2.62	500	10		
		25		200	25		
		21		1,236	25		
				1,936 R	60	10.3	15.9
BWLF-7	2-26	21	2.25	750	15		
		25		136	17		
		21		2,003	40		
				2,889 R	72	12.3	20.5
BWLF-9	7-24	21	2.21	1,104	20		
		25		136	17		
		21		1,610 I	32		
BWLF-10	2-27	21	2.47	1,006	20		
		25		136	17		
		21		900 I	18		
BWLF-8	7-23	21		750	15		
		25		136	17		
		21		360 I	7		
BWLF-6	7-22	21	3.11	500	10		
		25		200	25		
		21		560 I	11		

[a]R = rupture; D = discontinued; I = in test.

[b]Elongation over 3 in. in BWC series; over 2 in. in BWR series.

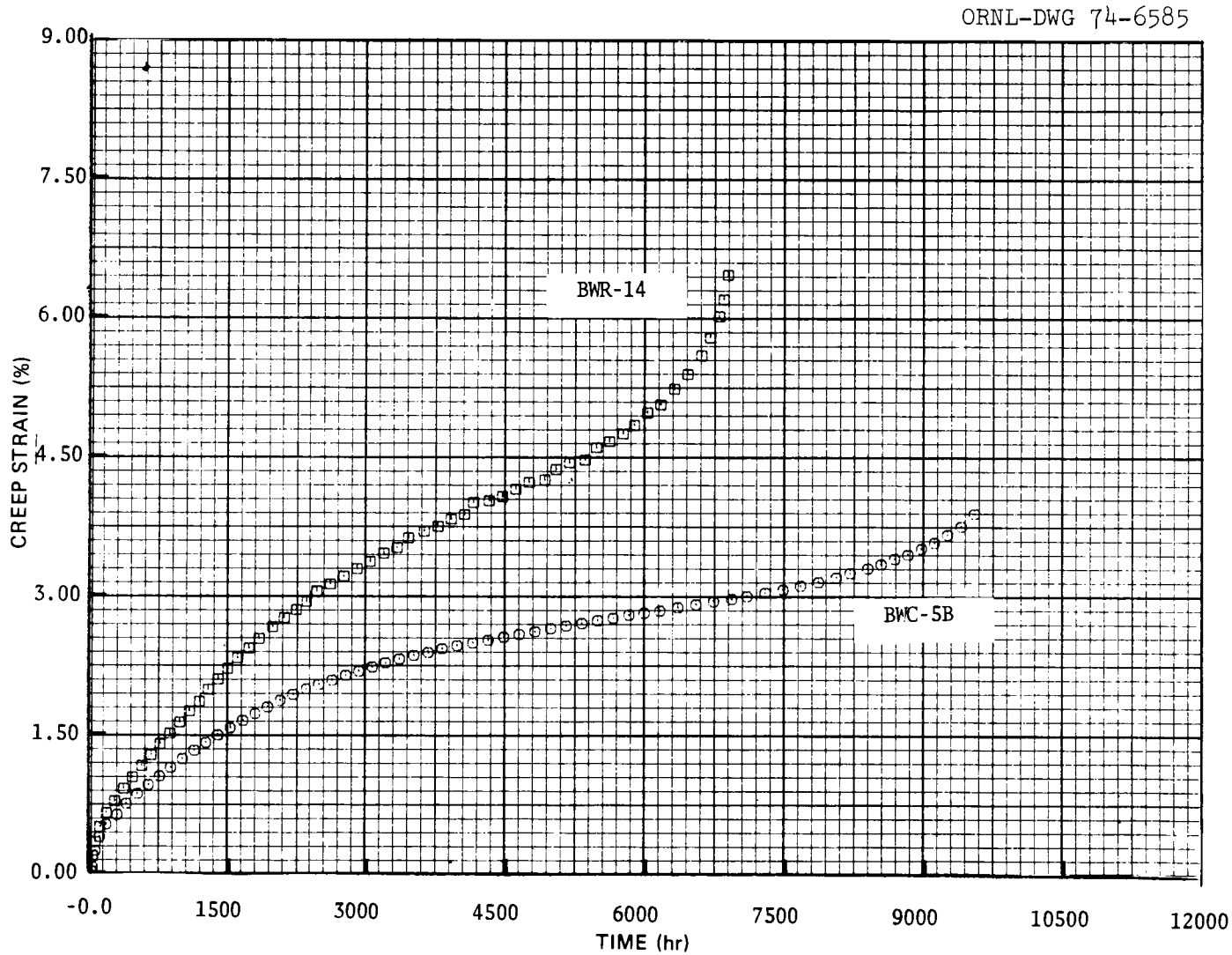

Fig. 5.92. Constant-Load Uniaxial Rupture Tests Loaded at 20 ksi at 593°C (1100°F). Type 304 Stainless Steel (Heat 9T2796) 5/8-in. Bar.

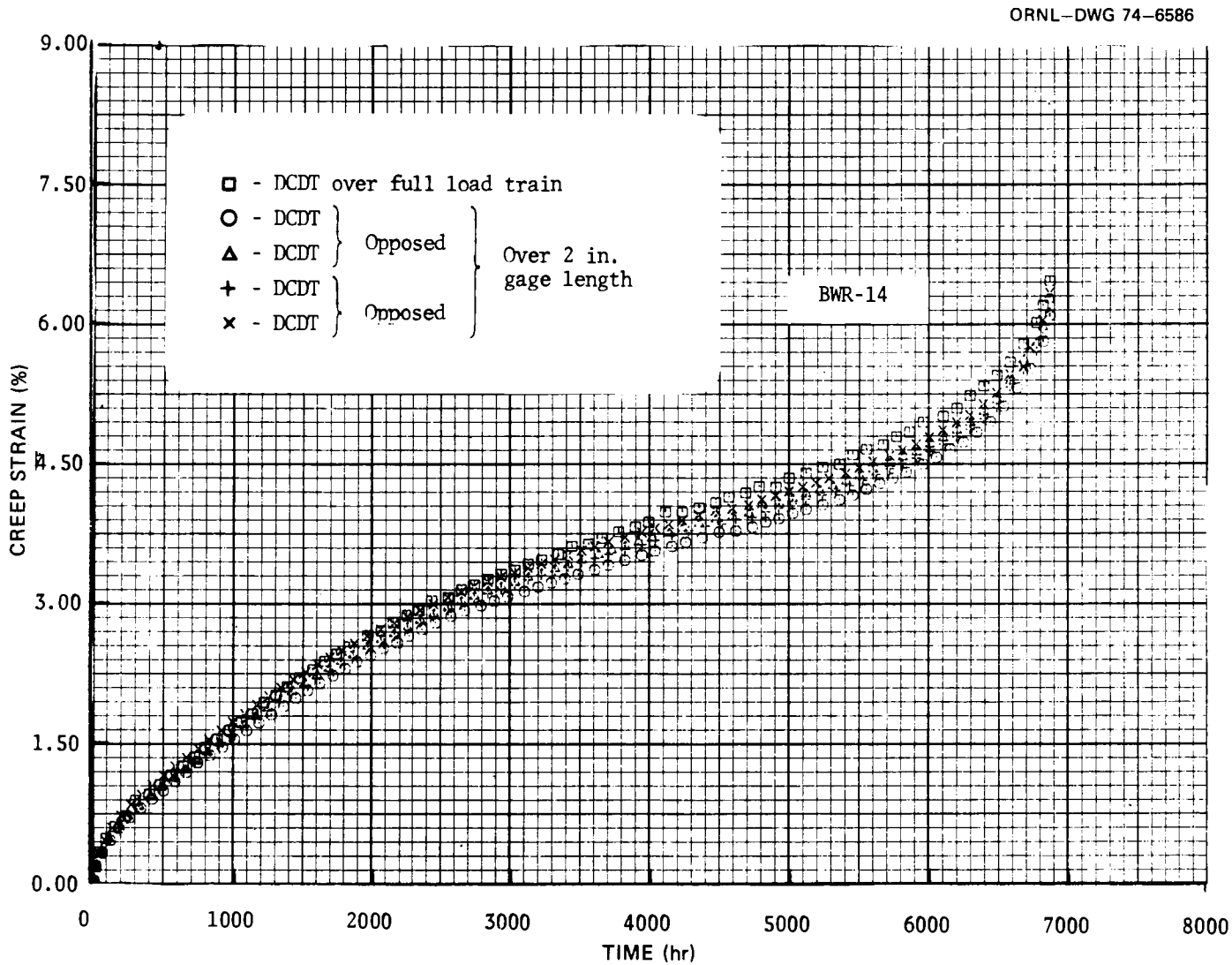

Fig. 5.93. Constant-Load Uniaxial Test to Evaluate Strain Outside of Gage Length and Bending in a Threaded Rupture Machine Specimen. Loaded at 20 ksi and 593°C (1100°F); Type 304 Stainless Steel (Heat 9T2796) 5/8-in. Bar.

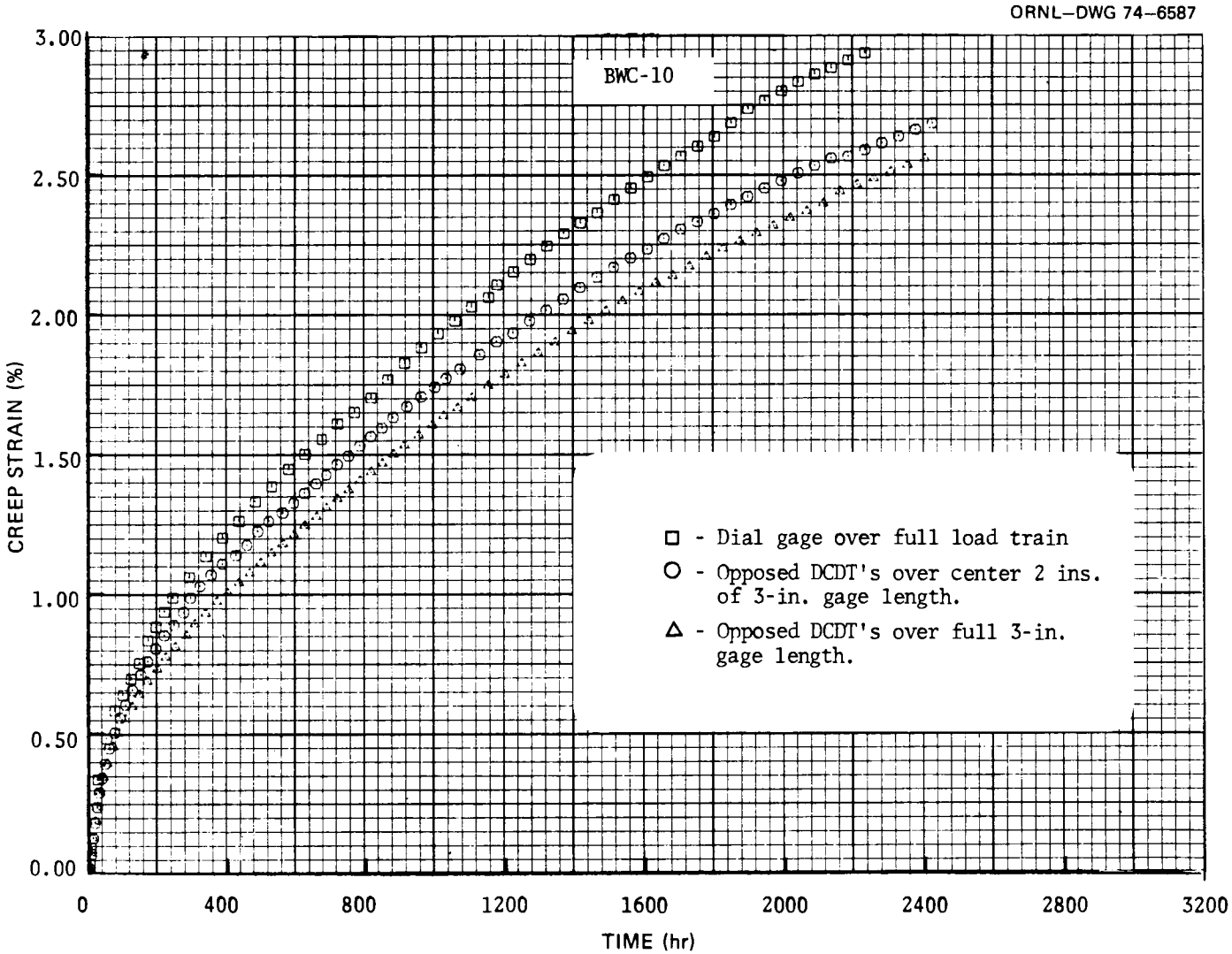

Fig. 5.94. Constant-Load Uniaxial Test to Evaluate Localization of Strain in 3-in. Button-Head Creep Machine Specimen. Loaded at 20 ksi and 593°C (1100°F); Type 304 Stainless Steel (Heat 9T2796) 5/8-in. Bar.

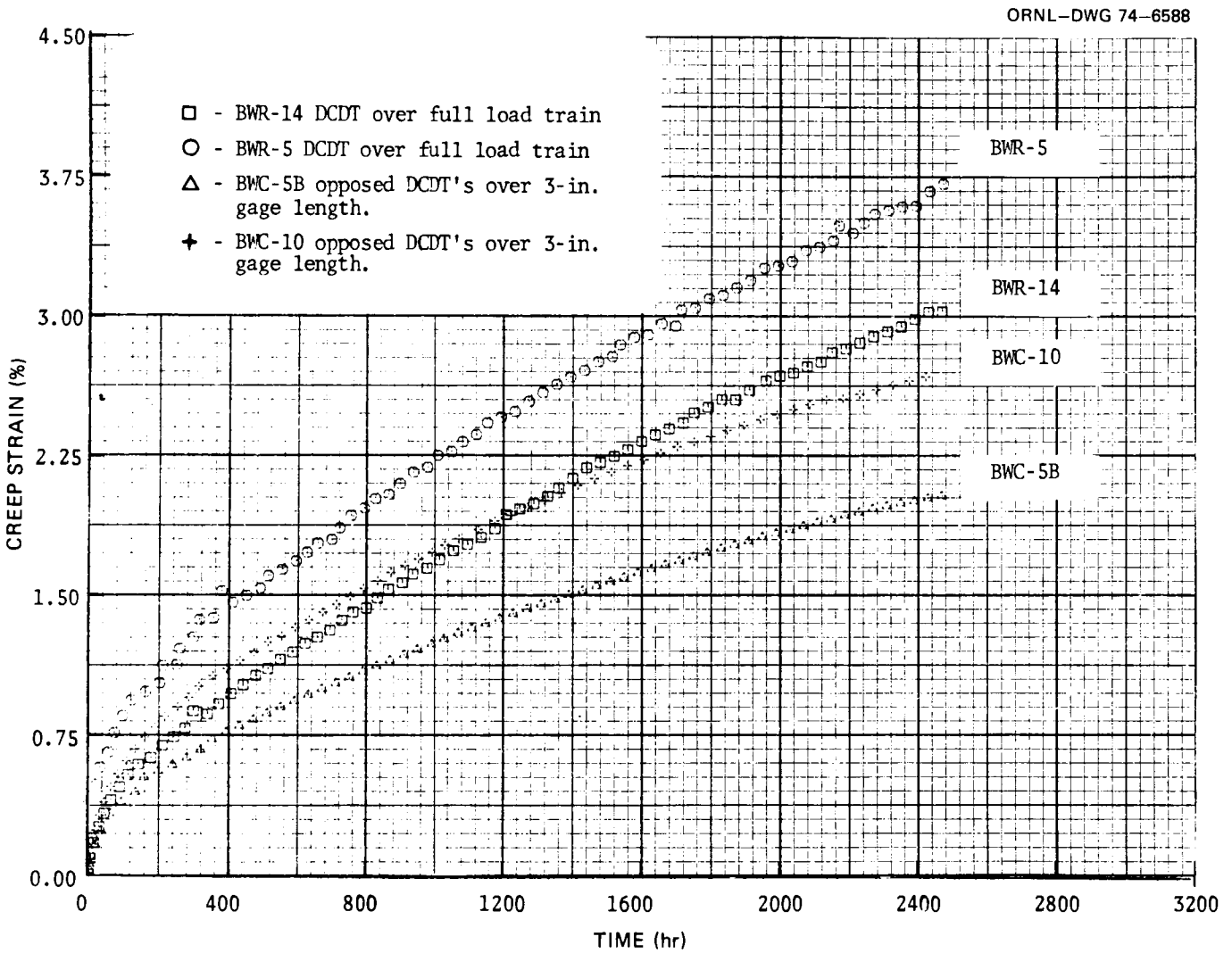

Fig. 5.95. Comparison of Uniaxial Tests Loaded at 20 ksi and 593°C (1100°F). Type 304 Stainless Steel (Heat 9T2796) 5/8-in. Bar.

for the first four of the tests at approximately 100% and the last two at nearly 150%. The strain-time results for these two tests are given in Figs. 5.96 and 5.97. The other step-load uniaxial test completed was BWLF-7, with a calculated life fraction of approximately 70%; the strain-time results are shown in Fig. 5.98. As shown in Table 5.28, step-load tests BWLF-6, BWLF-8, and BWLF-10 were initiated during this reporting period.

The variations seen in rupture lives in both constant- and step-load tests cannot be attributed to either load history or type of specimen and/or testing machine; hence, they must be a result of the grain size variation reported for other specimens in the last quarterly report.[51] We have continued this posttest determination of grain size and concluded that the mixture of coarse and fine grains is evident, to some degree, in most of our tested specimens. As a result, we have now expanded this effort to determine the cause and solution. The results of this effort will be reported when completed.

Three specimens (6-1, 6-2, and 6-3) were loaded at 19.5 ksi as a part of the interrupted uniaxial test series and have now been in test for more than 1400 hr. The initial three specimens loaded in this test series (6-4, 6-5, and 6-6) have now been in test over 8000 hr at 19.5 ksi.

Two tubular specimens (tests BWTR-2 and BWTR-4) ruptured during this reporting period. Test BWTR-2 was loaded by internal pressure only with a circumferential stress of 21,850 psi (based on the mean diameter formula) and ruptured in 1713 hr. Posttest specimen measurements for strain determination have not been completed. Visual inspection showed that the thermocouples (held in place by wire wraps around the specimen) greatly interfered with the radial growth; this test procedure is being revised. The axial strain-time results are shown in Fig. 5.99. Test BWTR-4 was loaded with internal pressure and an axial load such that the axial stress (21,850 psi) was twice the circumferential stress (10,925 psi). This specimen ruptured after 3336 hr under load. The axial strain-time results appear in Fig. 5.100. The reduction in creep rate at about 1500 hr was due to a reduction in load that went undetected for about 150 hr.

Figure 5.101 summarizes the constant-load rupture data including the tubular specimen data, which are plotted on the basis of maximum principal stress. The effective stress for both tests BWTR-2 and BWTR-4 was 18,920 psi.

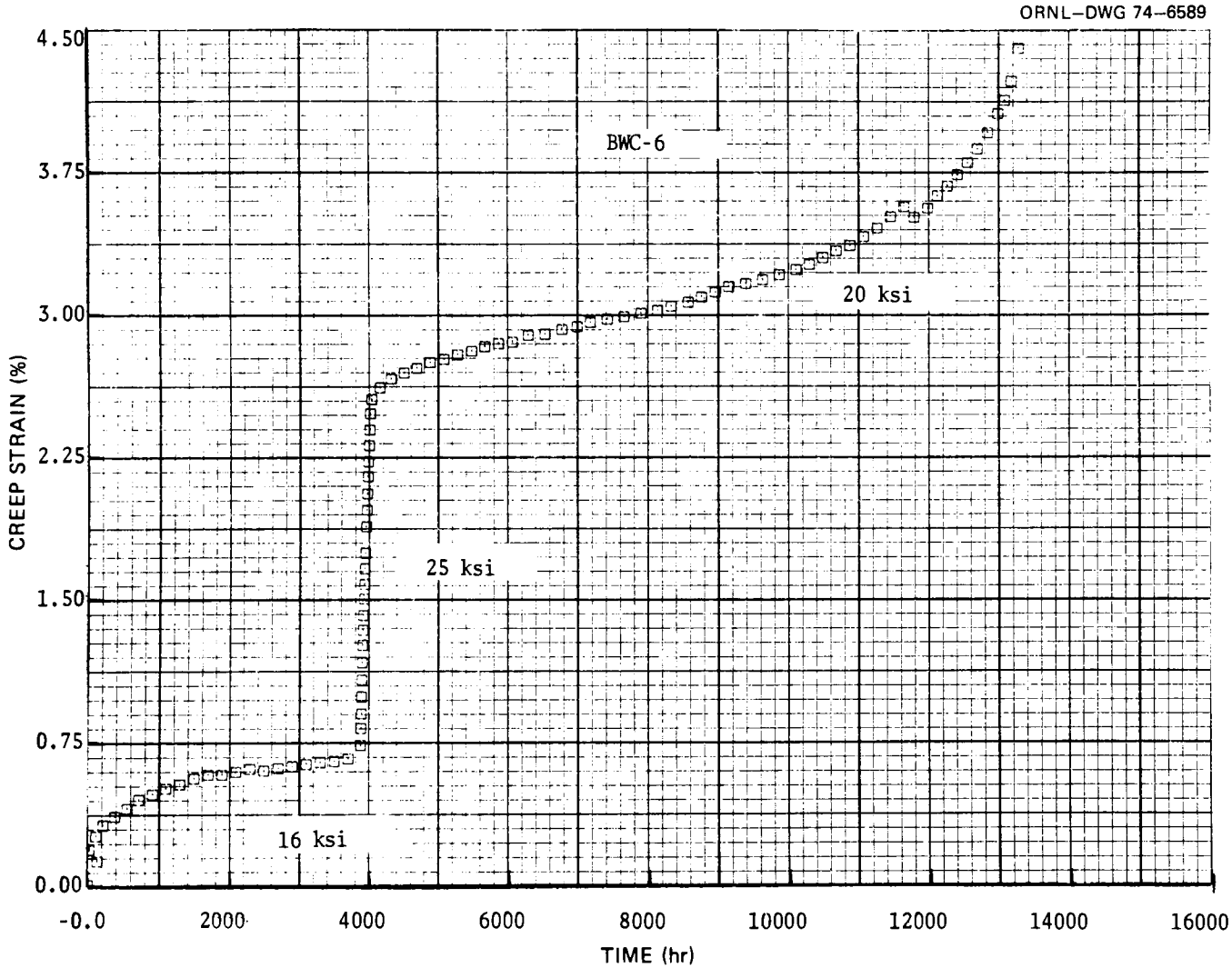

Fig. 5.96. Step-Load Uniaxial Rupture Test at 593°C (1100°F). Type 304 Stainless Steel (Heat 9T2796) 5/8-in. Bar.

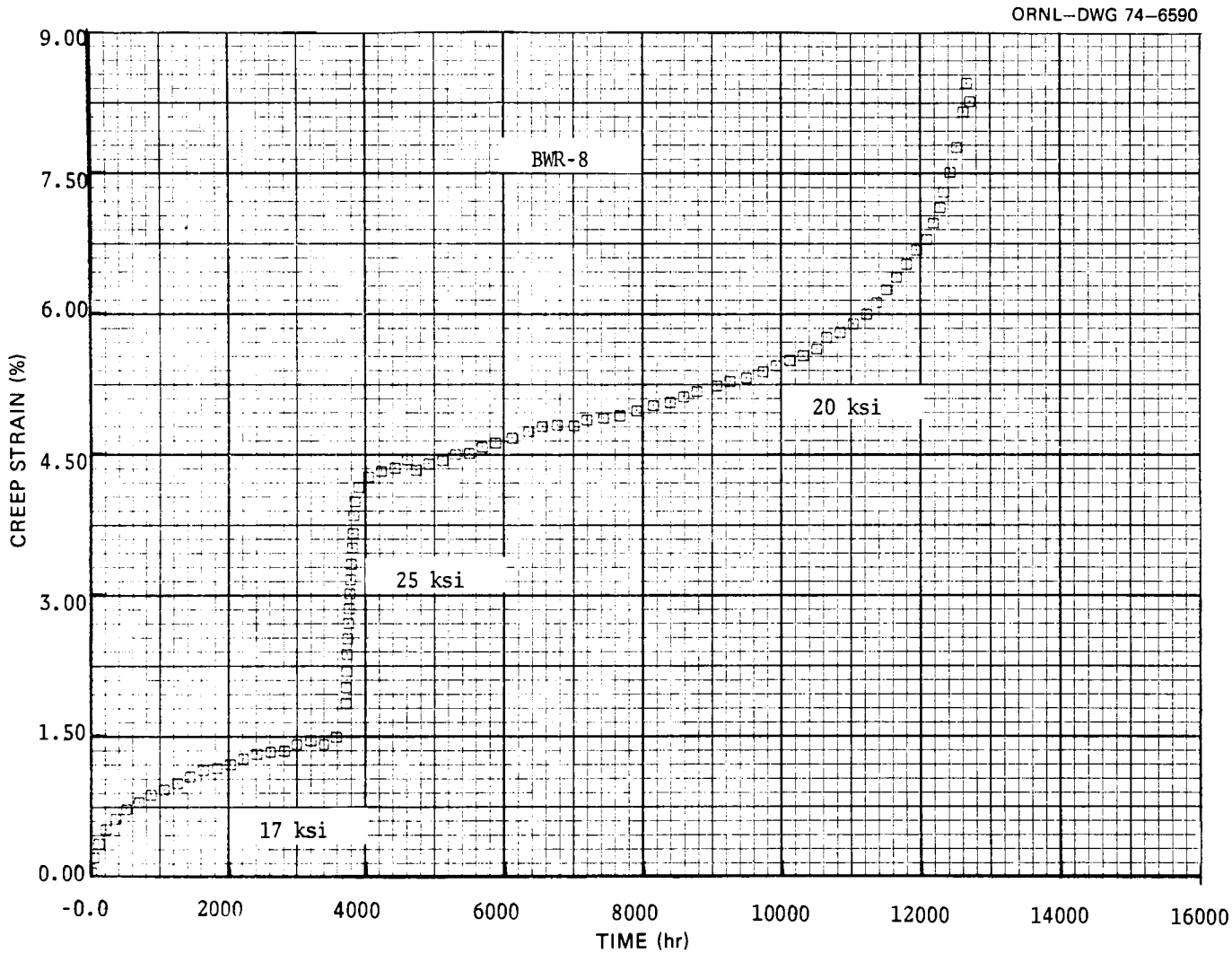

Fig. 5.97. Step-Load Uniaxial Rupture Test at 593°C (1100°F). Type 304 Stainless Steel (Heat 9T2796) 5/8-in. Bar.

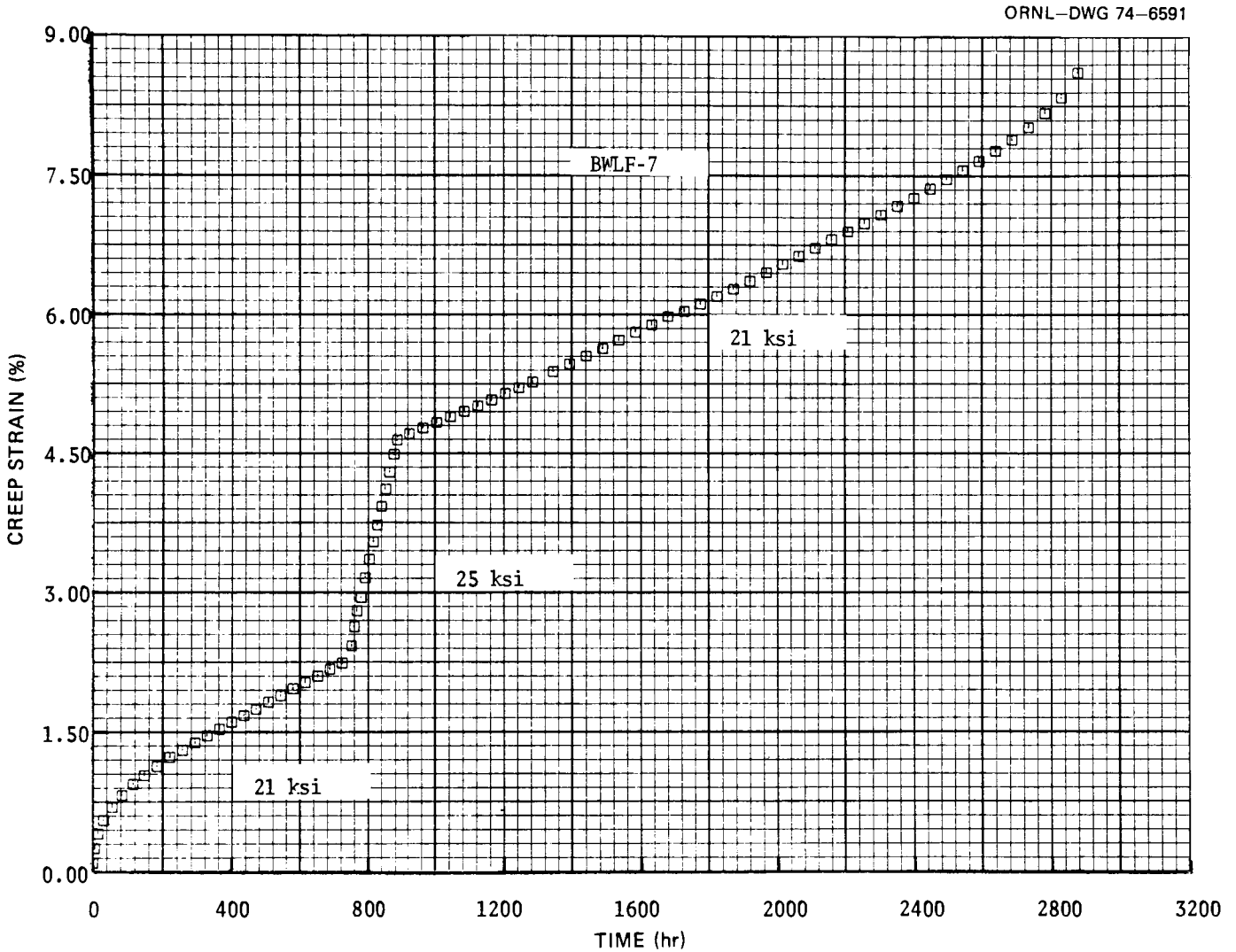

Fig. 5.98. Step-Load Uniaxial Rupture Test at 593°C (1100°F). Type 304 Stainless Steel (Heat 9T2796) 5/8-in. Bar.

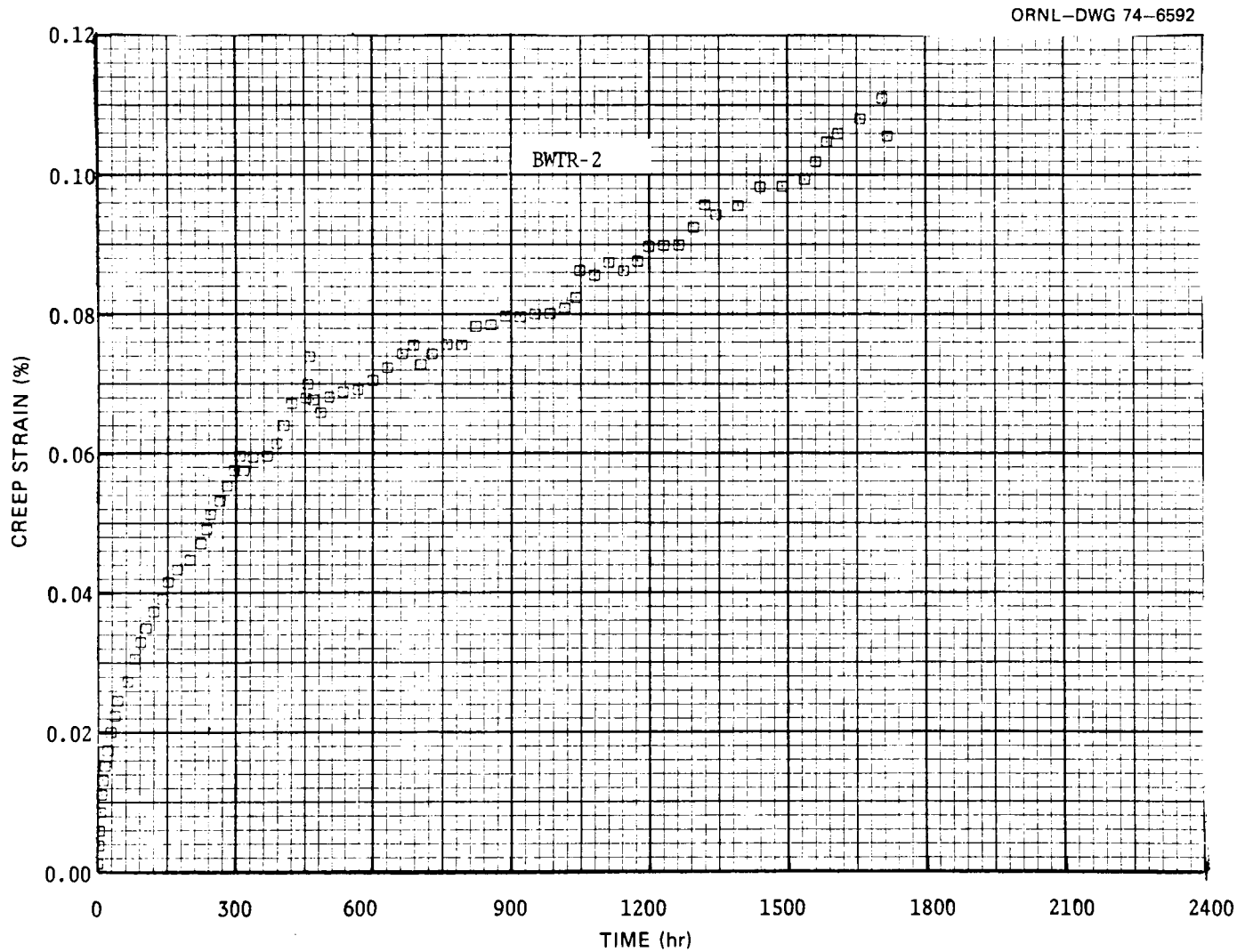

Fig. 5.99. Axial Creep Strain in Constant-Load Biaxial Rupture. Tubular Specimen with Internal Pressure; Circumferential Stress of 21,850 psi and Axial Stress of 10,925 psi; 593°C (1100°F). Type 304 Stainless Steel (Heat 9T2796) 1.927-in. Bar (1.50 in, OD, 0.075 in. Wall Thickness).

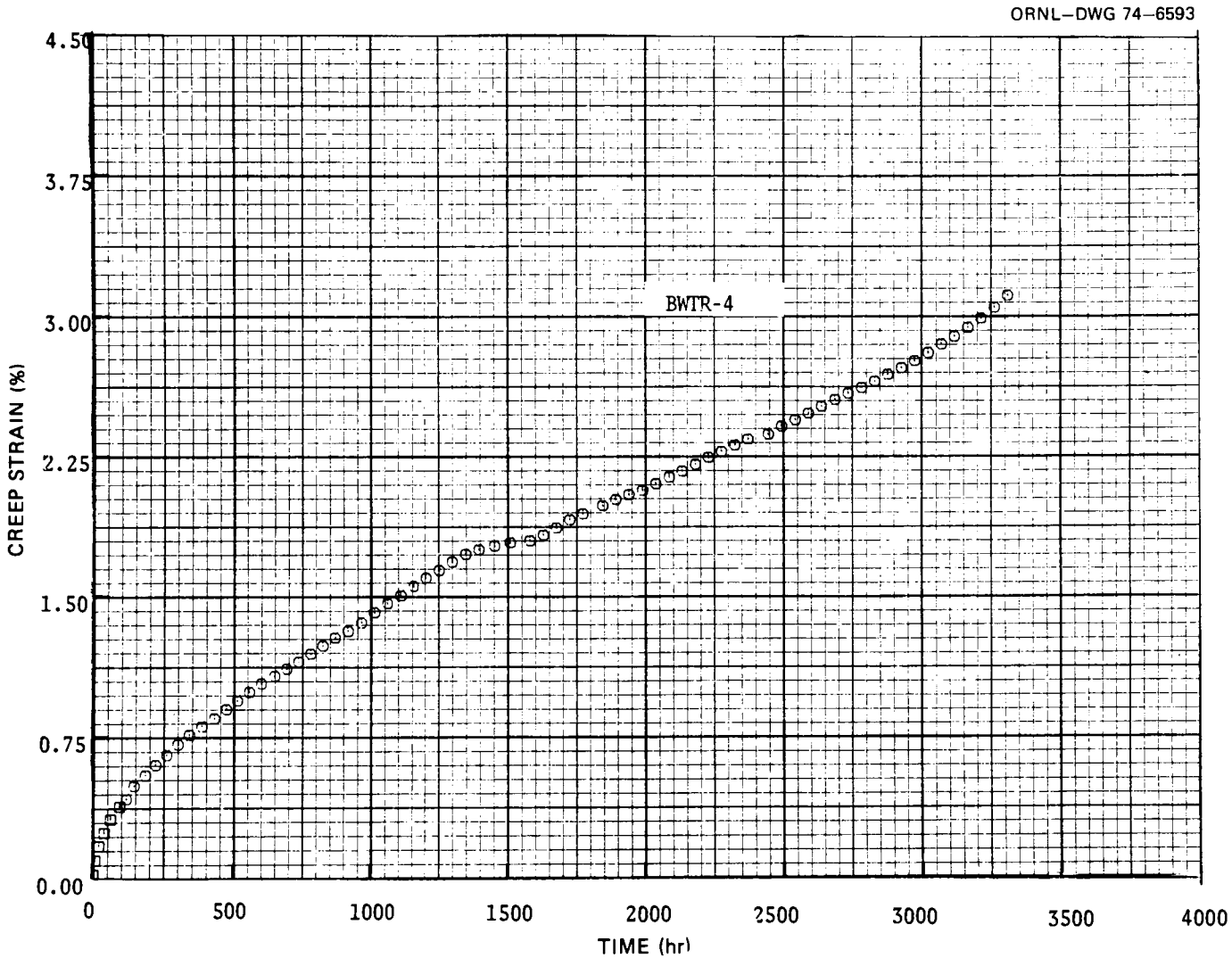

Fig. 5.100. Axial Creep Strain in Constant-Load Biaxial Rupture. Tubular Specimen with Internal Pressure and Additional Axial Load; Circumferential Stress of 10,925 psi and Axial Stress of 21,850 psi; 593°C (1100°F). Type 304 Stainless Steel (Heat 9T2796) 1.927-in. Bar (1.50 in. OD, 0.075 in. Wall Thickness).

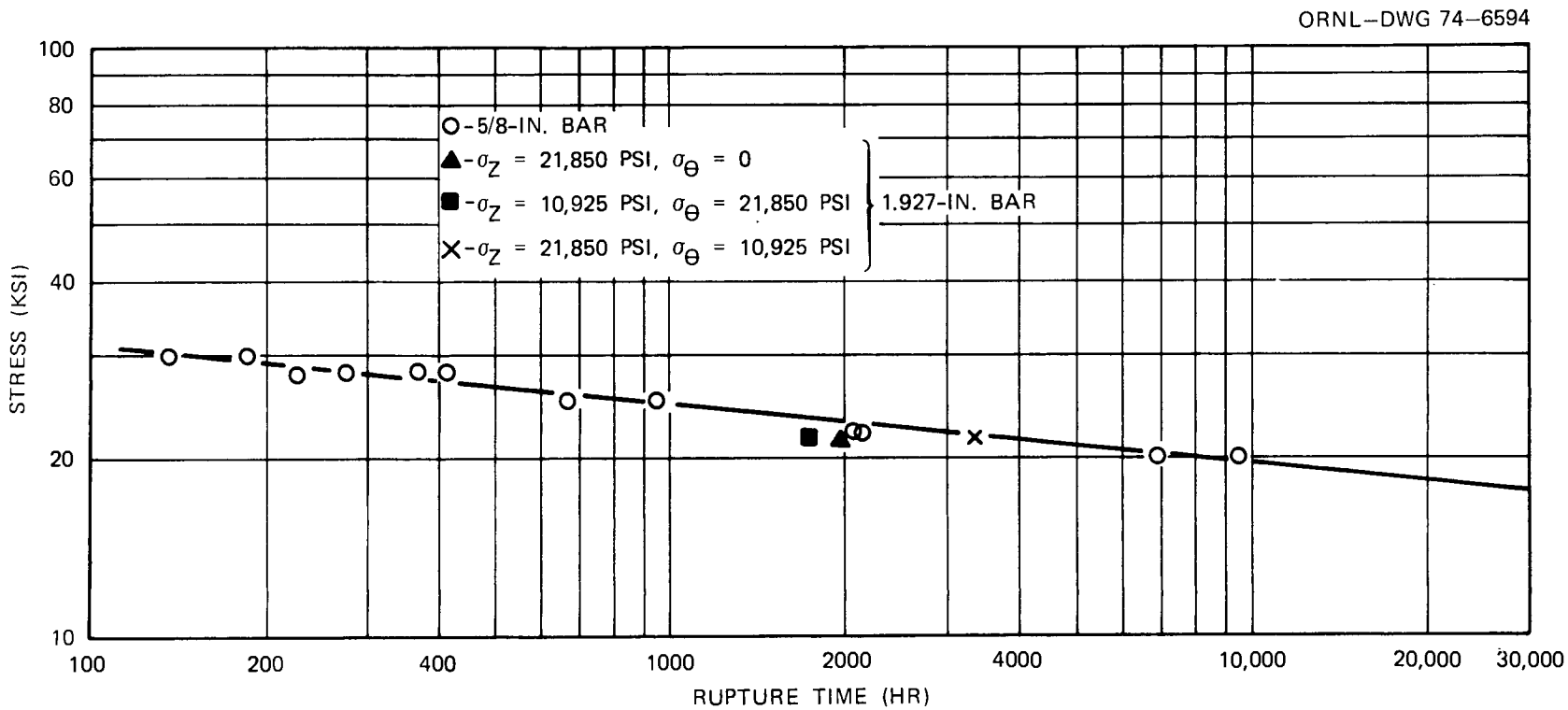

Fig. 5.101. Stress-Rupture Data for Constant-Load Uniaxial and Biaxial Tests at 593°C (1100°F). Type 304 Stainless Steel (Heat 9T2796).

5.6 MECHANICAL PROPERTIES OF HTGR STEAM GENERATOR AND PRIMARY CIRCUIT MATERIALS — P. L. Rittenhouse

The scope and purpose of this program were described previously.[52] During this quarter we have continued a number of tasks preparatory to the initiation of mechanical property determinations on HTGR materials in an environment of simulated primary coolant helium.

5.6.1 Materials

The status of procurement of HTGR materials required for out tests in FY 1975 and beyond is summarized in this paragraph. We currently have on hand material from three lots of 2 1/4 Cr-1 Mo steel (used in the steam generator and in the primary coolant circulator closure),* one lot of Hastelloy X (hot duct and thermal barriers), one lot of 9 Cr-1 Mo steel, and two lots of Hastelloy S. (The latter two materials are not presently in HTGR design but are being evaluated for several potential applications.) General Atomic Company is to provide sufficient Incoloy 800 (steam generator and control rods) to satisfy our FY 1975 testing schedule while plans are being formulated for the purchase of a reference heat of this material. Inconel 617 (possible uses in hot duct and steam generator) has been ordered; procurement of 1010/1020 steel (low-temperature thermal barrier) and stabilized high-alloy ferritic steels (steam generator) will procede in FY 1975.

5.6.2 Mechanical Property Testing

Tensile and creep specimens have been fabricated from all the materials (see Sect. 5.6.1) that are on hand. Tensile testing of the three lots of 2 1/4 Cr-1 Mo steel (pipe) and one lot of 9 Cr-1 Mo steel (plate) is essentially complete, and data reduction is in progress. These tests were conducted at room temperature and at 260 to 593°C (500 to 1100°F) in 55.6°C (100°F) increments. The temperatures experienced by these materials in the HTGR will range from approximately 260 to 566°C (500 to 1050°F). Both steels were isothermally annealed [i.e., austenitized at 927°C (1700°F),

---

*Typical HTGR applications of the material listed are given in parentheses following the material call out.

and held for 2 hr at 704°C (1300°F) with controlled cooling rates, both from the austenitizing temperature to 704°C (1300°F) and to room temperature]. Hastelloy X and Hastelloy S will be tensile tested in the solution-annealed condition.

A test matrix is currently being prepared for our FY 1975 creep-rupture experiments. Ten environmental (i.e., atmosphere of simulated HTGR primary coolant helium) creep machines and six conventional (air environment) machines are committed to this program for FY 1975. Allowing time for system shakedown and assuming a nominal test duration of 3000 hr, slightly more than 30 tests are to be included in the matrix. Tests will emphasize 2 1/4 Cr-1 Mo steel, Incoloy 800, and Hastelloy X in the range 482 to 816°C (900 to 1500°F).

Matrices for stable crack growth testing are also being prepared. Testing during FY 1975 will be devoted to 2 1/4 Cr-1 Mo steel and Incoloy 800. Tests will be conducted both in simulated HTGR helium and in steam at temperatures to 593°C (1100°F) for 2 1/4 Cr-1 Mo and to 816°C (1500°F) for Incoloy 800.

5.6.3 Environmental Facilities

Reactions between the materials of construction of the HTGR steam generator and primary circuit and the gaseous impurities in the primary coolant helium could degrade mechanical properties and behavior. Therefore, elevated-temperature testing of HTGR materials must include these effects. To this end, we are providing simulated HTGR helium as the environment in creep-rupture, fatigue, and crack growth tests. The impurity species and their ranges under consideration are H_2 at 50–5000 μatm,* CH_4 at 10–50 μatm, and $H_2O + CO + CO_2 + O_2$ not to exceed 500 μatm. Ratios of H_2 to H_2O from 10 to 1000 are of interest. Levels of N_2 up to 25 μatm may also be of interest.

The supply and control of these gaseous mixtures is a demanding task, and we are currently taking two approaches. First, we are setting up five of our ten environmental creep chambers with gas supply from a

---

*1 μatm is defined as the equivalent of 1 ppm at 1 atmospheric pressure.

dynamic mixing system in which H_2, CO, CH_4, and others can be micrometered into a helium stock that has been purified in-line by passage through an activated charcoal trap cooled by liquid nitrogen. This system is of a design successfully employed by General Atomic Company.

The remaining five systems will employ and evaluate the use of tank mixtures of simulated HTGR helium. In this regard, we have recently received encouraging results relative to the stability of such mixtures. A tank containing controlled additions of CO, CH_4, and H_2 to He was prepared and bled from 1000 psi (7 MPa) to 50 psi (0.35 MPa) over a 600-hr period. This gas was analyzed daily; the results at start and finish are shown in Table 5.29.

Table 5.29. Analysis of Simulated HTGR Helium in 600-hr Bleed Test

Time of Analysis	Concentration, ppm				
	H_2	CO	CH_4	O_2	N_2
Start	122	34	26	7	28
Finish	114	34	26	8	30

These results suggest that our earlier concerns about settling of the gas mixture and preferential sticking of gas molecules to the tank walls were largely unfounded. The relatively high O_2 and N_2 contents of the gas mixture resulted from similarly high contents in the helium supply. However, ultrapure helium (1.9 ppm total impurities including 0.5 ppm H_2O, 0.2 ppm N_2, and 0.05 ppm O_2) is available as a starting gas.

The environment in all elevated-temperature tests (creep-rupture, fatigue, etc.) will be monitored by a combination of an on-line chromatograph (H_2, CO, CO_2, N_2, CH_4, and O_2 determinations), a trace moisture analyzer (H_2O), and a solid-state oxygen-potential meter. This equipment is on hand.

5.7 REFERENCES

1. C. R. Brinkman, *Mechanical Properties Test Data for Structural Materials Quart. Progr. Rep. Jan. 31, 1974*, ORNL-4948, pp. 221–26.
2. C. R. Brinkman, *Mechanical Properties Test Data for Structural Materials Quart. Progr. Rep. April 30, 1974*, ORNL-4963, pp. 119–26.
3. L. D. Blackburn, Hanford Engineering Development Laboratory, private communication, November 1973.
4. R. W. Swindeman and C. E. Pugh, Symposium on Elevated Temperature Properties of Austenitic Stainless Steels, The American Society of Mechanical Engineers, New York, June 1974.
5. R. K. Penny and D. L. Marriott, *Design for Creep*, McGraw-Hill, New York, 1971.
6. A. Kirsch, Paper 62, pp. 1-81 to 1-89, *Joint International Conference on Creep*, The Institute of Mechanical Engineers, London, 1963.
7. H. E. McCoy, *Mechanical Properties Test Data for Structural Materials Quart. Progr. Rep. April 30, 1974*, ORNL-4963, pp. 110–23.
8. *Effects of Residual Elements on Properties of Austenitic Stainless Steels, Spec. Tech. Publ.* 418, American Society for Testing and Materials, Philadelphia, 1967.
9. K. I. Irvine, T. Gladman, and F. B. Pickering, "The Strength of Austenitic Stainless Steels," *J. Iron Steel Inst.* 207: 1017–28 (1969).
10. D. J. Dyson and B. Holmes, "Effect of Alloying Additions on the Lattice Parameter of Austenite," *J. Iron Steel Inst.* 208: 469–74 (1970).
11. P. Soo and W. H. Horton, *The Effect of Carbon and Nitrogen on the Short-Term Tensile Behavior of Solution-Treated Types 304 and 316 Stainless Steels*, WARD-NA-3045-2 (July 1973).
12. J. V. Heger and G. V. Smith, eds., *Elevated Temperature Properties as Influenced by Nitrogen Additions to Types 304 and 316 Austenitic Stainless Steels, Spec. Tech. Publ.* 522, American Society for Testing and Materials, Philadelphia, 1973.
13. K. Natesan, T. F. Kassner, and Che-Yu Li, "Effect of Sodium on Mechanical Properties and Friction-Wear Behavior of LMFBR Materials," *Reactor Technol.* 15: 244–77 (Winter 1972–73).

14. J. W. Woods, *Mechanical Properties Test Data for Structural Materials Quart. Progr. Rep. Jan. 31, 1974,* ORNL-4948, pp. 226–30.

15. J. P. Hammond and M. W. Moyer, *Mechanical Properties Test Data for Structural Materials Quart. Progr. Rep. April 30, 1974,* ORNL-4963, pp. 126–33.

16. J. A. Clinard and J. S. Crowell, *ORNL User's Manual for CREEP-PLAST Computer Program,* ORNL-TM-4062 (November 1973).

17. C. E. Pugh, et al., *Currently Recommended Constitutive Equations for Inelastic Design Analysis of FFTF Components,* ORNL-TM-3602, (September 1972).

18. S. P. Timoshenko and J. M. Gere, *Theory of Elastic Stability,* 2nd ed., McGraw-Hill, New York, 1961.

19. R. T. King and G. M. Goodwin, *Fuels and Materials Development Program Quart. Progr. Rep. Sept. 30, 1972,* ORNL-TM-4055, pp. 5.14–5.16.

20. B. Dewey, ibid., pp. 5.53–5.55.

21. R. G. Berggren and R. T. King, *Mechanical Properties Test Data for Structural Materials Quart. Progr. Rep. April 30, 1974,* ORNL-4963, pp. 143–51.

22. R. T. King and E. Bolling, *Fuels and Materials Development Program Quart. Progr. Rep. Sept. 30, 1972,* ORNL-TM-4055, pp. 5.24–5.27.

23. R. T. King, J. O. Stiegler, and G. M. Goodwin, *Properties of Thick Type 308 Stainless Steel Welds with Controlled Residual Elements,* ORNL-TM-4206 (June 1974).

24. R. T. King and G. M. Goodwin, *Fuels and Materials Development Program Quart. Progr. Rep. Dec. 31, 1971,* ORNL-TM-3703, pp. 209–15.

25. R. T. King, R. E. Adams, and G. M. Goodwin, *Fuels and Materials Development Program Quart. Progr. Rep. Mar. 31, 1972,* ORNL-TM-3797, pp. 210–20.

26. R. T. King, J. K. Alley, and E. Bolling, *Fuels and Materials Development Program Quart. Progr. Rep. Mar. 31, 1973,* ORNL-TM-4250, pp. 139–51.

27. R. T. King and E. Bolling, *Mechanical Properties Test Data for Structural Materials Quart. Progr. Rep. April 30, 1974,* ORNL-4963 pp. 140–43.

42. P. Patriarca, "CRBRP Steam Generator Meeting," minutes of a meeting held at Oak Ridge National Laboratory, June 5–6, 1974.

43. R. L. Klueh, *Effect of Carbon on the Mechanical Properties of 2 1/4 Cr-1 Mo Steel*, ORNL-4922 (November 1973).

44. J.G.Y. Chow, *Quarterly Progress Report on High Cycle Fatigue of LMFBR Materials Sponsored By the Division of Reactor Development and Technology, USAEC, July 1–September 30, 1972*, BNL–50376, pp. 1–7.

45. D. O. Hobson and T. L. Hebble, *Fuels and Materials Development Program Quart. Progr. Rep. Mar. 31, 1974*, ORNL-TM-4620, pp. 44–47.

46. P. L. Rittenhouse, D. O. Hobson, and T. L. Hebble, *Fuels and Materials Development Program Quart. Progr. Rep. Dec. 31, 1973*, ORNL-TM-4524, pp. 48–52.

47. G. J. Lieberman and R. G. Miller, Jr., "Simultaneous Tolerance Intervals in Regression," *Biometrika* 50: 155–68 (1963).

48. R. L. Klueh, *Fuels and Materials Development Program Quart. Progr. Rep. Mar. 31, 1974*, ORNL-TM-4620, pp. 36–46.

49. R. W. Swindeman, "Exploratory Testing to Identify Behavioral Features," in *Mechanical Properties Test Data for Structural Materials Quart. Progr. Rep. April 30, 1974*, ORNL-4963, pp. 174–95.

50. C. E. Jaske, *High-Temperature Structural Design Methods for LMFBR Components Progr. Rep. Oct. 1972–Mar. 1973*, ORNL-TM-4089, pp. 231–39.

51. C. C. Schultz, "Investigations of Creep Failure under Uniaxial and Multiaxial Conditions," *High-Temperature Structural Design Methods for LMFBR Components Progr. Rep. July–December 1973*, ORNL-4947, pp. 75–103.

52. P. L. Rittenhouse, *Mechanical Properties Test Data for Structural Materials Quart. Progr. Rep. April 30, 1974*, ORNL-4963, pp. 195–97.

28. *Interpretations of ASME Boiler and Pressure Vessel Code, Case 1331-8,* The American Society of Mechanical Engineers, New York, 1973.

29. D. O. Hobson and T. L. Hebble, *Mechanical Properties Test Data for Structural Materials Quart. Progr. Rep. Oct. 31, 1973,* ORNL-4936, pp. 111–18.

30. R. L. Klueh, *Fuels and Materials Development Program Quart. Progr. Rep. Mar. 31, 1974,* ORNL-TM-4620, pp. 26–32.

31. J. H. Holloman, "Tensile Deformation," *Trans. AIME* 162: 268 (1945).

32. P. Ludwik, *Elemente der Technologischen Mechanik,* Springer, Berlin, 1900.

33. E. Voce, "The Relationship Between Stress and Strain for Homogeneous Deformation," *J. Inst. Metals* 74: 537 (1948).

34. D. C. Ludwigson, "Modified Stress-Strain Relation for FCC Metals and Alloys," *Met Trans.* 2: 2825 (1971).

35. R. L. Klueh, *Fuels and Materials Development Program Quart. Progr. Rep. Dec. 31, 1973,* ORNL-TM-4524, pp. 37–45.

36. G. V. Smith, *Supplement Report on the Elevated-Temperature Properties of Chromium-Molybdenum Steels (an Evaluation of 2 1/4 Cr-1 Mo Steel), ASTM Data Ser. Publ.,* DS 6-S2, American Society for Testing and Materials, Philadelphia, March 1971.

37. R. L. Klueh, *Fuels and Materials Development Program Quart. Progr. Rep. Mar. 31, 1974,* ORNL-TM-4620, pp. 33–35.

38. L. H. Kirschler, R. H. Hiltz, and S. J. Rodgers, *The Effect of High-Temperature Sodium on the Mechanical Properties of Candidate Alloys for the LMFBR Program Final Report,* MSAR-70-76 (May 1970).

39. R. H. Hiltz, L. H. Kirschler, and R. C. Andrews, *Tensile Strength of Standard 2 1/4 Cr-1 Mo Steel after 20,000-hr Exposure in 1050°F Sodium,* MSAR-71-78 (April 1971).

40. R. H. Hiltz, L. H. Kirschler, and R. C. Andrews, *Tensile Strength of Standard 2 1/4 Cr-1 Mo Steel after 10,000, 20,000, and 26,000-hr Exposures in 1050°F Sodium,* MSAR-72-286 (December 1972).

41. R. H. Hiltz and L. H. Kirschler, *Effect of High-Temperature Sodium on the Mechanical Properties of Candidate Alloys for the LMFBR Program,* MSAR-69-139 (July 1969).

6. WESTINGHOUSE ADVANCED REACTORS DIVISION

E. C. Bishop

6.1 INTRODUCTION

The program being performed at Westinghouse Advanced Reactors Division (ARD) is entitled "Validation of High Temperature Design Methods and Criteria," (189a No. 04165). Two of the tasks in this program are "Basic Specimen Testing" and "Tubular Specimen Testing". The objective of these tasks is to design and test specimens of increasing complexity to determine the inelastic behavior and strain tolerances of Types 304 and 316 stainless steel under complex stress distributions. This report covers the work performed during the period from March 1, 1974 to May 31, 1974.

6.2 BASIC SPECIMEN TESTING - N. J. Ettenson, M. Manjoine (Westinghouse Research Laboratories)

A variety of specimen designs have been selected for this task, as shown in Table 6.1 and Figure 6.1. Data obtained to date are presented in Table 6.2.

6.2.1 Uniaxially Loaded Specimen Models with Uniform Gage Section (304 SS, Heat 9T2796)

6.2.1.1 Test Piece Description

Types A, B, and G test piece designs, as shown in Table 6.1, are used for this part of the test program.

6.2.1.2 Current Results

The A, B, and G type test pieces were completed during the current period with test results shown in Table 6.2. A comparison of the data is shown in Figure 6.2. The rupture data for the plane stress specimen, Type A, is practically the same as the ORNL data; the B type with some degree of plane strain due to the width to thickness ratio of 10, and the G type with a lateral restriction at the ends of the gage sections of

Table 6.1 Model Types

Specimens From Base Material

Code Designation	Description
A.	Plane Stress Specimen 1/3 x 2/3 x 3 in. (8.5 x 17 x 76.2 mm) gage section.
B.	Plate Specimen 1/3 x 10/3 x 3 in. (8.5 x 85 x 76.2 mm) gage section.
C.	Plate Specimen with Central Hole of 1/3 in. (8.5 mm) Diameter, 1/3 x 10/3 x 3 inc. (8.5 x 85 x 76.2 mm) plate section.
D.	Round Circumferentially Notched Specimen, Major Diameter = 0.96 in. (24.4 mm), Minor Diameter = 0.64 in. (16.2 mm), K_t = 4, Root Radius = 0.018 in. (0.46 mm), Two nearly identical notches in specimen.
E.	Plate Specimen in bending and tension, 1/3 x 10/3 x 2 in. (8.5 x 85 x 50.8 mm) plates section, eccentric load
F.	Designation generally refers to failure or fracture; therefore, it is not used to identify a type of model.
G.	Plane Strain Specimen 1/3 x 10/3 x 1 in. (8.5 x 85 x 26 mm) gage section, Ends constrained in transverse direction
H.	Biaxially Loaded Notched Plates, Wedge-opening-loaded Plates with 1/3 in. (8.5 mm) Diameter Notch.

Specimen With Welds

BTW - B-type plate specimen with transverse weld at mid-length of gage section.

BAW - B-type plate specimen with axial weld at center of gage section.

CTW - C-type specimen with hole through transverse weld

CAW - C-type specimen with hole through axial weld

DTW - D-type specimen with notch root in transverse weld

DZTW - D-type specimen with notch root at weld fusion line of heat affected zone.

GTW - G-type specimen with transverse weld at mid-gage length.

GAW - G-type specimen with axial weld at center of gage section.

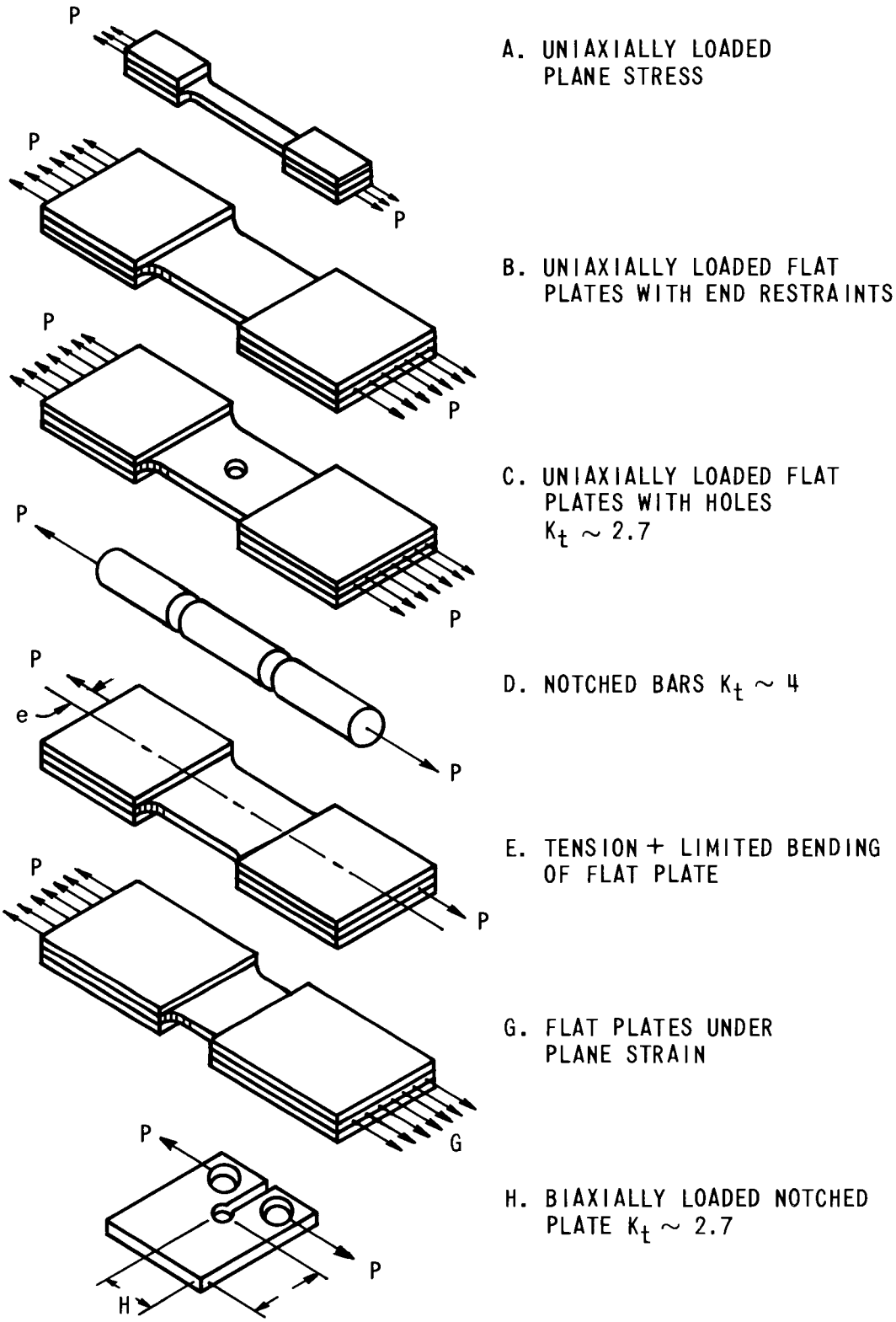

Figure 6-1 Basic Specimen Types

Table 6.2 Summary of Creep Data, Type 304 Stainless Steel* at 1100°F (593°C)

Test No. (Gage Section)	Loading Data			Creep Data					
	Stress		Plastic Strain	Creep Rate	Increment		Accumulated		Permanent Strain
	(ksi)	(MPa)	(%)	(%/hr)	Strain (%)	Time (hr)	Strain (%)	Time (hr)	(%)
A1	21.0	144.8	4.66	2.2×10^{-3}	1.10	303	1.10	303[a]	5.76
(1/2x2/3x3 in)				2.2×10^{-3}	0.89	403	1.99	706[a]	6.65
(8.5x17x76.2mm)							3.47	1250[b]	8.13
							3.65	1270[c]	8.31
							7.34	1826	12.00[d]
A2	10.0	68.95	0.215	8.5×10^{-5}	0.228	2180	0.228	2180[a]	0.443
(1/3x2/3x3 in)				6.2×10^{-5}	0.028	405	0.256	2585[e]	0.471
(8.5x17x76.2mm)	11.0	75.84	0	8.6×10^{-5}	0.124	1349	0.380	3934[e]	0.595
	12.5	85.68	0	2.0×10^{-4}	0.213	1002	0.593	4936[e]	0.808
	15.0	103.4	0.014	2.5×10^{-4}	0.811	1848	1.404[a]	6784[e]	1.619
	21.0	144.8	0.646	4.5×10^{-3}	28.75	4266	30.15	11050[h]	31.0
B1	21.0	144.8	5.34	1.4×10^{-3}	1.76	666	1.76	666[a]	7.10
(1/3x10/3x3 in)				8.8×10^{-4}	1.03	1005	2.79	1671[a]	
(8.5x85x76.2mm)				1.7×10^{-3}				3000[c]	
					1.72	1587	4.51	3258[a]	9.85[g]
								3525[h]	
B2	10.0	68.95	0.273[i]	8.6×10^{-5}	0.31	1644	0.31	1644[a]	0.58
(1/3x10/3x3 in)	j			9.0×10^{-5}	0.14	1462	0.45	3106[e]	0.72
(8.5x85x76.2mm)	11.0	75.84	0	1.1×10^{-4}	0.16	1804	0.61	4910[e]	0.88
	12.5	85.68	0	2.0×10^{-4}	0.33	1364	0.94	6274[e]	1.21
	15.0	103.4	0.051	4.7×10^{-4}	1.00	1302[a]	1.93	7576[e]	1.98
	21.0	144.8	1.88	8.4×10^{-3}	16.47	1563	18.40	9139[h]	20.33

*HT 9T2796, annealed 2000F (1094C)

[a]Interrupted for photographic measurement

[b]Transition at 0.2% OFFSET

[c]Transition at double minimum rate

[d]Rupture, R

[e]Stress raised (step-loaded test)

[f]Test in progress

[g]Crack initiated

[h]Test terminated, crack tearing

[i]Strain gage average, bending noted

[j]Specimen rotated 180° to investigate bending

[k]Net Section Stress, Gross Section Stress = 0.9 N.S.S.

[l]Time at final strain

[m]Average overall strain

[p]Test in preparation

[q]Specimen to be sectioned to determine damage at 78% of estimated rupture life

[r]Deflection of notch, inches (25.4 mm)

[t]True strain = In(Ao/A)

[u]Test interrupted, 1/2 of specimen continued

Table 6.2 (Continued)

Test No. (Gage Section)	Loading Data			Creep Data					
	Stress		Plastic Strain	Creep Rate	Increment		Accumulated		Permanent Strain
	(ksi)	(MPa)	(%)	(%/hr)	Strain (%)	Time (hr)	Strain (%)	Time (hr)	(%)
C1	23.3[k]	160.6	8[n]		1.7[n]	100[c]			
(1/3x10/3x3in)							22.9[n]	138[d]	
(8.5x85x76.2mm)									
Central Hole									
1/3in(8.5mm)dia.									
C2	10.0[k]	68.95	0.14[n]		0.62[n]	2808[a]	0.62[n]	2808[e]	0.76[n]
Same as C1	11.0[k]	75.84	0		0.40[n]	1290	1.02[n]	4098	1.16[n]
	12.5[k]	85.68	0		0.50[n]	1300[a]	1.52[n]	5398	1.66[n]
	15.0[k]	103.4	0.28[n]		0.82[n]	1148	2.34[n]	6546	2.76[n]
	18.0[k]	124.1	0.06[n]		3.31[n]	1630[a]	5.65[n]	8176[g]	6.13[n]
					0.89[n]	791[a]	6.54[n]	8967	7.02[n]
					1.05[n]	944[a]	7.59[n]	9911	8.07[n]
					1.12[n]	1339[a]	8.71[n]	11250	9.19[n]
					1.60[n]	1468 6172[l]	10.30	12718[h]	10.79
C3	21.0[k]	144.8	4.4[n]		1.5[n]	325[c]			
Same as C1							4.1[n]	397[h]	8.5[n]
D1	30.0	206.8							
D=.96 in(24.4mm)									
d=.64 in(16.2mm),									
R=.19 in(0.46mm)									
D1-1	30.0	206.8	2.60[t]		0.30[t]	137	0.30[t]	137	2.90[t]
					0.20[t]	102	0.50[t]	239[g]	3.10[t]

[*] HT 9T2796, annealed 2000F (1094C)

[a] Interrupted for photographic measurement

[b] Transition at 0.2% OFFSET

[c] Transition at double minimum rate

[d] Rupture, R

[e] Stress raised (step-loaded test)

[f] Test in progress

[g] Crack initiated

[h] Test terminated, crack tearing

[i] Strain gage average, bending noted

[j] Specimen rotated 180° to investigate bending

[k] Net Section Stress, Gross Section Stress = 0.9 N.S.S.

[l] Time at final strain

[m] Average overall strain

[p] Test in preparation

[q] Specimen to be sectioned to determine damage at 78% of estimated rupture life

[r] Deflection of notch, inches (25.4 mm)

[t] True strain = In(Ao/A)

[u] Test interrupted, 1/2 of specimen continued

Table 6.2 (Continued)

Test No. (Gage Section)	Loading Data			Creep Data					
	Stress		Plastic Strain	Creep Rate	Increment		Accumulated		Permanent Strain
	(ksi)	(MPa)	(%)	(%/hr)	Strain (%)	Time (hr)	Strain (%)	Time (hr)	(%)
D1-2	30.0	206.8	2.20[t]		0.26[t]	137	0.26[t]	137	2.46[t]
					0.22[t]	113	0.48[t]	250[c]	2.68[t]
							10.92[t]	305[d]	13.12[t]
D2-1	25.0	172.4	0.009[r]				0.006[r]	1371	0.015[r]
								1371[g]	2.17[t]
D2-2	25.0	172.4	0.009[r]				0.006[r]	1240[c]	
								1371[d]	5.3[t]
D3	21.0	144.8	0.002[r]					5499[h]	
D4	10.0	68.95	0			406		406[e]	
	11.0	75.84	0			477		883[e]	
	12.5	85.68	0			434		1317[e]	
	15.0	103.40	0			404		1721[e]	
	21.0	144.80	0.001[r]		0.004[r]	433		2154[e]	
	25.0	172.40	0.003[r]		0.033[r]	1581[g]		3735[u]	
D4-1	One Notch of Specimen D4 to Be Sectioned.								
D4-2	25.0	172.40				2904[h]		5058[h]	
D5	23.0	158.4				1681[g]		1681	
D5-1	One Notch of Specimen D5 to Be Sectioned.								
D5-2	23.0	158.4				150		1831[d]	
D6	20.0	137.9			1.0[t]	4023[u]			

[*] HT 9T2796, annealed 2000F (1094C)

[a] Interrupted for photographic measurement

[b] Transition at 0.2% OFFSET

[c] Transition at double minimum rate

[d] Rupture, R

[e] Stress raised (step-loaded test)

[f] Test in progress

[g] Crack initiated

[h] Test terminated, crack tearing

[i] Strain gage average, bending noted

[j] Specimen rotated 180° to investigate bending

[k] Net Section Stress, Gross Section Stress = 0.9 N.S.S.

[l] Time at final strain

[m] Average overall strain

[p] Test in preparation

[q] Specimen to be sectioned to determine damage at 78% of estimated rupture life

[r] Deflection of notch, inches (25.4 mm)

[t] True strain = In(Ao/A)

[u] Test interrupted, 1/2 of specimen continued

Table 6.2 (Continued)

Test No. (Gage Section)	Loading Data: Stress (ksi)	Stress (MPa)	Plastic Strain (%)	Creep Data: Creep Rate (%/hr.)	Increment: Strain (%)	Increment: Time (hr)	Accumulated: Strain (%)	Accumulated: Time (hr)	Permanent Strain (%)
G1	25.0	172.4	2.00[i]		0.88[i]	47[a]	0.88	47	2.47
				3.5×10^{-3}	1.12[i]	268[a]	2.00	315	4.00
				——	0.90[i]	170[a]	2.90[c]	485[g]	4.90
				——	0.65[i]	83	3.55	568[h]	5.60
G2	21.0	144.8	0.43	3.9×10^{-4}	1.34	1195[a]	1.34	1195	1.77
(1/3x10/3x1 in)			0	1.0×10^{-4}	0.83	5520[a]	2.17	6715[e]	2.60
(8.5x85x25mm)	25.0	172.4	0.01	2.3×10^{-3}	1.80	700	——	7415	——
				——	2.50	450[c]	4.67	7865	——
				——	4.43	283[a]	6.60	8148	——
				——	——	1827[l]	——	8552[d]	——
BAW-1	25.0	172.4	0.25	8.3×10^{-3}	4.35[n]	477[a]	4.35	477	4.60[g]
B Type Specimen				1.1×10^{-2}	8.32[n]	765[a]	12.67	1242	12.92
With Central Axial				1.5×10^{-2}	3.42[n]	216[a]	16.09	1458	16.34
Weld				——	2.35[n]	71	18.44	1529	18.69
				——	——	——	——	1532[d]	——
CAW-1	18.0	124.1	0.05	——	0.42	791[f]	——	——	——
C Type Specimen									
With Central Axial									
Weld									
GAW-1	23.0	158.6	0.10[n]	5.1×10^{-3}	1.56[n]	1882	1.56[n]	188	1.65[n]
G. Type Specimen				4.2×10^{-3}	1.93[n]	452[a]	3.59[n]	640	3.69[n]
With Axial				5.3×10^{-3}	1.64[n]	307[a]	5.13[n]	947	5.23[n]
Weld				5.3×10^{-3}	2.00[n]	379[a]	7.13[n]	13269	7.23[n]
				——	2.21[n]	456[a]	9.34[n]	1782	9.44[n]
					0.64[n]			1901[f]	
BTW-1	21.0	144.8	0.17[n]	3.2×10^{-3}	1.29[n]	339[a]	1.29[n]	339	1.47[n]
B Type Specimen			0.01	3.2×10^{-3}	2.35[n]	718[a]	3.64[n]	1057[g]	3.82[n]
With Transverse					1.25[n]	474[a]	4.89[n]	1531	5.07[n]
Weld							5.67[n]	1724	
								1734[d]	
GTW-1	25.0	172.4	0.09	4.7×10^{-3}	1.62[n]	240[a]	1.62	240	1.71
G Type Specimen				——	——	208	——	448[d]	——
With Transverse Weld									

[*] HT 9T2796, annealed 2000F (1094C)

[a] Interrupted for photographic measurement

[b] Transition at 0.2% OFFSET

[c] Transition at double minimum rate

[d] Rupture, R

[e] Stress raised (step-loaded test)

[f] Test in progress

[g] Crack initiated

[h] Test terminated, crack tearing

[i] Strain gage average, bending noted

[j] Specimen rotated 180° to investigate bending

[k] Net Section Stress, Gross Section Stress = 0.9 N.S.S.

[l] Time at final strain

[m] Average overall strain

[p] Test in preparation

[q] Specimen to be sectioned to determine damage at 78% of estimated rupture life

[r] Deflection of notch, inches (25.4 mm)

[t] True strain = In(Ao/A)

[u] Test interrupted, 1/2 of specimen continued

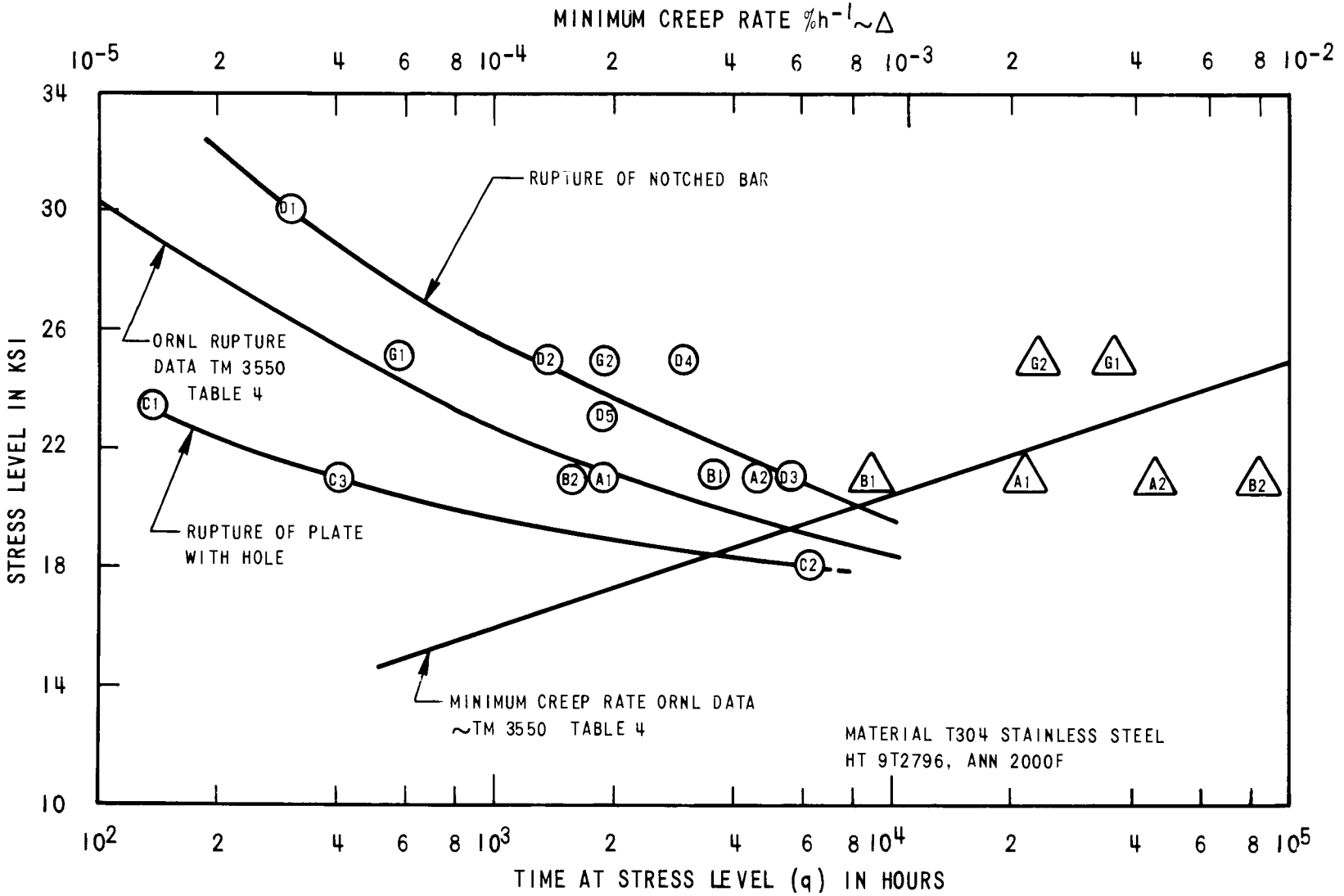

Figure 6-2 Basic Specimen Creep Data at 1100°F

3 and 1 inches, have higher rupture and creep strengths when tested under single constant load. The effects on the rupture and creep strengths for the step loading test of B and G specimens were inconsistent and may be a result of the non-uniform time at the various increasing stress levels.

6.2.2 Uniaxially Loaded Specimen Models with Non-Uniform Gage Section

6.2.2.1 Test Piece Description

Types C, D, and E test piece designs, as shown in Table 6.1, are used for this part of the test program.

6.2.2.2 Current Results

Current results are presented in Table 6.2.

The Type C specimens show a lower strength than for the Type B specimen that are tested at the same net section stress. It is hypothesized that the lower strength is caused by the high strain concentration at the edges of the hole where biaxial stresses are generated and, therefore, less reduction of effective stress. The major damage is an exhaustion of ductility by the high local strains. Further analysis will be used to evaluate the damage functions presented in the quarterly report WARD-HT-3045-4.[1] Another test is planned for the Type C specimen that will be loaded to a constant net section stress of 18 ksi.

The circumferentially notched bars, Specimen D, show a notch strengthening over the range of stresses investigated. The ratio of the notch strength to that of the unnotched after 8000 hours of testing is estimated to be about 1.08 for the notch with an elastic stress concentration factor of 4. This strengthening is a result of the relaxation of peak stresses due to the plastic flow-on loading and the creep strains, which generate triaxially and lower effective stresses without

initiating fracture.

6.2.3 Specimens with Welds (304 SS Heat 9T2796)

6.2.3.1 Test Piece Description

The weld specimens are described in Table 6.1 and Figure 6.1.

6.2.3.2 Current Results

The data for the welded specimens are illustrated in Figure 6.3. The rupture curves for the base metal and the all-weld-metal are presented with the minimum creep rate curve for the base metal. Although the amount of data is minimal, the axial welded specimens appear to be stronger than the transverse welded specimens and the composite specimens are weaker than the all-weld-metal specimens.

Specimen DZTW was tested at 25 ksi and 1100°F and failure appeared to initiate in the heat affected zone after 978 hours. The fracture propagated around the minimum cross-section until the final failure occurred through the weld metal.

6.2.4 Topical Report

A topical report is being prepared to present all of the results and interpretation from specimen types A, B, and G.

6.3 TUBULAR SPECIMEN TESTING - K. C. Thomas, P. C. S. Wu

6.3.1 Test Piece Description

The tubular test pieces used in this program are 304SS, Heat 9T2796, 1.8 inch OD and 1.6 inch ID and 8.7 inch length. However, thinner wall (1.7 inch OD and 1.6 inch ID) test pieces are being considered for use in future tests to reduce the stress variation through the wall thickness during multiaxial testing.

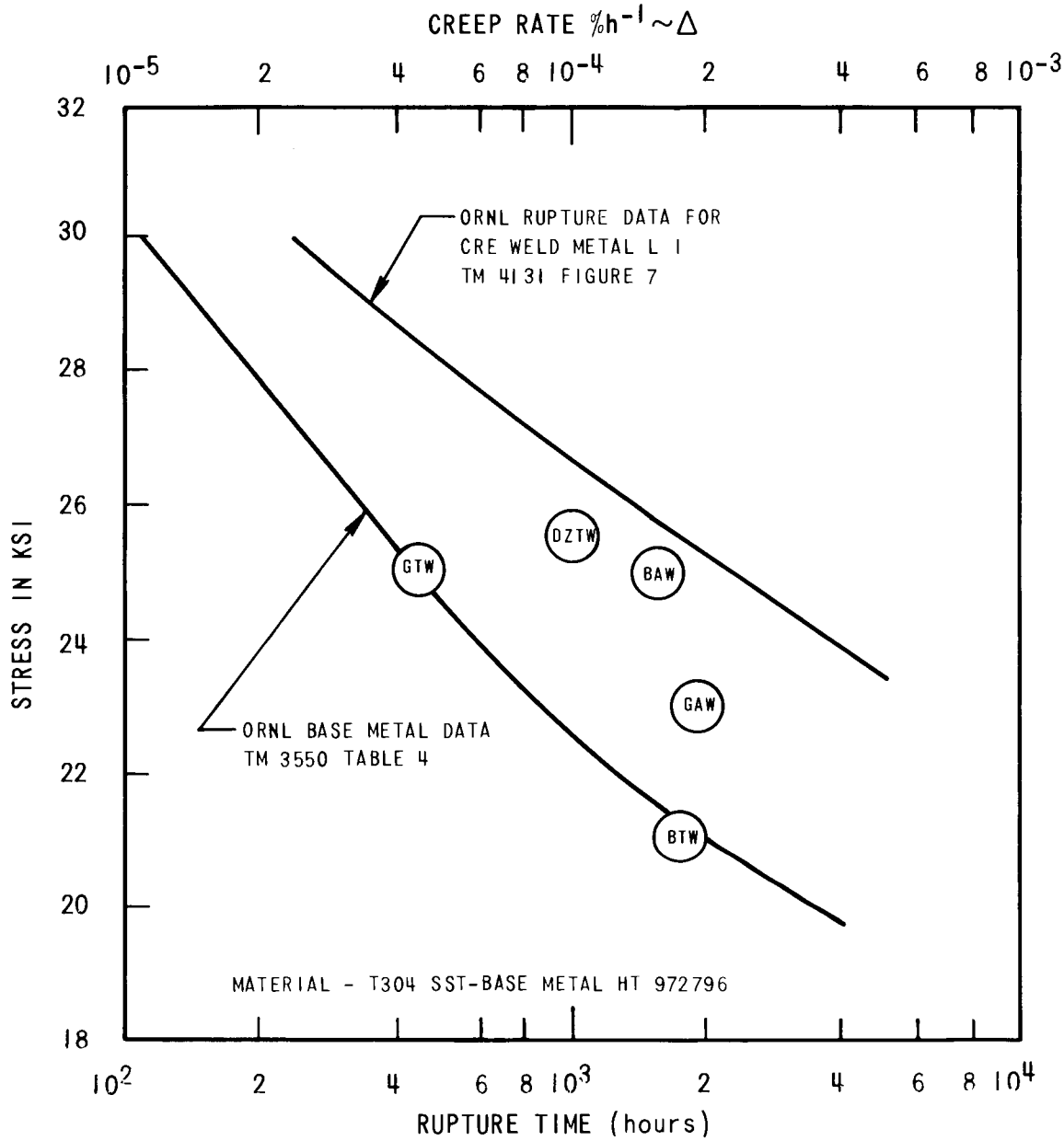

Figure 6-3 Basic Specimen Creep Data for Welds at 1100°F

6.3.2 Test Results and Planning (304SS, Heat 9T2796 ORNL Reference Heat)

The test plan for the Uniaxial Tubular Specimen Testing Program and current status are shown in Table 6.3. At the present time, all of the original uniaxial creep tests including the additional tests have been completed. The tests were carried out at 1100°F (866°K) with the stress level ranging from 5000 to 25,000 psi (447×10^7 to 1.723×10^8 Pascal). Preliminary analyses of the uniaxial creep data for the tubular specimens have shown that the constants ε_t and $\dot{\varepsilon}_m$ in Equation (1)

$$\varepsilon - \varepsilon_L = \varepsilon_t (1-e^{-rt}) + \dot{\varepsilon}_m t \qquad (1)$$

are both continuous functions of stress ranging from 7,700 to 25,000 psi (5.308×10^7 to 1.723×10^8 Pascal) at 1100°F (866°K). However, the constant r is a continuous function of stress only above 10,000 psi (6.894×10^7 Pascal). At 7,700 psi (5.308×10^7 Pascal) the value of r does not follow the extrapolation of high stress values. The results obtained on uniaxial creep test, No. 3D12, at 5,000 psi (3.447×10^7 Pascal) are being analyzed and the information obtained will better clarify the stress dependence of the constant r. The results obtained for the uniaxial creep tests are summarized in Table 6.4. Uniaxial creep test No. 3F at a stress level of 15,000 psi (1.034×10^8 Pascal) is still tentative at the present time and this test will be carried out if additional machine time should become available before testing Type 316 stainless steel specimens.

The effective stress for all the tests shown in the original multiaxial creep test matrix for the Type 304 stainless steel tubular specimens was calculated based on thick cylinder formula.[1] Since thin cylinder formula has been used in effective stress calculations at the other institutions involved in the same test program,and also thin wall specimens will be used to reduce the stress variation across the specimen wall, thin cylinder formula was used to calculate the effective stress for all the tests yet to be carried out. The final test matrix

Table 6.3 Final Test Matrix for Tubular Specimens[d]

(Test Plan - Uniaxial Constant Load Specimens)

Test Number	Effective Stress σ_e[a] (psi)	Stress Ratio $\sigma_{hoop}/\sigma_{axial}$ (σ_θ/σ_z)	Loads to Obtain Nominal Desired Stresses		Nominal Test Temperature T (°F)	Nominal Test Duration t (hours)	Test Status	Remarks
			Int. Pressure p (psi)	Axial Load P (lbs)				
1A	25,000.0	0.0	0.0	6,872.2	1100	100	b	Terminated due to over temperature
1B	25,000.0	0.0	0.0	6,872.2	1100	100	b	0.050" wall thickness
2A	10,000.0	0.0	0.0	5,340.1	1100	2,000	b	Cold drawn sample
2B	10,000.0	0.0	0.0	5,340.1	1100	2,000	b	
3A	20,000.0	0.0	0.0	10,681.4	1100	2,000	b	Terminated due to pull rod failure
3B	20,000.0	0.0	0.0	10,681.4	1100	2,000	b	
3C	7,700.0	0.0	0.0	4,112.3	1100	2,000	b	Additional test
3D	5,000.0	0.0	0.0	2,670.4	1100	2,000	b	Additional test
3F	15,000.0	0.0	0.0	8,011.1	1100	2,000	c	Tentative

(a) $\sigma_e = \sigma_z = \frac{P}{2\Pi r_{av} t}$

where: r_{av} = Average radius of the tube

t = Thickness of the tube

(b) Test complete

(c) Test to be initiated

(d) All test specimens, except 1A and 1B, have 0.100" wall thickness. They are annealed at 2000°F for 30 minutes except specimen 2A which is cold drawn.

Table 6.4 Test Results - Uniaxial Creep Test

Test No.	Nominal Test Temperature (°F)	Axial Stress (psi)	Test Hours Accumulated	Axial Loading Strain (%)	Axial Creep Strain[a] (%)	Total Axial Strain (%)
1B	1100	25,000	241.5	0.7988	3.5572	4.3660
2A	1100	10,000	2016	0.0490	0.0697	0.1187
2B	1100	10,000	2000	0.0780	0.0880	0.1660
3A	1100	20,000	336	- - -	0.9591	- - -
3B	1100	20,000	1990	0.1783	2.7468	2.9251
3C	1100	7,700	2002	0.0461	0.0534	0.0995
3D	1100	5,000	1721.3	0.0253	0.0089	0.0342

(a) Average of two readings.

for multiaxial creep tests of Type 304 stainless steel specimen has been completed. The test plan is shown in Table 6.5. Currently, five multiaxial creep tests are completed and three are in progress and the test results are summarized in Table 6.6. The test plan for multiaxial, variable load conditions, is shown in Table 6.7.

Multiaxial creep test No. 7A11 and uniaxial creep test No. 3D12 were completed during this report period. It was observed from the test measurements, shown in Figure 6.4, that significant discrepancies exist among the various measurements for a given test. One factor which was identified during the last report period as affecting test results significantly is fluctuations in the ambient (room) temperature. Because of the double tube construction of the extensometers, temperature changes in the inner tube lag temperature changes in the outer tube as the ambient temperature varies. This lag has been determined to be the major factor in causing the large scattering in measurements shown in Figure 6.4. A plastic enclosure was designed and constructed to encompass all machines so that ambient temperature variations will be insignificant. The extremely small amount of scattering among the test measurements shown in Figure 6.5 for multiaxial creep test No. 8 has demonstrated the intended function of the plastic enclosure.

In addition to the ambient temperature variation, other factors which might have contributed to the observed discrepancies among the measurements will also be thoroughly evaluated. A definitive plan is being established to analyze the potential factors using the "research" test setup. Knowledge obtained on these studies will have immediate impact on the Tubular Test Program concerning the refining of test specimens, equipment and test procedures.

The set of laboratory data sheets, which was developed specifically for the tubular specimen testing program, was revised and demonstrated to be very useful in facilitating the data acquisition process in the

Table 6.5 Final Test Matrix for Tubular Specimens

(Test Plan - Multiaxial Constant Load Specimens)

Test Number	Effective Stress σ_e [a] (psi)	Stress Ratio $\sigma_{hoop}/\sigma_{axial}$ (σ_θ/σ_z)	Loads to Obtain Nominal Desired Stresses: Int. Pressure p (psi)	Loads to Obtain Nominal Desired Stresses: Axial Load P (lbs)	Nominal Test Temperature T (°F)	Nominal Test Duration t (hours)	Test Status	Remarks
4	10,000.0 [e]	2.0	1209.5	323.0	1100	2,000		Terminated due to malfunction of strain measuring system
4A	10,000.0 [e]	2.0	1209.5	323.0	1100	2,000	(b)	Test No. 4 repeated
5	15,000.0 [e]	2.0	1814.3	484.0	1100	2,000	(b)	
6	20,000.0 [f]	2.0	2716.9	0.0	1100	2,000	(c)	
7	10,000.0 [e]	1.5	1180.0	1211.0	1100	2,000		Terminated due to malfunction of strain measuring system
7A	10,000.0 [e]	1.5	1180.0	1211.0	1100	2,000	(b)	Test No. 7 repeated
8	15,000.0 [f]	1.5	2000.0	1515.0	1100	2,000	(c)	
9	20,000.0 [f]	1.5	2668.4	2018.6	1100	2,000	(d)	
10	10,000.0 [e]	1.0	1049.4	2670.0	1100	2,000	(b)	
11	15,000.0 [e]	1.0	1574.0	4005.0	1100	2,000	(b)	
12	20,000.0 [f]	1.0	2353.0	5340.7	1100	2,000	(c)	

(a) Effective stress calculated as per thick cylinder formula is given by:

$$\sigma_e = \frac{1}{2}\left[(\sigma_z-\sigma_\theta)^2 + (\sigma_\theta-\sigma_r)^2 + (\sigma_r-\sigma_z)^2\right]^{1/2}$$

where: $\sigma_z = \sigma_{axial} = \frac{P}{A} + p\,\frac{a^2}{b^2-a^2}$

$\sigma_\theta = \sigma_{hoop} = p\,\frac{a^2(b^2+r^2)}{r^2(b^2-a^2)}$

$\sigma_r = \sigma_{radial} = p\,\frac{a^2(b^2-r^2)}{r^2(b^2-a^2)}$

A = Cross-sectional area of the tube

t = Thickness of the tube

a = Inside radius of the tube

b = Outside radius of the tube

r = Radius at the point under consideration. r = a, is used to calculate the maximum σ_e which occurs at the inside fiber of the tube.

Effective stress calculated as per thin cylinder formula is given by:

$$\sigma_e = \left[\sigma_\theta^2 + \sigma_z^2 - \sigma_\theta\sigma_z\right]^{1/2}$$

where: $\sigma_\theta = p\,\frac{r_{av}}{t}$

$\sigma_z = \frac{pr_{av}}{t} + \frac{P}{2\Pi r_{av} t}$

r_{av} = Average radius of the tube

t = Thickness of the tube

(b) Test completed

(c) Test in progress

(d) Test to be initiated

(e) Thick cylinder formula used to calculate σ_e

(f) Thin cylinder formula used to calculate σ_e

(g) All test specimens are annealed to 2000°F for 30 minutes

Table 6.6 Test Results - Multiaxial Creep Test

Test No.	Nominal Test Temp. (°F)	Axial Load (lbs)	Nominal Internal Pressure (psi)	Nominal Effective Stress (psi)	Nominal Principal Stress Ratio (σ_θ/σ_z)	Test Time (hours)	Average[a] Loading Strain (%)		Nominal Average Creep Strain[a]			
							Axial	Hoop	Radial	Hoop	Axial	Effective
4A	1100	323	1209.5	10,000	2.0	1965.7	0.01048	0.02174	-0.12711	0.12466	0.00245	0.14536
5	1115	484	1814.3	15,000	2.0	1998.0	0.09208	0.08499	-0.57795	0.54670	0.03125	0.64996
7[b]	1100	1211	1180.0	10,000	1.5							
7A	1100	1211	1180.0	10,000	1.5	1648.0	0.04240	0.03521	-0.02101	0.01360	0.00741	0.02110
10	1100	2670	1049.4	10,000	1.0	2033.8	0.04363	0.01994	-0.06130	0.03890	0.03330	0.06000
11	1100	4005	1574.0	15,000	1.0	2012.9	0.03288	0.07339	-0.48900	0.21100	0.27800	0.47200
6	1100	0	2716.9	20,000	2.0	304.6	0.13321	2.71103	-0.85149	0.84610	0.00539	0.5658
8	1100	1515	2000.0	15,000	1.5	209.2	0.19414	0.80047	-0.39800	0.32500	0.07300	0.42400
12	1100	5340.7	2353.0	20,000	1.0	112.3	1.82117	0.99892	-0.68300	0.34900	0.33400	0.67500

(a) The axial loading strain is the average of two readings.
The loop strain is the average of three readings.

(b) Test terminated due to instability of the strain measuring system.

Table 6.7 Final Test Matrix for Tubular Specimens

(Test Plan - Multiaxial, Variable Load (Step Loaded) Specimen)

Test Number	Effective Stress σ_e (a) (psi)	Stress Ratio $\sigma_{hoop}/\sigma_{axial}$ (σ_θ/σ_z)	Loads to Obtain Nominal Desired Stresses		Nominal Test Temperature T (°F)	Nominal Test Duration t (hours)	Test Status
			Int. Pressure p (psi)	Axial Load P (lbs)			
13	10,000.0 (e)	1.5	1180.0	1211.0	1100	1100	(d)
13 (Cont'd.)	15,000.0 (f)	1.5	2000.0	1515.0	1100	500	(d)
13 (Cont'd.)	20,000.0 (f)	1.5	2668.4	2018.6	1100	200	(d)
13 (Cont'd.)	20,000.0 (e)	1.0	2353.0	5340.7	1100	200	(d)
14	15,000.0 (f)	2.0	1814.3	484.0	1100	500	(d)
14 (Cont'd.)	15,000.0 (e)	1.5	2000.0	1515.0	1100	500	(d)
14 (Cont'd.)	15,000.0 (e)	1.0	1574.0	4005.0	1100	500	(d)
14 (Cont'd.)	15,000.0 (e)	2.0	1814.3	484.0	1100	500	(d)
15	10,000.0 (f)	2.0	1209.5	323.0	1100	1150	(d)
15 (Cont'd.)	15,000.0 (f)	1.5	2000.0	1515.0	1100	500	(d)
15 (Cont'd.)	20,000.0 (e)	1.0	2353.0	5340.7	1100	200	(d)
15 (Cont'd.)	15,000.0	2.0	1814.3	484.0	1100	200	(d)

(a) For effective stress formulas see note (a) in Table 4-3.

(d) Test to be initiated.

(e) Thick cylinder formula used to calculate σ_e; See Table 4-3 Note (a).

(f) Thin cylinder formula used to calculate σ_e; See Table 4-3 Note (a).

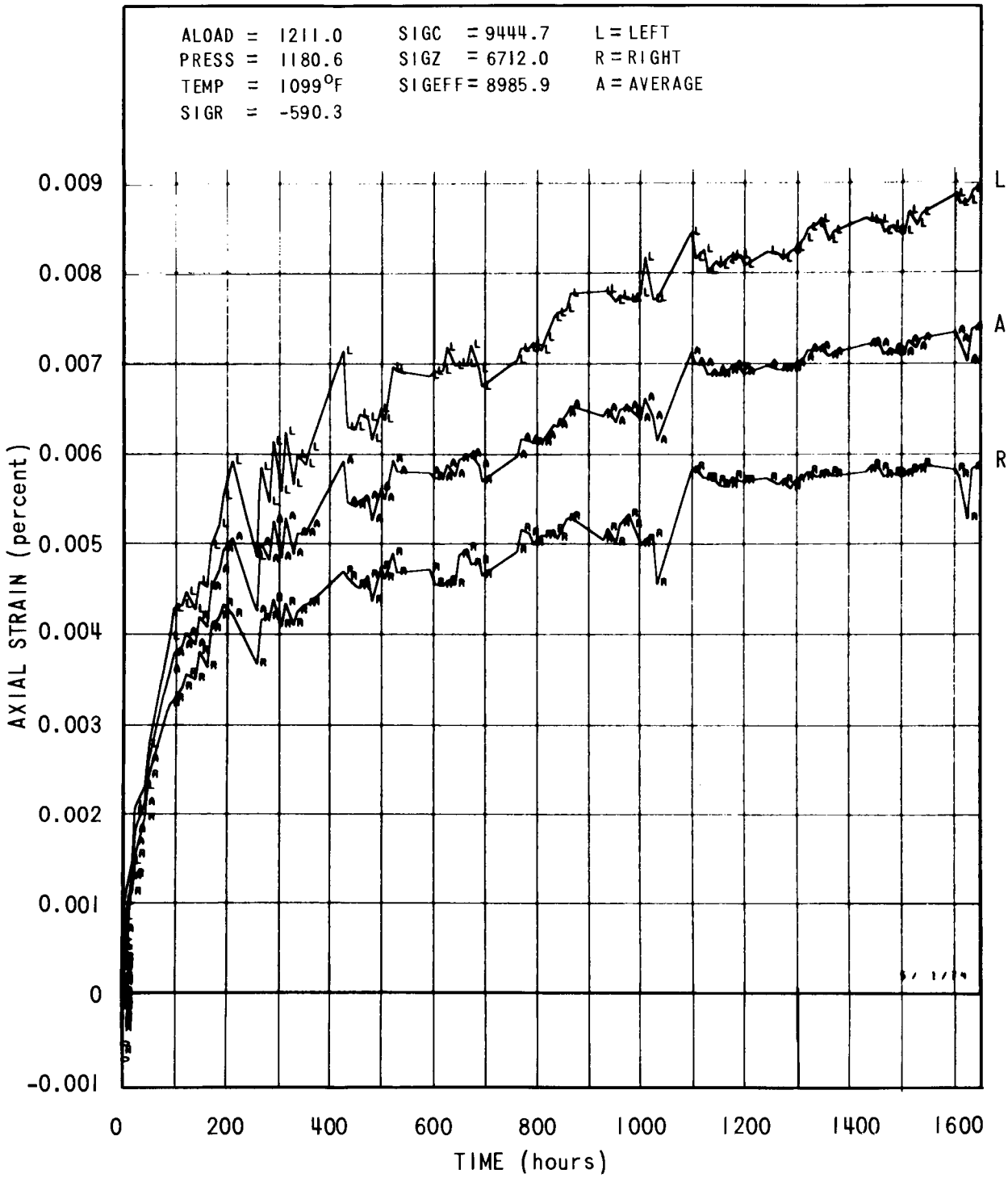

Figure 6-4 Cylindrical Specimen Creep Test 7 A11

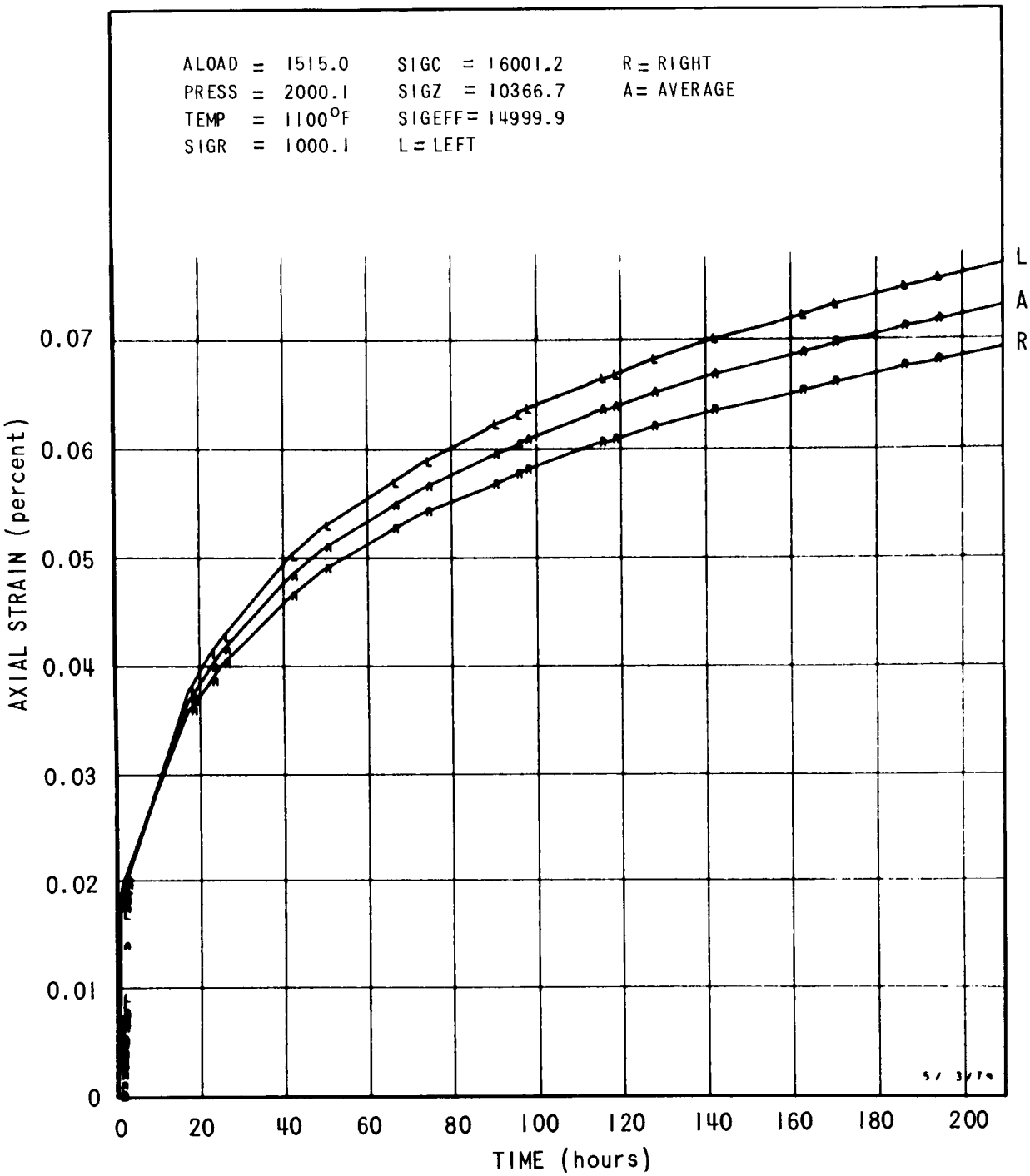

Figure 6-5 Cylindrical Specimen Creep Test 8 13

tubular specimen testing program. Measurements obtained from the completed tests, as well as from the tests in progress, are continuously compiled in the computer through the use of the newly developed semi-automatic data acquisition system.

6.3.3 Data Reduction and Analysis

A data package for the tubular specimen test program has been prepared. In this data package complete and detailed information is provided for all tests completed or in progress at WARD. The information, concerning sample histogram, geometry, fabrication and quality control, equipment and instrumentation, test conditions, etc., recorded for each test is intended to be comprehensive and sufficient to facilitate data reduction and evaluation. There are three sections in this data package. The results obtained on uniaxial and multiaxial creep tests on the Tubular Specimen Test Program are given in Section II and III, respectively. Information reported by other institutions obtained through the literature is included in Section IV so that a comparison can be made with the experimental data obtained at ARD.

Graphical displays of the results of the basic data reduction calculations of all tests completed or in progress are compiled in the Tubular Specimen Test Program Data Package. Due to the large volume of graphical displays generated, only the effective strain versus time graphs for all tests are shown in Figure 6.6 to Figure 6.17. Curve 1 is the effective strain versus time graph for the present results. Curves 2 and 3 are based on the ORNL models[2] derived from all and the 1000 hours test data respectively. Curve 4 is derived from the creep model given in the LMFBR Materials Handbook[3]. Curve 5 is based on the Blackburn 1973 creep model[4].

The test results available for uniaxial creep test covered a stress range of 5000 to 25,000 psi at 1100°F. Preliminary analyses of the test results obtained at the stress range from 7,700 to 25,000 psi were conducted and curve fitting to the creep-time data was also

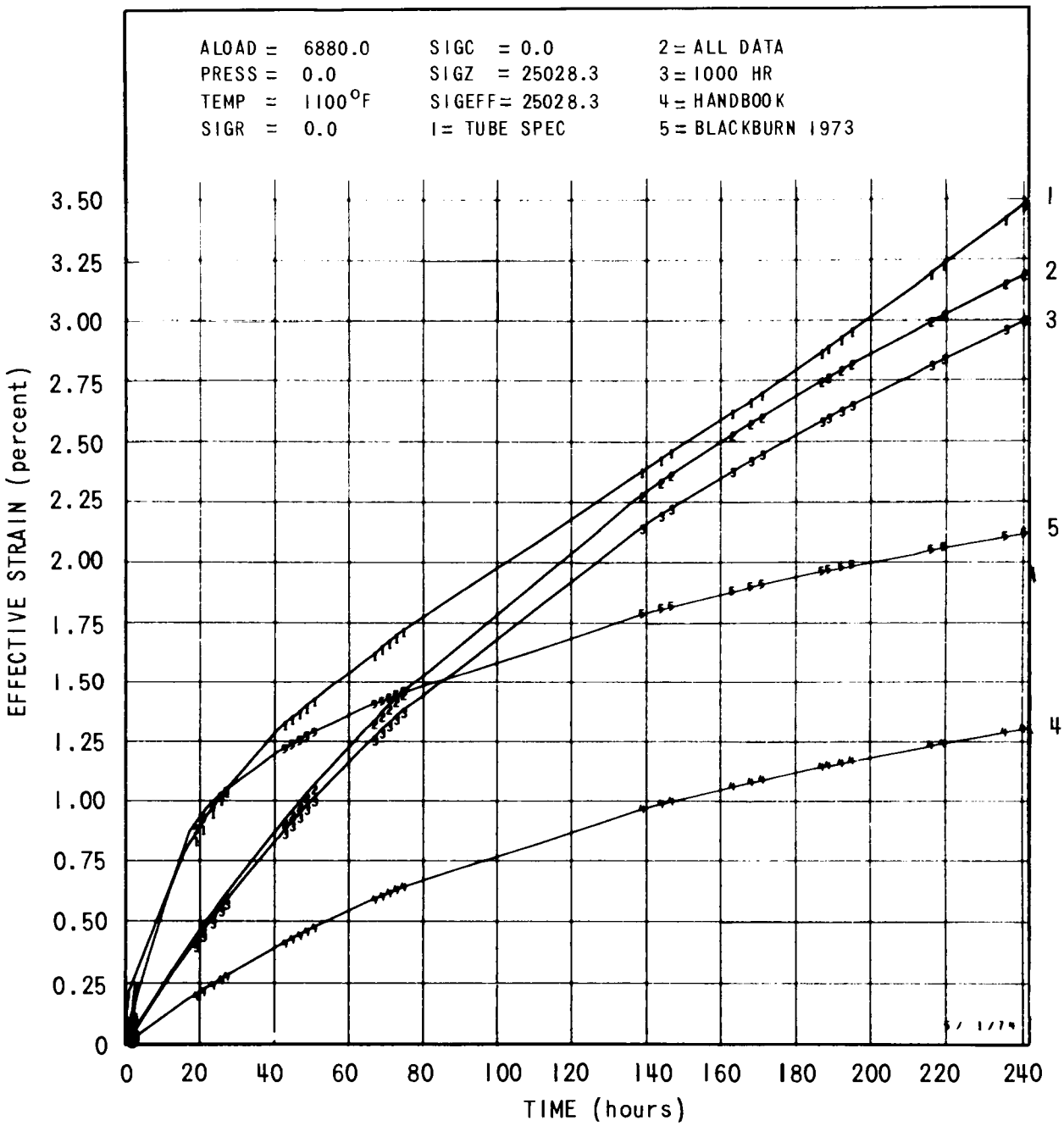

Figure 6-6 Cylindrical Specimen Creep Test 1 B51

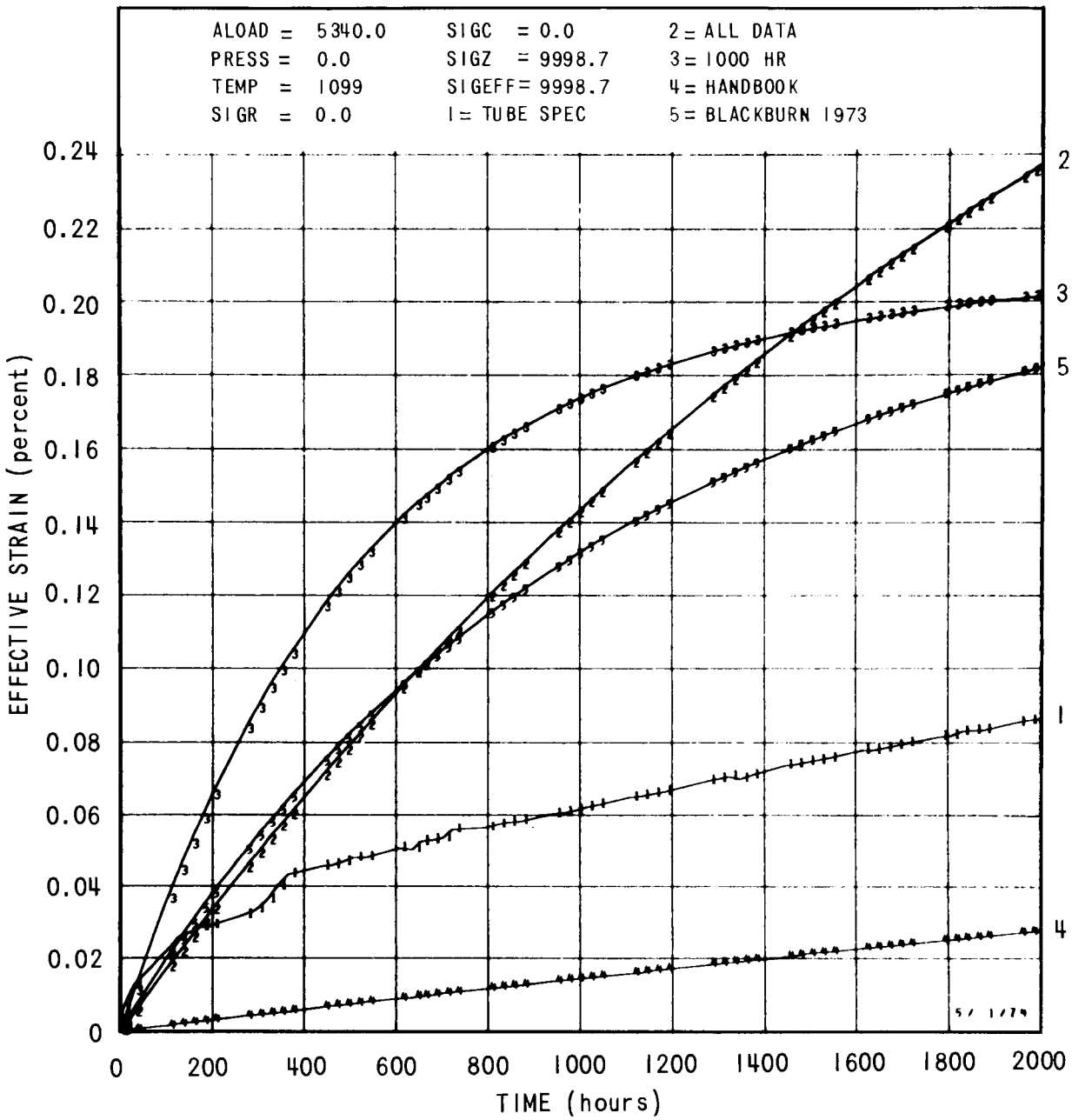

Figure 6-7 Cylindrical Specimen Creep Test 2 B54

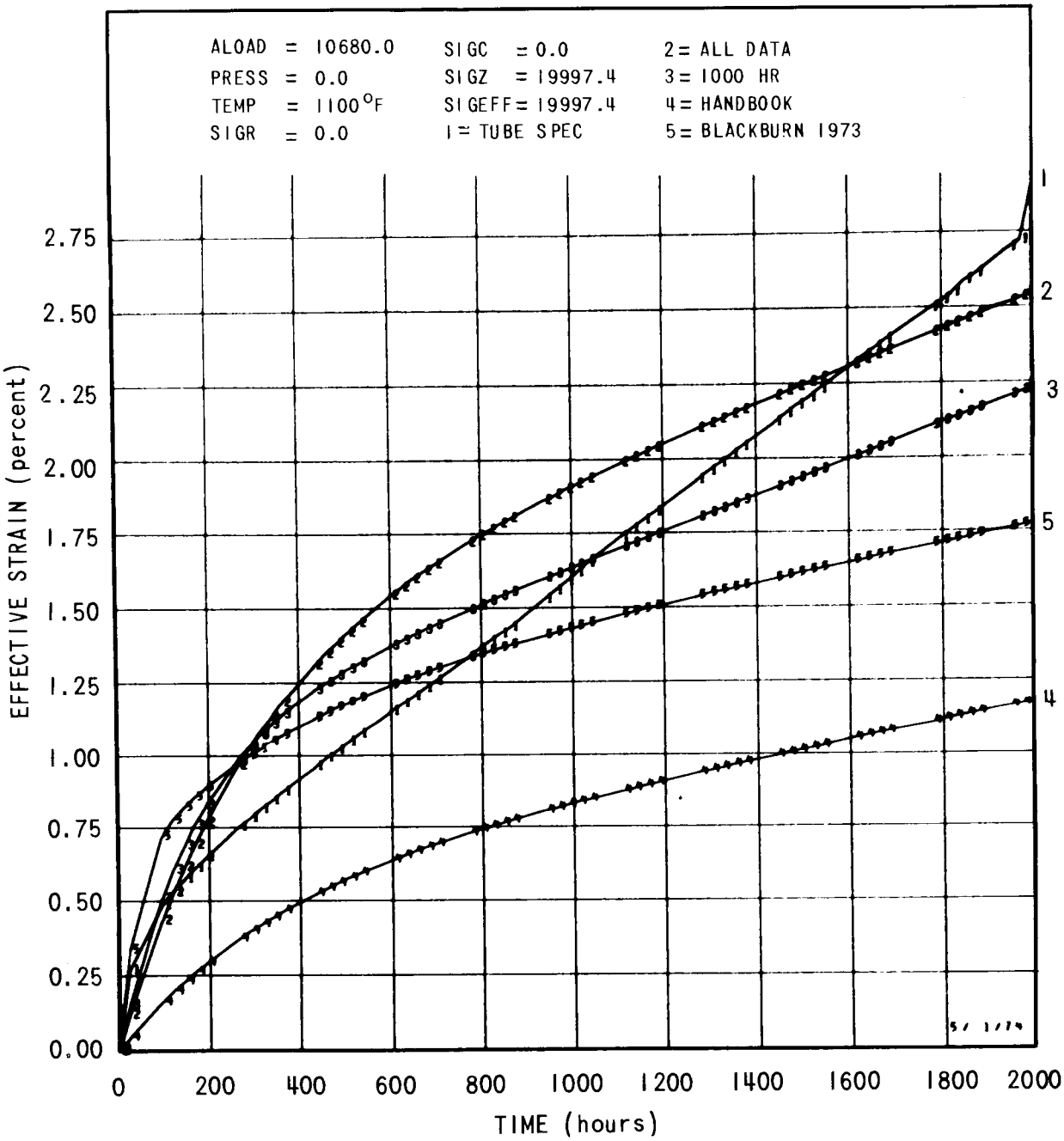

Figure 6-8 Cylindrical Specimen Creep Test 3 B52

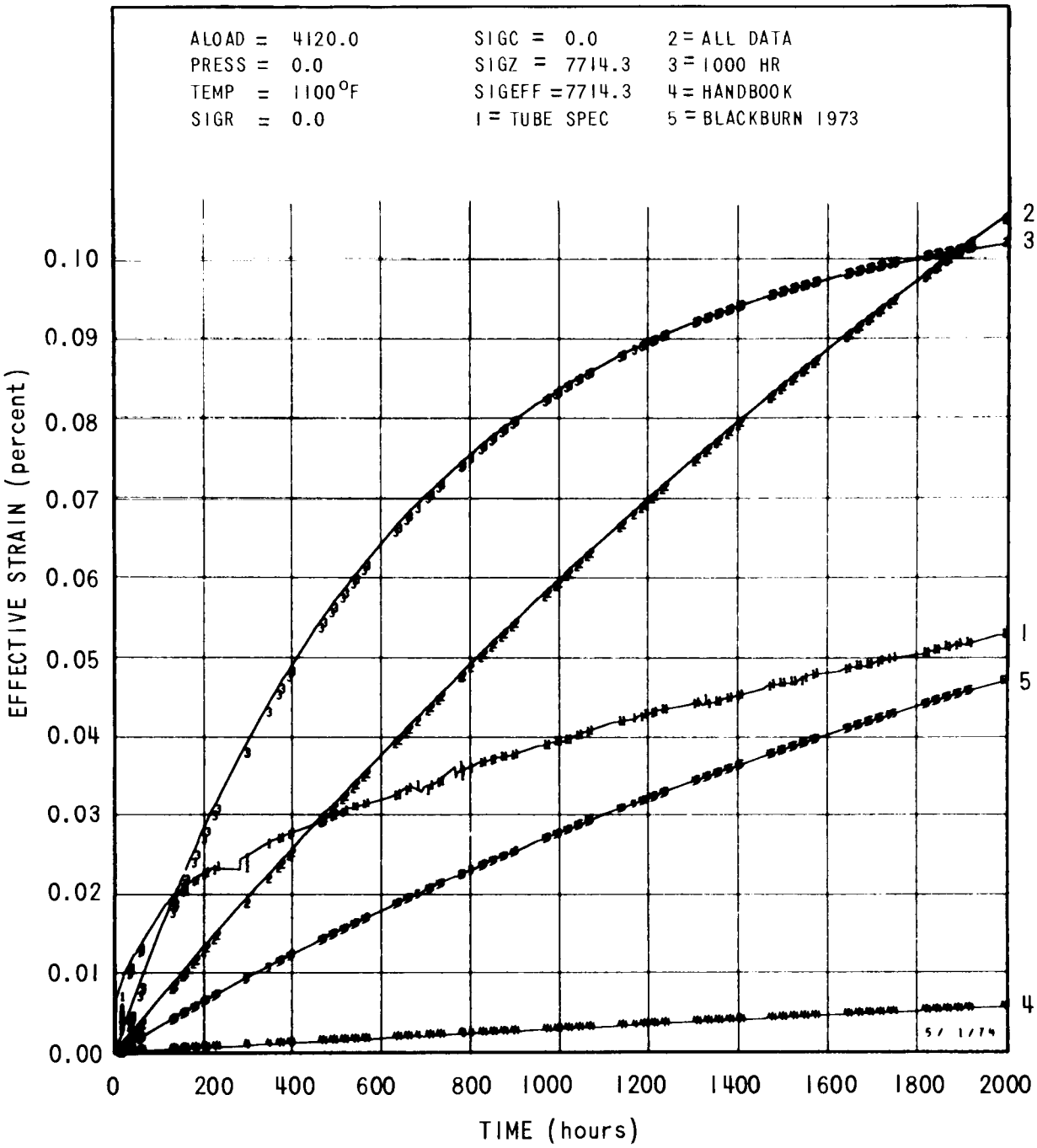

Figure 6-9 Cylindrical Specimen Creep Test 3 C53

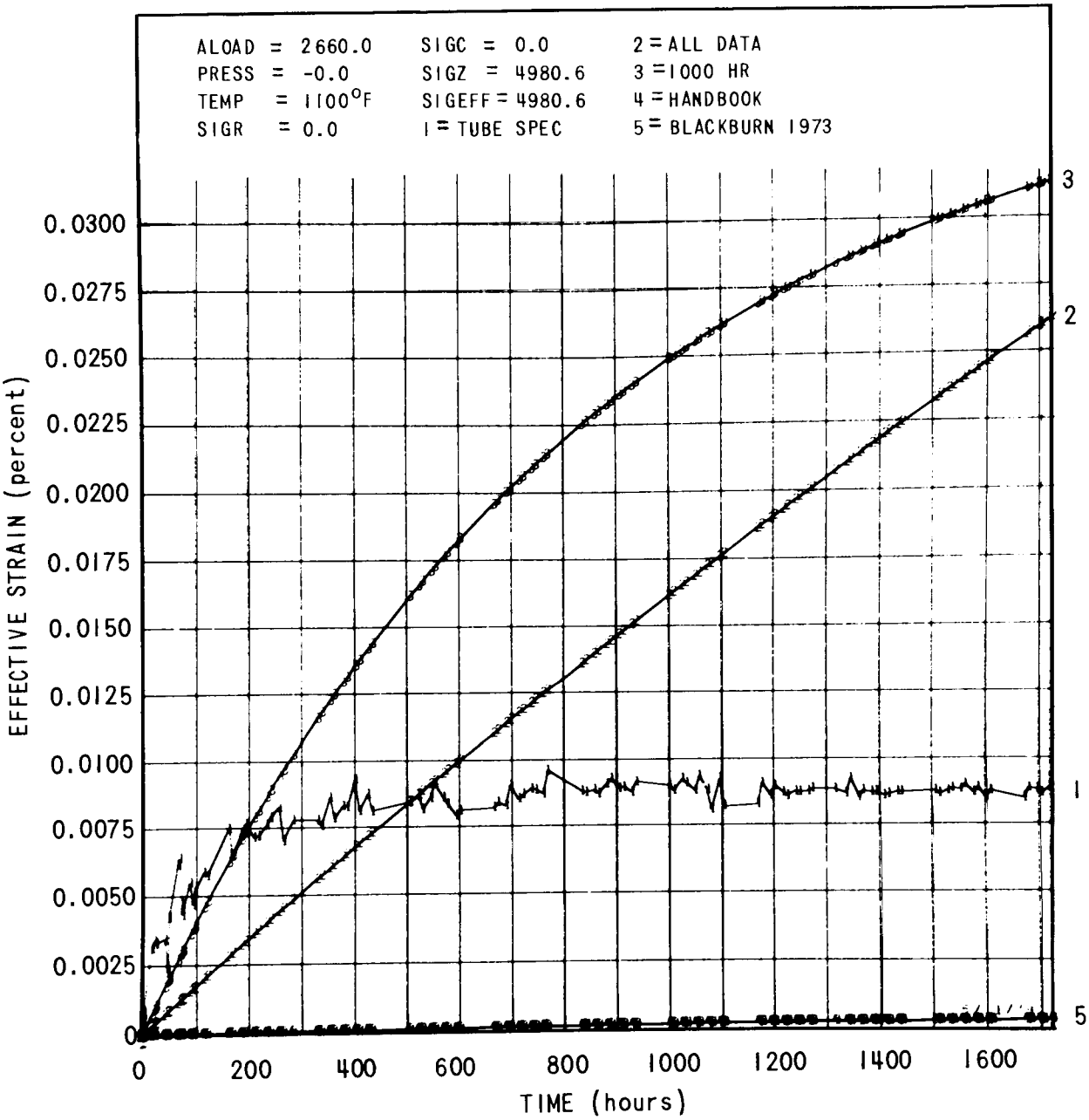

Figure 6-10 Cylindrical Specimen Creep Test 3 D12

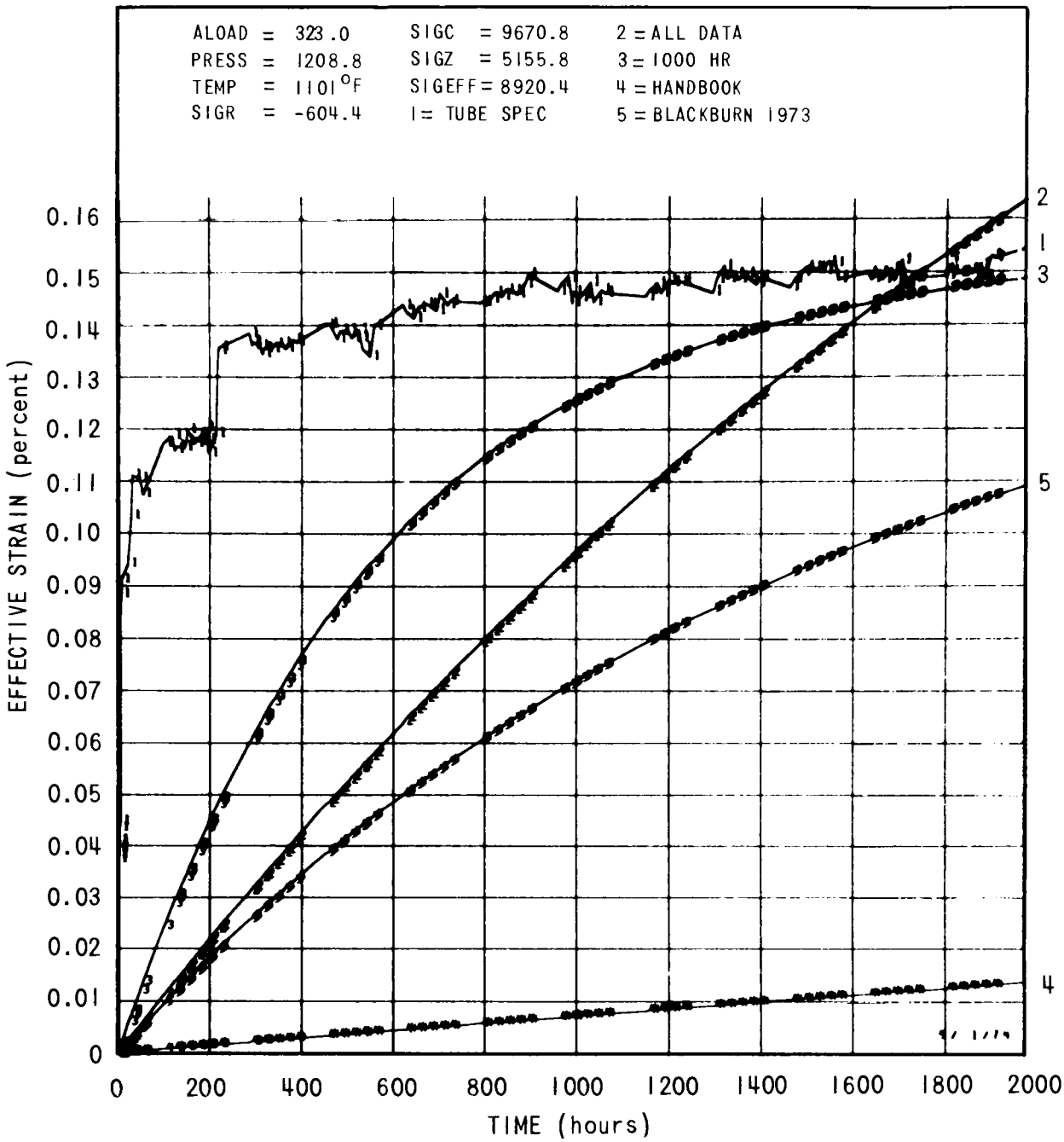

Figure 6-11 Cylindrical Specimen Creep Test 4 A 4

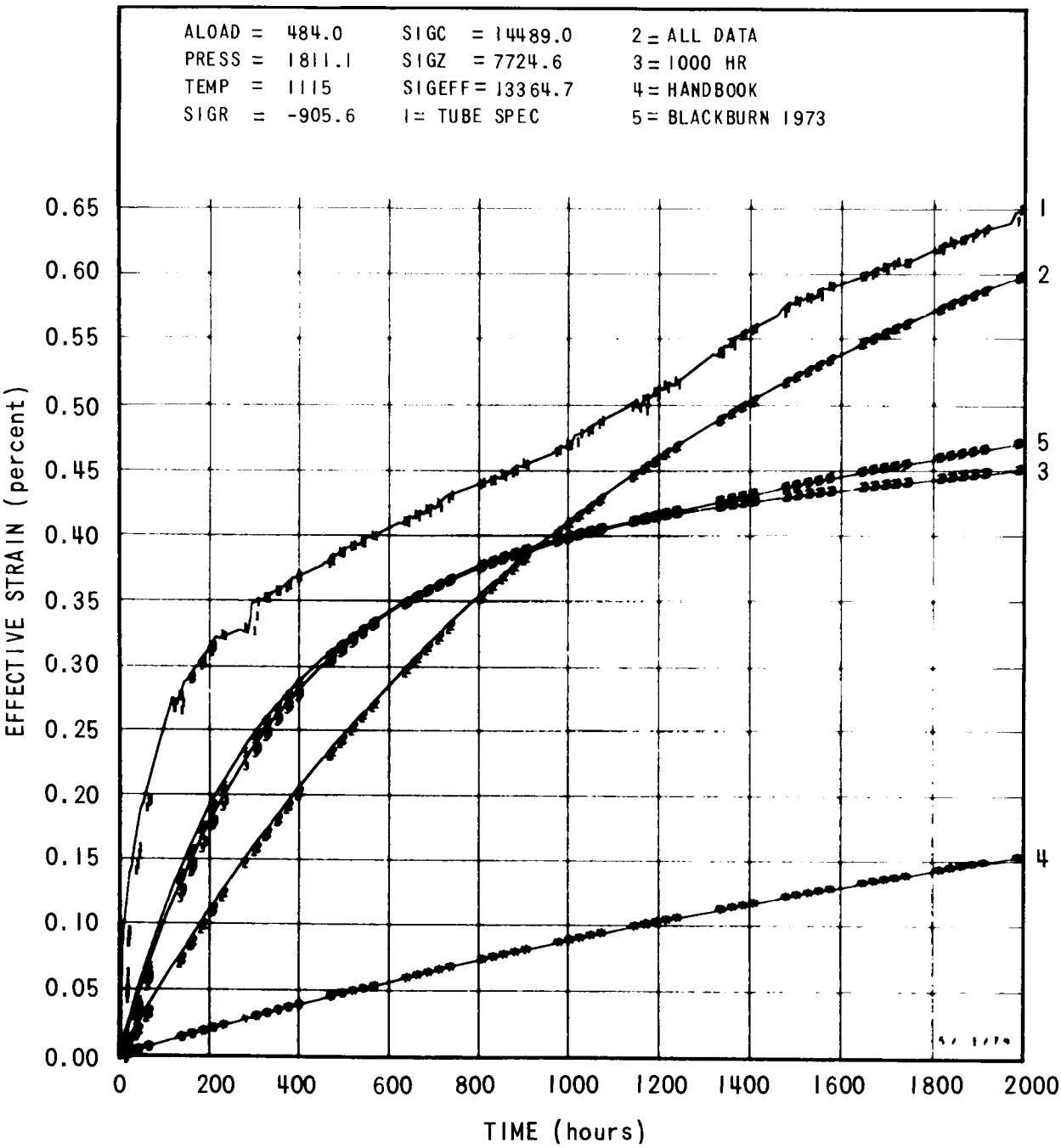

Figure 6-12 Cylindrical Specimen Creep Test 5 5

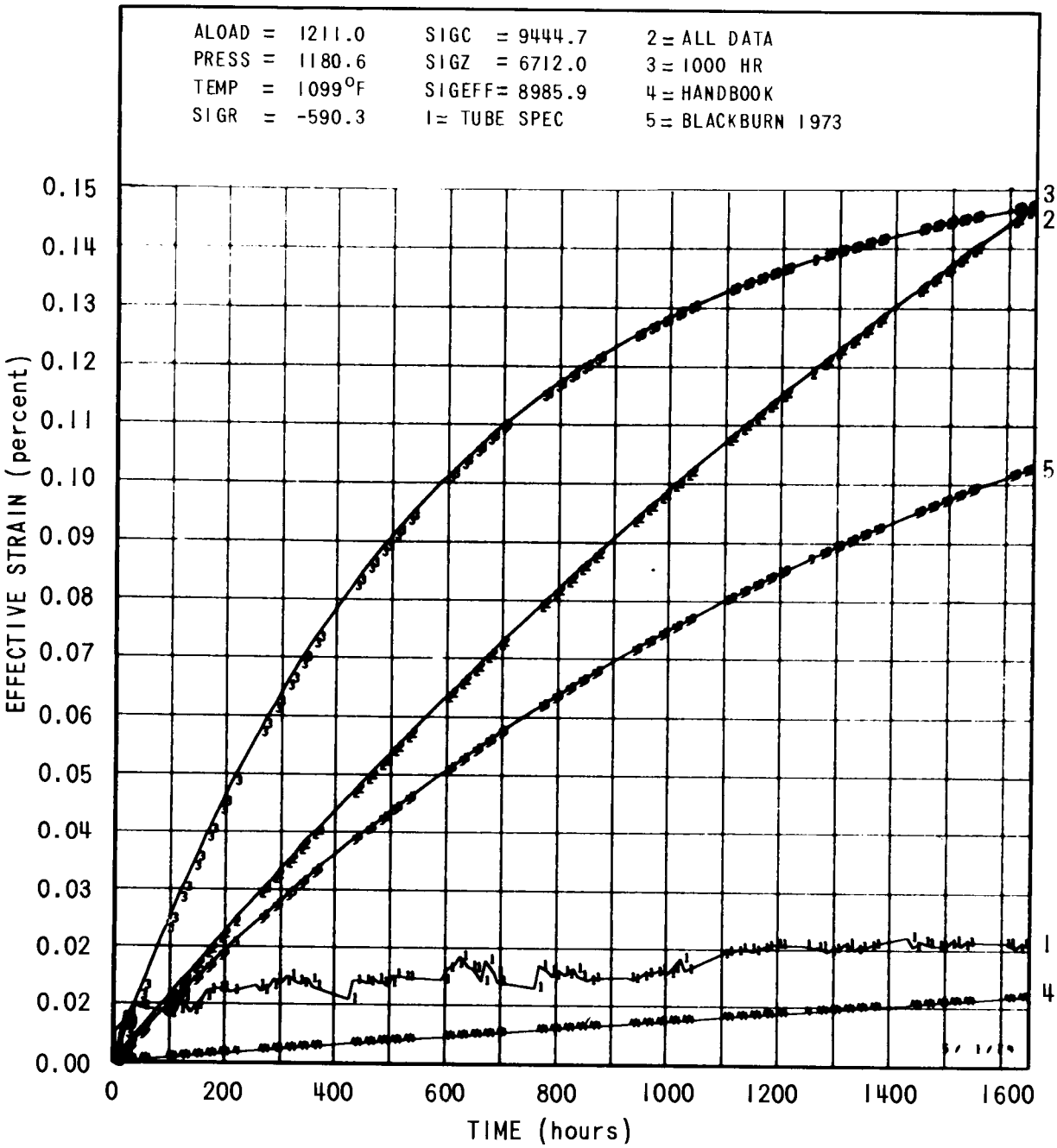

Figure 6-13 Cylindrical Specimen Creep Test 7 A11

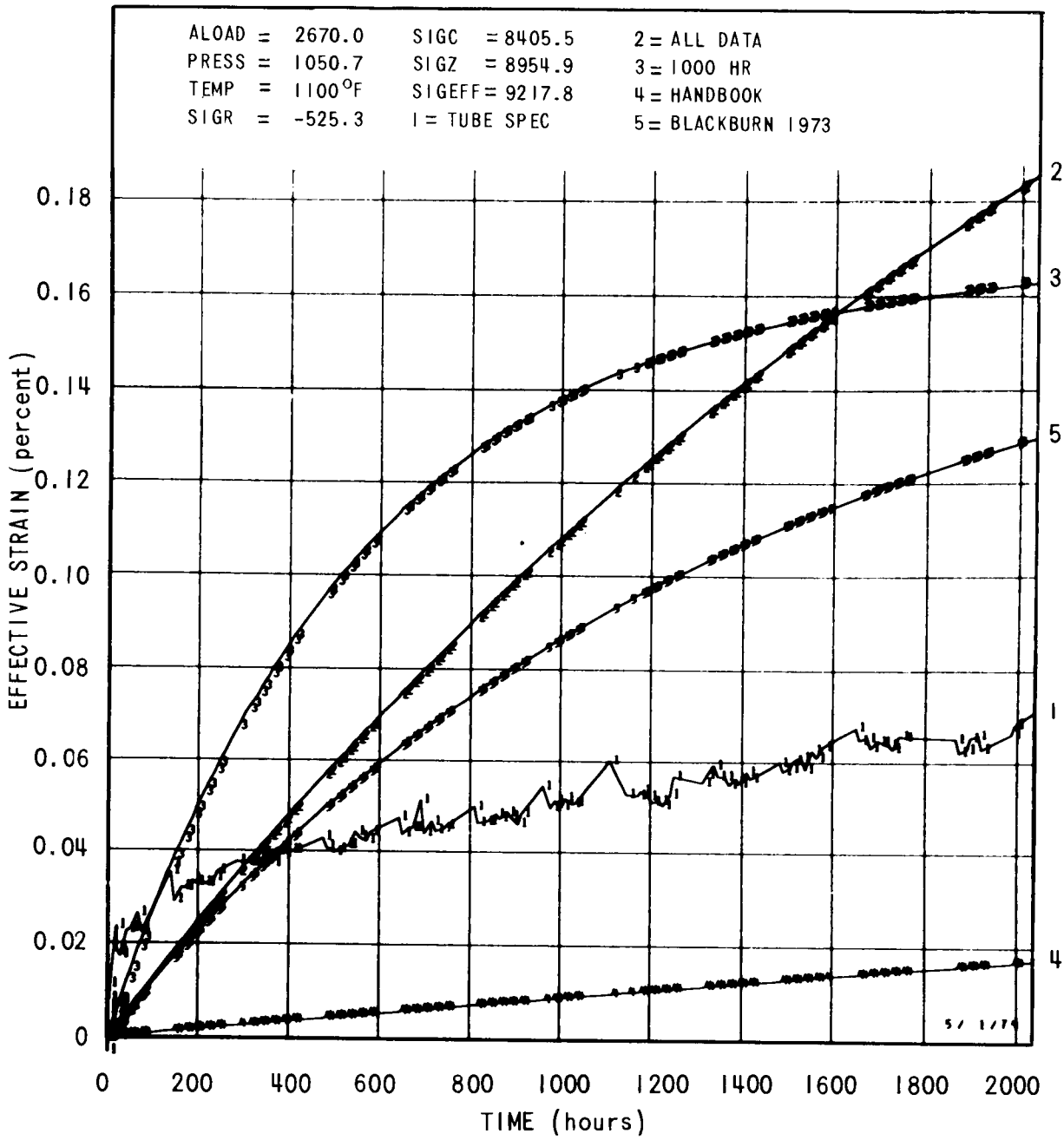

Figure 6-14 Cylindrical Specimen Creep Test 10 9

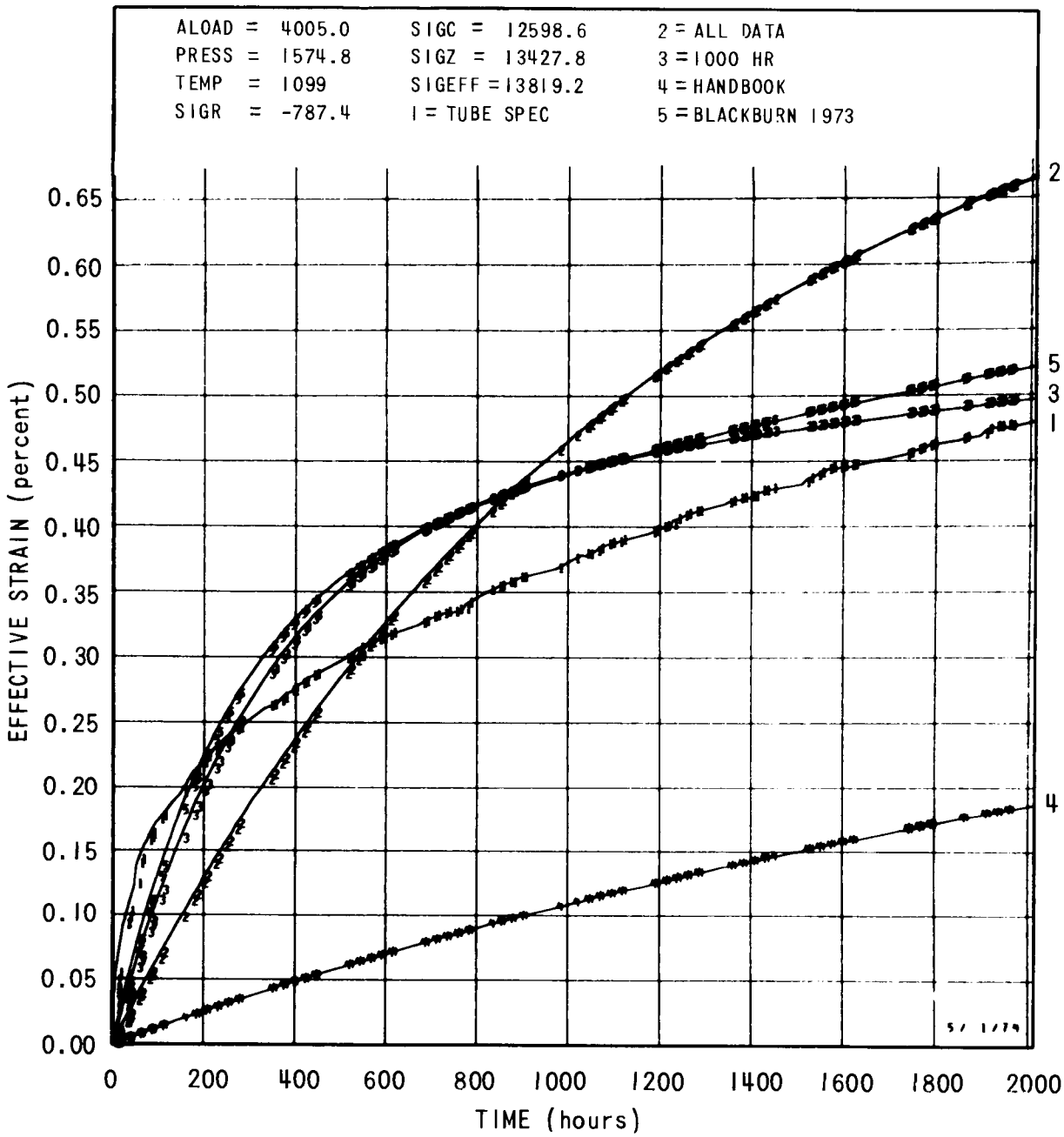

Figure 6-15 Cylindrical Specimen Creep Test 11 10

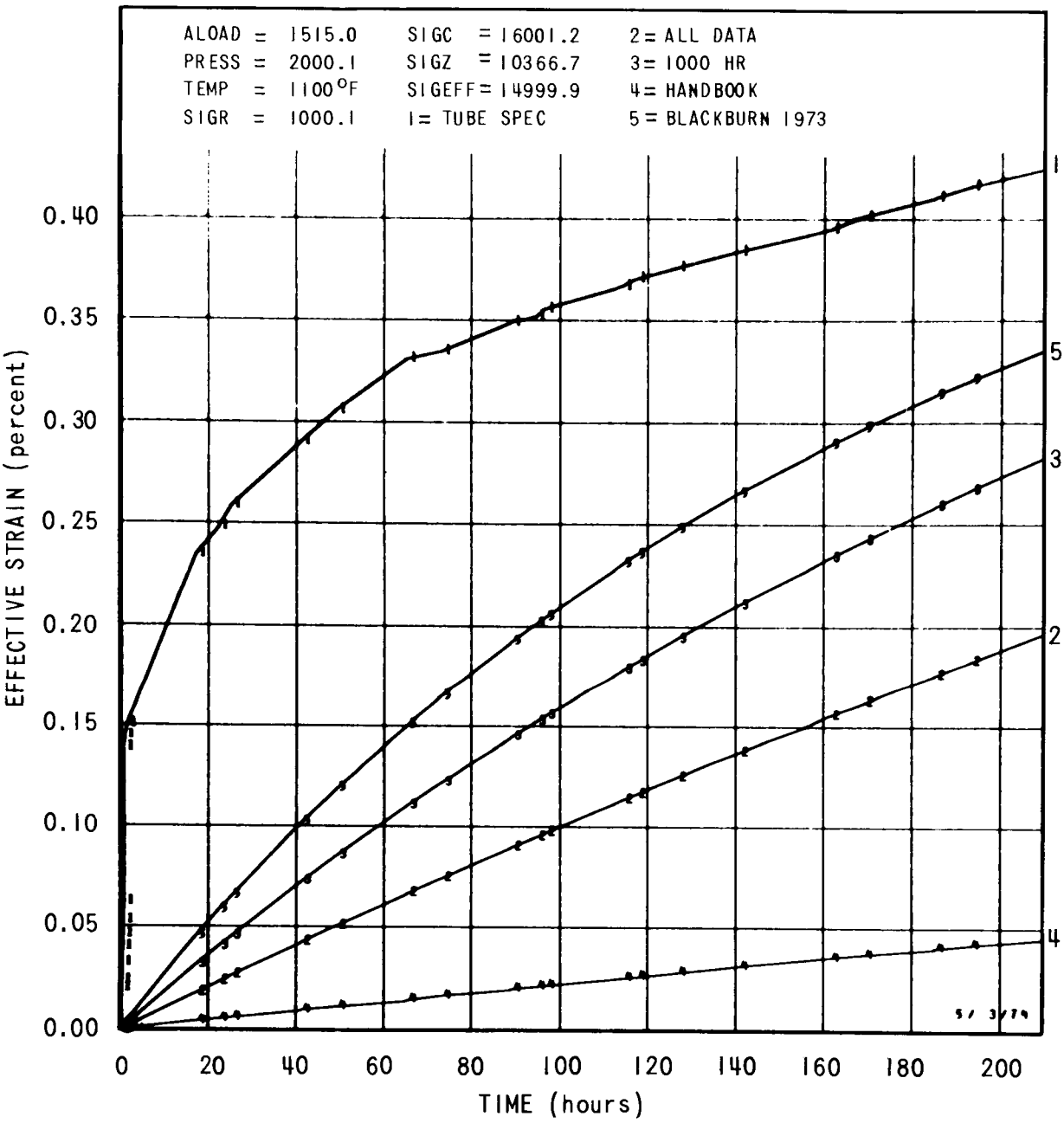

Figure 6-16 Cylindrical Specimen Creep Test 8 13

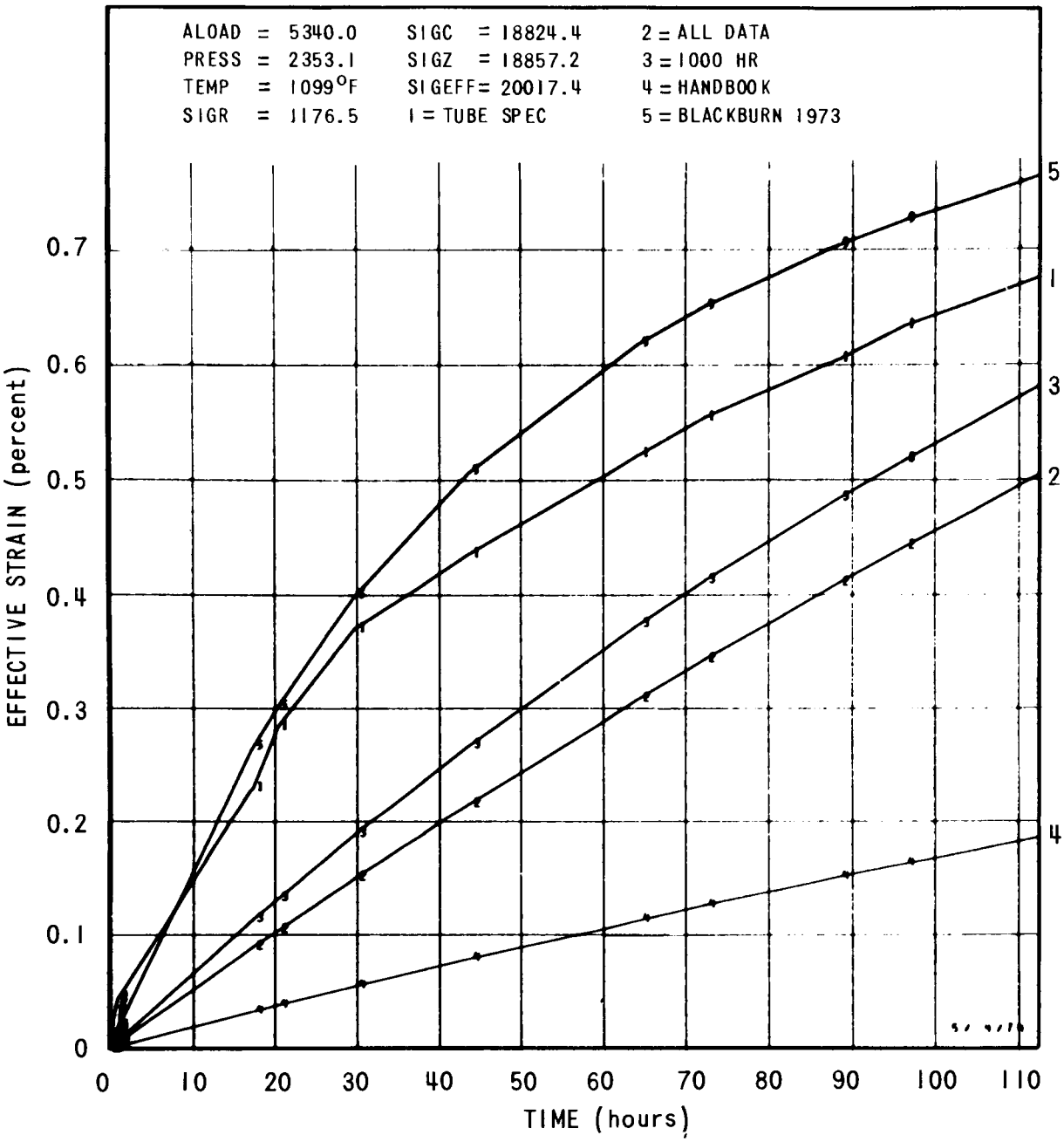

Figure 6-17 Cylindrical Specimen Creep Test 12 14

presented for each stress level according to the following equation:

$$\varepsilon - \varepsilon_L = \varepsilon_t \ (1-e^{-rt}) + \dot{\varepsilon}_m t \qquad (1)$$

where : ε = total strain (in/in)

ε_L = initial loading strain (in/in)

t = test time (hrs)

ε_t, r and $\dot{\varepsilon}_m$ are constants

The three constants in Equation (1) were also obtained for uniaxial test 3D at 5000 psi by using the computer program CREEP-FIT transmitted from ORNL. These values along with those derived for the other uniaxial creep tests are shown in Table 6.8.

A general model for creep strain behavior involves dependence upon temperature and stress as well as time. The primary objective of the present investigation is the determination of the dependence of creep strain upon stress and tubular specimens are tested over a wide range of stress. Because of the inherently nonuniform distributions of stress and strain, a knowledge of the stress dependence is essential to a detailed analysis of high temperature creep behavior of the tubular specimens.

The functional form of the stress-dependent model for creep behavior presently being considered is that form used in the LMFBR Materials Handbook, i.e.,

$$\varepsilon_c \ (\sigma,t) = \varepsilon_t \ (\sigma) \ [1-e^{-r(\sigma)t}] + \dot{\varepsilon}_m(\sigma)t \qquad (2)$$

$$r \ (\sigma) = b_1 \ [\mathrm{Sinh} \ (c_1\sigma)]^{d_1} \qquad (2a)$$

$$\dot{\varepsilon}_m \ (\sigma) = b_2 \ [\mathrm{Sinh} \ (c_2\sigma)]^{d_2} \qquad (2b)$$

$$\varepsilon_t \ (\sigma) = b_3 \ \frac{\dot{\varepsilon}_m(\sigma)}{r \ (\sigma)} \qquad (2c)$$

In Figures 6.18 to 6.21 the three constants, ε_t, r, and $\dot{\varepsilon}_m$, derived for the experimental data obtained at B&W and in the present investi-

Table 6.8 ε_t, r, and ε_m Derived for Uniaxial Creep Tests

Data Source	Test Type	Test No.	Test Temp. (°F)	Stress (ksi)	Constants $\dot{\varepsilon}_t$	Constants r	Constants ε_m	Remarks
				5.0	0.0085	0.0113	1.53×10^{-7}	
ARD	Uniaxial		1100	7.7	0.0227	0.0156	1.65×10^{-5}	
				10.0	0.0379	0.00604	2.52×10^{-5}	
				20.0	0.4882	0.0569	1.16×10^{-3}	
				25.0	0.9125	0.010	1.075×10^{-3}	
ORNL 1000 Hr. Data	Uniaxial Creep		1100	7.7	0.1025	0.1605	1.85×10^{-6}	Constants are derived from calculated values at the given stress level
				10.0	0.0379	4.51×10^{-5}	6.06×10^{-6}	
				20.0	1.358	0.00343	5.51×10^{-3}	
				25.0	2.05	0.00946	5.51×10^{-3}	
BLACKBURN 1970	Uniaxial		1100	7.7				Constants are derived from calculated values at the given stress level
				10.0	0.180	2.02×10^{-4}	4.54×10^{-6}	
				20.0	1.073	0.010	1.422×10^{-3}	
				25.0	1.923	0.0375	9.02×10^{-3}	
B&W	Uniaxial Creep and Rupture	BWR-5	1100	20.0	1.01	0.0117	1.15×10^{-3}	Tested in rupture machine
		BWR-6		19.0	0.932	0.00731	6.87×10^{-4}	
		BWR-7		16.0	0.371	0.00378	2.13×10^{-4}	
		BWR-8		17.0	0.583	0.00702	3.13×10^{-4}	
		BWR-9		18.0	0.655	0.00647	5.75×10^{-4}	
		BWR-10		16.0	0.634	0.00893	2.37×10^{-4}	
		BWR-11B		17.0	0.539	0.0113	4.13×10^{-4}	
		BWC-5B		20.0	0.720	0.00501	5.47×10^{-4}	Tested in creep machine
		BWC-6		16.0	0.391	0.00669	1.0×10^{-4}	
		BWC-7		17.0	0.571	0.00597	2.37×10^{-4}	
		BWC-8		18.0	0.470	0.00786	2.75×10^{-4}	

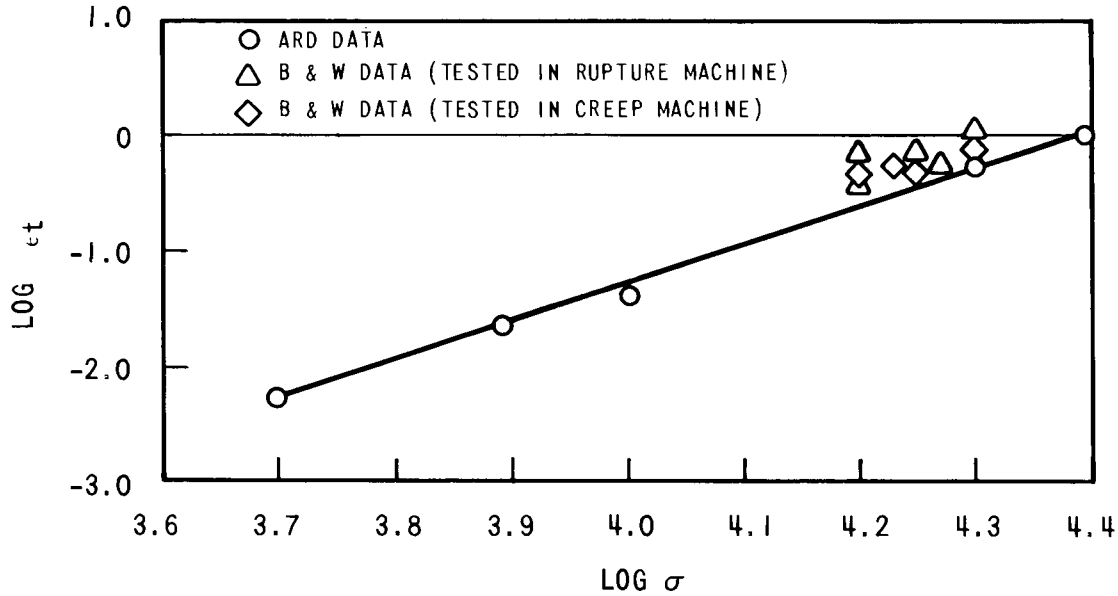

Figure 6-18 ϵ_t as a Function of Stress

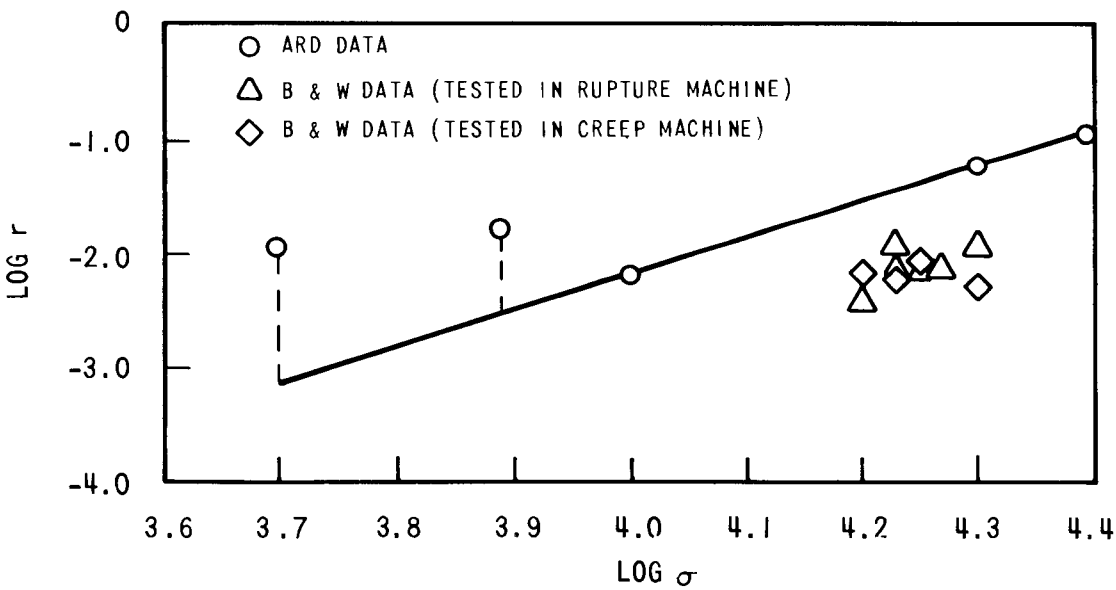

Figure 6-19 r as a Function of Stress

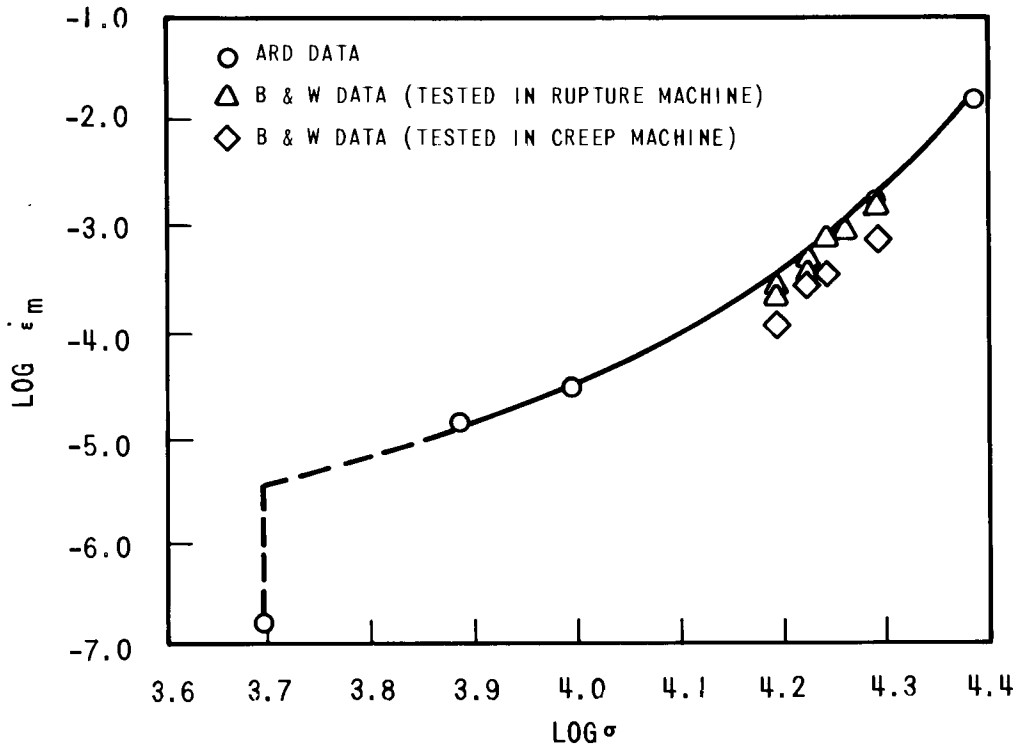

Figure 6-20 $\dot{\varepsilon}_m$ as a Function of σ

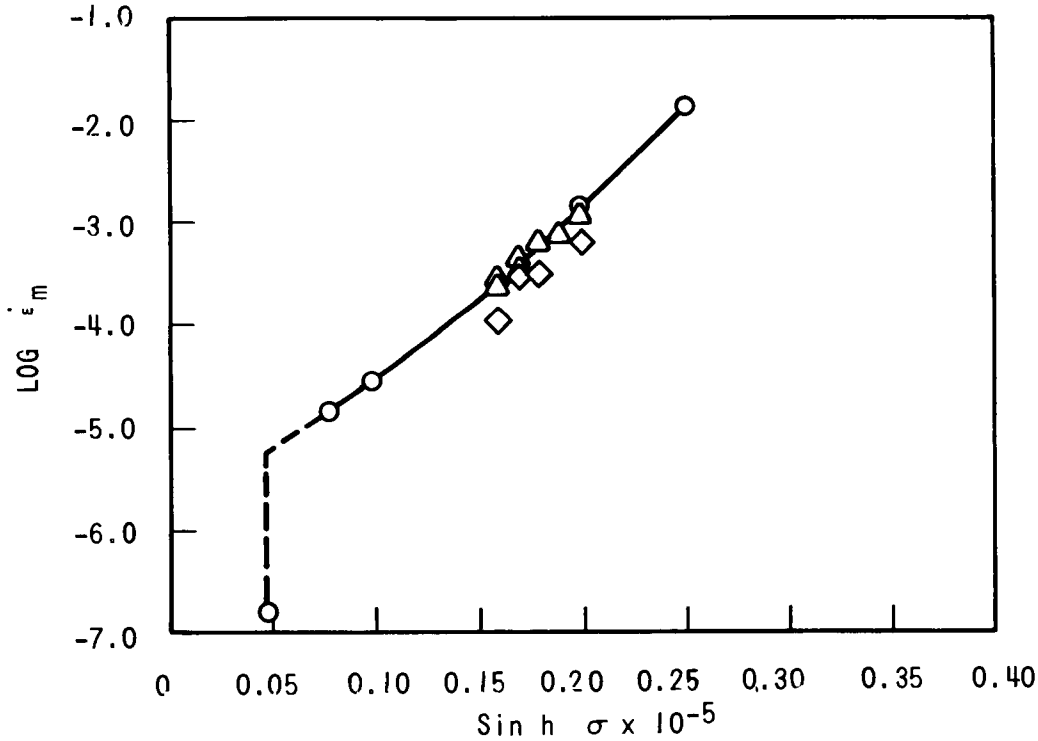

Figure 6-21 ε_m as a Function of σ

gation, are plotted as a function of stress. It is encouraging to note that the logrithm of the transient creep strain (ε_t) in the present investigation follows a linear relationship with the logrithm of the stress. In addition, the B&W data agree reasonably well with present data. Consequently, a very good estimate of the transient creep strain ε_t, can be made within the stress range from 5000 to 25,000 psi (3.447 x 10^7 to 1.723 x 10^8 Pascal) shown in Figure 6.14.

The constant r is a continuous function of stress above 10,000 psi (6.894 x 10^7 Pascal), as shown in Figure 6.15, while the values derived from the 5000 psi (3.447 x 10^7 Pascal) and 7,700 psi (5.308 x 10^7 Pascal) test results do not follow the extrapolation of high stress values. It is also noted that the agreement between the values derived from the B&W test results and those obtained from the present investigation is not as good as in the case of ε_t.

In Figures 6.20 and 6.21 the minimum creep rate, $\dot{\varepsilon}_m$, is plotted as a function of stress. It is noted that the $\dot{\varepsilon}_m$ values of the present investigation are consistent at stress level above 7,700 psi (5.308 x 10^7 Pascal). However, the value obtained from the 5000 psi (3.447 x 10^7 Pascal) test results does not follow the general trend established by the values obtained from the high stress test results. The exact reason for this is not apparent at the present time. However, the relatively short test period (2000 hours) may have a significant effect in establishing the minimum creep rate, $\dot{\varepsilon}_m$, particularly at the low stress level such as 5000 psi (3.447 x 10^7 Pascal). Additional tests at stress levels between 5000 and 10,000 psi (3.447 x 10^7 to 6.894 x 10^7 Pascal) have to be carried out to better define the stress dependence of the constants r and $\dot{\varepsilon}_m$.

6.3.4 316SS Tubular Testing

It was decided during a program review meeting held on May 7 at ORNL that test of Type 304 stainless steel models with discontinuities

be postponed and testing of Type 316 stainless steel models be initiated instead. In addition, it was agreed that tests to failure should be included in the Type 316 stainless steel model test program. A tentative test matrix for Type 316 stainless steel testing, shown in Table 6.9 and 6.10 has been completed. It is expected that the piping from the Type 316 stainless steel reference heat will be received during the month of October, 1974. Fabrication of the test models will be initiated immediately upon receiving of this material.

6.4 REFERENCES

1. Validation of High Temperature Design Methods and Criteria, Quarterly Progress Report for Period Ending August 31, 1973. WARD-HT-3045-4.
2. W. L. Greenstreet, J. C. Corum and C. E. Pugh, "High Temperatures Structural Design Methods for LMFBR Components Quarterly Progress Report for Period Ending September 30, 1972", ORNL-TM-4058, January, 1973.
3. Handbook, "LMFBR Material Properties Handbook", HEDL-TME-71-32 Data Sheet 3045S-23, Dated July 30, 1971.
4. Letter, E. A. Evans to W. H. Harms, "LMFBR Materials Handbook Creep and Tensile Behavior Representations," Proposed Data Sheet 3045S-23 Dated January 17, 1973, W/FFTF 734612, June 8, 1973.

Table 6.9 Proposed Test Matrix for Additional Type 316 Stainless Steel Tubular Specimens

(Test Plan - Uniaxial Constant Load Specimens)

Test Number	Effective Stress σ_e (a) (psi)	Stress Ratio $\sigma_{hoop}/\sigma_{axial}$ (σ_θ/σ_z)	Loads to Obtain Nominal Desired Stresses		Nominal Test Temperature T (°F)	Nominal Test Duration t (hours)	Test Priority	Remarks
			Int. Pressure p (psi)	Axial Load P (lbs)				
101	25,000.0	0.0	0.0	6479.5	1100.0	2000.0	(b)	Test to Failure
102	20,000.0	0.0	0.0	5183.6	1100.0	2000.0	(d)	
103	15,000.0	0.0	0.0	3887.7	1100.0	2000.0	(b)	
104	10,000.0	0.0	0.0	2591.8	1100.0	2000.0	(b)	Test to Failure with Stepped Loading
105	7,700.0	0.0	0.0	1995.7	1100.0	2000.0	(c)	

(a) $\sigma_e = \sigma_z = \frac{P}{2\pi r_{av} t}$

where: r_{av} = average radius of the tube

t = thickness of the tube

(b) These tests should be initiated before tests 102 and 105.

(c) Test 105 can be omitted if machine time is not available.

(d) Test 102 need not be performed. It is given here only as a comparison test for Type 304 stainless steel Test No. 3.

Table 6.10 Proposed Test Matrix For Additional Type 316 Stainless Steel Tubular Specimens

(Test Plan - Multiaxial, Constant Load Specimens)

Test Number	Effective Stress σ_e (a) (psi)	Stress Ratio $\sigma_{hoop}/\sigma_{axial}$ (σ_θ/σ_z)	Loads to Obtain Nominal Desired Stresses		Nominal Test Temperature T (°F)	Nominal Test Duration t (hours)	Test Priority	Remarks
			Int. Pressure p (psi)	Axial Load P (lbs)				
106	20,000.0	2.0	1399.6	0.0	1100.0	2000.0	(c)	
107	20,000.0	1.0	1212.1	2591.8	1100.0	2000.0	(c)	
108	15,000.0	2.0	1049.7	0.0	1100.0	2000.0	(b)	
109	15,000.0	1.0	909.1	1943.9	1100.0	2000.0	(b)	
110	12,500.0	2.0	874.8	0.0	1100.0	2000.0	(b)	
111	12,500.0	1.0	757.6	1619.9	1100.0	2000.0	(b)	
112	10,000.0	2.0	699.8	0.0	1100.0	2000.0	(b)	Test to Failure
113	10,000.0	1.0	606.1	1295.9	1100.0	2000.0	(b)	with Stepped Loading

(a) Effective stress calculated as per thin cylinder formula is given by:

$$\sigma_e = [\sigma_\theta^2 + \sigma_z^2 - \sigma_\theta \sigma_z]^{1/2}$$

where: $\sigma_\theta = p \frac{r_{av}}{t}$

$\sigma_z = p \frac{r_{av}}{t} + \frac{P}{2\Pi r_{av} t}$

r_{av} = average radius of the tube

t = thickness of the tube

(b) These tests should be initiated before tests 106 and 107.

(c) Tests 106 and 107 can be omitted if machine time is not available.

7. UNIVERSITY OF CINCINNATI

J. Moteff

7.1 INTRODUCTION

The objective of this program is to (a) evaluate the time, temperature and stress dependent properties of several austenitic stainless steels, (b) determine the relation of these properties to the microstructure as observed principally with a 200 kV transmission electron microscope and (c) show the contribution of grain boundary microcracking to the plastic deformation behavior at high temperature. Special consideration has been given to operating conditions typical of LMFBR applications, including the knowledge that the radiation environment can influence the substructure of these metals leading to significant changes in the mechanical property behavior. Related substructure studies on other metals and alloys are also being investigated.

7.2 EXPERIMENTAL PROGRAM

Transmission electron microscopy has been used to study the deformation substructure resulting from fatigue, tensile and creep deformation at elevated temperatures. Special studies have been initiated on the comparison of the substructure developed in Incoloy 800 following both a push-pull and a bend fatigue testing mode. Preliminary work was started on the evaluation of the substructure developed in 304 stainless steel tested in a creep-fatigue (hold-time) mode. Creep data from ORNL (Heat Number 9T2796) was evaluated through

regression analysis in preparation for the correlation with the substructure results. Hot hardness measurements were employed to determine an activation energy for the creep process.

The work in progress will be presented according to the separate mini-research programs for convenience. A general description and a brief discussion will be given on several of the programs that are presently active.

7.2.1 Characterization of the Creep and Tensile Substructure of 304 Stainless Steel, Reference Heat 9T2796

(R. Bhargava)

The characterization of the substructure of specimens* fabricated from Reference Heat number 9T2796 of AISI 304 stainless steel tested in the creep and tensile mode has been initiated. The results obtained from this study will be compared with the previous substructure information obtained at the University of Cincinnati and the published literature. In the period of this report, the substructure evaluation of three specimens was completed. These specimens were tested in tension at 650°C at various strain rates. The tensile properties and the correlation with the microstructural features e.g. cavities and grain boundary sliding and grain boundary migration etc. has been presented elsewhere.[1]

---

* Tested specimens furnished by the Metals and Ceramics Division of the Oak Ridge National Laboratory, Oak Ridge, TN.

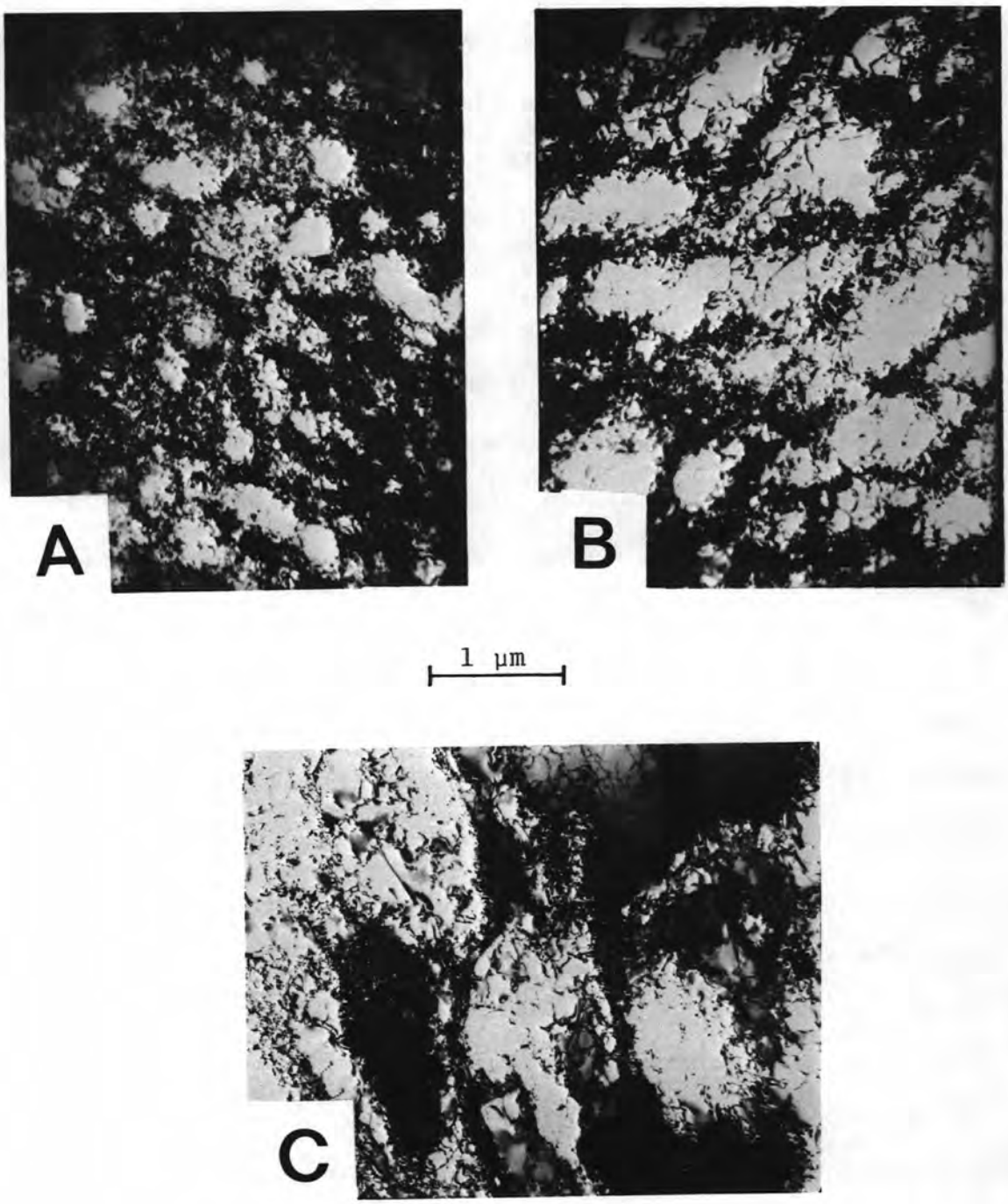

Fig. 7.1 Typical Photmicrographs of the Substructure Developed in Tension at 650°C, (A) $\dot{\varepsilon}=8.33\times10^{-4}$ $(Sec.)^{-1}$, (B) $\dot{\varepsilon}=8.33\times10^{-5}(Sec.)^{-1}$, (C) $\dot{\varepsilon}=8.33\times10^{-6}(Sec.)^{-1}$ (AISI 304 Stainless Steel, Reference Heat 9T2796).

Figure 1, shows typical photomicrographs of the cells* and subgrains* formed in the three specimens. The effect of the strain rate on substructure is manifested in two ways. As the strain rate is reduced with a corresponding reduction in the flow stress, the cell or subgrain size becomes larger again confirming the inverse relationship of λ with the stress. Another effect of strain rate is that at the fast strain rates, the substructure consists of cells whose walls are tangles of dislocations and the inside is more or less void of dislocations. At the slow strain rates, the substructure tends to approach that typical of a subgrain structure where the well defined sub-boundary becomes thinner as compared to the cell walls. Because longer times are involved at the lower flow stress, the dislocations may move slower with little cross slip and seem to develop into these low angle sub-boundaries. In Figure 2, the subgrain or cell intercept, λ, is plotted versus the modulus compensated true stress, σ/G. The error bands on the data points represent the 2σ 95% confidence limit. In this the previously published and reported data has also been plotted.[2] It is becoming more obvious that at the high strain rates and higher

---

* The term cell is used to describe the modulated substructure having poorly defined walls consisting of dislocation tangles and subgrains for those having well defined regular networks of dislocations. Generally, the cells are typical of deformations which occur below $\sim 0.5\ T_m$ and subgrains for those above.

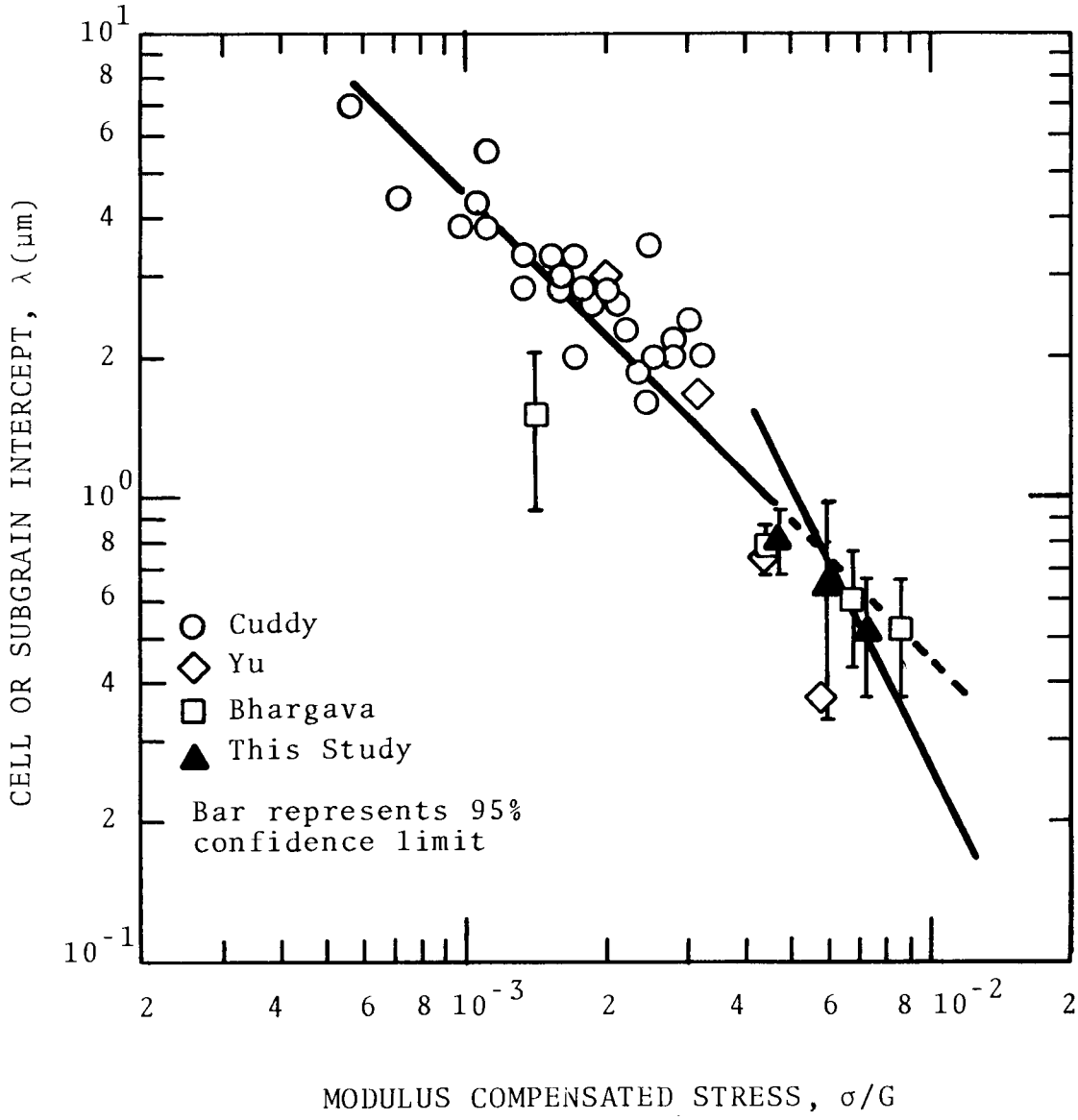

Fig. 7.2 Plot of Cell or Subgrain Intercept Versus Modulus Compensated Stress (AISI 304 Stainless Steel).

stress levels (typical of a short term tensile test) the substructure consists of a cellular structure and at the lower stress levels and therefore longer times on test, the dislocations rearrange into well defined sub-boundaries. The temperature should be sufficiently high to permit the required dislocation mobility by permitting climb over obstacles. The work is being continued and the results will be reported in future progress reports.

7.2.2 Analysis of Relationships of Creep Rate, Stress and Temperature for 304 Stainless Steel - (R. Bhargava)

The analysis of the creep data to determine the relationship between the steady-state creep rate, temperature and stress for AISI 304 stainless steel (Reference Heat Number 9T2796) is being continued. The preliminary results were reported previously.[3] Further analysis of the data in light of recent creep theories is being carried out. In order to compare the results with the various theoretical models involving constant stress creep testing, the applied stress was changed to an effective true stress by correcting for the reduction in area occurring during the secondary stage of creep. Assuming constant volume conditions, then the cross sectional area becomes proportional to the strain. The strain used for the above correction was determined, as a first approximation, according to the following equation,

$$\varepsilon = \varepsilon_{plastic} + \varepsilon_{primary} + 1/2\ \varepsilon_{creep} \qquad (1)$$

where $\varepsilon_{plastic}$ is the strain on loading, $\varepsilon_{primary}$ is the strain in the primary stage and ε_{creep} is the strain in the secondary stage of creep. Moreover, in order to separate the effect of temperature on the stress levels, a parameter σ_T/E (Modulus Compensated True Stress) was evaluated where E is the Young's modulus at the given test temperatures.

The steady-state creep rate, $\dot{\varepsilon}_s$ has been plotted in Figure 3 versus the modulus compensated true stress, σ_T/E. At all the test temperatures, a straight line of slope 7 can be drawn. The computer analysis also showed the values of n to be 7 $\pm$ 1. From Figure 3, the values of $\dot{\varepsilon}_s$ at constant values of σ_T/E, and therefore supposedly constant substructure, (6×10^{-4}, 1.0×10^{-3} and 1.5×10^{-3}) were obtained for the various test temperatures. These values are then plotted in Figure 4. The various values of the apparent activation energy for creep, Q_c, obtained were 80.3 $\pm$ 1.5, 85.1 $\pm$ 2.8 and 90.3 $\pm$ 1.8 (kcals/mole). These values of Q_c are in good agreement with the values of 87 kcals/mole reported previously.[4] Thus, the steady-state creep rate $\dot{\varepsilon}_s$ can be given by a relation,

$$\dot{\varepsilon}_s = A(\sigma_T/E)^{7\pm1} \exp(-85\pm5/RT) \qquad (2)$$

Work is continuing on determination of the value of the constant A and on the uncertainties in the value of the creep rate $\dot{\varepsilon}_s$ based on the experimental uncertainties.

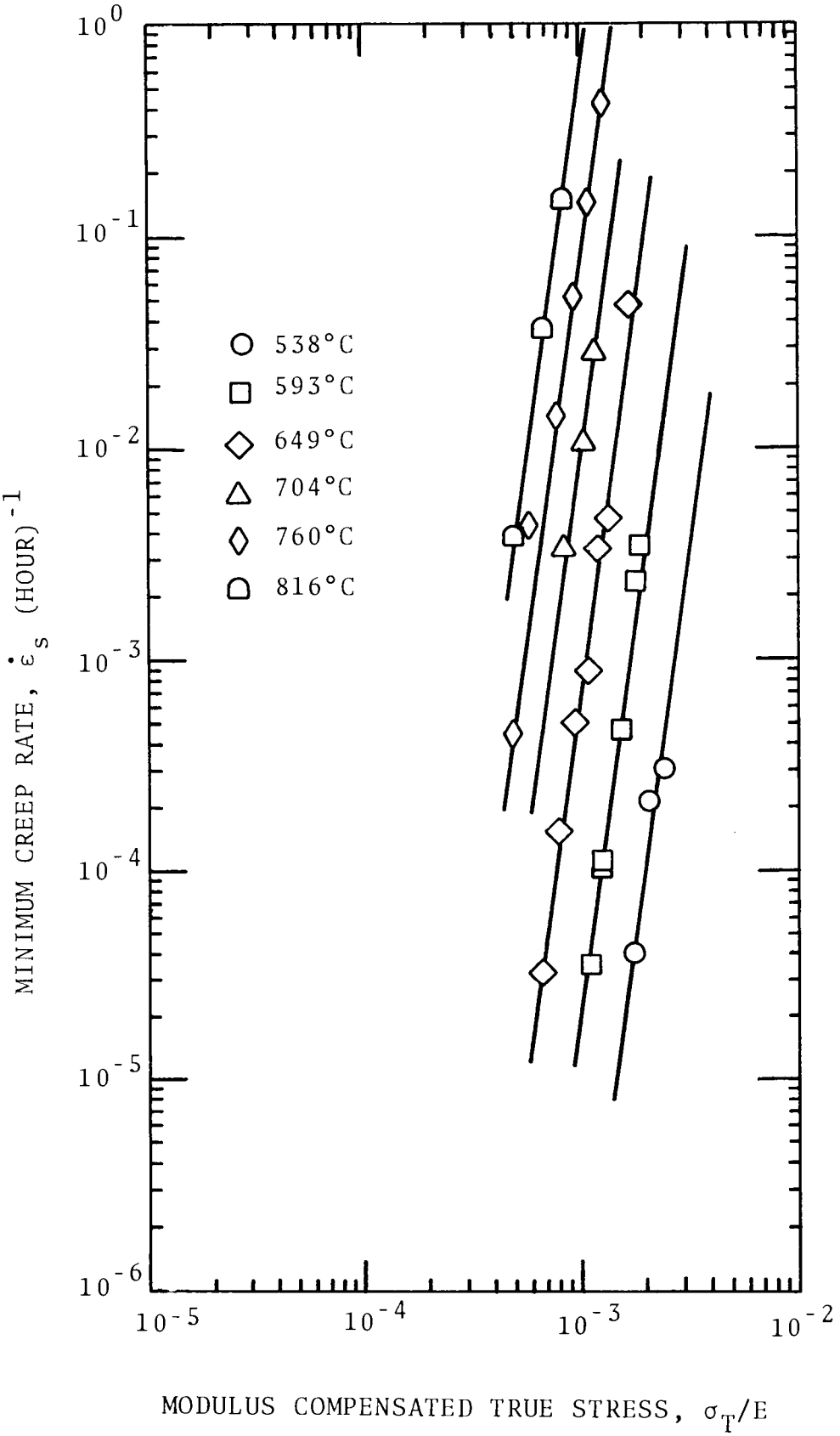

Fig. 7.3 Plot of Minimum Creep Rate Versus Modulus Compensated True Stress (AISI 304 Stainless Steel, Reference Heat 9T2796).

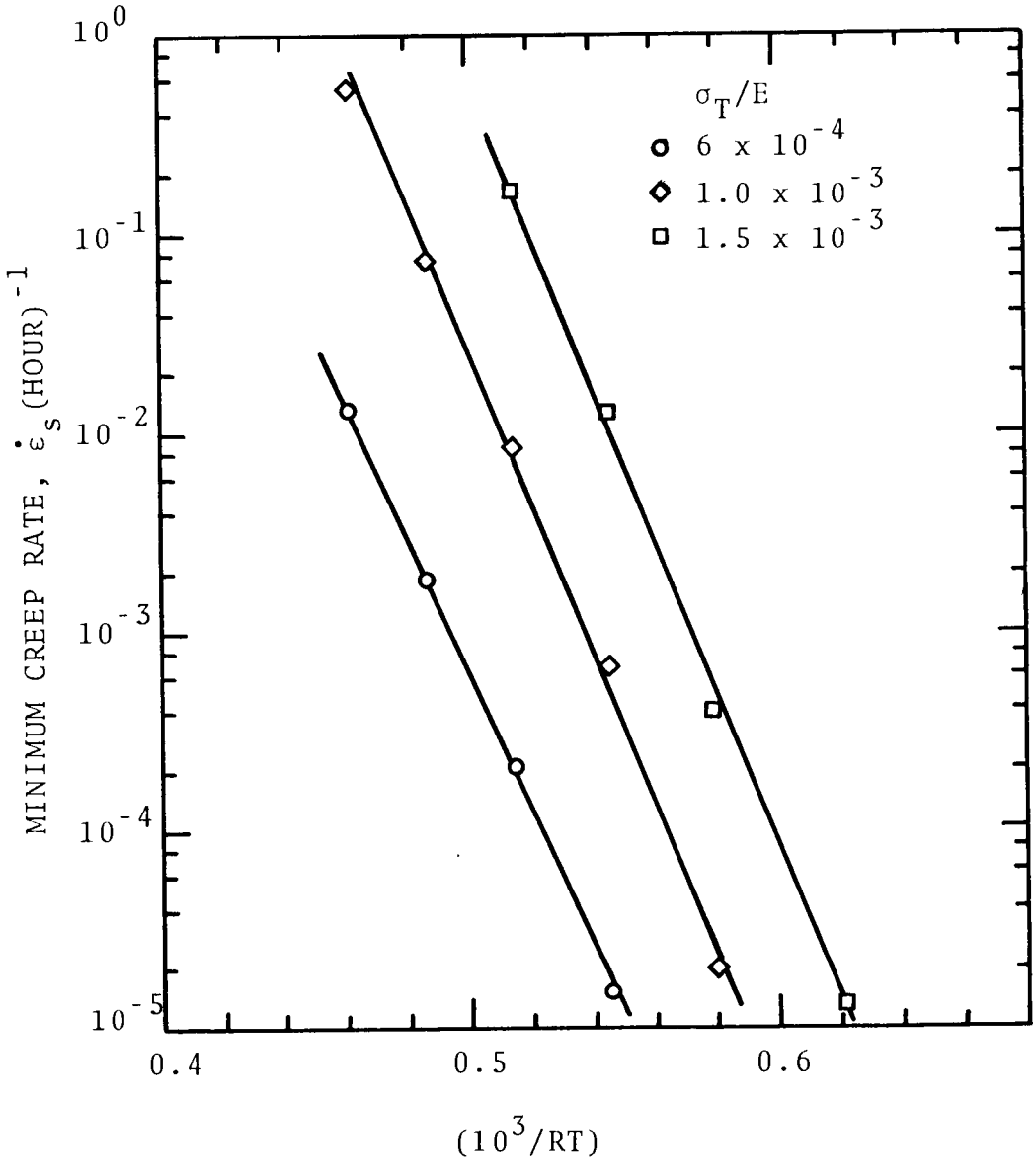

Fig. 7.4 Plot of Minimum Creep Rate Versus Reciprocal Temperature Parameter (AISI 304 Stainless Steel, Reference Heat 9T2796).

Recently Sherby and co-workers[5] have proposed a relationship of the form,

$$\dot{\varepsilon}_s = A'\lambda^3 D\ (\sigma_T/E)^7 \tag{3}$$

suggesting that in metals where subgrains form during creep testing, the stress exponent value of 7 can be explained by taking into account the relationship of subgrain size, λ and the modulus compensated stress, σ/E. The factor D is equivalent to $D_o \exp(-Q_c/RT)$. Since

$$\lambda = K(\sigma_T/E)^{-1} \tag{4}$$

for deformation occurring in the creep range, then Equation 3 reduces to,

$$\dot{\varepsilon}_s = A''D\ (\sigma_T/E)^4 \tag{5}$$

This approach yields stress dependencies for the creep process which are in better accord with the theoretical predictions of n values close to 3.5.

7.2.3 <u>The Role of Twin Boundary - Grain Boundary Intersections on Microcracking Behavior of AISI 304 Stainless Steel Deformed in Slow Tension and Creep at 650°C</u> - (H. Nahm)

Studies of intergranular crack formation in metals at elevated temperatures have shown that triple points may provide both preferential sites for the nucleation of

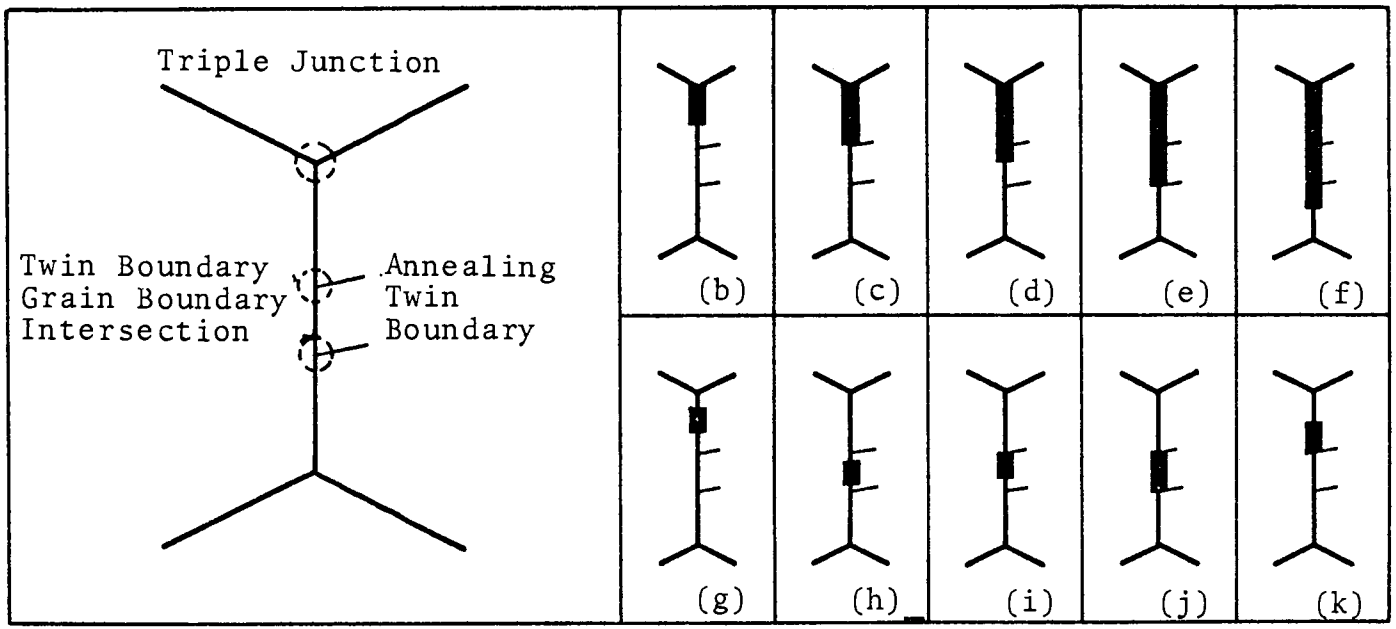

Fig. 7.5 Schematics Showing Various Types of Cracks

cracks and barriers to their propagation.[6-10] Although it has been shown that the growth of cracks originating at grain boundary triple junctions may be arrested or interrupted at twin boundary - grain boundary intersections[11-12], relatively little is known concerning the influence of these intersections on the crack propagation process in austenitic stainless steel.

Recent work has shown evidence for the formation of cracks and cavities along twin boundaries in 304 stainless steel.[13] These results suggest that the twin boundaries may behave in a manner similar to grain boundaries under the proper conditions.

The purpose of this study is to report quantitative observations concerning the influence of twin boundary - grain boundary intersections (hereafter referred to as TGI) on the intergranular cracking behavior in AISI 304 stainless steel deformed in the slow tension and creep rupture modes at 650°C. Figure 5 describes the crack morphology that will be used in this analysis.

In addition to those cracks whose lengths, in terms of grain boundary facets, fall in the interval $\ell \leq 2$ and are not terminated at TGI[10], a non-negligible number of triple point cracks were also observed to terminate at TGI (See Figure 5-c and 5-e). Cracks not associated with triple junctions but associated with TGI's were observed as well. These cracks are shown in Figure 5 - (i to k). Secondary

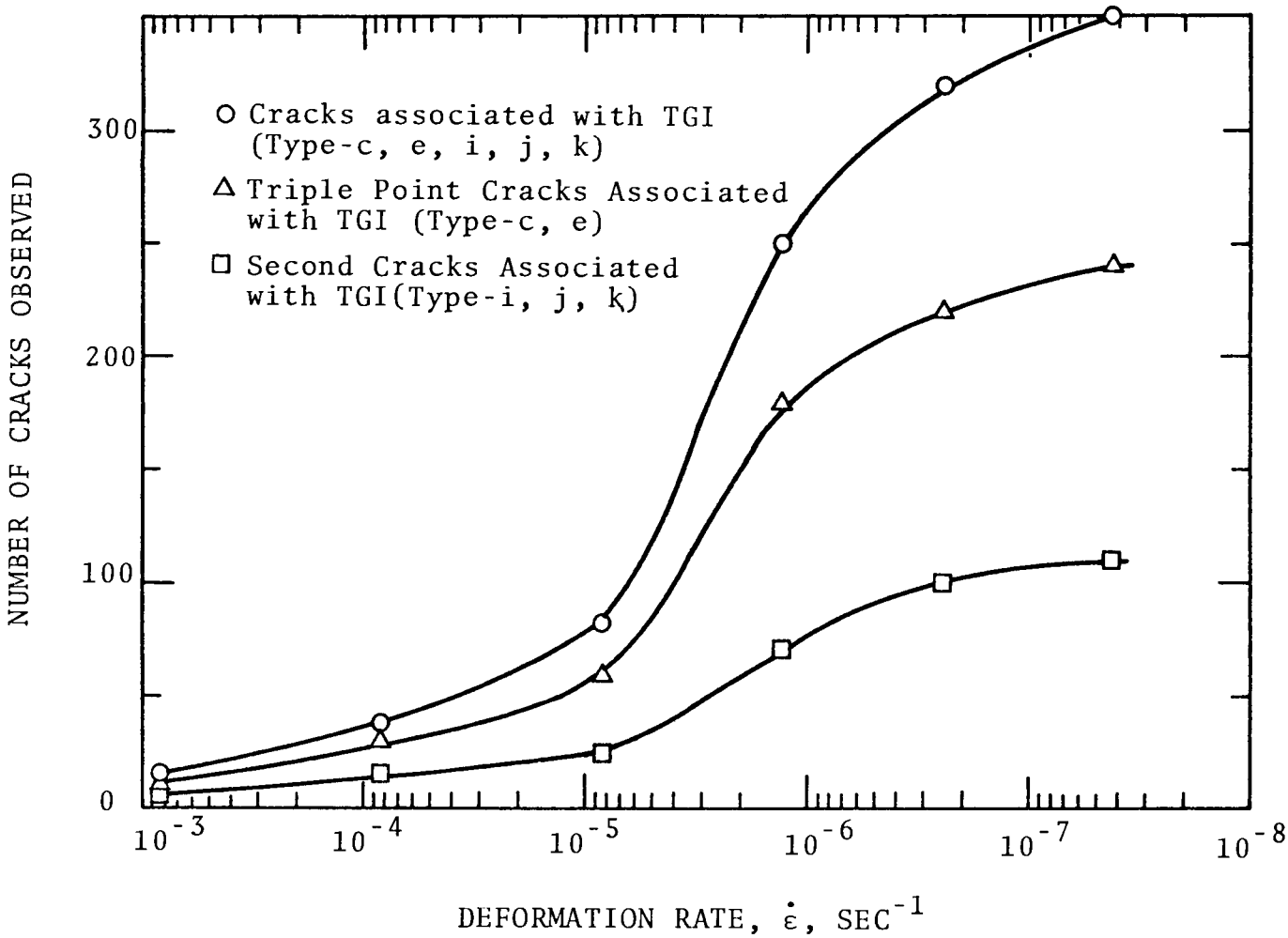

Fig. 7.6 Distribution of Intergranular Cracks Associated With Twin Boundary - Grain Boundary Intersection (TGI) as a Function of Deformation Rate.

cracks[14] are defined as those which are not associated with triple points (Figure 5 - g to k). The cracks in both of these groups were therefore evaluated in a manner similar to that used for the triple point cracks previously discussed.[15] Relatively few cracks with lengths $\ell > 2$ were observed to terminate at TGI.[15] The distribution of cracks terminated at TGI's and secondary cracks associated with TGI's are plotted in Figure 6 as a function of deformation rate. It is apparent that both the intergranular cracks related to TGI's and the secondary cracks increase with decreasing deformation rate (i.e. decreasing stress levels). This is consistent with the overall intergranular crack results for these specimens where triple junctions are involved.[10]

There is a strong indication that the propagation of triple point cracks may be interrupted at TGI's. This is mainly based on the observation that there are non-negligible number of triple point cracks which occupy sites between triple points and TGI (as shown in Figure 5-c, e, and Figure 6). Although it is difficult to visualize the actual cracking process, it can be safely assumed that the intergranular cracks have a greater tendency to nucleate at or near the triple point and then proceed toward the TGI and the next triple point. This circumstance may be explained from the fact that the surface energy[16], and stress concentration due to the applied stress at triple junctions

are higher than those at TGI's. The majority of cracks observed are triple point cracks which again supports this idea. Figure 7-A shows the angular incidence with respect to the applied stress of triple point cracks which are filled between the triple junction and TGI (Figure 5-c). Cracks with a length of less than one boundary facet are plotted in this Figure. The angular orientation of these cracks is consistent with those triple point cracks which are not associated with TGI.[10]

There is a further experimental result indicating that the secondary cracks appear, at times, to originate from TGI. Approximately 1 ∿ 3 percent of the total population of cracks observed in each specimen are found to be secondary cracks which occupy sites between TGI. And 1 ∿ 4 percent are found to be those lying between TGI and boundaries not associated with TGI (Figure 5-i, k). From the above observations, it is concluded that the role of the TGI appears to be similar to that of the triple point junction in the normal cracking process.

However, the extent of the role of TGI acting as a barrier to crack growth as well as being a nucleation site for cracks in the creep fracture behavior is certainly dependent on many factors such as the grain size, temperature, deformation rate, impurity levels, etc. along with the surface energy and the grain orientation relative to the applied stress for both the grain boundary and the twin boundary considera-

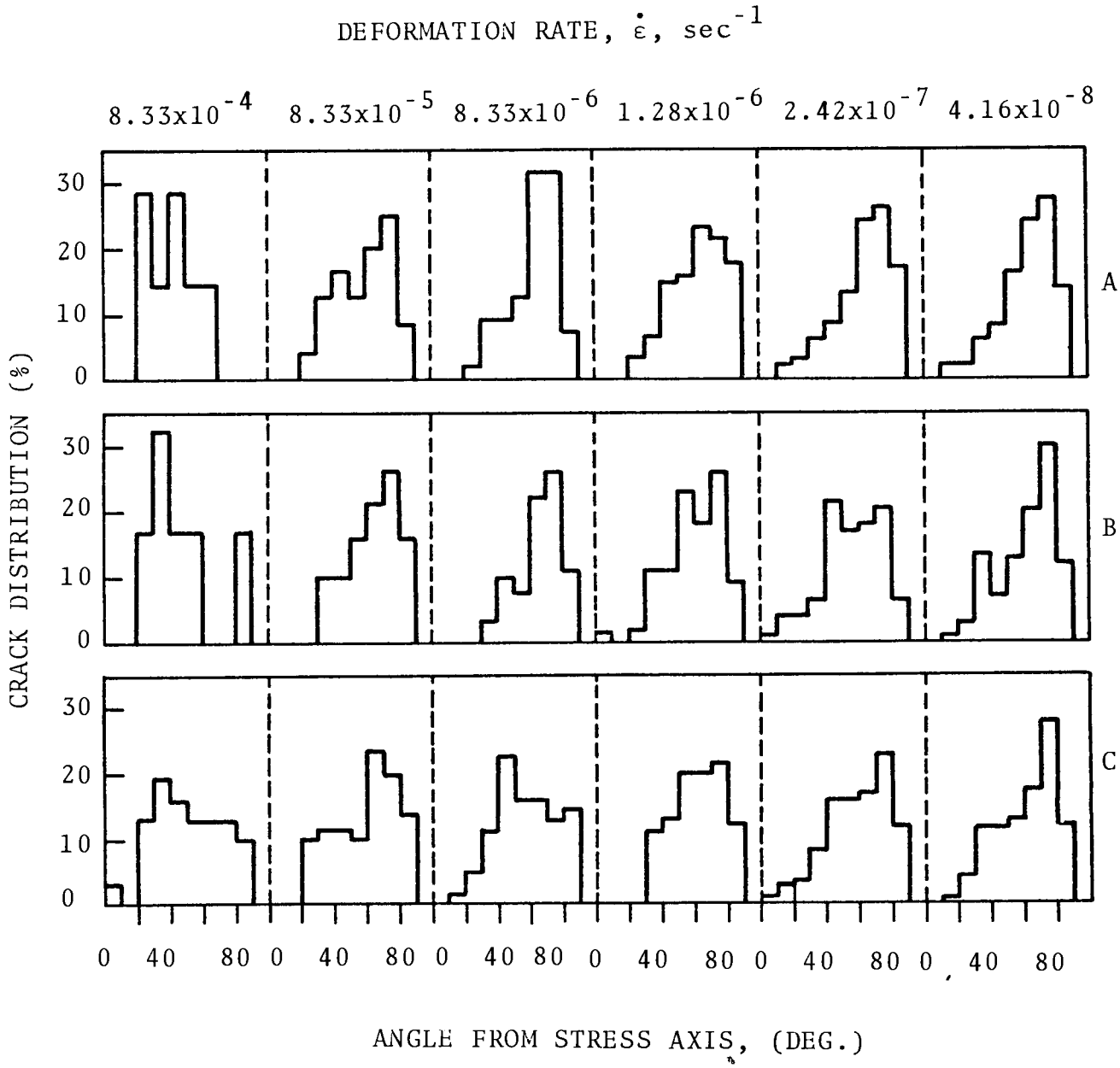

Fig. 7.7 Angular Percentage Distribution of Different Types of Intergranular Cracks: (A) Type c and e; (B) Type i, j and k; (C) Type g to k in Reference to Fig. 7.5.

tions.

Slow deformation at elevated temperature has been known to be a competitive process between intergranular deformation and grain boundary sliding. In the 304 stainless steel employed in this study, it is found that the ratio of grain boundary sliding strain to total elongation is increased when the deformation rate (i.e. stress level) is decreased.[15] This is consistent with the results shown in Figure 6 in the sense that the number of triple point cracks and secondary cracks, regardless of their relationship with TGI is increased when the grain boundary sliding component of the strain is increased with the decrease in the deformation rate.

In one study of secondary cracks which were formed in copper, Gittins and Williams[14] suggested that the secondary cracking may be affected by the triple point cracking because of the plastic strain field ahead of the triple point cracks. However, in this study of 304 stainless steel, careful examination shows that there is a predominance of secondary cracks formed along the boundary facet where no triple point cracks were observed to occur. Furthermore, as shown in Figure 7-Band C, the angular orientation of secondary cracks shows the same behavior as that of triple point cracks.[10] From the preceding observations together with the result that the considerable number of secondary cracks are related to TGI, it appears that the secondary cracking

mode is essentially the same as the triple point cracking mode. It is a reasonable conclusion since the role of TGI is quite similar to that of triple junction in the cracking behavior. It would be especially true in the case of coarse grain size materials such as the 210 μm size employed in this study. This cracking behavior could be different in fine grain size materials because there are more triple points available sites for cracking.

It is worth noting that approximately 5 percent of the intergranular cracks are found to be pure secondary cracks (Figure 5-g, h). This clearly demonstrates that the triple points and TGI's are not necessarily the only nucleation sites for crack formation. The degree of cracking follows from triple junctions, TGI, grain boundary, to twin boundary. It is interesting to note that the interfacial energies most likely also follow in that order.

7.2.4 Comparison of the Fatigue Induced Microstructure in Incoloy 800 When Tested in the Bend and Push-Pull Modes - (H. Nahm)

In order to better interpret and to apply the results of experimental data of elevated temperature mechanical properties, it is important to understand the testing technique and the specimen geometry employed in the various types of deformation modes. It is also very important to know which microstructural changes will affect the mechanical properties. For instance, a marked difference in hardness distribution

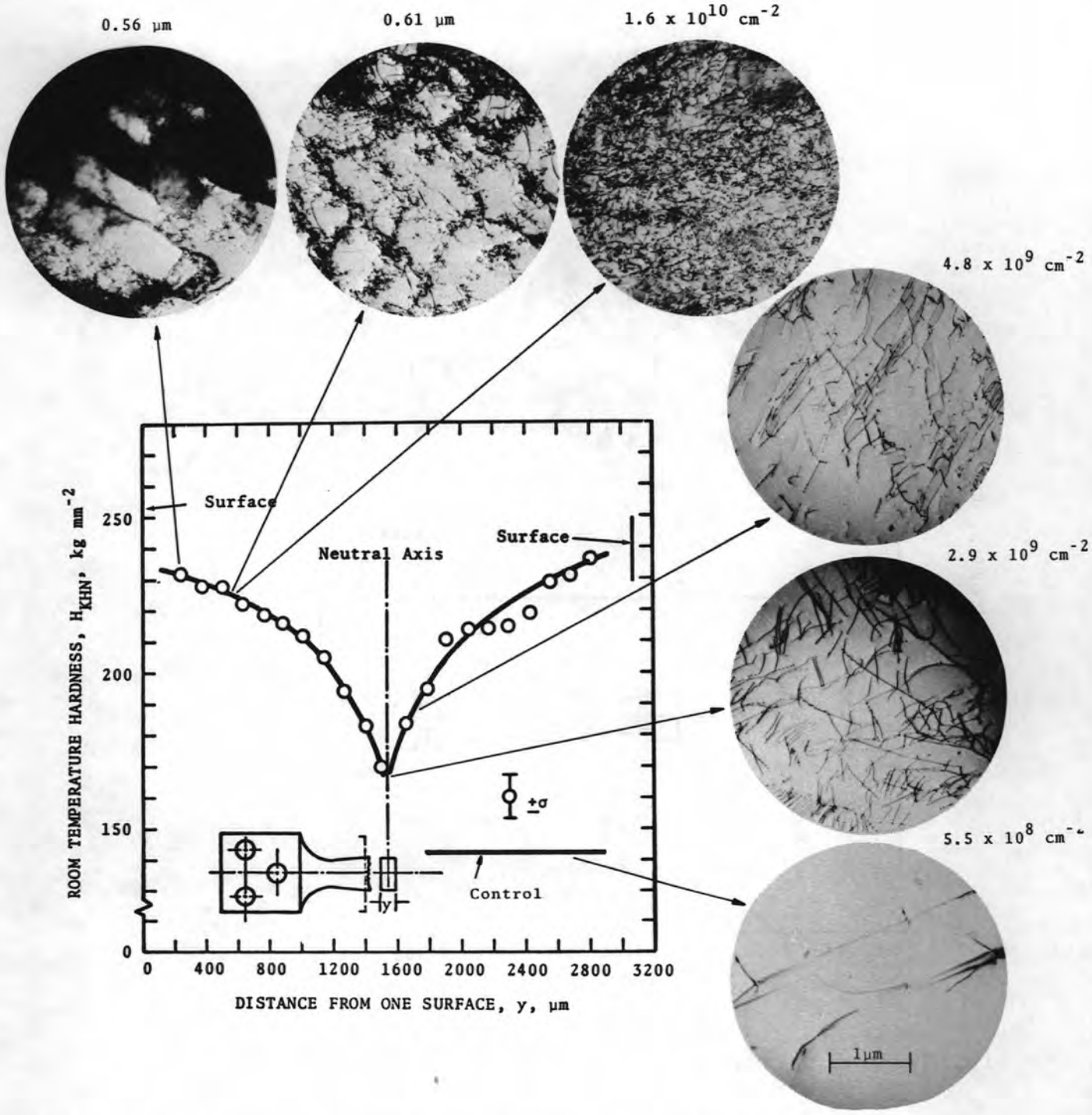

Fig. 7.8 Transverse Hardness Distribution in Incoloy 800 of Bend Fatigue Specimen on Plane Parallel to Fracture Surface with Corresponding Substructure. Strain Rate: 4×10^{-3} $(Sec)^{-1}$, Total Strain Range: 2 Percent, Fatigue Life: 260 Cycles, at 1300°F.

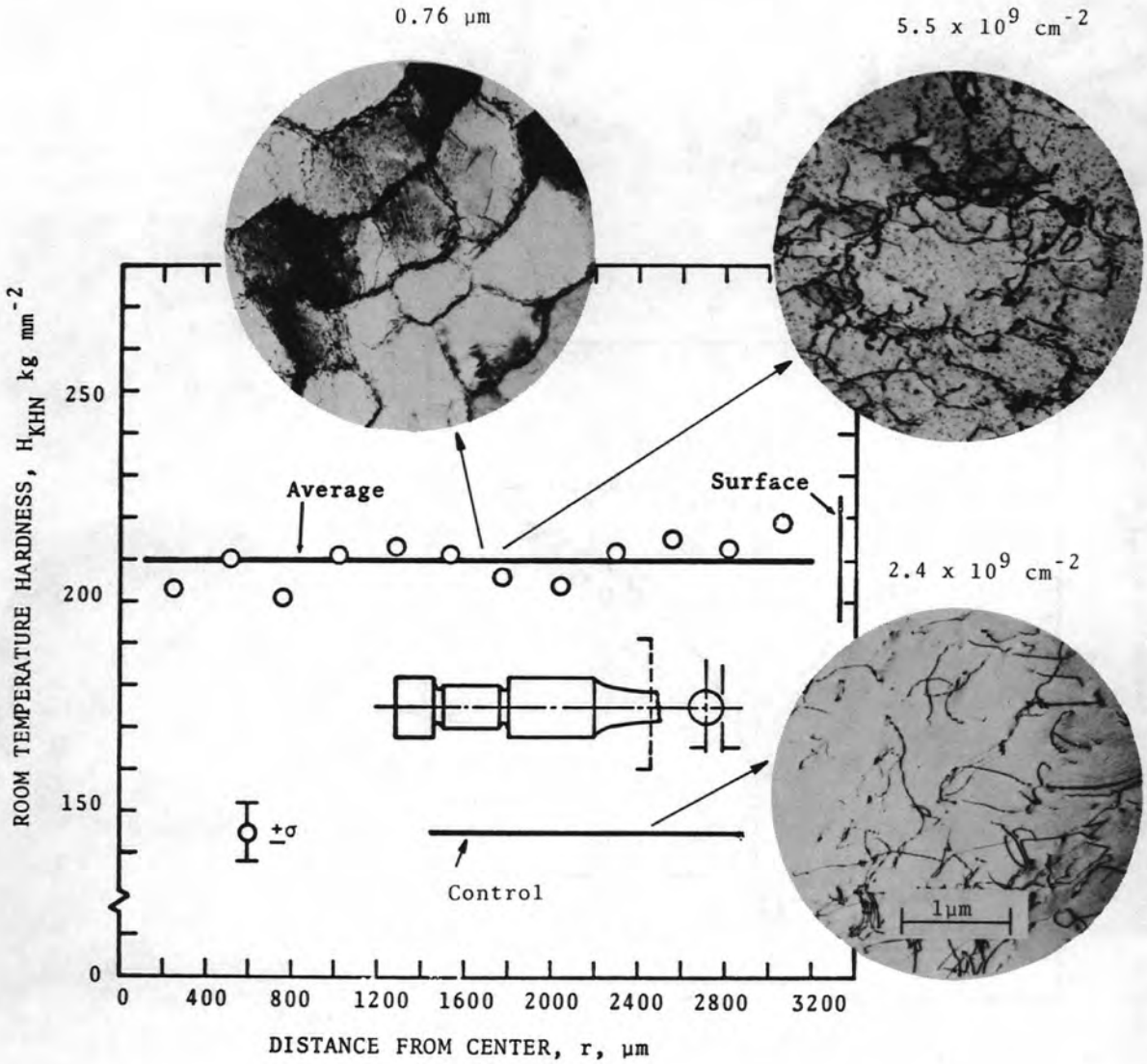

Fig. 7.9 Diametrical Hardness Distribution in Incoloy 800 of Push-Pull Fatigue Specimen on Plane Parallel to Fracture Surface with Corresponding Substructure. Strain Rate: $4 \times 10^{-3}(\text{Sec})^{-1}$, Total Strain Range: 2 Percent, Fatigue Life: 407 Cycles, at 1300°F.

was observed between the specimens tested in the bend and the push-pull mode at 650°C as shown in the previous progress report.[17] Transmission electron microscopy has been performed to show the substructural changes which occur when specimens are tested in these two types of deformation modes. The preliminary results are now presented.

Figure 8 and 9 show the dislocation substructure developed from the bend and push-pull fatigued specimen, respectively. Figure 8 shows that the substructure varies as a function of the position on a plane perpendicular to the neutral axis. The dislocation density increases from the neutral axis (essentially zero strain) toward the specimen surface ($\Delta\varepsilon_p \simeq 2\%$). A modulated dislocation substructure consisting of cells are formed near the surface. The dislocation density obtained from the shoulder portion of the specimen is very low. In principle the dislocation density in the neutral axis should be the same as that of the shoulder portion, but the observed difference is apparently due to the fact that the neutral axis continuously shifts around the mid-point of the specimen during the cyclic bending thereby inducing a small amount of residual internal stress in the form of dislocations.

Compared to the case of the bend fatigued specimen in Figure 8, there is little change in deformation substructure across the diameter of the hour-glass shaped push-pull fatigue specimen shown in Figure 9. Stress and strain distribution

on the minimum cross section seem to remain uniform during the push-pull fatigue mode testing.

In summary, the preliminary results suggest that the stress levels in the region of the surface of the bend specimens were slightly higher (Approximately 14 percent) than that along the diameter of the push-pull specimens although they were tested at the same strain range. The estimated increase in stress level was based on the observed subgrain sizes and is consistent with the measured increase in hardness and dislocation density. This larger stress level near the surface of the bend specimen may therefore account for the reduction in the fatigue life when both types are compared on the basis of the same strain range.

7.3 REFERENCES

1. H. Nahm, D. J. Michel and J. Moteff, J. of Mat. Sci. 8, 104 (1973).

2. COO-2107-10, "Correlation of Substructure with the Mechanical Properties of Plastically Deformed AISI 304 and 316 Stainless Steel," Progress Report for the Period Ending December 31, 1973; March 15, 1974, University of Cincinnati, Figure 13.

3. ORNL-4963, "Mechanical Properties Test Data for Structural Materials," Quarterly Progress Report for Period Ending April 30, 1974; p. 242.

4. ORNL-4963, "Mechanical Properties Test Data for Structural Materials," Quarterly Progress Report for Period Ending April 30, 1974; p. 249.

5. S. L. Robinson, C. M. Young and O. D. Sherby, J. of Mat. Sci. 9, 341 (1974).

6. U. Lindborg, Acta Met. 17, 157 (1969).

7. U. Lindborg and B. O. Gustafssson, Fracture 1969 (ed. Pol. Pratt), Chapman and Hall, London, p. 457 (1969).

8. R. Soderberg, Fracture 1969 (ed. Pol. Pratt), Chapman and Hall, London, p. 450 (1969).

9. J. S. Waddington and K. Lofthouse, J. Nucl. Mat. 22, 205 (1967).

10. H. Nahm, D. J. Michel and J. Moteff, J. Mat. Sci. 8, 104 (1973).

11. D. McLean, J. Inst. of Metals 85, 468 (1957).

12. C. W. Weaver, J. Inst. of Metals 87, 126 (1959).

13. D. J. Michel, H. Nahm and J. Moteff, Mat. Sci. Eng. 11, 97 (1973).

14. A. Gittins and J. A. Williams, Scripta Met. 3, 209 (1969).

15. H. Nahm, D. J. Michel and J. Moteff, To be submitted for publication.

16. L. E. Murr, G. I. Wong and R. J. Horylev, Acta Met. 21, 595 (1973).

17. ORNL-4963, "Mechanical Properties Test Data for Structural Materials," Quarterly Progress Report for Period Ending April 30, 1974; p. 237.

8. UNIVERSITY OF CALIFORNIA, LOS ANGELES

K. Ono, A.J. Ardell and A.S. Tetelman

8.1 Microstructure and High Temperature Deformation of Cr-Mo Steels for LMFBR Heat Exchanger (P. A. Chalco and K. Ono)

8.1.1 Introduction

During the past three years, we have examined microstructural variations as a function of time and temperature, and the concomitant effects on mechanical behavior, in 2-1/4Cr-1Mo steels of different initial carbon content. This study has been performed in conjunction with the research program being undertaken at Oak Ridge National Laboratory. Our major goals were: 1) to identify the metallurgical changes during the long-term exposure to reactor operating temperatures; 2) to characterize the mechanical properties of the exposed alloys; 3) to correlate the strength degradation to observed microstructural changes.

In a previous report,[1] the microstructure of long-term-tempered Alloy L (0.009%C) was presented. In this report, we present the microstructure of Alloys I (0.03%C) and H (0.12%C) in the long-term-tempered condition after normalizing and tempering at 1300°F for 1 hr. (N&T). As reported earlier,[2,3] in the N&T condition, Alloy H contained mostly granular bainite, while Alloy I contained a mixture of regular ferrite (80%) and granular bainite (20%).

8.1.2 Microstructures of Intermediate Carbon (0.03%) 2-1/4Cr-1Mo Alloy

8.1.2.1 Long-Term-Tempered at 850°F

The normalized and tempered, intermediate carbon material (Alloy I) was additionally tempered at 850°F for 4 to 19 months. In general, even very long tempering at 850°F did not produce any significant grain growth or reduction in the amount of bainite present. The average grain size of these materials remained to be 21μm, while the amount of bainite averaged around 17%. Figure 1a shows a bainitic region via thin foil TEM. It can be seen that polygonization or subgrain formation has occurred in the bainite. The subgrains average about 0.5μm in diameter and contain spheroidal carbides about 300-1000Å in diameter. Carbide coalescence and/or "in site" transformation can be observed in some regions. Needle shape carbides were also found in the bainite. Even after a year of tempering at 850°F, carbide precipitation in the bainite still continues and the larger carbides show a tendency to coalesce.

In the regular ferrite regions, dislocation substructures were observed very often in materials tempered for one year at 850°F. Although some dislocations may have annealed out, a large number of them still remain in the regular ferrite as seen in Figures 1b and 1c. These figures also show the heavy carbide precipitation that has occurred in and near the grain boundaries. Small groups of needles (Figure 1b) and

Fig. 1a Electron micrographs of Alloy I tempered at 850°F for 4 months, showing bainite.

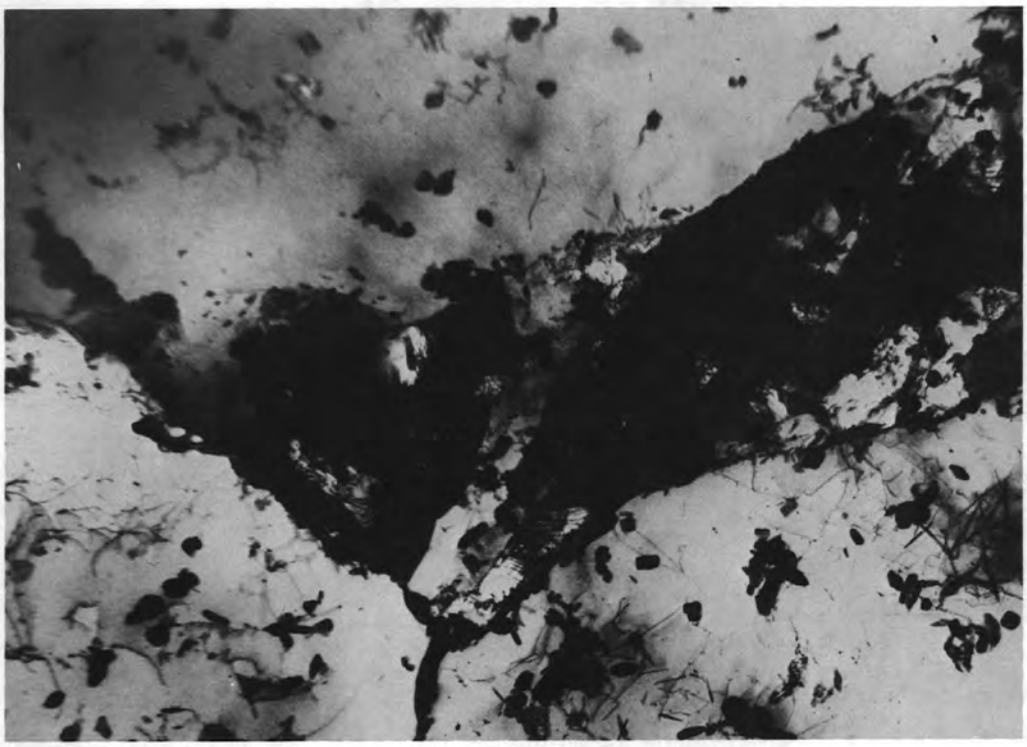

1μm

Fig. 1b Tempered at 850°F for 8 months, regular ferrite and bainite.

1 μm

Fig. 1c 8 months, regular ferrite.

some isolated ones were seen frequently. These were identified as M_2C particles having $a_o = 2.94 \pm .01\mathring{A}$ and $C_o = 4.54 \pm 0.01\mathring{A}$. Other particles were identified as M_7C_3. A common feature, observed in these materials, was the presence of "in situ" carbide transformation taking place throughout the ferrite matrix.

8.1.2.2 Long-Term-Tempered at 950°F

Tempering at 950°F of N&T Alloy I, produced gradual but significant microstructural changes. No grain growth occurred even after 19 months of tempering where the average grain size was about 20μm. However, bainitic zones were observed to shrink and disappear as tempering took place. After 19 months, less than 5% bainite remains. The bainite a microstructure which consists of dislocation substructures and carbides. As shown in Figure 2a, the carbides in the bainite were of two types. One type has a needle shape. The size of these carbides is 1000Å long, 50 to 100Å thick after four months of tempering, and slightly larger after eight months. The other type of carbides were coarser and ellipsoidal in shape, having dimensions of the order of 0.5μm. It appears that the coalescence of these particles produces their irregular appearance. As tempering time increased, it progressively became more difficult to find the bainitic zones. Very coarse carbides were commonly observed in previous bainitic regions, and also in regions where tempered bainite still showed its presence.

(a)

0.5 μm

(b)

0.5 μm

Fig. 2 Electron micrographs of Alloy I tempered at 950°F for 8 months. (a) Bainite, (b) Regular ferrite.

In the proeutectoid ferrite region no drastic microstructural changes were observed as shown in Figure 2b. Dislocations are seen to persist in these materials even after 8 months tempering. "In situ" carbide transformations were also commonly observed in materials tempered at 950°F as it is clearly seen in Figure 2b.

8.1.2.3 Long-Term-Tempered at 1050°F

The microstructural changes that occurred in Alloy I when tempered at 1050°F were more severe than the changes observed in a similar material tempered at 850 or 950°F. After the first month of tempering, the amount of tempered bainite was reduced to less than 10%. Tempering for longer times caused the almost complete disappearance of bainitic grains and the concurrent appearance of dark regions within some of the ferrite grains. These areas were identified by TEM as colonies of large M_2C needles. Grain growth did occur at slow rates. It was clearly detected after eight months of tempering when the grain size reached an average of 27μm.

The microstructural changes occurring in these materials were followed in more detail with electron microscopy. After one month of tempering, the regular ferrite did not show any significant changes from the initial N&T condition. However, isolated colonies of 10-20 needles were occasioally observed in some regions. Tempered bainite regions were seldom encourtered. The bainitic carbides averaged about 1000Å in diameter, but no M_2C carbide colonies were observed in the bainite.

Further tempering caused the formation of large colonies of M_2C needles carbides in the proeutectoid ferrite (Figure 3a), and the formation of subgrain structure and carbide coarsening in the bainite (Figure 3b). The M_2C needles were 1-2μm long, 800Å wide, and 100-200Å thick. In the bainite, the subgrains were 1-2μm in diameter, while the precipitates were blocky and irregular in shape. Some of these particles reached a size on the order of 1μm. Some clear evidence of what appears to be an "in situ" $M_2C \longrightarrow M_6C$ transformation were observed. This observation is very similar to the one made by McCann and Ridal,[4] who also observed M_2C needles being decorated by M_6C spheroids.

8.1.3 Microstructure of High Carbon (0.12%) 2-1/4Cr-1Mo Alloy

8.1.3.1 Long-Term-Tempered at 850 and 950°F

As shown in Figures 4a and b, the tempering of Alloy H at 850 or 950°F, up to 12 months, did not cause any significant changes in the microstructure. As in the N and N&T condition optical micrographs did not reveal much of the internal structure of these materials as electron micrographs did. However, it was observed in optical micrographs that a very fine grain structure, of the order of 5-10μm exist in these materials. At higher magnifications, electron micrographs, such as Figures 4a and b, show that M_2C needles and other coarser carbides exist in these materials in amounts and quality which are comparable to those in the N&T condition.

(a)

0.5μm

(b)

1 μm

Fig. 3 Electron micrographs of Alloy I tempered at 1050°F for 12 months. (a) Regular ferrite, (b) Bainite.

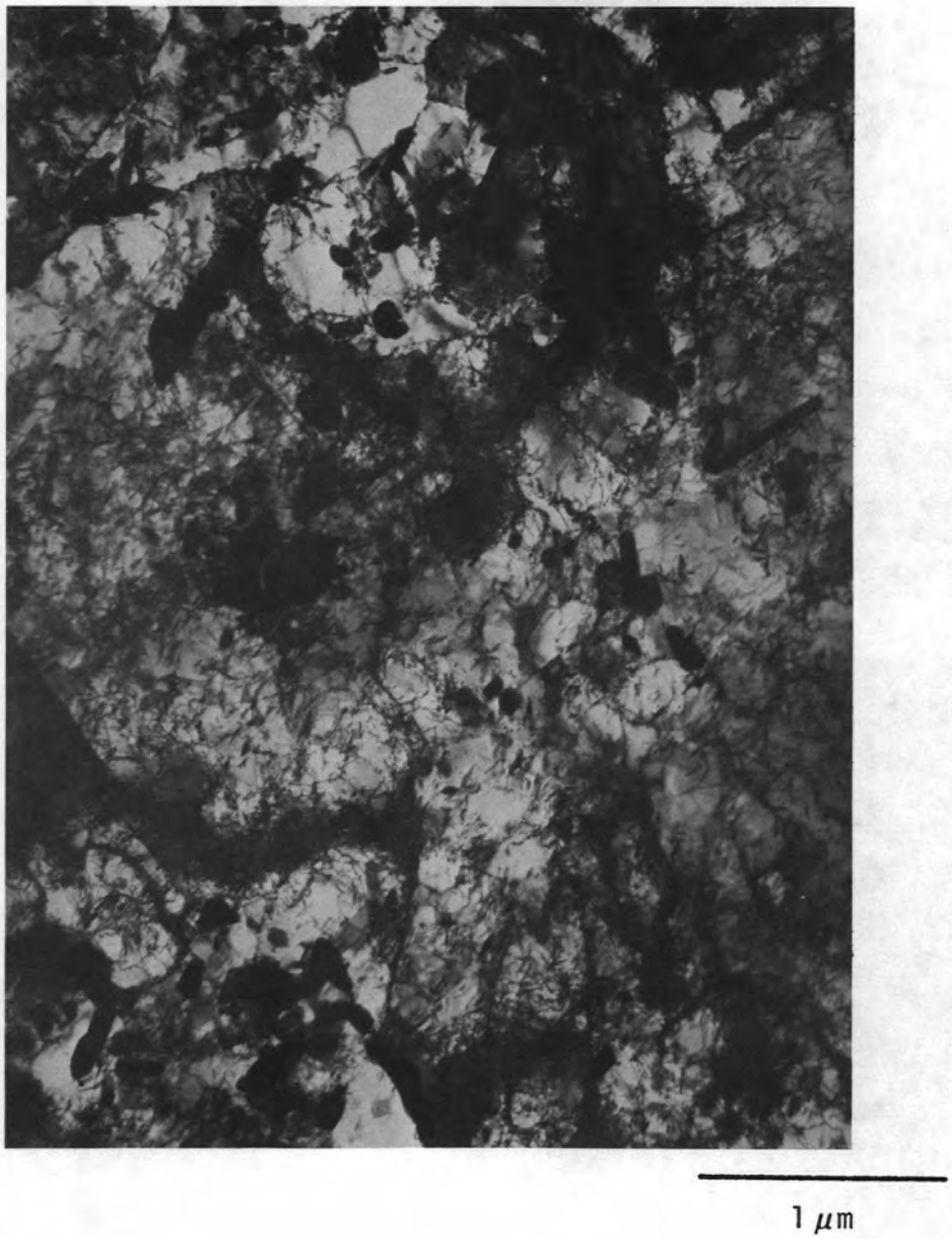

Fig. 4a Electron micrographs of Alloy H tempered for 12 months at 850°F.

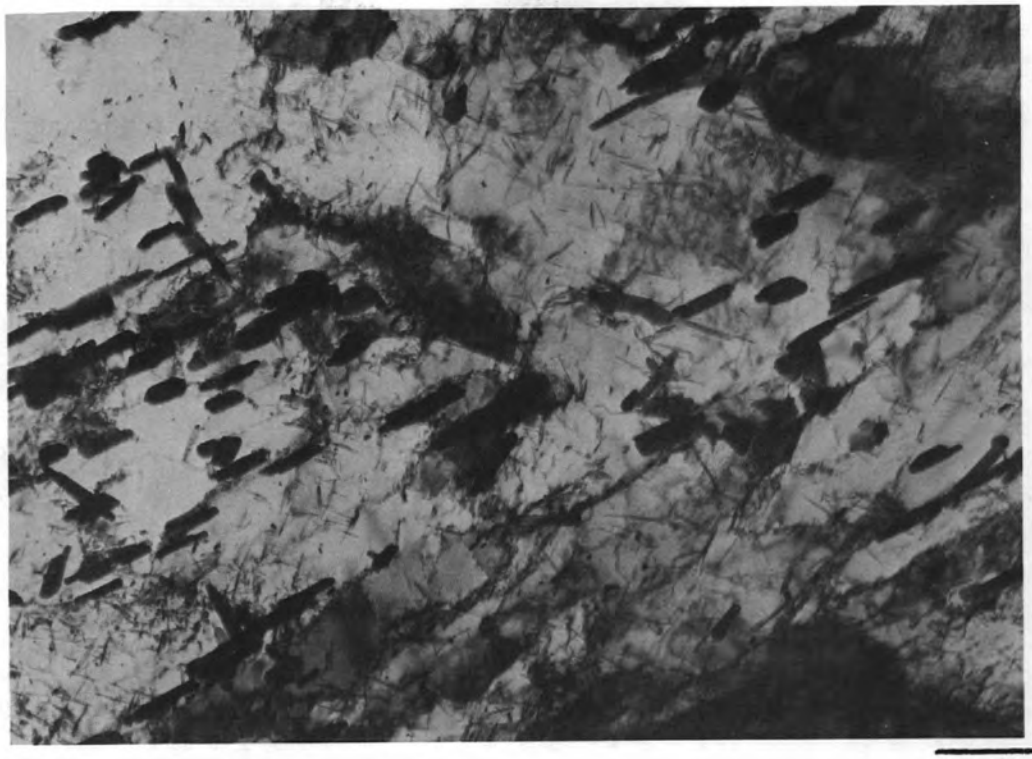

0.5 μm

Fig. 4b. Electron micrographs of Alloy H tempered for 12 months at 950°F.

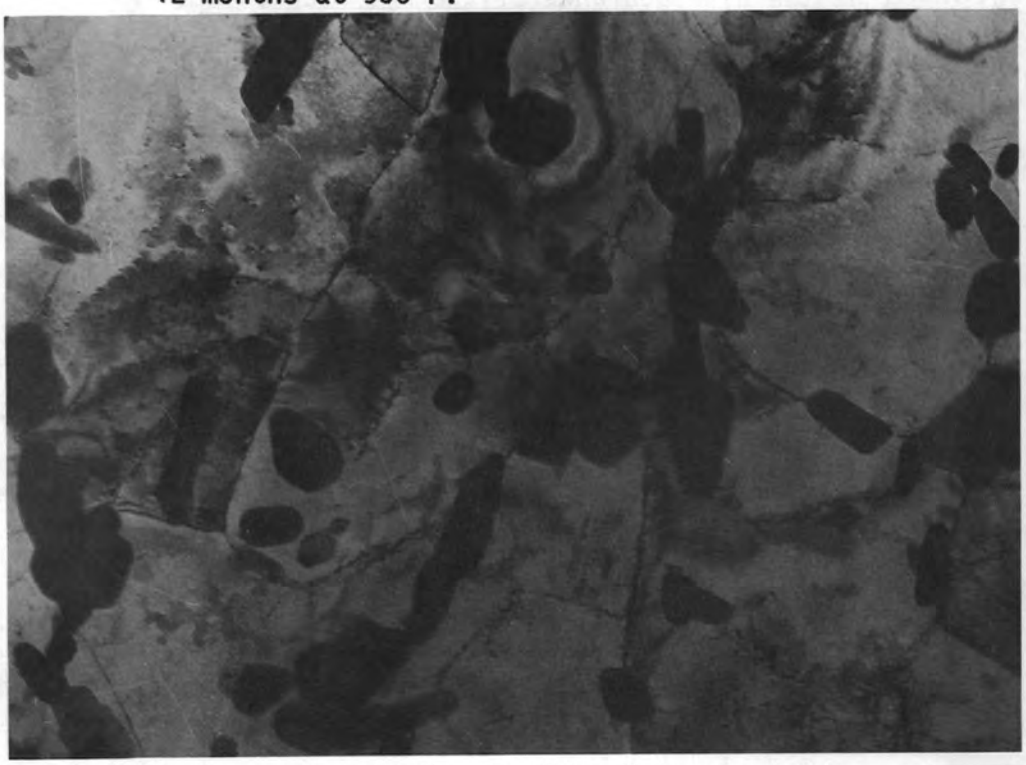

0.5 μm

Fig. 4c. Electron micrographs of Alloy H tempered for 12 months at 1050°F.

8.1.3.2 Long-Term-Tempered at 1050°F

Tempering at 1050°F produced severe internal microstructural changes in these materials. These variations cannot be appreciated at all in optical micrographs. However, it can be seen in electron micrographs (Figure 4c) that the M_2C needles are completely gone when this material is tempered for 12 months at 1050°F. The new microstructure is very uniform and is composed of a ferrite matrix containing subgrains, 0.6μm in diameter, and coarse carbides (0.2 - 1μm diameter). Some of which are preferentially located at subgrain boundaries. Also dislocation networks are seen to be contained not only in the subgrain boundaries, but also within the subgrains. Since the microstructure of materials tempered for 1-8 months was not studied by TEM, we can only assume that the disappearance of the M_2C needles occurred gradually through the 1-12 months tempering period.

8.2. Creep Studies in Lightly Cold-Worked Stainless Steels (O. Ajaja and A.J. Ardell)

8.2.1 Introduction

In this research program, the influence of small amounts of cold work (0-10%) on the elevated temperature creep kinetics of austenitic stainless steels (types 316 and 304) is being studied. Previous experiments on 316[5] have shown that an optimum level of cold work exists for which the creep rupture life is maximized, and suggested that there exists a much lower level of cold work (in the

range 0-10% for our present test conditions) for which the rupture life is a minimum. This latter observation has provided the impetus for the present experiments, in which the effect of small amounts of cold work on the creep characteristics of types 304 and 316 will be investigated for various temperatures and stresses.

8.2.2 Experimental Details

8.2.2.1 Testing Equipment

A constant stress creep apparatus[6,7] has been built for creep rupture testing. This consists of a constant radius wheel linked to a constant-stress cam-type lever arm via a roller chain. The other end of the chain is connected to the linkage bearing the test specimen. Strain measurements are made with a linear variable differential transformer (LVDT) whose output is recorded on a strip chart recorder. Displacements of 0.001 in. have been accurately measured. The strain in the linkage is determined by applying the same load to the linkage (without the specimen) at the same testing conditions, and noting the extension. This is subsequently corrected for in computing the values of true strain from the elongation data. The lever-arm was calibrated for constant stress prior to testing, the maximum deviation from the initial stress value being approximately ± 2%. Specimens will be tested at temperatures in the range 1000°F-1400°F under a helium atmosphere to minimize oxidation.

8.2.2.2 Test Material and Specimen Preparation

We are currently running tests on type 316 stainless steel whose composition is shown in Table 1. This material was supplied to us in the form of 0.250 in. diameter rods by M. M. Paxton at HEDL. The rods were swaged down to approximately 0.22 in. diameter from which cylindrical test specimens were machined. The specimens are threaded on both ends to fit into the internally threaded linkage-grips. All specimens are being solution annealed in a helium furnace at 1040 ± 4°C for 1 hr. and quenched into a refrigerated 10% NaOH solution. Cold work (0-10%) is introduced by straining in an Instron tensile machine at room temperature. The initial gauge lengths vary from 1.00 in. to 1.10 in., depending on the initial level of prestraining.

TABLE 1

Composition of the type 316 stainless steel test material

C	Mn	P	S	Si	Ni	Cr	Mo	Co	Cu	N_2	Fe %
0.040	1.76	0.010	0.008	0.58	13.65	17.27	2.37	0.03	0.03	0.0109	Balance

8.2.3 Results and Discussion

8.2.3.1 Steady-State Creep and Rupture Behavior

Short duration tests (less than 50 hr.) have been run at 1400°F and stress levels of 25 and 19 Ksi. The creep curves for the 19 Ksi

tests are shown in Fig. 5. The creep curves are classical in most regards, although there appear to be some unusual fluctuations. These may be due to instabilities in the voltage supply for the LVDT, or in the temperature controller, and will be investigated further to find out whether the effect is real. Values of steady state creep rate ($\dot{\epsilon}_s$), rupture life (t_R), rupture elongation (ϵ_R), and reduction of area at fracture (R.A.) are summarized in Tables 2 and 3. The following are noted from the results:

(i) The values of $\dot{\epsilon}_s$ do not vary appreciably with the cold work level;

(ii) The values of ϵ_R and R.A. decrease as the level increases, implying a loss of ductility;

(iii) No appreciable change in t_R was observed in this range of prestraining (0-10%). A special test conducted on a sample with 20% cold work (Table 3) at 25 Ksi shows that both the rupture life and the steady state creep rate differ considerably from those observed in the 0-10% range. The sample was more creep resistant and less ductile.

8.2.3.2 Transient Creep Behavior

The major effect of prior cold work lies in the appreciable difference in transient creep behavior, which is responsible for the displacements in the creep curves observed in Fig. 5. The curves diverge out from the origin and become reasonably parallel in the

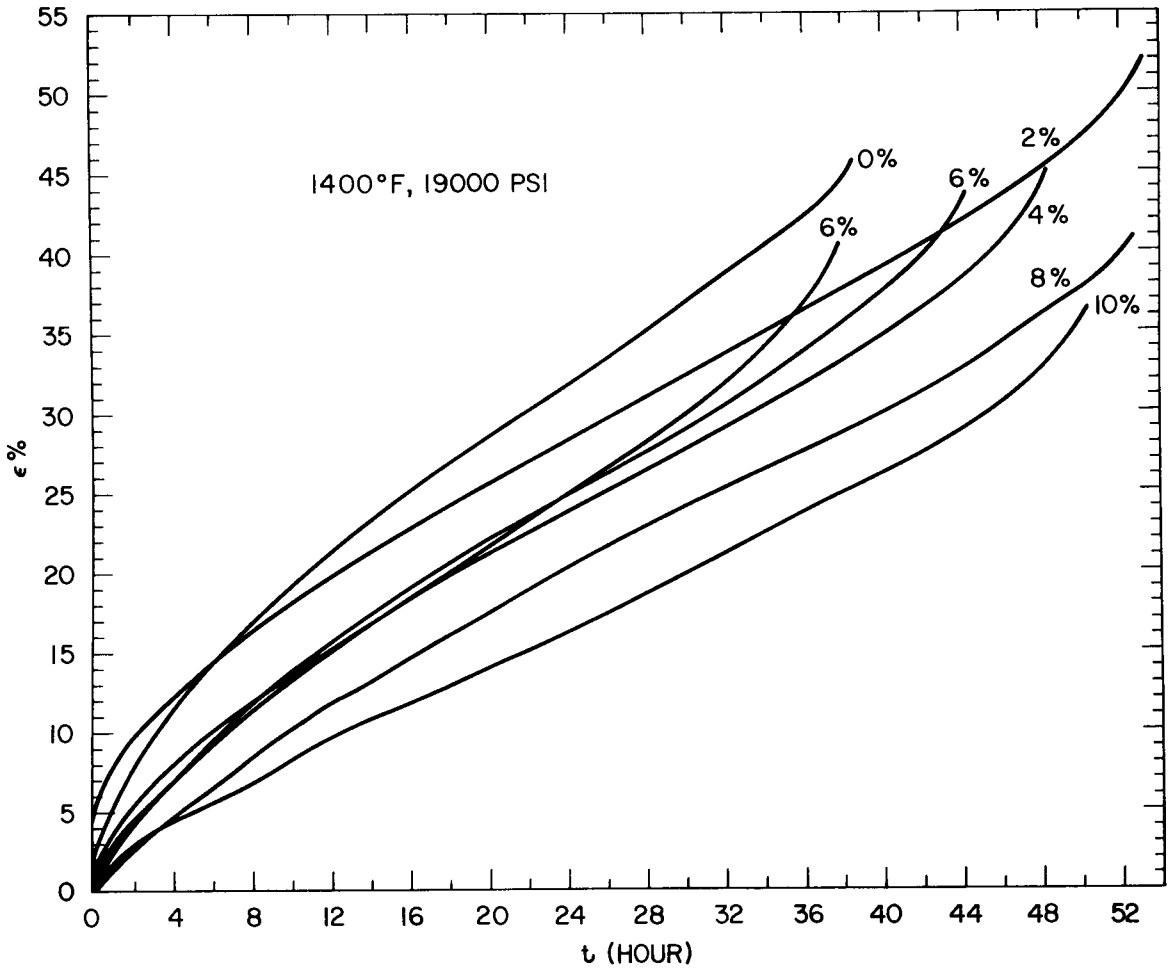

Fig. 5 True strain vs. time curves for type 316 stainless steel tested under a constant stress of 19,000 psi at 1400°F. The numbers next to each curve indicate the prestrain applied to each sample at room temperature.

TABLE 2

Creep parameters for type 316 stainless steel tested at 1400°F and 19 Ksi

% Cold Work	$\dot{\epsilon}_s$ (hr.$^{-1}$)	t_R(hr.)	ϵ_R (%)	R.A. (%)
0	0.0084	36.9	56.55	58.4
2	0.0067	48.6	68.18	65.5
4	0.0067	43.1	56.89	62.7
6	0.0082	33.6	49.94	63.1
6	0.0070	40.8	54.59	58.4
8	0.0062	49.2	50.33	49.9
10	0.0060	46.3	43.94	46.2

TABLE 3

Creep parameters for type 316 stainless steel tested at 1400°F and 25 Ksi

% Cold Work	$\dot{\epsilon}_s$ (hr.$^{-1}$)	t_R (hr.)	ϵ_R (%)	R.A. (%)
0	0.0586	6.4	67.85	71
2	0.0584	6.0	60.51	63
4	0.0547	5.6	53.74	67
6	0.0568	6.1	53.59	58
8	0.0597	5.4	52.68	61
10	0.0507	6.2	46.66	54
20	0.0336	8.0	31.22	38

steady state region. A curve-fitting computer program was run using the test data, and all the data were described quite accurately by a creep equation of the type[8-11]

$$\epsilon = \epsilon_o + \epsilon_t[1 - e^{-rt}] + \dot{\epsilon}_s t \quad , \tag{1}$$

where ϵ_o is the strain imposed on loading, ϵ_t is the so-called limiting transient creep strain, r is a constant related to the rate at which the transient creep disappears. The curve fitting was excellent, even taking the fluctuations seen in Fig. 5 into account.

As can be seen from the results in Table 4, the parameters ϵ_o, ϵ_t and r all vary with the prior cold work level. Both ϵ_o and ϵ_t decrease slowly as the cold work level increases, whereas r appears to

TABLE 4

Transient creep parameters at 1400°F obtained by appling Eq. (1) to the data in Fig. 5

% Cold Work	19 ksi			25 ksi		
	ϵ_o	ϵ_t	r	ϵ_o	ϵ_t	r
0	0.0212	0.095	0.253	0.0282	0.087	1.498
2	0.0454	0.072	0.317	0.0195	0.063	1.983
4	0.0124	0.062	0.284	0.0191	0.093	1.931
6	0.0043	0.048	0.306	0.0122	0.048	2.132
8	0.0016	0.045	0.156	0.0222	0.044	1.376
10	0.0022	0.022	0.570	0.0084	0.041	0.746

go through a broad maximum (with the exception of the one data point for the 10% cold work sample tested at 1400°F, 19 ksi). It is hoped that further experiments at lower temperatures and stresses will produce a more consistent set of data.

Tests are now being run at 1200°F and many more will be run at even lower temperatures on 316 and later, 304 stainless steels. Meanwhile the testing equipment is being modified so that we can run six tests (in the same furnace) simultaneously using six lever arms. If the influence of light cold work on the creep properties proves significant, we intend to conduct studies of the microstructures of the test specimens at various stages of creep and correlate these with the mechanical properties.

8.3 The Effects of Carbon on the Elevated Temperature Tensile Properties of Type 316 Stainless Steel (P.L. Jones and A.S. Tetelman)

8.3.1 Introduction

The effect of carbon on the elevated temperature tensile properties and fracture behavior of type 316 stainless steel has been studied. Sheet tensile specimens, all machined from the same heat, were carburized in a gas reaction furnace using hydrogen and methane. Tensile tests were performed at 760°C (1400°F). Yield strength, ultimate tensile strength, true fracture strength, and tensile ductility were correlated as a function of bulk carbon content and/or volume

fracture of carbon case. A model has been developed to describe the fracture behavior of case carburized type 316 stainless steel.

8.3.2 Experimental Procedures

8.3.2.1 Specimen Preparation

Sheet tensile specimens were machined from well characterized type 316 stainless steel supplied by the Hanford Engineering Development Laboratory, Richland, Washington. The steel, Heat No. 65808, was produced by the Allegheny Ludlum Steel Corporation, Pittsburgh, Pennsylvania. A chemical analysis supplied with the material is given in Table 5.

TABLE 5

Chemical Analysis of Material

	C	Mn	P	S	Si	Cr	Ni	Mo	Fe
wt.%	0.059	1.72	0.016	0.009	0.44	17.30	13.55	2.34	Balance

The as-received alloy bar was cut into 0.25 in. (6.35 mm) sections and subsequently cold rolled to an average thickness of 0.020 in. (0.508 mm). In all cases the original rolling direction was preserved. Coupons 0.5 in. (12.7 mm) by 3.25 in. (82.55 mm) were sheared from the rolled sheet and machined to the final specimen geometry using a carbide cutter. To remove cold work, specimens were heat treated at 1038°C

(1900°F) in a 25 μ vacuum furnace for 30 min. and air cooled before breaking vacuum.

Case hardening of specimens was carried out in a gas reaction furnace shown schematically in Fig. 6. A gas mixture consisting of 96% hydrogen and 4% methane was passed through the system at a flow rate of 400 cc/min. The specimen temperature was maintained at 900 ± 5°C and the case depth was controlled by varying the time at which specimens were exposed to the carburizing atmosphere.

8.3.2.2 Mechanical Test Procedures

Tensile tests were performed on the as-annealed and case carburized specimens at 760°C (1400°F) using a clam-shell resistance wound tube furnace in conjunction with an Instron testing machine. A cross-head speed of 0.05 in./min. was used in all tests. Both ends of the furnace were covered with fibered asbestos insulation to prevent heat loss and thermal gradients. The test temperature varied less than ± 3°C. To minimize oxidation, helium gas was passed through the furnace for the entire testing cycle. Specimens were tested using Inconel 700 flat wedge grips. Load-elongation curves were used to determine yield and fracture strength.

The yield strength was taken to be the 0.2% offset strain. Ultimate tensile strength was calculated from the maximum load and the initial cross-sectional area of the specimen. Fracture strength was determined using the load at specimen separation and the final cross-sectional area. Fracture strain, defined as the natural log of the

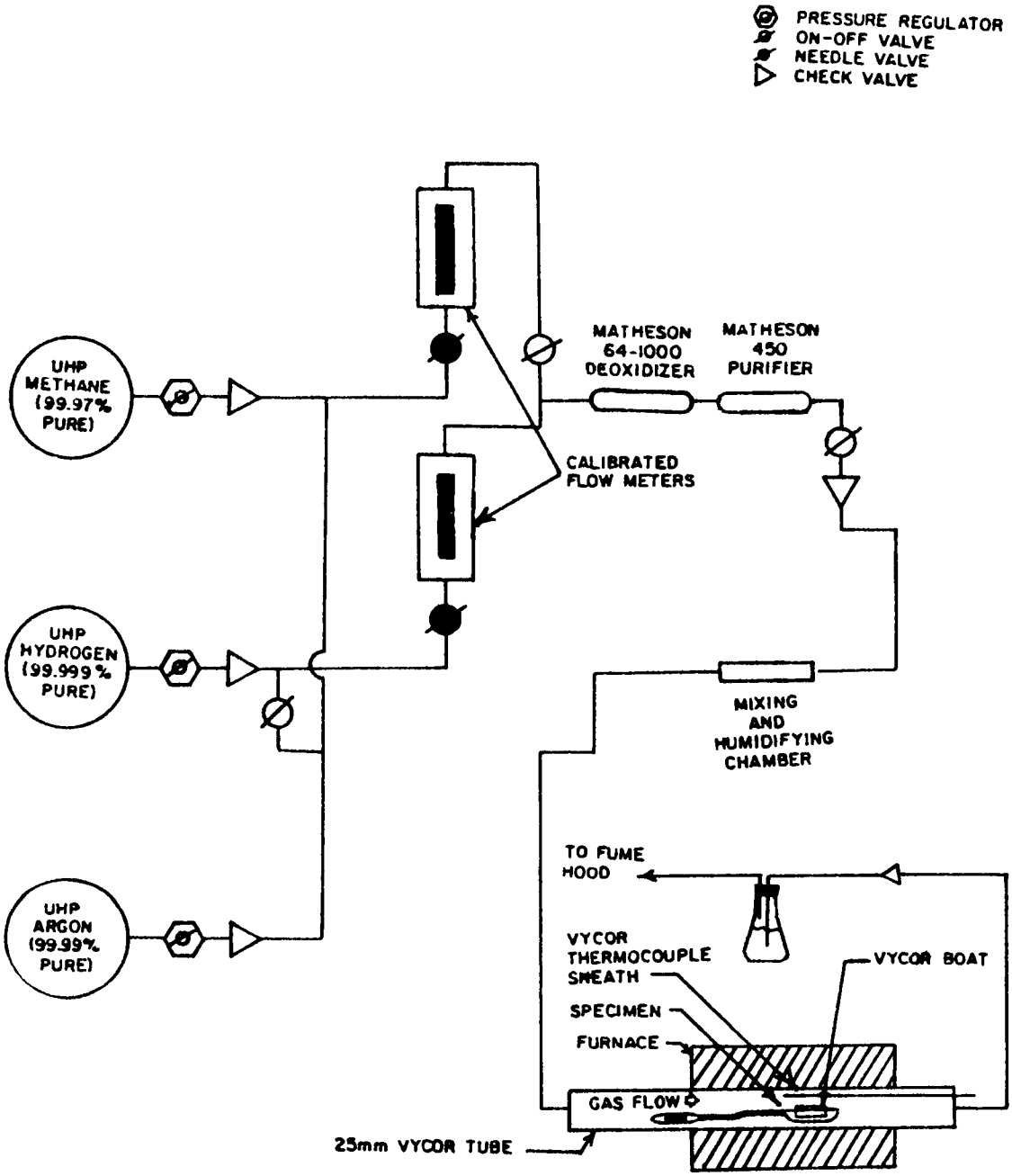

Fig. 6 Gas carburizing system

original cross-sectional area divided by the final cross-sectional area, was used as a measure of the tensile ductility.

Specimen thickness and width were measured three times to the nearest 0.0005 in. (0.01 mm) using a cathetometer before and after testing. The final width and thickness of tensile specimens were measured on the fracture surface. The average values of these parameters were used to calculate initial and final cross-sectional areas.

8.3.2.3 Carbon Analysis

Carbon analyses were performed on carburized specimens both before and after tensile testing. A Leco model 515-000 carbon analyzer was used together with an Ecco model PO-3D power oscillator. The reproducibility was ± 5% using a 1 gram sample. No significant loss of carbon occurred during the elevated temperature tensile testing. The initial carbon content of the as-received alloy was furnished by HEDL.

8.3.2.4 Measurement of Volume Fraction of Carbon Case

Optical micrographs of failed carburized specimens were used to measure the volume fraction of the carbon case. The volume fraction was calculated using the relation

$$V_B = \frac{L_1 + L_2}{t_f} \qquad (2)$$

where L_1 and L_2 are the surface depths of carbon penetration and t_f is the thickness of the specimen (see Fig. 7). The values of these parameters

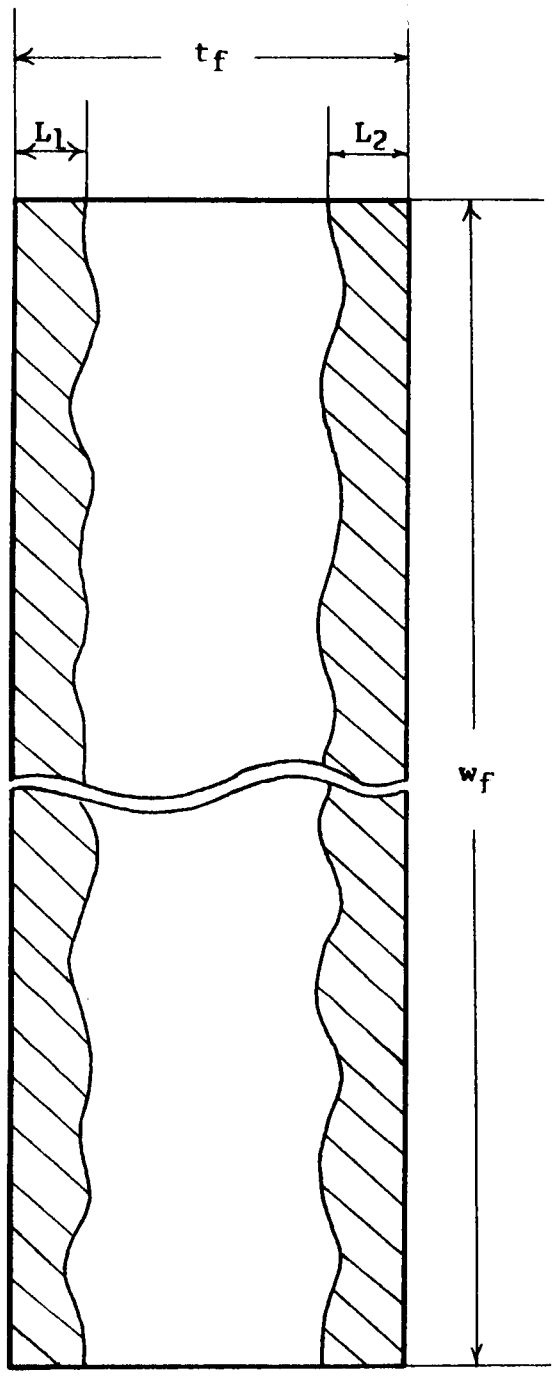

Fig. 7 Parameters used to calculate case depth and volume fraction.

used in the subsequent analysis represent the average of six measurements taken along the cross-sections of failed specimens near the fracture surface.

8.3.3 Results

8.3.3.1 Mechanical Properties vs. Bulk Carbon Content

A correlation of mechanical properties with bulk carbon content confirmed the general trends described by other researchers[12-15] (Figs. 8 and 9). Both the yield and fracture strength increase while the ductility decreases over the range 0.058 wt.% to 1.820 wt.%C. A linear relationship of the form

$$\epsilon_f = 0.134 - 0.237 \log_{10} (\text{wt.\%C}) \quad . \tag{3}$$

was observed when ductility was plotted as a function of the log of the bulk carbon content in this thickness material. Because the carbon added by gas carburization is not homogeneously distributed throughout the sample, but is present in a relatively shallow case, it is unrealistic to relate mechanical properties to the bulk carbon content of the sample. The remainder of this paper will be concerned with the volume fraction of carbon case.

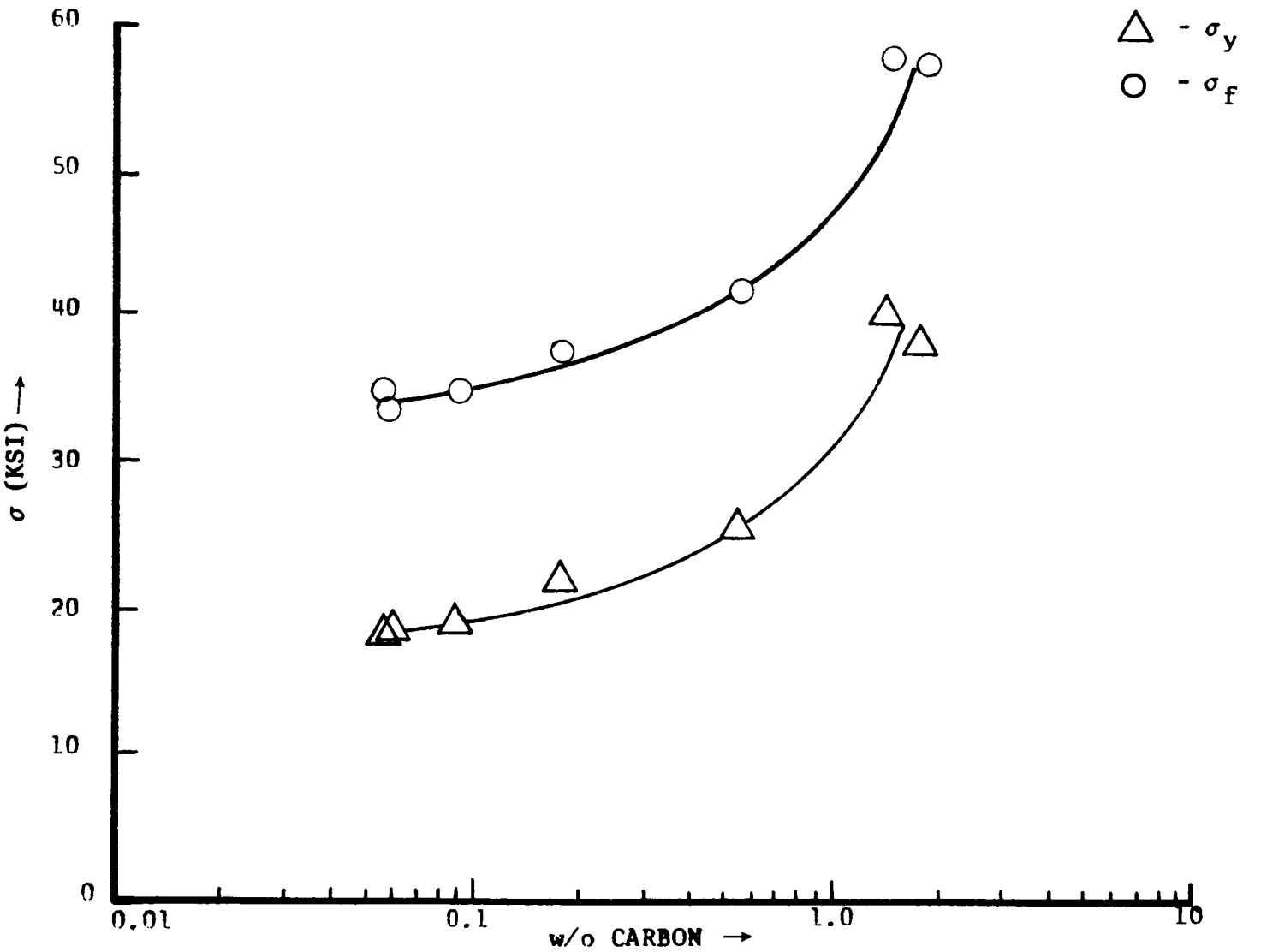

Fig. 8 Yield and fracture strength vs. bulk carbon content

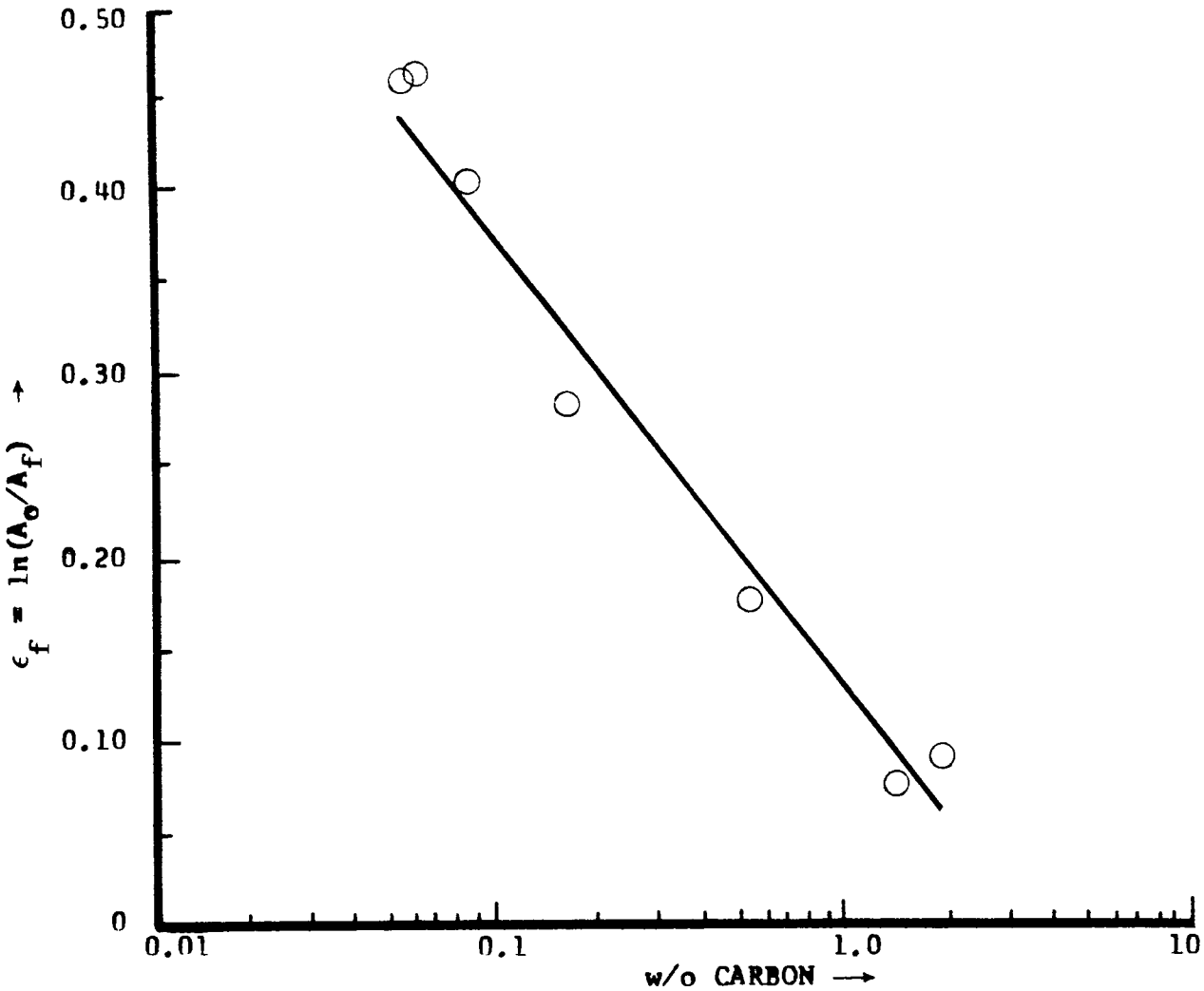

Fig. 9 Tensile ductility vs. bulk carbon content

8.3.3.2 Mechanical Properties vs. Volume Fraction of Case

A plot of the mechanical properties as a function of volume fraction of the carbon case provides a dimensionless comparison of the mechanical properties and case depth. The results are presented in Figs. 10 and 11. The volume fraction ranged from 0 to 0.628. Yield and true fracture strength increase in a linear manner as the case depth increases. The slopes of these curves, taken from a least squares fit, are approximately equal.

An interesting phenomenon is observed when the reduction in cross-sectional area is compared to the volume fraction of the carbon case (Fig. 11). The ductility decreases slightly for volume fractions ranging from 0 to 0.121. Increasing the volume fraction from 0.121 to 0.246 results in a 63% decrease in ductility. The ductility again decreases linearly as the volume fraction is increased from 0.246 to 0.628.

8.3.4 Fracture Model

A model has been developed to describe the fracture behavior of case carburized type 316 stainless steel. A continuous fibered composite model has been successfully used to predict UTS as a function of volume fraction of case and the results extended to describe the embrittlement that occurs over a relatively narrow range of volume fraction.

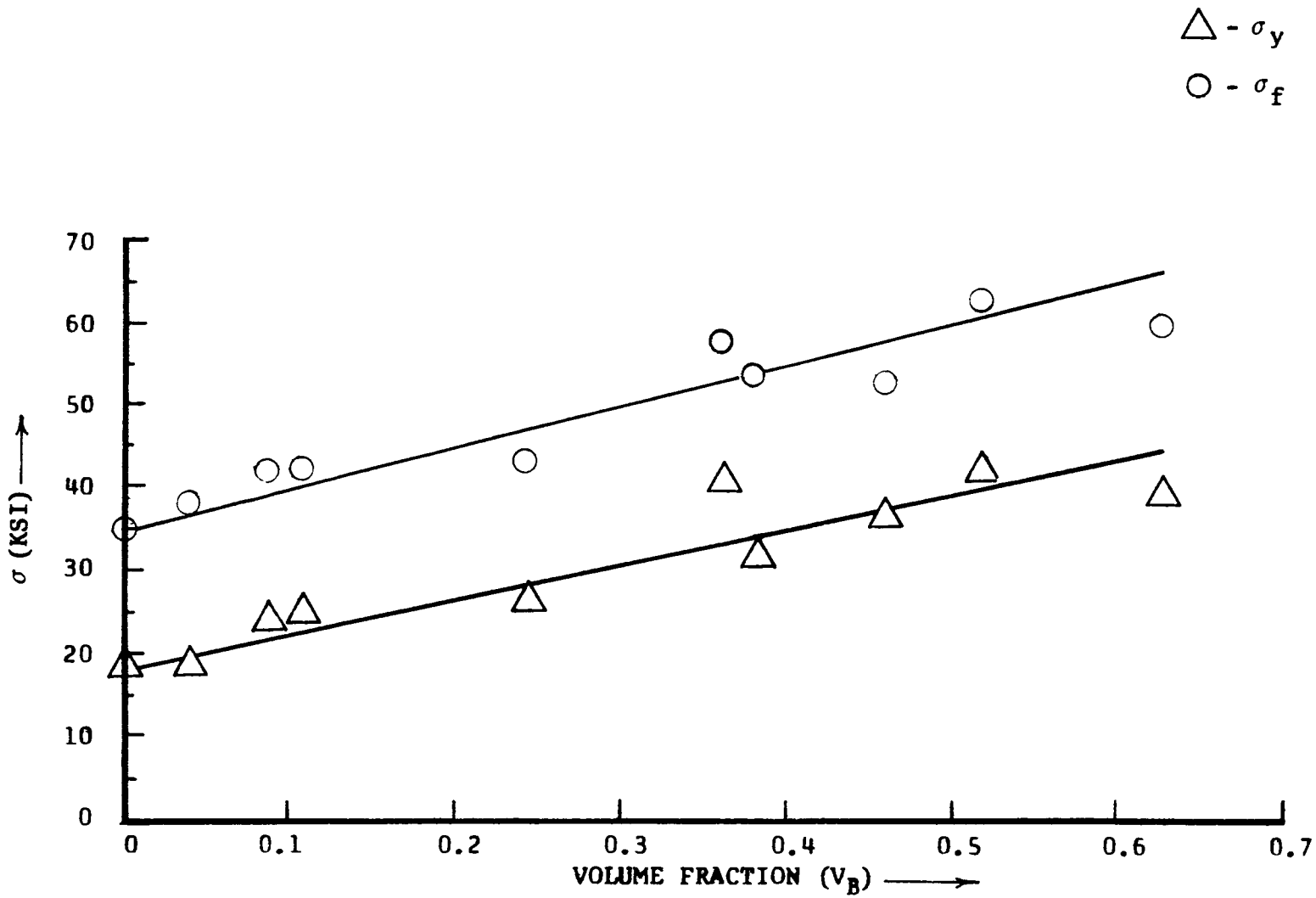

Fig. 10 Yield and fracture strength vs. volume fraction of case

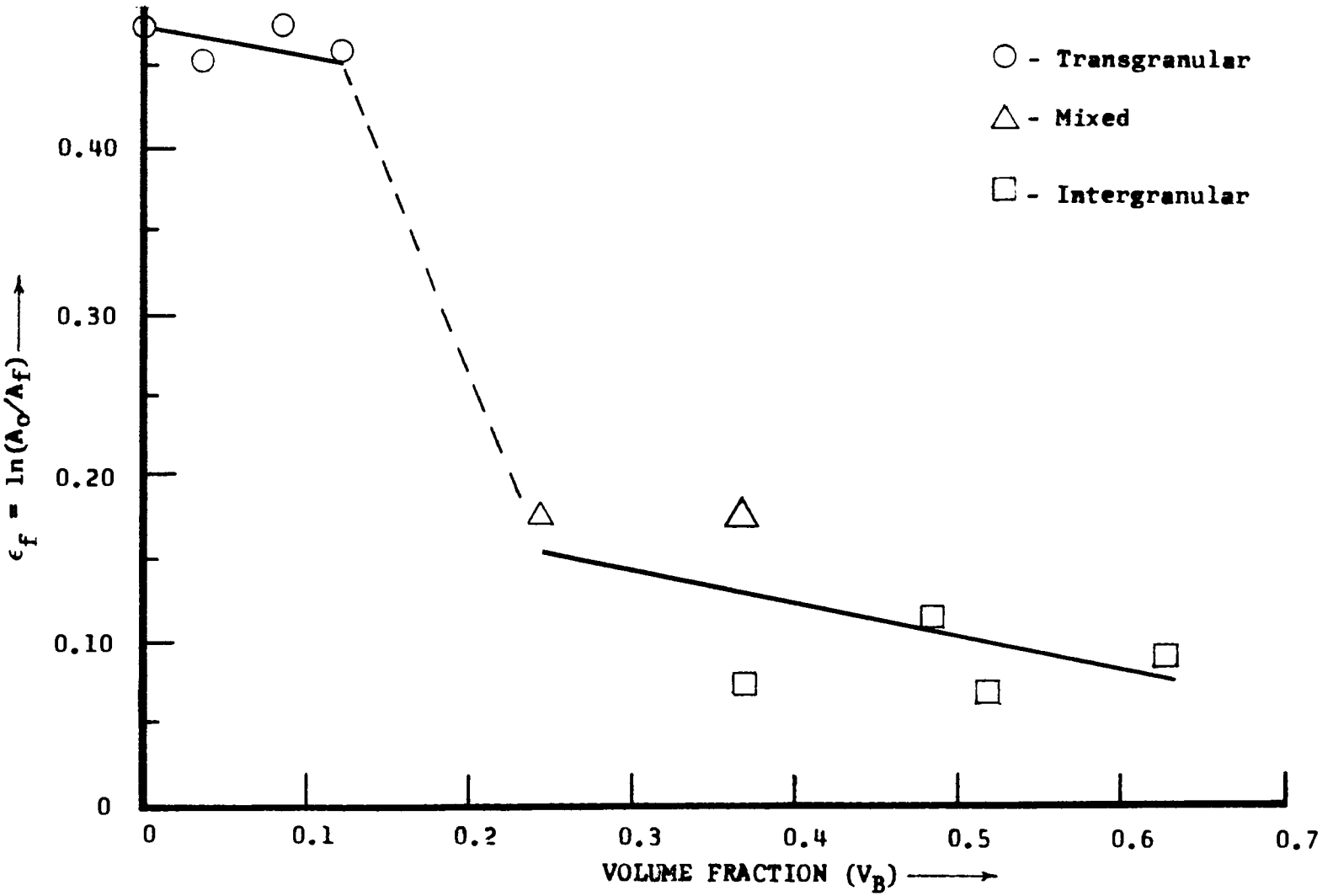

Fig. 11 Tensile ductility compared to volume fraction and fracture mode

8.3.4.1 Fibered Composite Model

An excellent correlation was obtained when the ultimate tensile strength of the case hardened material was compared to that predicted using a continuous fibered composite model. There are two assumptions involved in the model used. First, it was assumed that the carbon case and the core display isostrain behavior.[16] At a given stress level, the core strain and case strain are equal. Second, it was assumed that when the volume fraction of case is greater than a critical value, failure of the case leads to immediate overload of the core.[17] Using the composite model the strength, σ_c of the carburized steel can be related to the volume fraction of the carbon case by the relation

$$\sigma_c = \sigma_{(UTS)B} V_B + \sigma_m' (1 - V_B) \qquad (4)$$

where $\sigma_{(UTS)B}$ is the ultimate tensile strength of the carbon case, V_B is the volume fraction of the carbon case, and σ_m' is the stress borne by the core at the fracture strain of the case (not the UTS of the core). $\sigma_{(UTS)B}$ was estimated by extrapolating the UTS as a function of case depth to the fully case carburized condition. σ_m' was obtained from a stress-strain curve developed for the core material. This procedure for obtaining σ_m' was justified by electron microprobe scans showing that the core carbon content did not significantly increase during carburization and by tensile tests performed on case carburized specimens with the case removed.

This composite model is valid for volume fractions greater than some critical value $V_{B(crit)}$. For volume fractions less than this critical value, the core is able to absorb the load that had been carried by the case before the case failed, and then plastically deform an additional amount before specimen failure occurs. In this regime, the UTS of the "composite" is related to the UTS of the core material by the relation

$$\sigma_c = \sigma_m V_m = \sigma_m (1 - V_B) \tag{5}$$

Substituting appropriate values for $\sigma_{(UTS)B}$, σ_m, σ_m' and solving for V_B yields a value of 0.094 for $V_{B(crit)}$. Results of comparing the UTS of the case hardened material to the UTS predicted by the composite model are shown in Fig. 12. As can be seen, the agreement is very good, which indicates that a continuous fibered composite model can be used to estimate the UTS of case carburized type 316 stainless steel.

8.3.4.2 Fracture Controlling Process

An attempt was made to relate the observed embrittlement to the change in the fracture controlling process describe above. In all carburized specimens, the first step in the fracture process is the cracking of the brittle case. The core will then either absorb the load and fail in a ductile mode after further deformation, or the core will fail by overload. The determining factor is the effective load bearing cross-sectional area of the core when the case cracks, which is governed by the case depth (volume fraction). If this is the sequence

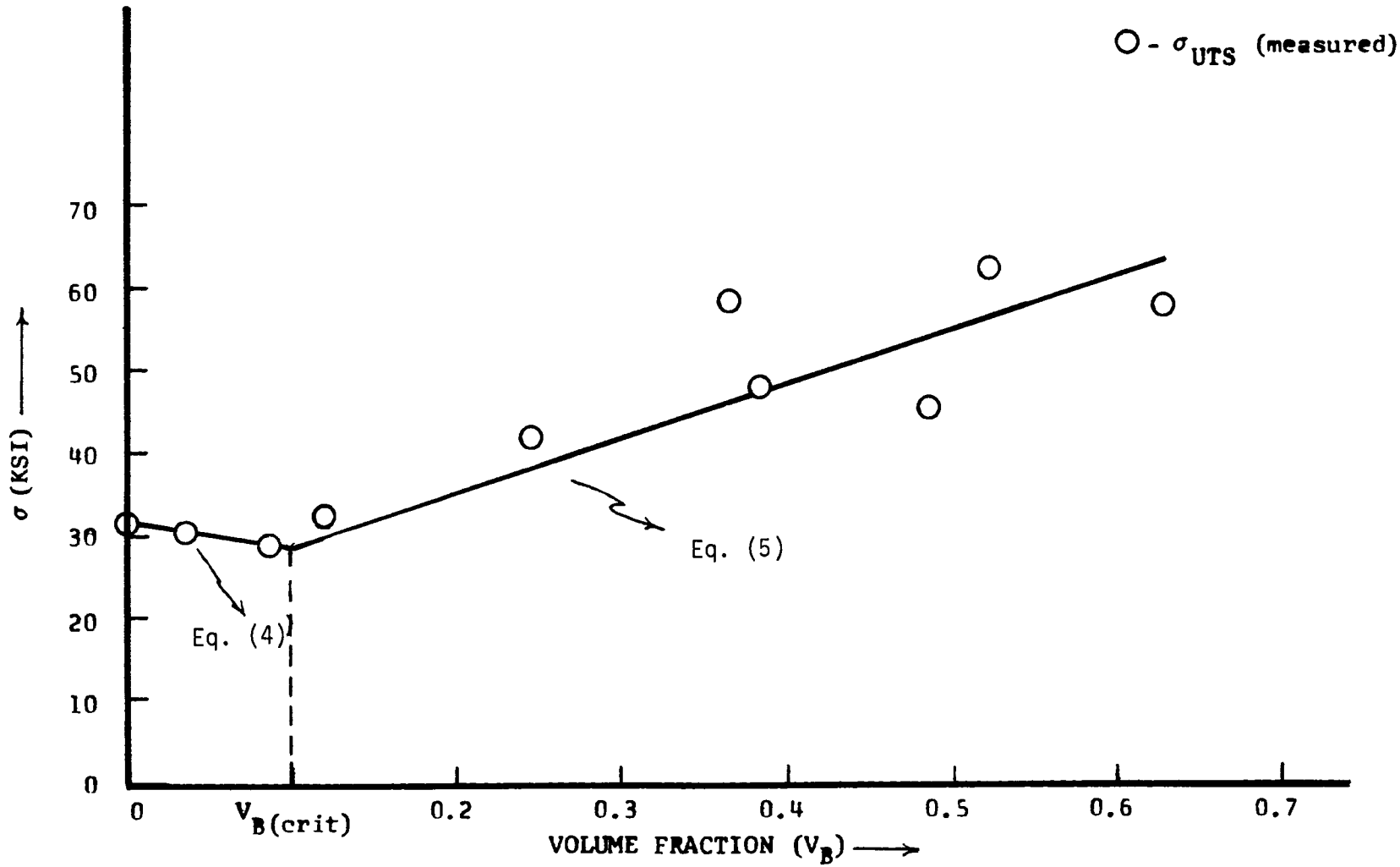

Fig. 12 Comparison of σ_c predicted and σ_{UTS} measured vs. volume fraction of case.

of events leading to failure, the critical case depth required to overload the core upon cracking of the carbon case can be estimated from tensile data obtained from the matrix of the case hardened material as follows:

$$\sigma_f(m) = \frac{L_f}{w\ t_{(crit)}} \quad , \tag{7}$$

where $\sigma_{(f)}m$ is the fracture strength of the core for a material case carburized to the critical depth, L_f is the failure load, w is the specimen width, and $t_{(crit)}$ is the critical thickness of the core required for overload when the carbon case fails. Substituting the appropriate values into the above equation gives a value of 0.016 in. as the critical core thickness required for failure of the core by overload. This implies that for a case depth greater than 0.002 in. on a specimen nominally 0.020 in. thick, failure of the carbon case leads to specimen failure immediately. This corresponds directly with the value of $V_{B(crit)}$ described above and is reflected in the decrease in ductility as the volume fraction (case depth) is increased (Fig. 11).

8.4 REFERENCES

1. P.A. Chalco and K. Ono, ORNL-4963, June 1974, p. 261.
2. K. Ono, A.J. Ardell, and A.S. Tetelman, Reactor Steels Studies Quarterly Progress Report, UCLA 34P177-16, April 1973.
3. K. Ono, A.J. Ardell, and A.S. Tetelman, Reactor Steels Studies Quarterly Progress Report, UCLA 34P177-17, August 1973.
4. J. McCann and K. A. Ridal, J.I.S.I. 202 (1964) 441.
5. K. Ono, A.J. Ardell and A.S. Tetelman, Reactor Steels Quarterly Progress Report, UCLA 34P177-18, August 1973.
6. F. Garofalo, O. Richmond and W.F. Domis, Journal of Basic Engineering 84 (1962) 287.
7. K. Ono, A.J. Ardell and A.S. Tetelman, Reactor Steels Quarterly Progress Report, UCLA 34P177-21, June 1974.
8. F. Garofalo, Fundamentals of Creep and Creep Rupture in Metals, McMillan (1965), p. 10.
9. F. Garofalo, W. Domis and F. Gemminger, Trans. AIME 230 (1964) 460.
10. N.S. Akulov, Acta Met. 12 (1964) 1195.
11. J.C.M. Li, Acta Met. 11 (1963) 1269.
12. H. Pearlman, Trans. Am. Nuc. Soc. 11 (1968) 126.
13. R.C. Andrews, Topical Report No. 4, MSAR-65-194 (1965) 135.
14. K. Natesan and T.F. Kassner, Report No. ANL 7646, Argonne National Laboratory (1969) 28.

15. H. Yoshida, R. Yoda, K. Koike, and K. Matuo, Tetsu-to-Hagane 56 (1970) 311.

16. A.S. Tetelman, and A.J. McEvily, Jr., Fracture of Structural Materials, Wiley, New York (1967) p. 637.

17. A. Kelly and G.J. Davies, Met. Rev. 10 (1965) 1.

SI CONVERSION TABLES AND FACTORS

The following information is presented as an aid to the conversion to the International System of Units (SI). It is in keeping with guidelines set forth by such organizations as the National Bureau of Standards and the American Society for Testing and Materials. Selected lists of unit abbreviations and conversion factors are followed by a table for converting stresses (or pressures) from ksi to megapascals.

Selected Unit Abbreviations

in.	- inch
lb	- pound force
ksi	- 1000 pounds per square inch
kg	- kilograms force
mm	- millimetre
m	- metre
N	- newton
MN	- meganewton
kN	- kilonewton
MPa	- megapascal
kPa	- kilopascal
kg/mm^2	- kilogram (force) per square millimetre
MN/m^2	- meganewton per square metre

Key Conversion Relationships

1 in.	= 0.0254 m (exactly)
1 mm	= 0.001 m (exactly)
1 lb	= 4.448 221 615 260 5 N (exactly)
1 lb	= 0.453 592 370 kg
1 kg(force)	= 9.806650 N (exactly)
1 ksi	= 0.70306958 kg/mm^2
1 ksi	= 6.894757 MN/m^2 (MPa)
1 psi	= 6.894757 kN/m^2 (kPa)
1 kg/mm^2	= 9.806650 MN/m^2 (MPa)
1 MN/m^2	= 1 MPa
1 kN/m^2	= 1 kPa
1 bar	= 0.1 MPa

Commonly Used SI Conversion Factors

Property	To Convert From English or Metric Units	To SI Units	Multiply By	SI Unit Abbreviation
Area	$inch^2$	$Metre^2$	6.451600×10^{-4}	m^2
	$foot^2$	$Metre^2$	9.290304×10^{-2}	m^2
Density	pound (mass) per $in.^3$	Kilogram per $metre^3$	2.767990×10^4	kg/m^3
	pound (mass) per ft^3	Kilogram per $metre^3$	1.601846×10^1	kg/m^3
	gram per cm^3	Kilogram per $metre^3$	1.000000×10^3	kg/m^3
Electrical resistivity	microhm-cm	Ohm-metre	1.000000×10^{-8}	Ω m
Energy	foot-pound (force)	Joule	1.355818×10^0	J
Force	pound (force)	Newton	4.448222×10^0	N
	kilogram (force)	Newton	9.806650×10^0	N
Stress intensity factors	($kilopound_f$ per $in.^2$) ($in.^{1/2}$)	Pascal $Metre^{1/2}$	1.098843×10^6	Pa $m^{1/2}$
Length	foot	Metre	3.048000×10^{-1}	m
	inch	Metre	2.540000×10^{-2}	m
Magnetic Coercive force	oersteds	Ampere per metre	7.957747×10^1	A/m
Magnetic induction	kilogauss	Tesla	1.000000×10^{-1}	T
Mass	pound (mass)	Kilogram	4.535924×10^{-1}	kg
	kilogram (mass)	Kilogram	1.000000×10^0	kg
Specific heat	BTU per (lb_mF)	Joule per kilogram-Kelvin	4.186800×10^3(b)	J kg^{-1} K^{-1}
		Joule per kilogram-Kelvin	4.184000×10^3(a)	J kg^{-1} K^{-1}
Stress or pressure (see separate table)	pound (force) per $inch^2$	Pascal	6.894757×10^3	Pa
	kilopound (force) per $inch^2$	Pascal	6.894757×10^6	Pa
	kilogram (force) per $metre^2$	Pascal	9.806650×10^0	Pa
Temperature	degree Celsius	Kelvin	$t_K = t_c + 273.15$	K
	degree Fahrenheit	Kelvin	$t_K = (t_F + 459.67)/1.8$	K
	degree Rankine	Kelvin	$t_K = t_R/1.8$	K
	degree Fahrenheit	Degree Celsius	$t_c = (t_F - 32)/1.8$	
	Kelvin	Degree Celsius	$t_c = t_K - 273.15$	
Thermal conductivity	BTU ft per (hr ft^2 F)	Watt per (metre-kelvin)	1.730735×10^0(b)	W m^{-1} K^{-1}
Thermal diffusivity	$foot^2$ per hour	$Metre^2$ per second	2.580640×10^{-5}	m^2/sec
Thermal expansion	in. per in. per°F	Metre per metre per Kelvin	5.555556×10^{-1}	/K
Torque or bending moment	inch-pound (force)	Newton-metre	1.129848×10^{-1}	Nm
	foot-pound (force)	Newton-metre	1.355818×10^0	Nm
Velocity	inches per minute	Metre per second	4.23333×10^{-4}	M/sec

(a) Thermochemical BTU values
(b) International steam table BTU values

Stress Conversion Table

English (ksi)	SI (MPa)	English (ksi)	SI (MPa)	English (ksi)	SI (MPa)
10.0	68.95	13.5	93.08	17.0	117.21
10.1	69.64	13.6	93.77	17.1	117.90
10.2	70.33	13.7	94.46	17.2	118.59
10.3	71.02	13.8	95.15	17.3	119.28
10.4	71.71	13.9	95.84	17.4	119.97
10.5	72.39	14.0	96.53	17.5	120.66
10.6	73.08	14.1	97.22	17.6	121.35
10.7	73.77	14.2	97.91	17.7	122.04
10.8	74.46	14.3	98.60	17.8	122.73
10.9	75.15	14.4	99.28	17.9	123.42
11.0	75.84	14.5	99.97	18.0	124.11
11.1	76.53	14.6	100.66	18.1	124.80
11.2	77.22	14.7	101.35	18.2	125.48
11.3	77.91	14.8	102.04	18.3	126.17
11.4	78.60	14.9	102.73	18.4	126.86
11.5	79.29	15.0	103.42	18.5	127.55
11.6	79.98	15.1	104.11	18.6	128.24
11.7	80.67	15.2	104.80	18.7	128.93
11.8	81.36	15.3	105.49	18.8	129.62
11.9	82.05	15.4	106.18	18.9	130.31
12.0	82.74	15.5	106.87	19.0	131.00
12.1	83.43	15.6	107.56	19.1	131.69
12.2	84.12	15.7	108.25	19.2	132.38
12.3	84.81	15.8	108.94	19.3	133.07
12.4	85.49	15.9	109.63	19.4	133.76
12.5	86.18	16.0	110.32	19.5	134.45
12.6	86.87	16.1	111.01	19.6	135.14
12.7	87.56	16.2	111.70	19.7	135.83
12.8	88.25	16.3	112.38	19.8	136.52
12.9	88.94	16.4	113.07	19.9	137.21
13.0	89.63	16.5	113.76	20.0	137.90
13.1	90.32	16.6	114.45	20.1	138.58
13.2	91.01	16.7	115.14	20.2	139.27
13.3	91.70	16.8	115.83	20.3	139.96
13.4	92.39	16.9	116.52	20.4	140.65

Stress Conversion Table (continued)

English (ksi)	SI (MPa)	English (ksi)	SI (MPa)	English (ksi)	SI (MPa)
20.5	141.34	24.0	165.47	27.5	189.61
20.6	142.03	24.1	166.16	27.6	190.30
20.7	142.72	24.2	166.85	27.7	190.98
20.8	143.41	24.3	167.54	27.8	191.67
20.9	144.10	24.4	168.23	27.9	192.36
21.0	144.79	24.5	168.92	28.0	193.05
21.1	145.48	24.6	169.61	28.1	193.74
21.2	146.17	24.7	170.30	28.2	194.43
21.3	146.86	24.8	170.99	28.3	195.12
21.4	147.55	24.9	171.68	28.4	195.81
21.5	148.24	25.0	172.37	28.5	196.50
21.6	148.93	25.1	173.06	28.6	197.19
21.7	149.62	25.2	173.75	28.7	197.88
21.8	150.31	25.3	174.44	28.8	198.57
21.9	151.00	25.4	175.13	28.9	199.26
22.0	151.68	25.5	175.82	29.0	199.95
22.1	152.37	25.6	176.51	29.1	200.64
22.2	153.06	25.7	177.20	29.2	201.33
22.3	153.75	25.8	177.88	29.3	202.02
22.4	154.44	25.9	178.57	29.4	202.71
22.5	155.13	26.0	179.26	29.5	203.40
22.6	155.82	26.1	179.95	29.6	204.08
22.7	156.51	26.2	180.64	29.7	204.77
22.8	157.20	26.3	181.33	29.8	205.46
22.9	157.89	26.4	182.02	29.9	206.15
23.0	158.58	26.5	182.71	30.0	206.84
23.1	159.27	26.6	183.40	30.1	207.53
23.2	159.96	26.7	184.09	30.2	208.22
23.3	160.65	26.8	184.78	30.3	208.91
23.4	161.34	26.9	185.47	30.4	209.60
23.5	162.03	27.0	186.16	30.5	210.29
23.6	162.72	27.1	186.85	30.6	210.98
23.7	163.41	27.2	187.54	30.7	211.67
23.8	164.10	27.3	188.23	30.8	212.36
23.9	164.78	27.4	188.92	30.9	213.05

Stress Conversion Table (continued)

English (ksi)	SI (MPa)	English (ksi)	SI (MPa)	English (ksi)	SI (MPa)
31.0	213.74	34.5	237.87	38.0	262.00
31.1	214.43	34.6	238.56	38.1	262.69
31.2	215.12	34.7	239.25	38.2	263.38
31.3	215.81	34.8	239.94	38.3	264.07
31.4	216.50	34.9	240.63	38.4	264.76
31.5	217.18	35.0	241.32	38.5	265.45
31.6	217.87	35.1	242.01	38.6	266.14
31.7	218.56	35.2	242.70	38.7	266.83
31.8	219.25	35.3	243.38	38.8	267.52
31.9	219.94	35.4	244.07	38.9	268.21
32.0	220.63	35.5	244.76	39.0	268.90
32.1	221.32	35.6	245.45	39.1	269.58
32.2	222.01	35.7	246.14	39.2	270.27
32.3	222.70	35.8	246.83	39.3	270.96
32.4	223.39	35.9	247.52	39.4	271.65
32.5	224.08	36.0	248.21	39.5	272.34
32.6	224.77	36.1	248.90	39.6	273.03
32.7	225.46	36.2	249.59	39.7	273.72
32.8	226.15	36.3	250.28	39.8	274.41
32.9	226.84	36.4	250.97	39.9	275.10
33.0	227.53	36.5	251.66	40.0	275.79
33.1	228.22	36.6	252.35	40.1	276.48
33.2	228.91	36.7	253.04	40.2	277.17
33.3	229.60	36.8	253.73	40.3	277.86
33.4	230.28	36.9	254.42	40.4	278.55
33.5	230.97	37.0	255.11	40.5	279.24
33.6	231.66	37.1	255.80	40.6	279.93
33.7	232.35	37.2	256.48	40.7	280.62
33.8	233.04	37.3	257.17	40.8	281.31
33.9	233.73	37.4	257.86	40.9	282.00
34.0	234.42	37.5	258.55	41.0	282.69
34.1	235.11	37.6	259.24	41.1	283.37
34.2	235.80	37.7	259.93	41.2	284.06
34.3	236.49	37.8	260.62	41.3	284.75
34.4	237.18	37.9	261.31	41.4	285.44

Stress Conversion Table (continued)

English (ksi)	SI (MPa)	English (ksi)	SI (MPa)	English (ksi)	SI (MPa)
41.5	286.13	45.0	310.26	48.5	334.40
41.6	286.82	45.1	310.95	48.6	335.09
41.7	287.51	45.2	311.64	48.7	335.77
41.8	288.20	45.3	312.33	48.8	336.46
41.9	288.89	45.4	313.02	48.9	337.15
42.0	289.58	45.5	313.71	49.0	337.84
42.1	290.27	45.6	314.40	49.1	338.53
42.2	290.96	45.7	315.09	49.2	339.22
42.3	291.65	45.8	315.78	49.3	339.91
42.4	292.34	45.9	316.47	49.4	340.60
42.5	293.03	46.0	317.16	49.5	341.29
42.6	293.72	46.1	317.85	49.6	341.98
42.7	294.41	46.2	318.54	49.7	342.67
42.8	295.10	46.3	319.23	49.8	343.36
42.9	295.79	46.4	319.92	49.9	344.05
43.0	296.47	46.5	320.61	50.0	344.74
43.1	297.16	46.6	321.30	50.1	345.43
43.2	297.85	46.7	321.99	50.2	346.12
43.3	298.54	46.8	322.67	50.3	346.81
43.4	299.23	46.9	323.36	50.4	347.50
43.5	299.92	47.0	324.05	50.5	348.19
43.6	300.61	47.1	324.74	50.6	348.87
43.7	301.30	47.2	325.43	50.7	349.56
43.8	301.99	47.3	326.12	50.8	350.25
43.9	302.68	47.4	326.81	50.9	350.94
44.0	303.37	47.5	327.50	51.0	351.63
44.1	304.06	47.6	328.19	51.1	352.32
44.2	304.75	47.7	328.88	51.2	353.01
44.3	305.44	47.8	329.57	51.3	353.70
44.4	306.13	47.9	330.26	51.4	354.39
44.5	306.82	48.0	330.95	51.5	355.08
44.6	307.51	48.1	331.64	51.6	355.77
44.7	308.20	48.2	332.33	51.7	356.46
44.8	308.89	48.3	333.02	51.8	357.15
44.9	309.57	48.4	333.71	51.9	357.84

Stress Conversion Table (continued)

English (ksi)	SI (MPa)	English (ksi)	SI (MPa)	English (ksi)	SI (MPa)
52.0	358.53	55.5	382.66	59.0	406.79
52.1	359.22	55.6	383.35	59.1	407.48
52.2	359.91	55.7	384.04	59.2	408.17
52.3	360.60	55.8	384.73	59.3	408.86
52.4	361.29	55.9	385.42	59.4	409.55
52.5	361.97	56.0	386.11	59.5	410.24
52.6	362.66	56.1	386.80	59.6	410.93
52.7	363.35	56.2	387.49	59.7	411.62
52.8	364.04	56.3	388.17	59.8	412.31
52.9	364.73	56.4	388.86	59.9	413.00
53.0	365.42	56.5	389.55	60.0	413.69
53.1	366.11	56.6	390.24	60.1	414.37
53.2	366.80	56.7	390.93	60.2	415.06
53.3	367.49	56.8	391.62	60.3	415.75
53.4	368.18	56.9	392.31	60.4	416.44
53.5	368.87	57.0	393.00	60.5	417.13
53.6	369.56	57.1	393.69	60.6	417.82
53.7	370.25	57.2	394.38	60.7	418.51
53.8	370.94	57.3	395.07	60.8	419.20
53.9	371.63	57.4	395.76	60.9	419.89
54.0	372.32	57.5	396.45	61.0	420.58
54.1	373.01	57.6	397.14	61.1	421.27
54.2	373.70	57.7	397.83	61.2	421.96
54.3	374.39	57.8	398.52	61.3	422.65
54.4	375.07	57.9	399.21	61.4	423.34
54.5	375.76	58.0	399.90	61.5	424.03
54.6	376.45	58.1	400.59	61.6	424.72
54.7	377.14	58.2	401.27	61.7	425.41
54.8	377.83	58.3	401.96	61.8	426.10
54.9	378.52	58.4	402.65	61.9	426.79
55.0	379.21	58.5	403.34	62.0	427.47
55.1	379.90	58.6	404.03	62.1	428.16
55.2	380.59	58.7	404.72	62.2	428.85
55.3	381.28	58.8	405.41	62.3	429.54
55.4	381.97	58.9	406.10	62.4	430.23

Stress Conversion Table (continued)

English (ksi)	SI (MPa)	English (ksi)	SI (MPa)	English (ksi)	SI (MPa)
62.5	430.92	66.0	455.05	69.5	479.19
62.6	431.61	66.1	455.74	69.6	479.88
62.7	432.30	66.2	456.43	69.7	480.56
62.8	432.99	66.3	457.12	69.8	481.25
62.9	433.68	66.4	457.81	69.9	481.94
63.0	434.37	66.5	458.50	70.0	482.63
63.1	435.06	66.6	459.19	70.1	483.32
63.2	435.75	66.7	459.88	70.2	484.01
63.3	436.44	66.8	460.57	70.3	484.70
63.4	437.13	66.9	461.26	70.4	485.39
63.5	437.82	67.0	461.95	70.5	486.08
63.6	438.51	67.1	462.64	70.6	486.77
63.7	439.20	67.2	463.33	70.7	487.46
63.8	439.89	67.3	464.02	70.8	488.15
63.9	440.57	67.4	464.71	70.9	488.84
64.0	441.26	67.5	465.40	71.0	489.53
64.1	441.95	67.6	466.09	71.1	490.22
64.2	442.64	67.7	466.78	71.2	490.91
64.3	443.33	67.8	467.46	71.3	491.60
64.4	444.02	67.9	468.15	71.4	492.29
64.5	444.71	68.0	468.84	71.5	492.98
64.6	445.40	68.1	469.53	71.6	493.66
64.7	446.09	68.2	470.22	71.7	494.35
64.8	446.78	68.3	470.91	71.8	495.04
64.9	447.47	68.4	471.60	71.9	495.73
65.0	448.16	68.5	472.29	72.0	496.42
65.1	448.85	68.6	472.98	72.1	497.11
65.2	449.54	68.7	473.67	72.2	497.80
65.3	450.23	68.8	474.36	72.3	498.49
65.4	450.92	68.9	475.05	72.4	499.18
65.5	451.61	69.0	475.74	72.5	499.87
65.6	452.30	69.1	476.43	72.6	500.56
65.7	452.99	69.2	477.12	72.7	501.25
65.8	453.68	69.3	477.81	72.8	501.94
65.9	454.36	69.4	478.50	72.9	502.63

Stress Conversion Table (continued)

English (ksi)	SI (MPa)	English (ksi)	SI (MPa)	English (ksi)	SI (MPa)
73.0	503.32	76.5	527.45	80.0	551.58
73.1	504.01	76.6	528.14	80.1	552.27
73.2	504.70	76.7	528.83	80.2	552.96
73.3	505.39	76.8	529.52	80.3	553.65
73.4	506.08	76.9	530.21	80.4	554.34
73.5	506.76	77.0	530.90	80.5	555.03
73.6	507.45	77.1	531.59	80.6	555.72
73.7	508.14	77.2	532.28	80.7	556.41
73.8	508.83	77.3	532.96	80.8	557.10
73.9	509.52	77.4	533.65	80.9	557.79
74.0	510.21	77.5	534.34	81.0	558.48
74.1	510.90	77.6	535.03	81.1	559.16
74.2	511.59	77.7	535.72	81.2	559.85
74.3	512.28	77.8	536.41	81.3	560.54
74.4	512.97	77.9	537.10	81.4	561.23
74.5	513.66	78.0	537.79	81.5	561.92
74.6	514.35	78.1	538.48	81.6	562.61
74.7	515.04	78.2	539.17	81.7	563.30
74.8	515.73	78.3	539.86	81.8	563.99
74.9	516.42	78.4	540.55	81.9	564.68
75.0	517.11	78.5	541.24	82.0	565.37
75.1	517.80	78.6	541.93	82.1	566.06
75.2	518.49	78.7	542.62	82.2	566.75
75.3	519.18	78.8	543.31	82.3	567.44
75.4	519.86	78.9	544.00	82.4	568.13
75.5	520.55	79.0	544.69	82.5	568.82
75.6	521.24	79.1	545.38	82.6	569.51
75.7	521.93	79.2	546.06	82.7	570.20
75.8	522.62	79.3	546.75	82.8	570.89
75.9	523.31	79.4	547.44	82.9	571.58
76.0	524.00	79.5	548.13	83.0	572.26
76.1	524.69	79.6	548.82	83.1	572.95
76.2	525.38	79.7	549.51	83.2	573.64
76.3	526.07	79.8	550.20	83.3	574.33
76.4	526.76	79.9	550.89	83.4	575.02

Stress Conversion Table (continued)

English (ksi)	SI (MPa)	English (ksi)	SI (MPa)	English (ksi)	SI (MPa)
83.5	575.71	87.0	599.84	90.5	623.98
83.6	576.40	87.1	600.53	90.6	624.66
83.7	577.09	87.2	601.22	90.7	625.35
83.8	577.78	87.3	601.91	90.8	626.04
83.9	578.47	87.4	602.60	90.9	626.73
84.0	579.16	87.5	603.29	91.0	627.42
84.1	579.85	87.6	603.98	91.1	628.11
84.2	580.54	87.7	604.67	91.2	628.80
84.3	581.23	87.8	605.36	91.3	629.49
84.4	581.92	87.9	606.05	91.4	630.18
84.5	582.61	88.0	606.74	91.5	630.87
84.6	583.30	88.1	607.43	91.6	631.56
84.7	583.99	88.2	608.12	91.7	632.25
84.8	584.68	88.3	608.81	91.8	632.94
84.9	585.36	88.4	609.50	91.9	633.63
85.0	586.05	88.5	610.19	92.0	634.32
85.1	586.74	88.6	610.88	92.1	635.01
85.2	587.43	88.7	611.56	92.2	635.70
85.3	588.12	88.8	612.25	92.3	636.39
85.4	588.81	88.9	612.94	92.4	637.08
85.5	589.50	89.0	613.63	92.5	637.77
85.6	590.19	89.1	614.32	92.6	638.45
85.7	590.88	89.2	615.01	92.7	639.14
85.8	591.57	89.3	615.70	92.8	639.83
85.9	592.26	89.4	616.39	92.9	640.52
86.0	592.95	89.5	617.08	93.0	641.21
86.1	593.64	89.6	617.77	93.1	641.90
86.2	594.33	89.7	618.46	93.2	642.59
86.3	595.02	89.8	619.15	93.3	643.28
86.4	595.71	89.9	619.84	93.4	643.97
86.5	596.40	90.0	620.53	93.5	644.66
86.6	597.09	90.1	621.22	93.6	645.35
86.7	597.78	90.2	621.91	93.7	646.04
86.8	598.46	90.3	622.60	93.8	646.73
86.9	599.15	90.4	623.29	93.9	647.42

Stress Conversion Table (continued)

English (ksi)	SI (MPa)	English (ksi)	SI (MPa)	English (ksi)	SI (MPa)
94.0	648.11	97.5	672.24	101.0	696.37
94.1	648.80	97.6	672.93	101.1	697.06
94.2	649.49	97.7	673.62	101.2	697.75
94.3	650.18	97.8	674.31	101.3	698.44
94.4	650.87	97.9	675.00	101.4	699.13
94.5	651.55	98.0	675.69	101.5	699.82
94.6	652.24	98.1	676.38	101.6	700.51
94.7	652.93	98.2	677.07	101.7	701.20
94.8	653.62	98.3	677.75	101.8	701.89
94.9	654.31	98.4	678.44	101.9	702.58
95.0	655.00	98.5	679.13	102.0	703.27
95.1	655.69	98.6	679.82	102.1	703.95
95.2	656.38	98.7	680.51	102.2	704.64
95.3	657.07	98.8	681.20	102.3	705.33
95.4	657.76	98.9	681.89	102.4	706.02
95.5	658.45	99.0	682.58	102.5	706.71
95.6	659.14	99.1	683.27	102.6	707.40
95.7	659.83	99.2	683.96	102.7	708.09
95.8	660.52	99.3	684.65	102.8	708.78
95.9	661.21	99.4	685.34	102.9	709.47
96.0	661.90	99.5	686.03	103.0	710.16
96.1	662.59	99.6	686.72	103.1	710.85
96.2	663.28	99.7	687.41	103.2	711.54
96.3	663.97	99.8	688.10	103.3	712.23
96.4	664.65	99.9	688.79	103.4	712.92
96.5	665.34	100.0	689.48	103.5	713.61
96.6	666.03	100.1	690.17	103.6	714.30
96.7	666.72	100.2	690.85	103.7	714.99
96.8	667.41	100.3	691.54	103.8	715.68
96.9	668.10	100.4	692.23	103.9	716.37
97.0	668.79	100.5	692.92	104.0	717.05
97.1	669.48	100.6	693.61	104.1	717.74
97.2	670.17	100.7	694.30	104.2	718.43
97.3	670.86	100.8	694.99	104.3	719.12
97.4	671.55	100.9	695.68	104.4	719.81

Stress Conversion Table (continued)

English (ksi)	SI (MPa)	English (ksi)	SI (MPa)	English (ksi)	SI (MPa)
104.5	720.50	108.0	744.63	111.5	768.77
104.6	721.19	108.1	745.32	111.6	769.45
104.7	721.88	108.2	746.01	111.7	770.14
104.8	722.57	108.3	746.70	111.8	770.83
104.9	723.26	108.4	747.39	111.9	771.52
105.0	723.95	108.5	748.08	112.0	772.21
105.1	724.64	108.6	748.77	112.1	772.90
105.2	725.33	108.7	749.46	112.2	773.59
105.3	726.02	108.8	750.15	112.3	774.28
105.4	726.71	108.9	750.84	112.4	774.97
105.5	727.40	109.0	751.53	112.5	775.66
105.6	728.09	109.1	752.22	112.6	776.35
105.7	728.78	109.2	752.91	112.7	777.04
105.8	729.47	109.3	753.60	112.8	777.73
105.9	730.15	109.4	754.29	112.9	778.42
106.0	730.84	109.5	754.98	113.0	779.11
106.1	731.53	109.6	755.67	113.1	779.80
106.2	732.22	109.7	756.35	113.2	780.49
106.3	732.91	109.8	757.04	113.3	781.18
106.4	733.60	109.9	757.73	113.4	781.87
106.5	734.29	110.0	758.42	113.5	782.55
106.6	734.98	110.1	759.11	113.6	783.24
106.7	735.67	110.2	759.80	113.7	783.93
106.8	736.36	110.3	760.49	113.8	784.62
106.9	737.05	110.4	761.18	113.9	785.31
107.0	737.74	110.5	761.87	114.0	786.00
107.1	738.43	110.6	762.56	114.1	786.69
107.2	739.12	110.7	763.25	114.2	787.38
107.3	739.81	110.8	763.94	114.3	788.07
107.4	740.50	110.9	764.63	114.4	788.76
107.5	741.19	111.0	765.32	114.5	789.45
107.6	741.88	111.1	766.01	114.6	790.14
107.7	742.57	111.2	766.70	114.7	790.83
107.8	743.25	111.3	767.39	114.8	791.52
107.9	743.94	111.4	768.08	114.9	792.21

Stress Conversion Table (continued)

English (ksi)	SI (MPa)	English (ksi)	SI (MPa)	English (ksi)	SI (MPa)
115.0	792.90	118.5	817.03	122.0	841.16
115.1	793.59	118.6	817.72	122.1	841.85
115.2	794.28	118.7	818.41	122.2	842.54
115.3	794.97	118.8	819.10	122.3	843.23
115.4	795.65	118.9	819.79	122.4	843.92
115.5	796.34	119.0	820.48	122.5	844.61
115.6	797.03	119.1	821.17	122.6	845.30
115.7	797.72	119.2	821.86	122.7	845.99
115.8	798.41	119.3	822.54	122.8	846.68
115.9	799.10	119.4	823.23	122.9	847.37
116.0	799.79	119.5	823.92	123.0	848.06
116.1	800.48	119.6	824.61	123.1	848.74
116.2	801.17	119.7	825.30	123.2	849.43
116.3	801.86	119.8	825.99	123.3	850.12
116.4	802.55	119.9	826.68	123.4	850.81
116.5	803.24	120.0	827.37	123.5	851.50
116.6	803.93	120.1	828.06	123.6	852.19
116.7	804.62	120.2	828.75	123.7	852.88
116.8	805.31	120.3	829.44	123.8	853.57
116.9	806.00	120.4	830.13	123.9	854.26
117.0	806.69	120.5	830.82	124.0	854.95
117.1	807.38	120.6	831.51	124.1	855.64
117.2	808.07	120.7	832.20	124.2	856.33
117.3	808.75	120.8	832.89	124.3	857.02
117.4	809.44	120.9	833.58	124.4	857.71
117.5	810.13	121.0	834.27	124.5	858.40
117.6	810.82	121.1	834.96	124.6	859.09
117.7	811.51	121.2	835.64	124.7	859.78
117.8	812.20	121.3	836.33	124.8	860.47
117.9	812.89	121.4	837.02	124.9	861.16
118.0	813.58	121.5	837.71	125.0	861.84
118.1	814.27	121.6	838.40	125.1	862.53
118.2	814.96	121.7	839.09	125.2	863.22
118.3	815.65	121.8	839.78	125.3	863.91
118.4	816.34	121.9	840.47	125.4	864.60

Stress Conversion Table (continued)

English (ksi)	SI (MPa)	English (ksi)	SI (MPa)	English (ksi)	SI (MPa)
125.5	865.29	129.0	889.42	132.5	913.56
125.6	865.98	129.1	890.11	132.6	914.24
125.7	866.67	129.2	890.80	132.7	914.93
125.8	867.36	129.3	891.49	132.8	915.62
125.9	868.05	129.4	892.18	132.9	916.31
126.0	868.74	129.5	892.87	133.0	917.00
126.1	869.43	129.6	893.56	133.1	917.69
126.2	870.12	129.7	894.25	133.2	918.38
126.3	870.81	129.8	894.94	133.3	919.07
126.4	871.50	129.9	895.63	133.4	919.76
126.5	872.19	130.0	896.32	133.5	920.45
126.6	872.88	130.1	897.01	133.6	921.14
126.7	873.57	130.2	897.70	133.7	921.83
126.8	874.26	130.3	898.39	133.8	922.52
126.9	874.94	130.4	899.08	133.9	923.21
127.0	875.63	130.5	899.77	134.0	923.90
127.1	876.32	130.6	900.46	134.1	924.59
127.2	877.01	130.7	901.14	134.2	925.28
127.3	877.70	130.8	901.83	134.3	925.97
127.4	878.39	130.9	902.52	134.4	926.66
127.5	879.08	131.0	903.21	134.5	927.34
127.6	879.77	131.1	903.90	134.6	928.03
127.7	880.46	131.2	904.59	134.7	928.72
127.8	881.15	131.3	905.28	134.8	929.41
127.9	881.84	131.4	905.97	134.9	930.10
128.0	882.53	131.5	906.66	135.0	930.79
128.1	883.22	131.6	907.35	135.1	931.48
128.2	883.91	131.7	908.04	135.2	932.17
128.3	884.60	131.8	908.73	135.3	932.86
128.4	885.29	131.9	909.42	135.4	933.55
128.5	885.98	132.0	910.11	135.5	934.24
128.6	886.67	132.1	910.80	135.6	934.93
128.7	887.36	132.2	911.49	135.7	935.62
128.8	888.04	132.3	912.18	135.8	936.31
128.9	888.73	132.4	912.87	135.9	937.00

Stress Conversion Table (continued)

English (ksi)	SI (MPa)	English (ksi)	SI (MPa)	English (ksi)	SI (MPa)
136.0	937.69	139.5	961.82	143.0	985.95
136.1	938.38	139.6	962.51	143.1	986.64
136.2	939.07	139.7	963.20	143.2	987.33
136.3	939.76	139.8	963.89	143.3	988.02
136.4	940.44	139.9	964.58	143.4	988.71
136.5	941.13	140.0	965.27	143.5	989.40
136.6	941.82	140.1	965.96	143.6	990.09
136.7	942.51	140.2	966.64	143.7	990.78
136.8	943.20	140.3	967.33	143.8	991.47
136.9	943.89	140.4	968.02	143.9	992.16
137.0	944.58	140.5	968.71	144.0	992.85
137.1	945.27	140.6	969.40	144.1	993.53
137.2	945.96	140.7	970.09	144.2	994.22
137.3	946.65	140.8	970.78	144.3	994.91
137.4	947.34	140.9	971.47	144.4	995.60
137.5	948.03	141.0	972.16	144.5	996.29
137.6	948.72	141.1	972.85	144.6	996.98
137.7	949.41	141.2	973.54	144.7	997.67
137.8	950.10	141.3	974.23	144.8	998.36
137.9	950.79	141.4	974.92	144.9	999.05
138.0	951.48	141.5	975.61	145.0	999.74
138.1	952.17	141.6	976.30	145.1	1000.43
138.2	952.86	141.7	976.99	145.2	1001.12
138.3	953.54	141.8	977.68	145.3	1001.81
138.4	954.23	141.9	978.37	145.4	1002.50
138.5	954.92	142.0	979.06	145.5	1003.19
138.6	955.61	142.1	979.74	145.6	1003.88
138.7	956.30	142.2	980.43	145.7	1004.57
138.8	956.99	142.3	981.12	145.8	1005.26
138.9	957.68	142.4	981.81	145.9	1005.95
139.0	958.37	142.5	982.50	146.0	1006.63
139.1	959.06	142.6	983.19	146.1	1007.32
139.2	959.75	142.7	983.88	146.2	1008.01
139.3	960.44	142.8	984.57	146.3	1008.70
139.4	961.13	142.9	985.26	146.4	1009.39

Stress Conversion Table (continued)

English (ksi)	SI (MPa)	English (ksi)	SI (MPa)	English (ksi)	SI (MPa)
146.5	1010.08	150.0	1034.21	153.5	1058.35
146.6	1010.77	150.1	1034.90	153.6	1059.03
146.7	1011.46	150.2	1035.59	153.7	1059.72
146.8	1012.15	150.3	1036.28	153.8	1060.41
146.9	1012.84	150.4	1036.97	153.9	1061.10
147.0	1013.53	150.5	1037.66	154.0	1061.79
147.1	1014.22	150.6	1038.35	154.1	1062.48
147.2	1014.91	150.7	1039.04	154.2	1063.17
147.3	1015.60	150.8	1039.73	154.3	1063.86
147.4	1016.29	150.9	1040.42	154.4	1064.55
147.5	1016.98	151.0	1041.11	154.5	1065.24
147.6	1017.67	151.1	1041.80	154.6	1065.93
147.7	1018.36	151.2	1042.49	154.7	1066.62
147.8	1019.05	151.3	1043.18	154.8	1067.31
147.9	1019.73	151.4	1043.87	154.9	1068.00
148.0	1020.42	151.5	1044.56	155.0	1068.69
148.1	1021.11	151.6	1045.25	155.1	1069.38
148.2	1021.80	151.7	1045.93	155.2	1070.07
148.3	1022.49	151.8	1046.62	155.3	1070.76
148.4	1023.18	151.9	1047.31	155.4	1071.45
148.5	1023.87	152.0	1048.00	155.5	1072.13
148.6	1024.56	152.1	1048.69	155.6	1072.82
148.7	1025.25	152.2	1049.38	155.7	1073.51
148.8	1025.94	152.3	1050.07	155.8	1074.20
148.9	1026.63	152.4	1050.76	155.9	1074.89
149.0	1027.32	152.5	1051.45	156.0	1075.58
149.1	1028.01	152.6	1052.14	156.1	1076.27
149.2	1028.70	152.7	1052.83	156.2	1076.96
149.3	1029.39	152.8	1053.52	156.3	1077.65
149.4	1030.08	152.9	1054.21	156.4	1078.34
149.5	1030.77	153.0	1054.90	156.5	1079.03
149.6	1031.46	153.1	1055.59	156.6	1079.72
149.7	1032.15	153.2	1056.28	156.7	1080.41
149.8	1032.83	153.3	1056.97	156.8	1081.10
149.9	1033.52	153.4	1057.66	156.9	1081.79

Stress Conversion Table (continued)

English (ksi)	SI (MPa)	English (ksi)	SI (MPa)	English (ksi)	SI (MPa)
157.0	1082.48	160.5	1106.61	164.0	1130.74
157.1	1083.17	160.6	1107.30	164.1	1131.43
157.2	1083.86	160.7	1107.99	164.2	1132.12
157.3	1084.55	160.8	1108.68	164.3	1132.81
157.4	1085.23	160.9	1109.37	164.4	1133.50
157.5	1085.92	161.0	1110.06	164.5	1134.19
157.6	1086.61	161.1	1110.75	164.6	1134.88
157.7	1087.30	161.2	1111.43	164.7	1135.57
157.8	1087.99	161.3	1112.12	164.8	1136.26
157.9	1088.68	161.4	1112.81	164.9	1136.95
158.0	1089.37	161.5	1113.50	165.0	1137.63
158.1	1090.06	161.6	1114.19	165.1	1138.32
158.2	1090.75	161.7	1114.88	165.2	1139.01
158.3	1091.44	161.8	1115.57	165.3	1139.70
158.4	1092.13	161.9	1116.26	165.4	1140.39
158.5	1092.82	162.0	1116.95	165.5	1141.08
158.6	1093.51	162.1	1117.64	165.6	1141.77
158.7	1094.20	162.2	1118.33	165.7	1142.46
158.8	1094.89	162.3	1119.02	165.8	1143.15
158.9	1095.58	162.4	1119.71	165.9	1143.84
159.0	1096.27	162.5	1120.40	166.0	1144.53
159.1	1096.96	162.6	1121.09	166.1	1145.22
159.2	1097.65	162.7	1121.78	166.2	1145.91
159.3	1098.33	162.8	1122.47	166.3	1146.60
159.4	1099.02	162.9	1123.16	166.4	1147.29
159.5	1099.71	163.0	1123.85	166.5	1147.98
159.6	1100.40	163.1	1124.53	166.6	1148.67
159.7	1101.09	163.2	1125.22	166.7	1149.36
159.8	1101.78	163.3	1125.91	166.8	1150.05
159.9	1102.47	163.4	1126.60	166.9	1150.73
160.0	1103.16	163.5	1127.29	167.0	1151.42
160.1	1103.85	163.6	1127.98	167.1	1152.11
160.2	1104.54	163.7	1128.67	167.2	1152.80
160.3	1105.23	163.8	1129.36	167.3	1153.49
160.4	1105.92	163.9	1130.05	167.4	1154.18

Stress Conversion Table (continued)

English (ksi)	SI (MPa)	English (ksi)	SI (MPa)	English (ksi)	SI (MPa)
167.5	1154.87	171.0	1179.00	174.5	1203.14
167.6	1155.56	171.1	1179.69	174.6	1203.82
167.7	1156.25	171.2	1180.38	174.7	1204.51
167.8	1156.94	171.3	1181.07	174.8	1205.20
167.9	1157.63	171.4	1181.76	174.9	1205.89
168.0	1158.32	171.5	1182.45	175.0	1206.58
168.1	1159.01	171.6	1183.14	175.1	1207.27
168.2	1159.70	171.7	1183.83	175.2	1207.96
168.3	1160.39	171.8	1184.52	175.3	1208.65
168.4	1161.08	171.9	1185.21	175.4	1209.34
168.5	1161.77	172.0	1185.90	175.5	1210.03
168.6	1162.46	172.1	1186.59	175.6	1210.72
168.7	1163.15	172.2	1187.28	175.7	1211.41
168.8	1163.83	172.3	1187.97	175.8	1212.10
168.9	1164.52	172.4	1188.66	175.9	1212.79
169.0	1165.21	172.5	1189.35	176.0	1213.48
169.1	1165.90	172.6	1190.04	176.1	1214.17
169.2	1166.59	172.7	1190.72	176.2	1214.86
169.3	1167.28	172.8	1191.41	176.3	1215.55
169.4	1167.97	172.9	1192.10	176.4	1216.24
169.5	1168.66	173.0	1192.79	176.5	1216.92
169.6	1169.35	173.1	1193.48	176.6	1217.61
169.7	1170.04	173.2	1194.17	176.7	1218.30
169.8	1170.73	173.3	1194.86	176.8	1218.99
169.9	1171.42	173.4	1195.55	176.9	1219.68
170.0	1172.11	173.5	1196.24	177.0	1220.37
170.1	1172.80	173.6	1196.93	177.1	1221.06
170.2	1173.49	173.7	1197.62	177.2	1221.75
170.3	1174.18	173.8	1198.31	177.3	1222.44
170.4	1174.87	173.9	1199.00	177.4	1223.13
170.5	1175.56	174.0	1199.69	177.5	1223.82
170.6	1176.25	174.1	1200.38	177.6	1224.51
170.7	1176.94	174.2	1201.07	177.7	1225.20
170.8	1177.62	174.3	1201.76	177.8	1225.89
170.9	1178.31	174.4	1202.45	177.9	1226.58

Stress Conversion Table (continued)

English (ksi)	SI (MPa)	English (ksi)	SI (MPa)	English (ksi)	SI (MPa)
178.0	1227.27	181.5	1251.40	185.0	1275.53
178.1	1227.96	181.6	1252.09	185.1	1276.22
178.2	1228.65	181.7	1252.78	185.2	1276.91
178.3	1229.34	181.8	1253.47	185.3	1277.60
178.4	1230.02	181.9	1254.16	185.4	1278.29
178.5	1230.71	182.0	1254.85	185.5	1278.98
178.6	1231.40	182.1	1255.54	185.6	1279.67
178.7	1232.09	182.2	1256.22	185.7	1280.36
178.8	1232.78	182.3	1256.91	185.8	1281.05
178.9	1233.47	182.4	1257.60	185.9	1281.74
179.0	1234.16	182.5	1258.29	186.0	1282.42
179.1	1234.85	182.6	1258.98	186.1	1283.11
179.2	1235.54	182.7	1259.67	186.2	1283.80
179.3	1236.23	182.8	1260.36	186.3	1284.49
179.4	1236.92	182.9	1261.05	186.4	1285.18
179.5	1237.61	183.0	1261.74	186.5	1285.87
179.6	1238.30	183.1	1262.43	186.6	1286.56
179.7	1238.99	183.2	1263.12	186.7	1287.25
179.8	1239.68	183.3	1263.81	186.8	1287.94
179.9	1240.37	183.4	1264.50	186.9	1288.63
180.0	1241.06	183.5	1265.19	187.0	1289.32
180.1	1241.75	183.6	1265.88	187.1	1290.01
180.2	1242.44	183.7	1266.57	187.2	1290.70
180.3	1243.12	183.8	1267.26	187.3	1291.39
180.4	1243.81	183.9	1267.95	187.4	1292.08
180.5	1244.50	184.0	1268.64	187.5	1292.77
180.6	1245.19	184.1	1269.32	187.6	1293.46
180.7	1245.88	184.2	1270.01	187.7	1294.15
180.8	1246.57	184.3	1270.70	187.8	1294.84
180.9	1247.26	184.4	1271.39	187.9	1295.52
181.0	1247.95	184.5	1272.08	188.0	1296.21
181.1	1248.64	184.6	1272.77	188.1	1296.90
181.2	1249.33	184.7	1273.46	188.2	1297.59
181.3	1250.02	184.8	1274.15	188.3	1298.28
181.4	1250.71	184.9	1274.84	188.4	1298.97

Stress Conversion Table (continued)

English (ksi)	SI (MPa)	English (ksi)	SI (MPa)	English (ksi)	SI (MPa)
188.5	1299.66	192.0	1323.79	195.5	1347.92
188.6	1300.35	192.1	1324.48	195.6	1348.61
188.7	1301.04	192.2	1325.17	195.7	1349.30
188.8	1301.73	192.3	1325.86	195.8	1349.99
188.9	1302.42	192.4	1326.55	195.9	1350.68
189.0	1303.11	192.5	1327.24	196.0	1351.37
189.1	1303.80	192.6	1327.93	196.1	1352.06
189.2	1304.49	192.7	1328.62	196.2	1352.75
189.3	1305.18	192.8	1329.31	196.3	1353.44
189.4	1305.87	192.9	1330.00	196.4	1354.13
189.5	1306.56	193.0	1330.69	196.5	1354.82
189.6	1307.25	193.1	1331.38	196.6	1355.51
189.7	1307.94	193.2	1332.07	196.7	1356.20
189.8	1308.62	193.3	1332.76	196.8	1356.89
189.9	1309.31	193.4	1333.45	196.9	1357.58
190.0	1310.00	193.5	1334.14	197.0	1358.27
190.1	1310.69	193.6	1334.82	197.1	1358.96
190.2	1311.38	193.7	1335.51	197.2	1359.65
190.3	1312.07	193.8	1336.20	197.3	1360.34
190.4	1312.76	193.9	1336.89	197.4	1361.03
190.5	1313.45	194.0	1337.58	197.5	1361.71
190.6	1314.14	194.1	1338.27	197.6	1362.40
190.7	1314.83	194.2	1338.96	197.7	1363.09
190.8	1315.52	194.3	1339.65	197.8	1363.78
190.9	1316.21	194.4	1340.34	197.9	1364.47
191.0	1316.90	194.5	1341.03	198.0	1365.16
191.1	1317.59	194.6	1341.72	198.1	1365.85
191.2	1318.28	194.7	1342.41	198.2	1366.54
191.3	1318.97	194.8	1343.10	198.3	1367.23
191.4	1319.66	194.9	1343.79	198.4	1367.92
191.5	1320.35	195.0	1344.48	198.5	1368.61
191.6	1321.04	195.1	1345.17	198.6	1369.30
191.7	1321.72	195.2	1345.86	198.7	1369.99
191.8	1322.41	195.3	1346.55	198.8	1370.68
191.9	1323.10	195.4	1347.24	198.9	1371.37

Stress Conversion Table (continued)

English (ksi)	SI (MPa)	English (ksi)	SI (MPa)	English (ksi)	SI (MPa)
199.0	1372.06	202.5	1396.19	206.0	1420.32
199.1	1372.75	202.6	1396.88	206.1	1421.01
199.2	1373.44	202.7	1397.57	206.2	1421.70
199.3	1374.13	202.8	1398.26	206.3	1422.39
199.4	1374.81	202.9	1398.95	206.4	1423.08
199.5	1375.50	203.0	1399.64	206.5	1423.77
199.6	1376.19	203.1	1400.33	206.6	1424.46
199.7	1376.88	203.2	1401.01	206.7	1425.15
199.8	1377.57	203.3	1401.70	206.8	1425.84
199.9	1378.26	203.4	1402.39	206.9	1426.53
200.0	1378.95	203.5	1403.08	207.0	1427.21
200.1	1379.64	203.6	1403.77	207.1	1427.90
200.2	1380.33	203.7	1404.46	207.2	1428.59
200.3	1381.02	203.8	1405.15	207.3	1429.28
200.4	1381.71	203.9	1405.84	207.4	1429.97
200.5	1382.40	204.0	1406.53	207.5	1430.66
200.6	1383.09	204.1	1407.22	207.6	1431.35
200.7	1383.78	204.2	1407.91	207.7	1432.04
200.8	1384.47	204.3	1408.60	207.8	1432.73
200.9	1385.16	204.4	1409.29	207.9	1433.42
201.0	1385.85	204.5	1409.98	208.0	1434.11
201.1	1386.54	204.6	1410.67	208.1	1434.80
201.2	1387.23	204.7	1411.36	208.2	1435.49
201.3	1387.91	204.8	1412.05	208.3	1436.18
201.4	1388.60	204.9	1412.74	208.4	1436.87
201.5	1389.29	205.0	1413.43	208.5	1437.56
201.6	1389.98	205.1	1414.11	208.6	1438.25
201.7	1390.67	205.2	1414.80	208.7	1438.94
201.8	1391.36	205.3	1415.49	208.8	1439.63
201.9	1392.05	205.4	1416.18	208.9	1440.31
202.0	1392.74	205.5	1416.87	209.0	1441.00
202.1	1393.43	205.6	1417.56	209.1	1441.69
202.2	1394.12	205.7	1418.25	209.2	1442.38
202.3	1394.81	205.8	1418.94	209.3	1443.07
202.4	1395.50	205.9	1419.63	209.4	1443.76

Stress Conversion Table (continued)

English (ksi)	SI (MPa)	English (ksi)	SI (MPa)	English (ksi)	SI (MPa)
209.5	1444.45	213.0	1468.58	216.5	1492.71
209.6	1445.14	213.1	1469.27	216.6	1493.40
209.7	1445.83	213.2	1469.96	216.7	1494.09
209.8	1446.52	213.3	1470.65	216.8	1494.78
209.9	1447.21	213.4	1471.34	216.9	1495.47
210.0	1447.90	213.5	1472.03	217.0	1496.16
210.1	1448.59	213.6	1472.72	217.1	1496.85
210.2	1449.28	213.7	1473.41	217.2	1497.54
210.3	1449.97	213.8	1474.10	217.3	1498.23
210.4	1450.66	213.9	1474.79	217.4	1498.92
210.5	1451.35	214.0	1475.48	217.5	1499.61
210.6	1452.04	214.1	1476.17	217.6	1500.30
210.7	1452.73	214.2	1476.86	217.7	1500.99
210.8	1453.41	214.3	1477.55	217.8	1501.68
210.9	1454.10	214.4	1478.24	217.9	1502.37
211.0	1454.79	214.5	1478.93	218.0	1503.06
211.1	1455.48	214.6	1479.61	218.1	1503.75
211.2	1456.17	214.7	1480.30	218.2	1504.44
211.3	1456.86	214.8	1480.99	218.3	1505.13
211.4	1457.55	214.9	1481.68	218.4	1505.81
211.5	1458.24	215.0	1482.37	218.5	1506.50
211.6	1458.93	215.1	1483.06	218.6	1507.19
211.7	1459.62	215.2	1483.75	218.7	1507.88
211.8	1460.31	215.3	1484.44	218.8	1508.57
211.9	1461.00	215.4	1485.13	218.9	1509.26
212.0	1461.69	215.5	1485.82	219.0	1509.95
212.1	1462.38	215.6	1486.51	219.1	1510.64
212.2	1463.07	215.7	1487.20	219.2	1511.33
212.3	1463.76	215.8	1487.89	219.3	1512.02
212.4	1464.45	215.9	1488.58	219.4	1512.71
212.5	1465.14	216.0	1489.27	219.5	1513.40
212.6	1465.83	216.1	1489.96	219.6	1514.09
212.7	1466.51	216.2	1490.65	219.7	1514.78
212.8	1467.20	216.3	1491.34	219.8	1515.47
212.9	1467.89	216.4	1492.03	219.9	1516.16

Stress Conversion Table (continued)

English (ksi)	SI (MPa)	English (ksi)	SI (MPa)	English (ksi)	SI (MPa)
220.0	1516.85	223.5	1540.98	227.0	1565.11
220.1	1517.54	223.6	1541.67	227.1	1565.80
220.2	1518.23	223.7	1542.36	227.2	1566.49
220.3	1518.91	223.8	1543.05	227.3	1567.18
220.4	1519.60	223.9	1543.74	227.4	1567.87
220.5	1520.29	224.0	1544.43	227.5	1568.56
220.6	1520.98	224.1	1545.12	227.6	1569.25
220.7	1521.67	224.2	1545.80	227.7	1569.94
220.8	1522.36	224.3	1546.49	227.8	1570.63
220.9	1523.05	224.4	1547.18	227.9	1571.32
221.0	1523.74	224.5	1547.87	228.0	1572.00
221.1	1524.43	224.6	1548.56	228.1	1572.69
221.2	1525.12	224.7	1549.25	228.2	1573.38
221.3	1525.81	224.8	1549.94	228.3	1574.07
221.4	1526.50	224.9	1550.63	228.4	1574.76
221.5	1527.19	225.0	1551.32	228.5	1575.45
221.6	1527.88	225.1	1552.01	228.6	1576.14
221.7	1528.57	225.2	1552.70	228.7	1576.83
221.8	1529.26	225.3	1553.39	228.8	1577.52
221.9	1529.95	225.4	1554.08	228.9	1578.21
222.0	1530.64	225.5	1554.77	229.0	1578.90
222.1	1531.33	225.6	1555.46	229.1	1579.59
222.2	1532.02	225.7	1556.15	229.2	1580.28
222.3	1532.70	225.8	1556.84	229.3	1580.97
222.4	1533.39	225.9	1557.53	229.4	1581.66
222.5	1534.08	226.0	1558.22	229.5	1582.35
222.6	1534.77	226.1	1558.90	229.6	1583.04
222.7	1535.46	226.2	1559.59	229.7	1583.73
222.8	1536.15	226.3	1560.28	229.8	1584.42
222.9	1536.84	226.4	1560.97	229.9	1585.10
223.0	1537.53	226.5	1561.66	230.0	1585.79
223.1	1538.22	226.6	1562.35	230.1	1586.48
223.2	1538.91	226.7	1563.04	230.2	1587.17
223.3	1539.60	226.8	1563.73	230.3	1587.86
223.4	1540.29	226.9	1564.42	230.4	1588.55

Stress Conversion Table (continued)

English (ksi)	SI (MPa)	English (ksi)	SI (MPa)	English (ksi)	SI (MPa)
230.5	1589.24	234.0	1613.37	237.5	1637.50
230.6	1589.93	234.1	1614.06	237.6	1638.19
230.7	1590.62	234.2	1614.75	237.7	1638.88
230.8	1591.31	234.3	1615.44	237.8	1639.57
230.9	1592.00	234.4	1616.13	237.9	1640.26
231.0	1592.69	234.5	1616.82	238.0	1640.95
231.1	1593.38	234.6	1617.51	238.1	1641.64
231.2	1594.07	234.7	1618.20	238.2	1642.33
231.3	1594.76	234.8	1618.89	238.3	1643.02
231.4	1595.45	234.9	1619.58	238.4	1643.71
231.5	1596.14	235.0	1620.27	238.5	1644.40
231.6	1596.83	235.1	1620.96	238.6	1645.09
231.7	1597.52	235.2	1621.65	238.7	1645.78
231.8	1598.20	235.3	1622.34	238.8	1646.47
231.9	1598.89	235.4	1623.03	238.9	1647.16
232.0	1599.58	235.5	1623.72	239.0	1647.85
232.1	1600.27	235.6	1624.40	239.1	1648.54
232.2	1600.96	235.7	1625.09	239.2	1649.23
232.3	1601.65	235.8	1625.78	239.3	1649.92
232.4	1602.34	235.9	1626.47	239.4	1650.60
232.5	1603.03	236.0	1627.16	239.5	1651.29
232.6	1603.72	236.1	1627.85	239.6	1651.98
232.7	1604.41	236.2	1628.54	239.7	1652.67
232.8	1605.10	236.3	1629.23	239.8	1653.36
232.9	1605.79	236.4	1629.92	239.9	1654.05
233.0	1606.48	236.5	1630.61	240.0	1654.74
233.1	1607.17	236.6	1631.30	240.1	1655.43
233.2	1607.86	236.7	1631.99	240.2	1656.12
233.3	1608.55	236.8	1632.68	240.3	1656.81
233.4	1609.24	236.9	1633.37	240.4	1657.50
233.5	1609.93	237.0	1634.06	240.5	1658.19
233.6	1610.62	237.1	1634.75	240.6	1658.88
233.7	1611.30	237.2	1635.44	240.7	1659.57
233.8	1611.99	237.3	1636.13	240.8	1660.26
233.9	1612.68	237.4	1636.82	240.9	1660.95

Stress Conversion Table (continued)

English (ksi)	SI (MPa)	English (ksi)	SI (MPa)	English (ksi)	SI (MPa)
241.0	1661.64	244.5	1685.77	248.0	1709.90
241.1	1662.33	244.6	1686.46	248.1	1710.59
241.2	1663.02	244.7	1687.15	248.2	1711.28
241.3	1663.70	244.8	1687.84	248.3	1711.97
241.4	1664.39	244.9	1688.53	248.4	1712.66
241.5	1665.08	245.0	1689.22	248.5	1713.35
241.6	1665.77	245.1	1689.90	248.6	1714.04
241.7	1666.46	245.2	1690.59	248.7	1714.73
241.8	1667.15	245.3	1691.28	248.8	1715.42
241.9	1667.84	245.4	1691.97	248.9	1716.11
242.0	1668.53	245.5	1692.66	249.0	1716.79
242.1	1669.22	245.6	1693.35	249.1	1717.48
242.2	1669.91	245.7	1694.04	249.2	1718.17
242.3	1670.60	245.8	1694.73	249.3	1718.86
242.4	1671.29	245.9	1695.42	249.4	1719.55
242.5	1671.98	246.0	1696.11	249.5	1720.24
242.6	1672.67	246.1	1696.80	249.6	1720.93
242.7	1673.36	246.2	1697.49	249.7	1721.62
242.8	1674.05	246.3	1698.18	249.8	1722.31
242.9	1674.74	246.4	1698.87	249.9	1723.00
243.0	1675.43	246.5	1699.56	250.0	1723.69
243.1	1676.12	246.6	1700.25	250.1	1724.38
243.2	1676.80	246.7	1700.94	250.2	1725.07
243.3	1677.49	246.8	1701.63	250.3	1725.76
243.4	1678.18	246.9	1702.32	250.4	1726.45
243.5	1678.87	247.0	1703.00	250.5	1727.14
243.6	1679.56	247.1	1703.69	250.6	1727.83
243.7	1680.25	247.2	1704.38	250.7	1728.52
243.8	1680.94	247.3	1705.07	250.8	1729.21
243.9	1681.63	247.4	1705.76	250.9	1729.89
244.0	1682.32	247.5	1706.45	251.0	1730.58
244.1	1683.01	247.6	1707.14	251.1	1731.27
244.2	1683.70	247.7	1707.83	251.2	1731.96
244.3	1684.39	247.8	1708.52	251.3	1732.65
244.4	1685.08	247.9	1709.21	251.4	1733.34

Stress Conversion Table (continued)

English (ksi)	SI (MPa)	English (ksi)	SI (MPa)	English (ksi)	SI (MPa)
251.5	1734.03	255.0	1758.16	258.5	1782.29
251.6	1734.72	255.1	1758.85	258.6	1782.98
251.7	1735.41	255.2	1759.54	258.7	1783.67
251.8	1736.10	255.3	1760.23	258.8	1784.36
251.9	1736.79	255.4	1760.92	258.9	1785.05
252.0	1737.48	255.5	1761.61	259.0	1785.74
252.1	1738.17	255.6	1762.30	259.1	1786.43
252.2	1738.86	255.7	1762.99	259.2	1787.12
252.3	1739.55	255.8	1763.68	259.3	1787.81
252.4	1740.24	255.9	1764.37	259.4	1788.50
252.5	1740.93	256.0	1765.06	259.5	1789.19
252.6	1741.62	256.1	1765.75	259.6	1789.88
252.7	1742.31	256.2	1766.44	259.7	1790.57
252.8	1742.99	256.3	1767.13	259.8	1791.26
252.9	1743.68	256.4	1767.82	259.9	1791.95
253.0	1744.37	256.5	1768.51	260.0	1792.64
253.1	1745.06	256.6	1769.19	260.1	1793.33
253.2	1745.75	256.7	1769.88	260.2	1794.02
253.3	1746.44	256.8	1770.57	260.3	1794.71
253.4	1747.13	256.9	1771.26	260.4	1795.39
253.5	1747.82	257.0	1771.95	260.5	1796.08
253.6	1748.51	257.1	1772.64	260.6	1796.77
253.7	1749.20	257.2	1773.33	260.7	1797.46
253.8	1749.89	257.3	1774.02	260.8	1798.15
253.9	1750.58	257.4	1774.71	260.9	1798.84
254.0	1751.27	257.5	1775.40	261.0	1799.53
254.1	1751.96	257.6	1776.09	261.1	1800.22
254.2	1752.65	257.7	1776.78	261.2	1800.91
254.3	1753.34	257.8	1777.47	261.3	1801.60
254.4	1754.03	257.9	1778.16	261.4	1802.29
254.5	1754.72	258.0	1778.85	261.5	1802.98
254.6	1755.41	258.1	1779.54	261.6	1803.67
254.7	1756.09	258.2	1780.23	261.7	1804.36
254.8	1756.78	258.3	1780.92	261.8	1805.05
254.9	1757.47	258.4	1781.61	261.9	1805.74

Stress Conversion Table (continued)

English (ksi)	SI (MPa)	English (ksi)	SI (MPa)	English (ksi)	SI (MPa)
262.0	1806.43	265.5	1830.56	269.0	1854.69
262.1	1807.12	265.6	1831.25	269.1	1855.38
262.2	1807.81	265.7	1831.94	269.2	1856.07
262.3	1808.49	265.8	1832.63	269.3	1856.76
262.4	1809.18	265.9	1833.32	269.4	1857.45
262.5	1809.87	266.0	1834.01	269.5	1858.14
262.6	1810.56	266.1	1834.69	269.6	1858.83
262.7	1811.25	266.2	1835.38	269.7	1859.52
262.8	1811.94	266.3	1836.07	269.8	1860.21
262.9	1812.63	266.4	1836.76	269.9	1860.89
263.0	1813.32	266.5	1837.45	270.0	1861.58
263.1	1814.01	266.6	1838.14	270.1	1862.27
263.2	1814.70	266.7	1838.83	270.2	1862.96
263.3	1815.39	266.8	1839.52	270.3	1863.65
263.4	1816.08	266.9	1840.21	270.4	1864.34
263.5	1816.77	267.0	1840.90	270.5	1865.03
263.6	1817.46	267.1	1841.59	270.6	1865.72
263.7	1818.15	267.2	1842.28	270.7	1866.41
263.8	1818.84	267.3	1842.97	270.8	1867.10
263.9	1819.53	267.4	1843.66	270.9	1867.79
264.0	1820.22	267.5	1844.35	271.0	1868.48
264.1	1820.91	267.6	1845.04	271.1	1869.17
264.2	1821.59	267.7	1845.73	271.2	1869.86
264.3	1822.28	267.8	1846.42	271.3	1870.55
264.4	1822.97	267.9	1847.11	271.4	1871.24
264.5	1823.66	268.0	1847.79	271.5	1871.93
264.6	1824.35	268.1	1848.48	271.6	1872.62
264.7	1825.04	268.2	1849.17	271.7	1873.31
264.8	1825.73	268.3	1849.86	271.8	1873.99
264.9	1826.42	268.4	1850.55	271.9	1874.68
265.0	1827.11	268.5	1851.24	272.0	1875.37
265.1	1827.80	268.6	1851.93	272.1	1876.06
265.2	1828.49	268.7	1852.62	272.2	1876.75
265.3	1829.18	268.8	1853.31	272.3	1877.44
265.4	1829.87	268.9	1854.00	272.4	1878.13

Stress Conversion Table (continued)

English (ksi)	SI (MPa)	English (ksi)	SI (MPa)	English (ksi)	SI (MPa)
272.5	1878.82	276.0	1902.95	279.5	1927.08
272.6	1879.51	276.1	1903.64	279.6	1927.77
272.7	1880.20	276.2	1904.33	279.7	1928.46
272.8	1880.89	276.3	1905.02	279.8	1929.15
272.9	1881.58	276.4	1905.71	279.9	1929.84
273.0	1882.27	276.5	1906.40	280.0	1930.53
273.1	1882.96	276.6	1907.09	280.1	1931.22
273.2	1883.65	276.7	1907.78	280.2	1931.91
273.3	1884.34	276.8	1908.47	280.3	1932.60
273.4	1885.03	276.9	1909.16	280.4	1933.29
273.5	1885.72	277.0	1909.85	280.5	1933.98
273.6	1886.41	277.1	1910.54	280.6	1934.67
273.7	1887.09	277.2	1911.23	280.7	1935.36
273.8	1887.78	277.3	1911.92	280.8	1936.05
273.9	1888.47	277.4	1912.61	280.9	1936.74
274.0	1889.16	277.5	1913.30	281.0	1937.43
274.1	1889.85	277.6	1913.98	281.1	1938.12
274.2	1890.54	277.7	1914.67	281.2	1938.81
274.3	1891.23	277.8	1915.36	281.3	1939.50
274.4	1891.92	277.9	1916.05	281.4	1940.18
274.5	1892.61	278.0	1916.74	281.5	1940.87
274.6	1893.30	278.1	1917.43	281.6	1941.56
274.7	1893.99	278.2	1918.12	281.7	1942.25
274.8	1894.68	278.3	1918.81	281.8	1942.94
274.9	1895.37	278.4	1919.50	281.9	1943.63
275.0	1896.06	278.5	1920.19	282.0	1944.32
275.1	1896.75	278.6	1920.88	282.1	1945.01
275.2	1897.44	278.7	1921.57	282.2	1945.70
275.3	1898.13	278.8	1922.26	282.3	1946.39
275.4	1898.82	278.9	1922.95	282.4	1947.08
275.5	1899.51	279.0	1923.64	282.5	1947.77
275.6	1900.20	279.1	1924.33	282.6	1948.46
275.7	1900.88	279.2	1925.02	282.7	1949.15
275.8	1901.57	279.3	1925.71	282.8	1949.84
275.9	1902.26	279.4	1926.40	282.9	1950.53

Stress Conversion Table (continued)

English (ksi)	SI (MPa)	English (ksi)	SI (MPa)	English (ksi)	SI (MPa)
283.0	1951.22	286.5	1975.35	290.0	1999.48
283.1	1951.91	286.6	1976.04	290.1	2000.17
283.2	1952.60	286.7	1976.73	290.2	2000.86
283.3	1953.28	286.8	1977.42	290.3	2001.55
283.4	1953.97	286.9	1978.11	290.4	2002.24
283.5	1954.66	287.0	1978.80	290.5	2002.93
283.6	1955.35	287.1	1979.48	290.6	2003.62
283.7	1956.04	287.2	1980.17	290.7	2004.31
283.8	1956.73	287.3	1980.86	290.8	2005.00
283.9	1957.42	287.4	1981.55	290.9	2005.68
284.0	1958.11	287.5	1982.24	291.0	2006.37
284.1	1958.80	287.6	1982.93	291.1	2007.06
284.2	1959.49	287.7	1983.62	291.2	2007.75
284.3	1960.18	287.8	1984.31	291.3	2008.44
284.4	1960.87	287.9	1985.00	291.4	2009.13
284.5	1961.56	288.0	1985.69	291.5	2009.82
284.6	1962.25	288.1	1986.38	291.6	2010.51
284.7	1962.94	288.2	1987.07	291.7	2011.20
284.8	1963.63	288.3	1987.76	291.8	2011.89
284.9	1964.32	288.4	1988.45	291.9	2012.58
285.0	1965.01	288.5	1989.14	292.0	2013.27
285.1	1965.70	288.6	1989.83	292.1	2013.96
285.2	1966.38	288.7	1990.52	292.2	2014.65
285.3	1967.07	288.8	1991.21	292.3	2015.34
285.4	1967.76	288.9	1991.90	292.4	2016.03
285.5	1968.45	289.0	1992.58	292.5	2016.72
285.6	1969.14	289.1	1993.27	292.6	2017.41
285.7	1969.83	289.2	1993.96	292.7	2018.10
285.8	1970.52	289.3	1994.65	292.8	2018.78
285.9	1971.21	289.4	1995.34	292.9	2019.47
286.0	1971.90	289.5	1996.03	293.0	2020.16
286.1	1972.59	289.6	1996.72	293.1	2020.85
286.2	1973.28	289.7	1997.41	293.2	2021.54
286.3	1973.97	289.8	1998.10	293.3	2022.23
286.4	1974.66	289.9	1998.79	293.4	2022.92

Stress Conversion Table (continued)

English (ksi)	SI (MPa)	English (ksi)	SI (MPa)	English (ksi)	SI (MPa)
293.5	2023.61	297.0	2047.74	300.5	2071.87
293.6	2024.30	297.1	2048.43	300.6	2072.56
293.7	2024.99	297.2	2049.12	300.7	2073.25
293.8	2025.68	297.3	2049.81	300.8	2073.94
293.9	2026.37	297.4	2050.50	300.9	2074.63
294.0	2027.06	297.5	2051.19	301.0	2075.32
294.1	2027.75	297.6	2051.88	301.1	2076.01
294.2	2028.44	297.7	2052.57	301.2	2076.70
294.3	2029.13	297.8	2053.26	301.3	2077.39
294.4	2029.82	297.9	2053.95	301.4	2078.08
294.5	2030.51	298.0	2054.64	301.5	2078.77
294.6	2031.20	298.1	2055.33	301.6	2079.46
294.7	2031.88	298.2	2056.02	301.7	2080.15
294.8	2032.57	298.3	2056.71	301.8	2080.84
294.9	2033.26	298.4	2057.40	301.9	2081.53
295.0	2033.95	298.5	2058.08	302.0	2082.22
295.1	2034.64	298.6	2058.77	302.1	2082.91
295.2	2035.33	298.7	2059.46	302.2	2083.60
295.3	2036.02	298.8	2060.15	302.3	2084.29
295.4	2036.71	298.9	2060.84	302.4	2084.97
295.5	2037.40	299.0	2061.53	302.5	2085.66
295.6	2038.09	299.1	2062.22	302.6	2086.35
295.7	2038.78	299.2	2062.91	302.7	2087.04
295.8	2039.47	299.3	2063.60	302.8	2087.73
295.9	2040.16	299.4	2064.29	302.9	2088.42
296.0	2040.85	299.5	2064.98	303.0	2089.11
296.1	2041.54	299.6	2065.67	303.1	2089.80
296.2	2042.23	299.7	2066.36	303.2	2090.49
296.3	2042.92	299.8	2067.05	303.3	2091.18
296.4	2043.61	299.9	2067.74	303.4	2091.87
296.5	2044.30	300.0	2068.43	303.5	2092.56
296.6	2044.98	300.1	2069.12	303.6	2093.25
296.7	2045.67	300.2	2069.81	303.7	2093.94
296.8	2046.36	300.3	2070.50	303.8	2094.63
296.9	2047.05	300.4	2071.19	303.9	2095.32

Stress Conversion Table (continued)

English (ksi)	SI (MPa)	English (ksi)	SI (MPa)	English (ksi)	SI (MPa)
304.0	2096.01	307.5	2120.14	311.0	2144.27
304.1	2096.70	307.6	2120.83	311.1	2144.96
304.2	2097.39	307.7	2121.52	311.2	2145.65
304.3	2098.07	307.8	2122.21	311.3	2146.34
304.4	2098.76	307.9	2122.90	311.4	2147.03
304.5	2099.45	308.0	2123.59	311.5	2147.72
304.6	2100.14	308.1	2124.27	311.6	2148.41
304.7	2100.83	308.2	2124.96	311.7	2149.10
304.8	2101.52	308.3	2125.65	311.8	2149.79
304.9	2102.21	308.4	2126.34	311.9	2150.47
305.0	2102.90	308.5	2127.03	312.0	2151.16
305.1	2103.59	308.6	2127.72	312.1	2151.85
305.2	2104.28	308.7	2128.41	312.2	2152.54
305.3	2104.97	308.8	2129.10	312.3	2153.23
305.4	2105.66	308.9	2129.79	312.4	2153.92
305.5	2106.35	309.0	2130.48	312.5	2154.61
305.6	2107.04	309.1	2131.17	312.6	2155.30
305.7	2107.73	309.2	2131.86	312.7	2155.99
305.8	2108.42	309.3	2132.55	312.8	2156.68
305.9	2109.11	309.4	2133.24	312.9	2157.37
306.0	2109.80	309.5	2133.93	313.0	2158.06
306.1	2110.49	309.6	2134.62	313.1	2158.75
306.2	2111.17	309.7	2135.31	313.2	2159.44
306.3	2111.86	309.8	2136.00	313.3	2160.13
306.4	2112.55	309.9	2136.69	313.4	2160.82
306.5	2113.24	310.0	2137.37	313.5	2161.51
306.6	2113.93	310.1	2138.06	313.6	2162.20
306.7	2114.62	310.2	2138.75	313.7	2162.89
306.8	2115.31	310.3	2139.44	313.8	2163.57
306.9	2116.00	310.4	2140.13	313.9	2164.26
307.0	2116.69	310.5	2140.82	314.0	2164.95
307.1	2117.38	310.6	2141.51	314.1	2165.64
307.2	2118.07	310.7	2142.20	314.2	2166.33
307.3	2118.76	310.8	2142.89	314.3	2167.02
307.4	2119.45	310.9	2143.58	314.4	2167.71

Stress Conversion Table (continued)

English (ksi)	SI (MPa)	English (ksi)	SI (MPa)	English (ksi)	SI (MPa)
314.5	2168.40	318.0	2192.53	321.5	2216.66
314.6	2169.09	318.1	2193.22	321.6	2217.35
314.7	2169.78	318.2	2193.91	321.7	2218.04
314.8	2170.47	318.3	2194.60	321.8	2218.73
314.9	2171.16	318.4	2195.29	321.9	2219.42
315.0	2171.85	318.5	2195.98	322.0	2220.11
315.1	2172.54	318.6	2196.67	322.1	2220.80
315.2	2173.23	318.7	2197.36	322.2	2221.49
315.3	2173.92	318.8	2198.05	322.3	2222.18
315.4	2174.61	318.9	2198.74	322.4	2222.87
315.5	2175.30	319.0	2199.43	322.5	2223.56
315.6	2175.99	319.1	2200.12	322.6	2224.25
315.7	2176.67	319.2	2200.81	322.7	2224.94
315.8	2177.36	319.3	2201.50	322.8	2225.63
315.9	2178.05	319.4	2202.19	322.9	2226.32
316.0	2178.74	319.5	2202.87	323.0	2227.01
316.1	2179.43	319.6	2203.56	323.1	2227.70
316.2	2180.12	319.7	2204.25	323.2	2228.39
316.3	2180.81	319.8	2204.94	323.3	2229.07
316.4	2181.50	319.9	2205.63	323.4	2229.76
316.5	2182.19	320.0	2206.32	323.5	2230.45
316.6	2182.88	320.1	2207.01	323.6	2231.14
316.7	2183.57	320.2	2207.70	323.7	2231.83
316.8	2184.26	320.3	2208.39	323.8	2232.52
316.9	2184.95	320.4	2209.08	323.9	2233.21
317.0	2185.64	320.5	2209.77	324.0	2233.90
317.1	2186.33	320.6	2210.46	324.1	2234.59
317.2	2187.02	320.7	2211.15	324.2	2235.28
317.3	2187.71	320.8	2211.84	324.3	2235.97
317.4	2188.40	320.9	2212.53	324.4	2236.66
317.5	2189.09	321.0	2213.22	324.5	2237.35
317.6	2189.77	321.1	2213.91	324.6	2238.04
317.7	2190.46	321.2	2214.60	324.7	2238.73
317.8	2191.15	321.3	2215.29	324.8	2239.42
317.9	2191.84	321.4	2215.97	324.9	2240.11

Stress Conversion Table (continued)

English (ksi)	SI (MPa)	English (ksi)	SI (MPa)	English (ksi)	SI (MPa)
325.0	2240.80	328.5	2264.93	332.0	2289.06
325.1	2241.49	328.6	2265.62	332.1	2289.75
325.2	2242.17	328.7	2266.31	332.2	2290.44
325.3	2242.86	328.8	2267.00	332.3	2291.13
325.4	2243.55	328.9	2267.69	332.4	2291.82
325.5	2244.24	329.0	2268.38	332.5	2292.51
325.6	2244.93	329.1	2269.06	332.6	2293.20
325.7	2245.62	329.2	2269.75	332.7	2293.89
325.8	2246.31	329.3	2270.44	332.8	2294.58
325.9	2247.00	329.4	2271.13	332.9	2295.26
326.0	2247.69	329.5	2271.82	333.0	2295.95
326.1	2248.38	329.6	2272.51	333.1	2296.64
326.2	2249.07	329.7	2273.20	333.2	2297.33
326.3	2249.76	329.8	2273.89	333.3	2298.02
326.4	2250.45	329.9	2274.58	333.4	2298.71
326.5	2251.14	330.0	2275.27	333.5	2299.40
326.6	2251.83	330.1	2275.96	333.6	2300.09
326.7	2252.52	330.2	2276.65	333.7	2300.78
326.8	2253.21	330.3	2277.34	333.8	2301.47
326.9	2253.90	330.4	2278.03	333.9	2302.16
327.0	2254.59	330.5	2278.72	334.0	2302.85
327.1	2255.28	330.6	2279.41	334.1	2303.54
327.2	2255.96	330.7	2280.10	334.2	2304.23
327.3	2256.65	330.8	2280.79	334.3	2304.92
327.4	2257.34	330.9	2281.48	334.4	2305.61
327.5	2258.03	331.0	2282.16	334.5	2306.30
327.6	2258.72	331.1	2282.85	334.6	2306.99
327.7	2259.41	331.2	2283.54	334.7	2307.68
327.8	2260.10	331.3	2284.23	334.8	2308.36
327.9	2260.79	331.4	2284.92	334.9	2309.05
328.0	2261.48	331.5	2285.61	335.0	2309.74
328.1	2262.17	331.6	2286.30	335.1	2310.43
328.2	2262.86	331.7	2286.99	335.2	2311.12
328.3	2263.55	331.8	2287.68	335.3	2311.81
328.4	2264.24	331.9	2288.37	335.4	2312.50

Stress Conversion Table (continued)

English (ksi)	SI (MPa)	English (ksi)	SI (MPa)	English (ksi)	SI (MPa)
335.5	2313.19	339.0	2337.32	342.5	2361.45
335.6	2313.88	339.1	2338.01	342.6	2362.14
335.7	2314.57	339.2	2338.70	342.7	2362.83
335.8	2315.26	339.3	2339.39	342.8	2363.52
335.9	2315.95	339.4	2340.08	342.9	2364.21
336.0	2316.64	339.5	2340.77	343.0	2364.90
336.1	2317.33	339.6	2341.46	343.1	2365.59
336.2	2318.02	339.7	2342.15	343.2	2366.28
336.3	2318.71	339.8	2342.84	343.3	2366.97
336.4	2319.40	339.9	2343.53	343.4	2367.66
336.5	2320.09	340.0	2344.22	343.5	2368.35
336.6	2320.78	340.1	2344.91	343.6	2369.04
336.7	2321.46	340.2	2345.60	343.7	2369.73
336.8	2322.15	340.3	2346.29	343.8	2370.42
336.9	2322.84	340.4	2346.98	343.9	2371.11
337.0	2323.53	340.5	2347.66	344.0	2371.80
337.1	2324.22	340.6	2348.35	344.1	2372.49
337.2	2324.91	340.7	2349.04	344.2	2373.18
337.3	2325.60	340.8	2349.73	344.3	2373.86
337.4	2326.29	340.9	2350.42	344.4	2374.55
337.5	2326.98	341.0	2351.11	344.5	2375.24
337.6	2327.67	341.1	2351.80	344.6	2375.93
337.7	2328.36	341.2	2352.49	344.7	2376.62
337.8	2329.05	341.3	2353.18	344.8	2377.31
337.9	2329.74	341.4	2353.87	344.9	2378.00
338.0	2330.43	341.5	2354.56	345.0	2378.69
338.1	2331.12	341.6	2355.25	345.1	2379.38
338.2	2331.81	341.7	2355.94	345.2	2380.07
338.3	2332.50	341.8	2356.63	345.3	2380.76
338.4	2333.19	341.9	2357.32	345.4	2381.45
338.5	2333.88	342.0	2358.01	345.5	2382.14
338.6	2334.56	342.1	2358.70	345.6	2382.83
338.7	2335.25	342.2	2359.39	345.7	2383.52
338.8	2335.94	342.3	2360.08	345.8	2384.21
338.9	2336.63	342.4	2360.76	345.9	2384.90

Stress Conversion Table (continued)

English (ksi)	SI (MPa)	English (ksi)	SI (MPa)	English (ksi)	SI (MPa)
346.0	2385.59	349.5	2409.72	353.0	2433.85
346.1	2386.28	349.6	2410.41	353.1	2434.54
346.2	2386.96	349.7	2411.10	353.2	2435.23
346.3	2387.65	349.8	2411.79	353.3	2435.92
346.4	2388.34	349.9	2412.48	353.4	2436.61
346.5	2389.03	350.0	2413.16	353.5	2437.30
346.6	2389.72	350.1	2413.85	353.6	2437.99
346.7	2390.41	350.2	2414.54	353.7	2438.68
346.8	2391.10	350.3	2415.23	353.8	2439.37
346.9	2391.79	350.4	2415.92	353.9	2440.05
347.0	2392.48	350.5	2416.61	354.0	2440.74
347.1	2393.17	350.6	2417.30	354.1	2441.43
347.2	2393.86	350.7	2417.99	354.2	2442.12
347.3	2394.55	350.8	2418.68	354.3	2442.81
347.4	2395.24	350.9	2419.37	354.4	2443.50
347.5	2395.93	351.0	2420.06	354.5	2444.19
347.6	2396.62	351.1	2420.75	354.6	2444.88
347.7	2397.31	351.2	2421.44	354.7	2445.57
347.8	2398.00	351.3	2422.13	354.8	2446.26
347.9	2398.69	351.4	2422.82	354.9	2446.95
348.0	2399.38	351.5	2423.51	355.0	2447.64
348.1	2400.06	351.6	2424.20	355.1	2448.33
348.2	2400.75	351.7	2424.89	355.2	2449.02
348.3	2401.44	351.8	2425.58	355.3	2449.71
348.4	2402.13	351.9	2426.26	355.4	2450.40
348.5	2402.82	352.0	2426.95	355.5	2451.09
348.6	2403.51	352.1	2427.64	355.6	2451.78
348.7	2404.20	352.2	2428.33	355.7	2452.47
348.8	2404.89	352.3	2429.02	355.8	2453.15
348.9	2405.58	352.4	2429.71	355.9	2453.84
349.0	2406.27	352.5	2430.40	356.0	2454.53
349.1	2406.96	352.6	2431.09	356.1	2455.22
349.2	2407.65	352.7	2431.78	356.2	2455.91
349.3	2408.34	352.8	2432.47	356.3	2456.60
349.4	2409.03	352.9	2433.16	356.4	2457.29

Stress Conversion Table (continued)

English (ksi)	SI (MPa)	English (ksi)	SI (MPa)	English (ksi)	SI (MPa)
356.5	2457.98	360.0	2482.11	363.5	2506.24
356.6	2458.67	360.1	2482.80	363.6	2506.93
356.7	2459.36	360.2	2483.49	363.7	2507.62
356.8	2460.05	360.3	2484.18	363.8	2508.31
356.9	2460.74	360.4	2484.87	363.9	2509.00
357.0	2461.43	360.5	2485.56	364.0	2509.69
357.1	2462.12	360.6	2486.25	364.1	2510.38
357.2	2462.81	360.7	2486.94	364.2	2511.07
357.3	2463.50	360.8	2487.63	364.3	2511.76
357.4	2464.19	360.9	2488.32	364.4	2512.45
357.5	2464.88	361.0	2489.01	364.5	2513.14
357.6	2465.57	361.1	2489.70	364.6	2513.83
357.7	2466.25	361.2	2490.39	364.7	2514.52
357.8	2466.94	361.3	2491.08	364.8	2515.21
357.9	2467.63	361.4	2491.77	364.9	2515.90
358.0	2468.32	361.5	2492.45	365.0	2516.59
358.1	2469.01	361.6	2493.14	365.1	2517.28
358.2	2469.70	361.7	2493.83	365.2	2517.97
358.3	2470.39	361.8	2494.52	365.3	2518.65
358.4	2471.08	361.9	2495.21	365.4	2519.34
358.5	2471.77	362.0	2495.90	365.5	2520.03
358.6	2472.46	362.1	2496.59	365.6	2520.72
358.7	2473.15	362.2	2497.28	365.7	2521.41
358.8	2473.84	362.3	2497.97	365.8	2522.10
358.9	2474.53	362.4	2498.66	365.9	2522.79
359.0	2475.22	362.5	2499.35	366.0	2523.48
359.1	2475.91	362.6	2500.04	366.1	2524.17
359.2	2476.60	362.7	2500.73	366.2	2524.86
359.3	2477.29	362.8	2501.42	366.3	2525.55
359.4	2477.98	362.9	2502.11	366.4	2526.24
359.5	2478.67	363.0	2502.80	366.5	2526.93
359.6	2479.35	363.1	2503.49	366.6	2527.62
359.7	2480.04	363.2	2504.18	366.7	2528.31
359.8	2480.73	363.3	2504.87	366.8	2529.00
359.9	2481.42	363.4	2505.55	366.9	2529.69

Stress Conversion Table (continued)

English (ksi)	SI (MPa)	English (ksi)	SI (MPa)	English (ksi)	SI (MPa)
367.0	2530.38	370.5	2554.51	374.0	2578.64
367.1	2531.07	370.6	2555.20	374.1	2579.33
367.2	2531.75	370.7	2555.89	374.2	2580.02
367.3	2532.44	370.8	2556.58	374.3	2580.71
367.4	2533.13	370.9	2557.27	374.4	2581.40
367.5	2533.82	371.0	2557.95	374.5	2582.09
367.6	2534.51	371.1	2558.64	374.6	2582.78
367.7	2535.20	371.2	2559.33	374.7	2583.47
367.8	2535.89	371.3	2560.02	374.8	2584.15
367.9	2536.58	371.4	2560.71	374.9	2584.84
368.0	2537.27	371.5	2561.40	375.0	2585.53
368.1	2537.96	371.6	2562.09	375.1	2586.22
368.2	2538.65	371.7	2562.78	375.2	2586.91
368.3	2539.34	371.8	2563.47	375.3	2587.60
368.4	2540.03	371.9	2564.16	375.4	2588.29
368.5	2540.72	372.0	2564.85	375.5	2588.98
368.6	2541.41	372.1	2565.54	375.6	2589.67
368.7	2542.10	372.2	2566.23	375.7	2590.36
368.8	2542.79	372.3	2566.92	375.8	2591.05
368.9	2543.48	372.4	2567.61	375.9	2591.74
369.0	2544.17	372.5	2568.30	376.0	2592.43
369.1	2544.85	372.6	2568.99	376.1	2593.12
369.2	2545.54	372.7	2569.68	376.2	2593.81
369.3	2546.23	372.8	2570.37	376.3	2594.50
369.4	2546.92	372.9	2571.05	376.4	2595.19
369.5	2547.61	373.0	2571.74	376.5	2595.88
369.6	2548.30	373.1	2572.43	376.6	2596.57
369.7	2548.99	373.2	2573.12	376.7	2597.25
369.8	2549.68	373.3	2573.81	376.8	2597.94
369.9	2550.37	373.4	2574.50	376.9	2598.63
370.0	2551.06	373.5	2575.19	377.0	2599.32
370.1	2551.75	373.6	2575.88	377.1	2600.01
370.2	2552.44	373.7	2576.57	377.2	2600.70
370.3	2553.13	373.8	2577.26	377.3	2601.39
370.4	2553.82	373.9	2577.95	377.4	2602.08

Stress Conversion Table (continued)

English (ksi)	SI (MPa)	English (ksi)	SI (MPa)	English (ksi)	SI (MPa)
377.5	2602.77	381.0	2626.90	384.5	2651.03
377.6	2603.46	381.1	2627.59	384.6	2651.72
377.7	2604.15	381.2	2628.28	384.7	2652.41
377.8	2604.84	381.3	2628.97	384.8	2653.10
377.9	2605.53	381.4	2629.66	384.9	2653.79
378.0	2606.22	381.5	2630.35	385.0	2654.48
378.1	2606.91	381.6	2631.04	385.1	2655.17
378.2	2607.60	381.7	2631.73	385.2	2655.86
378.3	2608.29	381.8	2632.42	385.3	2656.55
378.4	2608.98	381.9	2633.11	385.4	2657.24
378.5	2609.67	382.0	2633.80	385.5	2657.93
378.6	2610.36	382.1	2634.49	385.6	2658.62
378.7	2611.04	382.2	2635.18	385.7	2659.31
378.8	2611.73	382.3	2635.87	385.8	2660.00
378.9	2612.42	382.4	2636.56	385.9	2660.69
379.0	2613.11	382.5	2637.24	386.0	2661.38
379.1	2613.80	382.6	2637.93	386.1	2662.07
379.2	2614.49	382.7	2638.62	386.2	2662.76
379.3	2615.18	382.8	2639.31	386.3	2663.44
379.4	2615.87	382.9	2640.00	386.4	2664.13
379.5	2616.56	383.0	2640.69	386.5	2664.82
379.6	2617.25	383.1	2641.38	386.6	2665.51
379.7	2617.94	383.2	2642.07	386.7	2666.20
379.8	2618.63	383.3	2642.76	386.8	2666.89
379.9	2619.32	383.4	2643.45	386.9	2667.58
380.0	2620.01	383.5	2644.14	387.0	2668.27
380.1	2620.70	383.6	2644.83	387.1	2668.96
380.2	2621.39	383.7	2645.52	387.2	2669.65
380.3	2622.08	383.8	2646.21	387.3	2670.34
380.4	2622.77	383.9	2646.90	387.4	2671.03
380.5	2623.46	384.0	2647.59	387.5	2671.72
380.6	2624.14	384.1	2648.28	387.6	2672.41
380.7	2624.83	384.2	2648.97	387.7	2673.10
380.8	2625.52	384.3	2649.66	387.8	2673.79
380.9	2626.21	384.4	2650.34	387.9	2674.48

Stress Conversion Table (continued)

English (ksi)	SI (MPa)	English (ksi)	SI (MPa)	English (ksi)	SI (MPa)
388.0	2675.17	391.5	2699.30	395.0	2723.43
388.1	2675.86	391.6	2699.99	395.1	2724.12
388.2	2676.54	391.7	2700.68	395.2	2724.81
388.3	2677.23	391.8	2701.37	395.3	2725.50
388.4	2677.92	391.9	2702.06	395.4	2726.19
388.5	2678.61	392.0	2702.74	395.5	2726.88
388.6	2679.30	392.1	2703.43	395.6	2727.57
388.7	2679.99	392.2	2704.12	395.7	2728.26
388.8	2680.68	392.3	2704.81	395.8	2728.94
388.9	2681.37	392.4	2705.50	395.9	2729.63
389.0	2682.06	392.5	2706.19	396.0	2730.32
389.1	2682.75	392.6	2706.88	396.1	2731.01
389.2	2683.44	392.7	2707.57	396.2	2731.70
389.3	2684.13	392.8	2708.26	396.3	2732.39
389.4	2684.82	392.9	2708.95	396.4	2733.08
389.5	2685.51	393.0	2709.64	396.5	2733.77
389.6	2686.20	393.1	2710.33	396.6	2734.46
389.7	2686.89	393.2	2711.02	396.7	2735.15
389.8	2687.58	393.3	2711.71	396.8	2735.84
389.9	2688.27	393.4	2712.40	396.9	2736.53
390.0	2688.96	393.5	2713.09	397.0	2737.22
390.1	2689.64	393.6	2713.78	397.1	2737.91
390.2	2690.33	393.7	2714.47	397.2	2738.60
390.3	2691.02	393.8	2715.16	397.3	2739.29
390.4	2691.71	393.9	2715.84	397.4	2739.98
390.5	2692.40	394.0	2716.53	397.5	2740.67
390.6	2693.09	394.1	2717.22	397.6	2741.36
390.7	2693.78	394.2	2717.91	397.7	2742.04
390.8	2694.47	394.3	2718.60	397.8	2742.73
390.9	2695.16	394.4	2719.29	397.9	2743.42
391.0	2695.85	394.5	2719.98	398.0	2744.11
391.1	2696.54	394.6	2720.67	398.1	2744.80
391.2	2697.23	394.7	2721.36	398.2	2745.49
391.3	2697.92	394.8	2722.05	398.3	2746.18
391.4	2698.61	394.9	2722.74	398.4	2746.87

Stress Conversion Table (continued)

English (ksi)	SI (MPa)	English (ksi)	SI (MPa)	English (ksi)	SI (MPa)
398.5	2747.56	402.0	2771.69	405.5	2795.82
398.6	2748.25	402.1	2772.38	405.6	2796.51
398.7	2748.94	402.2	2773.07	405.7	2797.20
398.8	2749.63	402.3	2773.76	405.8	2797.89
398.9	2750.32	402.4	2774.45	405.9	2798.58
399.0	2751.01	402.5	2775.14	406.0	2799.27
399.1	2751.70	402.6	2775.83	406.1	2799.96
399.2	2752.39	402.7	2776.52	406.2	2800.65
399.3	2753.08	402.8	2777.21	406.3	2801.34
399.4	2753.77	402.9	2777.90	406.4	2802.03
399.5	2754.46	403.0	2778.59	406.5	2802.72
399.6	2755.14	403.1	2779.28	406.6	2803.41
399.7	2755.83	403.2	2779.97	406.7	2804.10
399.8	2756.52	403.3	2780.66	406.8	2804.79
399.9	2757.21	403.4	2781.34	406.9	2805.48
400.0	2757.90	403.5	2782.03	407.0	2806.17
400.1	2758.59	403.6	2782.72	407.1	2806.86
400.2	2759.28	403.7	2783.41	407.2	2807.55
400.3	2759.97	403.8	2784.10	407.3	2808.23
400.4	2760.66	403.9	2784.79	407.4	2808.92
400.5	2761.35	404.0	2785.48	407.5	2809.61
400.6	2762.04	404.1	2786.17	407.6	2810.30
400.7	2762.73	404.2	2786.86	407.7	2810.99
400.8	2763.42	404.3	2787.55	407.8	2811.68
400.9	2764.11	404.4	2788.24	407.9	2812.37
401.0	2764.80	404.5	2788.93	408.0	2813.06
401.1	2765.49	404.6	2789.62	408.1	2813.75
401.2	2766.18	404.7	2790.31	408.2	2814.44
401.3	2766.87	404.8	2791.00	408.3	2815.13
401.4	2767.56	404.9	2791.69	408.4	2815.82
401.5	2768.24	405.0	2792.38	408.5	2816.51
401.6	2768.93	405.1	2793.07	408.6	2817.20
401.7	2769.62	405.2	2793.76	408.7	2817.89
401.8	2770.31	405.3	2794.45	408.8	2818.58
401.9	2771.00	405.4	2795.13	408.9	2819.27

Stress Conversion Table (continued)

English (ksi)	SI (MPa)	English (ksi)	SI (MPa)	English (ksi)	SI (MPa)
409.0	2819.96	412.5	2844.09	416.0	2868.22
409.1	2820.65	412.6	2844.78	416.1	2868.91
409.2	2821.33	412.7	2845.47	416.2	2869.60
409.3	2822.02	412.8	2846.16	416.3	2870.29
409.4	2822.71	412.9	2846.85	416.4	2870.98
409.5	2823.40	413.0	2847.53	416.5	2871.67
409.6	2824.09	413.1	2848.22	416.6	2872.36
409.7	2824.78	413.2	2848.91	416.7	2873.05
409.8	2825.47	413.3	2849.60	416.8	2873.73
409.9	2826.16	413.4	2850.29	416.9	2874.42
410.0	2826.85	413.5	2850.98	417.0	2875.11
410.1	2827.54	413.6	2851.67	417.1	2875.80
410.2	2828.23	413.7	2852.36	417.2	2876.49
410.3	2828.92	413.8	2853.05	417.3	2877.18
410.4	2829.61	413.9	2853.74	417.4	2877.87
410.5	2830.30	414.0	2854.43	417.5	2878.56
410.6	2830.99	414.1	2855.12	417.6	2879.25
410.7	2831.68	414.2	2855.81	417.7	2879.94
410.8	2832.37	414.3	2856.50	417.8	2880.63
410.9	2833.06	414.4	2857.19	417.9	2881.32
411.0	2833.75	414.5	2857.88	418.0	2882.01
411.1	2834.43	414.6	2858.57	418.1	2882.70
411.2	2835.12	414.7	2859.26	418.2	2883.39
411.3	2835.81	414.8	2859.95	418.3	2884.08
411.4	2836.50	414.9	2860.63	418.4	2884.77
411.5	2837.19	415.0	2861.32	418.5	2885.46
411.6	2837.88	415.1	2862.01	418.6	2886.15
411.7	2838.57	415.2	2862.70	418.7	2886.83
411.8	2839.26	415.3	2863.39	418.8	2887.52
411.9	2839.95	415.4	2864.08	418.9	2888.21
412.0	2840.64	415.5	2864.77	419.0	2888.90
412.1	2841.33	415.6	2865.46	419.1	2889.59
412.2	2842.02	415.7	2866.15	419.2	2890.28
412.3	2842.71	415.8	2866.84	419.3	2890.97
412.4	2843.40	415.9	2867.53	419.4	2891.66

Stress Conversion Table (continued)

English (ksi)	SI (MPa)	English (ksi)	SI (MPa)	English (ksi)	SI (MPa)
419.5	2892.35	423.0	2916.48	426.5	2940.61
419.6	2893.04	423.1	2917.17	426.6	2941.30
419.7	2893.73	423.2	2917.86	426.7	2941.99
419.8	2894.42	423.3	2918.55	426.8	2942.68
419.9	2895.11	423.4	2919.24	426.9	2943.37
420.0	2895.80	423.5	2919.93	427.0	2944.06
420.1	2896.49	423.6	2920.62	427.1	2944.75
420.2	2897.18	423.7	2921.31	427.2	2945.44
420.3	2897.87	423.8	2922.00	427.3	2946.13
420.4	2898.56	423.9	2922.69	427.4	2946.82
420.5	2899.25	424.0	2923.38	427.5	2947.51
420.6	2899.93	424.1	2924.07	427.6	2948.20
420.7	2900.62	424.2	2924.76	427.7	2948.89
420.8	2901.31	424.3	2925.45	427.8	2949.58
420.9	2902.00	424.4	2926.13	427.9	2950.27
421.0	2902.69	424.5	2926.82	428.0	2950.96
421.1	2903.38	424.6	2927.51	428.1	2951.65
421.2	2904.07	424.7	2928.20	428.2	2952.33
421.3	2904.76	424.8	2928.89	428.3	2953.02
421.4	2905.45	424.9	2929.58	428.4	2953.71
421.5	2906.14	425.0	2930.27	428.5	2954.40
421.6	2906.83	425.1	2930.96	428.6	2955.09
421.7	2907.52	425.2	2931.65	428.7	2955.78
421.8	2908.21	425.3	2932.34	428.8	2956.47
421.9	2908.90	425.4	2933.03	428.9	2957.16
422.0	2909.59	425.5	2933.72	429.0	2957.85
422.1	2910.28	425.6	2934.41	429.1	2958.54
422.2	2910.97	425.7	2935.10	429.2	2959.23
422.3	2911.66	425.8	2935.79	429.3	2959.92
422.4	2912.35	425.9	2936.48	429.4	2960.61
422.5	2913.03	426.0	2937.17	429.5	2961.30
422.6	2913.72	426.1	2937.86	429.6	2961.99
422.7	2914.41	426.2	2938.55	429.7	2962.68
422.8	2915.10	426.3	2939.23	429.8	2963.37
422.9	2915.79	426.4	2939.92	429.9	2964.06

Stress Conversion Table (continued)

English (ksi)	SI (MPa)	English (ksi)	SI (MPa)	English (ksi)	SI (MPa)
430.0	2964.75	433.5	2988.88	437.0	3013.01
430.1	2965.43	433.6	2989.57	437.1	3013.70
430.2	2966.12	433.7	2990.26	437.2	3014.39
430.3	2966.81	433.8	2990.95	437.3	3015.08
430.4	2967.50	433.9	2991.64	437.4	3015.77
430.5	2968.19	434.0	2992.32	437.5	3016.46
430.6	2968.88	434.1	2993.01	437.6	3017.15
430.7	2969.57	434.2	2993.70	437.7	3017.84
430.8	2970.26	434.3	2994.39	437.8	3018.52
430.9	2970.95	434.4	2995.08	437.9	3019.21
431.0	2971.64	434.5	2995.77	438.0	3019.90
431.1	2972.33	434.6	2996.46	438.1	3020.59
431.2	2973.02	434.7	2997.15	438.2	3021.28
431.3	2973.71	434.8	2997.84	438.3	3021.97
431.4	2974.40	434.9	2998.53	438.4	3022.66
431.5	2975.09	435.0	2999.22	438.5	3023.35
431.6	2975.78	435.1	2999.91	438.6	3024.04
431.7	2976.47	435.2	3000.60	438.7	3024.73
431.8	2977.16	435.3	3001.29	438.8	3025.42
431.9	2977.85	435.4	3001.98	438.9	3026.11
432.0	2978.54	435.5	3002.67	439.0	3026.80
432.1	2979.22	435.6	3003.36	439.1	3027.49
432.2	2979.91	435.7	3004.05	439.2	3028.18
432.3	2980.60	435.8	3004.74	439.3	3028.87
432.4	2981.29	435.9	3005.42	439.4	3029.56
432.5	2981.98	436.0	3006.11	439.5	3030.25
432.6	2982.67	436.1	3006.80	439.6	3030.94
432.7	2983.36	436.2	3007.49	439.7	3031.62
432.8	2984.05	436.3	3008.18	439.8	3032.31
432.9	2984.74	436.4	3008.87	439.9	3033.00
433.0	2985.43	436.5	3009.56	440.0	3033.69
433.1	2986.12	436.6	3010.25	440.1	3034.38
433.2	2986.81	436.7	3010.94	440.2	3035.07
433.3	2987.50	436.8	3011.63	440.3	3035.76
433.4	2988.19	436.9	3012.32	440.4	3036.45

Stress Conversion Table (continued)

English (ksi)	SI (MPa)	English (ksi)	SI (MPa)	English (ksi)	SI (MPa)
440.5	3037.14	444.0	3061.27	447.5	3085.40
440.6	3037.83	444.1	3061.96	447.6	3086.09
440.7	3038.52	444.2	3062.65	447.7	3086.78
440.8	3039.21	444.3	3063.34	447.8	3087.47
440.9	3039.90	444.4	3064.03	447.9	3088.16
441.0	3040.59	444.5	3064.72	448.0	3088.85
441.1	3041.28	444.6	3065.41	448.1	3089.54
441.2	3041.97	444.7	3066.10	448.2	3090.23
441.3	3042.66	444.8	3066.79	448.3	3090.92
441.4	3043.35	444.9	3067.48	448.4	3091.61
441.5	3044.04	445.0	3068.17	448.5	3092.30
441.6	3044.72	445.1	3068.86	448.6	3092.99
441.7	3045.41	445.2	3069.55	448.7	3093.68
441.8	3046.10	445.3	3070.24	448.8	3094.37
441.9	3046.79	445.4	3070.92	448.9	3095.06
442.0	3047.48	445.5	3071.61	449.0	3095.75
442.1	3048.17	445.6	3072.30	449.1	3096.44
442.2	3048.86	445.7	3072.99	449.2	3097.12
442.3	3049.55	445.8	3073.68	449.3	3097.81
442.4	3050.24	445.9	3074.37	449.4	3098.50
442.5	3050.93	446.0	3075.06	449.5	3099.19
442.6	3051.62	446.1	3075.75	449.6	3099.88
442.7	3052.31	446.2	3076.44	449.7	3100.57
442.8	3053.00	446.3	3077.13	449.8	3101.26
442.9	3053.69	446.4	3077.82	449.9	3101.95
443.0	3054.38	446.5	3078.51	450.0	3102.64
443.1	3055.07	446.6	3079.20		
443.2	3055.76	446.7	3079.89		
443.3	3056.45	446.8	3080.58		
443.4	3057.14	446.9	3081.27		
443.5	3057.82	447.0	3081.96		
443.6	3058.51	447.1	3082.65		
443.7	3059.20	447.2	3083.34		
443.8	3059.89	447.3	3084.02		
443.9	3060.58	447.4	3084.71		

INDEX

Test	Material	Page
Chemical Analysis		
	type 316 SS	167
Creep Test Data		
Base-Line Data		
	type 304 SS	120–21, 132–34
	type 304 SS plate	263–72
	type 304 SS welded plate	272
	overlaid type 304 SS forging	225–31
	type 304 SS tube	272–300
	type 316 SS tube	300–3
	type 316 SS, 20% cold worked	75
	type 316H SS	84
	type 308 CRE SS weld metal	187–97
	2 1/4 Cr-1 Mo	202–8
Correlations		
	2 1/4 Cr-1 Mo	223–25
	type 304 SS	120–31, 310–14
Crack Growth		
	type 304 SS	314–22
Cyclic Creep		
	decarburized 2 1/4 Cr-1 Mo	207–12
	type 304 SS	236–38
Dislocation Mechanisms		
	types 304 and 316 SS	305–10
Effect of Aging		
	type 304 SS	141–43
	type 316 SS	143–45
Effect of Cold Work		
	type 316 SS	340–47

Test	Material	Page
Creep Test Data (continued)		
Effect of Sodium Environment		
	types 304, 316, and Ti-modified SS	49–50
	2 1/4 Cr-1 Mo	207–12
Effect of Strain Cycling		
	type 304 SS	239–40
Effect of Test Method		
Theoretical Analysis		175–78
	type 304 SS	241–55
Heat-to-Heat Variation		
	type 304 SS	132–34, 141–43
	type 316 SS	143–45
	type 316 SS, 20% cold worked	97
Intergranular Cracking		
	type 304 SS	314–27
Multiaxial Data		
	type 304 SS	241–55
Strain Limits		
	type 304 SS	120–31
Fatigue Test Data		
Cyclic Fatigue Test Data		
	type 304/308 SS welds	22–28
Biaxial		
	2 1/4 Cr-1 Mo	219–22
Correlations		
	type 304 SS	15–22
Effect of Hold Time		
	type 316 SS	1–11
Strain-Controlled Tests		
	2 1/4 Cr-1 Mo	213–19
	Inconel 718	12–14

Test	Material	Page
Fatigue Test Data (continued)		
Crack Growth Rate Data		
Effect of Stress Intensity Factor		
	types 304 and 316 SS	103–10
	type 304/308 SS welds	28–35
	type 308 SS weld metal	103–10
Effect of Temperature		
	types 304 and 316 SS	103–10
	type 308 SS weld metal	103–10
	Incoloy 800	55–63
Effect of Test Variables		
	ASTM SA-351, Grade CF-8	90
Effect of Thermal Aging		
	types 304 and 316 SS	103–10
	type 304/308 SS welds	28–35
	type 308 SS weld metal	103–10
Microstructure		
	2 1/4 Cr-1 Mo	207–12, 329–40
	type 304 SS	303–10
	Incoloy 800	322–26
Relaxation		
	type 304 SS	238
Tensile Test Data		
Base-Line Data		
	types 304, 316, and Ti-modified SS	35–41, 167
	2 1/4 Cr-1 Mo	197–201
	type 304 SS welded plate	178–87
Correlations		
	type 316 SS	155–63
	2 1/4 Cr-1 Mo	224–25

Test	Material	Page
Tensile Test Data (continued)		
Effect of Aging		
	type 304 SS	63, 73, 132–42
	type 316 SS	143–55
Effect of Carbon		
	type 316 SS	347–62
Effect of Prior Creep		
	type 304 SS	120–23
Effect of Sodium Environment		
	types 304, 316, and Ti-modified 316 SS	41–50
Effect of Strain Rate		
	type 304 SS	63–73
Effect of Varying Conditions During Test		
	type 304 SS	232–37
Heat-to-Heat Variations		
	type 304 SS	132–42, 155–63
	type 316 SS	143–63
Toughness		
J Integral		
	type 316 SS (forging and weld)	110–15

☆U.S. GOVERNMENT PRINTING OFFICE: 1974-747-302/43

ORNL-4998
UC-79b, -h, -k
(Liquid Metal Fast
Breeder Reactors)

INTERNAL DISTRIBUTION

(3) Central Research Library
ORNL — Y-12 Technical Library
Document Reference Section
(10) Laboratory Records Department
Laboratory Records, ORNL RC
ORNL Patent Office
R. J. Beaver
M. Bender
R. G. Berggren
M. K. Booker
C. R. Brinkman
D. A. Canonico
J. Corum
W. R. Corwin
F. L. Culler
J. E. Cunningham
J. H. DeVan
D. P. Edmonds
G. Fee
M. H. Fontana
W. R. Gall
B. L. Greenstreet
J. C. Griess, Jr.
J. P. Hammond
W. O. Harms
R. L. Heestand
(5) M. R. Hill
D. O. Hobson
F. J. Homan
H. Inouye
P. R. Kasten
J. F. King
R. T. King
R. L. Klueh
K. C. Liu
C. T. Liu
A. L. Lotts
(20) W. R. Martin
W. J. McAfee
H. E. McCoy
H. C. McCurdy
C. J. McHargue
J. Merkle
P. Patriarca
S. Peterson
H. Postma
C. E. Pugh
P. L. Rittenhouse
T. Roche
J. L. Scott
Myrtleen Sheldon
V. K. Sikka
G. M. Slaughter
W. J. Stelzman
J. P. Strizak
R. W. Swindeman
D. B. Trauger
T. N. Washburn
J. R. Weir, Jr.
G. D. Whitman
T. Yahr
Walter Kohn (consultant)
W. C. Leslie (consultant)
John Moteff (consultant)
J. W. Prados (consultant)
G. V. Smith (consultant)

EXTERNAL DISTRIBUTION

USAEC DIVISION OF REACTOR RESEARCH AND DEVELOPMENT, Washington, DC 20545

(2) Director

USAEC OAK RIDGE OPERATIONS OFFICE, P.O. Box E, Oak Ridge, TN 37830

Research and Technical Support Division
Director, Reactor Division

USAEC TECHNICAL INFORMATION CENTER, Office of Information Services, P.O. Box 62, Oak Ridge, TN 37830

For distribution as shown in TID-4500 Distribution Category, UC-79b (Fuels and Materials Engineering Development); UC-79h (Structural Materials and Design Engineering); UC-79k (Components)